

CONDENSERS: THEORY AND PRACTICE

Organised by the Institution of Chemical Engineers and the Heat Transfer and Fluid Flow Service Harwell, in conjunction with the Heat Transfer Society and the Institution of Mechanical Engineers, and held at the University of Manchester Institute of Science and Technology, 22–23 March 1983.

Organising Committee

Mr. D. Butterworth	{HTFS, Harwell}
Dr. B.J. Davidson	{CERL, Leatherhead}
Dr. Y.R. Mayhew	{University of Bristol}
Dr. M.J. Moore	{CERL, Leatherhead}
Mr. G.H. Walter	{The Lummus Company Ltd}
Dr. D.R. Webb	{UMIST, Manchester}

**THE INSTITUTION OF CHEMICAL ENGINEERS
SYMPOSIUM SERIES No. 75**

ISBN 0 85295 152 3

All Rights Reserved. No part of this publication may be reproduced, stored in a retrieval system or transmitted in any form or by any means: electronic, electrostatic, magnetic tape, mechanical, photocopying, recording or otherwise, without permission in writing from the copyright owner.

First edition 1983 — ISBN 0 85295 152 3

MEMBERS OF THE INSTITUTION OF CHEMICAL ENGINEERS (Worldwide)
SHOULD ORDER DIRECT FROM THE INSTITUTION

Geo. E. Davis Building, 165–171 Railway Terrace, Rugby, Warks CV21 3HQ.

Australian orders to:

R.M. Wood, School of Chemical Engineering and In
University of New South Wales, PO Box 1, Kensington

*Distributed throughout the world (excluding Austr.
Ltd, except to IChemE members.*

MBM LIBRARY



61254

U.K.	Pergamon Press Ltd. Oxford OX3 0BW, England
U.S.A.	Pergamon Press Inc., Maxwell House, Fairview Park, Elmsford, New York 10523, U.S.A.
CANADA	Pergamon Press Canada Ltd., Suite 104, 150 Consumers Rd., Willowdale, Ontario M2J 1P9, Canada
FRANCE	Pergamon Press SARL, 24 rue des Ecoles, 75240 Paris, Cedex 05, France
FEDERAL REPUBLIC OF GERMANY	Pergamon Press GmbH, 6242 Kronberg- Taunus, Hammerweg 6, Federal Republic of Germany

British Library Cataloguing in Publication Data

Condensers: theory and practice. — (The Institution of Chemical Engineers
symposium series)

1. Condensers (Steam) — Congresses

621.1'97 TJ557

ISBN 0-08-028772-7

Library of Congress Cataloguing in Publication Data

Condensers, theory and practice — (The Institution of Chemical Engineers
symposium series; no. 75)

1. Condensation — Congresses. 2. Condensers (Vapors and gases) —
Congresses. I. Butterworth, D. (David), II. Institution of Chemical Engineers
(Great Britain), III. University of Manchester. Institute of Science and
Technology. IV. Series: Symposium series (Institution of Chemical Engineers
(Great Britain)).

TP156.C6066 1983

660.2'8423

83-6305

ISBN 0-08-028772-7

Printed by The Chameleon Press Limited, 5–25 Burr Road, London SW1B 4SG

Preface

The purpose of the Symposium is to stimulate the exchange of information between researchers into condensation and the designers and users of condensers. The Proceedings are classified into four categories: Theory and Practice as applied in the Power and Process industries. The organising committee has sought to assemble a programme of papers that will be of interest to a wide audience and within each session there is a keynote presentation of a review nature to place the individual papers in a broader context. Inevitably certain topics of current interest or importance receive stronger emphasis. Of note are heat transfer enhancement, computer modelling of flow and prediction of performance and multicomponent condensation.

Cover Illustration

Section of a computer drawing of condenser tube layout, derived from the HTFS program OPTU3 (by courtesy of the Heat Transfer and Fluid Flow Service, AERE, Harwell).

ERRATA

			error	correct version
Paper 1	p.4, line 28; p.8, line 31;		50<Re<100 one-half	; 50<Re<1000 ; twice
Paper 2	p.28, line 13;		0.5mm	; 0.2mm
Paper 24	p.409, line 3 ; line 11; line 32; p.411, line 4 ; line 37; p.412, line 12/13; line 32; line 35;		Ref(10) Ref(11) Ref(12) Ref(13) Ref(15) No Reference; Ref(16) Ref(17)	; Ref(11) ; Ref(12) ; Ref(13) ; Ref(14) ; Ref(18) below ; Ref(17) ; Ref(15) ; Ref(16)
	Ref(18)	Robertson, J.M., Review of Boiling, Condensing and Other Aspects of Two-Phase Flow in Plate-Fin Heat Exchangers, ASME Winter Annual Meeting, Chicago, HTD-Vol.10, pp17-27, 1980.		
Paper 30	p.480, line 14;		$\phi_g^2 \Delta_{p\ell}$; $\phi_{\ell}^2 \Delta_{p\ell}$

Contents

	<i>Page No.</i>
Power Condensers — Theory	
1. Keynote Address — Condensation in Tube Banks T. Fujii (Kyushu University, Kasuga-Shi, Japan)	3
2. The Potential of Heat Transfer Enhancement in Surface Condensers P.J. Marto and R.H. Nunn (Naval Postgraduate School, Monterey, California, USA)	23
3. Enhancement of Naval Condenser Performance D.W. Butcher (NE London Polytechnic) and D.C.P. Birt (Admiralty Marine Technology Establishment, Dorset, UK)	40
4. Air Entrainment in Steam Condensers J.G. Andrews, R.T. Deam and J. Smalley (CEGB, Marchwood Engineering Laboratories, UK)	48
5. A Computer Model for Detailed Calculation of the Flow in Power Station Condensers S. Al-Sanea, N. Rhodes, D.G. Tatchell (CHAM Ltd, Wimbledon, UK) and T.S. Wilkinson (NEI Parsons, Newcastle, UK)	70
6. Numerical Computation of Steam Flow in Power Plant Condensers C. Caremoli (Electricité de France, Chatou, France)	89
7. The Use of Computer Programs to Improve Condenser Performance G. Beckett, B.J. Davidson and J.A. Ferrison (Central Electricity Research Laboratories, Leatherhead, UK)	97
Power Condensers — Practice	
8. Keynote Address — Power Plant Condensers; Recent CEGB Experience M. Rowe (CERL, Leatherhead, UK)	113
9. A Design Method of Condenser Tube Arrangement for Large Power Stations T. Ozeki, Y. Miura and M. Miyoshi (Toshiba Corporation, Japan)	135
10. A Computerised Analysis of Power Condenser Performance Based upon an Investigation of Condensation H.L. Hopkins, J. Loughhead and C.J. Monks (GEC, Manchester, UK)	152
11. A New Condenser Test Code and Associated Measurement Techniques C.A.E. Clay and Z.W. Sochaczewski (CEGB, Midlands, UK)	171
12. Condenser Macrofouling Control Methods I.A. Diaz-Tous (EPRI) and Y.G. Mussalli (Stone and Webster Engineering Corporation, California, USA)	184
13. Seawater Biofouling Countermeasures for Spirally Enhanced Condenser Tubes R.W. Kornbau, C.C. Richard and R.O. Lewis (US Naval Academy, Annapolis, Maryland, USA)	200
14. Aeration and De-Aeration in a Condenser I. Olikar and D. Katsman (Burns and Roe Inc, New Jersey, USA)	213
15. Auxiliary Condensers versus Main Condenser for Boiler Feed Pump Turbine Drivers B. Bornstein (Bechtel Corporation, California, USA)	225
16. Assessing the Effect of Stainless Steel Tubes on Condenser Performance and Integrity J.R. Maurer and F.H. Berendsen (Allegheny Ludlum Steel Corporation, Pennsylvania, USA)	239
17. The Wylfa Condensers — Construction and Operational Problems at a Nuclear Power Station F.J.L. Bindon (Wylfa Power Station, N Wales, UK)	250

Process Condensers — Theory	Page No.
18. Keynote Address — A Review of Some Recent Developments in Condensation Theory R.G. Owen and W.C. Lee (HTFS, Harwell, UK)	261
19. Forced Convection Condensation of Refrigerants inside a Vertical Annulus A. Cavallini, S. Frizzerin and L. Rossetto (University of Padova, Italy)	309
20. Effect of Pitch-Diameter Ratio and Bypass Lanes on Pressure Loss in Condenser Tube Banks N.K. Lee, Y.R. Mayhew and M.A. Hollingsworth (University of Bristol, UK)	323
21. Comparison of Calculation Methods for Non-condensing Gas Effects in Condensation on a Horizontal Tube W.C. Lee and J.W. Rose (Queen Mary College, London, UK)	342
22. Condensation of Single and Mixed Vapours from a Non-condensing Gas in Flow over a Horizontal Tube Bank A.K. Shah and D.R. Webb (UMIST, Manchester, UK)	356
23. A Newton-like Algorithm for the Efficient Estimation of Rates of Multi-Component Condensation by a Film Model R. Taylor, A. Lucia and R. Krishnamurthy (Clarkson College, Potsdam, New York, USA)	380
Process Condensers — Practice	
24. Keynote Address — Trends in Design and Application of Condensers in the Process Industries K.J. Bell (Oklahoma State University, USA)	401
25. Gravity Controlled Condensation on a Horizontal Low-Fin Tube R.G. Owen, R.G. Sardesai, R.A. Smith and W.C. Lee (HTFS, Harwell, UK)	415
26. Condensation of Pure Fluids on Horizontal Finned Tube Bundles K.I. Ishihara and J.W. Palen (HTRI, Alhambra, California, USA)	429
27. An Assessment of Design Methods for Multi-component Condensation against Data from Experiments on a Horizontal Tube Bundle J.M. McNaught (National Engineering Laboratory, East Kilbride, Glasgow, UK)	447
28. A Method of Improving the Performance of an In-Tube Condenser J.A.R. Henry, I.D.R. Grant and C.D. Cotchin (National Engineering Laboratory, East Kilbride, Glasgow, UK)	459
29. The Prevention of Failure in High Integrity Condensers P.D. Hills, D. Henderson and R.R. Cowell (ICI, Norwich, Cheshire, UK)	469
30. Condensation Duties in Plate Heat Exchangers H. Kumar (APV Company, Sussex, UK)	478
Discussion Section	489

POWER CONDENSERS

Theory

CONDENSATION IN TUBE BANKS

Tetsu Fujii*

This report treats condensation phenomena in small, simple tube banks as a basic problem for research and development on turbine condensers. Current studies are described on the effect of air upon heat transfer, characteristics of pressure drops and mechanism of inundation, while referring to future problems. Then, variations in condensation characteristics in the directions of the steam flow and of the tube axis are predicted by a simple calculation, and a bank consisting of enhanced tubes is compared with that of smooth tubes regarding the number of rows, tube length, and depth of the bank.

INTRODUCTION

Technology for steam surface condensers was generally completed in the 1930's as seen in references (1) – (6). A synopsis of claims in patents before that time reveals that improvements on the condensers in terms of the layout of tubes had been made in accordance with the following objectives (Fujii and Uehara (7)): [1] to have steam distributed evenly and smoothly in all tubes (to prevent air pockets), [2] to reduce the thickness of liquid film on tubes (to prevent inundation), and [3] to prevent the sub-cooling of condensate (to increase thermo-cycle efficiency). These objectives are still valid today. However, condensers have been growing in capacity, rendering these objectives infeasible without concrete design schemes, more advanced basic studies on condensation, and mathematical techniques for integrating their results.

The author (8) has made suggestions as to the development of turbine condensers on the basis of his historical consideration and laboratory experience. The outline of his suggestions is as follows: [1] Design a shell or a special device so that water droplets in steam can be separated between the turbine exhaust and the condenser tube nest; [2] Cause steam to flow horizontally through in-line banks where the speed is high; [3] Provide individual tube nests for the high-speed steam, low-speed steam, and air-cooling zones, and connect them in series; and [4] Duly consider variations in characteristics in the tube axis direction. Furthermore, he has suggested that the flow field should be calculated independently for the tube nest zones and spaces between the tube nests and the shell, and that the boundary conditions in these calculations could be met on circumference of the tube nests. Most of the concepts in these suggestions have been adopted in design policy for the bell-type condenser developed by Toshiba Corporation, whose high performance are represented by Ozeki et al. (9).

Davidson and Rowe (10) and others discussed computer modeling at the workshop held in

*Research Institute of Industrial Science, Kyushu University, Japan

Monterey, California in 1980, proving that it was very effective in the diagnosis of defects in condensers in operation

Both in the pursuit of designs and in diagnosis of existing condensers, the reliability of mathematical estimation depends on the reliability of numerical values concerning characteristics of heat transfer and steam flow in tube banks. Although such values should be reduced from the measurements on actual condensers, the values obtained by simple tube banks on a laboratory scale are more reliable at present. This report, confined to the latter case, intends to recognize the latest progress on research activities, while pointing out problems awaiting solution

EFFECT OF AIR

Chisholm (11) reviewed the heat and mass transfer of steam-air mixture and its application to condenser designs and performance. In this review a classic method based on stagnant film models and their modifications was used. Rachko (12), Berman (13, 14, 15), Fuks and Zernova (16) and Buglaev et al (17, 18, 19) studied the relevant subject for tube banks, and presented empirical formulas obtained by using the classic method and dimensional analysis. The physical meaning of their formulas is not quite clear, because they contain an inundation term, which is related to thickness of the liquid film but will have scarcely a direct effect on mass transfer. The method used by Rose (20) of applying the boundary layer theory to the condensation of steam-air mixture on a single tube will be superior to the classic method. Here is presented a more simple method for tube banks based on the boundary layer theory

Theoretical Prediction of Mass Transfer

Average heat transfer coefficient for laminar forced convection to a single-phase flow along a flat plate is given by the equation

$$Nu_d^+ = 0.664 Re_d^{1/2} Pr^{1/3} \quad (1)$$

On the other hand, average heat transfer coefficients of a single-phase flow for tube banks with in-line, and staggered arrangements are derived from references (21) – (23) as

$$Nu_d^+ = 0.52 Re_d^{1/2} Pr^{1/3} \text{ (in-line)} \quad (2)$$

$$Nu_d^+ = 0.70 Re_d^{1/2} Pr^{1/3} \text{ (staggered)} \quad (3)$$

in the range $50 < Re_d < 100$. The ratios of equations (1) to (2) and equations (1) to (3) yield the following relations, respectively

$$L = 1.63D \text{ (in-line)} \quad (4)$$

$$L = 0.90D \text{ (staggered)} \quad (5)$$

These mean that equations (1) and (2), and equations (1) and (3) can be converted with equations (4) and (5) respectively.

The mass transfer coefficient obtained by a theoretical analysis of laminar forced convection condensation of a steam-air mixture on a flat plate is given by Fujii et al (24) as

$$Sh_q = 0.92f(\omega, Sc)Re_q^{\frac{1}{2}} \dots \dots \dots (6)$$

$$\text{where } f(\omega, Sc) = (1+\omega)^{-0.48} \omega^{-0.52} Sc^{0.32} \dots \dots \dots (7)$$

Since equation (6) is derived from the characteristics of the vapour phase boundary layer, it can be assumed that the same conversion as that with the single-phase flow is possible with respect to a representative length. Thus, by converting equation (6) with equations (4) and (5), mass transfer in tube banks can be predicted by the equations

$$Sh_d = 0.72f(\omega, Sc)Re_d^{\frac{1}{2}} \text{ (in-line)} \dots \dots \dots (8)$$

$$Sh_d = 0.97f(\omega, Sc)Re_d^{\frac{1}{2}} \text{ (staggered)} \dots \dots \dots (9)$$

The validity of this method has been proved by experimental results with single tubes by Fujii and Kato (25), and the thus obtained equation coincides numerically with Rose's equation. Also, an equation corresponding to body force convection condensation can be obtained by using a similar method. It reveals that the velocity of the main flow has such a strong effect on mass transfer, that presumably, equations (8) and (9) can be applied when $u_\infty^2 T_\infty / g_\eta D (T_\infty - T_i) \geq 10$.

Comparison Between Theory and Experiment

Figure 1 shows experimental results for heat transfer of steam containing air in a tube bank ($D = 14\text{mm}$, $L = 100\text{mm}$, $P_T/D = 22/14$, 15 rows 5 lines) by Fujii and Oda (26). The solid lines in the Figure denote average curves for data for pure steam obtained with the same equipment (Fujii and Oda (27)). The chain lines represent a theoretical solution by Fujii et al. (28) as

$$Nu = 0.69 \left(\frac{GaPr_L}{Ph} \right)^{\frac{1}{4}} \dots \dots \dots (10)$$

for body force convection condensation of pure steam on a single tube with uniform surface heat flux density. Where the solid lines lie below the chain lines, there exists an effect of inundation. Different runs are identified by such symbols as \circ , \square , \diamond , \triangle , and ∇ . Various patterns appearing in each symbol such as \circ , Φ , ... \bullet represent ranges of the mass concentration of air $x_{g\infty}$ as shown in the Figure. The left and right ends of data for the same run correspond to the inlet and outlet of the tube bank. The data corresponding to a few tube rows from the inlet coincide with those for pure steam. In addition, the effects of Pr_L / Fr_{Ph} and $x_{g\infty}$ on $Nu / \sqrt{Re_L}$ display similar trends with those for a single tube.

Figure 2 shows Sh obtained from the data given in Fig. 1. In calculating the values of Sh , temperature T_i at the vapour-liquid interface was obtained by substituting the measured values of \dot{q} and T_w and the calculated value α , which is obtained by substituting $T_i = T_g$ into empirical formulas that represent solid lines drawn in Figure 1, into $\dot{q} = \alpha(T_i - T_w)$. In other words, T_i corresponding to x_{gi} was obtained on the assumption that characteristics of the liquid film are not affected by the mixed air.

Thick solid lines in the Figure represent average lines for data drawn in parallel with thin lines corresponding to equations (8) and (9). Data shows dispersion to an extent of about $\pm(20 \sim 30)\%$ of the average lines. This depends on the accuracy of equations for pure steam as well as on the accuracy of the actual data in Fig. 1. Experimental values are about $30 \sim 50\%$ higher than the theoretical estimations for horizontal flow, about 40% for vertical down flow, and about 25% for vertical

up flow. These differences may be considered to be caused by turbulence in the main flow. In addition, note that $x_{g\infty}$ to be used in the calculation of data was calculated as a value averaged over the widest cross section.

When the condensation rate ratio of the experimental value to the theoretically estimated value corresponding to the experimental conditions T_{∞} , u_{∞} , $x_{g\infty}$, and T_w was calculated, it averaged about 1.2 for the horizontal flow and downflow, and about 1.1 for the upflow.

Method of Application

Within a limited operational range of turbine condensers, an equation for calculating Nu without repeated calculation can be obtained. An example is shown for downflow through an in-line bank. Heat transfer by pure steam is given by the equation which represents the corresponding solid line in Fig. 1.

$$Nu_s = 0.77 \left(\frac{Pr_L}{FrPh} \right)^{0.15} Re_L^{0.5} \dots \dots \dots (11)$$

Sh is given by the following equation in reference to Fig. 2

$$Sh = 1.4 \times 0.72 f(\omega, Sc) Re^{0.5} \dots \dots \dots (12)$$

Repeated calculation with a combination of equations (11) and (12) gives numerical values of Nu for given conditions of steam and cooling tube. Such kind of data can be approximated within an accuracy of a few per cent by the equation—

$$\frac{Nu}{Nu_s} = A \exp(-mx_{g\infty}) + B \exp(-nx_{g\infty}) \dots \dots \dots (13)$$

where $A = 0.83(T_{\infty} - T_w)^{-0.15} + 0.19 nu_{\infty}$, $B = 0.21(T_{\infty} - T_w)^{0.25} - 0.092 nu_{\infty}$, $m = 3.7 u_{\infty}^{-0.12}$ and $n = 19(T_{\infty} - T_w)^{0.2} u_{\infty}^{-0.3}$; applicable ranges are $0 < x_{g\infty} < 0.3$, $2 < u_{\infty} < 20$ m/s, $0 < T_{\infty} - T_w < 15K$, $20 < T_{\infty} < 40^\circ C$ and $D = 14$ mm.

The problem that remains to be solved in this section may be to discover experimentally the effect of the tube arrangement on equations (8) and (9). It will be related to the turbulent diffusion of air in theory.

PRESSURE DROP

Since it is still difficult to strictly mathematically solve turbulent flow with suction in a tube bank, only empirical knowledge is available.

Drag coefficient ξ is defined by the equation—

$$\xi = \frac{\bar{p}}{2n\dot{m}_{\max}^2} \left\{ (p_i - p_j) + \left(\frac{\dot{m}^2}{\rho} \right)_i - \left(\frac{\dot{m}^2}{\rho} \right)_j \right\} \dots \dots \dots (14)$$

Note here that equation (14) was derived, within a control volume surrounded by i-th and j-th widest cross sections and side walls, from the momentum law on the assumptions that [1] on cross sections i and j, pressure is uniform (variations in pressure in the cross sections are very small compared with $p_i - p_j$); [2] on cross sections i and j, the patterns of steam velocity distribution are identical (this does not hold true with the first and the last tube rows); [3] force of the side walls on the fluid is negligible in comparison with force of the tubes on the fluid; [4] momentum change of the condensate is

negligible in comparison with that of steam.

Experimental Results for Drag Coefficient ξ

Figure 3 shows experimental results for local value of ξ obtained by Fujii and Oda (29). The data have a large dispersion as shown in the Figure (the accuracy of measurement is estimated to be about $\pm 20\%$ with higher Re , and about $\pm 40\%$ with lower Re). However, it is clear that the value for the first row is high, and that there is a characteristic difference between the in-line and staggered banks in comparison with ξ_D for dry tubes in the core part. It seems certain that data on upflow, which is not shown in the Figure because of its low reliability, will be higher than ξ_D in the Figure. This may be due to the effect of inundation.

Table 1 lists measured values of ξ_D for the first row and the exit of tube banks without condensation in relation to those for the core part. The fact that the values of ξ_D for the first row differ among researchers may be due to accuracy of the measurement.

TABLE 1 - Drag Coefficients at the 1st and last Rows against Those in the Core Part for dry Tube Banks.

Authors	Fluid	Tube Arrangement	D (mm)	P_T/D	1st Row	Core Part	Last Row
Fujii et al. (31, 32)	air	in-line	15.6	1.6	3.5	1	-1.7
		staggered	15.6	1.6	2.0	1	-0.8
Fujii et al. (29)	steam	in-line	14.0	1.57	3	1	—
Nicol et al. (33)	steam	in-line	9.525	1.736	2.2	1	—

Table 2 lists relative values of ξ to ξ_D obtained by Fujii and Oda (29), Nicol et al. (33), Lee et al. (34) and Lee (35). The values for the former two obtained with condensation of steam are qualitatively identical. Particularly, the prominent decrease of ξ for the in-line banks is quite characteristic. Also, the ratio of ξ for the first row to that for core part becomes lower as a result of condensation (cf. Table 1). The test by Lee et al. consists of a simulation of condensation with the suction of air through seven rows of porous tubes. The results agree qualitatively with the above two

TABLE 2 - Drag Coefficients in Condensation of Steam and Suction of Air against Those without Condensation and Suction.

Authors	Tube Arrangement	D (mm)	P_T/D (trans./longi.)	1st Row	Core Part	
					Horizontal	Downflow
Fujii et al. (29) (condensation at $Re = 10^4$)	in-line	14.0	1.57/1.57	$2.3\xi_D$	$0.4\xi_D$	$0.35\xi_D$
	staggered	14.0	1.57/1.57	$1.8\xi_D$	ξ_D	$0.85\xi_D$
Nicol et al. (33) (condensation at $Re = 10^4$)	in-line	9.525	1.736/1.736	$1.4\xi_D$	$0.27\xi_D$	—
	staggered	9.525	1.58/1.80	—	$0.75\xi_D$	—
Lee (35) (suction at $Re = 2.5 \times 10^4$)	in-line	19.0	1.25/1.25	—	ξ_D or more	
	staggered	19.0	1.25/1.083	—	$0.9\xi_D$	
	staggered	19.0	1.25/0.935	—	$(0.85-0.9)\xi_D$	

cases for the staggered bank, while ξ for the in-line bank is increased by suction (this characteristic is independent of the representative value of \dot{m}_{\max} in equation (14).)

The foregoing results raise the problem as to whether or not condensation can be simulated by suction. There is a possibility that the change of shape of liquid-vapour interface promoted a drastic decrease of the value of ξ for the in-line bank. This doubt will be resolved by an experiment with the same tube arrangement, the same Reynolds number, and the same suction rate as those of the condensation case.

Comparison with Recommended Values for Pressure Drop

Figure 4 shows experimental results obtained by Fujii and Oda (29) for pressure distribution in small tube banks, whose dimensions are shown in Table 2. These data are compared with predicted values. The prediction is made by substituting recommended values of Δp_f into the equation

$$p_{j+1} = p_j - \left[\Delta p_f - \left\{ \left(\frac{\dot{m}}{\rho} \right)_j - \left(\frac{\dot{m}}{\rho} \right)_{j+1} \right\} \right] \quad (15)$$

The values expressed by solid lines in the Figure were obtained by substituting the values of ξ in the 1st and second lines in Table 2 into $\Delta p_f = 2\xi \dot{m}_{\max}^2 / \rho$. The slight difference between the measured and the predicted values is attributed to the fact that the values of ξ in the Table have been roughly determined. The values expressed by symbols + and x were obtained by using the values of Δp_f which were derived from experiments with adiabatic two-phase flow of air and water by Diehl and Unruh (36) and Ishihara et al. (37) respectively. In every calculation the values of \dot{m}_j were obtained from calculated values of heat exchange for individual runs.

While the recommended values by Ishihara et al. offer a fairly good approximation for the staggered bank, they cannot be applied to the in-line bank. Note here that the experimental data for runs SA and SB were obtained with pressure at the exit of the tube bank greatly lowered. Calculations with an increasing number of tube rows show that the temperature of steam approaches that of cooling water before the completion of condensation. In other words, pressure drop per row as large as those will not occur under actual conditions.

The equation of total pressure drops for tube banks with n rows presented by Rowe et al. (38) can be transformed as

$$p_0 - p_n = 0.0667 \left\{ \frac{\dot{m}_0 p_T}{(p_T - D)} \right\}^2 \frac{n}{\rho} \quad (16)$$

The values obtained by this equation compare fairly well with pressure drops for the staggered bank, which are obtained by extending such curves as shown in Fig. 4 (except for Runs SA and SB) to the complete condensation, but predict nearly one-half the values of those for the in-line bank.

In short, existing knowledge makes it possible to estimate pressure drops in the staggered bank fairly accurately. On the other hand, experimental data is insufficient to estimate pressure drops in the in-line bank. Considering that the latter tube arrangement is very effective in its application to actual condensers, there is a great demand for detailed measurement of the effect of pitch to diameter ratio upon the ξ value. Moreover, there are a few problems to be studied, such as tube arrangements in a central flow-type condenser and with various kinds of by-pass lanes.

INUNDATIONModification of Nusselt's Solution

The basic assumption in Nusselt's (39) inundation theory on a vertical row of horizontal tubes laid in stagnant vapour is that all droplets of condensate from the n -th tube from the top tube are caught by the $(n+1)$ th tube and spread uniformly over the top of the latter tube. Therefore, calculation was made with the physical model by assuming that the condensate continuously falls, forming a sheet between n -th and $(n+1)$ th tubes. The disagreement of this model with real phenomena was described in detail by Young and Wohlenberg (40), and has been reconfirmed by a number of observant researchers. While selecting only the extent of the droplet spread over the tube surface out of the complicated behavior of the liquid film, Fujii and Oda (41) proposed the two simple models shown in Fig. 5.

[Model I] If the heat transfer rate per unit tube length of the first tube is represented by \dot{Q}_1 , then the flow rate of falling condensate is given by $\dot{M}^+ = \dot{Q}_1 / \Delta h_v$. When the condensate reaches to the 2nd tube, $\dot{M}_1 = \xi \dot{M}^+$ spreads axially, $(1-\xi)\dot{M}_1^+$ flows to the tube bottom without affecting thickness of the liquid film. These join with the condensate $\dot{Q}_2 / \Delta h_v$ generated on the 2nd tube, amounting to $\dot{M}_2^+ = (\dot{Q}_1 + \dot{Q}_2) / \Delta h_v$ and falls down to the 3rd tube. Of this amount, $\dot{M}_2 = \xi \dot{M}_2^+$ spreads axially, $(1-\xi)\dot{M}_2^+$ without affecting the liquid film thickness. Further, it proceeds likewise.

Upon determination of an integral constant for the solution of Nusselt's equation on the basis of this model, $(Nu_n)_I$ for the n -th tube is given by the equation

$$(Nu_n)_I = \left(\xi \sum_{i=1}^{n-1} Nu_i \frac{Ph_i}{Ph_n} \right) \left[1 + \frac{\left(\frac{Ph_1}{Ph_n} \right)^{\frac{1}{3}} Nu_1^{\frac{4}{3}}}{\left(\xi \sum_{i=1}^{n-1} Nu_i \frac{Ph_i}{Ph_n} \right)^{\frac{4}{3}}} \right]^{\frac{3}{4}} - 1 \dots \dots \dots (17)$$

[Model II] On the assumption that the fraction $(1-\xi)$ of condensate falling from any tube passes over the tube bank without affecting film thickness on the subsequent tubes, $(Nu_n)_{II}$ is given, similarly to Model I, by the equation

$$(Nu_n)_{II} = \sum_{i=1}^{n-1} \xi^{n-i} Nu_i \frac{Ph_i}{Ph_n} \left[1 + \frac{\left(\frac{Ph_1}{Ph_n} \right)^{\frac{1}{3}} Nu_1^{\frac{4}{3}}}{\left(\sum_{i=1}^{n-1} \xi^{n-i} Nu_i \frac{Ph_i}{Ph_n} \right)^{\frac{4}{3}}} \right]^{\frac{3}{4}} - 1 \dots \dots \dots (18)$$

Values of $(Nu_n)_I$ and $(Nu_n)_{II}$ in equations (17) and (18) can be successively calculated from

$$(Nu_1)_I = (Nu_1)_{II} = 0.725 \left(\frac{Ga Pr_L}{Ph_1} \right)^{\frac{1}{4}} \dots \dots \dots (19)$$

, and both agree with Nusselt's solution when $Ph_n = Ph_1$ and $\xi = 1$.

Figures 6 (a) and (b) show calculations with $Ph_n = Ph_1$ in equations (17) and (18) respectively, and Figures 6 (c) and (d) show average Nusselt numbers $(\bar{Nu}_n)_I$ and $(\bar{Nu}_n)_{II}$ obtained from these

equations for the 1st through the n-th tube respectively. As the values of ξ decrease, Nusselt numbers become higher than Nusselt's solution ($\xi = 1$). Model II reveals this effect more prominently with the increase of n , showing a different trend from the Nusselt's solution.

Comparison Between Theory and Experiment

Figures 7 and 8 show existing experimental data (Young and Wohlenberg (40), Katz and Geist (42), Short and Brown (43), Katz et al. (44), Young and Briggs (45) and Smirnov and Lukanov (46)) and recommended equations (Kern (47) and Kutateladze (48)) for $Nu_n/(Nu_1)_{th}$ and $\bar{Nu}_n/(Nu_1)_{th}$ respectively. In Fig. 7 average values from experiments with R-12 by Young and Wohlenberg fairly agree with the values of Model I using $\xi = 0.3$. In Fig. 8, the equation recommended by Kern

$$\bar{Nu}_n = \alpha_1 n^{-\frac{1}{6}} \dots\dots\dots (20)$$

nearly agrees with Model I using $\xi = 0.4$. Butterworth (49) has pointed out that equation (20) nearly agrees with the test results by Grand and Osmet (50), represented by the equation

$$\frac{Nu}{(Nu_1)_{th}} = \left(\frac{\Sigma \dot{m}_n}{\dot{m}_n}\right)^{-0.332} \dots\dots\dots (21)$$

As a matter of course, nearly the same relationship as equation (21) can be derived from the solution of Model I using $\xi = 0.4$. In Figs. 7 and 8, no similar data characteristic of Model II can be found.

Figure 9 compares experimental results for R-12 by Gogonin et al. (51) with $(\bar{Nu}_n)_{II}/(Nu_1)_{th}$ in Model II. Symbols \circ , \square , \diamond , and ∇ in the Figure denote data under conditions $\theta_s = 40^\circ\text{C}$, $\theta_s - \theta_w = 3 - 6^\circ\text{C}$ and $\dot{q}_w = 6 - 13 \text{ kW/m}^2$, \bullet , \blacksquare , \blacklozenge , and \blacktriangledown under conditions $\theta_s = 40^\circ\text{C}$, $\theta_s - \theta_w = 8 - 21^\circ\text{C}$, and $\dot{q}_w = 12 - 32 \text{ kW/m}^2$ and $+$, \times , γ , τ , and \vee under conditions $\theta_s = 90^\circ\text{C}$, $\theta_s - \theta_w = 21 - 56^\circ\text{C}$, and $\dot{q}_w = 31 - 76 \text{ kW/m}^2$. Let us designate these three groups as A, B, and C. The data in groups A and B and most of the data in group C nearly agree with theoretical solutions using $\xi = 0.6$ and 0.1 in the 3rd through the 10th row.

As shown in Figs. 7 to 9, existing experimental results disagree so widely with each other that it is difficult to proceed with further comparison with theory. Either pattern of condensation—Model I or Model II—can occur. In the future, it will be possible to discover unknown factors to be introduced by closely observing phenomena in highly accurate experiments that can vary such factors as heat flux density, surface tension, and geometrical patterns of tube rows.

Trends of Studies on Inundation

Inundation without vapour shear can only be applied to a part of a large-capacity condenser and to a small-capacity condenser, because the effect of steam velocity is added in large-capacity condensers. However, most of the experimental results are represented in the same form as equation (20) without this distinction, as—

$$\alpha_n = \alpha_1 n^{-\gamma} \quad \text{or} \quad \bar{\alpha}_n = \alpha_1 n^{-\gamma'} \dots\dots\dots (22), (23)$$

where the values of the indices, which are related to the level of steam velocity and the inundation rate, are in the ranges of $\gamma = 0 - 0.15$ and $\gamma' = 0 - 0.25$. Some of the experimental results on inundation are plotted in terms of $\alpha_n(v^2/g_n)^{1/3}/\lambda$ versus $\pi D \Sigma \dot{q}_i/(\rho v \Delta h_v)$. However, the accuracy of the correlation is of the same order as that in equation (22) or (23).

Judging that inundation in shear-controlled condensation differs in nature from that in gravity-controlled condensation, McNaught (52) has adopted an equation of two-phase forced convection heat transfer for the former and equation (21) for the latter, to prove that an equation as a combination of these can correlate Nobbs' (53) data within an accuracy of $\pm 25\%$. This may be a new concept. However, the author's experience tells that the accuracy of estimation by two-phase forced convection is not high even with condensation heat transfer in tubes. The accuracy of estimates for pressure drops, to which the empirical formula for heat transfer is closely related, is very low.

In general, experimental results in respect to inundation vary widely among researchers. This suggests that unknown conditions exist which can diminish the effect of inundation. One of these may be that which confines the flow of condensate to a part of the tube bank. If this can be realized with a certain reproducibility, a correct theoretical prediction can be realized by developing the ideas shown in this section.

NUMERICAL PREDICTION OF CONDENSATION CHARACTERISTICS IN TUBE BANKS

Characteristics concerning condensation on a plane containing a steam flow and tube axes directions are predicted by a numerical calculation on several assumptions. A model of such a plane in a tube bank is shown in Fig. 10, where the tubes are numbered 1, 2, ... n successively from the steam inlet, the steam flow is tentatively divided by unit length ΔL ($= 1\text{ m}$), and the divided sections are numbered I, II, ... N successively from the cooling water inlet. The assumptions used are as follows: [1] steam flows perpendicularly to tubes; [2] pressure, temperature, and air concentration of steam are uniform at the inlet; [3] pressure of steam is uniform at the outlet; [4] steam is saturated throughout; and [5] the effect of inundation is neglected.

An equation for a single tube by Fujii (54) as condensation heat transfer of pure steam, equation (12) as effect of air, equation (15) and Fujii's data shown in Table 2 as pressure drop, and the equation of Dittus and Boelter (55) as convective heat transfer inside tubes are simultaneously solved step by step for every tube from the inlet of steam. The number of tube rows n is determined so that the steam $\theta_o = 33^\circ\text{C}$ and $x_{go} = 3 \times 10^{-5}$ at the inlet of section I can be $p_{1n} = 3.89 \times 10^3\text{ Pa}$ and $u_{1n} \approx 1\text{ m/s}$ at the outlet. At the same time u_{1o} is also determined. With the fixed n, identical calculations for section II, III, ... are continued until the average temperature rise of cooling water reaches about 8°C .

The result of an in-line bank of titanium tubes, where tube diameter $D = 31.75\text{ mm}$, tube thickness 0.5 mm , lateral and longitudinal pitches between tubes $P_T = 1.4D$, cooling water temperature at the inlet $\theta_{co} = 20^\circ\text{C}$, and cooling water velocity $u_c = 2.4\text{ m/s}$, is shown in Fig. 11 for (a) steam velocity u_{∞} , (b) steam pressure p, (c) cooling water temperature θ_c , and (d) heat flux density q_w and overall heat transfer coefficient α_{ov} in distributions in the direction of cooling water with a parameter of tube rows, where α_{ov} is defined based on heat flux density averaged over the tube surface area and the logarithmic temperature difference between θ_{so} , θ_{co} and $\bar{\theta}_{CN}$, and where the value averaged from the cooling water inlet to a tube length is plotted at the corresponding abscissa. This result possesses some irrational features; that is, steam velocity at the outlet varies markedly in the direction of cooling water as shown in Fig. (a), and pressure in the tube bank is not uniform in the direction of cooling water as shown in Fig. (b). The former depends on assumption [3] and the latter implies that assumption [1] is unsatisfactory. However, assuming that the distribution of cooling water temperature and heat flux density as shown in Figs. (c) and (d) differ only slightly from those in actual condensers, further discussion is made.

When identical calculation was effected for a tube bank composed of enhanced tubes where

heat transfer coefficients of both the shell and the tube sides were given as three times those of smooth tubes, a result with almost the same tendency as that shown in Fig. 11 was obtained. Values of n , L , $(\sum \dot{Q})/P_T \Delta h_v$ (condensation rate per unit depth of the tube bank), and α_{ov} from the result are shown in Table 3 together with those of smooth tubes.

Table 3 reveals that the condenser with enhanced tubes is about one-half in n and L , and therefore about one-fourth in cooling surface in comparison with those having smooth tubes. However, $(\sum \dot{Q})/P_T \Delta h_v$ is also about one-half. This means that twice the depth is necessary for condensing the same amount of steam. In other words, the adoption of enhanced tubes not only renders the condenser compact, but also changes the shape of the tube bank. Incidentally, n becomes larger, keeping L almost the same, with the increase of P_T/D , while the increased condensation rate per unit depth is not large enough to change the shape of the tube bank.

TABLE 3 - Comparison between Banks with smooth and enhanced Tubes on Number of Rows n , Tube Length L , Condensation Rate per Unit Depth $(\sum \dot{Q})/P_T \Delta h_v$, and overall Heat Transfer Coefficient α_{ov} - Sample Calculation -

Tube	Cooling Water Temperature Rise (K)	n	$L = N$ (m)	$(\sum \dot{Q})/P_T \Delta h_v$ 10^6 (W/m)	α_{ov} 10^3 (W/m ²)
smooth	4.17	40	9	2.78	3.21
enhanced	4.4	21	4	1.53	7.61
smooth	8.0	40	24	5.35	2.96
enhanced	7.9	21	10	2.77	6.96

CONCLUSION

This report has reviewed current studies on small tube banks, while pointing out their future trends. For the effect of air on heat transfer and the characteristics of pressure drops, it is necessary to find empirically their variations with tube arrangements. For the latter, data for the in-line bank, in particular, is inadequate. There is little reliable data on inundation. The method of simulating general characteristics in actual tube banks should be checked with actual condensers, particularly with respect to steam conditions at the inlet and outlet of tube banks. In addition, the study of wet steam containing water droplets, which is not discussed in this report and which has been studied only by Nicol (56), is one of the problems that remain to be studied.

SYMBOLS USED

c_p = specific heat capacity (J/kgK)

D = diameter (m)

$Fr = \frac{u_\infty^2}{g_n D}$ = Froude number (-)

$f(\omega, Sc)$ = function of ω and Sc , equation (7) (-)

$Ga = \frac{g_n D^3}{\nu_L^2}$ = Galileo number (-)

g_n = acceleration of gravity (m/s²)

Δh_v = specific latent heat of condensation (J/kg)

L = plate length, or tube length (m)

\dot{M} = mass flow rate per unit tube length (kg/ms)

\dot{M}^+ = mass flow rate falling from upper tube per unit tube length (kg/ms)

\dot{m} = mass velocity of steam at widest section, or mass flux density in condensation (kg/m²s)

\dot{m}_{\max} = mass velocity of steam at narrowest section (kg/m²s)

$Nu = \frac{\alpha D}{\lambda_L}$ = Nusselt number for condensation heat transfer (—)

$Nu_d^+ = \frac{\alpha D}{\lambda} =$ Nusselt number for single-phase heat transfer (—)

$Nu_L^+ = \frac{\alpha L}{\lambda} =$ Nusselt number for single-phase heat transfer (—)

n = total number of tubes in a control volume, or total number of tube rows, or n -th row from the inlet or from the top (—)

$Ph = \frac{c_{pL}(T_i - T_w)}{\Delta h_v} = \frac{c_{pL}(T_s - T_w)}{\Delta h_v} =$ phase change number (—)

Pr = Prandtl number (—)

P_T = pitch between tubes (m)

p = pressure (N/m²)

Δp_f = pressure drop without momentum change (N/m²)

\dot{Q} = heat flow rate per unit tube length (W/m)

\dot{q} = heat flux density (W/m²)

$Re_d = Re = \frac{u_{\infty} D}{\nu} =$ Reynolds number (—)

$Re_L = \frac{u_{\infty} L}{\nu} =$ Reynolds number (—)

$Re_L = \frac{u_{\infty} D}{\nu_L} =$ Two-phase Reynolds number (—)

Sc = Schmidt number (—)

$Sh_f = \frac{\delta L}{\delta} =$ Sherwood number (—)

$Sh_d = Sh = \frac{\delta D}{\delta} =$ Sherwood number (—)

T = temperature (K)

u = velocity (m/s)

x_g = mass fraction of air (kg/kg)

1, II, . . . N = number of steam flow sections in Figure 10 (—)

1, 2, . . . n = number of tube rows (—)

α = heat transfer coefficient ($W/m^2 K$)

α_{ov} = overall heat transfer coefficient ($W/m^2 K$)

β = mass transfer coefficient (m/s)

δ = diffusivity (m^2/s)

ζ = fraction of condensate spreading over tube surface (—)

$\theta = T - 273.2$ = Celsius temperature ($^{\circ}C$)

λ = thermal conductivity (W/mK)

ν = kinematic viscosity (m^2/s)

ξ = drag coefficient (—)

ξ_D = drag coefficient for dry tube (—)

ρ = mass density (kg/m^3)

$\omega = \frac{x_{g\infty}}{x_{gi}}$ (—)

Superscript

— = averaged

Subscripts

c = cooling water

i = interface between vapour and condensate film

i, j = i-th and j-th widest section from the inlet of a tube bank

L = physical properties of liquid

o = inlet of tube bank, or inlet of cooling water

s = pure steam

th = theoretical or calculated

w = tube wall

I, II = Model I and Model II

I, II, . . . N = number of steam flow sections in Figure 10

1, 2, . . . n = number of tube rows

∞ = main stream

REFERENCES

1. Hoefer, K., 1925, "Die Kondensation bei Dampfkraftmaschinen", Julius Springer, Berlin, Germany.
2. Sim, J., 1925, "Steam Condensing Plant in Theory and Practice", Blackie & Son, London, England.
3. Wright, A.R., 1928, "Modern Practice in Steam Condensing Plants", Crosby Lockwood & Son, London, England.
4. Six Leading Condenser Manufacturers Approve, 1932, "Commercial Factors for Designing Surface Condensers", Power 76, 133.
5. Guy, H.L., and Winstanley, E.V., 1934, Engineering 137, 159, 204 and 275.
6. Pendred, B.W., 1935, "The Surface Condenser", Sir Isaac Pitman & Sons, London, England.
7. Fujii, T., and Uehara, H., 1974, "Development of Steam Condenser and Heat Transfer" (In Japanese), Studies of Machinery 26, 455.
8. Fujii, T., 1975, "A Proposal of Research and Development for Turbine Condensers" (In Japanese), J.Japan Soc.Mech.Engrs. 78, 529.
9. Ozeki, T., Miura, Y., and Miyoshi, M., 1983, "A Design Method of Condenser Tube Arrangement for Large Power Stations", submitted to this Symposium.
10. Davidson, B.J., and Rowe, M., 1981, "Simulation of Power Plant Condenser Performance by Computational Methods: An Overview" in "Power Condenser Heat Transfer Technology", ed. Marto, P.J., and Nunn, R.H., Hemisphere, Washington, USA.
11. Chisholm, D., 1981, "Non-Condensable Gases: An Overview" in "Power Condenser Heat Transfer Technology", ed. Marto, P.T., and Nunn, R.H., Hemisphere, Washington, USA.
12. Rachko, V.A., 1957, Soviet Physics—Technical Physics 1, 564, and 579.
13. Berman, L.D., and Fuks, S.N., 1958, Teploenergetika 5, 66.
14. Berman, L.D., 1964, Teploenergetika 11, 74.

15. Berman, L.D., 1969, Teploenergetika 16, 68.
16. Fuks, S.N., and Zernova, E.P., 1970, Teploenergetika 17, 59.
17. Buglaev, V.T., Andreev, M.M., and Kleshchevnikov, V.P., 1971, Teploenergetika 18, 14.
18. Buglaev, V.T., Andreev, M.M., Nikolaev, G.V., and Pakhomov, V.A., 1971, Teploenergetika 18, 87.
19. Buglaev, V.T., and Kazakov, V.S., 1975, Heat Transfer—Soviet Research 7, 135.
20. Rose, J.W., 1980, Int.J.Heat Mass Transfer 23, 539.
21. Kays, M.W., London, A.L., and Lo, R.K., 1954, Trans.Am.Soc.Mech.Engrs. 76, 387.
22. Bergelin, O.P., Brown, G.A., Hull, H.L., and Sullivan, F.W., 1956, Trans.Am.Soc.Mech.Engrs. 72, 881.
23. E.S.D.U., 1973, Data item number 73031, Engineering Science Data Unit, London, England.
24. Fujii, T., Uehara, H., Mihara, K., and Kato, Y., 1977, "Forced Convection Condensation in the Presence of Noncondensables" (In Japanese), Report of Research Institute of Industrial Science, Kyushu University, 66, 53.
25. Fujii, T., and Kato, Y., 1980, "Condensation of Steam Containing Air—An Analogy Between Flat and Cylindrical Surfaces—" (In Japanese), Proc.17th Japan Heat Transfer Symposium, 433.
26. Fujii, T., and Oda, K., 1982, "Effect of Air on Condensation of Steam Flowing Through Tube Banks" (In Japanese), Proc.19th Japan Heat Transfer Symposium, 373
27. Fujii, T., and Oda, K., 1982, Trans.Japan Soc.Mech.Engrs., 48, 1580, (In Japanese).
28. Fujii, T., Uehara, H., and Oda, K., 1972, Heat Transfer—Japanese Research 1, 76.
29. Fujii, T., and Oda, K., 1983, Trans.Japan Soc.Mech.Engrs. 49, (In Japanese).
30. Zukauskas, A., 1972, "Heat Transfer from Tubes in Crossflow" in "Advanced Heat Transfer, vol.8", ed. Irvine, T.F., and Hartnett, J.P., Academic Press, New York, USA.
31. Fujii T., Nagata, T., and Shinzato, K., 1977, Refrigeration 52, 1059, (In Japanese).
32. Fujii, T., Nagata, T., and Shinzato, K., 1982, Refrigeration 57, 78, (In Japanese).
33. Nicol, A.A., Aidoun, Z., and Mussa, M.N., 1982, "Condensation and Pressure Drop for Crossflow of Steam in Small Tube Bundles", Proc.7th Int.Heat Transfer Conf. 5, 133.
34. Lee, N.K., Hollingsworth, M.A., and Mayhew, Y.R., 1982, "Simulation of Condenser Pressure Losses by Porous Tubes with Suction", Proc.7th Int.Heat Transfer Conf. 5, 107.

35. Lee, N.K., 1981, "Simulation of Condenser Pressure Losses by Porous Tubes with Suction", PhD Thesis, University of Bristol, England.
36. Diehl, J.E., and Unruh, C.H., 1958, Petroleum Refiner 37, 124.
37. Ishihara, K., Palen, J.W., and Taborek, J., 1980, heat transfer engineering 1, 23.
38. Rowe, M., Davidson, B.J., Andrews, E.F.C., Ferrison, J.A., and Taylor, B.J., 1979, "Heat Transfer and Air Blanketing in Steam Condensers", Proc. of the Conf. on Steam Turbines for the 1980s, Inst.Mech.Engrs., 153.
39. Nusselt, W., 1916, Z.Ver.D.Ing. 60, 569.
40. Young, F.L., and Wohlenberg, W.J., 1942, Trans.Am.Soc.Mech.Engrs. 64, 787.
41. Fujii, T., and Oda, K., 1981, "On the Inundation in Condensation of Quiescent Vapour" (In Japanese), Proc.19th Japan Heat Transfer Symposium, 343.
42. Katz, D.L., and Geist, J.M., 1948, Trans.Am.Soc.Mech.Engrs. 70, 907.
43. Short, B.E., and Brown, H.E., 1951, "Condensation of Vapors on Vertical Banks of Horizontal Tubes", Proc.General Discussion on Heat Transfer, Sec. I, ASME-IME, London, 27.
44. Katz, D.L., Young, E.H., and Balekjian, G., 1954, Petroleum Refiner 33, 175.
45. Young, E.H., and Briggs, D.E., 1966, J.Am.Inst.Chem.Engrs. 12, 31.
46. Smirnov, G.E., and Lukanov, I.I., 1972, Heat Transfer—Soviet Research 4, 51.
47. Kern, Q.K., 1958, J.Am.Inst.Chem.Engrs. 4, 157.
48. Kutateladze, S.S., 1963, "Fundamentals of Heat Transfer", Edward Arnold, London, England.
49. Butterworth, D., 1981, "Inundation without Vapour Shear" in "Power Condenser and Heat Transfer Technology", ed. Marto, P.J., and Nunn, R.H., Hemisphere, Washington, USA.
50. Grant, L.D.R., and Osmet, B.D.J., 1968, "The Effect of Condensate Drainage on Condenser Performance", NEL Report No.350.
51. Gogonin, I.I., Dorokhov, A.R., and Sosunov, V.I., 1977, Teploenergetika 24, 33.
52. McNaught, J.M., 1982, "Two-Phase Forced Convection Heat Transfer During Condensation on Horizontal Tube Bundles", Proc.7th Int.Heat Transfer Conf. 5, 125.
53. Nobbs, D.W., 1975, "The Effect of Downward Vapour Velocity and Inundation on the Condensation Rate on Horizontal Tubes and Tube Banks" PhD Thesis, University of Bristol, England.

54. Fujii, T., 1981, "Vapor Shear and Condensate Inundation: An Overview" in "Power Condenser Heat Transfer Technology", ed. Marto, P.T., and Nunn, R.H., Hemisphere, Washington, USA.
55. Dittus, F.W., and Boelter, L.M.K., 1930, "Heat Transfer in Automobile Radiators of the Tubular Type", Univ.Calif.Publs.Engng. 2, 443.
56. Nicol, A.A., and Dempsey, M.J., 1982, Int.J.Multiphase Flow 8, 207.

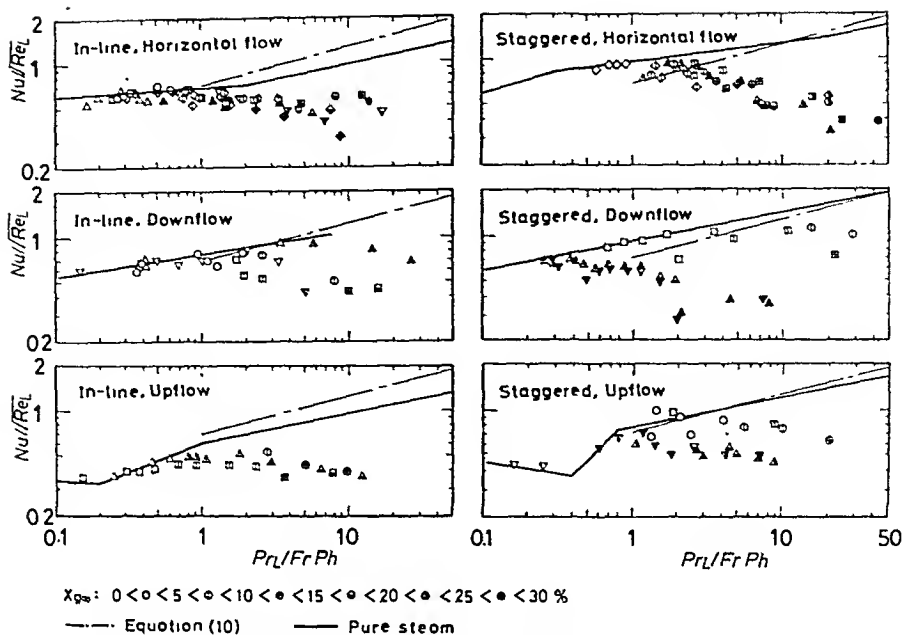


Figure 1 Local heat transfer of steam-air mixture in tube banks

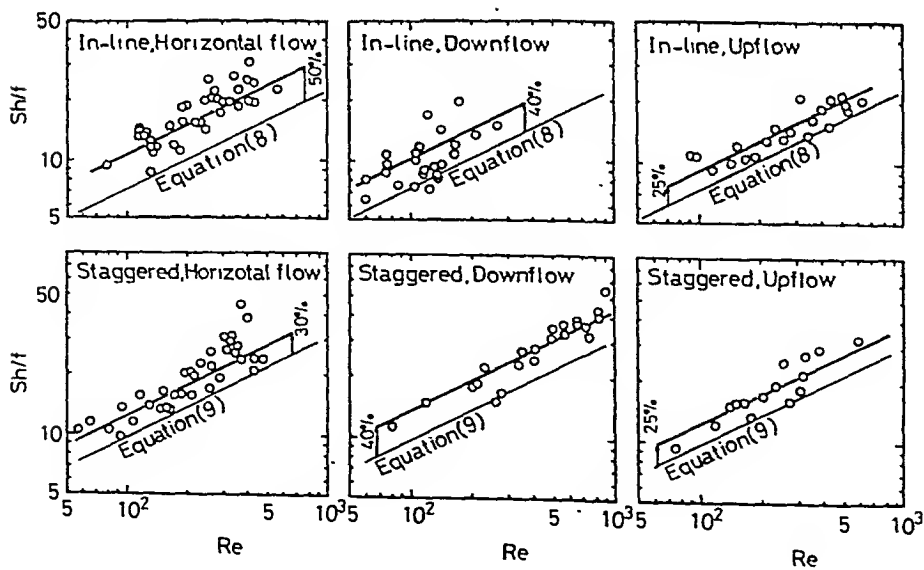


Figure 2 Comparison between theory and experiment for mass transfer in tube banks

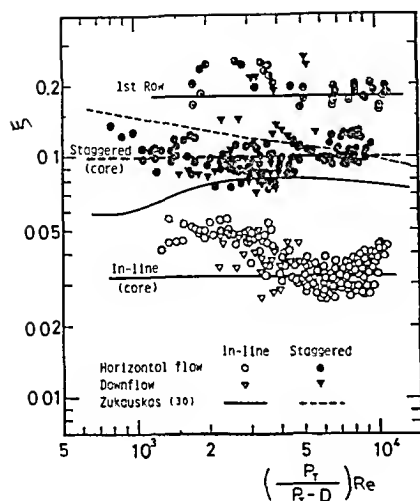


Figure 3 Local drag coefficient

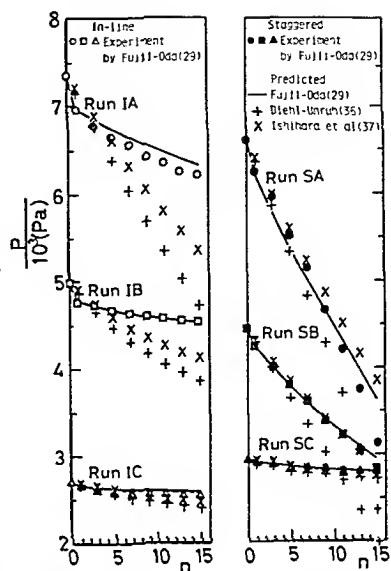


Figure 4 Pressure distributions in tube banks

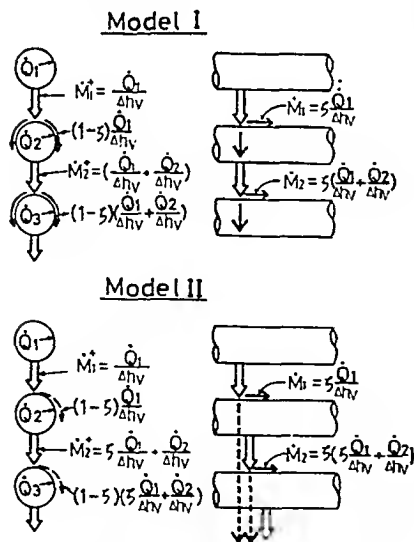


Figure 5 Physical model for innundation without vapour shear

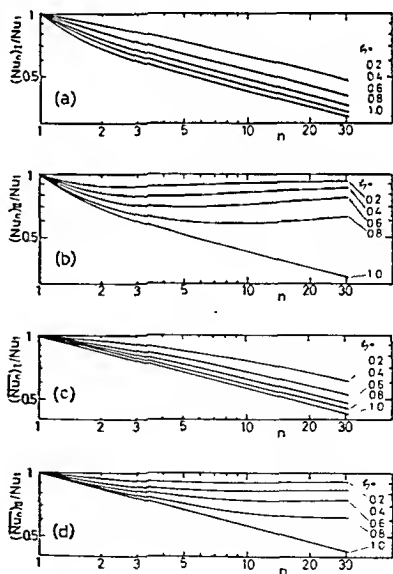


Figure 6 Theoretical results for Models I and II

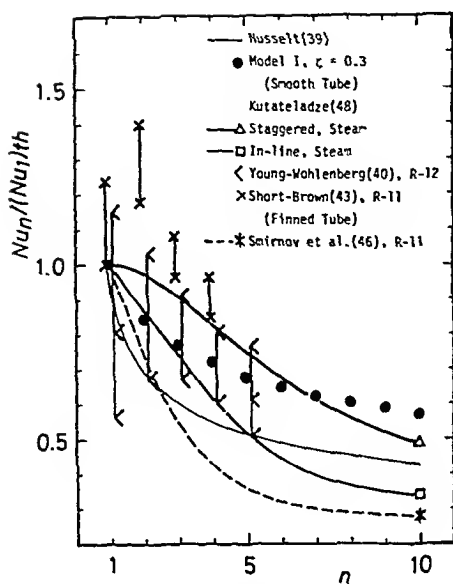


Figure 7 Comparison between theory and experiment for $Nu_n/(Nu_1)_{th}$

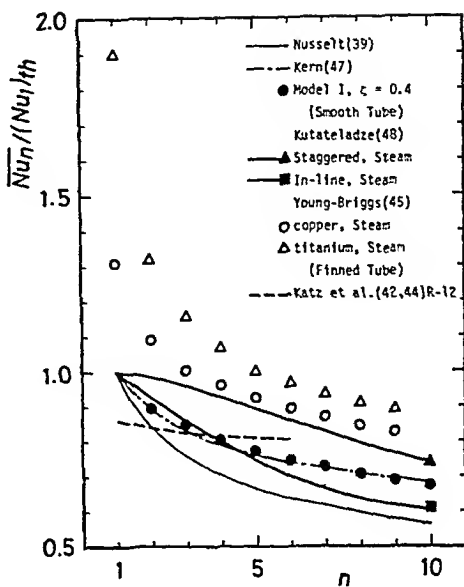


Figure 8 Comparison between theory and experiment for $Nu_n/(Nu_1)_{th}$

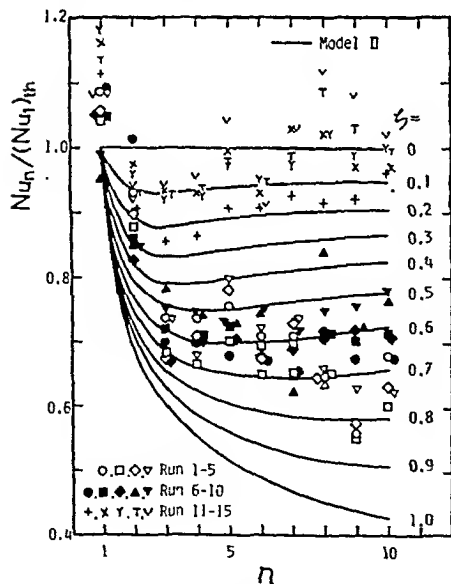


Figure 9 Theoretical result by Model II and experimental data by Gogonin et al.

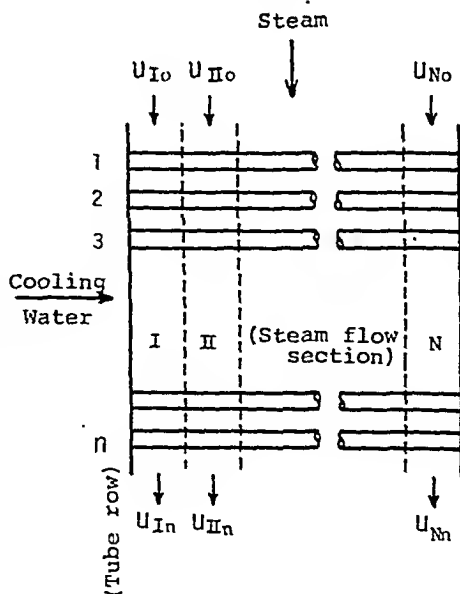
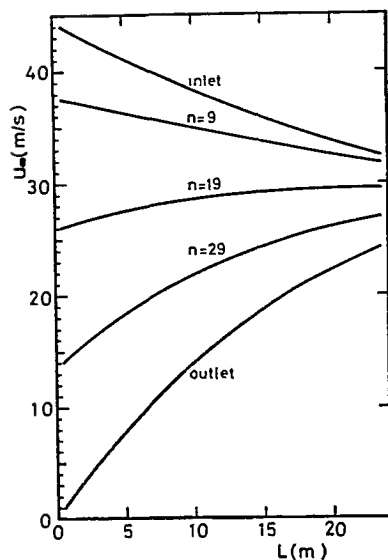
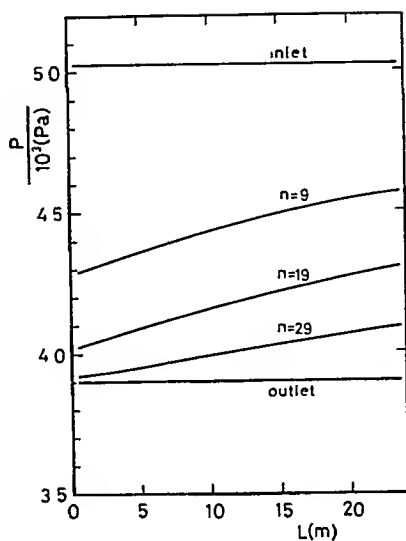


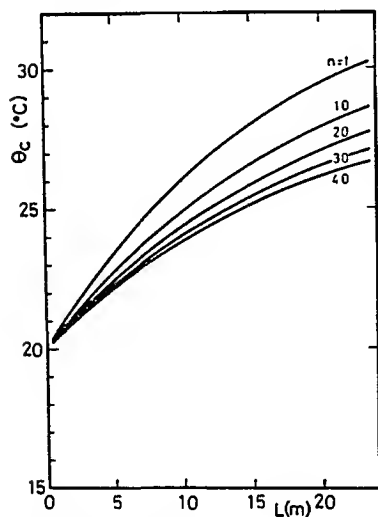
Figure 10 A model for calculating characteristics in a tube bank



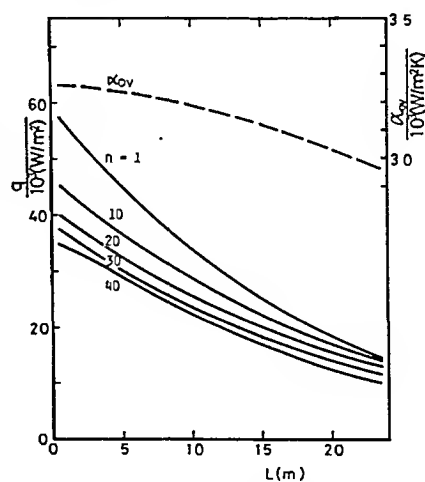
(a) Steam velocity



(b) Steam pressure



(c) Cooling water temperature



(d) Heat flux density and overall heat transfer coefficient

Figure 11 Two-dimensional distributions of u_w , p , θ_c , \dot{q} and α_{OV} in a tube bank

THE POTENTIAL OF HEAT TRANSFER ENHANCEMENT IN SURFACE CONDENSERS

P. J. Marto* and R. H. Nunn*⁺

Various heat transfer enhancement techniques are reviewed for use in condensers. Enhancement factors obtained from the literature for single tubes or small tube bundles are used in a condenser rating one-dimensional code to predict the benefits that are possible for a steam condenser having a circular tube bundle with radial flow on the steam side. The complex effects of condensate inundation and vapor shear, and their influence upon enhancement, are examined. It is estimated that a 30 percent decrease in condenser volume and weight is possible through enhancement.

INTRODUCTION

Surface condensers play an important role in steam power systems whether in use for electricity production, or marine propulsion. Improved heat transfer in a steam condenser can reduce condenser size, and therefore cost, for a given heat load. Alternatively, an existing condenser incorporating enhanced heat transfer can reduce the turbine back pressure, and increase the thermodynamic efficiency of the plant. With fuel costs rising at an alarming rate, even very small increases in efficiency can lead to significant reductions in plant operating cost.

In recent years, there has been an increased interest regarding the use of enhanced heat transfer surfaces in the design of heat exchangers (1, 2, 3, 4, 5, 6). Webb in 1980 provided an excellent review of enhancement methods for particular use in condensers (7). In general, these methods may be divided into tube-side enhancement (on the cooling-water side) and shell-side enhancement (on the steam side) techniques. While these methods have been examined for a single tube or in small tube bundles (8), few attempts have been made to predict the overall effect these enhancement methods would have on an operating condenser.

The purpose of this paper is to review promising heat transfer enhancement schemes which are suitable for use in surface condensers, and to show, with the use of a condenser rating code, how these heat transfer enhancement schemes may lead to smaller, lighter condensers of the future.

*Department of Mechanical Engineering, Naval Postgraduate School.

⁺Presently Visiting Research Fellow, Royal Naval Engineering College, Manadon.

TUBE-SIDE ENHANCEMENT

In general, the largest resistance to heat flow in conventional surface condensers is usually on the tube side, where single phase turbulent forced convection occurs. In such cases, tube-side enhancement may be expected to be of primary benefit in increasing condenser performance. Several promising techniques are described below.

Rough-Walled Tubes

It is well known that surface roughness, either in the form of random sand grains or regular geometric shapes, can be used to increase turbulent heat transfer. A recent patent by Fenner and Ragi (9) describes a method of using three-dimensional roughness to enhance heat transfer. A single discontinuous layer of randomly distributed metal bodies is bonded to the inside of the tube wall. Results for water at a Reynolds number of 35,000 and a Prandtl number of 10 show that as the average height of the roughness bodies increases, heat transfer is enhanced by factors of up to 2.5, corresponding to a relative roughness (e/d_i) near 0.016. This increase in heat transfer occurs, of course, at the expense of an equivalent amount of energy to overcome fluid friction. Beyond a relative roughness of 0.016, no further improvement in heat transfer is observed but a continued increase in frictional resistance lowers the performance ratio (α/α_s)/(f/f_s) below unity.

The repeated-rib surface has been studied by Webb et al. (10), and this work provides generalized correlations for both heat transfer and friction which depend upon roughness element height and spacing. More recently, Han et al. (11) showed that repeated ribs at a 45° angle of attack gave better performance than ribs oriented normal to the flow, with heat transfer enhancement factors as large as 3.0 being possible.

Withers and Rieger (12) describe a commercially available tube (TURBO-CHIL) which has an inner surface containing multiple-helix ridging as shown in Figure 1(a). Based upon experimental data obtained by Withers (13), the following tube-side correlations for this type of tubing are proposed:

$$\sqrt{\frac{f}{8}} = - \frac{1}{2.46 \ln[r + (7/Re)^m]} \quad (1)$$

and

$$St = \frac{\sqrt{f/8}}{5.68 (e/p)^{1/8} \sqrt{Pr} [(e/d_i) Re \sqrt{f/8}]^{0.136} + \gamma} \quad (2)$$

where

r and m are determined empirically for each tube, and

$$\gamma = - [2.5 \ln (2e/d_i) + 3.75].$$

Equations (1) and (2) predict heat transfer enhancement factors as large as 2.5.

Helically Corrugated Tubes

A wide variety of helically corrugated tubes can be manufactured with varying shapes and flute depths. Figure 1(b) shows a representative sample of a mildly corrugated or "roped" tube which shows promise for condenser use. This tube, because of its mild deformations, can be manufactured out of most materials, including titanium. Also, it is easily cleanable, and can be readily furnished with smooth lands spaced at appropriate intervals to accommodate the tube support plates. Withers (14) described one such tube (KORODENSE), and obtained data (15) which could be correlated by equations similar to equations (1) and (2) above. Gupta and Rao (16) compared the heat transfer and friction characteristics of a similar type of indented tube to smooth behavior. It was found that the performance ratio $(\alpha/\alpha_s)/(f/f_s)$ varied with a "severity factor", $\phi = e^2/pd_i$, and the highest performance occurred for ϕ equal to 0.002 (i.e., a very mildly indented tube), Figure 2. For this case, the heat transfer enhancement factor α/α_s was 1.75 for water. A similar type of "roped" tubing is available from Yorkshire Imperial Metals, Ltd. in Great Britain. Their product brochure (17) recommends the widely used correlation

$$St = C_1 Re^{-0.2} Pr^{-2/3} \quad (3)$$

where C_1 varies with the tube geometry (C_1 is 0.027 for smooth tubes). Values of C_1 for these enhanced tubes are plotted in Figure 3, and it is easily seen that enhancements of 3-4 are possible as groove depth increases and pitch decreases (i.e., the grooves have a tighter spiral).

Numerous other studies have occurred with a variety of tube geometries (18, 19, 20, 21). As a result, it appears that, at present, the most promising technique to enhance heat transfer on the tube side is with one of the commercially available helically corrugated tubes. With a mildly indented tube, internal heat transfer enhancement factors of from 1.5 to 3.0 may be expected with a somewhat larger amplification of friction factor. No one "best" surface exists and final selection will depend upon fouling characteristics, costs, and structural considerations, as well as the intended application.

SHELL-SIDE ENHANCEMENT

Since the analysis performed by Nusselt in 1916 (22), many analytical and experimental investigations have been conducted to further understand the condensation process. From these works, it

is well known today that during condensation a large thermal resistance occurs due to conduction of heat across the condensate film, and anything that can be done to thin or disturb this film is generally beneficial to heat transfer. For horizontal condenser tubes, this thinning may occur by promoting dropwise conditions, by using finned or fluted surfaces, or by improving condensate drainage. Condensation heat transfer enhancement by shell-side surface geometry modification has been recently reviewed by Cooper and Rose (23).

Dropwise Condensation on Tubes

In a review of dropwise condensation, Tanasawa (24) discusses the methods of promoting dropwise conditions, and states that finding how to promote dropwise conditions for long periods of time is one of the most important problems to be solved before practical application of this mechanism can be accomplished. Tanasawa further concludes that of all the promoting techniques, the use of a thin coating of organic polymer (such as Teflon) is the most promising in regard to economic feasibility. (While the injection of a promoting material into the steam has been shown to be effective, there remains a serious concern about the effect that this promoter will have upon boiler feedwater.) With the use of an organic polymer, however, two major problems must be addressed: (1) organic coatings have poor thermal conductivities and must, therefore, be applied in the form of an ultra-thin film, in order to reduce their conduction resistance, and (2) techniques must be developed to apply these ultra-thin films so that they are strongly adherent to the condenser tube, and have a toughness to withstand industrial conditions during assembly and use.

A variety of investigations have been conducted using Teflon to promote dropwise condensation conditions on horizontal tubes (25, 26, 27, 28). Results so far obtained show that using a permanent organic coating to promote dropwise conditions may give enhancements of the steam condensing heat transfer coefficient for single horizontal tubes in the range of from 1.4 to perhaps 3.0. This range of increase is substantially less than the factors of from 10 to 20 obtained for monolayer promoters on vertical surfaces (24, 29), and suggests perhaps that the potential for steam-side enhancement using organic-coated tubes has yet to be realized.

Finned Tubes

During film condensation on finned tubes, the fins not only serve to increase the heat transfer surface area, but also to increase the film condensation heat transfer coefficient by thinning the condensate film. As originally described by Gregorig (30) in 1954, the fins generate surface tension forces which tend to thin the condensate film near the tips of the fins and to thicken the film in the channels, or troughs, between fins. Alternatively, for widely spaced fins, the presence of the fins will draw the condensate to the base of each fin, thinning the film along the tube wall. In either case, the result is that the condensing heat transfer coefficient is increased over that for the smooth tube.

Staub (31) reported on some experimental work in 1961 which included film condensation of steam on horizontal finned tubes at both atmospheric and sub-atmospheric pressures. All data were obtained with 15.9 mm OD, copper tubes. External heat transfer coefficients for a fine pitch tube (1.0 mm spacing between fins) at a steam pressure of 0.05 bar were about 2.5 to 3 times the smooth tube values at a heat flux comparable to surface condenser designs (approximately 75 kW/m^2). Results with a coarse-pitch tube (1.5 mm spacing) for the same conditions were only 2 times the smooth tube results, indicating that fin pitch is an important variable. Karkhu and Borovkov (32) obtained condensation data for steam on four horizontal tubes containing different configurations of trapezoidally shaped fins. All these data were taken at pressures slightly higher than atmospheric, and it was discovered that for transverse fins with large Weber numbers (i.e., large surface tension forces in relation to gravity forces), the average condensation heat transfer coefficient increased by 50 to 100 percent, whereas for low Weber numbers, there was little, or no improvement. There is recent evidence also for finely spaced fins that the thermal conductivity of the tube wall is an important variable (33).

In designing finned tubes for use with steam, the relatively large surface tension of water requires that special care be exercised to avoid bridging of the gap between fins by the condensate. As shown schematically in Figure 4, the fin geometry must be chosen with the particular working fluid in mind (34). In the case of steam, the fins must be spaced far enough apart to avoid this bridging phenomenon, otherwise the thermal performance will be severely deteriorated. For refrigerants (with low surface tension), tubes with a fin spacing of 0.8 mm have been shown to be most effective (35). Some recent data for water indicate that the optimum fin spacing with this high surface tension fluid may be near 2.5 mm (36).

Corrugated Tubes

Mildly indented, corrugated tubes of the type shown in Figure 1(b) appear attractive for condenser use because enhancement of heat transfer occurs on both sides of the tube wall, and the mild indentation may permit easy internal cleaning as noted above. In 1975, Young et al. (37) reported on some measurements using mildly corrugated (KORODENSE) tubes with a groove depth near 0.76 mm. Three 25 mm OD 90-10 copper-nickel tubes with flute spacings of 6.4, 8.5 and 12.7 mm were tested at atmospheric and sub-atmospheric steam conditions. It was found that at atmospheric conditions the heat transfer enhancement factors were between 1.3 and 1.7, whereas under vacuum conditions, the enhancement factors were lower at 1.3 - 1.4. Catchpole and Drew (38) tested a family of corrugated tubes having different groove depths and spacings. All tests were on 15.9 mm OD 70-30 copper-nickel tubes at a steam pressure of 0.14 bar. These results are reproduced in Figure 5.

Correlation of the experimental results led to an external enhancement factor given by the following relationship:

$$E_0 = 1.17 (We \cdot \cos \eta)^{0.076} \quad (4)$$

where

We = Weber Number, a function of condensate density and surface tension, as well as enhancement geometry and dimensions, and

η = helix angle of the grooves measured from the perpendicular to the tube axis.

Catchpole and Drew therefore concluded that it is desirable to design the corrugation so that a large Weber number exists, and a small helix angle exists. In fact, when $\eta = 0$, i.e., when the grooves are vertical, the best performance would occur. The highest enhancement factor measured was 1.7, corresponding to a tube with grooves 0.5 mm deep, spaced 2.0 mm apart. It should be noted here that a disadvantage of these mildly indented tubes is that an optimum configuration on each side of the tubes will not be possible because the geometry is altered both on the shell side as well as on the tube side in a single rolling operation.

Other recent measurements with mildly indented tubes have shown enhancement factors between 1.05 and 1.4 (20, 21, 39). Placing micro-grooves on a mildly indented surface improved the shell-side enhancement factor to near 2.0 (21). Other techniques, such as helically wrapped wires (40), and non-wetting strips (41, 42) also show promise for steam condensation on horizontal tubes.

COMPUTER EVALUATION OF ENHANCED-TUBE CONDENSERS

The performance of a condenser tube within a tube bundle is strongly influenced by the history of the vapor/gas mixture prior to arrival at the tube in question. Conversely, the performance of any given tube can have a profound effect upon the thermal behavior of tubes located downstream. The complexity of these interactions may lead to a degree of depression in the mind of the researcher who would predict overall bundle performance. On the other hand, these inadequacies in understanding may be viewed as challenges and, even in our present state of ignorance, we can answer questions in a relative way. For instance, qualitative trends due to enhancement may be identified and relative improvements due to enhancement may even be quantified within a precision of perhaps 10-20%. As Mayhew has put it (43), "Theory, if it cannot provide an accurate design tool, can at least show how to progress from one design to a better one."

In order to conduct such comparative studies, the authors have utilized the code MORCON (44) which is an adaptation of the code ORCON1 (45, 46) developed at the Oak Ridge National Laboratory. MORCON is restricted to use with circular tube bundles and in the calculation procedure the inlet steam/gas mixture is distributed in such a way that there is no circumferential pressure gradient at the condenser outlet (air-cooler inlet). The flow

in such a condenser is radially inward and, in this sense, the computational field in MORCON is one-dimensional.

Internal tube-side thermal resistances are calculated using the well-known Dittus-Boelter correlation for fully-developed turbulent flow. On the steam side, the standard Nusselt formula for columns of tubes (22) is corrected first for vapor shear effects and then for condensate inundation. Vapor shear enhancement is modelled using the correlations of Fujii et al. (47), and the effects of condensate inundation are included by means of a modified Nusselt exponent applied to the number of tubes resident above a given location in the bundle ($\bar{x}_n/\alpha_l = n^{-0.2}$). This latter result is further modified to include the favorable effects of side drainage as proposed by Eissenberg (48, 44). Finally, an iterative procedure is utilized to account for the added thermal resistance due to the presence of noncondensable gases. (In cases of primary interest to the authors, the noncondensable gas concentrations in the inlet steam flow are small enough to be inconsequential from a thermal resistance point of view.)

Enhancement is taken into account by multiplying the tube-side and shell-side heat transfer coefficients by user-specified enhancement factors, E_i and E_o . No attempt has been made to adjust the vapor shear and condensate inundation models to include a dependency upon enhancement.

RESULTS OF COMPUTER EXPERIMENTS

The following computations are based upon a "baseline" smooth-tube condenser that is of a radial design, symmetrical about a vertical centerline, with a vertical cooler section extending upwards from a central collecting point, Figure 6. Table 1 further describes the baseline design.

TABLE 1 - Input Data and Computed Performance for the Smooth-Tube Baseline Condenser.

<u>Input Values</u>	<u>Computed Values</u>
Inlet steam: 23.8 kg/s saturated at 330K (1.7×10^4 N/m ²)	Tube length for 0.05% exit fraction: 5.72 m Condenser bundle dimensions: 1.26m OD, 0.1m ID
Tubes: 1646 tubes in each of two passes, 6% in cooler; 70-30 CuNi, 16mm OD 16 BWG; fouling resistance: $R_F = 5.8 \times 10^{-5}$ m ² K/W	Area avg. q_{bv} 3014 W/m ² K LMTD, 19.9K Heat removal rate, 56.4×10^6 W Cooling surface area, 938 m ²
Coolant: Water with 3.5% salt by weight; inlet temp., 292K, velocity 2.44 m/s.	Steam velocity, m/s: Condenser inlet, 36.8 Cooler exit, 1.1 Shell side ΔT , 19.0K Shell side ΔP , 868 N/m ² Avg. CW ΔT , 27.8K CW flow, 510 kg/s

Effect of Internal and External Enhancement on Bundle Length

Figure 7 illustrates the predicted effect of internal and external enhancement in terms of the length of tubes necessary to maintain the baseline heat duty. (Constant heat duty is obtained by iteratively varying the tube length to obtain a fixed fraction of 0.05% of the baseline inlet steam flow.) Figure 7 indicates enhancement factors of some commercially available enhanced tubes and it is seen that combined internal and external enhancement can be expected to lead to bundle length (and volume and weight) reductions on the order of 25 - 35%. Table 2 gives information describing the enhanced tubes considered in this study. The smooth-tube baseline is, as is typical, controlled in thermal resistance by the tube-side film coefficient. For this reason internal enhancement is relatively more effective (about 2:1) than external enhancement.

Variations in Thermal Resistance through the Bundle

The importance of considering the limiting thermal resistance is illustrated in Figures 8a and 8b. Figure 8a illustrates the row-by-row variation in internal and external resistances for a condenser with no external enhancement. Without internal enhancement, the thermal circuit is unbalanced (dominated by the internal resistance) throughout the condenser. External enhancement in this case would clearly be gilding the thermal lily. With an internal enhancement of 2.0, however, the two film resistances are more-nearly balanced. Such would be the approximate case for the KL tube of Figure 7.

TABLE 2 - Characteristics of Some Commercially-Available Enhanced Tubes.¹

Tube	Groove Geometry		Thermal Enhancement Factors		Head Loss Factor ²
	Pitch Dia	Depth Dia	Internal	External	
KL	0.543	0.025	2.14	1.05	2.03
KM	0.543	0.040	2.51	1.14	3.26
YL1	0.250	0.013	1.44	1.35	1.56
YL2	0.250	0.013	1.44	1.94	1.47
YM1	0.125	0.0215	2.70	1.38	6.02
YM2	0.125	0.0215	2.70	1.94	5.69

Notes:

1. Tubes KL and KM are products of Wolverine Division, UOP Inc. (49). Tubes YL1, YL2, YM1, and YM2 are products of Yorkshire Imperial Metals, LTD (17).
2. Figures shown are ratios of cooling water head loss values to the smooth-tube case for the baseline conditions.

If external enhancement is to be applied, on the other hand, such as in the case of YM2 in Figure 7, additional internal enhancement is to be recommended. Such a case is illustrated in Figure 8b where, again, a relative balance is obtained between the two film resistances by using an inside enhancement factor $E_i = 3.0$ and an outside enhancement factor $E_o = 1.5$. It should be noted that in Figure 8b the film resistances have been lowered below the thermal resistances due to fouling (R_f) and tube wall (R_k). In such a case, attempts to optimize the bundle design further must consider all of the thermal resistance elements (except that due to noncondensable gases, which is in this case negligible).

Figures 8a and 8b also illustrate the complicated nature of the shell-side resistance across the bundle. The dashed lines indicate the distribution of external resistance in sectors I, IV, and VI of the condenser, with sector I at the top of the bundle (center ray at 150°) and proceeding clockwise in 30° increments to sector VI (see Figure 6). In sector I, a procession radially inward from row 1 to row 30 is in the direction of gravity and each successive row is inundated by the row above - thus, the continuous increase in R_o in sector I. In sector VI, however, each row radially inward is subject to less inundation so that a general improvement is realized from the point of view of condensate inundation. In every sector, however, the vapor velocity is decreasing in a radially inward direction and the beneficial effect of vapor shear is correspondingly less in regions toward the center of the bundle. In the top sector (sector I), condensate inundation and vapor shear effects change in the same direction with resistance increasing radially inward. In the bottom sector (sector VI), the inundation and vapor shear change oppositely and there is an approximate balance.

Influence of Vapor Shear and Condensate Inundation

Figures 9a and 9b illustrate the potentially deceptive nature of the influence of vapor shear and condensate inundation in condenser bundles. Figure 9a examines the relative influence of the two effects upon required tube length and their dependency on internal enhancement. In this case the favorable effect of vapor shear is roughly balanced by that of inundation, and in terms of required bundle length they are by no means independent of each other. Without enhancement the two effects are essentially equivalent so that the standard HEI method (50), which neglects them both, appears to be adequate (for rather serendipitous reasons). With enhancement, however, when tube-by-tube thermal performance must be considered, the neglect of either vapor shear or condensate inundation can lead to erroneous results (e.g., the neglect of vapor shear would indicate no improvement with an internal enhancement of about 1.7). Figure 9b shows that when external enhancement is large, these effects are less important because of the dominance of thermal resistances other than those due to the shell-side film.

CONCLUSIONS

1. Using mildly indented condenser tubing which is commercially available today, heat transfer enhancement factors of 1.5 to 3.0 on the tube side and 1.1 to 1.7 on the shell side are possible.
2. With mildly indented condenser tubing, and with some reservations regarding uncertain penalties, it is estimated that a 30 percent decrease in condenser volume and weight is possible.
3. In utilizing enhanced heat transfer techniques in large condenser tube bundles, care must be exercised in balancing each of the thermal resistances. Different regions of the condenser may be limited by the tube-side or shell-side resistance.
4. A strong need exists to conduct a tube-by-tube analysis when using external (shell-side) enhancement techniques. The effects that vapor shear, condensate inundation and noncondensable gas concentration have upon heat transfer enhancement and two-phase pressure drop must be determined.

REFERENCES

1. Junkhan, G.H., Bergles, A.E., and Webb, R.L., 1979, "Research Workshop on Energy Conservation Through Enhanced Heat Transfer", HTL-21, Iowa State University, Ames, Iowa.
2. Bergles, A.E., 1978, Proceedings of the Sixth International Heat Transfer Conference 6, Toronto, 89-108.
3. Bergles, A.E., 1978, Previews of Heat and Mass Transfer 4, No. 2, January.
4. Bergles, A.E., 1978, Previews of Heat and Mass Transfer 4, No. 4, July.
5. Bergles, A.E., Webb, R.L., Junkhan, G.H., and Jensen, M.K., 1979, "Bibliography on Augmentation of Convective Heat and Mass Transfer", HTL-19, Iowa State University, Ames, Iowa.
6. Bergles, A.E., and Jensen, M.K., 1977, "Enhanced Single-Phase Heat Transfer for Ocean Thermal Energy Conversion Systems," HTL-13, Iowa State University, Ames, Iowa.
7. Webb, R.L., 1981, Power Condenser Heat Transfer Technology, Marto, P.J. and Nunn, R.H. (Editors), Hemisphere Publishing Corp., Washington, D.C., 287-324.
8. Marto, P.J. and Nunn, R.H., 1982, "A Critical Review of Heat Transfer Enhancement Techniques for Use in Marine Condensers," NPS Report 69-82-006, Naval Postgraduate School, Monterey, California.

9. Fenner, G.W. and Ragi, E.G., 1979, "Enhanced Tube Inner Surface Heat Transfer Device and Method," U.S. Patent No. 4,154,293.
10. Webb, R.L., Eckert, E.R.G. and Goldstein, R.J., 1971, Int. J. Heat and Mass Transfer 14, 601-617.
11. Han, J.C., Glicksman, L.R. and Rohsenow, W.M., 1978, Int. J. Heat and Mass Transfer 21, 1143-1156.
12. Withers, J.G. and Rieger, K.K., 1974, "Heat Transfer Tube Having Multiple Internal Ridges," U.S. Patent No. 3,847,212.
13. Withers, J.G., 1980, Heat Transfer Engineering 2, No. 2, 43-50.
14. Withers, J.C., 1977, "Heat Exchange Apparatus and Method of Controlling Fouling Therein," U.S. Patent No. 4,007,774.
15. Withers, J.C., 1980, Heat Transfer Engineering 2, No. 1, 48-58.
16. Gupta, R.K. and Rao, M.R., 1979, Adv. in Enhanced Heat Transfer, ASME, New York, 103-114.
17. "YIM Heat Exchanger Tubes: Design Data for Horizontal Roped Tubes in Steam Condensers," Technical Memorandum 3, Yorkshire Imperial Metals, Ltd., Leeds, England.
18. La Rue, J.C., Libby, P.A. and Yampolsky, J.S., 1981, "Fluid Mechanics and Heat Transfer Spirally Fluted Tubing," GA-A16541, General Atomic Company.
19. Reilly, D.J., 1978, "An Experimental Investigation of Enhanced Heat Transfer on Horizontal Condenser Tubes," M.S. Thesis, Naval Postgraduate School, Monterey, California.
20. Marto, P.J., Reilly, D.J. and Fenner, J.H., 1979, Adv. in Enhanced Heat Transfer, ASME, New York, 1-9.
21. Ciftci, H., 1979, "An Experimental Study of Filmwise Condensation on Horizontal Enhanced Condenser Tubing," M.S. Thesis, Naval Postgraduate School, Monterey, California.
22. Nusselt, W., 1916, VDI Zeitung 60, 541-546, and 569-575.
23. Cooper, J.R. and Rose, J.W., 1981, "Condensation Heat-Transfer Enhancement by Vapour-Side Surface Geometry Modification," HTFS Research Symposium, Harwell, England.
24. Tanasawa, I., 1978, Proceedings of the Sixth International Heat Transfer Conference 6, Toronto, 393-405.
25. Topper, L. and Baer, E.J., 1955, J. of Colloid Science 10, 225.

26. Smith, G.G., 1956, "Promotion of Dropwise Condensation by Teflon Coated Condenser Tubes," Evaluation Report 030038B, NS-643-078, U.S. Naval Engineering Experiment Station, Annapolis, Maryland.
27. Depew, C.A., and Reisbig, R.L., 1956, I&EC Process Design and Development 3, No. 4, 365-369.
28. Brown, A.R. and Thomas, M.A., 1966, Proceedings of the Third International Heat Transfer Conference 2, Chicago, 300-305.
29. Graham, C., 1969, "The Limiting Transfer Mechanisms of Dropwise Condensation," Ph.D. Thesis, Department of Mechanical Engineering, M.I.T., Cambridge, Massachusetts.
30. Gregorig, R., 1954, Zeitschrift fur angewandte Mathematik und Physik 5, 36-49 (Translation by D.K. Edwards, UCLA).
31. Staub, F.W., 1961, "Heat Transfer for Film Condensation on Vertical and Horizontal Fluted Tubes," General Electric Report No. 61GL175, Schenectady, New York.
32. Karkhu, V.A. and Borovkov, V.P., 1971, Heat Transfer-Soviet Research 3, 183-191.
33. Shklover, G.G., Milman, O.O., Baskov, V.S. and Ankudinov, G.A., 1981, Heat Transfer-Soviet Research 13, No. 2, 108-114.
34. Taborek, J., 1974, Heat Exchangers: Design and Theory Sourcebook, Afgan, N. and Schlunder, E.V. (Editors), Scripta Book Company, Washington, D.C., 1974, 69.
35. Carnavos, T.C., 1980, "An Experimental Study: Condensing R-11 on Augmented Tubes," ASME Paper No. 80-HT-54, 19th National Heat Transfer Conf., Orlando, Florida.
36. Yau, K.K., 1982, "Condensation Heat-Transfer Enhancement by Vapour-Side Geometry Modification," Project Report, Mechanical Engineering, Queen Mary College, Univ. of London.
37. Young, E.H., Withers, J.G. and Lampert, W.B., 1975, "Heat Transfer Characteristics of Corrugated Tubes in Steam Condensing Applications," AIChE Paper No. 3, 15th National Heat Transfer Conference, San Francisco, California.
38. Catchpole, J.P., and Drew, B.C.H., 1976, Steam Turbine Condensers, Report No. 619, National Engineering Laboratory, East Kilbride, Glasgow, U.K.
39. Mehta, M.H. and Rao, M.R., 1979, Adv. in Enhanced Heat Transfer, ASME, New York, 11-22.
40. Thomas, A., Lorenz, J.J., Hillis, D.L., Yung, D.T. and Sather, N.F., 1979, "Performance Tests of the LMW Shell-and-Tube Heat Exchangers for OTEC," Sixth OTEC Conf., Washington, D.C.

41. Glicksman, L.R., Mikic, B.B. and Snow, D.F., 1973, AICHE Journal 19, No. 3, 636-637.
42. Desmond, R.M. and Karlekar, B.V., 1980, "Experimental Observations of a Modified Condenser Tube Design to Enhance Heat Transfer in a Steam Condenser," ASME Paper No. 80-HT-53, 19th National Heat Transfer Conference, Orlando, Florida.
43. Mayhew, Y.R., 1981, Power Condenser Heat Transfer Technology, Marto, P.J. and Nunn, R.N. (Editors), Hemisphere Publishing Corp., Washington, D.C., 230.
44. Nunn, R.H. and Marto, P.J., 1982, "Performance Rating of Enhanced Marine Condensers," NPS Report 69-82-005, Naval Postgraduate School, Monterey, California.
45. Hafford, J.A., 1973, "ORCON1: A Fortran Code for the Calculation of a Steam Condenser of Circular Cross Section," ORNL-TM-4248, Oak Ridge National Laboratory, Tennessee.
46. Eissenberg, D.M. and Noritake, H.M., 1970, "Computer Model and Correlations for Prediction of Horizontal Tube Condenser Performance in Seawater Distillation Plants," Report ORNL-TM-2972, Oak Ridge National Laboratory, Tennessee.
47. Fujii, T., Honda, H. and Oda, K., 1979, Condensation Heat Transfer, ASME, New York, 35-43.
48. Eissenberg, D.M., 1972, "An Investigation of the Variables Affecting Steam Condensation on the Outside of a Horizontal Tube Bundle," Ph.D. Dissertation, Univ. of Tennessee.
49. Korodense Bulletin 4020, 1976, Wolverine Division, Decatur, Alabama.
50. Standards for Steam Surface Condensers, 1970, Heat Exchange Institute, New York.

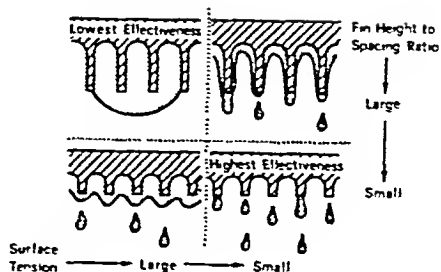
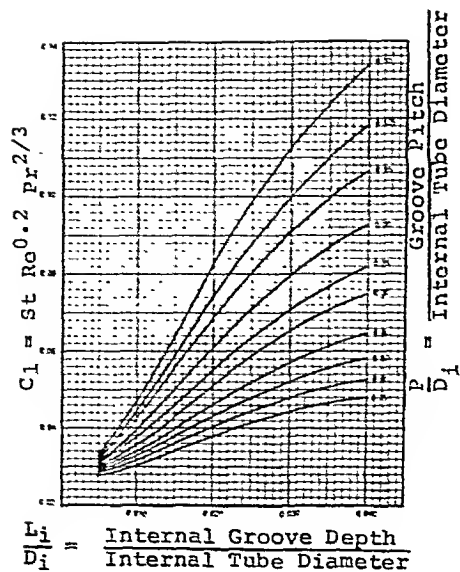


Figure 3 Estimated convective coefficient, C_1 (17)

Figure 4 Condensate retention on various fins (34)

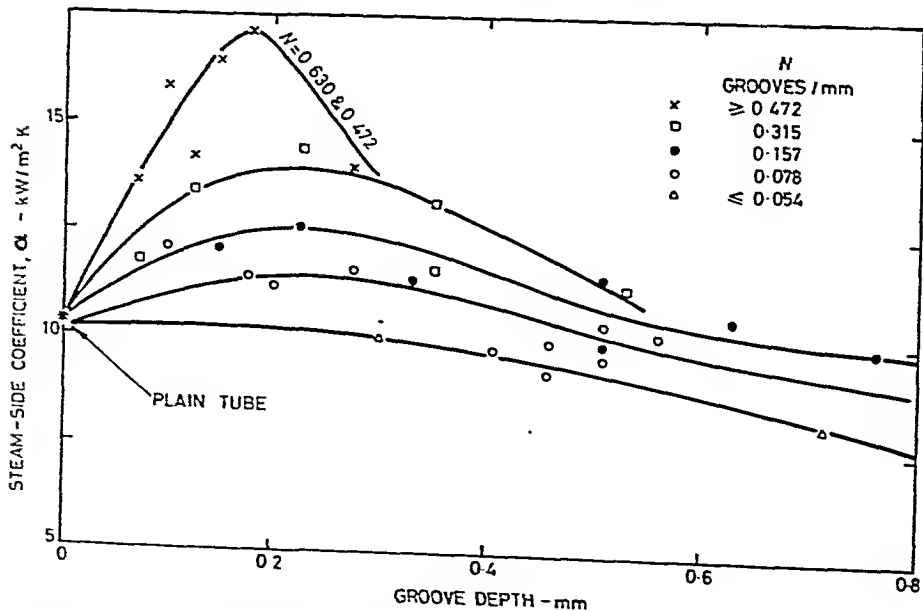


Figure 5 Steam side coefficient versus groove depth and pitch (38)

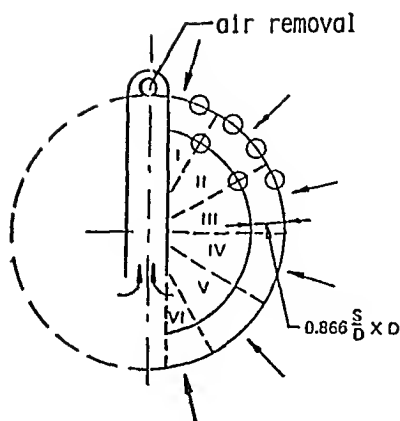


Figure 6 Sketch of bundle geometry

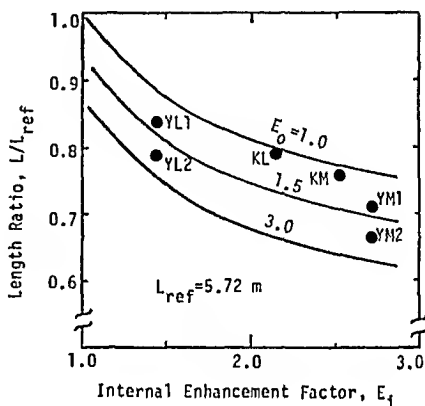
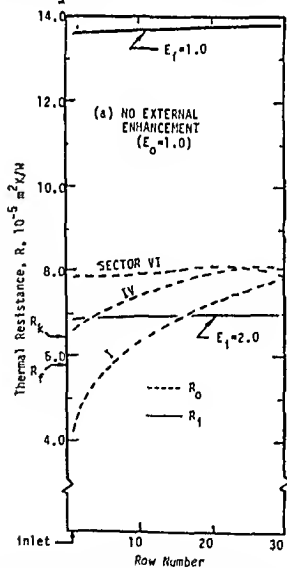


Figure 7 Bundle length reduction due to internal and external enhancement



(b) EXTERNAL ENHANCEMENT
 $E_o = 1.5$

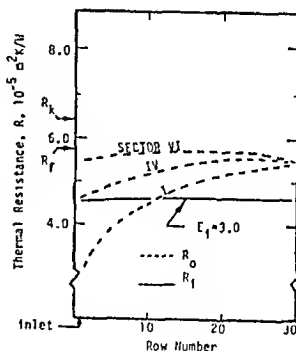


Figure 8 Row-by-row variations of thermal resistances

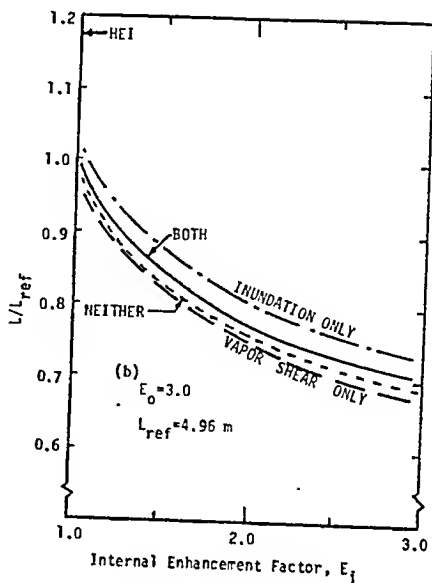
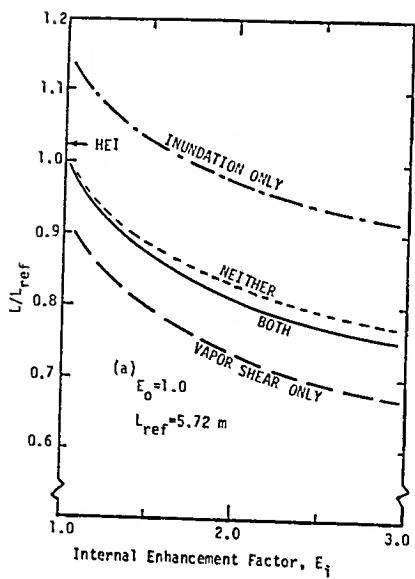


Figure 9 Effects of vapor shear and condensate inundation with various degrees of enhancement

ENHANCEMENT OF NAVAL CONDENSER PERFORMANCE

D.W.Butcher* and D.C.P.Birt†

Summarised results of tests using dropwise condensation techniques on naval steam condensers are presented. Injected promoters applied to condensers with heat transfer areas of 3.19, 21.18 and 425.5 m² resulted in variable improvements inconsistent with the results using single tubes. The performance of a condenser fitted with PTFE coated tubes was impaired by the presence of a hydrophilic deposit formed during some 4000 hours steaming.

A shipboard trial on a condenser retubed with grooved tubing - Kydensa - has shown that some 19% fewer tubes give the same thermal performance as plain tubes.

INTRODUCTION

Plant and equipment designed for use in warships must be reliable, robust and compact. In the case of steam turbine driven vessels, condensers are usually larger than the turbines to which they are fitted even though they are made more compact than land based condensers by the use of smaller tubes and greater coolant velocities. In order to achieve additional reductions in size, methods of improving steam and water side film coefficients of heat transfer have been investigated by the Ministry of Defence (MOD). Although the possible naval applications have diminished in recent years due partly to the development of the marine gas turbine, the research has revealed aspects of behaviour that are considered of interest in other applications.

Laboratory tests using single tubes have shown that the overall coefficient of heat transfer could be improved by some 10-50% using either dropwise condensation techniques to improve steamside coefficients, or corrugated tubing (Kydensa) to improve coolant film coefficients. Following the success of the laboratory tests, a series of trials using full-scale condensers was undertaken, the findings being summarised below. Momentum and heat transfer correlations for Kydensa tubing are also given.

The immediate aim of each of the trials using dropwise condensation promoters was to show that the change in the mode of condensation from filmwise to dropwise would result in a reduction in heat transfer area (and hence condenser volume) for otherwise similar operating conditions. Thus no attempt was made to measure either the concentration of non-condensables in the steam or its inlet velocity in any of the trials, for they were considered independent of the mode of condensation in each of the trials, which are summarised in

*School of Chemical & Systems Engineering, N.E.London Polytechnic.

†Admiralty Marine Technology Establishment, Holton Heath, Poole.

I.CHEM.E. SYMPOSIUM SERIES NO. 75

chronological order to help explain the development of the trials programme.

TRIAL NO.1. - CONDENSER HEAT TRANSFER AREA 425.5 m²

The condenser was fitted with 2800 Admiralty brass tubes 15.88 mm od, through which sea water was pumped at a velocity of 0.91 m/s. Dropwise condensation was successfully promoted using a 2% solution of tetrakis-dodecanethiosilane (C₁₂H₂₅S)₄ Si in carbon tetrachloride.

TABLE 1 - Results for Trial 1 - Condenser Area 425.5 m²

Condensation mode	Shell pressure kN/m ²	Temperatures °C				Steam flow kg/h	Overall htc W/m ² k
		Coolant in	Condenser shell		Condensate		
			1	2			
Filmwise	84.75	10.0	88.9	92.2	29.4	19545	432
	88.14	10.0	92.2	94.4	60.0	44545	954
	100.00	10.0	94.4	97.8	87.8	51364	1022
Dropwise	84.75	10.6	88.9	92.2	29.4	19545	432
	84.75	"	92.2	94.4	54.4	41818	897
	88.99	"	92.8	95.0	61.1	48182	1016
	89.84	"	92.8	95.6	75.6	60909	1340
	91.53	"	93.3	96.7	82.8	63636	1363

The results of Birt & Brunt (1) summarised in Table 1 reveal that the lack of improvement in overall heat transfer coefficients at low steam loadings was due to the limitation of condensation to part of the condenser, the remainder being used to undercool the condensate. At high steam flowrates the undercooling was less significant, resulting in higher values of overall coefficient.

TRIAL NO.2. - CONDENSER HEAT TRANSFER AREA 3.19 m²

The condenser was fitted with 118 Cu/Ni tubes 15.88 mm od arranged in two tube passes, through which water was pumped at a velocity of 1.48 m/s. Table 2 shows the improvements in overall heat transfer coefficient reported by Birt et al (2) at different condenser loadings after dropwise condensation had been promoted using three 20 ml injections of a solution of 10% by weight of montan wax in liquid paraffin (light liquid petrolatum).

As shown in Table 2, the results were more marked than those in the first trial due to the greater heat loading per unit surface area in the small condenser.

Values of steam-side coefficient calculated by the method given in Appendix I were in the range 9370-16230 for filmwise condensation. Values for dropwise condensation were in general at least five times greater. Values are not quoted

TABLE 2 - Results for Trial 2 - Heat Transfer Area 3.19 m^2

Condensation mode	Trial No.	Condenser pressure kN/m^2	Steam temperature $^{\circ}\text{C}$	Specific heat flux kW/m^2	Overall htc $\text{W/m}^2\text{k}$
Filmwise	1	32.21	70.6	155.0	3157
	1	40.68	76.2	177.9	3344
	1	50.85	81.7	204.2	3583
	1	61.02	86.4	224.1	3708
	1	67.80	88.9	233.4	3747
	2	32.21	70.6	156.2	3361
	2	40.68	76.2	181.9	3486
	2	50.85	81.7	203.8	3617
	2	61.02	86.4	223.7	3730
	2	67.80	88.9	233.1	3765
Dropwise	5	33.90	71.9	192.5	4236
	5	40.68	76.2	216.0	4474
	5	50.85	81.7	246.0	4616
	5	61.02	86.4	275.0	4906
	5	67.80	88.9	293.7	5082
	6	30.51	69.3	180.2	4077
	6	40.68	76.2	220.6	4366
	6	50.85	81.7	245.1	4548
	6	61.02	86.4	276.2	4866
	6	67.80	88.9	290.9	5122

due to uncertainty about the effects of the steam at high flow rates on the condensate level at the bottom of the condenser.

TRIAL NO.3. - CONDENSER HEAT TRANSFER AREA 21.18 m²

Following the success of Trial No. 2, reproducibility of the results was investigated by Butcher et al (3) in a trial on a larger condenser of a type common to a number of ships. The condenser was that of a 350 kVA auxiliary turbo-generator, having a condensing area of 21.18 m² provided by 632 Kunifer 30 tubes each 12.70 mm, 20 SWG, arranged in four equal tube passes side by side.

The mode of condensation could not be assessed visually because observation ports were not fitted to the shell side of the condenser. The effectiveness of the injected promoter could thus be made only by comparison of overall heat transfer coefficients before and after treatment. Although a total of seventy-three runs were made at different steam loads on the condenser, the results were far less conclusive than those of Trial No. 2. No general improvement followed seven 50 ml injections and one 100 ml injection of fatty acid/liquid paraffin promoter. An additional single injection of 800 ml was required before a significant improvement was shown by an increase in the condenser vacuum under otherwise similar operating conditions. It is noteworthy that the runs were at a generator loading of 400 kW, and coolant inlet temperatures of 20°C. Values of α_{ov} were 3776 W/m²K and 4145 W/m²K for the filmwise and dropwise runs respectively, showing an improvement of some 10%.

TRIAL NO.4. - CONDENSER HEAT TRANSFER AREA 46.45 m²

Because of the uncertainty of inducing dropwise condensation by steam injectable promoters, a thin PTFE coating was applied to the condenser tubes of a 1000 kW turbogenerator set, with the knowledge that dropwise condensation would be assured, and that the thickness of the PTFE coating (2.54×10^{-4} cm) would make a negligible addition to the overall thermal resistance.

The shipboard condenser contained four water passes each of 191 Kunifer 30 (70/30 Cu/Ni) tubes, 15.88 mm od, 1.22 m heat transfer length, supplied with sea water at 5000 l/min, giving a linear velocity of approximately 3.05 m/s. The performance of the condenser was compared with that of a similar condenser with uncoated tubes, at nominal loads of 800 and 1000 kW.

The results obtained by Butcher (4) summarised in Table 3 showed only marginal improvements (< 5%) at each loading, suggesting that the condenser was underloaded due to overdesign. To increase the specific heat flux with the same steam flow rates, tubes were removed from the bottom of each pass of the condenser to reduce the overall heat transfer area from 46.45 to 35.49 m². The summarised results given in Table 3 show no significant improvement, and at 800 kW loading the condenser with the coated tubes performed less satisfactorily than the untreated condenser.

In order to investigate the reason for the disappointing results, some of the coated tubes were examined under laboratory conditions. Fouling was observed on both sides of each tube but that on the steam side - although only some 2.913×10^{-5} (W/m²K)⁻¹ was more significant in that it reduced the quality of the condensation to a mixture of grades from filmwise to part dropwise. The appearance of the deposit was that of a slightly greasy reddish brown powder, suggesting the presence of metal oxides whose hydrophilic nature would explain the change in condensation mode.

TABLE 3 - Comparison of condensers with uncoated & PTFE coated tubes

Heat transfer area - m^2	46.45				35.49							
Coolant inlet temp - $^{\circ}C$	19.4 ± 0.6				18.6 ± 0.3				14.7 ± 0.3			
Nominal load kW	800		1000		800		1000		800		1000	
Tubes coated/ uncoated	U	C	U	C	U	C	U	C	U	C	U	C
Actual load kW	823	823	1003	966	818	822	998	998	813	815	1011	1008
ohfc α_o kW/ m^2K	2629	2754	2814	2904	2794	2695	2734	2805	2689	2648	2720	2862
% difference	+4.75		+3.23		-3.56		+2.60		-1.53		+5.22	

The test condenser had operated for approximately 4000 hours in contrast to the 18000 hours steaming experienced by the reference plant, so it is likely that fouling in the latter would have been at least as severe as that in the former.

After cleaning the sample tubes both externally and internally, their heat transfer performance became comparable with that of a clean reference tube.

The findings of Trials 3 and 4 point to the probability that the erosive effect of steam passing through the turbines at high velocity resulted in contamination of the steam by small quantities of metallic oxides which were subsequently deposited on the condenser tubes. In contrast, steam used in laboratory tests had been raised at a much lower pressure (550 kN/m^2) than the turbine inlet pressures (3200 and 2240 kN/m^2) applicable in Trials 3 and 4 respectively.

TRIAL NO.5. - USE OF EXTENDED SURFACE TUBING

Concurrent with the work on dropwise condensation promoters, a laboratory evaluation of extended surface condenser tubes was undertaken by Birt et al (5).

Low Fin Integron was found to be unsuitable, so the manufacturers (IMI Ltd) developed a form of tube into which a single helical groove was rolled, giving a pitch of some 0.3 cm^{-1} in tubes of 12.70 and 15.88 mm od.

Heat transfer measurements were made using tubes approximately 1 metre long, condensing steam at 101.3 kN/m^2 and 13.56 kN/m^2 absolute pressure at water velocities up to 6.84 m/s . The results of the Wilson (6) method of determining film coefficients of heat transfer are presented in Table 4 which shows the significant improvement in waterside coefficient achieved by the use of Kydensa tubing. Condensers operating at a water velocity of 3.05 m/s will thus show values of α_1 a factor of $10^{0.8}$ ($= 6.3$) greater than those shown in Table 4, giving improvements in overall coefficient of 20-70% under the same condensation conditions.

TABLE 4 - Film coefficients of heat transfer for Kydensa tubing
 Values of α_i and α_o based on tube internal diameter

Tube Type & Diameter (mm)	Condensation mode	Steam at 101.3 kN/m ²		Steam at 13.56 kN/m ²	
		α_i at $u_i = 0.305$ m/s W/m ² K	α_o W/m ² K	α_i at $u_i = 0.305$ m/s W/m ² K	α_o W/m ² K
Plain 12.70	Filmwise	2072	15274	2044	16353
	Dropwise	2072	44402	2044	76653
Kydensa 12.70	Filmwise	5337	18170	4770	20725
	Dropwise	5337	44743	4770	61663
Plain 15.88	Filmwise	2101	17148	1931	18510
	Dropwise	2101	162390	1931	66035
Kydensa 15.88	Filmwise	5337	19703	4088	19192
	Dropwise	5337	45083	4088	42017

To obtain such improvements, increased pumping power was required. The head loss per unit length of tubing was investigated using straight tubes with flow lengths at least 1.5 m between pressure tapings fitted to allow adequate entry length for flow development. The ratio was found to be $0.161 u_i^{1.7}$ for the 12.70 mm diameter tubing, and $0.117 u_i^{1.7}$ for the 15.88 mm plain tubing. The comparable expressions for Kydensa were $0.651 u_i^{2.05}$ and $0.470 u_i^{2.05}$ respectively. An alternative expression for Kydensa tubing has been given by Butcher (7) in the form

$$\phi = 0.0022 \text{ Re}^{0.15} \quad \text{for } 8000 < \text{Re} < 40000,$$

which incorporates the expressions for the two separate tubes with an accuracy of $\pm 3\%$.

At a constant heat flux of 56.79 kW/m² Butcher (7) also obtained expressions

$$\text{St} = 0.071 \phi^{0.5} \text{Pr}^{-0.6} \quad \text{and} \dots\dots\dots (1)$$

$$\text{St} = 0.0032 \text{Re}^{0.08} \text{Pr}^{-0.6} \quad \dots\dots\dots (2)$$

which compared favourably with those given by Davies & Shawki (8) for tubing with a different geometry.

The laboratory work on single tubes was extended by replacing the 632 plain tubes by 512 Kydensa tubes in a condenser of the type described in Trial No. 3. The coolant flow rate was reduced from 2.669 m³/min to 1.864 m³/min, giving an acceptable increase in pumping power necessary for the same thermal performance.

Further work has led to the development of multi-start grooved tubes with smaller indentation depths, showing certain similarities with those described by Newson & Hodgson (9).

CONCLUSIONS

1. The improvements in condensation heat transfer coefficients obtained by the use of drop-wise promoters in laboratory experiments have not been comprehensively realised in trials on full-scale condensers.
2. There is evidence to suggest that hydrophilic steam-borne contaminants can cause a hydrophobic substrate to become wettable, thereby decreasing its effectiveness as a condensing surface.
3. Grooved tubing of the type exemplified by Kydensa give overall heat transfer coefficients at least 30% greater than those shown by plain tubes of the same nominal diameter.
4. The improvements shown with single tubes have been realised in tests on a 350 kW turbogenerator condenser, which required 19% fewer Kydensa tubes to achieve the same thermal performance as that given by plain tubes.

APPENDIX I

Calculation of steamside heat transfer coefficients - Trial 2

Assuming clean tubes, the relationship between film and overall coefficients is:

$$\frac{1}{\alpha_{ov} A_o} = \frac{1}{\alpha_i A_i} + \frac{\Delta R}{\lambda_t A_t} + \frac{1}{\alpha_o A_o} \dots\dots\dots (3)$$

$$\text{giving } \frac{1}{\alpha_o} = \frac{1}{\alpha_{ov}} - \left(\frac{1}{\alpha_i} + \frac{\Delta R}{\lambda_t} \cdot \frac{D_o}{D_i} \right) \dots\dots\dots (4)$$

Values of α_i may be calculated for different coolant conditions from:

$$Nu = 0.023 Re^{0.8} Pr^{0.4} \dots\dots\dots (5)$$

$$\text{giving } \alpha_i = 0.023 \frac{\lambda_w}{D_i} Re^{0.8} Pr^{0.4} \dots\dots\dots (6)$$

Values of α_o were thus calculated using observed values of α_{ov} and the corresponding predicted values of α_i , making due allowance for the changing physical properties of the coolant.

SYMBOLS USED

- A = heat transfer area, m²
 D = diameter - m
 R = radius - m
 ΔR = wall thickness, m

u = velocity - m/s

Greek

α = heat transfer coefficient - W/m^2K

λ = thermal conductivity - W/mK

ϕ = friction factor

Subscripts

i = inside (water)

m = mean

o = outside (steam)

ov = overall

t = tube

w = water

REFERENCES

1. Birt, D.C.P., and Brunt, J.J., 1959, "Condenser trials using dropwise promoters Pt I", AML Report No B/93 (W).
2. Birt, D.C.P., Brunt, J.J., and Honour, C.W., 1961, "Condenser trials using dropwise promoters Pt II", AML Report No A/79 (W).
3. Butcher, D.W., Birt, D.C.P., and Honour, C.W., 1964, "Condenser trials using dropwise promoters Pt III", AML Report No A/86 (W).
4. Butcher, D.W., Unpublished MOD report.
5. Birt, D.C.P., Butcher, D.W., Honour, C.W., and Manson, P., "Laboratory tests on Kydensa and Low Fin Integron condenser tubing", AML Report No B/115 (W).
6. Wilson, E.E., 1915, Trans. ASME 37, 47.
7. Butcher, D.W., 1976, "An assessment of Kydensa tubing for use in steam condensers", MSc Thesis.
8. Davies, J.T., and Shawki, A.M., 1973, The Chemical Engineer 279, 528-532.
9. Newson, I.H., and Hodgson, T.D., 1974, Desalination 14, 291-324.

AIR ENTRAINMENT IN STEAM CONDENSERS

J.G. Andrews, R.T. Deam and J. Smalley *

The physical mechanisms for the transport of air inside steam condensers are by convection, diffusion and entrainment in an air-rich boundary layer adjacent to the condensate. The effect of air entrainment is shown to be significant, provided the condensate film remains continuous. In contrast, air entrainment by detached droplets of condensate is much weaker and it is in such regions that the formation of large air blankets is a potential threat. Experimental measurements of the air entrainment by falling drops support the theory.

INTRODUCTION

It is well established that the accumulation of air in steam condensers can seriously degrade their performance (see, e.g. Rowe and Ferrison (1)). Air leakage are inevitable, due to the low vapour pressure (20-60 mb) of the working fluid (water) at the heat rejection temperatures in power stations. In order to remove the air efficiently it is necessary to understand how the air is transported through the condenser and this requires good modelling of the flow of steam, air and condensate.

Modelling of condensers has been attacked by two radically different approaches. The traditional one has been to study the detailed process of film condensation on an isolated cooled surface such as a vertical plate or cylinder, under both natural and forced convection. The other approach, developed during the last decade with the advent of large computers, has been to treat the condenser as a whole. In this method, the complexity of the tube geometry is grossly simplified by representing the steam condensation in terms of some equivalent 'smeared-out' sink throughout the volume of the condenser, the strength of the sink being deduced from empirical correlations of the local heat transfer rates.

In this paper we show that there is a strong coupling between the air and the falling condensate in a thin boundary layer, irrespective of whether the condensate is attached to a cooled surface. As this effect has been apparently overlooked in the large-scale models, it is of interest to estimate its impact on these models and the possible consequences for future condenser design. We also describe laboratory scale experiments designed to investigate and quantify the magnitude of air entrainment associated with a falling drop of condensate.

* C.E.G.B., Marchwood Engineering Laboratories, Marchwood, Southampton.

BULK MODELS OF CONDENSERSExisting Models

The first global model of a condenser is due to Patankar and Spalding (2). They introduced the idea of the 'porous body model', in which the complex array of condenser tubes is replaced by a 'fictitious' porous medium, with a distributed heat transfer rate and non-linear resistance per unit volume. This has subsequently been developed by a number of workers, notably Davidson (3), Wilkinson and Blackburn (4), Murray (5) and McNaught (6). The physical assumptions in these models are broadly similar, though the numerical methods adopted tend to differ. Davidson favours using a 'control volume' finite difference method, in which the mass and momentum fluxes are conserved within elemental volumes, though others prefer to use finite elements.

The role of the condensate in these global models is ignored, apart from its effect on heat transfer in the inundated parts of the condenser. Also, the transport of air is assumed to be determined solely by convection and diffusion in the body of the steam-air mixture. Boundary layer effects do not arise because the cooling surfaces are not considered. The choice of diffusion coefficient is an important feature, since molecular diffusion alone is apparently too weak to explain air blankets observed in real condensers. To explain the observed size of air blankets, it has been found necessary to employ a turbulent diffusion coefficient, some two orders of magnitude or so greater than that for molecular diffusion. At first sight, since the tubes are tightly packed in modern condensers, the invoking of turbulence does not seem unreasonable. However, for flow over bluff bodies with 'suction' of the vapour by condensation at the surface, the onset of separation of the boundary layer is somewhat suppressed. Hence, the critical Reynolds Number for the onset of turbulence is higher than in the usual situation without suction. In any case, in stagnant regions of the condenser where the formation of air blankets is most likely, we expect the Reynolds Number to be low and it is not obvious that the use of a turbulent diffusion coefficient can be justified.

Effect of Air Entrainment

In the existing models discussed above, there are two mechanisms for transporting air, i.e. by convection with the bulk flow of vapour and by diffusion. In the next section we shall show that air is also transported by the falling condensate. To assess the impact of this effect on the existing models we consider a simple one-dimensional model. The mass transport equations for the steam and air are

$$\frac{d}{dx}(\rho_s u - D \frac{d\rho_s}{dx}) = -\rho C \quad (1)$$

and

$$\frac{d}{dx}(\rho_a u - D \frac{d\rho_a}{dx}) = -\rho S \quad (2)$$

respectively, where ρ = density, u = velocity, D = diffusion coefficient, C

= condensation rate per unit volume and S = sink strength per unit volume for air removal.

Later we discuss the detailed physical mechanism for air entrainment in a boundary layer attached to a condensate surface. We show that air is removed from the bulk at a rate proportional to the air density in the bulk and to the rate of condensation. Hence, in the context of a 'porous body' model, it is appropriate to take S to be of the form

$$S = \lambda C \phi \quad (3)$$

where $\phi = p_a / (p_s + p_a)$ is the air mass fraction; the constant of proportionality will be called the 'air entrainment coefficient'. Adding (1) and (2), assuming that $(p_s + p_a) = \text{constant}$, we obtain

$$\frac{d\phi}{dx} = -C(1 + \lambda\phi) \quad (4)$$

and substituting for p_a and S in (2), we have

$$\frac{d}{dx} \left(\phi u - D \frac{d\phi}{dx} \right) = -\lambda C \phi \quad (5)$$

We neglect the $\lambda\phi$ term in (4) since $\lambda\phi \ll 1$, typically, and the resulting problem is then linear in ϕ .

In the absence of diffusion ($D = 0$), the solution is simply obtained as

$$\frac{\phi}{\phi_0} = (1 - X)^{\lambda-1} \quad (6)$$

where $X = Cx/u_0$ and u_0 is the velocity at the inlet to the condenser, $X=0$. For $0 < \lambda < 1$, the solution blows up at $X=1$, i.e. when the flow stops and all the air has been removed, as shown in Figure 1. When $\lambda=1$ the air fraction is removed in proportion with the steam fraction and the air density is uniform throughout. When $\lambda > 1$ the air density falls.

The inclusion of diffusion produces an air flux in the upstream direction which has the effect of softening the curvature and removing singularities of air density. Thus we impose the boundary conditions

$$\frac{d\phi}{dX} = 0 \quad \text{at} \quad X = 1 \quad (7)$$

and

$$\frac{\phi}{\phi_0} = 1 \quad \text{at} \quad X = 0 \quad (8)$$

The solution is

$$\frac{\phi}{\phi_0} = \frac{Z(a, Pe(1-X))}{Z(a, Pe)} e^{\frac{1}{4}Pe^2 X(2-X)} \quad (9)$$

where

$$Pe = \frac{u_0}{(CD)^{1/2}}, \quad a = \lambda - \frac{1}{2},$$

Pe being the appropriate Peclet No and

$$Z(a, b) = U(a, b)V'(a, 0) - V(a, b)U'(a, 0), \quad (10)$$

where U and V are parabolic cylinder functions. The air mass fraction at $X=1$ has a finite maximum, now that diffusion has been included, given by

$$\frac{\phi_{\max}}{\phi_0} = \frac{\left(\frac{2}{\pi}\right)^{\frac{1}{2}} e^{\frac{1}{4} Pe^2}}{Z(\lambda - \frac{1}{2}, Pe)} \quad (11)$$

Table 1 gives the variation of ϕ_{\max}/ϕ_0 with the air entrainment coefficient, λ , for different values of Pe . Table 2 lists the corresponding variation of the fraction of air removed by air entrainment with λ for various values of Pe . In both tables we note that air removal by entrainment is significant compared with that due to diffusion, even at modest Peclet Numbers. In power station condensers, the Peclet Number is typically of order $10^4 \sim 10^5$, so that the effect of even a very small amount of entrainment is likely to be significant.

TABLE 1 - Variation of (normalised) peak air density, ϕ_{\max}/ϕ_0 , with air entrainment coefficient, λ , and Peclet No. $Pe = u_s/(CD)^{1/2}$, for a 1-D porous body model with air entrainment.

$Pe \backslash \lambda$	0	0.1	0.5	1
1	1.65	1.56	1.26	1
2	7.39	5.04	2.00	1
3	90.0	16.0	2.79	1
5	2.68×10^5	32.9	3.78	1

TABLE 2 - Variation of air fraction removed by air entrainment for a 1-D porous body model

$Pe \backslash \lambda$	0	0.1	0.5	1
1	0	0.14	0.58	1
2	0	0.32	0.78	1
3	0	0.72	0.92	1
5	0	0.96	0.98	1

FACULTY OF ENGINEERING, LIBRARY

THE UNIVERSITY OF MUMBAI

Acc. No. 51. 61284

Call No. 24.24

M3

To be more realistic, we should recognise that the condensation rate effectively vanishes when the air concentration reaches some 'saturation' value. To illustrate this effect, consider the case where the condensation rate is assumed to be step function

$$C = \begin{cases} C_0, & \phi_0 < \phi < 1 \\ 0, & \phi = 1 \end{cases} \quad (12)$$

By inspection of the solution above, for $C = \text{constant}$ throughout the condenser, we can patch (9) in the region $0 < X < 1$ to the trivial solution

$$u = 0, \quad \phi = 1 \quad (X \geq 1) \quad (13)$$

Thus, the condenser is air-blanketed in the region $X \geq 1$, in which no condensation takes place.

From (11) and (13) we put

$$\frac{1}{\phi_0} = \left(\frac{2}{\pi}\right)^{\frac{1}{2}} e^{\frac{1}{2} Pe^{\frac{1}{2}}} / Z(\lambda - \frac{1}{2}, Pe) \quad (14)$$

In principle, given λ , equation (14) fixes Pe and hence relates u_0 and C_0 . Hence, the rate of entrainment controls the position of the air blanket $x = u_0/C_0$ ($X=1$). The assumption of a simple switch-like form for C is reasonable provided $Pe \gg 1$, since the main increase in ϕ occurs in a layer of thickness of $O(Pe^{-1})$ near $X=1$, as shown in Figure 1.

FILM CONDENSATION AND AIR ENTRAINMENT

We have shown that the effect of including an air sink term in the porous body models of whole condensers could be very significant. We will now investigate the physical mechanisms for air entrainment on various condensing surfaces of interest.

The classic theory of film condensation is due to Nusselt (7), in which he derived the heat transfer coefficient from the thickness of the film of falling condensate. Important developments of the Nusselt model have included: The detailed boundary layer solution of the condensate (Sparrow and Gregg, (8) & (9)); the inclusion of the vapour boundary layer (Chen, (10)), and the inclusion of a non-condensable gas such as air (Sparrow and Eckert, (11)). During the last twenty years or so there have been several improvements to models of condensation in the presence of a non-condensable gas, for natural and forced convection, for both plates and cylinders. It should be emphasised that these models apply only to condensate films which are attached to a cooled surface. Also, they focus attention on the effect of air on the heat transfer coefficient and tend not to calculate explicitly the amount of air entrainment within the boundary layer.

When a vapour is drawn towards a condensing surface, non-condensables will be carried along with the vapour and concentrate in a thin boundary layer adjacent to the condensate. Some air will diffuse out of the boundary layer back into the free stream, but the remainder will flow in a

direction parallel to the condensing surface due to viscous shear forces set up by the moving condensate. Also, since air is more dense than steam, buoyancy forces will enhance the downward flow of air. Hence, air will accumulate along the boundary layer and reach a maximum in the regions where the condensate detaches from the cooled surface. In the steady state, the rate at which air is removed must equal the rate at which air arrives over the entire surface, less that which diffuses back into the free stream

When condensate detaches from the cooled surface it will still be cooler than the surrounding vapour and continue to condense vapour. However, the total amount of heat removed by 'detached condensate' will be small compared with that removed through the condensate film attached to the cooled surface. Nonetheless, the condensation rate per unit area will be comparable with that for the 'attached condensate', at least for some period of time, so that detached condensate will tend to sustain an air-rich atmosphere close to its surface due to the persistence of vapour suction. The timescale for this process to be effective depends on the size of the detached condensate and its speed relative to the surrounding vapour. In practical condensers (in which the inter-tube spacing is of the same order as the tube diameter) the issue is whether the air atmosphere remains attached to the falling condensate up to the point when the condensate strikes another tube and the whole process can be renewed. To get an estimate of the size of the air entrainment coefficient, λ , and the relevant timescales, we now consider the detailed air entrainment processes for (a) a condensate film attached to various simple cooled surfaces, (b) a continuous jet of detached condensate and (c) an isolated droplet of detached condensate.

CONDENSATE ATTACHED TO A COOLED SURFACE

A suitable definition of the air entrainment coefficient, λ , which can be directly related to that used in the fictitious porous body model already described is

$$\lambda = \frac{\dot{m}_a}{\phi_a \dot{m}} \quad (15)$$

where $\phi_a = \rho_a/\rho$ is the mass fraction of air in the body of the mixture, \dot{m} is the mass condensation rate and \dot{m}_a is the mass flux of air flowing into the viscous boundary layer adjacent to the falling condensate. Note, that the thickness of the concentration boundary layer, d , is always greater than that of the viscous boundary layer Δ (Schlichting (12)). Note that \dot{m}_a represents the net mass flux of air entering the viscous boundary layer, which is not transported back into the bulk flow.

Forced Convection Past a Flat Plate

There have been several attempts to model the forced convection of a mixture of condensing and non-condensing gases past a flat plate. We concentrate on the paper by Sparrow et al. (13) (where references to other models can be found), because their analytical treatment in terms of

similarity variables and dimensionless groups is easily manipulated to obtain the air entrainment coefficient. Their primary interest was in the effect of non-condensing gases on the heat transfer coefficient. By contrast, we are more concerned with the entrained air flow, which they do not explicitly calculate. We have used their results, to determine the air entrainment coefficient, λ . We found that as the 'driving force' tends to zero, i.e. condensation disappears, the air becomes entrained in a conventional viscous boundary layer and λ , as defined, blows up. For large values of the 'driving force' the suction effect destroys the outward diffusive flux and $\lambda \rightarrow 1$. For steam with a Schmidt No. $Sc = 0.55$, λ has a minimum value of $\lambda = 0.61$ at a 'driving force' of about 17, though this point will be out of the range of conditions inside a power station condenser. Typically, however, we can assert that the air entrainment coefficient for a flat plate in forced convection is of order unity, so that the ratio of the rates of removal of air and steam is comparable with the air mass fraction in the bulk.

Natural Convection Past a Vertical Plate

We now consider natural convection past a vertical plate. In this case the condensate falls due to gravity and there is also a buoyancy force in the gas-vapour boundary layer due to a variation of the air density in the vertical direction. A similarity solution of this problem along the same lines as in (13) has been obtained by Sparrow and Lin (14). Using their results, we calculated in all cases that λ is of order unity, the variation with 'driving force' being noticeably less than that for forced convection. Thus the ratio of the rate of air removal by entrainment to that of vapour removal by condensation is of the same order as the ratio of their concentrations in the bulk.

Condensation on a Cylinder

It is well known that flow separation occurs for flow around a cylinder, even at moderate Reynolds' numbers. However, when suction (due to condensation) is present the onset of separation is delayed (e.g. (12)). According to Prandtl (15), separation is completely suppressed if there is a uniform radially inward 'suction velocity', u_r , such that

$$u_r > 4.33 u_\infty / Re^{1/2} \quad (16)$$

In practice, of course, the suction velocity varies around the cylinder and the complete two-dimensional boundary layer solution must be found. Fujii (16) has analysed the case of separated flow of a condensing vapour over a cylinder at large Reynolds' numbers, which is relevant in the strong vapour shear part of a condenser where the incoming vapour stream meets the first few rows of tubes. In the body of a condenser, where the crossflow velocity is much reduced, it is possible that separation is significantly suppressed. Unfortunately, this important regime does not appear to have been considered to date and we are restricted to considering approximate models.

Let us first examine the case of . radially-symmetric condensation on a cylinder in an air-steam mixture, where the effects of cross-flow and gravity are ignored. The solution for the steady-state density distribution is simply

$$\frac{\phi}{\phi_c} = \left(\frac{r_c}{r}\right)^{Pe} \quad (17)$$

The Peclet No, Pe is given by $Pe = r_c \dot{m} / \rho D$, where \dot{m} is the mass condensation rate per unit area and r_c is the radius of the tube. (We note, in passing, that the steady-state breaks down as $r_c \rightarrow \infty$).

The effect of gravity is to make the film thickness on the underside of a cylinder much greater than that on the top. Hence, the radial in-flow speed (and the associated Peclet No.) will vary substantially around a tube. To get a rough idea of the variation, we considered the results obtained in reference (9) for the natural convection condensation on a horizontal axis cylinder. However, given a more detailed model of condensation on a cylinder in the presence of air, we expect the variation to be even greater because the accumulation of air underneath the tube further reduces the heat transfer. The modelling at the bottom of the tube ($\theta = 180^\circ$), is clearly unrealistic since the condensate detachment mechanisms tend to preclude the stability of a thin sheet. In practice, three-dimensional effects become important and the condensate runs along the tube either to a tube support plate or to some point where it detaches as a continuous stream or as an intermittent drip. These mechanisms are discussed in the next section.

Another important effect in a real condenser is the possibility of 'air-bridging' between adjacent tubes. That is, the air boundary layer on the underside of a tube might merge with the tube below it, thereby providing a continuous pathway for air to be 'entrained' in a downward flow of condensate (see Figure 2). Condensate drips from the underside of one tube at point A and strikes the tube beneath at point B. Air is transported around the upper tube by viscous shear forces in the air/vapour boundary layer, by the same processes as those described for a flat plate. Air accumulates at A and, even if only a small fraction of air is transported by the droplets, we can expect some air to be drawn towards B since the vapour suction on the topside of the lower tube is much larger there than that towards the underside of the upper tube. Thus air can be transported downwards through a vertical tube bank provided that at least a small amount of condensation exists. Clearly, if condensation stops altogether then this mechanism ceases and an air blanket develops, surrounding several tubes.

AIR ENTRAINMENT OF DETACHED CONDENSATE

We now continue the argument to condensation on detached condensate. As mentioned already, we dismiss the possibility of detachment in the form of a continuous two-dimensional sheet, on the grounds of hydrodynamic stability. Instead, the condensate on a cooled surface will tend to accumulate and detach in the form of isolated droplets or as a continuous jet. In general, the detached condensate will be subcooled relative to the surrounding vapour and condensation will persist.

Continuous Jet

We consider first the case of a continuous jet of subcooled condensate. The argument applies up to the point where the jet breaks up due to the Rayleigh instability (Rayleigh, (17); Curry and Portig, (18)). The jet is simply a continuous extension of the condensate on the cooled surface and air in the boundary layer in contact with the moving condensate will be continuously dragged by viscous shear forces. For consistency, we keep our previous notion of entrainment, i.e. the entrained air is that confined to the viscous boundary layer, i.e. we do not include that which diffuses into the (outer) concentration boundary layer since this region is more susceptible to fluctuating aerodynamic forces in the free stream. Now, according to the standard boundary layer concepts outlined in (12), the ratio of the thickness of the viscous boundary layer, Δ , to that of the concentration boundary layer, d , is $O(Sc)$ if suction (i.e. condensation) is significant but $O(Sc^{1/2})$ without suction. Since $Sc=O(1)$ for steam/air mixtures, the numerical difference between the two ratios is only slight. From our examination of entrainment on a flat plate in both natural and forced convection, we found that the ratios Δ/d , and the entrainment coefficient, λ , were indeed of order unity. These two problems are qualitatively similar to the present problem of a detached jet and we therefore expect similar results for the entrainment coefficient. We conclude that the continuous jet is an efficient means of transporting air from a cooled surface. The precise details of the process are not considered here. When the jet finally breaks up, either due to Rayleigh instability or impact with another surface, it becomes necessary to consider isolated droplets. Heating of the jet (and, hence, loss of suction) will typically be negligible in practical condensers.

Spherical Droplet

The fluid mechanics for the removal of condensate from a condensing surface is a complicated interaction between non-linear capillary waves, which we do not attempt to consider here. It is important to recognise that there will be large internal motions within the droplet as it breaks away from the condensate film. We therefore expect it to be well-mixed and sub-cooled. Condensation will thus be enhanced for a short period of time, during which an air-rich atmosphere will cling to the droplet, the air being gathered from the local region through which the droplet is falling.

For simplicity we assume radial symmetry, so that the convective diffusion equation for the air is

$$\frac{D}{r^2} \frac{\partial}{\partial r} \left(r^2 \frac{\partial \phi}{\partial r} \right) = \frac{\partial \phi}{\partial t} + u \frac{\partial \phi}{\partial r} \quad (18)$$

By mass continuity

$$u = - \dot{M} / 4\pi r^2 \rho \quad (19)$$

where \dot{M} is the total mass condensation rate. Normalising

$$\zeta = \frac{r}{r_s}, \quad \tau = \frac{Dt}{r_s^2}, \quad Pe = \frac{\dot{M}}{4\pi D_P r_s}, \quad (20)$$

where r_s is the radius of the droplet, (18) becomes

$$\phi_{\zeta\zeta} + \left(\frac{2}{\zeta} + \frac{Pe}{\zeta^2} \right) \phi_{\zeta} = \phi_{\tau} \quad (21)$$

where the subscripts denote partial differentiation. At large distances, $\phi \rightarrow \phi_{\infty}$ as $\zeta \rightarrow \infty$. At the surface of the droplet, $\zeta = 1$, the net transfer of air is zero, so that

$$\phi_{\zeta} + Pe \cdot \phi = 0 \quad \text{on} \quad \zeta = 1. \quad (22)$$

In the steady-state with $Pe = \text{constant}$ and $\partial/\partial\tau = 0$, the solution is

$$\frac{\phi}{\phi_{\infty}} = e^{\frac{Pe}{\zeta}}. \quad (23)$$

The extra fraction of air surrounding the droplet is

$$\int_1^{\infty} (\phi - \phi_{\infty}) 4\pi \zeta^2 d\zeta,$$

which blows up as $\zeta \rightarrow \infty$. Thus, the 'potential' amount of air which a droplet can entrain is arbitrarily large. In practice, the particle will be exposed to an air-rich region near the cooled surface of the condenser for only a finite time and the mass condensation rate, \dot{M} , will diminish as the droplet heats up. However, since we anticipate the mixing to be efficient within the droplet, the thermal inertia will be large and the rate of temperature rise will be small. Thus, the timescale for heating will be large compared with the lifetime of a droplet before it collides with some other surface. The assumption of constant \dot{M} (and hence Pe) therefore seems reasonable in solving equation (21).

From our steady-solution, it is useful to introduce the (non-dimensional) e-folding thickness, δ_a , of the enhanced air fraction, $\phi - \phi_{\infty}$, given by

$$\delta_a = \frac{Pe}{\ln\{1 + (e^{Pe} - 1)/e\}} - 1 \quad (24)$$

For $Pe \ll 1$,

$$\delta_a \approx e - 1 \approx 1.7 \quad (25)$$

and for $Pe \gg 1$,

$$\delta_a \approx \frac{1}{Pe}. \quad (26)$$

The total mass of air inside the boundary layer, M_a , can be written in the form

$$M_a = \frac{4}{3} \pi r_s^3 \rho_{\infty} \chi(Pe) \quad (27)$$

where $\rho_{\infty} = \rho \phi_{\infty}$ is the air density in the bulk of the air-vapour mixture and $\chi(Pe)$ is the ratio of the volume of air removed to the volume of the

droplet, given by

$$\chi(P_e) = 3 \int_1^{1+\delta_a} \zeta^2 e^{\frac{P_e}{\zeta}} d\zeta \quad (28)$$

The ratio for the excess air entrained, which was measured in experiments, is given by

$$\chi'(P_e) = 3 \int_1^{1+\delta_a} \zeta^2 \left[e^{\frac{P_e}{\zeta}} - 1 \right] d\zeta = \chi - \left[(1+\delta_a)^3 - 1 \right] \quad (29)$$

which is readily computed. For $Pe \ll 1$, we have

$$\chi \approx 19 - 9.5 Pe, \quad \chi' \approx 9.6 Pe$$

and for $Pe \gg 1$, we have

$$\chi = 3 e^{P_e/P_e}, \quad \chi' \approx \chi \quad (30)$$

The variation of χ and χ' with Pe for $0 < Pe < 5$ is given in Figure 3, which exhibits a minimum of $\chi_{min} \approx 14$ at $Pe \approx 1.2$. Thus, the droplet has the capacity to attract a volume of air many times its own volume. At large values of Pe (i.e. strong suction), this air is concentrated inside a thin boundary layer, of thickness a/Pe , where a is the radius of the droplet. For as long as strong suction persists, such a boundary layer could be expected to remain largely intact.

In practice, a freshly created droplet will be exposed to the air-rich region surrounding the condenser tube for only a finite time interval, so the interest is in how much air will have been attracted during that period. We restrict our attention to the case where $Pe \ll 1$. By inspection of equation (21), we observe that the boundary layer establishes a thickness of $O(Pe^{-1})$ in a timescale of $O(Pe^{-2})$. Hence, provided the droplet is exposed to the air-rich mixture in the gas-vapour boundary layer surrounding the condenser tube for a timescale which is significantly larger than $O(Pe^{-2})$, then we can expect our steady-state solution to be appropriate. For example, taking $r \approx 3$ mm, $D \approx 5 \times 10^{-6}$ m/s, we would require $Pe^2 \delta_v^2 \gg 1$, where δ_v (mm) is the thickness of the air-vapour boundary layer surrounding the tube.

To estimate a lower bound on Pe , we employ equation (23) at $\zeta=1$ to give

$$Pe = \ln(\phi_i / \phi_\infty) \quad (31)$$

In principle, given the pressure and the subcooling of the droplet, it is possible to calculate ϕ_i from the steam tables. Typically, ϕ_i / ϕ_∞ varies from around 10^1 to 10^3 , so that Pe varies from about 2 to 7. From Figure 3 and equation (30), we then find that the 'air enhancement factor', χ , varies from about 15 to 500.

It is then more pertinent to calculate the air entrainment coefficient, λ , for an isolated droplet leaving a condensing surface. From equations (15) and (27), we have

$$\lambda \approx \frac{P_{as} \chi}{\phi_\infty \rho_L}$$

where $\rho_{a,b}$ is the air density in the bulk of the air blanket, ρ_L is the density of water and $\phi_{a,b} = \rho_{a,b}/\rho$ is the air mass fraction in the bulk of the air/steam mixture. Substituting for $\phi_{a,b}$, we have

$$\lambda = \frac{\rho_{a,b}}{\rho_{a,\infty}} \frac{\rho}{\rho_L} \chi \quad (32)$$

Typically, $\rho_{a,b}/\rho_{a,\infty} = O(10^1)$, $\rho/\rho_L = O(10^{-5})$ and $\chi = O(10^1 - 10^2)$, so that $\lambda = O(10^{-3} - 10^{-2})$. Hence, the air entrainment coefficient for a detached droplet falling from a cooled surface is two or three orders of magnitude lower than that on the cooled surface itself. Preliminary measurements (discussed below) using a mass spectrometer in a single tube condensation experiment with air present, confirm the order of magnitude of this prediction. Nonetheless, in a bank of tubes immersed in a large air blanket, the size of the blanket may be controlled by the rate at which droplets fall through the region.

EXPERIMENTAL ARRANGEMENT

Boiler/Condenser

In an attempt to retain simplicity the experiment was contained in a single vessel, Figure 4. This consisted of a stainless steel boiler section containing 3 x 2.75 kW heating elements, controlled by Variacs to heat de-ionised water. This was covered by a lid through which 3 chimneys fed steam into the condenser region above, and consisted of a 300 mm dia x 350 mm high QVF glass cylinder fitted with sidearms. Two diametrically opposed sidearms were used to seal a 0.5 metre length of 1" diameter bronze condenser tube. This was slightly bowed in order to concentrate the returning condensate to a single dripping point. The condenser tube was fed with cooling water at 0.15 l/s from the water mains at a temperature of between 8 and 10°C.

The vessel was operated at reduced pressure by evacuating through either one of two 15 mm dia pumping pipes fitted through gland seals in the base of the boiler. One of these terminated under the condensate drip in a catcher volume of 31 mm dia and 80 mm height. The other pumping pipe terminated in a similar sized tube but was located at the same height as the catcher volume (to avoid stratification effects), also underneath the condenser tube but displaced such that it was pumping from the 'space' away from the falling condensate. The measured volumetric pumping speed of either of these pipes was 0.77 litres per second.

Instrumentation

The lid was provided with penetrations to enable the total pressure to be measured with a capsule gauge and the temperature with chromel-alumel thermocouples whose position within the vessel could be adjusted. Gas could be admitted through a control valve and metered by a flow gauge.

Another sidearm was positioned at right angles to the tube to enable a moveable probe to be inserted and adjusted to sample the atmosphere close to the falling droplet. Two other gas probes were positioned above the space pumping tube and the catcher volume so that the probes could be moved vertically either just inside or just outside the respective volumes. These probes (1.9 mm bore x 1.5 m long) heated to prevent condensation, sampled the steam/gas mixture for measurement in a Q7 Quadrupole mass spectrometer (MS) using inlet techniques previously described by Bloomer and Smalley (19) to ensure the rapid but undistorted introduction of gas mixtures.

The walls of the condenser were heated by means of thermal tapes to prevent condensation on the walls. Freedom from air inleakage was demonstrated by monitoring the air partial pressure after isolating the vessel from the pumps for a long period. Typically this would only rise by 1 or 2 mbar overnight - negligible for the duration of a series of measurements.

MEASUREMENTS AND RESULTS

In operation a steady stream of droplets was obtained within a few minutes of starting the cooling water flow. After the tube had wetted, condensate flowed to the lowest point where the droplets detached and fell into the catcher volume at a rate depending on air pressure and steam temperature.

Steam/Gas Concentration (Air Blankets)

Vertical scans were carried out to measure the concentration gradient adjacent to the catcher volume and the space volume. The subscripts P_1 , P_2 denote the pressures measured by probes 1 and 2 in the space and catcher planes respectively and the subscripts s and v denote which pumping pipe was being employed. Thus P_{2s} is the pressure at the catcher volume when being pumped through the 'space' pumping pipe etc. Figure 5 shows a plot of the air concentration (in terms of the MS ion current) as a function of height above the base of the condenser. The position of the condenser tube and the pumping levels are indicated. The latter was arrived at after preliminary measurements had established the extent of the blanket to ensure that the pumping pipe was not immersed in the blanket and thus distorting it by pumping air away directly. The cooling water flow in all cases was 0.15 l/s.

Air Entrainment Measurements in Falling Droplet

Before the series of measurements was commenced the boiler was adjusted to the required temperature and allowed to stabilise with the cooling water flowing in the condenser tube. A steady drip rate was quickly established which depended on the boiler temperature and the air concentration. The latter could be ascertained from the measured air flow rate and pumping speed.

After steady conditions had been established the horizontal probe was adjusted to a position close to the line of fall of the droplets (2-3 mm). With the mass spectrometer tuned to the $m/e = 28$ peak (nitrogen being representative of air) a steady pulsation was noted. The frequency of increase of air pressure coincided with the dripping rate, although retarded by the delay time in the probe (about 2 secs). Figure 6 shows three sections of chart illustrating:

- The probe in front of the drop showing rise in pressure,
- the probe behind the drop showing a fall in pressure in the blanket as air is drawn towards the drop,
- the vertical probe positioned at the base of the condenser close to the falling drop showing the rise in pressure as the air is released on impact of the drop. (N.B. the sensitivity is not the same for all traces).

For Figure 6c the drop was allowed to fall to the base of the condenser. When, however, it fell into the catcher volume the air associated with a single drop could be quantified by measuring the increase in air peak height over the background. The product of this quantity and a representative volume is then a measure of the entrained air. Probing measurements showed that the pulse height decreased as the probe was raised from the bottom of the volume towards the open top but a reasonable estimate of the excess air is obtained when the probe is positioned 50 mm into the catcher and the volume is taken as 50 ml. From a calibration relating the MS ion current to air partial pressure the pressure increase can be deduced and the quantity of air entrained per drop estimated and hence the equivalent mass evaluated from the density. Table 3 shows a typical set of results for a range of air throughputs.

TABLE 3 - Typical Results with Water Drops

Boiler Temp. °C	Total Pressure mb	Air Throughput mbar s	Drip Rate s	Entrained Air mbar l/drop*
26	31	0.5	0.49	7.4×10^{-3}
25	31	0.82	0.52	5.23×10^{-3}
25	28.5	1.5	0.38	1.1×10^{-3}
25.2	29	2.0	0.30	1.0×10^{-2}
25.9	29.5	3.0	0.26	1.5×10^{-2}
25.8	30.5	4.0	0.20	6.1×10^{-3}
25.8	31.2	6.0	0.16	7.5×10^{-3}
26	36	8.5	0.17	1.3×10^{-2}

* $1 \text{ mbar l} \equiv 1.2 \times 10^{-3} \text{ gm air at } 20^\circ\text{C}$

The excess air entrained, χ' , is given by

$$\chi' = \frac{m_a}{m_d} \frac{RT}{M_a P_a} P_L$$

where m_a and m_d are the mass of air and droplet respectively, R is the universal gas constant, T , the absolute temperature, M_a the molecular weight of air, P_a the air partial pressure outside the air blanket and ρ_l the density of the liquid. In practice P_a was taken to be the equilibrium pressure for an air throughput, \dot{Q}_a , being pumped at a rate S_p (measured to be 0.77 l s^{-1}).

This experimental method can measure only the excess air entrained, χ' , rather than the total air entrained, χ . The experimental values of χ' have been calculated and are shown, together with those obtained from several other runs, in Figures 7, as a function of the air throughput.

Air Entrainment at a Continuous Jet

The analysis showed that the effect of entrainment by a continuous jet should be much greater than that for detached droplets. In an attempt to simulate this experimentally a straight 1 mm wire was attached to the condenser tube with the free end in the catcher volume. Now the condensate ran down the wire, still in discrete droplets but the wire was wetted and a continuous flow of water was observed, even between droplets. No pulses of air were seen in the catcher volume, P_{2s} , as in the case of the falling droplets. A comparison of the air partial pressures at P_a and P_v showed the difference to be much less than for the free droplet case. However, no way was found of estimating the flow of entrained air.

DISCUSSION

In this section we tentatively discuss the significance of these results on power station condensers, indicating areas where further work is needed and speculate on improvements in design.

Experimentally it has been found that the ratio of entrainment for detached droplets (the product of entrained air/drop and drip rate, Table 3) is almost constant at $3 \times 10^{-3} \text{ mbar l s}^{-1}$ over the range of air flows studied. The excess air entrained (χ') decreases however with the air throughput as shown in Figure 7. If the Peclet number, Pe , is expressed as the logarithm of the ratio of the local air fraction to that at infinity, equation (31), then it can be estimated from measurements of the air blanket like Figure 5. If this is done for the two air throughputs measured $Pe = 1.6$ and 0.7 are obtained. Corresponding theoretical values of χ' are 10 and 5 which compare with the experimental values of about 20 and 7 and are in remarkably good agreement considering theoretical assumptions made and the limitations of the experimental techniques.

Theoretically, we have found that air entrainment in a thin boundary layer next to the falling condensate is a powerful effect provided the condensate stream remains continuous, but in an isolated droplet the effective rate of entrainment is comparatively low. Also if falling condensate collides with another condenser tube, say, it may be broken up into a spray of small droplets. The vapour pressure associated with a

small droplet can be significantly higher than that on a plane surface. The relationship between the enhanced vapour pressure, p^* , and the equilibrium radius, r_s , is given by Kelvin's formula (Mason, (20)).

$$\ln \left(\frac{p^*}{p_\infty} \right) = \frac{2M\sigma}{p_\infty R T r_s}$$

where p_∞ is the equilibrium vapour pressure (at temperature T) over a plane surface, σ is the specific surface energy of the liquid/vapour interface, ρ_L is the density of the liquid, M is the molecular weight of the liquid and R is the universal gas constant. In a region of locally high evaporation the air concentration will be correspondingly lower than 'normal', so air is effectively de-entrained from the small droplets. However, a fraction of the vapour will recondense on the lower cooled surface and air will again be entrained by the air/vapour boundary layer. The mechanisms of de-entrainment and recondensation are beyond the scope of the present study but are clearly relevant in a multitube power station condenser. Even so, we can still infer that the process will lead to a general downward flow of air through a tube bank. This is also true in the 'air bridging' regime (Figure 2), and that where a continuous stream of condensate links successive tubes, which is likely to be the case in the lower inundated tubes. Thus the trend is still for air to be transported downwards through the tube bank.

On the other hand, it is still feasible for an isolated air blanket to arise in the body of a bank of condenser tubes if there is insufficient condensate falling through the region from the tubes above. One possible remedy would be to inject a stream of cold water through the affected region in order to entrain air and reduce the overall dimensions of the air blanket. The power required to pump the water to a suitable point above the air blanket would normally be much less than the power lost due to inefficient condensation in the air blanket.

The broad picture emerging from our discussion is that the present design of condensers may be improved from the point of view of air removal by condensate. The indiscriminate nature of condensate dripping from horizontal condenser tubes, the problems of de-entrainment, due to splashing, and the fact that the amount of air entrainment is very sensitive to whether condensate falls as isolated droplets or as continuous streams, makes condensers prone to instability and the siting of air suction ports a hit-and-miss affair.

An alternative design philosophy, if the condensate entrainment mechanism is found to be significant in practice, would be to attempt to ensure that condensate remains intact on cooled surfaces, so that the air flow would largely follow the condensate. For example, if the tubes were inclined or even vertical, rather than horizontal, then condensate would be more likely to run to the end of tubes instead of dripping at random points along their length. The condensate streams could be channelled into conduits, with minimal splashing or turbulence, from which the air could be extracted with reasonable efficiency. The measurements reported in reference (1) of the distribution of steam and cooling water temperature in a power station condenser exhibited a strong periodic variation with the positions of the sagging plates (see Figure 8, which is from Rowe and Ferrison's paper). That the plate might have been wetted by falling condensate and shrouded by an air-rich boundary layer seems to be a

plausible explanation and is circumstantial evidence that air may be transportable in the way suggested.

The overall pressure drop and heat transfer correlations for banks of vertical tubes are not significantly different from those for horizontal tubes. In general, however, the air transport properties of vertical tubes (with their more continuous condensate films) would appear to be better than those of horizontal tubes. Experiments are needed to confirm these ideas for the various ranges of conditions, which can exist in a large condenser. Also, the manufacturing and maintenance aspects of vertical versus horizontal designs would need to be examined for a global cost-benefit assessment.

CONCLUSIONS

The transport of air through a steam condenser is not solely determined by the convective motion and diffusion of vapour in the bulk of the flow. A theoretical analysis indicates that a significant proportion of air is entrained in an air-rich boundary layer attached to the flowing condensate, the air being dragged along with the condensate by viscous shear forces in the boundary layer, and that the effect should not be ignored in global condenser models. Provided the condensate film remains continuous, the boundary layer will also remain continuous, favouring the transport of a significant fraction of air along with the condensate. Provided this effect is validated experimentally, it could be exploited practically by designing the condenser in such a way that condensate films remain intact, so that air can be guided into convenient air removal ports. However, if the condensate detaches from the tubes in the form of droplets, the net removal of air is dramatically reduced. Air will be 'de-entrained' from the spray of fine droplets formed when condensate strikes other tubes though some of the de-entrained air will be re-entrained on the next tube and so on. A possible palliative for existing designs which suffer from air blanketing might be to inject a stream of water (from the hot-well, say), into the air blanket. Experiments are needed to test these ideas and the associated practical problems must be evaluated.

ACKNOWLEDGEMENTS

The authors wish to record their appreciation for discussions with various colleagues, notably Mr. R.N. Bloomer, Dr. B.J. Davidson, Mr. J.A. Ferrison, Dr. M. Rows. This paper is published by permission of the Central Electricity Generating Board.

REFERENCES

1. ROWE, M. & FERRISON, J.A., 1975, 'Air removal problems in condensers', Symposium on Steam Condenser Performance, CERL, Leatherhead, England.
2. PATANKAR, S.V. & SPALDING, D.B., 1974, 'A calculation procedure for the transient and steady-state behaviour of shell-and-tube heat exchangers', In Afgan, N. & Schlunder, E.V. (Eds), 'Heat Exchanger -

Design and Theory Sourcebook', 155-176, Scripta Book Co., Washington, DC, USA.

3. DAVIDSON, B.J., 1975, 'Condenser Performance assessment by computer', Symposium on Steam Condenser Performance, CERL, Leatherhead, England.
4. WILKINSON, T.S. & BLACKBURN, W.S., 1976, 'A finite element method for calculating the distribution of air in power station condensers', R & D Publication No 26, C.A. Parsons & Co. Ltd., Newcastle-upon-Tyne.
5. MURRAY, W.L., 1979, 'Numerical solutions of the diffusion-convection equation in steam condenser flow modelling', Int. Conf. Numerical methods in Thermal Problems, Swansea, University of Wales, Wales.
6. McNAUGHT, J.M., 1981, 'Finite element methods in the simulation of power condensers', HTFS Research Symposium, Harwell, England.
7. NUSSELT, W., 1916, 'Die Oberflächenkondensation des Wasserdampfes', Z. ver.deut. Ing., 60, 541-580.
8. SPARROW, E.M. & GREGG, J.L., 1959, 'A boundary layer treatment of laminar film condensation', J.Heat Transfer (Trans. ASME), 81C, 13-18.
9. SPARROW, E.M. & GREGG, J.L., 1959, 'Laminar condensation heat transfer on a horizontal cylinder', J. Heat Transfer (Trans. ASME), 81C, 291-296.
10. CHEN, M.M., 1961, 'An analytical study of laminar film condensation; Part 2 - Single and multiple horizontal tubes', A.I.Ch.E Journal, 7, 473-477
11. SPARROW, E.M. & ECKERT, E.R.G., 1961, 'Effects of superheated vapour and non-condensable gases on laminar film condensation', A.I.Ch.E. Journal, 7, 473-477.
12. SCHLICHTING, H., 1960, 'Boundary Layer Theory' (4th Edition), McGraw-Hill, New York.
13. SPARROW, E.M., MINKOWICZ, W.J. & SADDY, M., 1967, 'Forced convection condensation in the presence of non-condensables and interfacial resistance', Int. J. Heat Mass Transfer, 10, 1829-1845.
14. SPARROW, E.M. & LIN, S.H. 1964, 'Condensation heat transfer in the presence of a non-condensable gas', J.Heat Transfer (Trans. ASME), 86C, 430-436.
15. PRANDTL, L., 1935, 'The mechanics of viscous fluids', In Durand, W.F., 'Aerodynamic Theory', 3, 34-208, Springer, Berlin.
16. FUJII, T., 1981, 'Vapour shear and condensate inundation: an overview', Power Condenser Heat Transfer Technology (Proc. Monterey Workshop), 193-223.
17. RAYLEIGH, J.W.S., 1878, 'On the instability of jets', Proc. London Math. Soc. 10, 4-13.

18. CURRY, S.A. & PORTIG, H., 1977, 'Scale model of an ink jet', IBM J. Res. Develop., 21, 10-20.
19. BLOOMER, R.N. & SMALLEY, J., 1972, CEGB Laboratory Note R/M/H653.
20. MASON, B.J., 1971, 'The physics of clouds' (2nd Edn), Clarendon, Oxford.

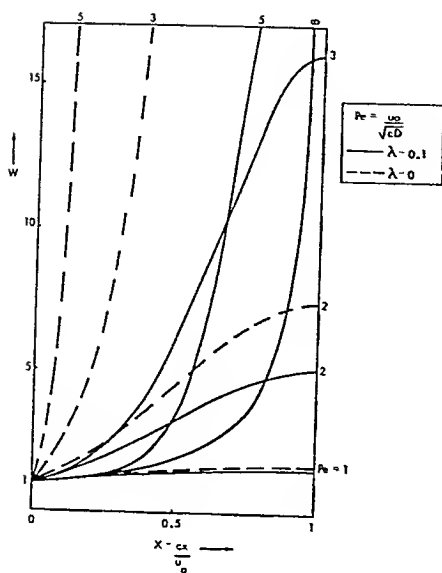


Figure 1 Variation of air density with position for $\lambda = 0$ and $\lambda = 0.1$.

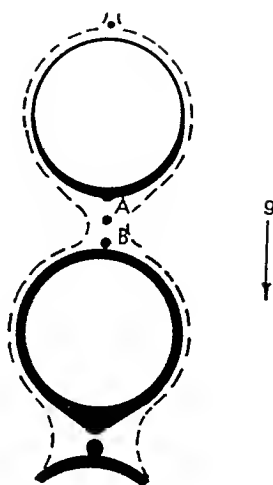


Figure 2 Bridging of air blanket between adjacent vertical tubes.

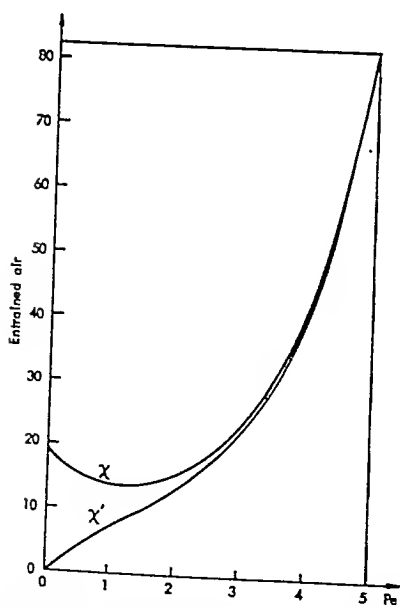


Figure 3 Variation of air enhancement factors λ and λ' with Pe .

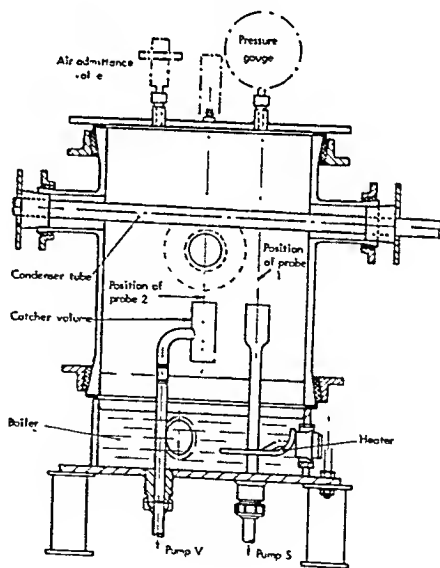


Figure 4 Diagram of apparatus.

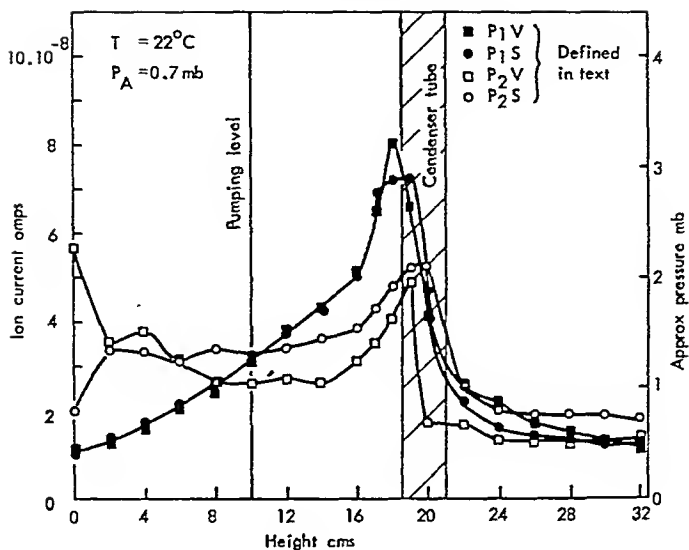


Figure 5 Measured concentration profiles of air.

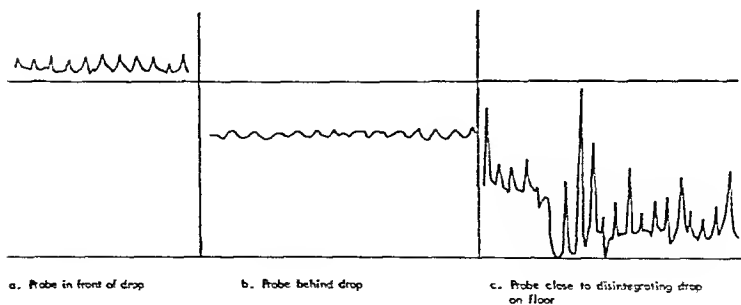


Figure 6 Measured variation of air concentration with time for passing droplets.

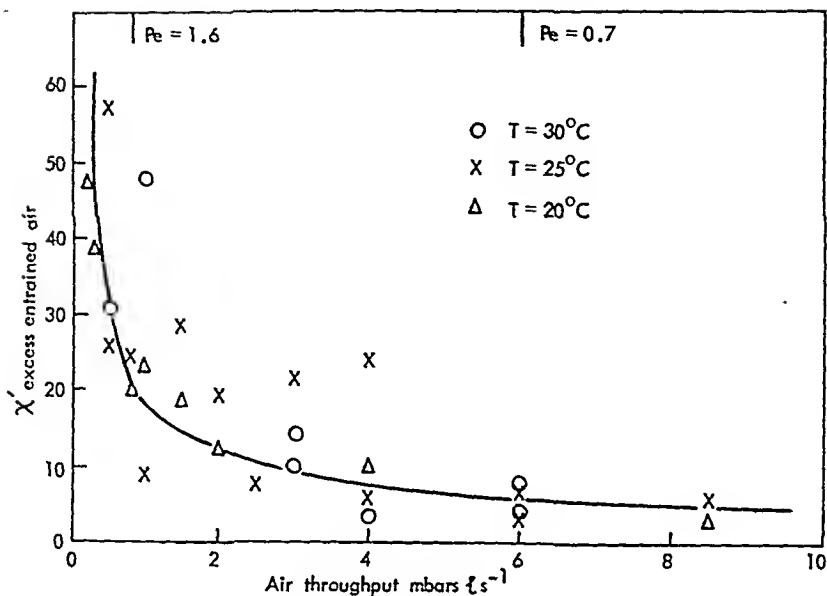


Figure 7 Variation of excess air enhancement (X') with air throughput.

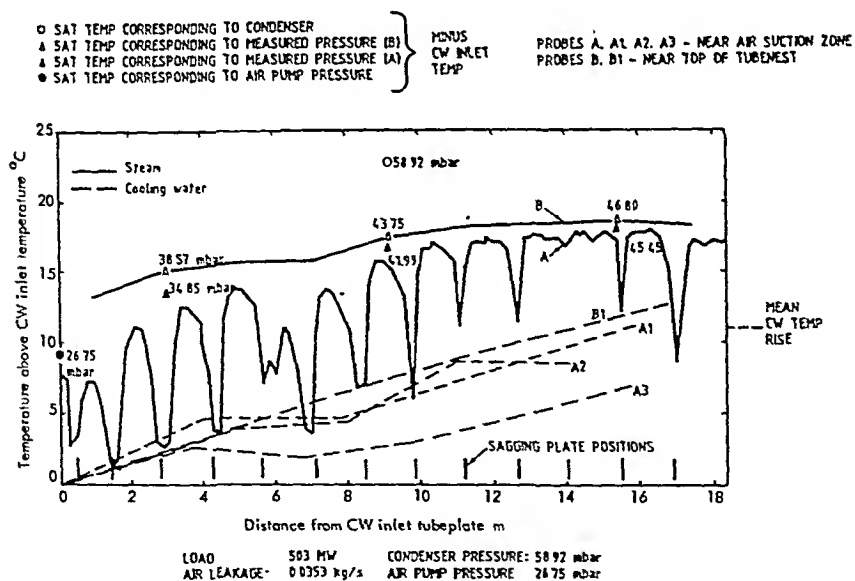


Figure 8 Distribution of steam and cooling water temperature along condenser (Reproduced by permission of CERL).

A COMPUTER MODEL FOR DETAILED CALCULATION OF THE FLOW IN POWER STATION
CONDENSERS

S. Al-Sanea*, N. Rhodes*, D.G. Tatchell* & T.S. Wilkinson†

A mathematical model of a condenser, developed using a general-purpose fluid-flow computer code, is described. The model assumes two-dimensional, steady flow, and equations are solved for continuity, momentum and species concentration. The use of different model representations of density diffusion coefficient and heat-transfer rate are examined. Model predictions obtained for an experimental condenser having a rectangular tube bank and two alternative venting arrangements are presented, and compared with experimental data.

INTRODUCTION

The complex heat and mass-transfer processes occurring in a condenser have led designers to rely heavily on empirical methods for predicting performance. Such methods are incorporated in design codes in which a mean heat-transfer coefficient is obtained from an empirical equation accounting for the velocity of the cooling water and its mean temperature. A description of several design methods is given by Rowe et al (1). These methods are based on an assessment of previous designs and in most cases take no account of the shape of the tube-nest.

However, the large capital cost of condensers, and the desire to improve efficiency and hence reduce operating costs, lead the designer to seek information regarding the fluid motion and thermal conditions at a more detailed level. A number of numerical schemes have been developed to provide information of this kind. That of Wilson (2) predicts the flow and heat-transfer between every tube row. A more practical approach, eg Davidson and Rowe (3), is to consider the tube nest as a porous medium, thus allowing a coarser computational grid to be used and hence economise on computer requirements. A common factor with all models is, of course, the empirical information required to calculate local heat and mass-transfer, pressure drop and similar parameters which depend on the local flow conditions. Reference to previous designs or experimental information is required to provide this information.

The advantage of a numerical method for prediction of condenser performance is that details of the tube nest shape can be accounted for, thus allowing the designer to investigate the effects of alternatives to the shape of the nest, placement of baffles and drip trays and other obstacles to flow. Such

* CHAM Ltd., Bakery House, 40 High Street, Wimbledon, SW19 5AU, England.

† NEI Parsons Ltd., Heaton Works, Newcastle-upon-Tyne, NE6 2YL.

studies can be carried out easily and economically, and expensive experimental validation can be kept to minimum. Models of this kind also provide detailed information on pressure, temperature, velocities and concentration distributions within the condenser.

Present Contribution

The present paper describes a condenser model which has been developed using a general-purpose, multi-dimensional, two-phase fluid flow computer code, PHOENICS, Spalding (4). The flow is assumed to be two-dimensional and steady, and equations are solved for continuity, momentum and species concentration. The model considers only the gaseous phase, the condensed water being assumed to vanish.

In respect of the assumption of two-dimensionality, and the treatment of the tube nest as a porous medium, the model is similar to that of Davidson and Rowe (3). The main differences in the present approach, are that diffusive terms are included in the modelled equations and, because of the general nature of the computer code employed, extension to three-dimensional cases and the inclusion of two-phase effects is possible.

The assumption of two-dimensional flow is usually made in condenser models, and solutions are obtained for the flow between tube-plates, which are assumed to preclude any strong three-dimensional effects. However, the flow in adjacent sections will differ due to the temperature rise of the cooling water, and the flow in the turbine exhaust, which is not constrained to be two-dimensional, will be influenced by the varying condenser performance in the third direction.

An additional feature of the present model is the two-phase flow solution capability available in the general computer code. Using this option, additional transport equations for the flow of condensate can in future be included, and the effects of the presence of condensate on the behaviour of the vapour flow and heat transfer can be studied in more detail than has previously been possible.

The model has been used to predict the two-dimensional, single-phase flow and heat-transfer in an experimental condenser having a rectangular tube bank, as shown in Figure 1. Calculations have been performed for two experimental cases, the first having an external vent, and the second an internal vent. The experimental condenser under consideration was designed to demonstrate the effects of air pockets and as such is not regarded as a good example of condenser design. However, the detailed measurements of heat-flux and air concentration, and the nature of the flows occurring in the two cases make them a good test of the condenser model. The externally vented case, for example, relies on turbulent diffusion as the mechanism by which non-condensable gas escapes from the tube nest to the vent. Models which do not include diffusion terms would fail to find a solution for this case.

The condenser model has been used to study the influence of grid size, and different modelling assumptions. Calculations are described which show the effect of density, diffusion coefficient and heat-transfer coefficient, both as fixed parameters and when allowed to vary with local conditions.

Calculations have also been performed for a power-station condenser, where the presence of baffles and drip-trays, and more complex tube-nest arrangements have an important effect on the flow. However, as there are no detailed experimental measurements available to compare with this case, the calculations are not reported here.

ANALYSIS AND SOLUTION METHODGoverning Differential Equations

The flow is treated as two-dimensional and steady; the governing equations are solved on a fixed and rectangular cartesian coordinate system. The coordinates are z (the axial direction) and y (the transverse direction). The variables solved for are:

- Gas velocities in the z and y directions, w and v
- Steam concentration, c
- Pressure, p

The equations solved are those representing the conservation of momentum in the z and y directions, steam concentration and mass continuity. They can be expressed in the common form:

$$\frac{\partial}{\partial y} (\rho v \phi) + \frac{\partial}{\partial z} (\rho w \phi) - \frac{\partial}{\partial y} \left(\Gamma_{\phi} \frac{\partial \phi}{\partial y} \right) - \frac{\partial}{\partial z} \left(\Gamma_{\phi} \frac{\partial \phi}{\partial z} \right) = S_{\phi} \quad \dots\dots\dots(2.1)$$

Where:

ϕ stands for v , w , c or 1 , the latter corresponding to the continuity equation

ρ is the mixture density

Γ_{ϕ} is the diffusion coefficient

S_{ϕ} is the source of ϕ per unit volume.

The "distributed resistance" method of Patankar & Spalding (9) is used in which the velocities in the above equations are those arising due to the reduced flow area in the tube nest. This method has been widely used for steam generator flow modelling, e.g. Singhal and Spalding (10).

The source terms which include the effect of pressure gradient, tube-friction and heat and mass transfer, are given in Table 1 in the integral form in which they appear in the finite-domain equations referred to later.

TABLE 1 - Integral Source Terms

Variable	Integral Source Term
v	$-\frac{\partial p}{\partial y} V - F_v$
w	$-\frac{\partial p}{\partial z} V - F_w$
c	$-K_c(c-c_s)$
Continuity	$-K_c(c-c_s)$

The symbols in Table 1 have the following meanings:

V = cell volume

$F_{v,w}$ = tube friction force

K_c = mass transfer rate per unit free volume per unit concentration gradient

c_s = saturation concentration of steam in air at a reference temperature.

Auxiliary Relationships

Physical Properties. The laminar viscosity has been assumed to have a constant value of 10^{-5} kg/ms, the Schmidt Number a value of unity. The density has been taken as either a constant equal to steam density, or has been allowed to vary locally according to the relation:

$$\frac{1}{\rho} = \frac{1-c}{\rho_{\text{air}}} + \frac{c}{\rho_{\text{steam}}} \dots\dots\dots(2.2)$$

Where ρ_{air} and ρ_{steam} have the values 0.162 kg/m³ and 0.091 kg/m³ for the external vent case and 0.33 kg/m³ and 0.1773 kg/m³ for the internal vent.

Tube Friction. For simplicity an extension of the losses for one-dimensional turbulent conditions is used. The tube friction integral source terms in the momentum equations have the forms:

$$F_v = 2f\rho v^2 N' A_y \delta_y \dots\dots\dots(2.3)$$

$$F_w = 2f\rho w^2 N' A_z \delta_z \dots\dots\dots(2.4)$$

Where:

f = Friction factor, given by

$$f = \left(0.23 + \frac{0.11}{\left(\frac{P}{d_0} - 1 \right)^{1.08}} \right) Re^{-0.15} \dots\dots\dots(2.5)$$

N' = number of tube rows per unit length in the direction in question

A_z, A_y = cell face areas normal to z and y directions

δ_y, δ_z = cell width and length.

Turbulent Diffusion. The diffusion coefficient, Γ_ϕ , is defined as:

$$\Gamma_\phi = \frac{\mu_t}{\sigma} \dots\dots\dots(2.6)$$

where:

μ_t = turbulent viscosity

σ = Schmidt Number for c-equation, unity for v and w equations

As σ is taken as unity in the model, we have $\Gamma_\phi = \mu_t$.

Studies have been carried out with fixed values of μ_t , in the range 1.7×10^{-3} kg/ms to 6.8×10^{-3} kg/ms, and with values varying locally as follows:

In the un-tubed region, μ_t is fixed and estimated from an application of the mixing length formula, ignoring the effects of extraction at the tube bank interfaces:

$$\mu_t = \rho \ell^2 \left(\frac{\partial v}{\partial y} \right) \dots \dots \dots (2.7)$$

where:

ℓ is a mixing length = $0.1 \times$ steam-lane width

$\frac{\partial v}{\partial y}$ is the mean velocity gradient across the lane, taken as an estimated mid velocity (taken as the inlet velocity) divided by the width.

In the tubed region, μ_t varies according to:

$$\mu_t = \rho \ell w' \dots \dots \dots (2.8)$$

where:

ℓ is a mixing length = $0.1 \times D_h$

w' is a fluctuating velocity, and has been estimated from an empirical correlation given by Weisman and Bowring (5) for the fluctuating flow rate per unit length of tube, \dot{M}' ;

$$\dot{M}' = a G D_h \text{Re}^{-0.1} \dots \dots \dots (2.9)$$

where:

G = fluid mass velocity

D_h = hydraulic diameter = $\frac{2\sqrt{3}p^2}{\pi d_o}$ - $d_o = .0275$ m

Re = Reynolds number based on D_h

a = constant = 15

Heat and Mass Transfer. Two methods of implementation of the source term in the steam-concentration and continuity equations, given in Table 1, have been examined. The first assumes that K_C and c_s remain constant. c_s is taken as the saturation concentration at the mean cooling water temperature of vapour in air and the condenser pressure and K_C is calculated using an estimated overall heat-transfer coefficient:

$$K_C = \frac{\alpha_{ov} A(T - T_s)}{\lambda (c - c_s)} \dots\dots\dots(2.10)$$

where:

α_{ov} = overall heat-transfer coefficient

A = Area per unit volume

λ = latent heat

The values used are given in Table 2.

TABLE 2 - K_C and c_s values

	K_C	c_s
External vent	5.3	0.072
Internal vent	6.4	0.056

In the second method, the values of K_C and c_s have been computed from local conditions, using a method described by Chisholm (6). It is assumed that the heat flux, q , and mass transfer, \dot{m} , are related through the latent heat by:

$$\dot{m} = \frac{q}{\lambda} \dots\dots\dots(2.11)$$

The heat flux can be expressed as a function of local temperatures of the vapour, T_v , condensate, T_s , outer wall, T_w , and cooling water, T_c and the corresponding heat-transfer coefficients between cooling water and outer tube wall, α_{wc} , across the condensate film, α_c , and the overall value between vapour and liquid, α_{ov} .

The mass transfer can be deduced from the temperature gradient between vapour, and condensate surface.

Combining the equations for heat and mass transfer, an equation for q is obtained:

$$q = (T_v - T_c) / \left(\frac{1}{B^{1/2}} + \frac{1}{c^{1/3}} + \frac{1}{\alpha_{wc}} \right) \dots\dots\dots(2.12)$$

where:

$$B = \frac{D_p}{d_o} \frac{Re_m^{0.5}}{\varepsilon^{0.6}} P^{1/3} \left\{ \frac{\lambda}{T_v V_v} \right\}^{2/3} \dots\dots\dots(2.13)$$

$$C = 0.725 \left(\frac{k_c^3 \lambda_g}{d_o \mu_c V_c} \right)^{1/4} (1 + 0.0095 Re_m^{11.8/\sqrt{Nu}}) \dots\dots\dots (2.14)$$

D_D , Re_m , ϵ , and V_V stand for the diffusion coefficient of steam in air Reynolds number of vapour gas mixture, volume ratio of air to mixture, and the specific volume of the mixture. k_c , μ_c and V_c stand for the conduction, viscosity and specific volume of the condensate. Equation (2.12) is solved iteratively, and the wall and condensate temperatures are then calculated. The vapour temperature, T_V , is taken as the local saturation temperature corresponding to the vapour pressure. The saturation concentration, c_s , is evaluated at the temperature of the condensate.

BOUNDARY CONDITIONS

A fixed mass flow is specified at the inlet boundary, the concentration being specified in this plane. At the vent, the pressure is fixed to zero. The walls of the condenser are assumed to be frictionless, impervious to flow and there is no loss of heat.

SOLUTION METHOD

The equations are solved using the standard finite-domain method embodied in the PHOENICS Code, Spalding (4). This involves the subdivision of the flow domain into rectangular grid cells and the derivation of algebraic finite-domain equations by integration of the differential equations over each grid cell. These equations are solved using a variation of the SIMPLE method of Patankar and Spalding (7).

PRESENTATION OF RESULTS

The Experimental Configuration

The condenser configuration is shown in Figure 1. Calculations have been performed for two experimental cases examined by McAllister (8), the first having an external venting arrangement, and the second an internal vent. Measurements were made of the cooling water temperature rise in each tube, and the air concentration along diagonals in the four planes across the axis of the tube nest, as shown in Figure 1.

As the vents are on the horizontal centre-line of the condenser, and the presence of condensate and its possible effects on performance are not included in the model, it has been assumed that the horizontal centre-line is a symmetry plane, and therefore calculations need only be performed for one half of the condenser.

Operating Conditions. The operating conditions for the two cases are given in Table 3.

TABLE 3 - Operating Conditions

	External Vent	Internal Vent
Pressure (N/m ²)	1.36×10^4	2.767×10^4
Steam inflow (kg/s)	0.792	2.032
Air inflow (kg/s)	2.69×10^{-4}	2.48×10^{-3}
Mixture outflow (kg/s)	2.87×10^{-3}	1.097×10^{-2}
Cooling water inlet temperature °C	13.1	17.8
Cooling water velocity (m/s)	1.177	1.19

Computational Details

Grid distribution. Grids of 5 x 11, 8 x 15, 11 x 20 and 16 x 30 cells in the transverse and axial directions respectively have been used for the external vent case. The two finer grids gave results which were virtually identical. The 11 x 20 grid was therefore deemed to give essentially grid-independent results, and has been used for subsequent calculations. The grid is non-uniform as shown in Figure 1, the cell sizes having been adjusted to suit the geometry of the condenser vent, steam lanes and tube bank. A 13 x 20 grid has been used in the internal vent case, as shown in Figure 1.

Convergence. 200 iterations of the equations were found to give adequate convergence; the sum of the absolute continuity errors was reduced to less than .01 % of the inflow.

Computer Requirements. A 200-iteration run required about thirty minutes on a Perkin-Elmer 3220 mini-computer. The memory requirements with all variables stored in core was 300 kbytes.

Runs Performed. Calculations were performed for both the internal and external vent cases to investigate the effects of different representations of density, viscosity and heat-transfer rate as described earlier. The runs reported for each case are:

- Fixed density, fixed viscosity, fixed K_C and c_s
- Variable density alone
- Variable viscosity alone
- Variable heat-transfer alone
- All variable options activated

The model employing all fixed options will hereafter be referred to as the "simple" model, that with all varying options the "complete" model.

Discussion of the Results

The results are shown in Figures 2 to 5 in the form of computer generated plots of velocity vectors and steam concentration contours. In Figures 6 to 11 comparison between predictions and measurement is shown for heat flux distributions along the central horizontal and vertical planes through the tube bank and air concentration distribution along diagonals in the tube bank.

Typical Results. The details of the flow for both cases can be best appreciated by consideration of the velocity vector and concentration contour plots shown in Figures 2 to 5. Both velocity-vector plots show the mixture entering from the side, there is some deflection of the flow away from the tube bank and down the steam lane, and the flow is turned around due to the presence of the rear wall and the suction effect of the tube bank. The velocities reduce to quite small values in the middle of the tube bank as the vapour condenses.

The vapour concentration contours are shown in Figures 4 and 5. The external vent case shows a sharp fall in concentration around the periphery of the tube bank, and a large air-bubble (ie a low steam concentration region) in the middle. The internally vented arrangement, Figure 5, shows a much smoother variation of concentration and the minimum value, c_s , is not reached, implying a much greater utilisation of the tube bank than in the externally vented case.

Comparison with Experimental Data. Figures 6 to 8 show the horizontal and vertical centre-line variations of heat flux, and the variation of air concentration along the diagonal, shown in Figure 1, for the externally vented case. The predictions obtained with the different modelling assumptions are compared with experimental measurements.

The large air bubble implied by the concentration contours in Figure 4 would be expected to reduce the heat transfer over much of the tube bank. This is confirmed in Figures 6 and 7, the heat flux being high at the periphery of the tube bank and falling rapidly to a low value well before the centre. All the models used tend to over-predict the heat flux at the periphery of the tube bank. The "complete" model gives the best agreement, with about 15 % maximum deviation from experiment. Comparing the models themselves, the calculation of a local heat-transfer coefficient appears to be the most important factor in moving the predictions towards the experimentally observed behaviour. The heat flux at inlet to the nest is reduced from 150 kW/m² for the simple model to 115 kW/m² for the complete model, compared with the experimental value of 100 kW/m². Allowing the density to vary locally makes virtually no difference to the results and use of a variable viscosity model has only a slight influence, reducing the heat flux at inlet by about 2 kW/m².

The air-concentration distribution along the diagonal, Figure 8, shows the four sets of experimental points corresponding to measurements at four locations in the third direction. The differences between these four sets therefore correspond to variations in the third dimension which are not modelled. The best that can be expected, therefore, is that the predictions lie within the range of the measured data, which they evidently do.

The predicted and experimental values of heat flux and air concentration for the internally vented case are shown in Figures 9 to 11. In this case the heat flux is under-predicted by the complete model by about 20 % at entry to the tube-nest, Figure 9. The simple model is in better agreement in this region. Overall, however, the complete model appears to follow the experimental data more accurately, the minimum value, about 50 kW/m², is closer to the experimental measurement than the other models, which predict much lower values.

Consideration of the vertical variation of heat flux, Figure 10, and also the air concentration distribution, Figure 11, shows that the measurements are not symmetric about the centre-plane. This is presumably due to some physical effect (probably associated with the condensate), which is not included in the present model. The region of maximum air concentration and minimum heat flux, now occurs in the upper part of the condenser. It is interesting to note that this asymmetry contradicts the usual expectation of the effect of inundation, i.e. of lowering the heat flux in the lower half. However, it would not be appropriate to pursue this matter here.

Figure 10 shows that all the calculations tend to over-predict the heat flux at the upper edge of the tube nest and, with the exception of the complete model, predict zero heat flux near the centre.

The concentration profiles in Figure 11 show that the simple model predicts the air concentration better in the upper half, and the complete model does better in the lower half. However, the main lesson to be learned from the comparison is that extension of the model is required to include the physical processes causing the asymmetry.

CONCLUDING REMARKS

A general-purpose fluid-flow computer program has been used to construct a two-dimensional mathematical model of a condenser. The effects have been investigated of the representation of density, diffusion coefficient and heat transfer, and the results of predictions compared with experimental data. The conclusions of the study may be summarised as follows:

- Allowing the mixture density to vary with the local concentration of steam and air has only a small effect on the predictions. This confirms the normal practice of neglecting variations of density except in the air-cooling section of a condenser.
- Allowing the diffusion coefficient to vary as a function of local conditions has a more pronounced effect on the results. The mechanism of turbulent diffusion itself is crucial for the external vent case, and consequently for any condenser liable to form an air pocket. The empirical correlation used to set the diffusion coefficient is worthy of further consideration, there being little available data on this topic.
- The incorporation of empirical data to calculate heat-transfer locally has the most significant effect on the results. Only one particular set of empirical correlations has been examined, and further studies using alternative sets would be useful.
- Allowing all parameters to vary locally results in the predictions which show the closest agreement with experiment. This would seem to imply that regardless of obvious doubts about particular empirical correlations, the allowance of local variations in parameters inevitably leads to a more realistic model.

Other work not reported in this paper includes application of the model to a two-dimensional study of a power station condenser. It is expected that in the future this will be extended to a full three-dimensional representation, and to a two-phase model including the motion and heat transfer of the condensate.

ACKNOWLEDGEMENTS

The authors wish to thank NEI-Parsons Limited and Concentration Heat and Momentum Limited for permission to publish this paper. The authors also acknowledge the encouragement and assistance of the experimentalists in the Mechanical Research Department of NEI-Parsons, led by Mr. D H McAllister, and the Condenser Design Department of NEI-Parsons, in particular Mr W R Reid for his guidance in the choice of heat-transfer correlations.

SYMBOLS USED

- A_y = cell-face area (m^2)
 A_z = cell-face area (m^2)
 a = constant in equation (2.9)
 B = parameter defined by equation (2.13)
 C = parameter defined by equation (2.14)
 c = steam concentration
 c_s = saturation concentration of steam in air
 D_h = hydraulic diameter (m)
 D_p = coefficient of vapour diffusion in air (kg/ms)/Pa
 d_o = outer tube diameter
 F_y = tube friction for y-momentum equation
 F_z = tube friction for w-momentum equation
 f = friction factor defined by equation (2.5)
 G = fluid mass velocity (kg/m^2s)
 K_c = mass transfer rate (kg/m^3s)
 k = thermal conductivity (W/mk)
 ℓ = mixing length (m)
 Nu = Nusselt number
 N' = number of tube rows
 P = tube pitch (m)
 p = pressure (N/m^2)
 q = heat flux (W/m^2)
 Re = Reynolds number
 S = source term in finite-domain equations

- T = temperature (K)
 V = volume (m^3)
 V_i = specific volume of 'i' (m^3/kg)
 v = velocity in y-direction (m/s)
 w = velocity in z-direction (m/s)
 y = transverse coordinate direction
 z = axial coordinate direction

Greek letters

- α = heat-transfer coefficient (W/m^2K)
 Γ_ϕ = exchange coefficient in finite-domain equations
 ϵ = volume ratio of air to mixture
 λ = latent heat (J/kg)
 μ = viscosity (kg/ms)
 ρ = density (kg/m^3)
 σ = Schmidt Number
 ϕ = general dependent variable

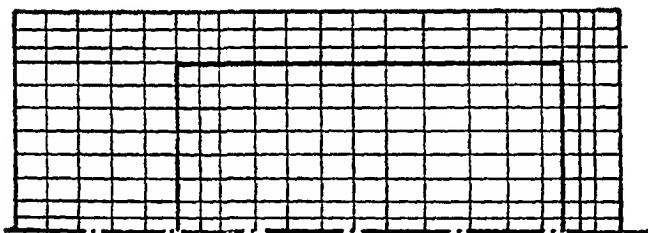
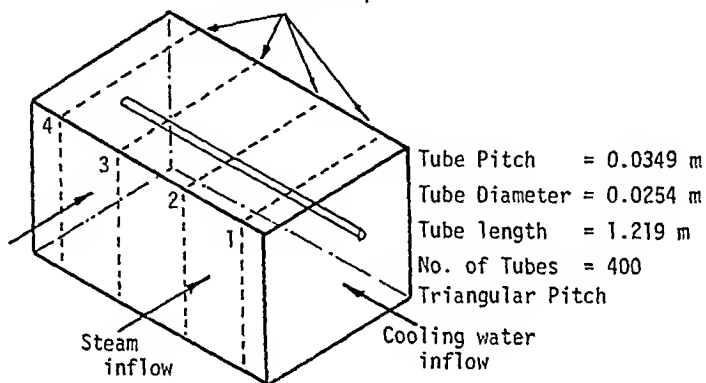
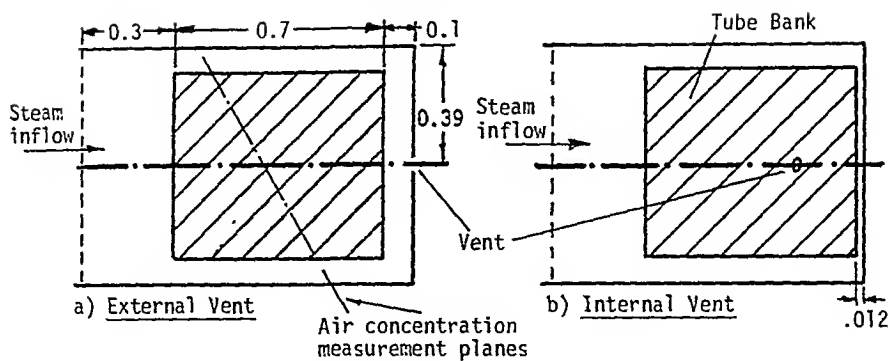
Subscripts

- c = condensate
 ℓ = liquid
 ov = overall
 v = vapour
 $w\ell$ = wall-to-liquid

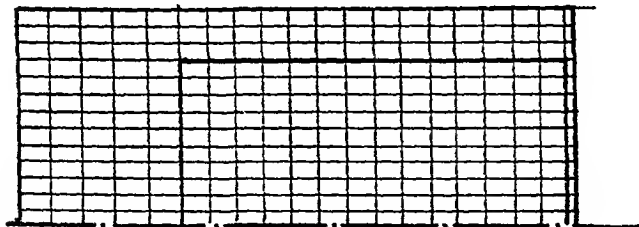
REFERENCES

1. Rowe, M., Davidson, B.J., Andrews, E.F.C., Ferrison, J.A., and Taylor, B.J., 1979, "Heat Transfer and Air Blanketing in Steam Condensers", Proc. of Conf. on Steam Turbines for the 1980s, I. Mech. E.
2. Wilson, J.L., 1972, "The Design of Condensers by Digital Computers", I. Chem. E. Symposium Series, No. 35.
3. Davidson, B.J. and Rowe, M., 1981, "Power Condenser Heat Transfer Technology", Hemisphere Publishing Corp.
4. Spalding, D.B., 1981, Mathematics and Computers in Simulation, XXIII, 267-276.

5. Weisman, J and Bowring, R W, 1975, Nuclear Science and Engineering, 57, 255-276.
6. Chisholm, D, 1981, 'Power Condenser Heat Transfer Technology', Hemisphere Publishing Corp.
7. Patankar, S.V. and Spalding, D B, 1972, Int. J. of Heat and Mass Transfer, 15, 1787-1806.
8. McAllister, D H, 1981, Unpublished work at NEI-Parsons Ltd.
9. Patankar, S.V. and Spalding D.B., 1975, "Heat Exchangers: Design and Theory Sourcebook", Ed. by H. Afgan and E.U. Schlunder, Scripta Book Company, Washington DC, pp 155-176.
10. Singhal A.K. and Spalding D.B., 1980, "Multiphase Transport: Fundamentals, Reactor Safety Applications", pp 373-406, Hemisphere Publishing Corp.



Grid Distribution: External Vent



Grid Distribution: Internal Vent

Figure 1 Experimental details and grid distribution

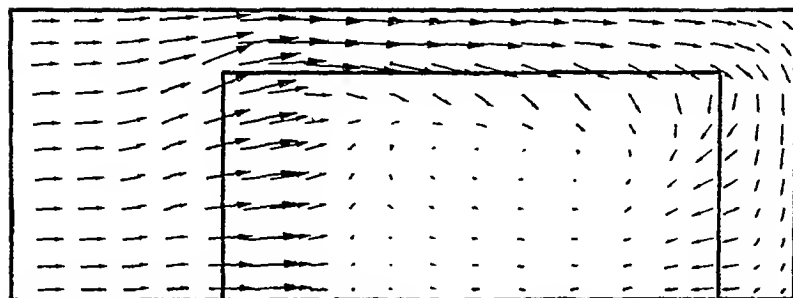


Figure 2 External vent - velocity vectors

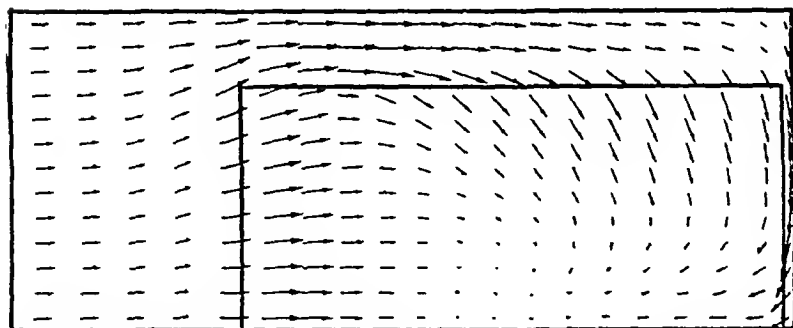


Figure 3 Internal vent - velocity vectors

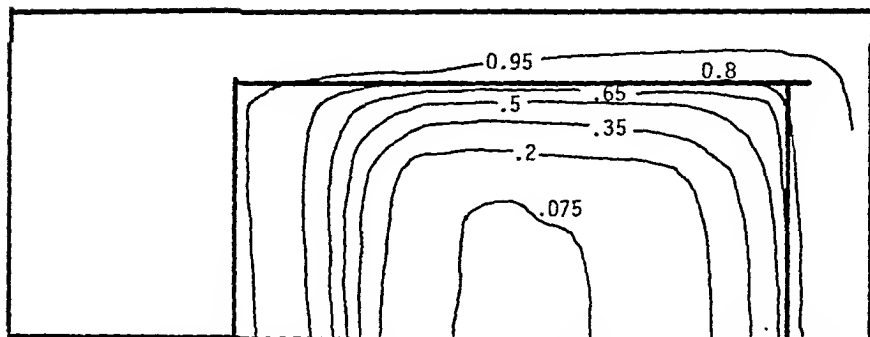


Figure 4 External vent - steam concentration contours

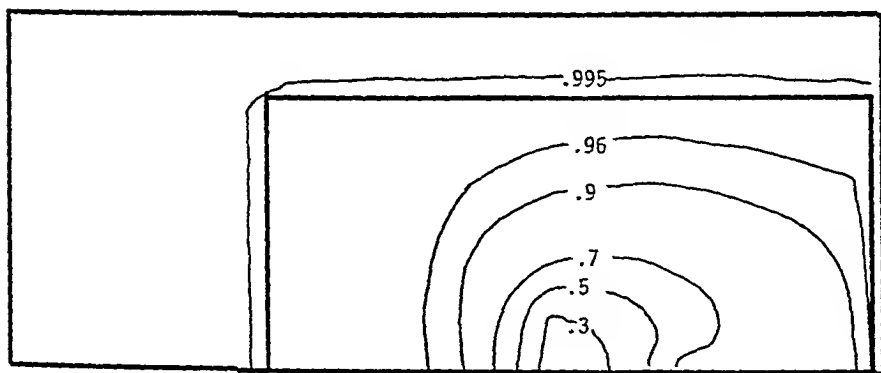


Figure 5 Internal vent - steam concentration contours

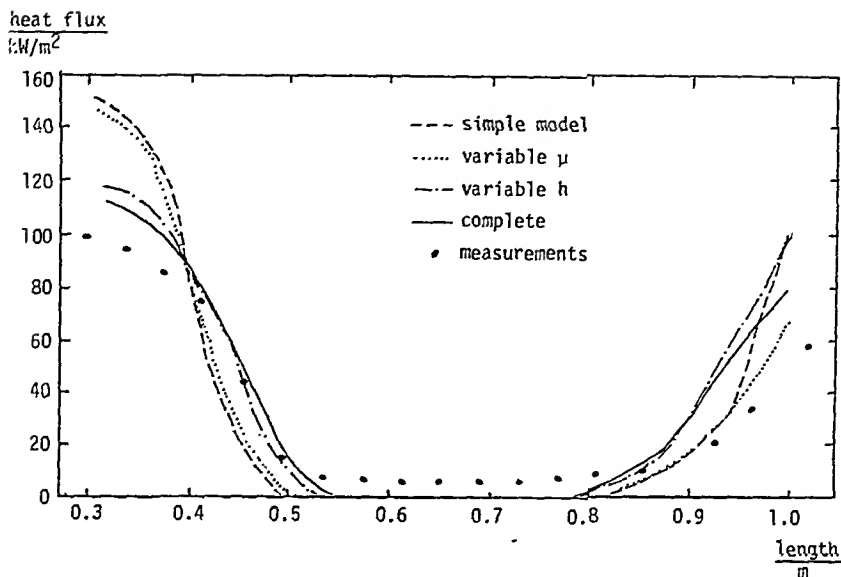


Figure 6 External vent - heat flux along horizontal centre-line

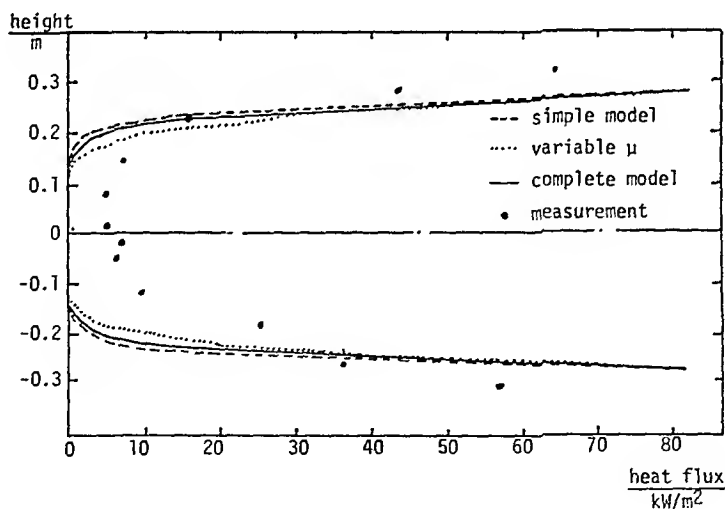


Figure 7 External vent - heat flux along vertical centre-line

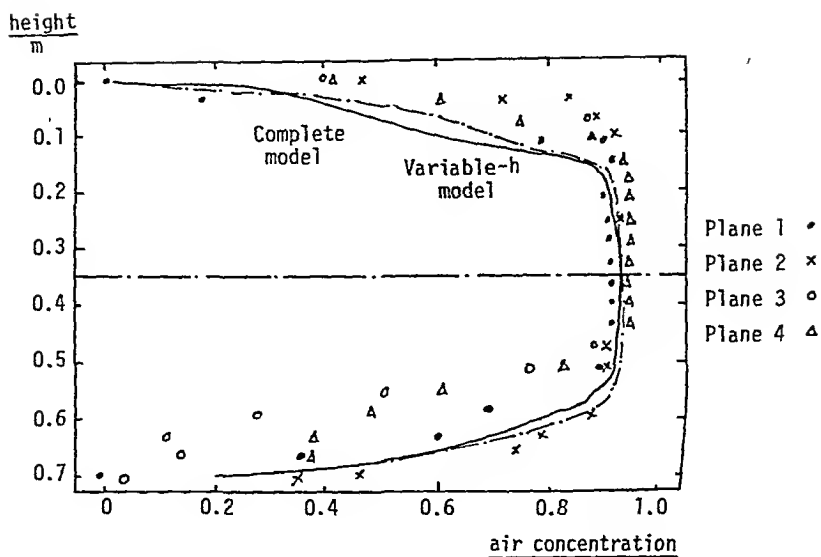


Figure 8 External vent - air concentration along diagonal

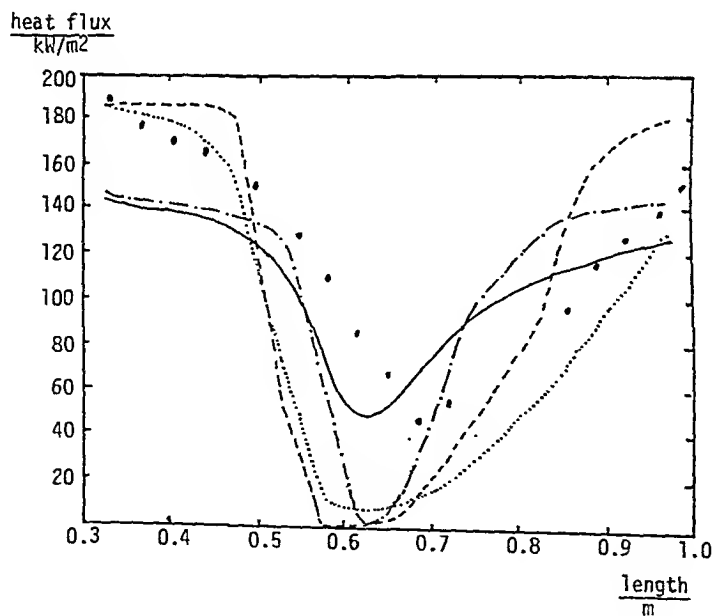


Figure 9 Internal vent - heat flux along horizontal centre-line

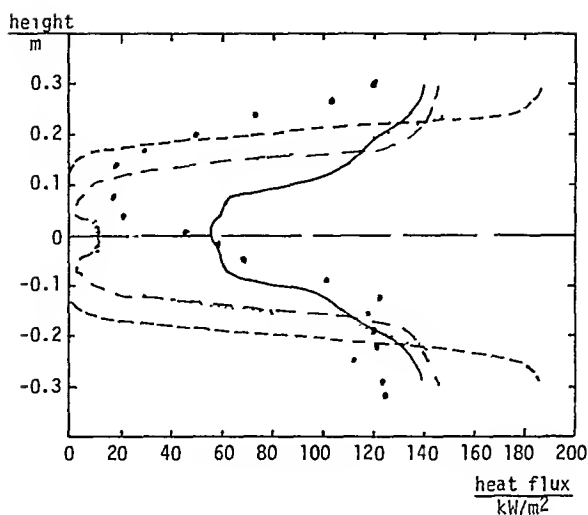


Figure 10 Internal vent - Heat flux along vertical centre-line

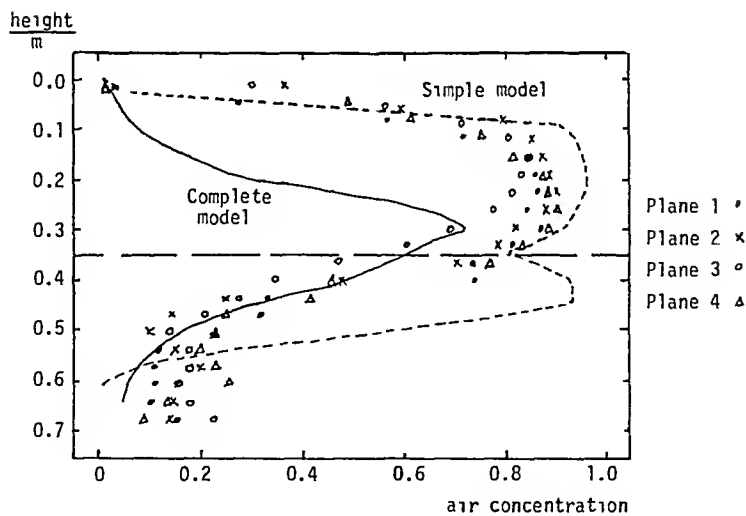


Figure 11 Internal vent - air concentration along diagonal

NUMERICAL COMPUTATION OF STEAM FLOW IN POWER PLANT CONDENSERS

C. Caremoli *

A computational method for evaluating the performance of power plant condensers is described. The program assumes that the flow is two dimensional over a cross section. A finite difference method is employed. The effects of inundation, vapour velocity, and non condensable gases are included in the condensation model. One example of calculation is presented.

INTRODUCTION

Codes of practice for the design of power plant condensers provide an overall mean heat transfer coefficient from which the heat transfer areas required are calculated. In determining this coefficient the only independent variables are the temperature and velocity of the cooling water and the dimensions and material of the tubes.

A two-dimensional computer code, called CALICO, has been developed by Electricité de France in order to simulate the steam flow in condensers. It calculates the pressure drop, the non condensable gas distribution and the heat transfer rate.

The complexity of the geometry is taken into account by means of a local volume averaging technique.

The interacting forces between the tubes and the fluid are modelled by empirical correlations and the heat and mass sources are calculated by a condensation model including the effects of inundation, vapour velocity and non condensable gases.

A semi implicit finite difference method is employed with the two velocity components, pressure and non condensable gas mass fraction as primary variables.

An application of the code to a nuclear power plant condenser is presented in this paper as an example of calculation.

* Electricité de France, Direction des Etudes et Recherches Département Transferts Thermiques et Aérodynamiques 6, quai Watier 78400 CHATOU. FRANCE.

Such predictions of the detailed flow pattern are useful to optimize some geometrical parameters with respect to vibration problems and overall thermal performance.

CODE DESCRIPTION

The prediction of the steam flow in condensers involves the solution of Navier-Stokes equations in tube bundles. When more than a few tubes are involved, the flow becomes too complex to be solved even numerically : consequently, the tube bundle is considered as an homogeneous medium.

The conservation equations are averaged over small control volumes surrounding each point. The proportion of fluid in each volume is the porosity defined as :

$$\epsilon = \frac{\text{Volume occupied by the fluid}}{\text{Total volume}}$$

However the averaging technique creates new terms in the equations. These terms can be calculated rigorously only if the local values are known. Some of them can be neglected. The others are modelled by empirical correlations.

Resulting equations

The main variables U_i , p and x_a are average quantities.

The mass conservation equation is given by :

$$\frac{\partial(\epsilon \rho)}{\partial t} + \frac{\partial}{\partial x_i} (\epsilon \rho U_i) = -m \quad (1)$$

The two momentum conservation equations can be written as :

$$\frac{\partial(\epsilon \rho U_i)}{\partial t} + \frac{\partial}{\partial x_j} (\epsilon \rho U_i U_j) = -\epsilon \frac{\partial p}{\partial x_i} + \epsilon \frac{\partial}{\partial x_j} \sigma_{ij} - m U_i + F_i \quad (2)$$

The air mass conservation equation is given by :

$$\frac{\partial(\epsilon \rho x_a)}{\partial t} + \frac{\partial}{\partial x_i} (\epsilon \rho U_i x_a) = \epsilon \operatorname{div}(\rho \delta \vec{\text{grad}} x_a) \quad (3)$$

Closure of the system

It is a very difficult problem because nearly all the existing correlations of data have been established for one dimensional flows. Therefore the models proposed for the terms F_i and m must be some kind of generalisation of these correlations.

Mass source term m . It is given by the general heat and mass transfer law :

$$q = m \Delta h_v = \frac{T_s - T_{cw}}{R} \quad (4)$$

The temperature of the vapor phase T_s is given by the equation of state. Δh_v is the latent heat, T_{cw} is the temperature of the cooling water.

The determination of the resistance R is obtained using various heat transfer correlations.

For the water side resistance the equation proposed by Dittus-Boelter (1) is used :

$$\frac{1}{R_w} = 0.023 \frac{\lambda_w}{d_i} Re^{0.8} Pr^{0.4} \quad (5)$$

The tube wall resistance is given by the standard equation :

$$R_t = \frac{d_o \log \frac{d_o}{d_i}}{2 \lambda_t} \quad (6)$$

The fouling resistance R_F is estimated. The resistance for film condensation is based on the equation proposed by Nusselt (2) :

$$\frac{1}{R_{Nu}} = 0.725 \left[\frac{\lambda_c^3 \rho_c (\rho_c - \rho_s) \Delta h_v g}{\eta_c d_o (T_{cs} - T_w)} \right]^{1/4} \quad (7)$$

Fuks (3), Grant and Osment (4), Wilson (5), Berman and Tumanov (6) proposed some corrective terms to take account of the effects of inundation and vapour shear :

$$\frac{1}{R_c} = \frac{1}{R_{Nu}} \left(\frac{W}{C} \right)^{-0.16} (1 + 0.0095 (Re_s)^{11.8/\sqrt{Nu}}) \quad (8)$$

The resistance to condensing heat transfer resulting from the presence of an air film is estimated via a mass transfer coefficient introduced by Berman and Fuks (7)

$$\frac{1}{R_s} = \frac{a \delta}{d_o} Re_s^{1/2} \left[\frac{P_s}{P_s - \pi_s} \right]^b P_s^{1/3} \left[\frac{\rho_s \Delta h_v}{T_s} \right]^{2/3} \frac{\Delta h_v}{(T_s - T_{cs})^{1/3}} \quad (9)$$

where $a = 0.52$ and $b = 0.7$ for $Re_s < 350$
and $a = 0.82$ and $b = 0.6$ for $Re_s > 350$

The resistance R is the sum of all the elementary resistances.

Momentum source term F_i . It is written on the general form :

$$F_i = - \epsilon \rho G U_i \quad (10)$$

G is the flow resistance depending on the main flow variables and on the bundle geometry. It is determined from one dimensional friction correlations obtained by Gunter and Shaw (8) for single phase flow.

$$G = \frac{f}{2} \left\| \bar{u} \right\| \frac{1}{D_v} \left(\frac{D_v}{S_T} \right)^{0.4} \left(\frac{S_l}{S_T} \right)^{0.6} \quad (11)$$

where

$$\frac{f}{2} = \frac{90}{Re_s} \quad \text{for } Re_s < 202.5$$

$$\text{and } \frac{f}{2} = 0.96 Re_s^{-0.145} \quad \text{for } Re_s > 202.5$$

Equation of state. Two assumptions are made : the steam is saturated throughout the condenser shell and the steam and the air are two perfect gases.

Solution procedure

Solution of equations (1), (2) and (3) are performed by finite difference method.

The calculation domain is divided into a finite number of main grid points where pressure and mass fraction of air are calculated. The two velocity components U_1 and U_2 are on the other hand calculated at grid locations situated midway between the main grid points. The conservation equations are integrated over control volumes surrounding grid points. This integration is performed by application of upwind differencing and semi-implicit formulation.

The result of this is a set of non linear algebraic equations which are solved by repeated use of the well known tridiagonal matrix algorithm. Special care has been taken to solve the pressure velocity coupling of the two momentum equations (2) and the mass balance equation (1). The "Simple Method" developed by Patankar and Spalding (9), (10) is used to solve this coupling.

This method introduces a new variable, the so-called pressure correction which corrects the velocity components so that they obey the continuity constraint. The pressure correction is determined by solution of a set of algebraic equations derived from the linearized momentum equations and the continuity equation.

A typical iteration sequence therefore contains the following main steps :

1. Calculate intermediate values of the velocities U_1 and U_2 based on the most recent pressure field.
2. Calculate necessary pressure correction so that the U_1 and U_2 fields obey continuity.
3. Update fields of velocities and pressure based on pressure correction field.
4. Calculate air mass fraction field.
5. Calculate the condensation rates, the new inlet flow, and the vent suction rate.
6. Check the convergence. a) If the convergence is not achieved continue to step n° 1 ; b) If it is, iteration process is finished.

Due to variations in the coefficients in the algebraic equations, under-relaxation of the variables must be used to obtain a converged solution.

EXAMPLE OF TWO DIMENSIONAL CALCULATION

The code has been applied to a power plant condenser containing 74000 titanium tubes in 6 tube banks. Each bank is a "fan-shaped" tube nest of 19 mm outside diameter tubes, 10.82 m long, with a 26 mm equilateral pitch. Only one half of a tube bank is modelled.

The main design parameters are :

Cooling water velocity = 2 m/s.
Cooling water inlet temperature = 11 °C.
Steam inlet pressure = 4600 Pa.

The finite difference grid comprises 1600 nodes.

Results of the calculation

The results presented are relative to the condenser operating at nominal conditions. Figure 1 shows the velocity field for one half of a tube bank. Figure 2 shows the contours of pressure and figure 3 the air mass fraction contours. The prediction of the condenser pressure is in good agreement with measured on site data. The velocity field (figure 1) gave some information about particular locations in the tube nest where excessive tube vibration may occur.

CONCLUSION

In its present stage of development, CALICO can be considered as a useful tool for the calculation of heat and mass transfer in tube bundle of condensers. The present two dimensional approach can be extended to three dimensions by a series of two dimensional calculations, each being for one slice between tube support plates. However it is not yet completely validated and other comparisons are needed with more detailed experimental data.

There are a number of assumptions which should be improved. The first is the assumption that friction factors are unaffected by condensation. The second point which needs further research is the model used for steam side heat transfer in tube banks (effects of inundation, velocity, and non-condensable gases).

SYMBOLS USED

- c = vapour condensed on a tube ($\text{kg/m}^3/\text{s}$)
 d_i = tube inside diameter (m)
 d_o = tube outside diameter (m)
 D_v = volumetric hydraulic diameter (m)
 F_i = momentum source term (N/m^3)
 g = acceleration due to gravity (m/s^2)
 Δh_v = latent heat (J/kg)
 m = mass source term ($\text{kg/m}^3/\text{s}$)
 Nu = Nusselt number based on Nusselt equation
 p = pressure (N/m^2)
 p_s = steam pressure (N/m^2)
 Pr = cooling water Prandtl number
 q = heat flux ($\text{J/m}^2/\text{s}$)
 R = thermal resistance ($\text{m}^2 \text{ K/W}$)
 R_c = condensate thermal resistance ($\text{m}^2 \text{ K/W}$)
 R_f = fouling resistance ($\text{m}^2 \text{ K/W}$)

- R_{Nu} = thermal resistance based on Nusselt equation ($m^2 \text{ K/W}$)
 R_t = tube wall thermal resistance ($m^2 \text{ K/W}$)
 R_w = cooling water thermal resistance ($m^2 \text{ K/W}$)
 Re = Reynolds number of the cooling water
 Re_s = Reynolds number of the steam flow
 S_L = longitudinal pitch (m)
 S_T = transversal pitch (m)
 T_{cs} = vapour - condensate interface temperature (K)
 T_{cw} = cooling water temperature (K)
 T_s = steam temperature (K)
 T_w = wall temperature (K)
 U_i = velocity component (m/s)
 x_a = air mass fraction
 W = condensate leaving a tube ($kg/m^2/s$)
 δ = diffusivity (m^2/s)
 ϵ = porosity
 λ_c = thermal conductivity of the condensate ($W/m/K$)
 λ_t = thermal conductivity of the material of the tube ($W/m/K$)
 λ_w = thermal conductivity for the cooling water ($W/m/K$)
 η_c = dynamic viscosity of the condensate ($kg/m/s$)
 π_s = partial pressure of the steam (N/m^2)
 ρ = mass density (kg/m^3)
 ρ_c = mass density of the condensate (kg/m^3)
 ρ_s = mass density of the steam (kg/m^3)
 σ_{ij} = viscous stress tensor ($kg/m/s^2$)

REFERENCES

1. Dittus F.W., and Boelter L.M.K., 1930, Publ. Eng. 2, 443.
2. Nusselt W., 1916, Z. Ver. dtsh. Ing. 60, 541.

3. Fuks S.N., 1957, Teploenergetika 4, 35.
4. Grant I.D.R., and Osment B.D.J., 1968, NEL Report N° 350.
5. Wilson J.L., 1972, I. Chem. E. Symp. Series 35, 21.
6. Berman L.D., and Tumanov Yu. A., 1962, Teploenergetika 9, 77.
7. Berman L.D., and Fuks S.N., 1958, Teploenergetika 5, 66.
8. Gunter A.Y., and Shaw W.A., 1945, Trans ASME, 643.
9. Patankar S.V., 1980, "Numerical Heat Transfer and Fluid Flow", Hemisphere, Washington.
10. Patankar S.V., and Spalding D.B., 1972, Int. J. Heat Mass Transfer 15, 1787.

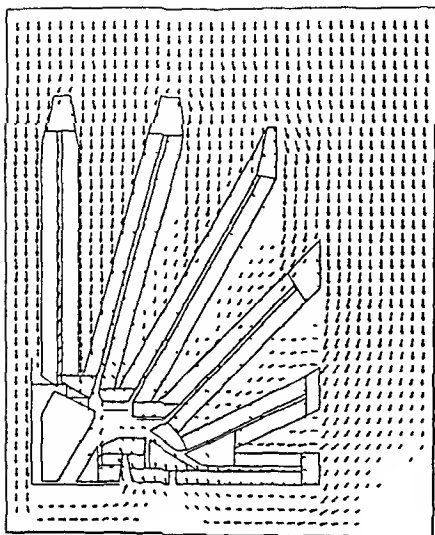


Figure 1 : Velocity field.

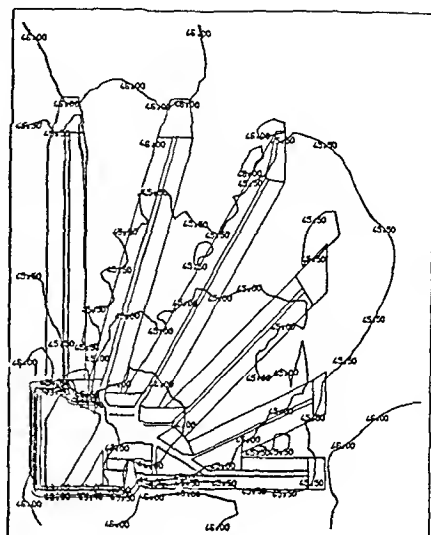


Figure 2 : Contours of pressure (mbar).

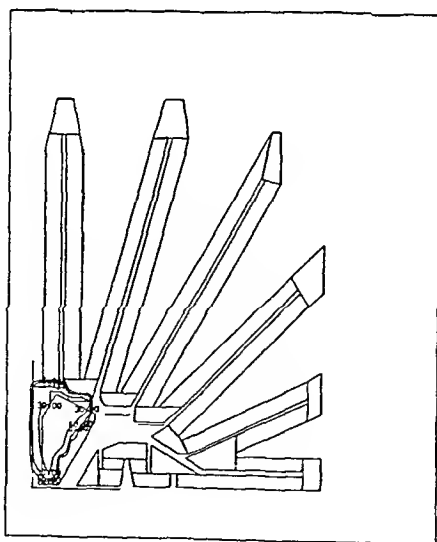


Figure 3 : Contours of air mass fraction.

THE USE OF COMPUTER PROGRAMS TO IMPROVE CONDENSER PERFORMANCE

G. Beckett, B.J. Davidson and J.A. Ferrison*

Three different forms of computer program have been developed at CERL to aid efforts to improve steam condenser performance. These are described and examples are presented in which the programs have been used to study condenser performance at CEBG power stations. Those programs which predict condenser performance agree well in general with measured data. However predicted values underestimate heat transfer coefficients in regions where both condensate inundation and steam velocities are high. Air leakage appears to have little influence on heat transfer coefficients outside air pockets, its role being solely to determine the air vent pressure. Improved methods of predicting the flows in steam access lanes are desirable.

INTRODUCTION

The increase in the speed of modern computers in recent years has led to a vast increase in the use of programs for solving some of the problems associated with large power plant steam condensers. In 'main frame machines' there are no longer the storage capacity problems which led to undesirable computational compromises. In addition the advent of the 'desk top' computer has seen the transfer of many of the simpler 'main frame' programs to these portable machines; this has resulted in considerable advantages in field work where there has been no access to a 'main frame'.

At the Central Electricity Research Laboratories three computer programs are used for studying the performance of steam condensers:

1. CONE (CONdenser Evaluation) is a 1D flow modelling program which produces condenser vacuum predictions over a range of operating conditions. Particular attention is paid to the interaction between the condenser and the air extraction system.
2. EPOC (Estimating the Performance Of Condensers) is a quasi-3D program which performs detailed multiple slice 2D flow field calculations to produce vacuum predictions; in addition velocities, heat transfer coefficients, temperatures, pressures and air concentration etc. are determined throughout the tubenest.
3. COLT (Condenser On Line Testing) is essentially a data reduction program for experimental work on full scale and model plant. Data is presented in tabular and graphical form. In addition test data is compared with standard test codes.

*C.E.G.B., Central Electricity Research Laboratories, Leatherhead, England.

This paper will consider the details of each of these programs and then consider a number of case studies where they have been used.

THE 'CONE' PROGRAM

Current design codes e.g. BEAMA (1) and HEI (2) do not take into account tube nest layout and the interaction of the condenser with the air pump or ejector system. They are therefore of limited use in predicting the performance of a particular design of condenser for a wide range of operating conditions. For example the codes would predict the same vacuum for condensers with deep tube nests - and high steam pressure losses - as for those with shallow nests. This is clearly not true. Likewise they cannot predict the influence of air leakage.

The CONE program has been developed to overcome these deficiencies. As shown in Figure 1, the condenser pressure will be determined by heat transfer considerations alone if the air suction pressure is sufficiently low. If the air removal device does not produce sufficient suction, air blanketing will occur in the condenser and the condenser pressure will be controlled by the air suction pressure. This is modelled in the program as follows. First an average heat transfer coefficient is used to determine the mean steam pressure in the tubenests. Then by using an estimated steam pressure drop the program derives the inlet steam pressure and the pressure at the air removal point. Thus

$$(p_1, p_{arp}) = f_1 (\text{CW temp, CW flow, heat load, fouling, geometry}) \quad \dots(1)$$

where CW refers to the cooling water, 1 is at the inlet to the condenser, arp refers to the air removal point in the condenser. This is compared with the characteristic for the air pumping system i.e.:

$$p_{axs} = f_2 (\text{air leakage rate, seal water temp, air steam ratio}) \quad \dots(2)$$

where axs refers to the air extraction system.

If $p_{arp} > p_{axs}$ then the air extraction system is considered adequate for the condenser to operate in an air free condition and the value of p_1 determined in equation (1) is taken as the condenser pressure.

If $p_{arp} < p_{axs}$, then it is assumed that regions of high air concentration exist within the tubenest and that a discrete boundary exists between those tubes with a high steam concentration and those with a high air concentration. Those with a high air concentration (the air blanketed ones) are assumed to perform no condensation and the equation (1) is recalculated iteratively with an increasing number of tubes air blanketed until $p_{arp} = p_{axs}$. The corresponding value of p_1 is then taken as the condenser pressure. This approach is valid for condensers where the regions of air blanketing can be reduced or removed by improved suction at the vent points. Isolated air pockets (i.e. those not connected to the vent points) are unlikely to be directly affected by improved suction and the CONE approach cannot be applied.

The mean steam pressure is calculated using an overall heat transfer coefficient, α_{ov} given by the expression:

$$\alpha_{ov} = 3.323 \left(\frac{U}{2}\right)^{0.4} f_3 (T) F_m F_c \quad \text{kW/m}^2\text{K}$$

where:

$$f_3(T) = 0.716 + 0.0236T - 0.00031T^2$$

These expressions are based on the CEGB Site Test Code 3 (3).

The tubenest pressure drop and its relationship with the mean pressure are determined from a 1D analysis, the complex shape of the nest being replaced by an equivalent one-dimensional 'nest description function':

$$n = f_4(z)$$

where n is the number of tubes per row and z is the row number. The total number of rows is obtained by estimating a mean path in terms of the number of tube rows over which the steam passes from inlet to air removal point. The number of tubes in each row is determined by selecting key positions in the tubenest where the value of n can clearly be established (e.g. the first and last rows, the beginning of the air cooling section etc.). Intermediate values of n are then determined by interpolation. A 'desk top' version of the program is now in use at some power stations for condenser performance monitoring.

THE 'EPOC' PROGRAM

The EPOC computer program simulates the fluid flow, heat transfer and air concentration process locally through a steam condenser. It is therefore more suitable than CONE as a tool for assessing or optimizing a condenser design. Briefly the space within the condenser shell (including both the access trunking and the tubenests) is divided into box shaped control volumes. The laws of conservation of mass, momentum and energy are applied to each control volume and the physical conditions within the control volumes are calculated for given conditions at the condenser inlet and vent points and given physical properties and geometrical data.

In detail, the presence of the tube support plates allows steam flows parallel to the tubes to be neglected. This reduces the problem of determining the steam flow pattern to two dimensions. Computations can be made for a number of planes perpendicular to the tube direction, a grid of rectangular control areas being superimposed on each plane. The condenser tubes are assumed to provide frictional resistance proportional to the number of tubes in each rectangle and flow sinks proportional both to the number of tubes in the rectangle and to the local heat transfer coefficient. The latter is dependent on local steam velocity and condensate inundation.

A principal part of the computations is the determination of the local pressure and velocity vectors. Equations for these quantities are derived for each grid rectangle, expressed in finite difference form and solved simultaneously. Iterations allow for changes in local heat transfer coefficient as the pressure and velocity fields vary. Other quantities such as steam temperature, local heat fluxes, cooling water (CW) temperature rise etc. can then be determined.

The program currently uses the Dittus-Boelter equation (4) for evaluating the water-side heat transfer coefficient. However recent information (5) suggests that the Petukhov-Popov equation may be more accurate and this may be incorporated in the program in the future.

The effect of air on the steam side heat transfer coefficient is allowed for by using the approximate theoretical equation proposed by Fujii (6). The equation of Rose (7) has been found to give similar results. Both these equations give better agreement over a wider range of conditions than the equation of Berman and Fuks (8).

The effect of inundation on heat transfer by additional condensate from other tubes has traditionally been accounted for using the correction term:

$$\frac{\alpha_n}{\alpha_{Nu}} = N^{-\gamma}$$

where α_{Nu} is the Nusselt value of the heat transfer coefficient and $N = (\dot{m}/C)$ is the ratio of total water flow rate over the tube to the condensation rate (assuming condensate drains downwards and the flow rate includes the amount of water which has condensed above the tube under consideration). The exponent γ has been ascribed constant values between 0.223 (Grant and Osment (9)) and 0.07 (Fuks (10)) to fit experimental data, high values of γ generally being associated with tests conducted at low Froude numbers (defined in terms of vapour intergap velocity) and vice versa. At present the value of 0.16 recommended by Wilson (11) is used in EPOC. An approach currently being reviewed is not to correlate against the total water flow rate \dot{m} but to define N in terms of the amount of water forming the film on the surface of the tube (Brickell (12)). In contrast to traditional methods where separate corrections are applied to α for vapour shear and inundation, a single correction incorporating both effects and their interaction is applied; for example less water is predicted on the tube at higher steam velocities.

The pressure drop, assumed to be isotropic, is calculated from the Engineering Sciences Data Unit (13) correlation for a dry tube bank. A single phase loss relation gives a reasonable indication of the two-phase loss although significant differences can occur with the upflow and downflow of vapour (Brickell (12)) particularly in a water hold-up situation. No allowance is made at present for the effect of outside tube fouling on pressure drop.

Because of the uncertainties which remain regarding the mechanisms by which high air concentrations exist in condensers and which are discussed in a companion paper (Al-Sanea et al (14)), a simpler model was desirable. From analytical studies (Davidson (15)) and steam side traversing of medium and large CEGB condensers it has been observed that a rapid transition occurs from a high steam fraction to a high air fraction, usually over 2 or 3 tube rows which is less than a typical finite difference cell length when modelling large plant. As a result a computationally faster program, EPOCB, has been developed from EPOC to predict the performance of condensers and the location of the air pockets by omitting the detailed programming in EPOC of such effects as air diffusion and air entrainment in condensate. Using a similar approach to that used in the CONE program it is assumed that regions of high air fraction exist within the tubenest and that a discrete boundary exists between those grid cells with a high steam fraction and those with a high air fraction. The high steam fraction tubes are assumed to be unaffected by the presence of air and the air blanketed tubes are assumed to perform no condensation. Location and size of air pockets are determined instead by an isobaric boundary condition at the air/steam interface. This pressure is normally equated to the air extraction vent pressure. For the purpose of predicting condenser pressure the errors associated with this approach are believed to be no greater than those which include diffusion etc. and attempt to model steep air gradients using a relatively coarse grid, particularly when

the magnitude of the turbulent diffusion coefficient is unknown. Further knowledge of diffusion, air entrainment etc. plus future improvement in computer speeds might make more precise modelling with finer grids more worthwhile.

The accuracy of the values predicted by EPOC and EPOCB depends on several additional factors such as the accuracy of the empirically derived heat transfer and pressure loss coefficients etc. In absolute terms the accuracy is believed to be about 2 mbar. Relatively, between computations for different data or small geometrical changes, the accuracy should be much better than this, probably better than 1 mbar.

THE 'COLT' PROGRAM

The 'COLT' program is used for conducting tests on full scale plant and on the Leatherhead condenser rig. A Hewlett-Packard 9835A 128K byte 'desk top machine' is used for this work. Within a few minutes of receiving the necessary information the program produces:

Contour plots (normally of CW temperature rises) - examples are given by Rowe (16)

Tabulation of key parameters

Data corrected to design conditions

Comparison with CEGB Site Test Code 3 (3)

Plots of selected parameters

The rapid presentation of information by the program has enabled the direction of tests to be altered interactively. In addition, defective instrumentation could be rapidly identified and remedial action taken.

CASE STUDIES

Ratcliffe

Ratcliffe Power Station has 500 MW (E) turbine-generators. One of the condensers was extensively instrumented for examining in detail the interaction of the condenser with the air extraction system. At the time of the test the CW inlet temperature was very steady. Figure 2 shows the effect of air leakage on condenser inlet pressure, together with the 'CONE' prediction which agrees closely. As shown, the pressure was constant until a 'critical' air leakage was reached when the pressure started to rise. This 'critical' air leakage is the point at which the air extraction system can no longer provide a sufficiently low suction pressure to prevent air blanketing. A different set of operating conditions would have a different 'critical' leakage. Of more interest was the fact that the same test was repeated with air being admitted at various locations and that the measured inlet pressures were independent of where the air was admitted. The condensation pattern as measured by tube temperature rises indicated extensive air blanketing at high air leakage but again these patterns were independent of where the air was admitted to the condenser. This is discussed in more detail by Rowe (16). These tests provide encouraging support for the simplistic approach adopted in both CONE and EPOCB where the degree of air blanketing in the condenser is considered to be a function of the vent pressure. The role of air leakage is solely to determine the vent pressure. It would be interesting to know whether this phenomenon were true for all large condensers, particularly those

The EPOCB program was used to assess proposed modifications as isolated air pockets can be reproduced without modelling the above mechanisms. The program automatically locates the area of high air concentration; the size of this being determined by the pressure boundary condition in the air pocket. To test the validity of the program, computer predictions using the 'as found' geometry were compared with the test data. As can be seen from Figures 6 and 7 the region of air blanketing located by the temperature traversing agrees well with that produced by the program.

Oldbury. Oldbury is one of the CEBG's Magnox gas cooled reactor stations using estuary water for the condensers. Tests have indicated large pressure drops through the tube bundles. Associated with this are areas where condensation rates are very low particularly when the cooling water temperature is low. (Figures 8 and 9).

When the condensers were constructed 70-30 cupro-nickel was used for the tubing. This material had shown signs of severe deterioration. During a summer outage in 1982 retubing with titanium was begun starting with one half of one condenser. The retubing exercise offered an opportunity to change the tubenest geometry.

Eight different geometries were studied using the EPOC program. Repositioning of baffles, provision of steam access lanes, condensate trays and additional vent points were all studied under a range of conditions. One of these geometries serves to illustrate how important it is to study the operating conditions of a condenser before implementing a modification.

Figure 10 shows the computed performance of a proposed modification which involved removing 9% of the tubes and providing central suction for the non-condensibles, with the objective of reducing the pressure drop through the nest. Predictions with 70-30 cupro-nickel and Titanium are shown. The prediction for the 'as found' geometry retubed in Titanium is shown for comparison. It can be seen clearly that the proposed modification performs better at low cooling water temperatures but is worse at the higher temperatures. This is because the steam pressure loss is less significant at the higher temperature and the reduction in surface area dominates.

The operating regime of any item of plant is determined mainly by its 'marginal' generation costs subject of course to safety and other technical considerations. Nuclear plant has in general high capital and low marginal costs and therefore is required to generate at its maximum permissible load for all times when maintenance is not being carried out. Consequently almost as much operation takes place at high cooling water temperatures (up to 15°C) as at low temperatures (down to 5°C); which makes this modification of no benefit.

Further geometries were studied and a configuration which was predicted to be of value at all cooling water temperatures was implemented. This involved the removal of a very small number of tubes to provide central air suction (Figure 11). The computer modelling indicated that central suction from upper and lower nests would be of benefit. However engineering constraints limited the modifications to the lower nests only. Preliminary tests carried out after the work was completed indicate an improved performance.

CONCLUSIONS

The computer programs described here have proved useful for assessing condenser performance at the design stage, for determining operating characteristics and for deciding on internal modifications. In general, comparison of the CONE and

EPOC programs with measured data shows good agreement. On an absolute scale, the programs predict condenser vacuum within approximately 2 mbar which is close to the tolerance in measurement. When using the EPOC program to distinguish between alternative possible modifications, a relative accuracy of about 1 mbar is estimated.

The EPOC program appears to underpredict the value for heat transfer coefficient in regions where both condensate inundation and steam velocities are high e.g. the lower parts of the tube nests in the Ince 'B' arrangement. This appears to be because the steam shear forces and velocity head are strong enough to displace the condensate perhaps causing some coalescence.

The EPOCB program which does not directly include air in its calculations does predict the position of air pockets quite closely. This apparent anomaly supports the supposition that air leaking into the condenser does not substantially effect the heat transfer coefficient outside an air pocket. The sole effect of the air leakage is to control the pressure of the air removal equipment and hence the pressure at the air removal point.

There is some uncertainty about the prediction of flows in access lanes. New experimental data on pressure loss coefficients in access lanes e.g. Lee et al (18) will need to be assessed and incorporated. Certainly this is an area for further work.

ACKNOWLEDGEMENT

The work was carried out at the Central Electricity Research Laboratories and the paper is published by permission of the Central Electricity Generating Board.

SYMBOLS USED

- C = condensation rate per tube ($\text{kg/m}^2 \text{s}$)
 F_C = cleanliness correction factor
 F_m = material correction factor
 f = function of
 N = inundation ratio
 n = number of cooling water, CW, tubes per row
 p = pressure (mbar)
 T = CW inlet temperature ($^{\circ}\text{C}$)
 u = CW flow velocity (m/s)
 \dot{m} = total water flowrate over a tube ($\text{kg/m}^2 \text{s}$)
 z = row number
 α = heat transfer coefficient, htc ($\text{kW/m}^2 \text{K}$)
 α_{Nu} = Nusselt htc ($\text{kW/m}^2 \text{K}$)

- α_n = steam side htc on the n th inundated tube ($\text{kW/m}^2\text{K}$)
 α_{ov} = overall htc ($\text{kW/m}^2\text{K}$)
 γ = exponent of inundation ratio

Subscripts

- arp = air removal point
 axs = air extraction system
 i = condenser inlet

REFERENCES

1. BEAMA, Recommended Practice for the Design of Surface Type Steam Condensing Plant, Publication No. 222, 1967.
2. HEI Standards for Steam Surface Condensers, 7th Edition, 1978.
3. CEGB Site Test Code Number 3, Performance of Surface-Type Steam Condensers, 1981 issue.
4. Dittus, F.N. and Boelter, L.M.K., 1930, University of California Publications Engng., 2(13), 443.
5. Lorenz, J.J. et al., 1981 An Assessment of Heat Transfer Correlations for Turbulent Pipe Flow of Water at Prandtl Numbers of 6.0 and 11.6, Argonne National Laboratory Memo. (draft).
6. Fujii, T., 1980, Vapour Shear and Condensate Inundation: An Overview. Condenser Workshop, Naval Postgraduate School, Monterey, California, Marto, P.J. and Nunn, R.H., Eds. (Hemisphere Publishing Corporation, 1981).
7. Rose, J.W., 1980, Condensation in the Presence of Noncondensing Gas. Condenser Workshop, Naval Postgraduate School, Monterey, California, Marto, P.J. and Nunn, R.H., Eds. (Hemisphere Publishing Corporation, 1981)
8. Berman, L.D. and Fuks, S.N., 1958, Mass Transfer in Condensers with Horizontal Tubes when the Steam Contains Air, Teplotenergetika, Vol. 5, No. 8, pp 66 - 74.
9. Grant, I.D.R. & Osment, B.D.J., 1968, The Effect of Condensate Drainage on Condenser Performance, NEL Report No. 350.
10. Fuks, S.N., 1957, Heat Transfer with Condensation of Steam Flowing in a Horizontal Tube Bundle, Teplotenergetika, 4(1), 35 - 39; English translation NEL 1041, National Engineering Laboratory, East Kilbride.
11. Wilson, J.L., 1972, The Design of Condensers by Digital Computers, I. Chem. E. Symposium Series, No. 35.
12. Brickell, G.M., 1980, Potential Problem Areas in Simulating Condenser Performance, Condenser Workshop, Naval Postgraduate School, Monterey, California, Marto, P.J. and Nunn, R.H., Eds. (Hemisphere Publishing Corporation, 1981).

13. Engineering Sciences Data Unit, 1979, Crossflow Pressure Loss Over Banks of Plain Tubes in Square and Triangular Arrays Including Effects of Flow Direction, No. 79034.
14. Al-Sanea, S., Rhodes, N., Tatchell, D.G. and Wilkinson, T.S., 1983, A Computer Program for Detailed Calculation of the Flow in Power Station Condensers. Proceedings of Conference on Condensers - Theory and Practice, UMIST, Manchester, England.
15. Davidson, B.J., 1981, Solutions of the Diffusion-Convection Equation in the Presence of Condensation. Proceedings of Conference on Diffusion-Convection, Sunderland Polytechnic, Sunderland, England, Caldwell, J. and Moscardini, A.O., Eds. (Pentech Press, Plymouth, 1982).
16. Rowe, M., 1983, Power Plant Condensers - Recent CEGB Experience. Proceedings of Conference on Condensers - Theory and Practice, UMIST, Manchester, England.
17. Rowe, M., Ferrison, J.A., Beckett, G and Taylor, B.J., 1981, Private Communication.
18. Lee, N.K., Mayhew, Y.R., Hollingsworth, M.A., 1983, Pressure Losses in Tube Banks with a By-pass Lane. Proceedings of Conference on Condensers - Theory and Practice, UMIST, Manchester, England.

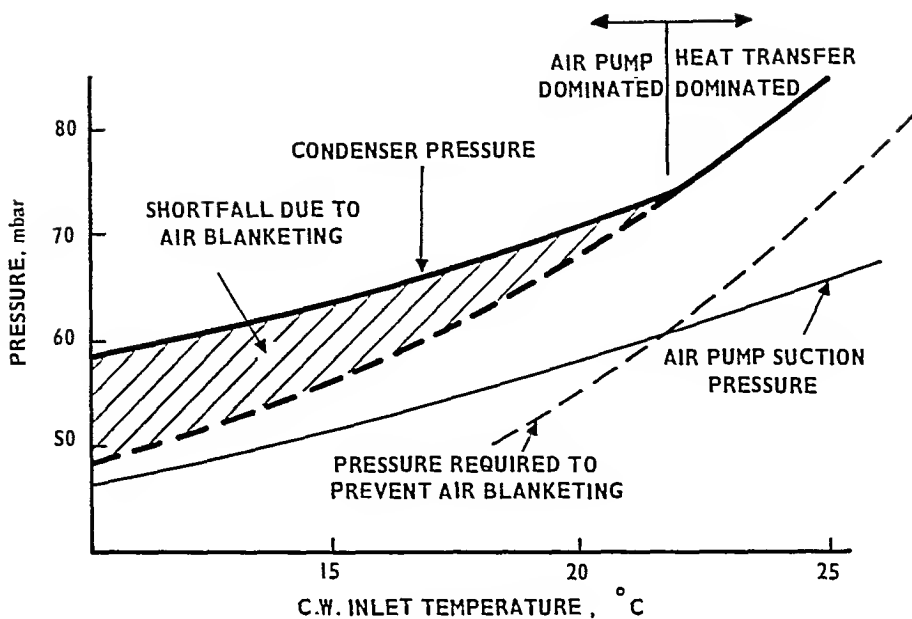


Figure 1 Typical 'CONE' prediction of condenser pressure

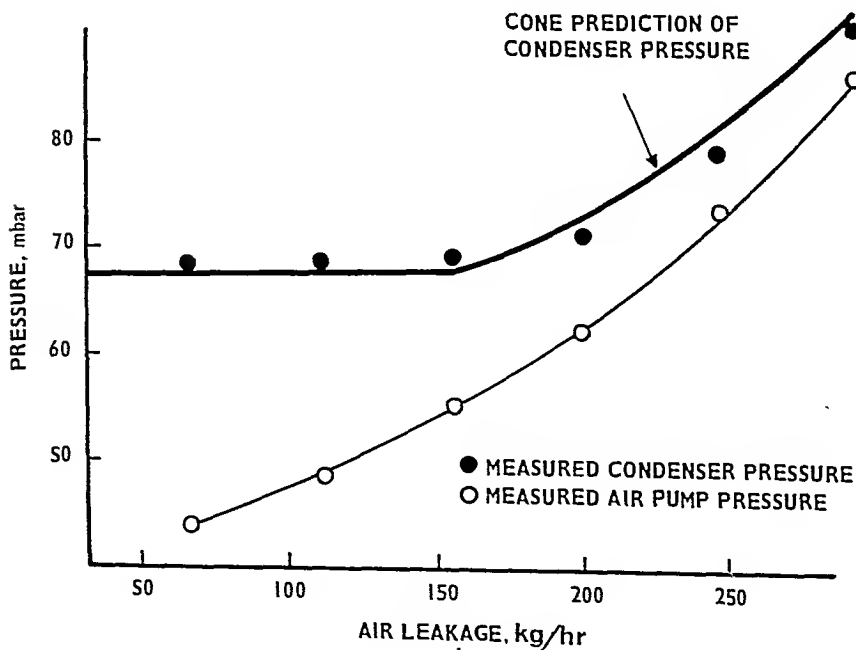


Figure 2 Ratcliffe - Effect of air leakage on condenser pressure

$\frac{\text{COMPUTED PRESSURE DROP}}{\text{MEASURED PRESSURE DROP}} = 0.98$

$\frac{\text{COMPUTED PRESSURE DROP}}{\text{MEASURED PRESSURE DROP}} = 1.15$

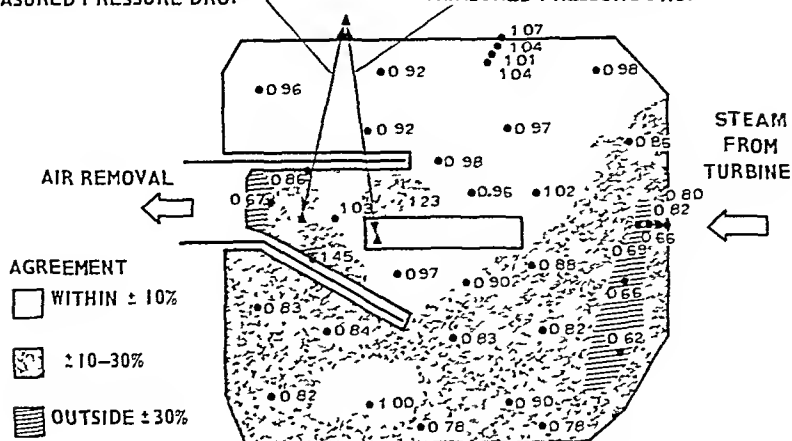


Figure 3 Ince 'B' - Comparison of computed and measured values of heat transfer coefficient and pressure drop

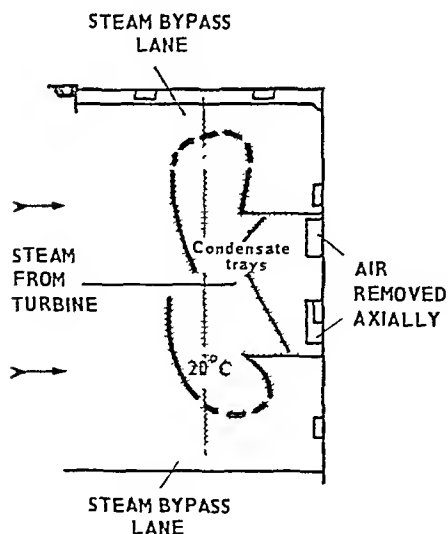


Figure 4 Aberthaw 'B' - Measured position of 20°C isotherm

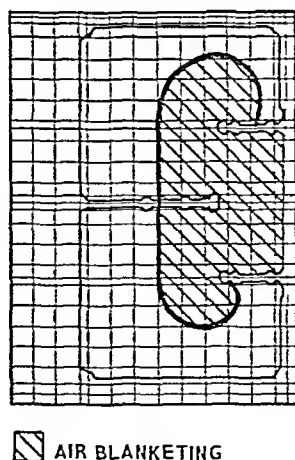


Figure 5 Aberthaw 'B' - Computed region of air blanketing

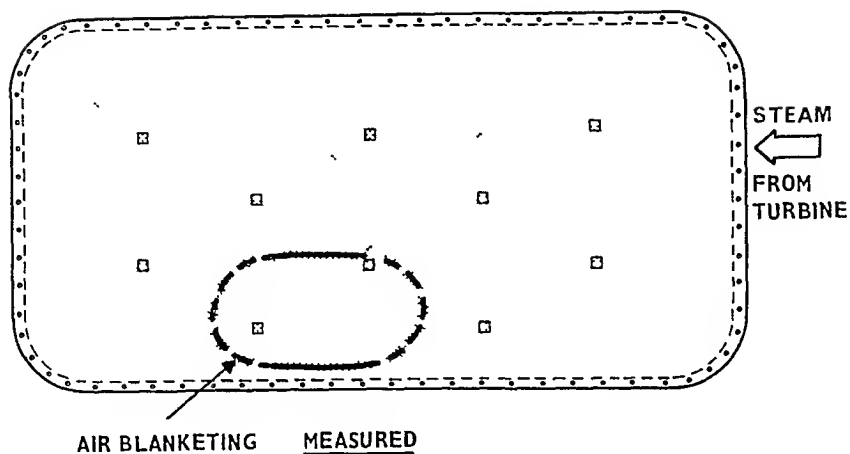


Figure 6 Didcot - Region of air blanketing measured by steam side temperature traversing

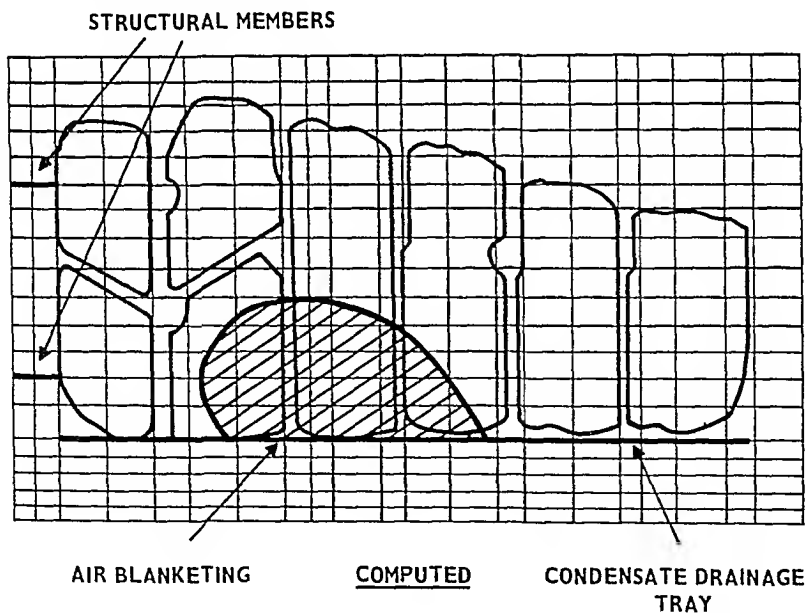


Figure 7 Didcot - Predicted region of air blanketing using the 'EPOCB' program

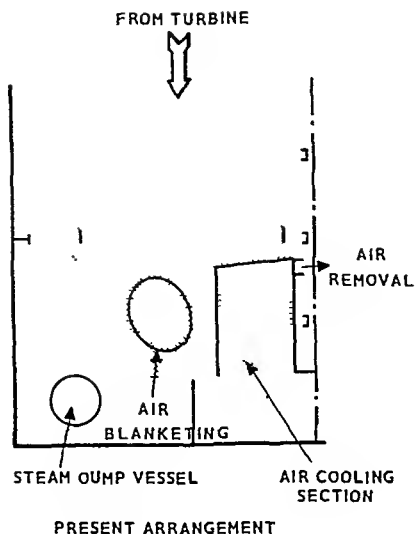


Figure 8 Oldbury - Measured location of air blanketing

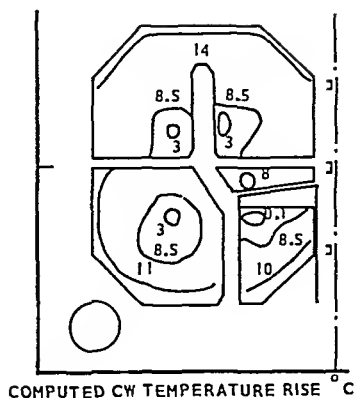


Figure 9 Oldbury - Computations showing regions of poor condensation

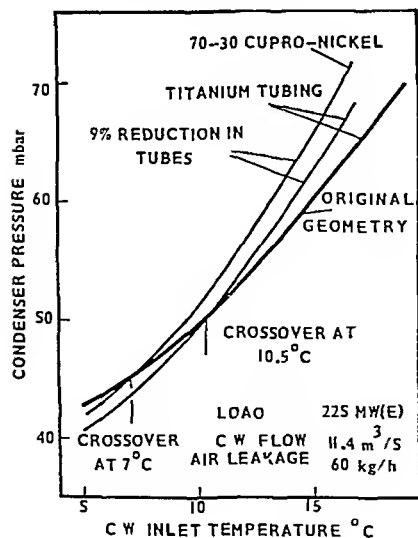


Figure 10 Oldbury - Computed effect of 9% tube removal

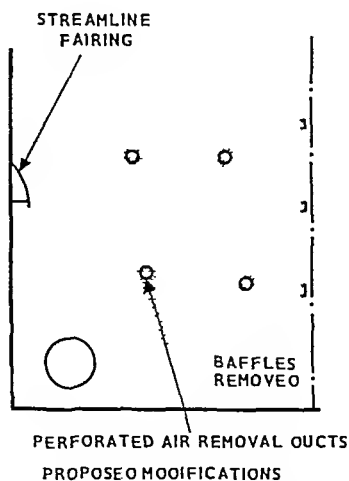


Figure 11 Oldbury - Provision of central air removal ducts

POWER CONDENSERS
Practice

POWER PLANT CONDENSERS - RECENT CEBG EXPERIENCE

M. Rowe*

This paper considers design trends, reliability and thermodynamic performance of condensing plant now operated by the CEBG. Emphasis is placed on recent work which has led to improved vacuum and higher power station thermal efficiency. Faults in older plant are identified. Plant recently installed is performing well. Possible future improvements including the use of roped condenser tubes are discussed.

INTRODUCTION

An important aim of this Symposium is to share practical experience on power plant condensers. Aspects of experience in the United States are expressed in papers by Diaz-Tous and Mussalli (1), Kornbau et al (2), Olikar and Katsman (3), Bornstein (4) and Maurer and Berendson (5). Japanese practical experience is described by Ozeki et al (6). The present paper concerns some experience with condensing plant in the larger turbine-generator units operating in Britain. Hopkins et al (7) provide some experience from a British manufacturer. Other details of British experience are provided by Beckett et al (8), Clay and Sochaczewski (9) and Bindon (10).

DESIGN TRENDS

Since 1966 the CEBG has installed 49 turbine-generator units of 500 MW output and 16 units of 660 MW output. Also 6 units in Magnox nuclear stations have condensers that are similar in size and design to those on the 500 MW plant. These units provide most of the electricity supply in England and Wales today. 7 further 660 MW units are under construction.

Before the introduction of the 500/660 MW plant most condensing plant was placed under the turbine in the, so called, underslung arrangement. The condenser tubes were placed horizontally transverse to the turbine shell. The 500 and 660 MW unit condenser designs (Figure 1) have evolved from this underslung arrangement in roughly the following order.

500 MW Transverse Underslung ('Bridge' Design)

In this arrangement the cooling water makes two passes through the condenser as in the earlier plant, the water entering by the bottom tube

* CEBG, Central Electricity Research Laboratories, Leatherhead, England.

nests and leaving by the top. There are however six separate cooling water flows in parallel, two for each low pressure turbine cylinder.

500 MW Axial Underslung. Contemporary with the bridge design were several single pass designs with the condenser tubes placed axially beneath the turbine. Such arrangements were possible because the combined length of three turbine cylinders was roughly twice the length of the tubes in the two-pass arrangement. A uniform vacuum was obtained along the condenser by allowing half the cooling water to flow in one direction, half in the other. Cost savings have resulted from the reduced number of tubeplates.

500 MW Axial Side-Mounted (Pannier). In this single-pass arrangement the condenser is split into two shells each mounted as panniers alongside and level with the turbine. The reduced overall height of the turbine plant allowed a corresponding reduction to be made in turbine-hall height with some saving in building costs. There is also an increased aperture for steam passing from the turbine to the condenser compared with the underslung design. A disadvantage to the operator is that the condenser steam space cannot be flooded, a useful feature when searching for tube leaks.

500 MW Axial Integral. This arrangement which is an alternative to the side-mounted arrangement has the low pressure turbine cylinders and the condenser tubes enclosed within a single box structure. In some cases the box is split transversely into compartments each containing one turbine cylinder. By allowing all the cooling water to flow in the same direction, a different vacuum forms in each compartment depending on the mean cooling water temperature in that compartment. This 'multivacuum' variation reduces fuel costs by about 0.2%

660 MW Axial. Both side-mounted and integral arrangements have been constructed the layouts being similar to the corresponding layouts on the 500 MW units. All but two of the 660 MW units with axial condensers are multivacuum units.

660 MW Transverse Underslung. The trend towards reducing plant costs by reducing the number of turbine low pressure cylinders (from three to two for this unit size) has meant a return to the transverse underslung condenser arrangement. This has also allowed development of the modular concept with each turbine cylinder having its own condenser. The single pass cooling water arrangement has been retained with the condensers projecting some distance on each side of the turbine.

Generally tubes of 25.4 mm outside diameter, 1.2 mm wall have been used in an equilateral triangle arrangement with pitch diameter of 1.375. Tube materials have varied from 70 - 30 brass in some inland stations to aluminium brass and 70 - 30 cupro-nickel in coastal stations. All new units from 1980 onwards have been fitted with titanium tubes (25.4 mm outside diameter, 0.7 mm wall) and some retubing of coastal stations with titanium has taken place. All units have double tubeplates.

Removal of non condensibles from the 500 MW unit condensers is effected by a bank of typically three air pumps. Some of these are of the Leblanc, water-jet type, some have an air driven ejector combined with a liquid-ring pump and others have a water driven ejector. The Magnox nuclear units with 500 MW type condensers are equipped with steam ejectors. On most of the 660 MW units, two air pumps have been provided (one as a stand-by), these being a steam ejector-liquid ring pump combination. During start-up operation an additional liquid-ring 'quick-start' pump enables the condenser pressure on most units to be reduced to about 100 mbar in 20 minutes.

RELIABILITY

Condensing plant commissioned recently has been very reliable. However a number of problems occurred on the early 500 MW plant and, while these have been largely overcome, they are worth mentioning briefly because of their influence on the more recent designs.

Tube Leakage

Erosion-Corrosion. Both aluminium brass and cupro-nickel tubes have been susceptible to erosion-corrosion in sea water cooled condensers. This problem has been cured by restricting the admission of debris or by dosing with ferrous sulphate. Nylon venturis inserted in the tube inlets have proved particularly effective at preventing inlet-end erosion and ensuring that debris which might have jammed further down the tube is excluded. A comprehensive summary of these remedial measures is provided by Parker and Ward (11). In some cases it has proved economic to retube with titanium. Heaton et al (12) consider some of the factors which have led to the adoption of titanium as a condenser tube material.

Ammonia Corrosion. This has caused tube leakage in the air cooling sections of some inland condensers. The cure has been to replace the brass tubes with tubes of 90 - 10 cupro-nickel.

Tube Vibration. There have been a few incidents of aerodynamically induced tube vibration on prominent tubes e.g. near the corners of a tube nest. In extreme cases adjacent tubes have clashed and perforated. Strapping the tubes at their mid points has effected a cure, the same procedure being used whenever brass or cupro-nickel tubes have been replaced by the thinner and thus more flexible titanium tubes.

Other Problems

Tubeplate Leakage. Leakage of cooling water through the tubeplates has occurred though infrequently and the practice of using double tubeplates has been vindicated.

Water Box Corrosion. The use of mild steel for water box construction has posed a problem where the cooling water is saline. Iron oxide readily detaches from mild steel as flakes, whereas on cast iron water boxes it remained intact. Cathodic protection systems have been tried in some water boxes but have not always been reliable. The most effective solution has been to coat the inside of the water box carefully with neoprene or coal tar epoxy. The same treatment has been applied to the water box side of the double tubeplates in condensers tubed with titanium as a precaution against galvanic interaction with the tubes.

THERMODYNAMIC PERFORMANCE

The vacuum achieved initially by some of the early 500 MW unit condensers was disappointing. Reliability problems with condensers and other plant components also meant that efforts to maximise plant thermal efficiency took second place. However the sharp rise in the cost of fuel in 1973 combined with improvements to plant availability produced a change of emphasis and greater attention was given to improving condenser vacuum if possible beyond the values intended by the designer. At today's prices, every millibar improvement in vacuum saves about £200,000 per annum in fuel costs on a high merit 2000 MW power station. A practical limit to what can be achieved will be reached when the terminal

temperature difference (condensing temperature minus cooling water outlet temperature) is about 3°C. Typically this temperature difference was as much as 7°C so that improvements of order 4°C - or in vacuum terms 10 mbar - appeared possible. A number of investigations were begun with CEGB staff working, in some cases, closely with the plant manufacturers.

Problem Areas and Early Modifications

The 500 MW unit condensers were designed in accordance with either the BEAMA (13) or the HEI (14) design guidelines. The problems which were identified as causing poor vacuum were largely outside the scope of these documents. The major problem areas were:

- (a) air leakage rates in excess of air pump or ejector handling capacity,
- (b) steam bypassing the air cooling section of the condenser and affecting the performance of the air pumps or ejectors,
- (c) air pockets at the centres of large tube nests,
- (d) high steam-side pressure losses resulting from narrow access lanes or tube nests that were too large,
- (e) tube fouling.

Air Leakage. Air leakage rates have been at times as high as 700 kg/h and as low as 35 kg/h on the 500 and 660 MW units. Where it was not possible to reduce leakage permanently to low levels extra air pumps or ejectors were added. Conversion of the quick-start air pumps to vacuum maintaining duty by adding an air operated ejector was a simple remedy in some cases. Leakage points have varied from plant to plant; condenser shell/turbine joint, low pressure cylinder half joints, turbine gland seals and housings, bursting discs, condensate level gauges have been typical examples. Generally, average leakage rates have risen on plant that is 'two-shifting' i.e. running for only a limited time each day.

Steam Bypassing. Steam bypassing the air cooling section has the same net effect as a high air leakage rate; insufficient suction is produced by the air pumps or ejectors and air pockets develop within the condenser. Blocking the direct path for steam to reach the air cooling section was found to be necessary in the side-mounted condensers installed at Fawley as shown in Figure 2. A more complex situation was remedied in the integral condensers at Cottam. Here steam bypassing was largely confined to the hotter end of the tube nests. By diverting the air ventilation route through a hole within each tube nest to a point near the cooling water inlet end (Figure 3) steam bypassing was eliminated, air cooling was increased and an improvement of some 2.5 mbar in vacuum was achieved. The tubes cut to create the new ventilation route were removed only partly so that restrictions were maintained at the division plates between the turbine cylinders. This was intended to maintain the multivacuum arrangement. However on other similar units the tubes were removed completely without any noticeable alteration to the multivacuum effect.

Air Pockets. In the absence of air, there will be a certain steam pressure distribution within the tube nests. The pressure will be lowest at points least accessible to the steam leaving the turbine. If air or other non-condensibles are added, they will collect at such low pressure points. If no escape route is provided, the air will accumulate as a pocket. An example of this is shown in Figure 2. Air was found to collect at the centres of the large

outer tube nests. Removal was effected by converting a small number of central tubes to air suction tubes.

Steam Pressure Drop. Tube nests too large for the steam to reach the innermost tubes without suffering a substantial pressure and temperature drop have been a problem in the underslung condensers of the type installed at Ratcliffe. Alternatively it could be argued that the condenser shells were too small for the duty intended. Some optimization has been possible by removing tubes in such a way that the net increase in heat transfer coefficient more than compensates for the reduction in condensing surface area. Figure 4 shows the sequence of modifications and the reported improvement in vacuum. These modifications were made before the development of computer programs which model the heat transfer and flow processes within condensers. Such programs would be useful if the modifications were to be carried out today. However their usefulness might be limited as the flow pattern is, in this example, very dependent on the frictional effects within the steam access lanes.

Tube Fouling. Water-side fouling is well known as a major contributor to poor condenser performance, the principal causes being phosphate or carbonate scale, silt and biological fouling (slime). The scale can be removed by adding sulphuric acid to the cooling water and the slime by chlorination. Silt and other debris can be removed by periodic brush cleaning or water hosing. An alternative technique which appears satisfactory for most causes of fouling is to circulate rubber balls through the tubes. Different methods have been tried in different power stations, the method adopted depending on the cause and severity of the fouling and on the cost. To quote an example (Ferrison et al (15)) measurements of heat transfer on specially cleaned tubes and tubes fouled with phosphate scale showed that the latter had decreased the overall 'clean' heat transfer coefficient by 58%. Acid cleaning reduced this to about 15%. The installation of a ball cleaning system reduced the fouling to near zero.

It has usually been assumed that fouling on the steam-side has a negligible effect on heat transfer. However some recent measurements at Ratcliffe (Rowe et al (16)) indicate that external fouling can be a problem particularly if the unit has been in service for a considerable time. For these measurements, three tubes were cleaned externally with emery cloth and the cooling water temperature rises through these tubes were compared with the corresponding rises in adjacent tubes. All the tubes were maintained clean on the inside with a ball cleaning system. The results are shown in Table 1. The Ratcliffe condensers have been in service for about 13 years. Obviously it is not possible to clean the outside of all the tubes mechanically. However chemical methods are under consideration and may be feasible.

TABLE 1 - Effect of External Tube Cleaning at Ratcliffe

Tube Position	Cooling Water Temperature Rise, °C			Increase in Tube Overall Transfer Coefficient
	Dirty Tube	Clean Tube	Difference	
Top tube, near outside	14.7	16.7	2.0	43%
Top tube, near centre	13.8	15.9	2.1	40%
Side tube, near centre	12.7	14.1	1.4	23%

Formal Testing

During the course of investigating condenser performance, it became necessary to examine and reappraise testing methods in order to assess as accurately as possible the thermal performance of particular plants.

Several methods for testing condensers have been published. The best known is that developed by the ASME (17). The general aim in a formal test is to refer the test data to some fixed set of operating conditions usually the design values of heat load, cooling water inlet temperature and flow rate. Some form of correction has to be applied to the measured vacuum because in most cases the test conditions are not the same as the reference conditions. The correction procedure does not normally take into account the geometrical layout of the condenser tubes. Identical corrections would thus be made for condensers with shallow tube nests where the steam temperature remains constant and for condensers with deep tube nests and a considerable variation in steam temperature. Errors have been found when correcting data from condensers with deep nests because the steam temperature variation (which results from frictional pressure losses) varies with operating condition.

A new test procedure, the CEBG Site Test Code 3 (18) attempts to rectify this situation by allowing for steam temperature variation when deriving the mean temperature difference between steam and cooling water in a manner similar to that considered by Guy and Winstanley (19) in 1934. Further details are given in the paper by Clay and Sochaczewski (9), together with some improved techniques for the measurement of cooling water flow and outlet temperature.

Diagnostic Testing

Tests with substantially more instrumentation than required for overall performance measurement have cast light on the internal physical behaviour of condensers. Beckett et al (8) show how the condenser pressure at Ratcliffe varied as the air leakage rate increased. Initially the condenser pressure remained constant - indicating that providing air does not stagnate, it does not affect the heat transfer coefficients within the tube nests. Then when the air leakage rate was high enough, the air pump pressure became too high for complete ventilation. Air pockets formed within the condenser and the condenser pressure rose to match the air pump pressure.

Interestingly, exactly the same effect was observed irrespective of where the air was injected. Three leakage routes were chosen in turn.

- (a) into the condenser shell above the tube nests and well distributed via the vacuum measurement grid,
- (b) into the condenser shell at one point just above the tube nests but not far from an air extraction position,
- (c) into the air suction manifold just ahead of the air pumps.

The same condenser pressure variation was obtained and, as shown in Figure 5, the same shape of air pocket as deduced from measurements of cooling water temperature rise distribution. From a design viewpoint these results show that no change in performance will result from diverting heater vents etc. from various points around the condenser shell to a common point near the air cooling section.

Another fact to emerge from these tests concerns the time required for test conditions to stabilize. It was observed that providing the condenser was unaffected by air pump pressure, stable conditions were reached quickly - within a minute or two - when the air leakage rate was changed. This is not

too surprising since the sole plant undergoing a change in condition was the bank of air pumps. However when the condenser was under the control of the air pumps, the stabilization time was much longer - of the order of 15 minutes. This is much longer than could be expected from any thermal lag effect. However by assuming that any change in air flow rate will be divided between the pumps and filling or emptying the air pockets within the condenser, it can be shown that the change in condenser pressure due to a step increase in air leakage follows an exponential rise of the form

$$p = p_0 + \Delta p(1 - e^{-t/\tau})$$

For the Ratcliffe tests the time constant τ was calculated as 4.2 minutes which means that 95% of the pressure change is completed in approximately 13 minutes, close to the observed value.

Observations by Bloomer (20) of the flow rate of air emerging from one of the condensers at Didcot during a change in load portray a similar feature, the rate of air removal varied depending on whether air pockets within the condenser were being inflated or deflated as the condenser adjusted to a change in heat load. The important point is that one should be careful that conditions have stabilized when making measurements on a condenser that is under the control of the air pumps.

Figure 6 shows measured zones of air blanketing in one panner of the side-mounted condensers at Ince 'B' when the air leakage rate had been substantially increased. The region to which the steam is penetrating is seen to vary from one tube nest to another. This variation is partly due to the disposition of the tube nests but mainly due to the influence of non uniformity in the turbine exhaust flow. In this case a broad jet of steam emerging from the turbine is directed from the lower inside corner of the condenser to the top outside corner. By comparing the degree of penetration into nests facing the turbine exhaust with that into nests that are in the 'shadow', the net effect of the turbine exhaust dynamic head can be established. In this case it amounts to some seven tube rows. Although it will depend on tube spacing and to some extent on nest shape, it is suggested that the side or top of a tube nest which faces the turbine exhaust should be thickened by approximately this number of tube rows for steam penetration to be even.

Internal inspection of condensers as part of a diagnostic investigation occasionally reveals an oddity. One such item is shown in Figure 7. It concerns the detailed arrangement for drainage from the air cooling section of a condenser tube nest. This would be satisfactory if there were no difference in pressure between the air pump and the condenser. However with a pressure difference, the condensate level in the manometric seal loop will rise. A pressure difference of 1 mbar corresponds to a water level difference of 1 cm. A typical pressure difference between condenser and air pump on this particular plant is 20 mbar which just causes the water level to rise and cut off the air flow route. Certainly there is evidence (Smalley and Deam (21)) that very little air is extracted from this nest. It is clearly an undesirable design detail.

Modifications Involving Computer Programs.

Computer programs which determine the flow and heat transfer variations within a condenser have usefully indicated the need for some modifications and the form they should take. The earliest example is probably that made at Cockenzie reported by Wilson (22). This consisted of baffles placed at the entrance to the air cooling sections in a similar manner to that employed at Fawley (see Figure 2).

Another modification of similar type at Sizewell is reported by Colquhoun-Lee and Bryan (23). As shown in Figure 8 the computed flow pattern indicates routes of unequal resistance to the air removal points. Suitable baffles were added to prevent steam taking the line of least resistance and swamping the air ejectors.

Oldbury Modifications. These modifications are mentioned by Beckett et al (8). However the redesign process is worthy of discussion in more detail. The problem was not steam bypassing, as e.g. in the Sizewell modification, but very deep tube nests. The task was thus to reduce as much as possible the average steam path length. Venting at the centre of the tube nests was the obvious answer but the real use of the computer program was to help decide on several geometrical options. These were:

- (a) whether to vent from both upper and lower nests - this was found to give better performance but was difficult to implement so only the lower nests were given central vents,
- (b) whether to include extra access lanes for the steam in the upper nests - it was found that the loss of surface outweighed the effect of a reduction in steam pressure loss,
- (c) whether condensate trays should be provided below the upper nests - it was found that the obstruction to the steam flow outweighed the effect of reduced condensate inundation.

Further design details required hand calculation. The central vents (Figure 9) were sized to carry an air-steam mixture of ten parts steam to one of air. It was assumed that the flow rate of the air-steam mixture entering the vent in any bay between adjacent tube support plates was proportional to the condensation rate in that bay. The pressure drop along the vent tubes was calculated by allowing for frictional effects and for the change in momentum as flows enter the vent tube and are accelerated (see Appendix A).

The vent holes in each bay were initially sized to carry the relevant mixture flow taking into account the local pressure drop from within the tube nest to the inside of the vent tube, the minimum pressure drop being set at 1 mbar. The hole sizes and pattern finally chosen were simplified to ease implementation. The holes were positioned near to the tube support plates. This followed observations by Rowe and Ferrison (24) that this is where air tends to collect. A small rig was built to determine the effect of condensate inundation on the vent holes. Gutters were found to be necessary to prevent condensate entering the holes. The best circumferential position of the holes was judged to be just below the horizontal centre-line. This was above the level of possible flooding inside the vent (flooding could be maintained by the pressure difference from outside to inside the vent tube).

Part of the first bay at the cooling water inlet end was used as an air cooling section; this allowed the former air cooling section which ran the whole length of the condenser to be converted to use as 'main condenser'. A check was made to ensure that there was sufficient tube surface area in the end bay to condense the air-laden steam emerging from the vent pipe. For this a heat transfer coefficient of half that in the main part of the condenser was assumed; also the temperature difference between steam and cooling water was assumed to be $0.5 \times (\text{steam condensing temperature at condenser inlet} - \text{cooling water inlet temperature})$. The baffling around the air cooling section was made as tight as possible.

Thus the redesign process contained a combination of sophisticated fluid mechanics computing, some physical modelling and other assumptions which in the absence of available data can only be described as educated guesses. The modification appears to have been successful. A higher vacuum is being obtained though to an extent this must be due to the fitting of new tubes (Wallace (25)). However the cooling water temperature rise distribution is much more even with none of the 'hollows' that had been noticed earlier. Because of the need to remove as few condenser tubes as possible, the vent tubes were sized to be no bigger than necessary for this particular modification. Vent tubes in a new design may need to be more generously sized to minimize overall pressure loss through the condenser.

RECENT PLANT

Evidence from recently installed CEBG plant suggests that the increased attention given to condenser plant design by manufacturers and others is beginning to pay off. Studies by Rowe et al (26) concluded that performances better than predicted by present design codes (BEAMA (13) or HEI (14)) should be possible with careful tubenest design, even in large condensers. Test data now confirms this. Measurements made at Ince 'B' show that these condensers are producing a vacuum that is over 4 mbar better than the guarantee value with a terminal temperature difference of 3.4°C. Moreover, corresponding vacua above target performance are being maintained over a wide range of cooling water temperatures and heat loads. Air leakage rates are low and condensate is leaving the condenser with a temperature very close to the steam condensing temperature. No special provision was made to promote good deaeration (the plant cycle includes a deaerator and direct-contact feed heaters) however a creditable level of 8 ppb is being achieved.

The condensers at Littlebrook 'D' are the first of the new traverse underslung design to be used by the CEBG. Exact performance details are not available but preliminary information suggests that high values of overall heat transfer coefficient are being obtained.

There are probably two main reasons for this general improvement. Firstly condenser shells have been more generously sized so that steam pressure losses are minimized and secondly air vents have been placed at the lowest pressure points within tube nests with the air extracted finally at the coldest point of the condenser. However, in addition, there has been greater attention to detail. Where possible strengthening girders have been placed on the outside of the shell to avoid interference with the steam flow, obstructions in the turbine exhaust region have been minimized and internal baffles made tight particularly around air cooling sections.

FUTURE IMPROVEMENTS

Recent tests tend to suggest that provided a condenser is given air pumps or ejectors of sufficient duty and that air is removed at the low pressure points, air blanketing should not be a problem. Tube cleanliness is a maintenance problem. Improvements must therefore lie in the direction of reducing the mean condensate thickness or increasing the water-side heat transfer, though if the latter is done by increasing turbulence there will be an increase in the frictional coefficient and a reduction in cooling water velocity. Additional condensate trays (made of Lexan) have been inserted at Ratcliffe and Ironbridge 'B' (Figure 10). Tests show that these improve the heat transfer coefficients on the tubes immediately below. However it may be necessary to add a series of trays to make a substantial change in the average heat transfer coefficient for the whole condenser.

A more radical change in new plant might be to slope the tubes to promote drainage via the tube support plates. Tests in which a bundle of 84 tubes (12 rows vertical, 7 horizontal) was rotated up to 18° from the horizontal have been reported by Shklover and Buevich (27). These showed that drainage via the tube support plates can be achieved with only a modest inclination of condenser tubes. At an inclination of 12° the increase in bundle heat transfer coefficient was about 25%. An angle of 5° was selected for design purposes.

Roped Tubes

The most obvious candidate for giving immediate improvement is the 'roped' or spiral grooved condenser tube and the CEGB has recently been considering its potential. The effect of the spiral groove is to promote higher turbulence on the water-side and to improve drainage of condensate on the steam-side. The principle variables are groove pitch and groove depth. Data on the enhancement of heat transfer and increase in friction factor are given in several papers e.g. Webb (28) and Cooper and Rose (29). A useful publication which correlates some of this data is provided by IMI (30).

However to determine the overall effect of roped tubes either as replacement tubes in an existing station or as part of a new design, it is necessary to take account of the flow/head characteristics of the cooling water circuit. Appendix B gives a method for doing this for a typical power station with cooling towers. The results (Figure 11) show that with the correct choice of tube (i.e. that for which the heat transfer effect dominates the additional water-side frictional resistance) it should be possible to improve the vacuum by up to 4 mbar in the case of tube replacement. In a new design, a condenser with roped tubes could be built up to 25% shorter than a similar condenser with plain tubes and give the same vacuum with the same cooling water pumping power.

Of course, the above results depend on the experimental data on heat transfer and pressure loss coefficients being accurate and on other factors such as how well the tubes can be kept clean. To answer this a two-fold approach has been adopted

- (a) to test a number of tube geometries around the predicted optimum geometry in the experimental condenser at the CEGB's Leatherhead laboratory, and
- (b) to install groups of roped tubes in operational condensers for evaluation.

In the first laboratory tests, a nest of 200 roped titanium tubes each 2 m long was tested simultaneously with a similar nest of 200 plain tubes placed alongside. The roped tube groove dimensions were: pitch/outside diameter, 0.2, depth/outside diameter, 0.015. All tubes were instrumented. The results which have been corrected for differences in cooling water velocity in the nests are shown in Figure 12. They show that at the top of the nests, the roped tubes have a mean heat transfer coefficient that is 40% greater than that for the plain tubes. At the bottom of the nest, the increase is 54% which shows up the improved condensate drainage characteristics of the roped tubes.

Power station evaluation has involved a small group of brass tubes installed several years ago at Pembroke, an estuarine station; a group of 400 titanium tubes all of the same geometry installed over 3 years ago at Kingsnorth also an estuarine station, and 48 tubes of 90 - 10 cupro-nickel comprising 6 different geometries which were installed in 1982 at Didcot, a cooling tower station with condensers fitted with ball cleaning systems.

The experience to date with operational condensers has shown that the mechanical integrity of roped tubes is just as good as that of plain tubes and, from a limited number of inspections, fouling rates do not appear to differ. An initial set of measurements has been made of the performance of the individual groups of roped tubes installed at Didcot (Ferrison et al (31)). The results are given in Figure 11 in terms of the relative effectiveness of the groups. The measurements are consistent with the predictions, the first and second most effective geometries being closest to the predicted optimum. The measurements will be repeated periodically to determine the effectiveness of the ball cleaning system.

CONCLUSION

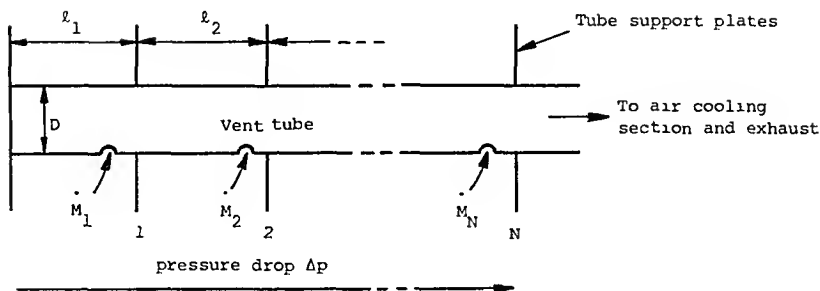
The need to maximize power station thermal efficiency has caused the CEBG to examine carefully the performance of its condensing plant. Faults in the early 500 MW unit condensers have been identified and modifications made where possible. This has brought improvements in vacuum of the order of 3 mbar. The reduction or elimination of tube fouling has also improved vacuum. The extent of this improvement depends on the severity of the fouling but improvements of up to about 4 mbar are typical. The net resulting saving in fuel costs amounts to several £ million per year. To an extent, plant improvement is a continuing process; there is often extra scope for internal modifications when tubes wear out and have to be replaced. A working party from all the CEBG operating regions is currently examining the performance of all large condensers over their complete range of operating conditions.

The experience gained by both the CEBG and the manufacturers in recent years has resulted in a much greater understanding of condenser behaviour. The experience with the early 500 MW unit condensers - largely untried designs - has influenced new designs. Plant coming into service now is reliable and from a thermal performance view point is exceeding expectations. Design improvements have resulted from improving steam access to the tube nests (the new transverse underslung arrangement is particularly good in this respect), from minimizing steam-side pressure losses, from better venting arrangements and the matching of condenser and air pumps, and finally from attention to constructional details. The use of titanium tubes has increased reliability. Computer programs have helped to optimize tube nest layout.

There are still gaps in our knowledge of condensing plant behaviour. How is condensate distributed within tube banks for example? The computer modelling of steam access lanes may need to be improved. The principle direction of improvement in condenser design would appear to be in minimizing the effects of condensate inundation. Roped tubes may help here. Initial site experience with these is encouraging and some of the water-side heat transfer enhancement may also be utilized providing pressure losses are not too great. A reduction of up to 25% in tube surface area for the same vacuum appears possible with capital costs being reduced accordingly. Modest inclination of the condenser tubes so that the condensate drains via the tube support plates also appears feasible in new designs.

ACKNOWLEDGEMENT

The author thanks many colleagues particularly from within the CEBG and from UK manufacturers for help and advice on the task of improving condensing plant performance. This paper is published by permission of the Central Electricity Generating Board.

APPENDIX A: PRESSURE DROP IN AIR VENT

For the geometry shown above, the pressure drop to the Nth tube support plate is given by:

$$\Delta p = \frac{16v}{\pi^2 D^4} \left[\left(\sum_{n=1}^N M_n^2 \right) + \frac{2c_f}{D} \sum_{n=1}^{N-1} l_{n+1} \left(\sum_{m=1}^n M_m^2 \right) \right] \quad N > 1 \quad \dots (A1)$$

where v = mean specific volume, M_n is the flow removal rate from bay n and c_f is the friction coefficient.

APPENDIX B: OPTIMUM CHOICE OF ROPED TUBESNew Design

The problem is to find which roped tube geometry allows the condenser to be designed with the smallest surface area (shortest tube length) and yet perform the same duty as a condenser with plain tubes. Duty in this context means heat load, vacuum and cooling water (CW) pumping power and inlet temperature.

Definitions. Suppose u and f are the augmentation factors for heat transfer and pressure defined by:

$$u = \frac{\text{overall heat transfer coefficient (roped tube)}}{\text{overall heat transfer coefficient (plain tube)}}$$

for the same CW flow velocity and,

$$f = \frac{\text{CW friction coefficient (roped tube)}}{\text{CW friction coefficient (plain tube)}}$$

Also let w and x be the relative CW flow velocity and tube length. These are defined by:

$$w = \frac{\text{CW velocity (in roped tubes)}}{\text{CW velocity (in plain tubes)}}$$

$$x = \frac{\text{tube length (roped tubes)}}{\text{tube length (plain tubes)}}$$

If h is defined as the effective heat transfer augmentation factor allowing for a change in CW velocity then, typically,

$$h = uw^\gamma \quad \dots (B1)$$

where γ for clean tubing and no air blanketing is ~ 0.5 .

Calculation of vacuum. For a given CW inlet temperature T_i and heat load Q , the steam temperature T_s (and hence the condenser pressure p_s) is given by:

$$T_s = T_i + \frac{Q}{M_{cw} c_p (1 - e^{-\beta})} \quad \dots (B2)$$

where M_{cw} = CW mass flow rate,

c_p = CW specific heat,

$$\beta = \frac{A \alpha_{ov}}{M_{cw} c_p},$$

α_{ov} = overall heat transfer coefficient,

A = condensing surface area.

If the vacuum is to remain the same in the condenser with roped tubes as in the condenser with plain tubes then:

$$M_{cw} c_p (1 - e^{-\beta}) = \text{constant}$$

i.e.

$$w(1 - e^{-\frac{Phx}{w}}) = (1 - e^{-P}) = C, \text{ say} \quad \dots (B3)$$

where:

$$P = \beta_{\text{plain tubes}}$$

substituting for h from equation (B1) and rearranging gives:

$$x = \frac{1}{w} \ln \left(\frac{1}{1 - \frac{C}{w}} \right) \quad \dots (B4)$$

Determination of CW Velocity. To eliminate w in equation (B4) it is necessary to consider the effect of the increase in friction in the roped tubes on the CW flow. For the range of operation involved i.e. $w \sim 1$, the CW pump efficiency remains nearly constant so that for constant pumping power,

$$p_h w = \text{constant} \quad \dots (B5)$$

where p_h is the head delivered by the CW pumps. The friction loss characteristic (head v. flow rate) of the CW flow circuit (condenser, culverts, cooling tower nozzles) is a quadratic of the form:

$$p_{CW} = j + kw^2 \quad \dots(B6)$$

where in the case of a station with cooling towers, j allows for lift to the tower nozzles. Typically half of k can be associated with the losses in the condenser. Inspection of test data from a station with cooling towers shows that equation (B6) can be linearized and represented approximately by

$$p_{CW} = \left[1 + \left(\frac{xf - 1}{4} \right) \right] Kw \quad \dots(B7)$$

where x and f allow for changes in tube length and friction and K is a constant. Equilibrium is reached when $p_{CW} = p_h$, hence applying equation (B5) gives.

$$\left[1 + \left(\frac{xf - 1}{4} \right) \right] w^2 K = \text{constant } K$$

and hence,

$$w = \left(\frac{4}{3 + xf} \right)^{\frac{1}{2}} \quad \dots(B8)$$

Determination of Tube Length. Substitution of equation (B8) into equation (B4) gives.

$$x = \frac{1}{uP} \left(\frac{4}{3 + xf} \right)^{\frac{1}{2}} \ln \left[\frac{1}{1 - C \left(\frac{3 + xf}{4} \right)^{\frac{1}{2}}} \right] \quad \dots(B9)$$

which may be solved by iteration to give x as a function of u and f . The optimum roped tubing will be that having values of u and f which give the lowest value of x .

Existing Condenser

A similar argument applies when choosing roped tubes to replace tubes in an existing condenser. Here however, $x = 1$ and the optimum tubing is that which produces the highest vacuum. From equation (B2), the change in condensing temperature produced by the roped tubes is:

$$\Delta T_s = \left[\frac{Q}{\dot{m}_{cw} c_p (1 - e^{-\beta})} \right]_{\text{roped tubes}} - \left[\frac{Q}{\dot{m}_{cw} c_p (1 - e^{-\beta})} \right]_{\text{plain tubes}}$$

$$= \left[\frac{C}{w(1 - e^{-\beta})} - 1 \right] (T_s - T_1)_{\text{plain tubes}} \quad \dots(B10)$$

Substituting for h and w from equations (B1) and (B8) with $x = 1$ and introducing the slope of the saturation line (dp_s/dT_s) gives the improvement in vacuum Δp_s as:

$$\Delta p_s = \left(\frac{dp_s}{dT_s} \right) \left[\frac{c \left(\frac{3+f}{4} \right)^{\frac{1}{4}}}{1 - e^{-Pu \left(\frac{3+f}{4} \right)^{\frac{1}{4}}}} - 1 \right] (T_s - T_1) \quad \text{plain tubes} \quad \dots (B11)$$

The optimum roped tubing will be that having values of u and f which give the highest (negative) value of Δp_s .

SYMBOLS USED

- A = condensing surface area (m^2)
 C = dimensionless constant
 D = vent tube internal diameter (m)
 K = constant (N/m^2)
 \dot{M} = mass flow rate (kg/s)
 N = tube support plate number
 P = $\beta_{\text{plain tubes}}$
 Q = condensing heat load (kW)
 T = temperature ($^{\circ}C$)
 ΔT = temperature change (K)
 c_f = friction coefficient
 c_p = specific heat (kJ/kgK)
 f = ratio of friction coefficient, roped : plain
 h = ratio of effective heat transfer coefficient, roped : plain
 j = constant (N/m^2)
 k = constant (N/m^2)
 ℓ = length between tube support plates (m)
 n = bay number
 p = pressure (N/m^2)
 p_h = cooling water pump head (N/m^2)
 Δp = pressure change (N/m^2)
 t = time (minutes)
 u = ratio of heat transfer coefficient, roped : plain

- v = specific volume (m^3/kg)
 w = ratio of flow velocities, roped : plain
 x = ratio of tube lengths, roped : plain
 α_{ov} = overall heat transfer coefficient ($\text{kW}/\text{m}^2\text{K}$)
 $\beta = A\alpha_{\text{ov}}/\dot{M}_{\text{cw}} c_p$
 γ = velocity exponent
 τ = time constant (minutes)

Subscripts

- i = cooling water inlet
 o = initial value
 s = steam
 cw = cooling water

REFERENCES

1. Diaz-Tous, I.A. and Mussallil, Y.G., 1983, "Condenser Macrofouling Control Methods", Proceedings of International Symposium on Condensers, UMIST, Manchester, England.
2. Kornbau, R.W., Richard, C.C. and Louis, R.O., "Sea Water Biofouling Countermeasures for Spirally Enhanced Condenser Tubes", Proceedings of International Symposium on Condensers, UMIST, Manchester, England.
3. Olike, I. and Katsman, D., 1983, "Aeration and Deaeration in a Condenser", Proceedings of International Symposium on Condensers, UMIST, Manchester, England.
4. Bornstein, B., 1983, "Auxiliary Condensers vs. Main Condenser for Boiler Feed Pump Turbine-Drivers", Proceedings of International Symposium on Condensers, UMIST, Manchester, England.
5. Maurer, J.R. and Berendsen, F.H., 1983, "Assessing the Effect of Stainless Steel Tubes on Condenser Performance and Integrity", Proceedings of International Symposium on Condensers, UMIST, Manchester, England.
6. Ozeki, T., Miura, T. and Miyoshi, M., 1983, "A Design Method of Condenser Tube Arrangement for Large Power Stations", Proceedings of International Symposium on Condensers, UMIST, Manchester, England.
7. Hopkins, H.L., Loughhead, J. and Monks, C.J., 1983, "A Computerised Analysis of Power Condenser Performance Based upon an Investigation of Condensation", Proceedings of International Symposium on Condensers, UMIST, Manchester, England.
8. Beckett, G., Davidson, B.J. and Ferrison, J.A., 1983, "The Use of Computer Programs to Improve Condenser Performance", Proceedings of International Symposium on Condensers, UMIST, Manchester, England.

9. Clay, C.A.E. and Sochaczewski, Z.W., 1983, "A Condenser Testing Code and Associated Measurement Techniques", Proceedings of International Symposium on Condensers, UMIST, Manchester, England.
10. Bindon, F.J.L., 1983, "Operational Problems with Condensing Plant at a Nuclear Power Station", Proceedings of International Symposium on Condensers, UMIST, Manchester, England.
11. Barker, S. and Ward, J.B.D., 1979, "Maintenance and Operational Aspects of Condenser Management", Paper C71/79, Conference on Cooling with Sea Water, Institution of Mechanical Engineers, London.
12. Heaton, W.E., Edgley, J., Andrews, E.F.C. and Patient, B., 1979, "A Review of the Factors Leading to the Use of Titanium as a Steam Condenser Tube Material within the CEGB", Paper C78/79, Conference on Cooling with Sea Water, Institution of Mechanical Engineers, London.
13. BEAMA, 1967, "Recommended Practice for the Design of Surface Type Steam Condensing Plant, Publication No. 222", British Electrical and Allied Manufacturing Association, London.
14. HEI, 1978, "Standards for Steam Surface Condensers", 7th Edition, Heat Exchange Institute, Cleveland, Ohio.
15. Ferrison, J.A., Rowe, M. and Richmond, J.W., 1980, Private Communication.
16. Rowe, M., Tagg, C. and Beckett, G., 1983, Private Communication.
17. ASME, Power Test Code, 12.2 - 1955, "Steam Condensing Apparatus", ASME, New York.
18. CEGB Site Test Code No. 3, "Performance of Surface-Type Steam Condensers", 1981 issue, CEGB London.
19. Guy, H.L. and Winstanley, E.V., 1934, "Some Factors in the Design of Surface Condensing Plant", Proc. I. Mech. E.
20. Bloomer, R.N., 1982, Private Communication.
21. Smalley, J. and Deam, R.T., 1982, Private Communication.
22. Wilson, J.L., 1972, "The Design of Condensers by Digital Computers", I. Chem. E. Symp. Series No. 35, pp 3:21 - 3:27.
23. Colquhoun-Lee, I. and Bryan, H.G., 1980, Private Communication.
24. Rowe, M. and Ferrison, J.A., 1976, "Steam-side Measurements in the Condenser of a 500 MW Turbine", NEL Report No. 619, Steam Turbine Condensers, East Kilbride, Scotland.
25. Wallace, G.N., 1982, Private Communication.
26. Rowe, M., Davidson, B.J., Andrews, E.F.C., Ferrison, J.A. and Taylor, B.J., 1979, "Heat Transfer and Air Blanketing in Steam Condensers", Paper C180/79, Conference on Steam Turbines for the 1980s, Institution of Mechanical Engineers, London.
27. Shklover, G.G. and Buevich, A.V., 1978, "Investigation of Steam Condensation

in an Inclined Bundle of Tubes", Teploenergetika 25, No. 6.

28. Webb, R.L., 1981, "The Use of Enhanced Surface Geometries in Condensers: An Overview", Power Condenser Heat Transfer Technology, P.J. Marto and R.H. Nunn, eds., Hemisphere Publishing Corporation, Washington D.C., USA.
29. Cooper, J.R. and Rose, J.W., 1981, "Condensation Heat-Transfer by Vapour-Side Surface Geometry Modification", HTFS Report RS402.
30. IMI, Tech. Memo 3, "YIM Heat Exchanger Tubes: Design Data for Horizontal Roped Tubes in Steam Condensers", Yorkshire Imperial Metals plc., Leeds, England.
31. Ferrison, J.A., Rowe, M. and Goodson, M.I., 1982, Private Communication.

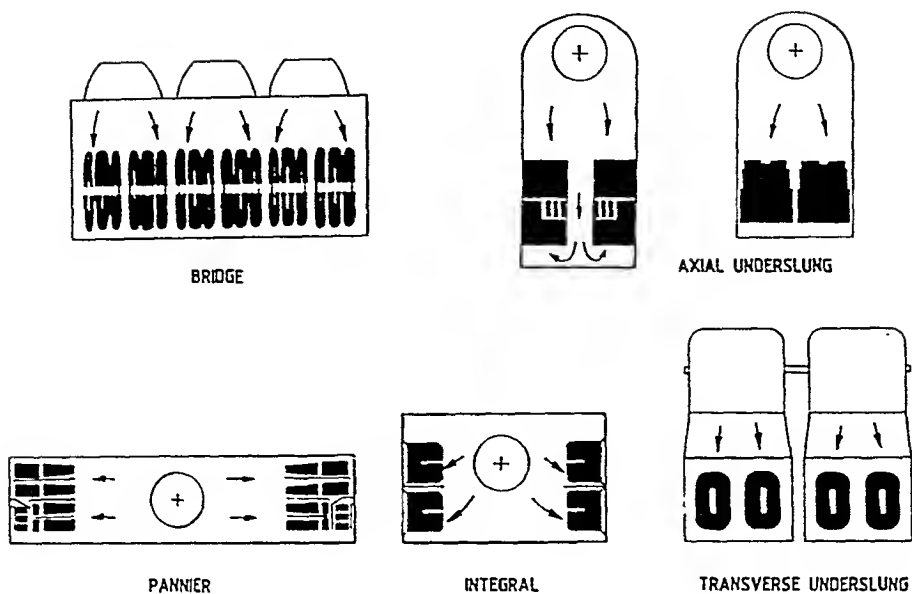


Figure 1 Types of Steam Condenser

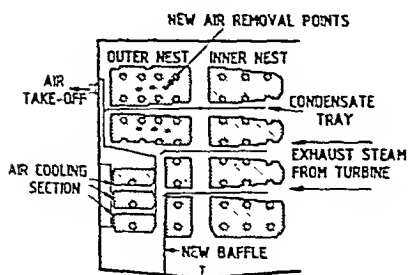


Figure 2 Pannier Condenser with Modifications

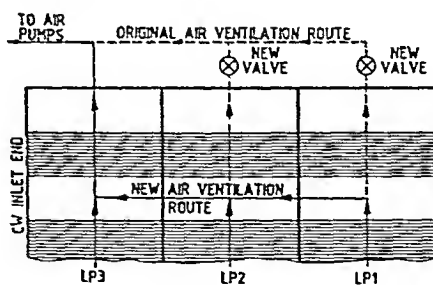


Figure 3 Modified Air Ventilation at Cottam

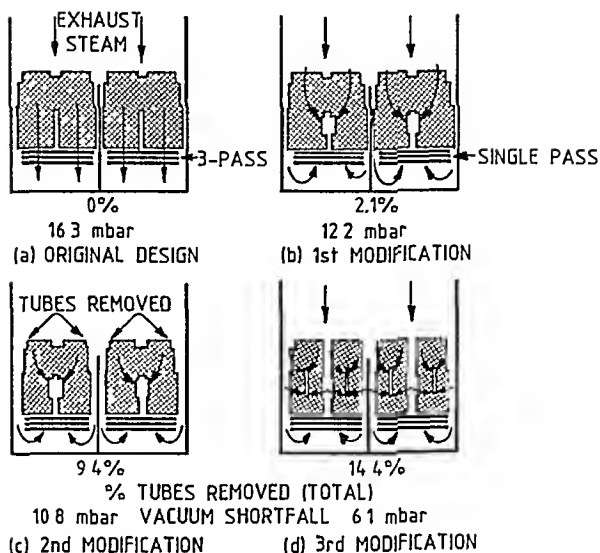


Figure 4 Ratcliffe Condenser Modifications

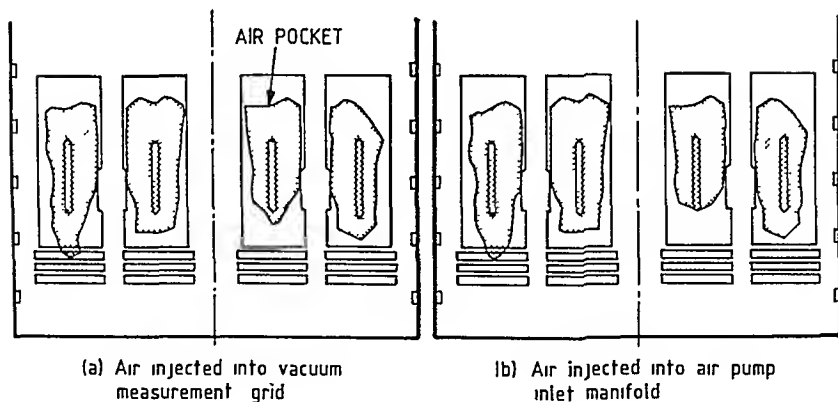


Figure 5 Air Blanketing in Ratcliffe Condensers

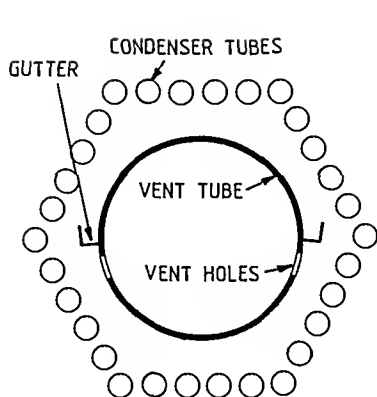


Figure 9 Air Vent Tube

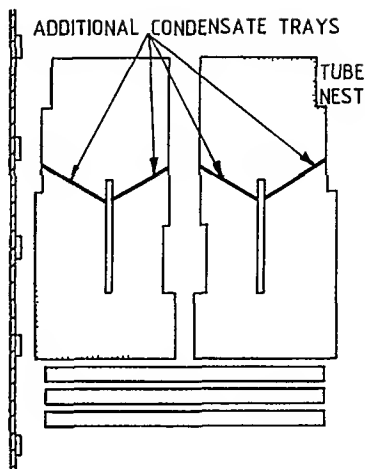
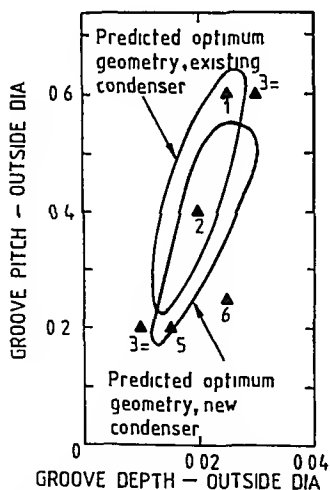
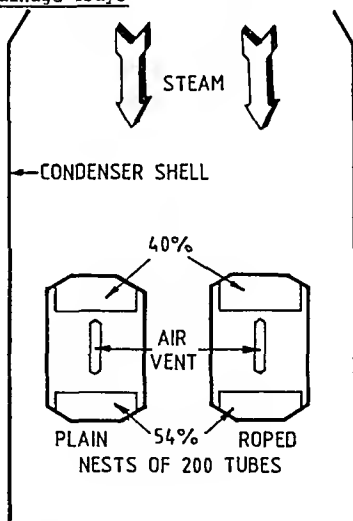


Figure 10 Additional Condensate Drainage Trays



Tubes tested number indicates order of merit, 1=best 6=worst

Figure 11 Optimum Roped Tube Geometry (Power Station with Cooling Towers)



Values show mean heat transfer enhancement for regions indicated

Figure 12 Heat Transfer Enhancement with Roped Tubes

A DESIGN METHOD OF CONDENSER TUBE ARRANGEMENT FOR LARGE POWER STATIONS

T. OZEKI*, Y. MIURA*, M. MIYOSHI*

On the larger condenser units for fossil power stations as well as nuclear plants, it is becoming increasingly important to pay careful attention to designing the tube arrangement of condensers.

This paper introduces a design method of the condenser tube arrangement based on the fundamental concepts which must be taken into account in the design stage. The results of a performance test on the actual condenser designed on the above-mentioned concepts are also presented.

INTRODUCTION

With the advent of large-capacity power plants, condensers are remarkably increasing in scale. The flow of steam around the cooling tubes on large scaled condensers is one of the most essential factors which determine condenser performance. Hence, the condenser tube arrangement is designed in accordance with the following basic policies:

- [1] To design a tube arrangement which provides a stable flow of low-pressure steam in tube bundles and high performance in heat transfer.
- [2] To calculate the pressure distribution around the outer circumference of a tube arrangement by the two-dimensional finite element method, while considering steam suction at the outermost circumference.
- [3] On the basis of the aforementioned pressure distribution, to calculate the number of cooling tubes on each section of the tube bundle so that noncondensable gas can be led into a non-condensable gas extractor without stagnation.

This paper describes a design method conforming to the above-mentioned design policies. Shaped similarly to a hanging bell, this tube arrangement is termed a "bell-type tube arrangement." This paper also shows a comparison between the result based on a calculation program prepared for evaluating the performance of each section of a large-scaled condenser and the result of a test on actual equipment. The comparison reveals that both results well coincide with each other.

* Heat Exchanger Research and Development Staff, Turbine Works, Toshiba Corporation, Japan

A DESIGN METHOD OF BELL-TYPE TUBE ARRANGEMENT

Steam Flow and Condensing Heat Transfer

BEAMA (1) and HEI (2) are recognized as general technical standards for designing condensers. These standards have been applied to the design of many condensers. However, in view of the fact that the scale of condenser increases with an increase in the unit capacity, it has become necessary to examine whether or not these technical standards are still applicable to the design of large-scaled condensers. That is, with an increase in the scale of tube bundles, the velocity of steam flowing from the outer circumference of the bundle thereinto increases, resulting in a large pressure loss of saturated steam passing through the bundle. Further, with the drop in pressure, the saturation temperature falls, causing a decrease in the heat transfer rate. This impairs the condenser performance, resulting in a possible rise in condenser pressure.

The overall heat transfer coefficient of condensers determined by BEAMA and HEI seems to be based on the filmwise condensing heat transfer coefficient of stationery steam on horizontal tubes given by Nusselt (3). In actual condensers, steam velocity at the outer circumference of the tube arrangement is high and decreases as it flows inside. While the condensing heat transfer coefficient of flowing steam becomes higher than that of the stationery steam (4), however, the steam decreases in saturation temperature owing to pressure loss caused when the steam passes through the tube bundle. As a result, the difference between the steam saturation temperature and the cooling water temperature decreases, so that the heat transfer rate is decreased, resulting in a possible failure in meeting performance requirements set forth in the standards.

The condensing heat transfer coefficient is also affected by the direction of steam flow passing through the outside tubes. It is surmised that horizontal flow, vertical-downward flow, and vertical-upward flow in the horizontally arranged tube bank decrease in condensing heat transfer coefficient in the order mentioned (4), (5). In designing a condenser tube arrangement, therefore, it is essential to consider the following (12):

- [1] To minimize pressure loss of steam passing through tube bundle.
- [2] To design a tube arrangement so that steam flows through the tube bundle in a horizontal or downward direction.
- [3] To precisely predict a steam flow pattern in which no stagnation of noncondensable gas is brought about in the tube bundle.

Steam Flow in Bell-type Tube Arrangement

In designing a condenser tube arrangement, it is very important to consider the flow of steam in the tube bundle as far as large-scaled condensers are concerned. The bell-type tube arrangement is a large-scaled condenser tube arrangement designed with the aforementioned three important items duly considered. Figure 1 shows an example of the bell-type tube arrangement. The turbine exhaust steam reaching the upper section of the condenser flows into the upper circular section of the tube arrangement and into the side section connected thereto; then, the steam flows through the tube bundle. To decrease the flow resistance of steam passing through the tube bundle, an access lane (laned section; LS) is provided on the outer circumference of the tube bundle. The tube bundle is provided on its center with a close-packed section (CPS) in which cooling tubes are uniformly arranged. In this arrangement, the steam arriving at the upper semicircular section flows down to the

center of the circle and the steam horizontally incoming from the side section directly flows into the steam aisle in the tube bundle. Upon reaching the steam aisle, the steam flows into an air cooling zone (ACZ) installed on the lowest section of the tube bundle. This ACZ is enclosed by partition plates to separate it from the LS and CPS.

Pressure Loss in Tube Bundles

To prevent a stagnation of noncondensable gas in the tube bundle, it is necessary to precisely estimate the pressure loss of steam passing through the tube bundle.

The pressure loss of steam passing through the tube bundle is calculated (4) by Equation—

$$P_{n-1} - P_n = 2Cl \rho_{sm} (\xi_1 u_{sm})^2 - \xi_2^2 \{ (\rho_s u_s) n^{-1}^2 - (\rho_s u_s) n^2 \} \dots \dots \dots (1)$$

where suffix n denotes the number of rows of cooling tubes arranged in the direction of steam flow, and suffix m denotes the average between a value for row $(n-1)$ and a value for n . For pressure loss in a regular arrangement such as CPS and ACZ, the pressure loss coefficient for condensing steam is modified 25% less than the coefficient for noncondensable gas (7), in accordance with the recommendations of Fujii et al (4). In actual condensers, irregular tube arrangement appears as in LS. Pressure loss coefficient in this case was experimentally determined by Hydraulic Analogue, as proposed by Drummond et al (8). Figure 2 shows the result. As to a regular tube arrangement, on the other hand, the result of Hydraulic Analogue is shown in Figure 3. The test result well coincides with the value of pressure loss coefficient estimated in accordance with the recommendation of Fujii et al (4). Therefore the pressure loss coefficient adopted for LS is considered to be adequate.

The calculation of pressure loss mentioned above is performed on the part of the horizontally arranged tube bundle; then the number of LS and CPS rows is adjusted to establish a pressure gradient in the steam aisle toward the inlet of ACZ as shown in Figure 1, whereby the final tube arrangement is determined.

Analysis of Pressure Distribution on the Outermost Circumference of Tube Bundle

The pressure loss of steam passing through the tube bundle can be calculated by the previously described method. Thus, it becomes necessary to calculate the pressure distribution on the outermost circumference of the tube arrangement. Turbine exhaust steam led into a condenser is drawn into the center of the tube bundle from the outermost circumference of tube arrangement. To calculate the pressure distribution, therefore, it is necessary to analyze the flow field associated with suction on the outermost circumference of tube arrangement as the boundary in the steam-side space in the condenser.

Figure 4 illustrates a model of the condenser section. Since the condenser is usually installed in the foundation of the turbine, turbine exhaust steam flows downward into the condenser from its upper shell. In large-scaled condensers, one condenser shell is provided with two tube bundles. The flow field around the outer circumference of a tube bundle is analyzed as a model half of a tube bundle as shown in Figure 5. The flow field of low-pressure steam around the outer circumference of the tube bundle is analyzed by the two-dimensional finite element method (FEM) as an ideal fluid. Figure 5 illustrates how space of the outer circumference of a tube bundle is split into mesh for the purpose of FEM analysis. This flow field is treated as a vortex-free potential flow. The velocity potential ϕ satisfies the following Laplace's equation:

$$\frac{\partial^2 \phi}{\partial x^2} + \frac{\partial^2 \phi}{\partial y^2} = 0 \quad \dots\dots\dots (2)$$

The following equation holds at the boundaries a-a and b-b:

$$1x \frac{\partial \phi}{\partial x} + 1y \frac{\partial \phi}{\partial y} + \bar{v} = 0 \quad \dots\dots\dots (3)$$

Calculation is carried out on the assumption that no fluid enters or leaves through other boundaries ($\bar{v} = 0$), and by the method proposed by Zienkiewicz (9).

The velocity at each point is calculated on the basis of the velocity potential at any point by equations—

$$v_x = \frac{\partial \phi}{\partial x} \quad \dots\dots\dots (4)$$

$$v_y = \frac{\partial \phi}{\partial y} \quad \dots\dots\dots (5)$$

Pressure distribution at the tube bundle outermost circumference is determined by subtracting the dynamic pressure at each point from the total pressure at the boundary of flow field a-a given as the reference pressure. The primary approximation of pressure field is obtained by assuming uniform suction at boundary b-b. Finally, the pressure field is determined by adopting steam suction at the boundary b-b corresponding to the condensing performance of cooling tubes.

Figure 6 shows an example of the calculation results. The parenthesized numerical values in the figure represent the values obtained by Hydraulic Analogue. As is evident from Figure 6, the result of calculation well coincides with the test result even though the flow field is assumed to be a potential flow. Thus, it is considered that the method for calculating the pressure field explained here causes no problem in practical use.

Calculation of Heat Transfer in Tube Bundle

Described so far is a method of calculating the pressure loss of steam passing through the tube bundle and pressure distribution on the outer circumference of the tube bundle. Since the quantity of steam flowing into the tube bundle is determined by the condenser performance of each part within the tube bundle, it is calculated by the following method.

The heat flux and the overall heat transfer coefficient at each part of the tube bundle are calculated as follows.

The heat flux is defined by the equation—

$$q = \alpha_{ov}(\theta_s - \theta_c) \quad \dots\dots\dots (6)$$

The overall heat transfer coefficient is given by the equation—

$$\frac{1}{\alpha_{ov}} = \frac{1}{\alpha_s} + \frac{1}{\alpha_c} \left(\frac{D_o}{D_i} \right) + \frac{D_o}{2\lambda_w} \ln \left(\frac{D_o}{D_i} \right) + Rf \left(\frac{D_o}{D_i} \right) \quad \dots\dots\dots (7)$$

The heat transfer coefficient of the cooling water side in a tube is determined by the equation of Dittus-Boelter (6) as follows:

$$\alpha_c = 0.023 \frac{\lambda_c}{D_i} \text{Re}^{0.8} \text{Pr}^{0.4} \quad \dots\dots\dots (8)$$

For the condensing heat transfer coefficient, the equation of Fujii-Uehara (10) is used, in which the effects of steam velocity and noncondensable gas are considered.

$$\alpha_s = \frac{\lambda L}{D_o} \left\{ X^4 (Re D_o) L^2 + 0.276 \frac{(Ga D_o) L \cdot Pr_L}{H} \right\}^{1/4} \exp(-5.4 W_G) \dots \dots \dots (9)$$

$$H = \frac{C_p L (\theta_s - \theta_{wo})}{\Delta h_s}$$

$$R = \left(\frac{\rho L \mu L}{\rho_s \mu_s} \right)^{1/2}$$

$$X = 0.9 \left(1 + \frac{Pr_L}{HR} \right)^{1/3}$$

Calculation is repeated until satisfactory results of heat transfer and pressure loss are simultaneously obtained, and condenser pressure is finally adjusted.

PERFORMANCE TEST ON ACTUAL EQUIPMENT

Measurement on an Actual Condenser

Figure 7 illustrates the bell-type tube arrangement applied to a 600 MW thermal power plant condenser. In this condenser, all cooling tubes are made of titanium and welded to titanium tube sheets. For performance evaluation of the condenser, both the temperature rise and the flow velocity distribution of cooling water at each part of the tube bundle were measured. Figure 8 shows devices for measuring the temperature of cooling water and the flow velocity in a tube. These thermocouples and pitot tubes are respectively installed by a special support on a tube plate at the cooling water outlet side. Figure 7 shows the locations of measuring points.

To compare with the result of the performance test on actual equipment with the result calculated, the hatched areas in Figure 9 are typically selected. The tube bundle is divided into five sections in the longitudinal direction of the condenser as shown in Figure 10. Figure 11 is a flow chart of the calculation. In the condenser subjected to the performance test, the cooling tubes are made of titanium highly resistant to corrosion and kept clean by the effective operation of sponge ball cleaners so that fouling on the tube side is negligible. Thus, the fouling thermal resistance in Equation (7) is assumed to be zero.

Comparison Between the Result of Performance Test and Calculated Value

Figure 12 shows a comparison between the result of calculation of temperature distribution on the cooling water outlet and the result of measurement. The result of calculation well agrees with the result of measurement; thus, validity of the calculation method described in this paper has been confirmed.

Table 1 shows a comparison between the measured value of the condenser overall heat transfer coefficient and the value calculated on the basis of the HEI standard. The measured overall heat transfer coefficient is approximately 10% greater than the value based on the HEI standard. Thus, it seems that performance of the bell-type tube arrangement is fairly excellent.

TABLE 1—Condenser Overall Heat Transfer Coefficient

		Measured value	HEI
Overall heat transfer coefficient	W/m ² K	3.45×10^3	3.13×10^3
Temp. at cooling water inlet	°C	13.75	
Temp. at cooling water outlet	°C	20.03	
Flow rate of cooling water	kg/h	9.65×10^7	
Heat transfer rate	kW	7.05×10^5	
Condenser pressure (at exhaust connection)	kPa	3.06	

CONCLUSION

In this paper a description has been presented on the design concept of condensers having a bell-type tube arrangement for large-capacity power stations, and a comparison has been made between the result of performance test on an actual 600 MW condenser and the result of calculation.

The resulting conclusion is as follows:

- [1] The result of the performance test on an actual condenser having a bell-type tube arrangement is better than the value based on the HEI standard by approximately 10%.
- [2] As a result of the performance test on actual equipment, validity of the design concepts of condensers introduced in this paper has been confirmed.
- [3] In designing the condenser tube arrangement, it is important to consider a drop in saturation temperature resulting from a pressure loss caused when steam passes through the tube bundle. That is, the greatest factor affecting condenser performance is a drop in saturation temperature attendant on pressure loss.

SYMBOLS USED

Cl = pressure loss coefficient (-)

C_{PL} = specific heat of condensate (J/kgK)

Di = inside diameter (m)

Do = outside diameter (m)

g = acceleration of gravity (m/s²)

G_a = mass flow of air pass through a calculating tube row (kg/s)

$Ga(Do)_L = \frac{g Do^3}{\nu_L^2}$ Galileo number (-)

G_s = mass flow of steam pass through a calculating tube row (kg/s)

H, R, X = factor (-)

Δh_s = specific latent heat of vaporization (J/kg)

i_x = x-directional cosine of vertical line perpendicular to the boundary (-)

i_y = y-directional cosine of vertical line perpendicular to the boundary (-)

P_o = pressure around tube bundle (Pa)

P_N = pressure at ACZ outlet (Pa)

ΔP = pressure loss in tube bundle (Pa)

Pr_c = Prandtl number of cooling water (-)

Pr_L = Prandtl number of condensate (-)

q = heat flux (W/m²)

$Re_c = \frac{D_i u_c}{\nu_c}$: Reynolds number (-)

$(Re_o)_L = \frac{D_o u_s}{\nu_L}$: Reynolds number (-)

R_f = fouling thermal resistance for inside surface of tube (m² k/W)

u_c = cooling water velocity (m/s)

u_s = oncoming air-steam mixture velocity (m/s)

v_x = x-directional component of velocity (m/s)

v_y = y-directional component of velocity (m/s)

\bar{v} = normal velocity at the boundary (m/s)

$WG = \frac{G_a}{G_a + G_s}$: mass flow ratio of air to air-steam mixture (-)

x, y = co-ordinate direction (m)

α_c	= cooling water-side heat transfer coefficient ($\text{W/m}^2 \text{K}$)
α_{ov}	= overall heat transfer coefficient ($\text{W/m}^2 \text{K}$)
α_s	= steam-side heat transfer coefficient ($\text{W/m}^2 \text{K}$)
θ_c	= bulk temperature of cooling water ($^{\circ}\text{C}$)
θ_s	= saturated temperature of steam ($^{\circ}\text{C}$)
θ_{wo}	= temperature of outside tube surface ($^{\circ}\text{C}$)
λ_c	= thermal conductivity of cooling water (W/mK)
λ_L	= thermal conductivity of condensate (W/mK)
λ_w	= thermal conductivity of tube wall (W/mK)
μ_L	= dynamic viscosity of condensate ($\text{N}\cdot\text{s/m}^2$)
μ_s	= dynamic viscosity of steam ($\text{N}\cdot\text{s/m}^2$)
ν_c	= kinematic viscosity of cooling water (m^2/s)
ν_L	= kinematic viscosity of condensate (m^2/s)
ν_s	= kinematic viscosity of steam (m^2/s)
ζ_1	= ratio of maximum flow area to minimum one (-)
ζ_2	= ratio of mean square velocity to u_s^2 (-)
ρ_L	= mass density of condensate (kg/m^3)
ρ_s	= mass density of steam (kg/m^3)
ϕ	= velocity potential

REFERENCES

1. BEAMA, 1975, "Recommended practice for the design of surface type steam condensing plant", British Electrical and Allied Manufacturers Association, London.
2. HEI, 1978, "Standard of steam surface condensers, 7th ed.", Heat Exchange Institute, New York.
3. Nusselt, W. 1916, "The surface condensation of steam", VDI.Z., 60, 541-546, 569-575.

4. Fujii. T., Uehara. H., Hirata. K., Oda. K., 1972, Int. J. Heat Mass Transfer 15, 247-260.
5. Machida. U., Fujii. T., Uehara. H., Oda. K., 1974, Preprint of 11th Japan Heat Transfer Symposium, 213-216, (in Japanese).
6. Dittus, F. W., and Boelter, L. M. K., 1930, "Heat Transfer in automobile radiators of the tubular type", Univ. Calif., Pubs. Eng., 443-461.
7. Zukauskas. A., 1972, "Advances in Heat Transfer, vol. 8", Academic Press, New York.
8. Drummond. W., Lorett. J. A., 1962, "Hydraulic Analogue for Condenser Design", Engineering, 1, June, 733-734.
9. Zienkiewicz, O. C., 1971, "The Finite Element Method in Engineering Science", McGraw-Hill, New York.
10. Fujii. T., Uehara. H., 1973, "Advanced Heat Transfer vol. 1, 1st ed.", Yokendo, Tokyo, (in Japanese).
11. Sakurai. K., Itabashi. Y., Komatsu. A., 1980, "Large Titanium Tubed Condensers with Welded Tube-to-Tubesheet Joints", Proceedings of the American Power Conference 42, 309-318.
12. Fujii. T., 1975, "A Proposal of Research and Development for Turbine Condensers", Journal of Japan Society of Mechanical Engineering 78, 529-533 (in Japanese).

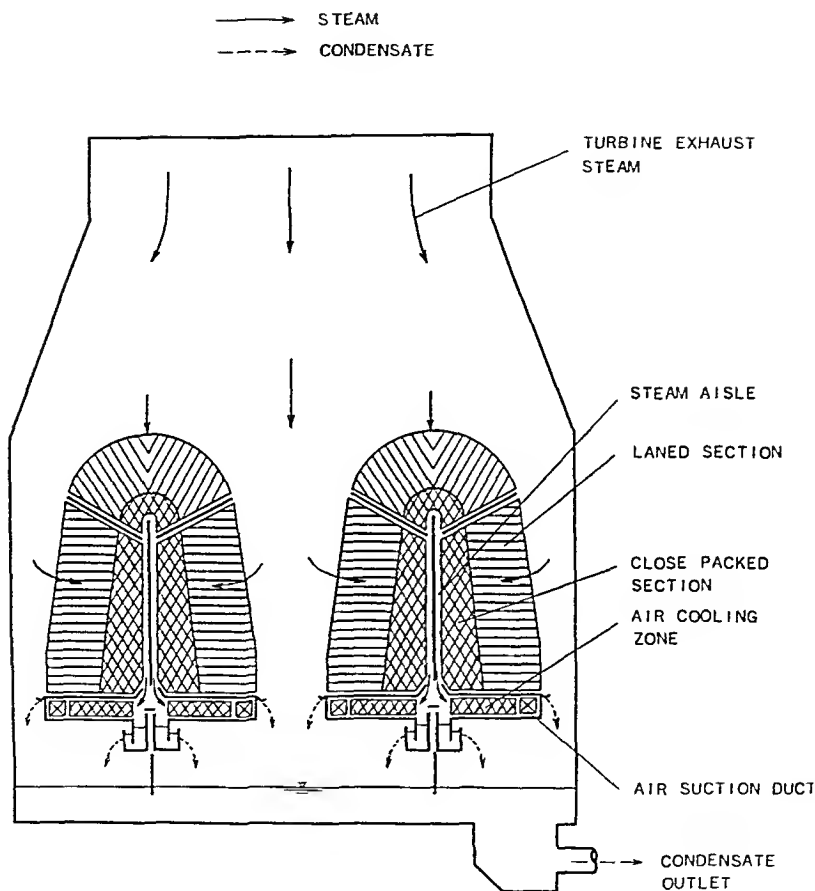


Figure 1 Bell-type tube arrangement and steam flow

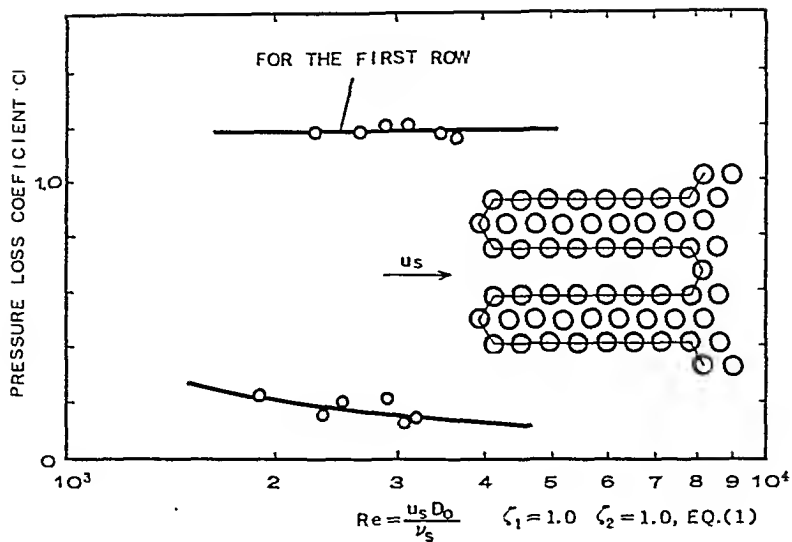


Figure 2 Pressure loss coefficient for Laned Section

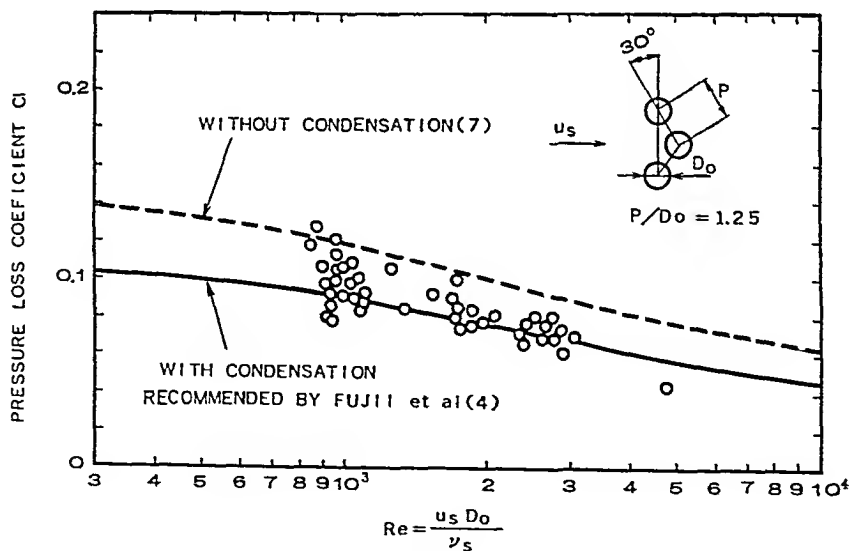


Figure 3 Pressure loss coefficient for Close Packed Section

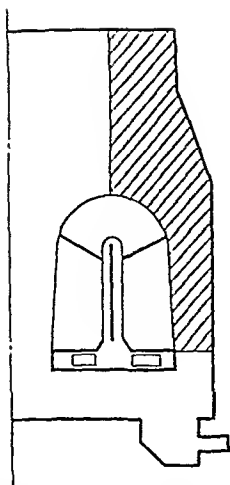


Figure 4 Flow field (hatched area) to be calculated around tube bundle

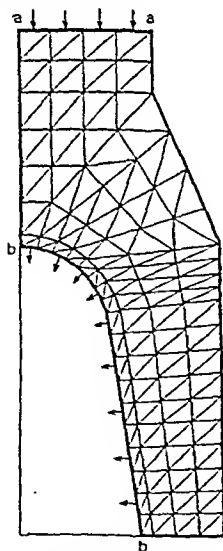


Figure 5 Flow field divided into mesh for FEM calculation

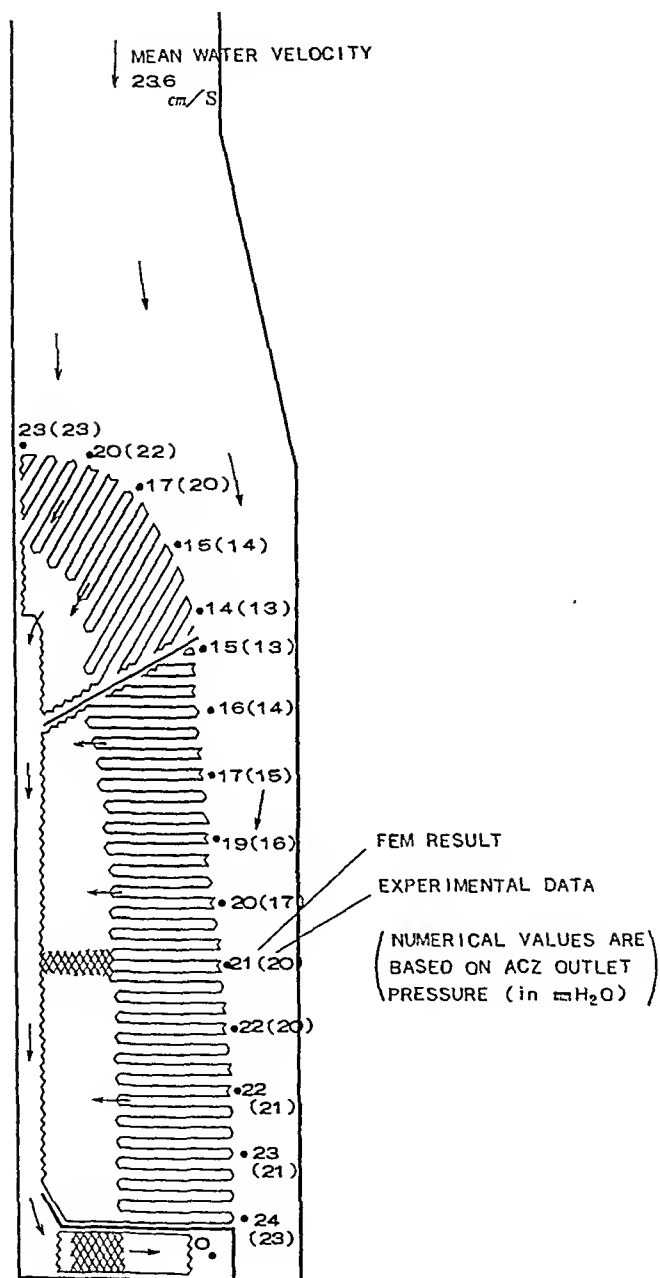


Figure 6 Comparison between FEM result and experimental data by Hydraulic Analogue

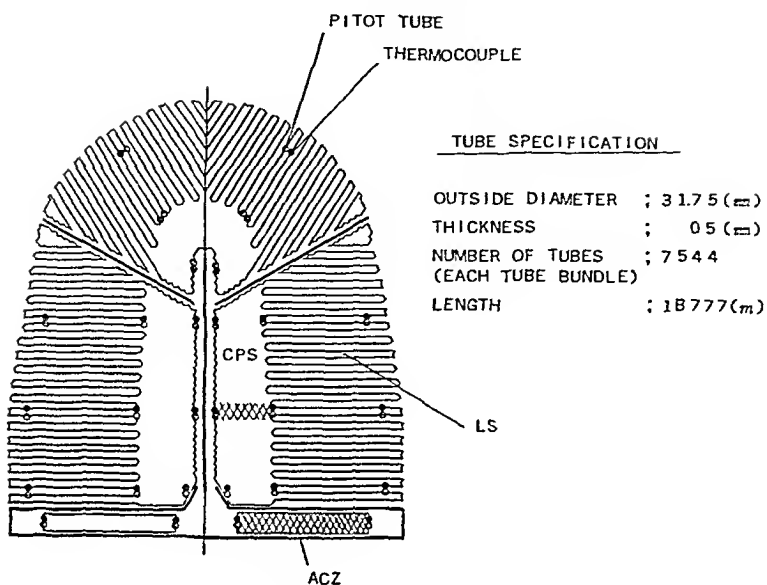


Figure 7 Tube arrangement for 600MW actual condenser

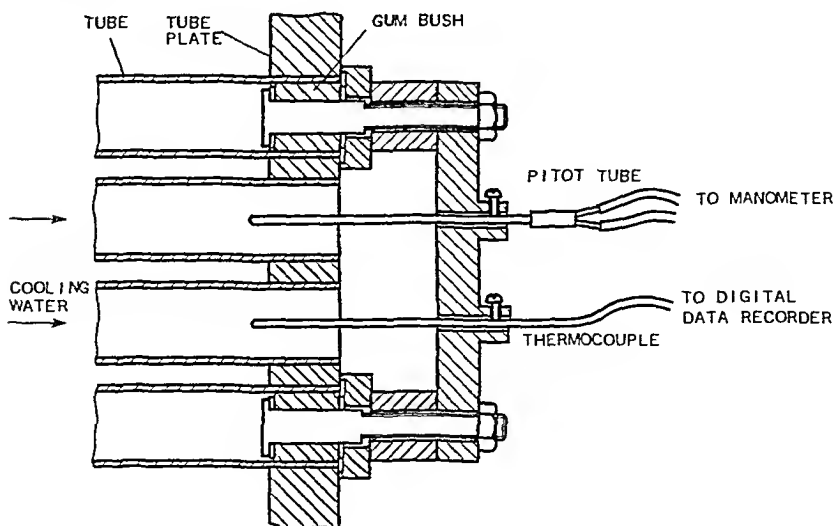


Figure 8 Details of measuring apparatus for cooling water temperature and velocity

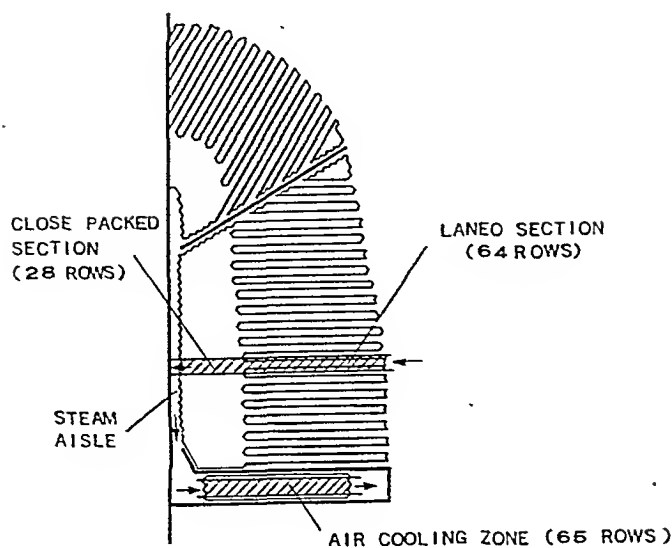


Figure 9 Typical calculating zone along steam flow

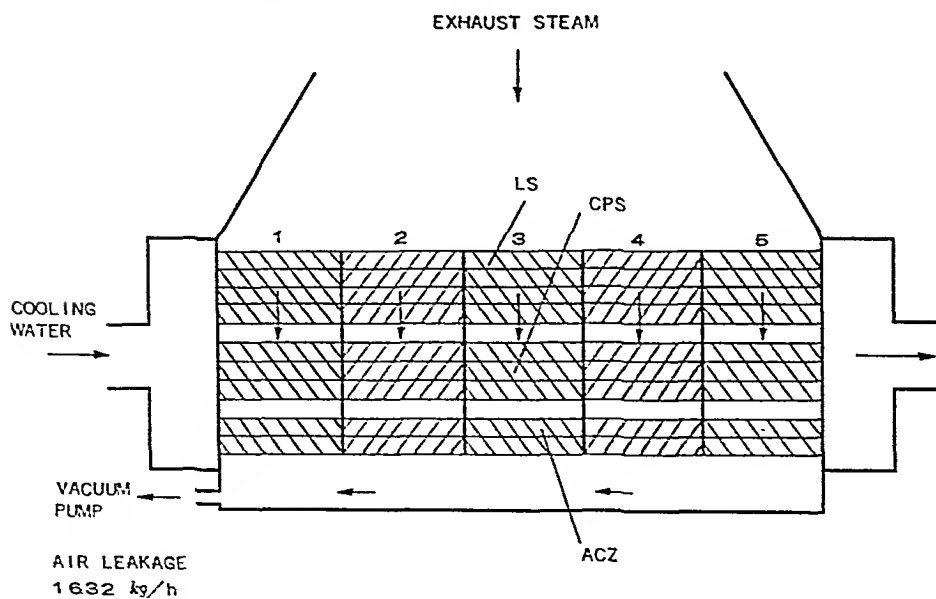


Figure 10 Division of cooling tubes along longitudinal direction

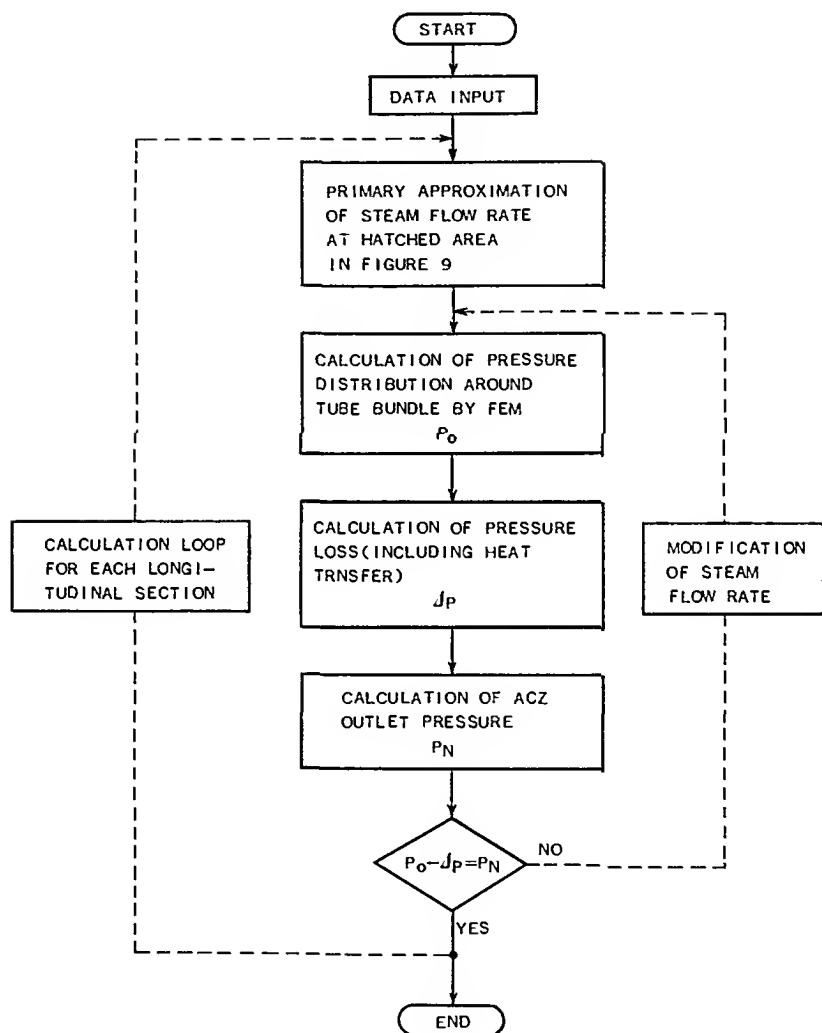


Figure 11 Flow chart of calculation

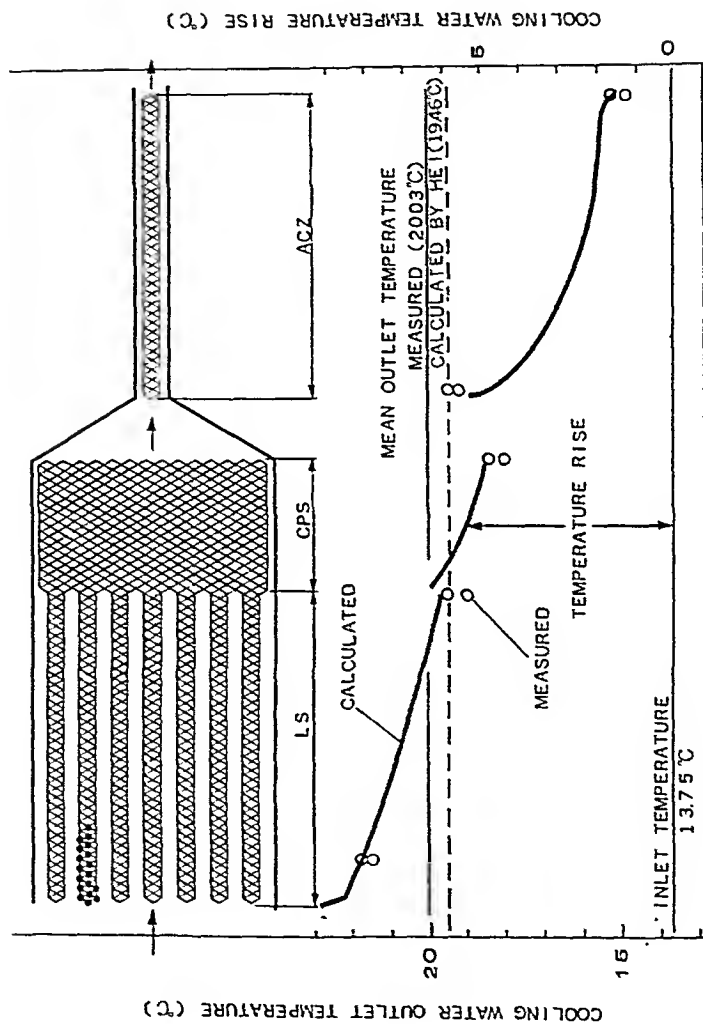


Figure 12 Temperature distribution of cooling water outlet

"A COMPUTERISED ANALYSIS OF POWER CONDENSER PERFORMANCE BASED UPON AN INVESTIGATION OF CONDENSATION".

H.L. Hopkins, J. Loughhead, C.J. Monks.

Whilst the condensers provided on recently commissioned large turbine generator plants have performance levels considerably better than HEI standard predictions the paper describes how, by a combination of experimental research and computer aided analysis, the designer can develop a better understanding of condenser operation which should lead to further improvements.

1. INTRODUCTION.

In the early 1970's the authors' company decided that their future designs of large turbine generator plant, above 200MW rating, would be based on a range of standardised low pressure turbine cylinders which would be associated with underslung condensers. The size and type of condenser would obviously be influenced by the heat rejection and also by the economics of operation. The most suitable design can, in some instances, be an axial arrangement, sometimes a two pass transverse arrangement, but for the majority of applications a single pass transverse condenser, as illustrated in Figure 1, is the best solution.

A standard design based on previous good experience and developed using the mathematical model and condensation theory then available, was adopted. The tubeplate arrangement shown in Figure 3 incorporates the following features:-

- (a) Central venting, which when combined with radial flow into the whole periphery of the tube nest ensures low velocities and low steam pressure drops.
- (b) Steam access to the bottom of the nest, which combined with steam lanes in the bottom of the nest minimises condensate undercooling and ensures good deaeration.
- (c) A large amount of horizontal steam flow which provides good heat transfer rates.
- (d) In-line open-pitched tubes in the outer rows to minimise pressure drop, and triangular close-pitched tubes in the inner region to promote good heat transfer rates.

- (e) Condensate collecting trays built into the nest to reduce inundation.
- (f) A nest design and venting system to ensure good steam distribution throughout the condenser, and thereby enabling the use of long tubes which often provide an economic advantage.

The central venting system, Figure 2, also takes account of the different rates of condensation along the tube length due to the variation in cooling water temperature. Steam and incondensibles, which penetrate the nest to the central vent duct at the warm end of the condenser are transported down the duct to the cold end where most of the steam is condensed. The residual steam and incondensibles are finally extracted, by the air pumps, via a boxed section adjacent to the inlet tubeplate. This is the coldest part of the condenser and therefore ensures the lowest possible mixture temperature.

In order to advance this design it was necessary to investigate the condenser operation in greater detail, using an improved analytical procedure. A systematic series of experiments to establish information on the condensation process was undertaken. The purpose was to incorporate the experimental results, together with operational experience, into a computer program to facilitate the detailed analysis and design of condensers.

2. EXPERIMENTAL INVESTIGATION.

The purpose of the investigation was to establish the heat transfer and pressure drop characteristics for condensing steam, in both square and triangular pitched geometries, for the flow directions as illustrated in Figure 3. The tests were carried out in a vacuum steam tunnel using test elements sized to give results applicable to the cells finally used in the computer simulation.

2.1 Experimental Facility.

The experimental rig is described by Davidson and Preston (1) and is illustrated schematically in Figure 4 (a).

The test section, shown in Figure 4(c), contains between 40 and 105 tubes, depending on geometry and pitch. It is supplied with cooling water at a nominal velocity of 2 m/s, which is typical of operating velocities in a power condenser. Orientation of the test section in the various positions shown in Figure 4(b) enables tests with up, down, horizontal and inclined steam flow.

By incorporating a downstream dump condenser, any desired fraction of the steam can be passed through the test section uncondensed. This, together with the inclusion of an artificial inundation system, allows simulation of the conditions prevailing at any point within the condenser tube nest.

Artificial inundation is achieved by pumping condensate on to the top most row of tubes, Figure 4(c). The condensate is initially carried in a small tube brazed inside the condenser tube and discharged via holes drilled at 25mm pitch in the top surface as shown in Figure 5. This allows the tube to continue to condense steam.

Condensation rates in the range 0-0.05kg/m²s; steam velocities across the tubes up to 250m/s are possible and are controlled by independently varying the cooling rate of both the test section and the dump condenser, and the heat supplied to the boiler.

2.2 Experimental Programme.

The experimental programme, involving nearly 900 runs, has provided data which allows direct calculation of condensation, steam flow, inundation rates, overall test section pressure drop and steam-side heat transfer coefficient. The results are checked quantitatively as the experimental programme progresses and areas of unexpected or non-uniform results are especially scrutinised. For example, the considerable variation of pressure drop and heat transfer rates for steam in an upflow direction resulted in these tests being given special attention and subsequently led to the establishment of criteria for condensate hold-up and for condensate flow reversal at high steam flow rates.

The computer-controlled data acquisition system allows each temperature measurement to be taken up to one hundred times per second. An interesting result from this facility is the plot, shown in Figure 6, of the variation in temperature difference between the tube wall and the steam around the circumference of a tube taken at half second intervals. This plot provides a good representation of the film indicating the thickening of the film at the bottom of the tube as the water drains away. The unsteadiness of the film, presumably due to disturbance by water splashing onto the tube, is clearly identified. Mean temperatures are obtained for the correlation work by averaging the many readings taken from each thermocouple.

2.3 Data Correlation.

2.3.1 Correlation Approach. Models of condensation have generally regarded the two-phase flow across the tube nest as consisting of two separate streams, namely the steam and a condensed water film, having different velocities. This 'two velocity model' is a simplification because it can be observed that a considerable amount of the water is carried as droplets between the tubes. It was found that the 'two velocity model' tends to underpredict some heat transfer coefficients and to produce unreliable predictions of upflow pressure drop.

A 'three velocity model' was developed which overcomes these problems by treating the steam, water film and the water droplets separately as illustrated in Figure 7. This model allows for hold-up of condensate droplets between tubes, which is especially important in some upflow situations where condensate does not drain but is held and ultimately carried upwards. The more accurate prediction of water loading on the tube also enables better heat transfer predictions.

2.3.2 Pressure Drop Correlation. The form of the equation for pressure drop in three velocity model is:-

$$-\Delta P_T = \frac{(\text{frictional term} + \text{gravitational term} + \text{momentum term})}{(1 + \text{compressibility term})} \quad \text{--- (1)}$$

where:-

$$\text{Frictional term} = -\Delta P_f \frac{\bar{x}_f^2}{\bar{x}_f}$$

$$\text{Gravitational term} = \pm g \sin \theta (\alpha \rho_g + (1 - \alpha) \rho_L) \Delta z$$

$$\text{Momentum term} = \frac{2W_f C}{A_{TS}^2} \left(\frac{x}{\alpha \rho_g} - \frac{1 - x - y}{\rho_L (1 - \alpha - \delta)} \right)$$

$$\text{Compressibility term} = \frac{W_r^2 X^2}{A_{\text{min}}^2 \alpha^2} \cdot \frac{\partial \partial_g}{\partial P}$$

The unknown quantities on the right hand side of the equation are :-

$-\Delta P_f$ The single phase frictional pressure drop

Φ_g^2 The frictional two phase multiplier

α The void fraction

γ The droplet area ratio

γ The droplet mass fraction

Appendix 1 contains more detailed definitions of these and other less familiar terms. The frictional and gravitational terms can be identified with change in total pressure as presented in section 3.2.

The single-phase frictional pressure drop $-\Delta P_f$ is taken from published literature, Zukauskas (2) Grant and Murray (3), whereas the remaining unknowns, obtained using three correlations derived by the authors are:-

(a) Φ_g^2 as a function of the Lockhart/Martinelli parameter

(b) α as a function of the steam Froude number, Fr

(c) Entrainment ratio, E, as a function of the steam Froude number Fr

E is the ratio of condensate present as droplets between the tubes to the total condensate flow. The value increases significantly as the steam velocity increases and more condensate is stripped from the tube by vapour shear. The value of the entrainment ratio results from dynamic equilibrium set up between:-

- a water film on the tube formed by condensation
- droplets redepositing on the tubes by splashing
- droplets leaving the film influenced by vapour shear and gravity.

Another consideration of condensate entrainment in the steam flow is that of large scale condensate transport through the tube nest. If not correctly accounted for, this will result in errors in the prediction of condensate loadings and incorrect predictions of pressure drop and heat transfer. Figure 8 depicts two sections from a condenser nest; where (a) and (b) relate to positions D and A in Figure 3, and indicate typical transport of condensate by the steam flow. The results from the tests show good agreement with the predictions of Eissenberg (4) and have been used to produce a correlation based on the Wallis (5) superficial volumetric flux parameter j_{G*}

The form of this correlation is

$$E_c = (1 - e^{-mj_g^*})^n \quad \text{--- (2)}$$

where m is a function of the number of tube rows in the vertical direction and N is the number of tube rows in the horizontal direction of the computational cell.

2.3.3. Heat Transfer Correlation. The correlations produced for the steam side heat transfer coefficient are based on the equation of Nusselt (6) for condensation of stationary vapour on a single horizontal tube. To apply the Nusselt heat transfer coefficient, h_{NU} , to a power condenser nest, correction factors must be used to account for:-

- a) condensate sub-cooling
- b) vapour shear
- c) inundation

The effect of condensate sub-cooling is accounted for by the correction proposed by Rosehow (7).

$$\frac{h}{h_{NU}} = \left(1 + \frac{0.68}{K}\right)^{0.25} \quad \text{--- (3)}$$

In a power condenser this factor is much less significant than the other two listed, because the value of K is of the order of one hundred and so the factor is close to unity.

When considering vapour shear and inundation in a tube bundle it becomes difficult to separate the two effects and to obtain independent correlations. To overcome this problem a published vapour shear correlation was used. Since the 'three velocity model' provides information on water loadings on tubes, an inundation correlation can be derived to match the measured heat transfer data.

The vapour shear correction factor is that of Berman (8), derived to describe the data of Berman and Tumanov (9), which considers a condensing tube imbedded in a bundle of dummy tubes, and is more appropriate in this case.

The inundation factor is in the same form as that used by Kutatela (10), Fuks (11), and Grant and Osment (12).

$$\frac{h}{h_{NU}} = N_I^{-n} \quad \text{--- (4)}$$

N_I was calculated for all the test data using the previously described entrainment correlations. The value of the exponent n is dependent on steam velocity and so it is correlated against Froude number, using an exponential form between two limiting values:-

- a) The lower limit, n_{min} , tends to the theoretical extension of Nusselt's equation for a single tube in stationary steam, assuming laminar film flow and no splashing.

$$\frac{h}{h_{NU}} = N_I^{0.75} - (N_I - 1)^{0.75} \quad \text{--- (5)}$$

- b) The upper limit, n_{\max} , is a function of N_f as the Froude number tends to infinity.

Figure 9 illustrates all the heat transfer mechanisms involved and summarises the correlations used to predict them.

3. COMPUTER PROGRAM.

The computer program is directed towards prediction of the performance of condensers typified by the design discussed in section 1. The overall performance is obtained by considering a series of successive axial slices of the condenser which are small enough to allow use of mid-span data to represent local steam conditions. For detailed analysis it is possible to analyse the span between each support plate and, consequently, a two-dimensional analysis is considered appropriate. The computational problem is then largely concerned with a calculation of separate successive two-dimensional flow fields connected by conditions of thermodynamic and flow continuity and heat balance.

It is assumed that each flow field is made up of two distinct but interrelating flow regimes, one corresponding to the area occupied by the tube nest and the other corresponding to the region external to the tube nest. Flow entering the outer region is distributed around the tube nest boundary, adjusting within some small zone to pass more or less normally through the gaps between the outer tubes. In the analysis this change in flow regime is assumed to take place abruptly, with a discontinuous jump in flow conditions across the interface at the periphery of the tube nest, while maintaining a continuity of flow. Calculated total pressure changes incorporate flow losses introduced by correlated viscous effects in the outer region and separate entry losses into the first row of tubes.

In the outer region the flow regime is typical of duct flow, where velocity components are continuously distributed over the region. Boundary conditions on the casing walls are satisfied by a zero normal velocity component. Any non-uniformity in the specified inlet flow distribution will result in vorticity being distributed throughout the region.

In the tube nest itself the flow field is not continuously distributed over the available space, but is confined to the gaps between tubes. Flow conditions are dominated by local condensation together with high viscous resistance from the tube drag. The application of correlated heat transfer and pressure loss data over a block of condensing tubes eliminates the necessity to calculate flow conditions local to each tube.

3.1 External Flow Solution.

The flow field in each axial slice of the outer region is computed using two-dimensional compressible flow equations. For a pressure-density relationship applicable to the steam/air mixture the equation of motion can be written in the form:

$$\frac{\partial^2 \psi}{\partial x^2} + \frac{\partial^2 \psi}{\partial y^2} = \frac{1}{\rho} \cdot \frac{\partial \psi}{\partial x} \cdot \frac{\partial \rho}{\partial x} + \frac{1}{\rho} \cdot \frac{\partial \psi}{\partial y} \cdot \frac{\partial \rho}{\partial y} - \left(\frac{\gamma}{\rho} \right) \rho^2 \dots (6)$$

where the vortex density term $\frac{\gamma}{\rho}$ is constant along each streamline. This equation represents a flow field with varying total pressure at inlet which is conserved along streamlines. The compressible stream function, ψ , is defined in the usual way:

$$v = -\frac{1}{\rho} \frac{\partial \psi}{\partial x} \quad ; \quad u = \frac{1}{\rho} \frac{\partial \psi}{\partial y}$$

and the vortex density is given by:

$$\frac{\gamma}{\rho} = -\frac{1}{\rho} \left(\frac{\partial v}{\partial x} - \frac{\partial u}{\partial y} \right)$$

Boundary conditions for the stream function and vortex density are:

- (i) Inlet flow boundary; ψ distribution derived from specified conditions.
- (ii) Outer region walls; ψ constant
- (iii) Outer region: tube nest interface; ψ is specified by the equivalent continuous distribution of mass flux crossing the interface and defined by a tube nest solution.
- (iv) Vortex density; γ/ρ derived as a function of ψ from specified data at inlet.

In the calculation procedure, the equation of motion is effectively linearised by evaluating the source of terms on the right hand side of equation (6) from the previous solution. Each linearised set of equations is solved by means of a finite difference approximation using a nodal mesh with uniform grid spacing.

3.2 Tube Nest Region.

Equivalent continuous equations relating mass flux and total pressure are solved in conjunction with the continuity condition, i.e.

$$\left[\frac{\partial P_t}{\partial z_{ij}} \right]_{\text{TP}} = \Phi_q \left[\frac{\partial P_t}{\partial z_{ij}} \right]_q + \text{Gravitational term.} \quad \text{--- (7)}$$

$$\sum \frac{\partial \dot{m}_{ij}}{\partial z_{ij}} = -Q \quad \text{--- (8)}$$

$$\text{where } \rho \left[\frac{\partial P_t}{\partial z_{ij}} \right]_q = F_1(\dot{m}_k, \dot{m}_l) \frac{\dot{m}_k}{|\dot{m}_k|} + F_2(\dot{m}_k, \dot{m}_l) \frac{\dot{m}_l}{|\dot{m}_l|} \quad \text{--- (9)}$$

F_1 and F_2 being quadratic equations in $|\dot{m}_k|$ and $|\dot{m}_l|$

\dot{m}_{ij} denotes the equivalent continuous components of mass flux in directions z_{ij} , and subscripts k and l relate to the direction of the tube pitch axes. Correlated values of the two-phase multiplier and the gravitational term are specified by data obtained from the experimental programme discussed earlier. In the horizontal direction the gravitational term is zero.

Single-phase pressure gradients are deduced from loss coefficient data which define the total pressure drop over a tube pitch in terms of mass flux. Loss coefficients for a range of pitching geometries for single phase flows normal to the tube pitch axes are taken from (2). The effect of crossflow is derived

from analysis of the detailed flow situation around individual tubes.

A general loss coefficient, matched to the standard data of (2), has been derived from the correlated data of Miller (13) and Idel'chik (14), assuming the flow to be analogous to that of a successive series of converging or diverging branch sections. From such an analysis the equivalent continuous derivatives are obtained in the form specified above.

The coefficients of functions F_1 and F_2 in equation (9) relate to specific tube pitch arrangements for flow in any particular direction and take account of the minimum loss achieved for steam flowing at the tube pitch angle.

The condensation rate required in the continuity equation is calculated by heat balance using local values of overall heat transfer coefficients. The correlated test data is used for the steam-side coefficients with the effect of air blanketing and the water-side coefficients, derived from standard expressions as shown in Figure 9.

To evaluate numerical solutions in the tube nest region finite difference techniques are used. The region is divided into a number of control volumes with pressure, condensation rate, and directional components of mass flux defined at the central or nodal points. Pressure gradients are calculated by first order differencing.

3.3. The Overall Procedure.

The computer program predicts the pressures at the turbine exhaust and in the central duct of the tube nest for specified conditions of steam, cooling water and air leakage.

The calculation integrates the results of each axial section where the inlet cooling water temperature is the outlet temperature from the preceding section. The total steam flow is, therefore, the summation of the steam flow into each section obtained by successive iterations between the external flow solution, which defines the pressure conditions at inlet to the nest, and the nest solution which defines the complementary mass flow distribution across the interface.

The procedure produces a balance of the uncondensed steam which flows into the central duct at the warm end of the tube nest, and the surplus condensing potential at the cold end of the tube nest, as illustrated in Fig (2). The maximum steam flow along the duct is thus predicted. The small steam flow to the air pumps is neglected.

The small air cooling zone, located adjacent to the inlet tubeplate, represents less than 2% of the total condenser surface and is not included in the computer analysis. It does, however, further reduce the temperature of the mixture discharged from the condenser. The pressure drop through this zone and across the preceding baffles, in the central vent duct, is a defined value and is not at this stage predicted by the calculation procedure.

4. APPLICATION.

The computer program is used to develop desirable features of condenser design, taking account of the wide variation in operating conditions experienced by such condensers. It is necessary, for the majority of applications, to retain an overall design concept and to achieve the desirable high performance by attention to the details of design.

Analysis includes the plotting of salient conditions for a tube nest as illustrated typically in Figure 10. The combination of tube size and pitch, the tube pattern, the location and shape of the central vent and the location of condensate collection trays, can all be adjusted to achieve an optimum design.

In such an analysis the effect of variation of external parameters such as the rate of steam flow, the steam flow pattern at the turbine exhaust, cooling water conditions, dimensions of the condenser shell, and air leakage can be assessed.

In the instances where detailed test results are available for comparison with this type of analysis, agreement is encouragingly good.

5. CONCLUSION.

By incorporating the results of related experimental research into a specifically designed computer program it has been possible to produce predictions of condenser performance which correlate well with actual condenser operation.

Use of the condenser analysis program will enable further improvements to be achieved by general design changes and by fine tuning of the designs for specific projects.

It is intended to continue the investigation of the condensation process with further consideration of the flow regimes around and entering the tube nest, of the overall distribution of condensate within the tube nest and of the operation of the air cooling zone. This may lead to further improvements in performance predictions and in condenser design.

6. ACKNOWLEDGEMENT.

The authors would like to acknowledge the work of their colleagues in the G.E.C. Turbine Generator Ltd and Power Group and especially the contribution of Mr. A. Jackson and Mr. C.J. Morgan in the production of the computer programming and research aspects of this paper.

7. APPENDIX.

1. Void fraction, α , the ratio of the cross sectional area occupied by the vapour phase to the total cross sectional area

$$\alpha = \frac{A_g}{A_T} \quad \text{OR} \quad (1 - \alpha) = \frac{A_L}{A_T}$$

2. Mass flow dryness fraction, X , the ratio of the mass flow of vapour to the total mass flow

$$X = \frac{W_g}{W_g + W_L} \quad \text{OR} \quad (1 - X) = \frac{W_L}{W_g + W_L}$$

3. Droplet mass fraction, Y , the ratio of the mass flow of the droplets to the total mass flow

$$Y = \frac{W_{Lf}}{W_g + W_{Ld} + W_{Lf}} \quad \text{OR} \quad (1 - X - Y) = \frac{W_{Ld}}{W_g + W_{Ld} + W_{Lf}}$$

4. Entrainment area ratio, E , the ratio of droplets to the total water flow, i.e. the fraction of the water at a point that is not on the tube as film but is entrained in the vapour stream as droplets

$$E = \frac{W_{Ld}}{W_{Ld} + W_{Lf}} = \frac{Y}{(1-X)}$$

5. Droplet area ratio, γ , the ratio of the cross sectional area occupied by the droplet liquid stream to the total cross sectional area

$$\gamma = \frac{A_{Ld}}{A_T} \text{ OR } (1-K-\gamma) = \frac{A_{Lf}}{A_T} \text{ OR } \gamma = E(1-K)$$

6. Average total space area, A_{TS} , the average flow volume per unit flow length, i.e. , the volume of the bundle per unit length, excluding the volume occupied by tubes.

7. Lockhart/Martinelli parameter, χ , the square root of the ratio of the pressure drop due to the liquid fraction flowing alone to the pressure drop to the vapour fraction flowing alone.

$$\chi = \left[\frac{\Delta P_L}{\Delta P_g} \right]^{0.5}$$

8. Two-phase multiplying factor, Φ_g^2 , used to scale the pressure drop due by vapour flowing alone, to give the two-phase frictional pressure drop.

$$\Phi_g^2 = \frac{\Delta P_{TP}}{\Delta P_g}$$

9. Horizontal condensate carryover ratio, E_1 , the ratio of the condensate which is moving horizontally, due to entrainment in horizontal steam flow, to the total amount of condensate present at a point.

10. Wallis superficial vapour flux parameter

$$j_g^* = W_g \cdot [g D \rho_g (\rho_L - \rho_g)]^{-0.5}$$

8. SYMBOLS USED.

Symbol	Description	Units
A	Area	m
C	Condensation rate	kg/s
C_1, C_2, C_3, C_4	Constants used in heat transfer correlations	-
C_p	Specific heat at constant pressure.	KJ/Kg.K
D	Tube outside diameter	m
d	Tube inside diameter	m
E	Entrainment ratio	-
E_1	Horizontal condensate carry-over ratio	-
F	Fouling resistance	K.m ² /KW
Fr	Mean steam Froude number based on minimum area, $\frac{U^2}{gD}$	-
F_1, F_2	Quadratic functions in \dot{m}_k and \dot{m}_l	--
g	Acceleration due to gravity	m/s ²
h	Heat transfer coefficient	KW/m ² .K

<u>Symbol</u>	<u>Description</u>	<u>Units</u>
h_{fg}	Latent heat of condensation	KJ/Kg
J_G^*	Wallis superficial volumetric flux parameter	-
k	Thermal conductivity	KW/m.K
L	Length	m
m	Exponent in expression for horizontal carry-over ratio	-
\dot{m}	Mass flux density	Kg/m ² .s.
N	Number of tube rows in horizontal direction	-
N_I	Inundation parameter	-
n	Exponent of N_I in heat transfer coefficients correction factor	-
P	Pressure	N/m ²
ΔP	Pressure drop	N/m ²
Pr	Prandtl number, $\frac{\mu C_p}{k}$	-
Q	Condensation per unit volume	kg/m ³ .s
Re	Reynolds number, $\frac{\rho U D}{\mu}$, used in heat transfer correlations	-
T	Temperature	K
U	Velocity	m/s
u	Component of velocity in horizontal direction	m/s
v	Component of velocity in vertical direction	m/s
W	Mass flow rate	Kg/s
X	Mass flow dryness fraction	-
x	Distance in horizontal direction	m
Y	Droplet mass fraction	-
y	Distance in vertical direction	m
z	Distance	m
α	Void fraction	-
Γ	Diffusion coefficient	m ² /s
δ	Droplet area ratio	-
ζ	Vorticity	-
θ	Angle of inclination to gravity	radians
K	Ratio of latent to sensible heat $\frac{h_{fg}}{C_p(T_g - T_w)}$	-
μ	Viscosity	kg/m.s
ν	Specific volume	m ³ /kg
π	Bernans velocity/condensation parameter, $\frac{Fr}{Pr \cdot K}$	-
ρ	Density	kg/m ³
Φ_2	Frictional two-phase multiplier	-
χ	Lockhart Martinelli parameter	-
ψ	Stream Function	-

Subscripts

C	Condensate
CW	Cooling water

Subscripts

G	Gas
i	Horizontal direction
j	Vertical direction
k,l	Direction of tube pitch axes
L	Liquid
Ld	Liquid drop
Lf	Liquid film
max	Maximum
min	Minimum
NU	Nusselt
S	Steam
T	Total
TP	Two-phase
TS	Total space
t	Tube
W	Tube wall

9. REFERENCES.

- Davidson, B.J., and Preston, S.B., 1976, "Heat and Mass Transfer in Condensers.", Anglo-Soviet Symposium
- Zukauskas, A., 1972, "Advances in Heat Transfer.", Volume 8" Academic, Press., New York.
- Grant, I.D.R., and Murray, I., "Shell side performance of segmentally baffled shell and tube heat exchangers by divided flow method.", HTFS, Design Report D.R.24.
- Eissenberg, D.M., 1974, "An investigation of the variables affecting steam condensation on the outside of a horizontal tube bundle.", prepared for the Office of Saline Water, PB232-365.
- Wallis, G.B., 1969, "One-dimensional two-phase flow.", McGraw Hill, New York.
- Nusselt, W., 1916, "Die oberflächen-Kondensation des Wasserdampfes." VDI.Z.60., 541-546 and 569-575.
- Rosenhow, W.M., 1956, "Heat transfer and temperature distribution in laminar film condensation.", Trans. ASME 78., 1645-1648.
- Berman, L.D., 1973, "Heat transfer with condensation of moving vapour on a horizontal tube.", Teploenergetika 20(8), 76-77.
- Berman, L.D. and Tumanov, Yu.A., 1962 "Condensation heat transfer in a vapour flow over a horizontal tube.", Teploenergetika 9(10), 77-84.
- Kutateladze, S.S., 1963, "Fundamentals of heat transfer.", Edward Arnold, London.
- Fuks, S.N., 1957, "Heat transfer with condensation of steam flowing over a horizontal tube bundle.", Teploenergetika 4(1), 35-38.

12. Grant, I.D.R., and Osment, B.D.J., "The effect of condensate drainage on condenser performance." N.E.L. Report No.350.
13. Miller, D.S., "Internal flow - A guide to losses in pipe and duct systems.", British Hydromechanic Research Association Report.
14. Idel'chik, I.E., 1966, "Handbook of Hydraulic Resistance - Coefficients of local resistance and friction." - Russian translation - U.S. Atomic Energy Commission.
15. Dittus, F.W. and Boelter, L.M.K., 1930, "Heat transfer in automobile radiators of the tubular type.", Univ. Calif. Pubs. Eng., 443-461.

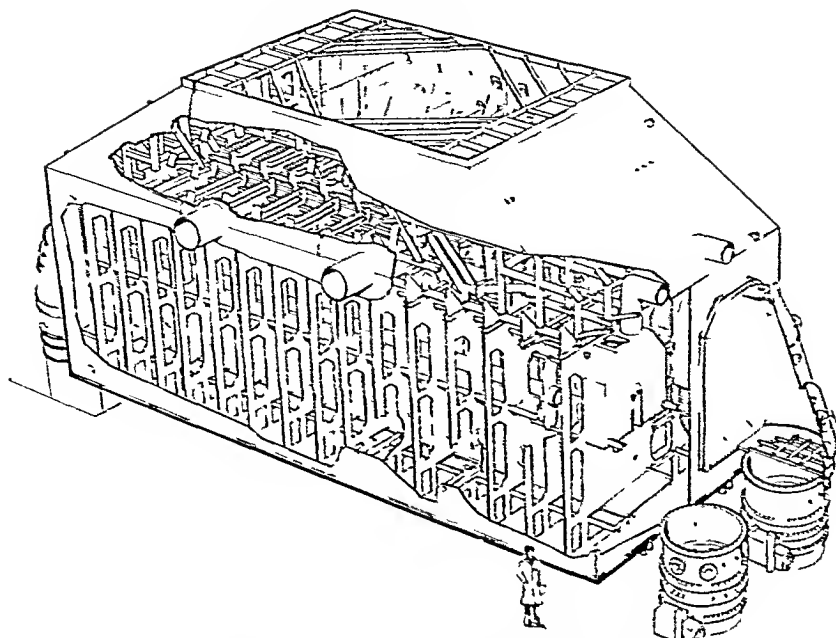


Fig1 SINGLE PASS TRANSVERSE CONDENSER

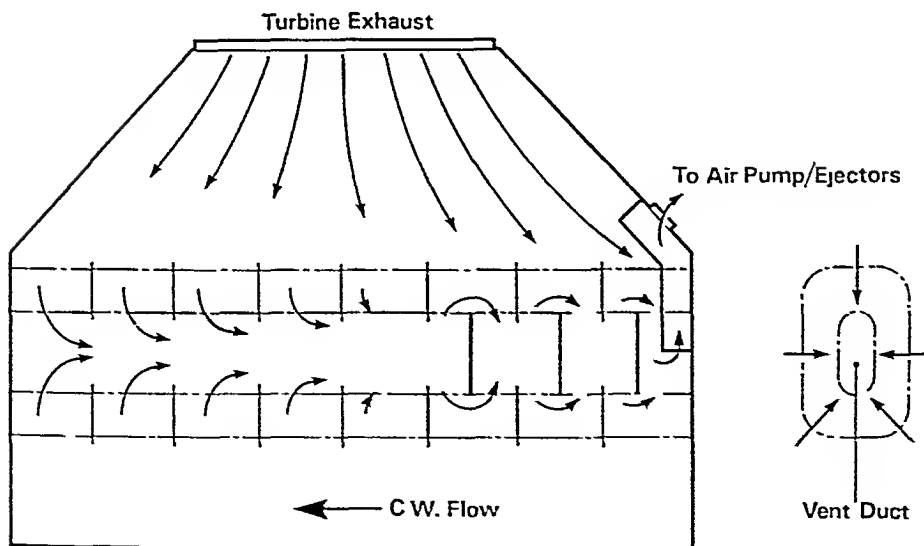


Fig.2 SINGLE PASS CONDENSER AIR SUCTION

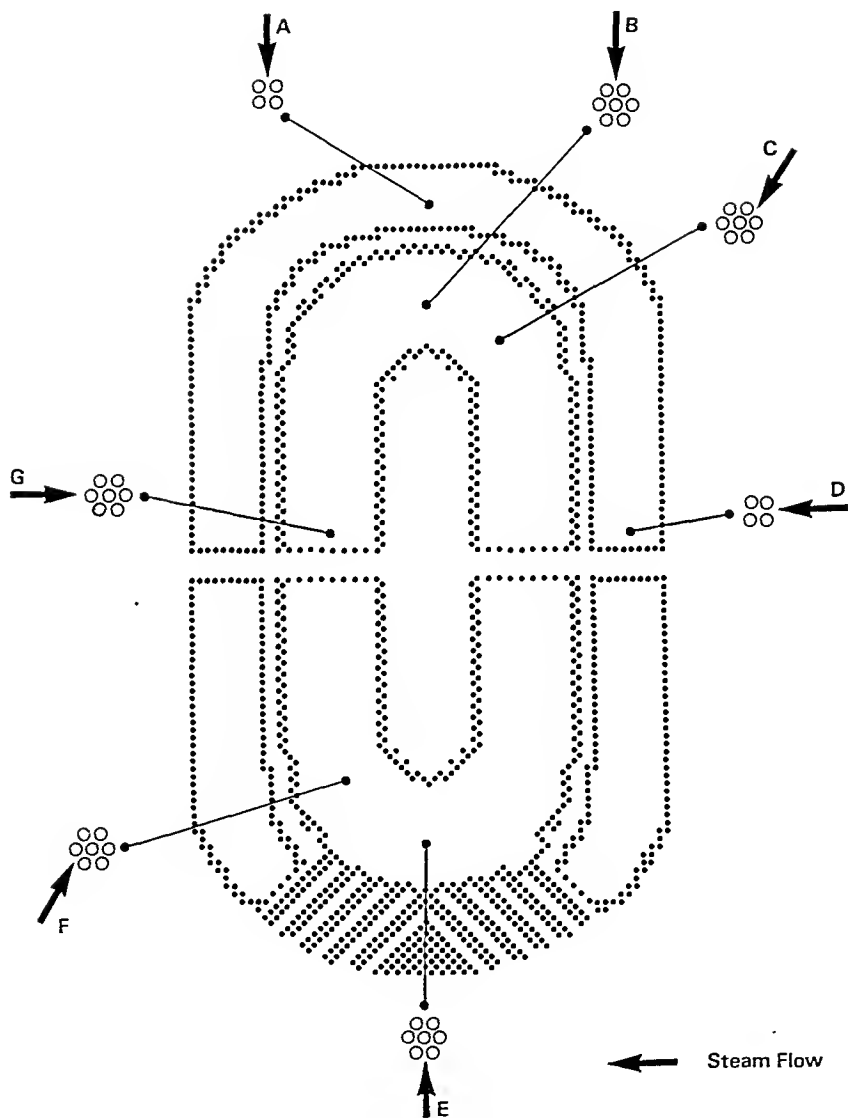
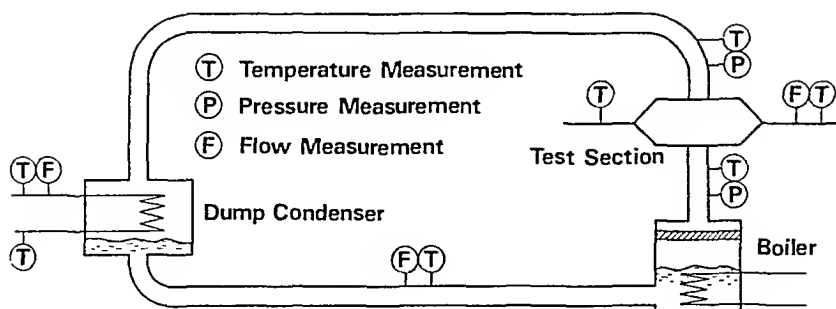
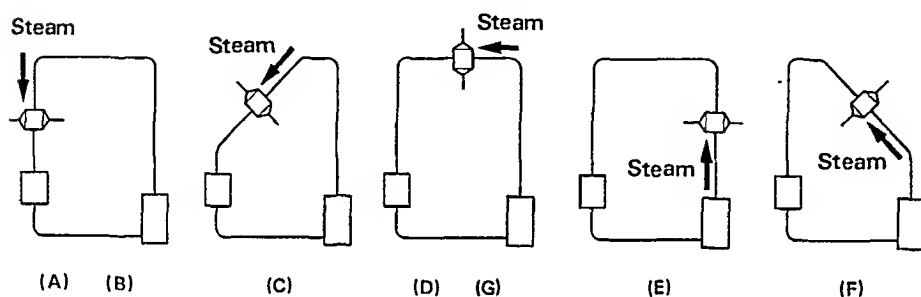
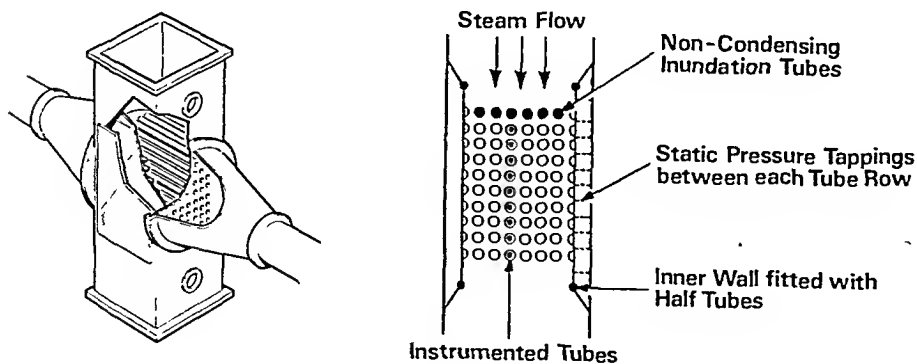


Fig.3 TYPICAL TUBEPLATE LAYOUT SHOWING SECTIONS WITH DIFFERING FLOW CONDITIONS



(a) Schematic Diagram of Experimental Rig

(b) Alternative Position of Test Section
(Reference are to Flow Directions of Fig 3)

(c) Details of Test Section

Fig.4 DETAILS OF EXPERIMENTAL RIG

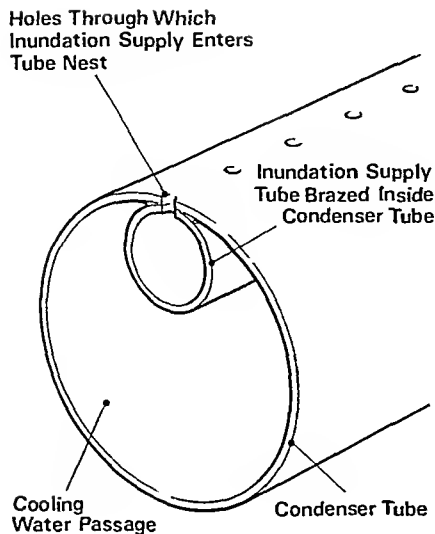


Fig. 5 CROSS SECTION THROUGH SPECIALLY CONSTRUCTED INUNDATION SUPPLY TUBE

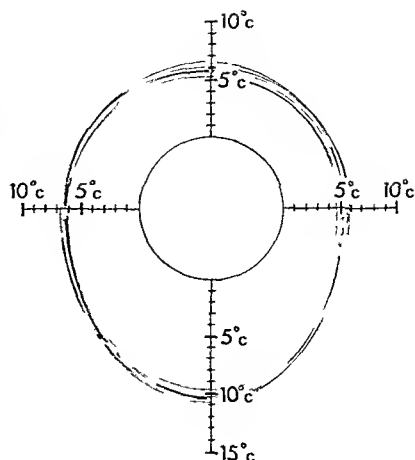


Fig. 6 TEMPERATURE DIFFERENCE BETWEEN THE TUBE WALL AND THE LOCAL STEAM

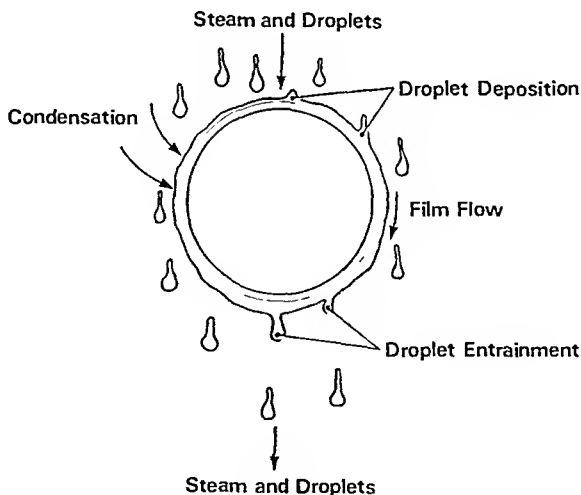


Fig. 7 THE 'THREE VELOCITY MODEL'

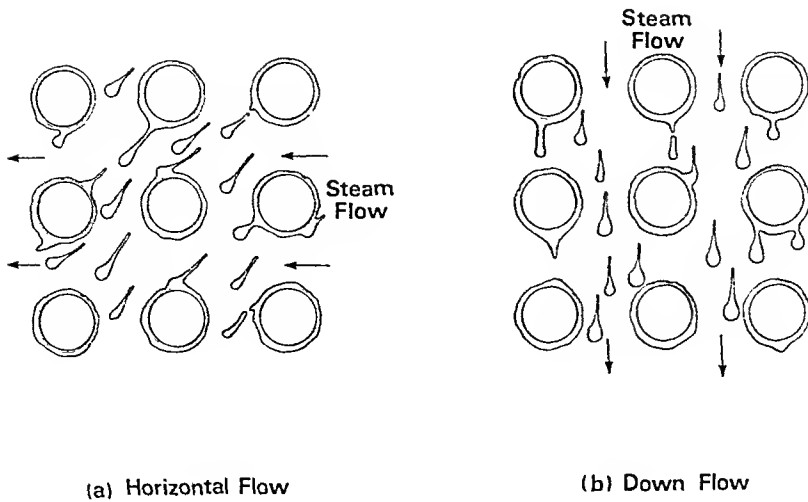
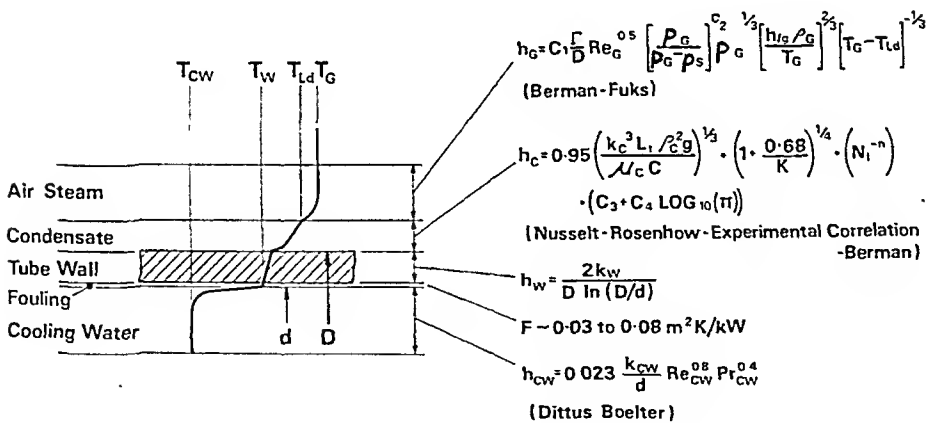


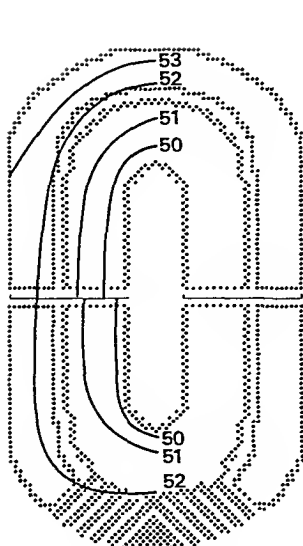
Fig.8 DIAGRAM SHOWING TYPICAL CONDENSATE DROPLET MOTION WITH STEAM FLOW



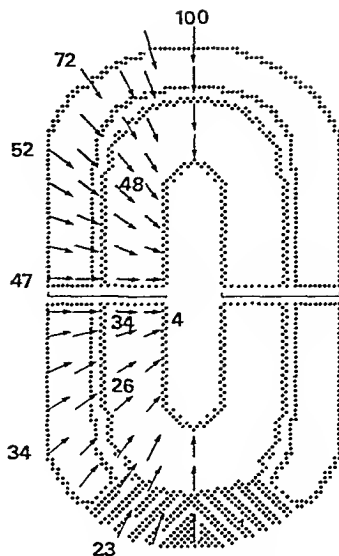
Overall heat transfer coefficient h defined by

$$\frac{1}{h} = \frac{D}{d h_{CW}} + \frac{1}{h_W} + F + \frac{1}{h_C} + \frac{1}{h_G}$$

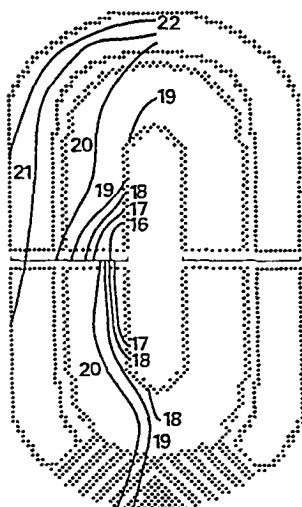
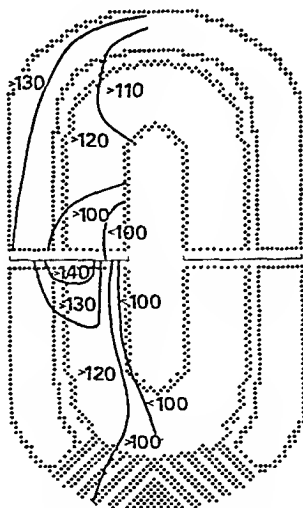
Fig.9 CONSTITUENT PARTS OF OVERALL HEAT TRANSFER COEFFICIENT



(a) Pressure Contours (m.bar)



(b) Variation in Velocity (% of Maximum)

(c) Variation in Cooling Water Temperature Rise ($^{\circ}\text{C}$)

(d) Variation in Heat Transfer Coefficient (% HEI Prediction)

Fig 10 TYPICAL GRAPHICAL REPRESENTATION OF COMPUTER PROGRAM RESULTS

A NEW CONDENSER TEST CODE & ASSOCIATED MEASUREMENT TECHNIQUES

C.A.E. Clay * & Z.W. Sochaczewski⁺

The CEGB's new Condenser Site Test Code is briefly described and its special features, including the determination of the testing accuracy, are highlighted. Details of novel methods for measuring cooling water outlet temperatures from and flowrates through condensers are given, together with some test results obtained using these techniques.

INTRODUCTION

When testing plant for acceptance or other purposes, it is necessary that the interested parties agree as to how the performance is to be assessed and how the plant is to be tested. This leads to a requirement for test codes which lay down general concepts and procedures.

It is the policy of the Central Electricity Generating Board (CEGB) to use whenever possible the appropriate International or National code, such as those produced by ISO, IEC, ANSI, BSI, etc., for guidance on plant testing. However, in many cases, due to rapid advances in technology and other factors, the existing codes either do not cover the specific requirements or are outdated, and the CEGB then has to prepare and publish codes to suit their particular requirements. (Because often the same specialists are involved it is not unusual for such a CEGB code to be used as a basis for a subsequent national code). The preparation of a testing code is not an easy matter as, apart from technical considerations, agreement is required between parties with sometimes different objectives and conflicting loyalties, and so it is often time consuming to reach mutually satisfactory agreement.

In the case of condenser performance assessment there was no national testing code, and the BEAMA document (reference 1) and foreign test codes previously used were not considered appropriate for the testing of condensers of current design. Consequently the preparation of Site Test Code No.3 (STC3) entitled "Performance of Surface-Type Steam Condensers" was authorised in 1977 and published in 1981 (2).

* Midlands Region, Central Electricity Generating Board, Solihull, U.K.

+ ex Midlands Region, CEGB.

This paper gives brief details of STC3, explains why various new ideas were introduced and describes in greater detail some of the instrumentation used for measuring the basic parameters involved in assessing condenser performance.

GENERAL DESCRIPTION OF STC3

Site Test Code No.3 is divided into three parts, Part 1 dealing with general aspects such as scope, definitions, test procedures and conditions; Part 2 gives information on measurement techniques and Part 3 deals with the calculation and presentation of results. A brief description of the contents of each Section and appendix is given in appendix A of this paper.

Particular items which are considered to be significantly different from other such codes, and are thought to be of considerable advantage, are detailed below:

a) For assessing the compliance with guarantee, two methods are available for comparing test results with the guaranteed performance. The first involves correcting the test measurement of condenser steam inlet pressure for differences between measured and specified values of:

- cooling water inlet temperature
- cooling water flowrate
- condenser heat load
- tube cleanliness and surface area (if necessary) .

This corrected pressure is then compared with the guaranteed or specified value. The second method is the converse of the first, whereby the guaranteed or specified condenser pressure is corrected for differences in the previously mentioned parameters between specified and test conditions, and this corrected value is then compared with the measured condenser pressure.

The first of the above methods was adopted for STC3 as it was considered that this approach would give more consistent results, particularly if a number of tests were carried out under significantly different conditions.

b) To minimise possible errors from applying unproven corrections for departure from specified conditions, close limits were set for permissible deviations in the main parameters during acceptance tests. If these limits are exceeded for any reason, validated tests are required, either on the particular condenser or an essentially similar one, to determine the shape and value of the correction factor for the parameter(s) involved. This applies particularly to:-

- cooling water inlet temperature
- cooling water flowrate (i.e. water velocity through tubes)

c) All necessary corrections are applied to the test logarithmic mean temperature difference (LMTD), calculated using the mean steam temperature rather than, as

previously employed, the inlet steam temperature. This change was necessary because certain condenser designs were found to have a higher steam side pressure drop than previously experienced. The mean steam temperature is the average of the saturation temperatures corresponding to the steam pressures at the condenser inlet and at a zone within the tube nest where most of the steam is condensed i.e. close to the air cooling section.

d) In addition to the usual corrections, the following additional corrections have been incorporated into the code and are permitted under special circumstances:

- for tube cleanliness, if this differs significantly and measurably from the cleanliness specified in the contract document; it is defined as the ratio of the average heat transfer coefficient of tubes in the condenser to that of a new acid-cleaned tube
- for condensing surface area, if tubes have been plugged or removed.
- for tube material, in cases where the condenser has been retubed either wholly or in part with tubes of different material from that specified.

e) STC3 gives also procedures for evaluating the uncertainties of the individual measurements and of the calculated results. The uncertainties are given in terms of systematic errors only, as the test procedure and frequency of measurement recommended should reduce any random errors to negligible proportions. Sensitivity coefficients are quoted for a typical type of condenser so that the parameters significantly affecting the overall uncertainty can be identified and actions taken to reduce their effect to a minimum. It is considered a significant step forward in this type of code not only to be able to assess the overall test accuracy but also to provide the means by which the test engineer can identify those parameters requiring care in measurement to meet the required accuracy.

This test code has been well received and used for both acceptance and routine condenser testing. Resulting from this experience certain minor corrections and improvements have been suggested and an amendment sheet has been issued.

MEASUREMENT TECHNIQUES

STC3 gives general guidance on techniques to be used for measuring all the main parameters required for assessing the thermal performance of a condenser. Two parameters which are particularly important to the overall accuracy of the assessment are cooling water outlet temperature and flowrate, and novel measurement techniques have been developed for these items as described below.

Cooling Water Outlet Temperature

The measurement of cooling water outlet temperature from a condenser to the required accuracy of about $\pm 0.1^{\circ}\text{C}$ or better can be difficult due to spatial variations in the rate of condensation in different parts of the condenser. This means that the cooling water leaving the water boxes can be significantly stratified so that single point temperature measurements are not adequate. In the past, to overcome this problem and to improve accuracy, multiple thermocouple devices have been

employed, distributed over the pipe cross-section, or water has been withdrawn through multi-hole probes to give a representative sample, the temperature of which was measured with a standard temperature measuring device such as a platinum resistance thermometer or mercury-in-glass thermometer. However, neither of these methods has proved to be completely satisfactory due mainly to their inadequate accuracy, lack of mechanical strength and the possibility of blockage of the holes. A new technique has therefore been developed which has given encouraging results. This involves the use of a number of extended platinum resistance thermometers (PRT's) capable of measuring the average temperature along their entire length, positioned on chordal paths across the pipe. Chordal paths were chosen in preference to the more usual radial paths as they give a better and more representative coverage of the cross-section (figure 1) leading to a more accurate average temperature measurement under stratified conditions. Experience has shown that the best compromise between adequate accuracy on the one hand and cost on the other is obtained by using four chordal paths.

Mechanical integrity is considered to be of paramount importance and therefore the tubes containing the PRT's are supported by either an existing grid or by specially installed rigid struts of narrow section facing the flow so as to reduce vortex shedding and vibration. The PRT containment tubes may be filled with oil if necessary to improve the thermal conductivity to the PRT elements.

The distributed PRT elements can be constructed by various methods. One such method specially developed for this application consists of winding a doubled fine enamelled platinum wire around an insulated copper wire which acts as a former, the whole assembly then being insulated before insertion into a thin walled stainless steel protective tube, typically two metres in length. Alternatively, a number of discrete PRT elements (such as short wound coils or the "Platfilm" type) can be spaced along the immersed length and connected in a series/parallel arrangement, figure 2. Prototype elements of these three types were constructed for calibration and evaluation purposes. A special temperature calibration rig was developed consisting of a 2.1 metre length of 100mm bore plastic pipe, through which water could be circulated from a constant temperature bath. Up to six PRT elements could be inserted into this pipe at any one time together with a standard PRT for measuring the true temperature.

Calibrations of the three prototype elements showed that they all gave stable results in the short term with repeatabilities of $\pm 0.02^\circ\text{C}$ or better. It was also found that the resistance/temperature relationship could be adequately defined by a linear regression over the required temperature range of 20°C to 45°C . These prototypes were then installed in tubes supported by chordal struts in the cooling water outlet pipes of one of the condensers at Ratcliffe-on-Soar power station (4 x 500MW units). After being in service for two months they were removed and recalibrated and were found to have held their calibration. It was decided to standardise on the long PRT element (type 4/21 in figure 2) as it was considered that this type should give a true average as it responds to the temperature distribution over its entire length.

All condensers at Ratcliffe-on-Soar power station have now been equipped with elements of this type as part of a thermal efficiency monitoring system for the whole plant. Recently two of the elements were removed for check calibrations after some

18 months of service. The original and latest calibration results are shown in figure 3, in which the graphs are based on the resistance/temperature formulae derived from the original calibrations. It can be seen that the maximum change in calibration was 0.04°C with most of the values being significantly better than this. It is reported that none of these elements has failed in service, this being attributable to the care taken by the power station staff involved in the design and installation of the supporting struts.

The resistance values of these PRT elements are measured by the four wire constant current/voltage drop method. It is possible to connect the four elements in a pipe in series (or series/parallel) with low resistance connections so that a single output is obtained giving an accurate mean cooling water temperature.

Cooling Water Flowrate

Site Test Code No.3 recommends that the heat load on the condenser should be determined either by calculating the heat rejected from the associated turbine generator or by measuring the heat absorbed by the cooling water. The latter method involves measuring the cooling water flowrate and its temperature rise. In practice this method is often preferable to the heat rejected approach which requires either a concurrent and resource consuming heat rate test on the turbine-generator or the use of recent test data in conjunction with corrections for changes in the turbine-generator terminal conditions.

Site Test Code No.3 summarises the main techniques available for cooling water flowrate measurement which are broadly categorised as:- tracer methods; velocity/area methods and differential pressure methods. The authors consider that the best way of measuring cooling water flowrate when the pipework layout permits, is by the use of an acoustic "time of flight" flowmeter, preferably of the multiple chordal path type. The potential advantages are as follows:-

- a) negligible pressure loss
- b) an accuracy of $\pm 1.0\%$ or better
- c) capability of the multiple path system of providing this accuracy even under certain distorted velocity profile conditions
- d) not essential to calibrate the system in-situ
- e) can be used to also measure average cooling water temperature (see later)

The general principle of operation of the multi-path ultrasonic flowmeter is illustrated in figure 4. Ultrasonic transducers are located at each end of four chordal paths positioned on an angled acoustic plane across the pipe. Acoustic energy pulses are transmitted both backwards and forwards between the pairs of transducers on each path and the times of travel of the pulses through the liquid are measured very precisely. The difference between these travel times is proportional to the average liquid velocity through the particular path involved, and by integrating the four average velocity values it is possible to accurately determine the mean velocity for the whole of the cross-section, and hence the flowrate.

The particular advantage of this technique is that the parameters, measurements and calculations are all fundamental in nature, so that no empirical factors or corrections are required. This means that if the whole system is shown to be accurate under one or more sets of conditions, then it should also be accurate under other conditions which differ only in terms of scale.

PRACTICAL APPLICATION OF THE CODE AND MEASUREMENT TECHNIQUES

An early application of the calculation procedures described in STC3 and the above measurement techniques was at Rugeley 'B' power station (2 x 500 MW units) as part of a turbine-generator efficiency monitoring system, described by Sochaczewski, Clay and Morris (3). This system measures the heat rejected to the condenser as the main parameter in determining the total heat input to the machine. To achieve this, the cooling water flowrates were measured in the two 1.8 metre bore cooling water outlet pipes using an acoustic flowmeter manufactured by Ocean Research Equipment which was connected to transducers mounted on four chordal paths in each pipe. The cooling water inlet and outlet temperatures were measured by PRTs to give the temperature rise. In addition, the mean outlet water temperatures were measured by employing the acoustic flowmeter's ability to measure the velocity-of-sound in water which varies in a known and repeatable way with change in water temperature. The cooling water outlet temperatures were measured well downstream of the condenser and beyond two non-coplanar bends so that adequate mixing was ensured. This avoided the necessity of shutting down and isolating the cooling water pipes to install the more elaborate elements detailed earlier in this paper.

Besides its basic function of continuously monitoring the performance of the turbine-generator, this "Thermal" system (from Turbine Heat Rate Monitoring by Assessment of Losses) was extended to also monitor the thermal performance of the condenser. This merely involved the addition of transducers to measure the steam pressure to the condenser, and extensions to the computer program to calculate and print out the required parameters. Some typical results printed out by this system are shown in Table 1. These are ten minute averages of the various parameters, with the heat load calculated from the cooling water flowrates and temperature rises, and the heat transfer coefficient calculated from the logarithmic mean temperature difference and the surface area of the tubes.

TABLE 1 - Typical performance results obtained on Rugeley "B" No. 6 condenser using the "Thermal" system

Water Inlet Temp. °C	Water Outlet Temp. °C	Water Flowrate m ³ /s	Condenser Heat Load MW	Condenser Pressure mbar	Heat Transfer Coeff. kW/m ² K
12.95	22.51	15.87	624.3	39.2	2.51
14.70	24.16	15.91	624.8	41.4	2.73
16.66	26.16	16.11	628.4	45.6	2.80
17.68	27.04	16.22	625.5	47.4	2.88
19.72	29.25	16.51	647.2	53.6	2.97
20.81	30.80	16.04	666.0	57.2	3.11
23.06	33.44	15.85	683.3	65.1	3.22
25.49	35.89	15.88	684.3	73.5	3.25

These results were obtained over a four week period and values have been selected which show the variations obtained with change in cooling water inlet temperature.

A more comprehensive set of results has been plotted in Figure 5 in terms of heat transfer coefficient against cooling water inlet temperature. Also given on this graph are the design lines abstracted from the BEAMA document (1) and the Heat Exchange Institute standard (4). It can be seen that the heat transfer coefficient falls more sharply than the design values at lower cooling water inlet temperatures, and this trend has been shown to be typical for large condensers.

CONCLUSIONS

The new condenser Site Test Code and its specific innovations have been briefly described. The combined use of the Code and the improved measuring techniques have shown the previously accepted relationship between cooling water inlet temperature and heat transfer coefficient to be inaccurate at the lower end of the cooling water temperature range.

The longer term application of this Code and the improved measuring techniques described should enable power plant operators to monitor condenser performance accurately, leading to improved overall energy conversion efficiency.

REFERENCES

- 1) British Electrical and Allied Manufacturers' Association Incorporated, 1967; Publication No.222; Recommended Practice for the Design of Surface Type Steam Condensing Plant.
- 2) C.E.G.B., 1981; Site Test Code No. 3; Performance of Surface Type Steam Condensers.
- 3) Sochaczewski, Z.W., Clay, C.A.E., and Morris, J.A., 1981.
Proc. I.Mech.E., 195; 295
- 4) Heat Exchange Institute, 1978; Standards for Steam Surface Condensers, seventh edition.

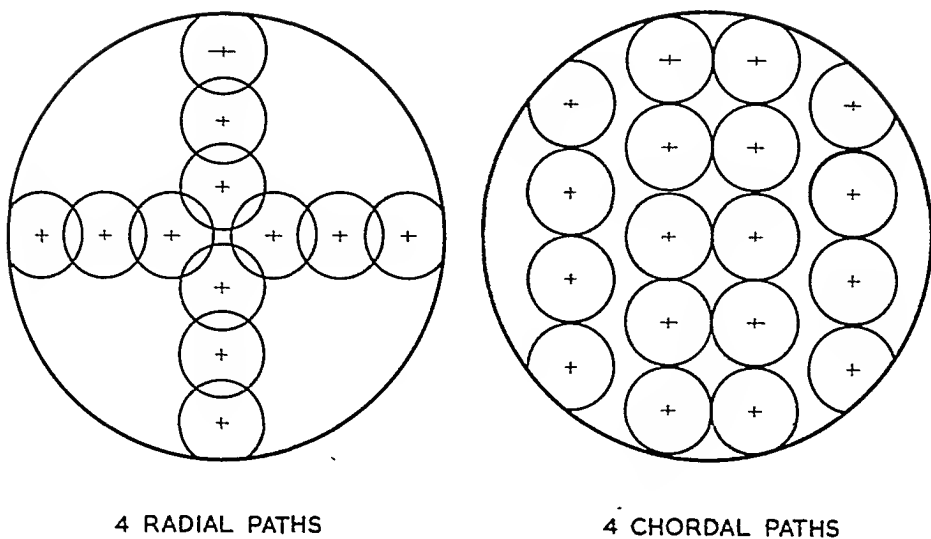


Figure 1 Comparison of radial and chordal temperature sensing paths

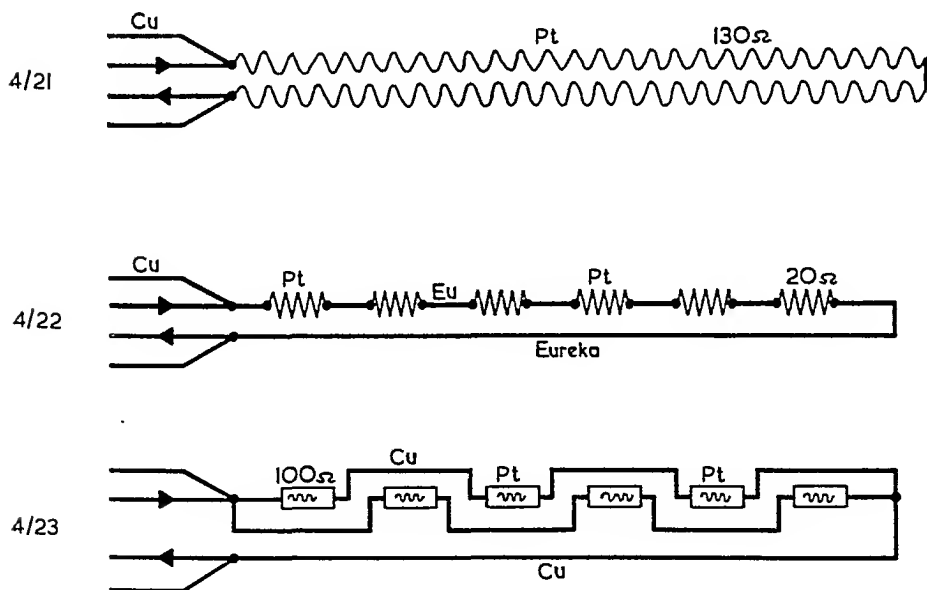


Figure 2 Three types of extended resistance elements

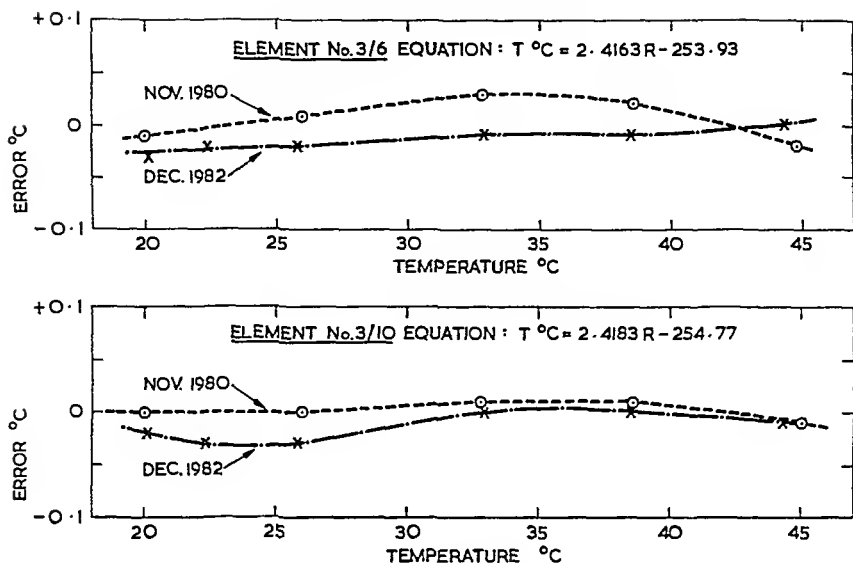


Figure 3 Calibration results on extended platinum resistance elements

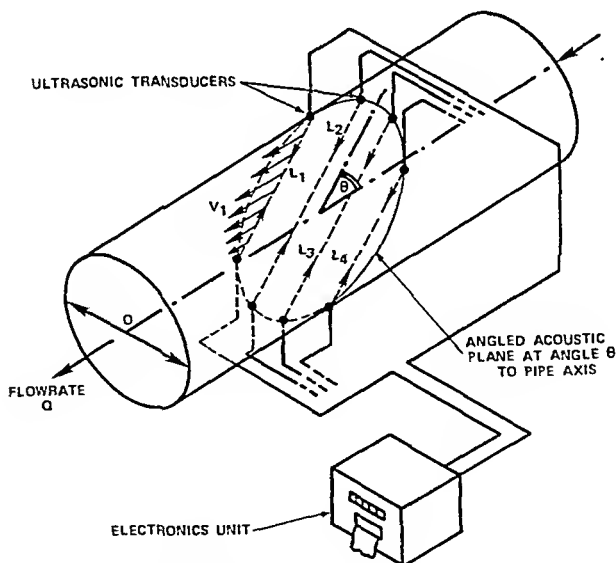


Figure 4 Diagram of four path ultrasonic flowmeter

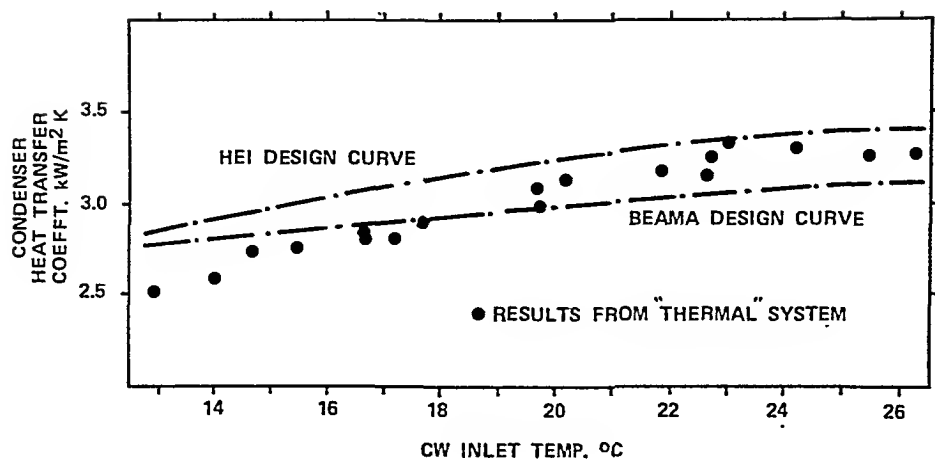


Figure 5 Heat transfer coefficient results for Rugeley "B" condenser

APPENDIX ACONTENTS OF SITE TEST CODE No.3

Part 1, General, consists of four sections which cover the scope of the Code, quote references, notations and definitions, and set down general test procedures, conditions and duration. Those items requiring agreement between all parties to the test before testing can proceed are clearly stated, including responsibility for provision and calibration of instrumentation and the division regarding test personnel. The permissible limits for deviations from specified conditions and extent of fluctuations in test parameters are laid down.

Part 2, Measurements, consists of seven sections the first three of which cover successively the measurement of pressures, temperature and flowrates. In the pressure section particular attention is paid to instrumentation and techniques for measuring the mean steam pressure in the duct(s) between the turbine-generator and the condenser. The actual planes of pressure measurement are defined for different types of plant and details are given of sensing holes, manifolds and connecting lines as well as suitable instruments and their calibration. The measurement of steam side pressure drop is also covered, together with a formula to be used for estimating the drop if for any reason it is not practical to measure it.

Measurement of temperature, an equally important parameter, is also covered in some detail, especially the measurement of cooling water outlet temperature including the technique described earlier in this paper.

The section on flow determination includes descriptions of the various techniques for measuring cooling water flowrate. A rough guide is given by listing the techniques in order of preference, but it is stressed that the best technique depends on a knowledge of all the factors relevant to a particular situation.

The determination of condenser heat load, which is another important parameter in the assessment of condenser performance, is covered in some depth, dealing separately with the calculations involved when concurrent test or derived heat rates are used. The heat absorbed by the condenser cooling water method is also covered and tables are given for the density and specific heat capacity of water with salinity ranging from 0 to 4%.

The section on tube cleanliness and air blanketing is of interest in that cleanliness factor is defined as the ratio of the average heat transfer coefficient of the tubes in the condenser to that of new acid cleaned tubes. The "brushed clean" condition is taken to have a cleanliness factor of 0.9. Methods are given for determining the cleanliness factor both on-load and off-load.

Other sections in this part of STC3 deal briefly with the measurement of condensate quality and equipment for data acquisition.

Part 3, Calibration and Presentation of Results, is divided into four sections covering the calculation procedures for both acceptance and routine tests, the

assessment of the accuracy of the test results and the presentation of acceptance test results; certain aspects of the calculation procedures were covered earlier in this paper. Regarding routine tests, the correction procedure is somewhat different in that the acceptance test results are corrected to the conditions on the particular routine test and the resulting calculated condenser pressure is then compared with the actual pressure obtained on the particular routine test.

The section on the assessment of accuracy describes how the basic statistical concepts given in appendix E are applied to the various measurements and calculated figures. Details are also given of the methods to be used for determining the uncertainties in the empirical corrections and the condenser heat load.

Appendices The major part of STC3 consists of six appendices, as follows:

Appendix A: Example of Acceptance Test Results (single pressure condenser). This appendix gives a complete set of results and calculations for a single pressure condenser. Design and specified data are listed, together with a set of test measurements. Detailed step by step calculations show the recommended method of producing the overall comparison with the specified condenser pressure, including the determination of tube cleanliness factor by the on-load method.

Appendix B: gives a virtually identical example to that given in appendix A, but for a multi-pressure condenser rather than for the single pressure condenser covered previously.

Appendix C: gives examples of the assessment of test result accuracies including typical figures for the sensitivity coefficients for the main parameter measurements.

Appendix D: Recommended Instrumentation for Condenser Testing. This appendix lists the various measurements required and details the recommended types of primary instruments, mounting arrangements, interconnections and secondary instrumentation.

Appendix E: Statistical Basis for Assessment of Test Result Accuracy. This appendix describes the basic concepts of systematic and random uncertainties and discusses the application of these methods to the particular case of condenser testing. The treatment of multiple measurements, short term drift and the application of the 'sensitivity coefficients' are given in some detail, together with a glossary of statistical terms.

Appendix F: Laboratory Determination of Tube Cleanliness Factor. This final appendix describes the off-load method of determining the cleanliness factor of condenser tubes, by removing sample tubes from the condenser and measuring their thermal resistance in a laboratory.

CONDENSER MACROFOULING CONTROL METHODS

ISIDRO A. DIAZ-TOUS* AND YUSUF G. MUSSALLI**

Macrofouling is a major cause of condenser failures. This paper examines several macrofouling control methods. Mechanical controls, including heavy-duty trash rakes, modified through-flow screens, alternate screen designs, fine-mesh screens, debris filters, and condenser backwash, are discussed. Other control methods discussed are thermal backwash, anti-fouling coatings, and hydraulics controls.

INTRODUCTION

The Electric Power Research Institute (EPRI) estimates that, for fossil-fired power plants over 600 MW, a 3.8 percent loss in unit availability is directly attributable to poor reliability of condenser systems(1). The direct loss in nuclear power plant availability attributable to condensers is of the same magnitude. A recent EPRI project, RP1689-2, using data from 415 fossil-fueled units, revealed that the major cause of condenser problems was macrofouling (blockage by debris and biogrowth) (2). Operational experience also indicates that condenser failures and performance are directly related to the amount of debris and biogrowth within the cooling water system. Excessive entrapment of debris and biogrowth, as shown in Figure 1, can be detrimental to unit operation in several ways:

1. Debris and biogrowth trapped inside condenser tubes can cause high water velocities, which can lead to tube erosion and corrosion through differential aeration;
2. Debris and biogrowth blockage of tubes results in a reduction in heat transfer rate, resulting in increased condenser back pressure and unit heat rate;
3. Clogging of the tube sheet will eventually lead to excessive head losses in the system, resulting in reduced cooling water flow, higher condenser temperature rise, and, consequently, increased unit heat rate and condenser back pressure;
4. Excessive debris and biogrowth adversely affects the optimum operation of tube cleaning equipment;

*ELECTRIC POWER RESEARCH INSTITUTE, **STONE & WEBSTER ENGINEERING CORPORATION

5. Entrained silt and sand can, due to turbulence in the condenser inlet box, lead to solid particle impingement and/or erosion of tube inlet connections of copper alloys;
6. Decomposition of trapped organic debris can generate compounds which cause stress cracking during outages and other corrosion problems with some tube alloys.

Operational and maintenance costs due to fouling effects can be significant. Plant performance losses from increased condenser backpressure significantly affect operating costs. These costs result from increased fuel consumption and the need for replacement power due to reduced capacity. Figure 2 illustrates the typical base-loaded coal-fired and nuclear units replacement energy costs as a function of backpressure.

Maintenance costs to clean the condensers can also be significant. For units averaging 300 MW, the cost is \$30,000 per year per condenser. Of course the ultimate maintenance cost for a steam surface condenser is the cost of complete retubing, which ranges from \$3,000,000 to \$15,000,000 and causes significant impact on plant maintenance outages(2).

Debris and silt or sand particle problems in the condenser are the result of an inadequate cooling water intake screening system. Biogrowth is usually in the form of barnacles, mussels, oysters, and Asiatic clams which grow and later detach from the walls of the screenwell and intake piping to clog the condenser. Asiatic clams, which grow in fresh water, have recently caused severe blockage problems of cooling water systems in the United States; methods to control them will be discussed.

This paper, which is a synopsis of EPRI project 1689-9, discusses several macrofouling control methods; these methods can be categorized as:

- Mechanical Controls
 - Heavy-duty trash rakes
 - Modified through-flow traveling water screens
 - Alternate screen designs, i.e., center- and dual-flow screens, and drum screens
 - Fine-mesh screens
 - Debris filters
 - Condenser backwash
- Thermal Backwash
- Materials Control
 - Anti-fouling paints
 - Toxic sheeting
- Hydraulic Controls
- Chlorination
 - Although chlorination is recognized as an effective biofouling control method, its use in the United States is restricted because of stringent environmental regulation. It will not be discussed in this paper.

MECHANICAL CONTROLS

Effective intake screening will help minimize some of the macrofouling in the condenser(3). Modifications to the conventional trash rakes and through-flow screens (which are used extensively in the United States) and the use of dual- or center-flow screens and drum screens (which are of European design), fine-mesh screens, debris filters, and condenser backwash can minimize debris carry-over and carry-through the screens and help prevent clogging of the condenser.

Heavy Duty Trash Rakes

For light debris loading, conventional vertical or inclined racks with bar spacing of 50 to 75 mm (2 to 3 in.) are used in the United States to protect the traveling screens from large debris. Cable-operated rakes pick the debris from the racks and dump it into a hopper at the deck.

For heavy debris loading such as grass, seaweed, trees, and so on, several designs have been used. One design is to install a heavy-duty clamshell-shaped rake, as shown in Figure 3. Another is to install traveling bar racks, similar to traveling screens, with bar spacings of 10 to 25 mm (1/2 to 1 in.) between the coarse spaced racks and the screens. This design has been used successfully at a power plant in Southern California. In Europe, heavy-duty traveling rakes with protruding teeth are used to pick the debris from the racks for dumping into a hopper at the deck. Recently an hydraulically operated rake of a clamshell design, as shown in Figure 4, has been used successfully to rake seaweed at a power plant in South Carolina. In Japan, a bar screen, with traveling plastic bars, has been used at power plants to screen jellyfish and seaweed. In the United States, this design has been used, so far, to filter screen wash refuse water from weeds and filamentous algae.

Modifications to Through-Flow Traveling Water Screens

Conventional vertical through-flow traveling water screens, which are used at most power plant intakes in the United States, commonly allow some debris to carry over or through the mesh into the cooling water system. There are several tried and tested design changes which can be applied to solve these problems. Screen modifications (as shown in Figure 5) can be retrofitted to the screens after installation or can be made in the factory before shipment to solve various screening problems as follows.

Debris Carry-over Problems Debris carry-over problems can be mitigated using a dual spray header, a debris deflector, or nozzle header strainers and brush.

With through-flow screens, the use of dual high pressure spray headers, as shown in Figure 5, can help remove firmly lodged debris.

The addition of a debris deflector, located near the downstream face of a through-flow screen, can reduce the gap between the screen face and the concrete deck, as shown in Figure 5.

One of the major problems that can lead to debris carry-over is

clogging of spray nozzles. The loss of only a few nozzles can create voids in the spray curtain large enough to allow carry-over of entangled debris. Frequent inspection of spray nozzles and filtering of spray water is recommended. A nozzle header brush could be installed on a long rod located inside the spray header and connected to a handwheel. The handwheel allows the brushes to be manually rotated for internal cleaning of the spray nozzles, thus preventing clogging.

Debris Carry-through Problems. Carry-through problems can be alleviated by changing the screen mesh size or configuration or by using sealing strips.

One cause of excessive debris carry-over can be the severe entanglement of string-like seaweed or jellyfish in the screen mesh. To reduce the potential entanglement and carry-through of debris, a change in mesh size from the conventional 3/8-inch (9.5 mm) is sometimes recommended. A 3/16-inch (5 mm) mesh size has been used successfully in several power stations on the West Coast. Other mesh configurations are also being investigated at this time. Oblong smooth top mesh 1/8-inch wide (3 mm) by 1-inch long (25 mm) and lightweight wedge-wire screens, both shown in Figure 5, may have potential in reducing entanglement and carry-through. The cost per square meter ranges from \$20.00 (\$2/ft²) for the 3/16-inch, to \$50.00 (\$5/ft²) for the oblong smooth top, to \$250.00 (\$25/ft²) for the wedge-wire.

Redwood sealing strips can be used to reduce the normal clearance between basket and plates and the main screen frame, thus further reducing the quantity of debris that can pass through.

Screen Blockage Problems. Problems associated with screen blockage can be alleviated by installing the debris lips, by increasing screen travel speed, or by using a boot loading leg.

In cases of heavy seaweed and jellyfish, the installation of debris lips at the midsection of each screen basket is recommended to increase the lifting capacity of the traveling screen. Toothed lips could also be installed to lift leaves, moss, kelp, and grass.

For light debris loading, screen travel speeds of 2.5 and 10 fpm (0.01 and 0.05 m/s) are usually used. For heavy debris loading, speeds of 10 and 20 fpm (0.05 and 0.10 m/s) are recommended. The faster speeds increase the debris lifting capacity of the screen. However, faster speeds require motors with more power.

A boot loading leg consists of a baffle plate welded to the front side of the boot section. It helps load debris onto basket lips, but it may cause sand to settle out in front of the screen or, at normal velocities, cause it to be carried beyond the screen boot section.

Continuous Operation Problems. Depending on the type and loading of debris, it may be desirable to operate the screens on a frequent or even continuous basis, during certain times of the year. Frequent or continuous screen operation can result in substantial wear of the flex joints of the chain, the headshaft bearings, and the footshaft bushings. To remedy these types of wear, the rollers, pins, and bushings should be made of tool-quality alloy. The headshaft bearing should be of the anti-friction roller type, and tool-quality Stoddy bushings and liners on the footshaft should be used to resist wear from continuous operation.

Alternate Screen Designs

Center-Flow Traveling Water Screens. The center flow screen (single entry, double exit) is a European design that is used in Germany. This screen (Figure 6) is set parallel to the approach flow with water entering a central entrance port and exiting through both the ascending and descending screen faces. The screen has an overhead spray system which washes debris into an internal trash trough. Since all water is screened internally, there is no possibility of debris carry-over, i.e., debris cannot enter the cooling water system without passing through the screen mesh. For a given screen width, a larger screening area is available than with a through-flow screen. This is because both the ascending and descending screening faces are used for debris removal.

In the United States, two power plants have recently used center-flow screens. The most interesting installation uses 1-mm mesh and has been operating successfully at a power plant intake for several years to screen out seaweed on the Gulf of Mexico in Corpus Christi, Texas. Two disadvantages of the screen in relation to fish protection are:

1. Dead-end trap for fish between the screen faces (Figure 6).
2. High entrance port velocities (in excess of 0.3 m/s (1 fps)) that could result in fish entrapment inside the screen.

These disadvantages have limited the use of this type of screen in the United States.

There are other design considerations which should be evaluated before selecting this type of screening device. Water exiting the screen faces discharges from the side ports as jets. The nonuniform flow patterns created in the pumpwell could affect pump performance. Baffles could be installed downstream of the screens to streamline the flow, or the pumps could be installed farther downstream from the screens. Due to the angle at which the approach flow streamlines enter the screen, the velocity distribution across the screen face is uneven, possibly affecting screening efficiency.

Dual Flow Traveling Water Screens Another screening arrangement of European design is the dual-flow (double-entry, single-exit) screen. The dual-flow screen is basically a through-flow screen placed parallel to the flow streamlines. Debris carry-over is virtually eliminated because debris must pass through the mesh in order to pass the screen. A variation of this screen, known as the no-well arrangement, has the screen exit connected directly to the pump suction, as shown in Figure 7. This eliminates the need for a typical screenwell. Screens of the no-well design are presently being operated successfully at power plants in Florida and Georgia. Dual-flow screens, in general, are subject to the same advantages and disadvantages, hydraulically and operationally, as the center-flow type. The no-well arrangement, however, has environmental advantages since it acts as a passive screen: fish can swim freely around the screen without being entrapped.

Rotating Drum Screen This type of screen, which is shown in Figure 8, is not used in the United States but has been used widely in Europe. Engineering advantages of these screens include simplicity, in that there are fewer moving parts than in the revolving through, center, or dual flow screens and ease of maintenance, in that at low water the axis is

dry and can be easily serviced. In addition, debris carry-over into the clean water side cannot occur. One disadvantage is that the size of the structure required to mount such a screen is substantially larger than would be required for traveling screens of similar capacity. Diameters up to 20 m (65 ft) have been installed, and diameters in the 12 and 15 m (40 and 50 ft) range are common.

Because of the large size of the supporting structure and because there is no advantage in fish protection over those screens already in use in the United States, utilities in the U.S. have not considered this type of screen for U.S. power plant intake applications.

In selecting which type of traveling screen to use in the United States (through-, center-, or dual-flow, or rotating drum), the environmental impact on aquatic organisms must be evaluated(4).

Fine-Mesh Screens

Recently, attention has been focused on the use of fine-mesh screening (0.5-mm mesh openings) for the collection and safe removal of small organisms(5). Fine-mesh screening can also remove stringy debris, jellyfish, etc., and protect the condenser.

Fine-mesh screening of cooling systems with mesh openings ranging from 1 to 3 mm (0.04 to 0.12 in.) has been used extensively at installations in Europe and the Middle East. In 1980, a dual-flow, fine-mesh screen was tested in Florida to evaluate the survival of organisms and clogging problems. The facility used a 600 mm (2 ft) wide screen installed on a platform in an intake channel. The screening medium was 0.5-mm (0.02 in.) polyester mesh with 49 percent open area. The screen was completely sealed between the baskets and between the baskets and guides, and operated continuously at a speed of 7 fpm (0.04 m/s), at a differential of 4 inches (100 mm) at a speed of 14 fpm (0.07 m/s), and at 6 inches (150 mm) at 28 fpm (0.14 m/s). The velocities at the face of the screen ranged from 0.25 to 1.5 fps (0.08 to 0.45 m/s). The debris spray wash pressure was 40 to 60 psi.(280 to 410 kPa)(6). The fine-mesh screen operated successfully with no major clogging problems. The jellyfish and detritus washed off easily. Horeseshoe crabs, which usually become entangled on 3/8-inch (9.5 mm) mesh could not do so on the 0.5-mm mesh.

The encouraging results obtained from the fine-mesh test facility led to intake backfit designs incorporating fine mesh screening into a nuclear power plant on the upper Mississippi River and into a coal-fired power plant in Florida.

Frequent operation of fine-mesh screen can result in substantial wear requiring upgrading of the bearing, bushings, and chains, and provisions for slack tensioning. To reduce the clogging potential, traveling screens could be fitted with easily replaceable screen baskets of different mesh size. In this way, finer mesh could be used only during periods of heavy occurrence of seaweed, jellyfish, etc. To protect the fine mesh from puncture by sticks and from overloading by heavy debris, the use of trash racks with spacing as small as 40 mm (1.5 in.) is recommended. More frequent raking of the racks would also be required.

Debris Filters

Another means of supplementing an effective screening system is the installation of an in-line strainer between the pump and the condenser inlet water box. This technology is European and has recently begun to be used in the United States. Currently, there are large strainers in six U.S. power plant cooling water pipelines. For large diameter pipe (up to 2.8 m [110 in.] and capacity of 15,000 l/s [245,000 gpm]), a debris filter (as manufactured by Taprogge), a perforated stainless steel screen (mesh size ranges from 1/4-inch to 3/8-inch [6.5 to 9.5 mm]) concentrically aligned within a rubber-lined steel casing, can be used. Cooling water enters the screen radially and passes through the cylindrical screen, leaving the filtered debris on the outside. The screen can be cleaned "on-line" by fully opening the normally closed debris bypass valve and throttling the large diameter butterfly valve located in the cooling water inlet piping. Since the valve is angled, turbulence lifts the debris from the screen surface, flushing it toward the discharge outlet. The normal cleaning time is from 5 to 15 minutes with only a small portion of the total cooling water used for flushing. Approximately 3 to 10 percent of the main flow is bypassed. Similar devices are available for small diameter pipes (as small as 300 mm [12 in.] and with a capacity of 12.6 l/s [200 gpm]) as well. The filters can be installed inside the turbine building, at the pump house, or in the yard between the pump and the condenser (Figure 9), employing a variety of mounting positions.

Filters will result in two disadvantages. The first is an increase in system head loss: a 450 mm (1.5 ft) increase with the filters clean and a 600 mm (2 ft) increase with the filters 30 percent fouled associated with a 3 m/s (9 fps) water velocity. When filters are retrofitted to an existing system, the main circulating water pumps will require additional horsepower per pump, thus increasing station pumping costs. The second disadvantage incurred after retrofitting involves a decrease in unit efficiency caused by a reduction in cooling water flow associated with higher system losses.

The ability of these filters to remove entrained debris and biogrowth (such as mussels, barnacles, and Asiatic clams) has been demonstrated at several power plant locations including Southern California, North Carolina (Figure 9), Ohio, and Connecticut. Debris filters have also been backfitted in many cooling water systems. When no chlorination was available, the installation of the filter usually improved condenser performance when used in conjunction with a tube cleaning system. An improvement in the tube cleanliness factor can more than compensate for a reduction in flow and offset the associated production penalties.

Condenser Backwash

Another means to supplement an effective screening system and to clean debris accumulation in the condenser water boxes and on the tube sheets is to backwash the condenser by periodically reversing the direction of flow of the circulating water. To allow condenser backwash, additional pipelines and valves must be provided around the condensers and the various valve positions in the circulating water lines and at the condenser must be controlled. Figure 10, which shows three examples of circulating water pipeline arrangements and their respective procedures of backwash, represents the present state of technology in the U.S.A.

THERMAL BACKWASH

Marine organisms, such as barnacles, mussels, and oysters, can be prevented from becoming a significant macrofouling problem if the temperature of the cooling water is raised sufficiently above ambient. Thermal control methodology should be based on the thermal tolerances and life stage development characteristics of the particular fouling organisms. Biofouling by mussels, for example, most likely will initiate when ambient water temperature exceeds 13°C (55°F).

The effectiveness of thermal backwash is largely a function of applying the appropriate temperature to the fouling organisms for a period of time long enough to ensure mortality (Figure 11). For example, the lethal temperature for mussels is 40°C (105°F) applied for 2 hours every 6 weeks. To achieve this temperature, the water is pumped through the condenser twice and then back to the intake pipes and/or tunnels or to the discharge tunnels (Figure 12).

Thermal backwashing should be frequent enough to ensure that marine organisms are killed while in the juvenile stage(7). By treating only juveniles, the size of the organisms will be small enough to pass through the condensers without blocking the tubes. This control method has been used successfully at several plants on the California coast and on Long Island Sound in New York.

MATERIALS CONTROL

Some utilities in Europe (Electricite De France, for example) use anti-fouling paint on power plant seawater intake structures to control biogrowth. Similarly, a few utilities in the United States use cuprous oxide based paints and have to repaint the structures every one or two years.

EPRI is currently evaluating several anti-fouling paints for power plant use under project RP1689-9. This nationwide effort is the most comprehensive power plant oriented evaluation of anti-fouling paints in the U.S.A. Each of these paints is formulated with an organotin toxicant. The organotin-based materials were chosen for their advantages over the more conventional copper oxide materials.

Due to a higher toxic efficiency, the amount of organotin toxicants needed to attain full algae and barnacle control is approximately one-tenth to one-twentieth of the amount of copper oxide required(8). Unlike the copper oxide paints, organotin formulations provide a constant toxicant delivery over long periods of time (5 to 6 years service life). The periodic reactivation or scrubbing associated with the copper oxide paints is not required for the organotins. Once released to the sea water, the organotins are converted to non-toxic tin compounds through hydrolysis, photolysis, and microbial degradation(9).

Each of the organotin-based materials being evaluated can be applied to concrete and steel surfaces of the intake systems components, such as screens, screenbay walls, and intake piping. Most of the materials have been registered with the U.S. Environmental Protection Agency for use on ships but would require additional approval for large-scale power plant applications.

A threefold test program has been developed under the sponsorship of EPRI to evaluate the feasibility of adapting the organotin anti-fouling

coatings to control power plant condenser macrofouling. The objectives of the test program are to:

1. Evaluate the anti-fouling/mechanical performance of selected coating systems of various power plants,
2. Evaluate the corrosion protection performance of those coating systems, and
3. Evaluate the feasibility of applying these coating systems to existing concrete surfaces within a power plant cooling water intake structure.

The macrofouling problems experienced by power plants differ considerably from one plant to another. Among the major variables causing such variety are climatic conditions, cooling water source, and predominant marine organisms present. The program consists of testing the coatings at selected power generating stations located throughout the United States. The test site locations include approximately three on the West Coast, six on the Gulf of Mexico, and ten on the East Coast, including four on Long Island Sound. The anti-fouling coatings selected for evaluation are the following:

1. Coal Tar Epoxy (Tributyltin Acetate-TETA)
2. Chlorinated Rubber (Tributyltin Fluoride-TBTF)
3. Polysiloxane-Tributyltin Polymer
4. Polysiloxane-Tributyltin Polymer with a co-toxin of cuprous oxide
5. Acrylate-Tributyltin Polymer
6. Acrylic-Tributyltin Polymer with a co-toxin of cuprous oxide

The anti-fouling coatings have been applied to concrete and steel test panels. Additionally, the coatings have been applied as test patches to existing concrete (Figure 13) and steel surfaces within power plant intake structures. Testing started in the spring of 1983. The performance of each coating will be evaluated over a three year period. Annual reports will be prepared to keep the utility industry informed of the test results.

In addition to the anti-fouling coatings, toxic sheeting materials (such as B. F. Goodrich NOFOUL cured sheets) are also being investigated by some utilities for power plant applications.

HYDRAULIC CONTROLS

Fouling organisms are unable to settle out and attach to conduit surfaces when the ambient water velocity exceeds certain minimum values. Conduit design should avoid low flow or stagnant areas upstream of the condensers.

CONTROL OF ASIATIC CLAMS

Asiatic clams are spreading rapidly throughout the U.S.A., causing flow blockage and reliability problems in many cooling systems. Conventional

freshwater biofouling control methods generally are inadequate for control of Asiatic clams. Methods for the control of Asiatic clams include continuous chlorination, heat treatment (45°C (110°F) for 30 minutes), straining clam larvae through 1-mm (1/23-inch) mesh screen, in-line strainers for the adult clams (Figure 9), and chemicals (sodium metabisulfite, $\text{Na}_2\text{S}_2\text{O}_5$, and hydrogen sulfide gas, H_2S) to deplete the oxygen in the bottom of the screenwell during scheduled outages(10).

CONCLUSION

No one control method is the panacea for all biofouling and macrofouling problems; therefore, combinations of alternative methods will be required. The selection of the alternative methods should be based on a cost-benefit analysis. Integration of the proper macrofouling control methods into the design of the cooling system is essential to minimize condenser problems with minimum impact on the environment.

REFERENCES

1. Anson, D., 1977, "Availability of Fossil-Fired Steam Power Plants", Electric Power Research Institute, Report No. EPRI FP-422-SR.
2. Bell, R. J., Impagliazzo, A.M., and Mussalli, Y.G., 1982, "Failure Cause Analysis-Condenser and Associated Systems", Volumes 1 and 2. Report prepared by Stone & Webster Engineering Corporation for the Electric Power Research Institute, Project RP-1689-2, Report No.: EPRI-CS-2378.
3. Torhin, R.N. and Mussalli, Y.G., 1979, "Cost Effectiveness of Alternate Condenser Biofouling Control Methods", Condenser Biofouling Control Symposium, sponsored by Electric Power Research Institute, Atlanta, Georgia, EPRI CS-1450, Ann Arbor Science Publishers, Inc., pp. 497-517.
4. American Society of Civil Engineers, 1982, Design of Water Intake Structures for Fish Protection", prepared by the Task Committee on Fish Handling Capability of Intake Structures, ISBN 0-87262-291-6.
5. Mussalli, Y.G., Taft, E.P., and Hofmann, P., 1978, "Biological and Engineering Considerations in the Fine Screening of Small Organisms", Proceedings of Workshop on Larval Exclusion Systems for Power Plant Cooling Water Intakes, San Diego, California, Argonne National Laboratories, NUREG/CP-002; ANL/ES-66, pp. 107-123.
6. Mussalli, Y.G., Williams, J., and Hockman, J., 1981, "Engineering Evaluation of a Dual-Flow Fine-Mesh Traveling Screen", Proceedings of Workshop of Advanced Intake Technology, San Diego, California.

Edited by P. Dorn and J.J. Johnson, sponsored by Electric Power Research Institute, Southern California Edison, et. al. pp. 177-192.
7. Graham, John W., Stock, Jay N., and Benson, Peter H., 1977, Further Studies on the Use of Heat Treatment to Control Biofouling in Sea-water Cooling Systems", IEEE Oceans pp. 23A 1-23A-5.
8. Gitlitz, M., 1980, Recent Developments in Marine Antifoulants". Presented at the 20th Annual Marine Offshore and Inland Waterways Conference, New Orleans, Louisiana.
9. Englehart, J.E. and Sheldon, A.W., 1975, "Organotin Antifoulants: Their Toxicology and Environmental Impact. Guidelines for Safe Handling in Chemical and Paint Manufacturing and Paint Removal". Presented at the 5th Annual Marine Coatings Conference, Point Clear, Alabama, February 7, 1975.
10. Smithson, J.A., 1981, "Control and Treatment of Asiatic Clams in Power Plant Intakes". Proceedings of the 43rd Annual Meeting of the American Power Conference, Vol. 43, pp. 1146-1151.



Figure 1 Macrofouling

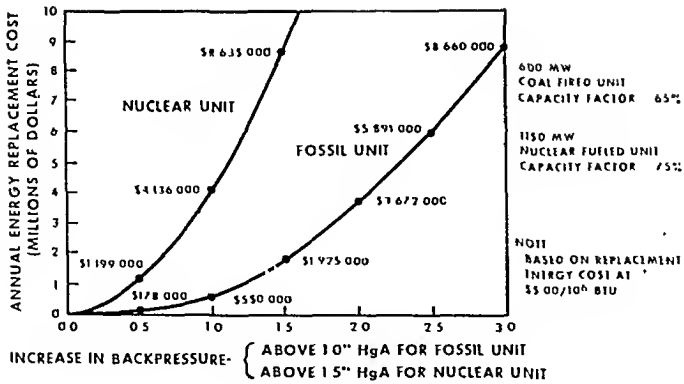


Figure 2 Annual replacement energy cost vs. increase in condenser backpressure

REFERENCES

1. Anson, D., 1977, "Availability of Fossil-Fired Steam Power Plants", Electric Power Research Institute, Report No. EPRI FP-422-SR.
 2. Bell, R. J., Impagliazzo, A.M., and Mussalli, Y.G., 1982, "Failure Cause Analysis-Condenser and Associated Systems", Volumes 1 and 2. Report prepared by Stone & Webster Engineering Corporation for the Electric Power Research Institute, Project RP-1689-2, Report No.: EPRI-CS-2378.
 3. Torbin, R.N. and Mussalli, Y.G., 1979, "Cost Effectiveness of Alternate Condenser Biofouling Control Methods", Condenser Biofouling Control Symposium, sponsored by Electric Power Research Institute, Atlanta, Georgia, EPRI CS-1450, Ann Arbor Science Publishers, Inc., pp. 497-517.
 4. American Society of Civil Engineers, 1982, Design of Water Intake Structures for Fish Protection", prepared by the Task Committee on Fish Handling Capability of Intake Structures, ISBN 0-87262-291-6.
 5. Mussalli, Y.G., Taft, E.P., and Hofmann, P., 1978, "Biological and Engineering Considerations in the Fine Screening of Small Organisms", Proceedings of Workshop on Larval Exclusion Systems for Power Plant Cooling Water Intakes, San Diego, California, Argonne National Laboratories, WUREG/CP-002; ANL/ES-66, pp. 107-123.
 6. Mussalli, Y.G., Williams, J., and Hockman, J., 1981, "Engineering Evaluation of a Dual-Flow Fine-Mesh Traveling Screen", Proceedings of Workshop of Advanced Intake Technology, San Diego, California.
- Edited by P. Dorn and J.J. Johnson, sponsored by Electric Power Research Institute, Southern California Edison, et. al. pp. 177-192.
7. Graham, John W., Stock, Jay N., and Benson, Peter H., 1977, Further Studies on the Use of Heat Treatment to Control Biofouling in Sea-water Cooling Systems", IEEE Oceans pp. 23A 1-23A-5.



Figure 1 Macrofouling

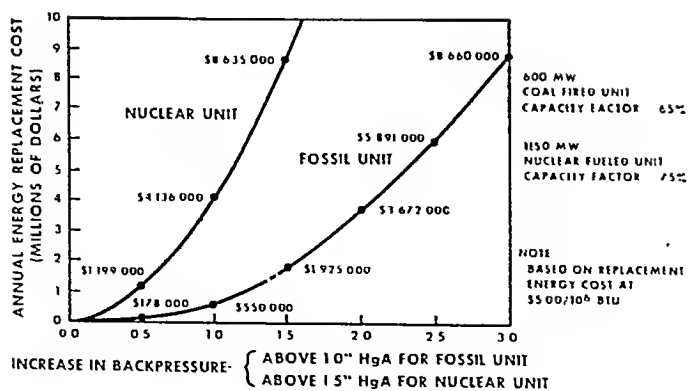


Figure 2 Annual replacement energy cost vs. increase in condenser backpressure

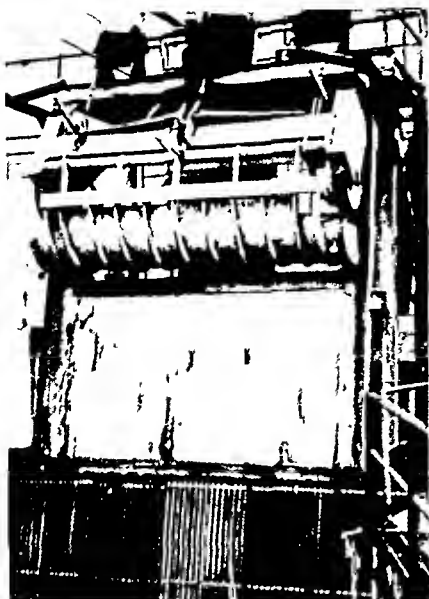


Figure 3 Clam-shell shaped rake

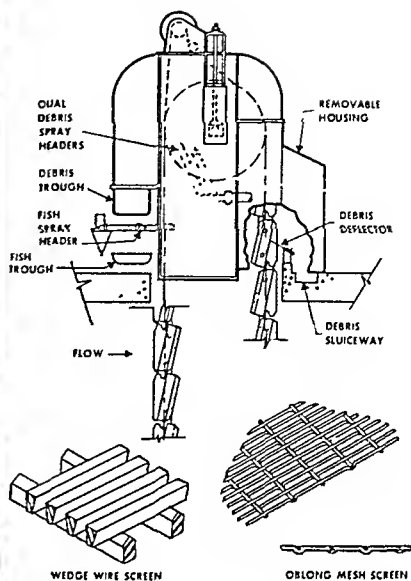


Figure 5 Through-flow traveling screen modifications

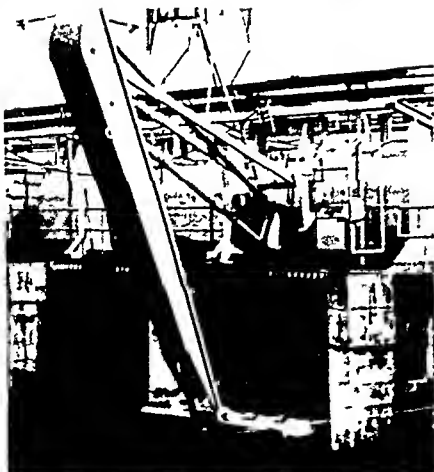
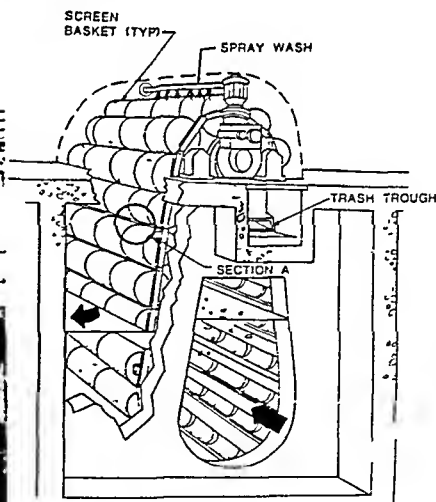


Figure 4 Hydraulic-operated rake



COURTESY OF PASSAVANT CORP.

Figure 6 Center-flow traveling screen

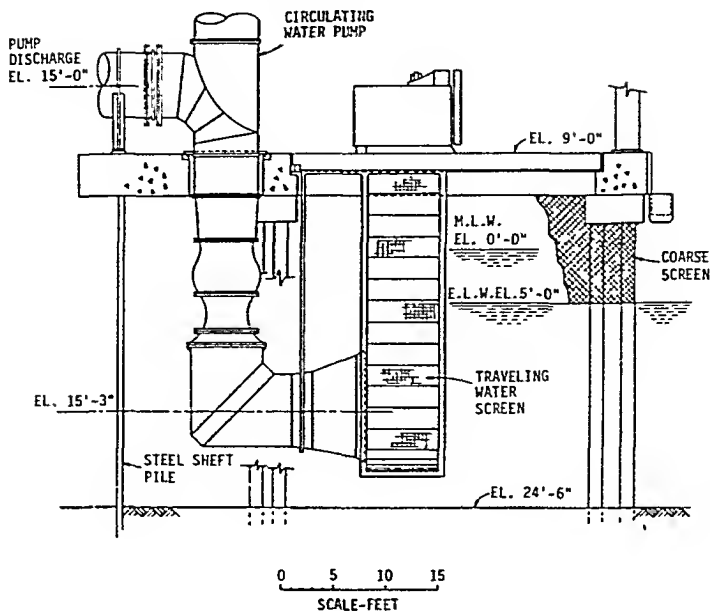


Figure 7 Dual-flow screenwell no-well arrangement

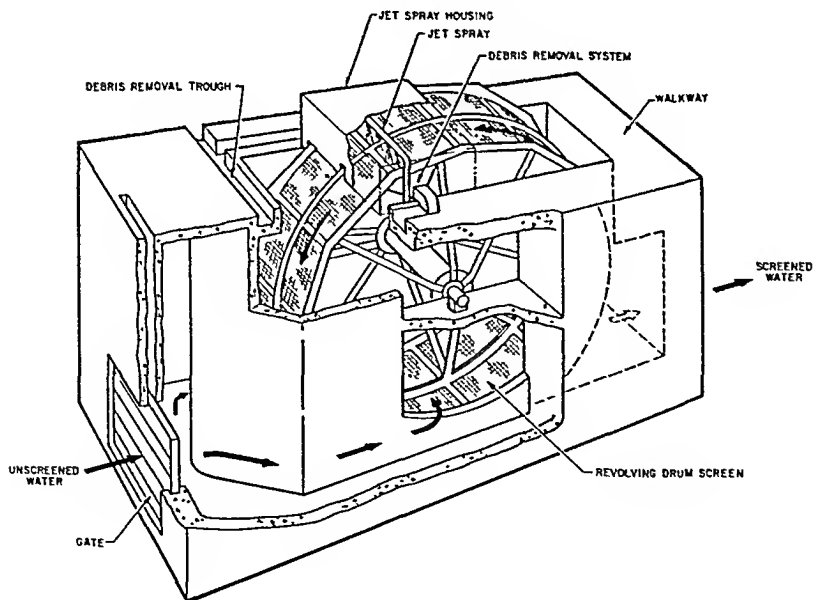


Figure 8 Rotating drum screen



Figure 9 Debris filter for Asiatic clams

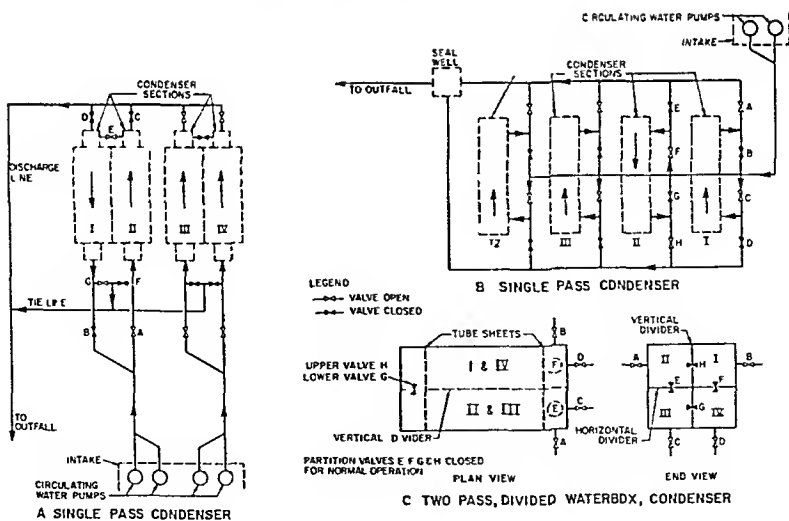


Figure 10 Condenser backwash arrangements

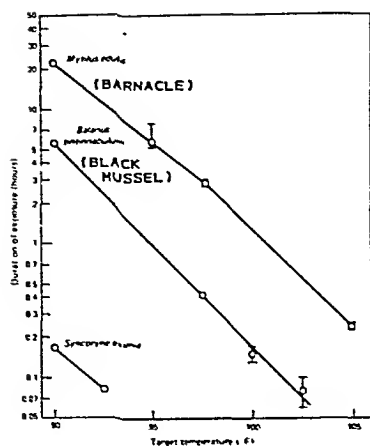


Figure 11 Temperature vs. exposure duration for heat treatment

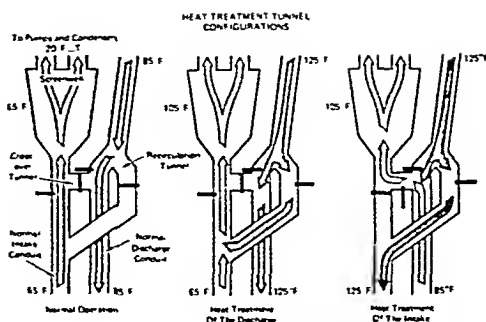


Figure 12 Circulating water system during the heat treatment process



Figure 13 Anti-fouling paint test patch in a concrete pipeline

SEAWATER BIOFOULING COUNTERMEASURES FOR SPIRALLY ENHANCED CONDENSER TUBES

R.W.Kornbau*, C.C.Richard**, and R.O.Lewis***

The effect of condenser tube surface enhancement on biofilm accumulation and heat transfer was evaluated for stainless steel (AL-6X) and pure titanium (CP-2) tube material in natural seawater. Both smooth and spirally grooved enhanced tubes were installed in electrical heat transfer monitoring devices which provided real time digital measurements of biofilm resistance under simulated condenser conditions. Biofouling rates were determined for equal pressure drop and equal velocity conditions between the smooth and enhanced tubes. A series of tests for three seawater cooling velocities demonstrated the effectiveness of fresh-water lay-up, high-velocity flushing, and chlorination cleaning.

INTRODUCTION

A multi-phase test program was initiated to identify the rate and extent of biofouling accumulation on condenser tubes with spiral grooves for internal heat transfer enhancement (manufactured by Wolverine Division of UOP, Inc.). A test plan was developed to compare biofilm accumulation on both smooth and enhanced condenser tubes as a function of seawater velocity and cleaning technique. This was accomplished through the use of heat transfer monitoring equipment at the LaQue Center for Corrosion Technology, (LaQue), Wrightsville, North Carolina, USA.

The Wolverine "Korodense" enhanced tube heat transfer monitor (HTM) was a one inch diameter AL-6X enhanced tube. For comparison of tube material and geometry, one inch diameter AL-6X and titanium smooth tube HTM's were installed in parallel with the enhanced tube AL-6X HTM. Heat transfer data from the HTM's provide an instantaneous measurement of biofilm thermal resistance as a function of surface enhancement, time of exposure, seawater velocity, tube cleaning technique and environmental variables.

TEST PROCEDURE

Apparatus

The Biofouling Countermeasures Laboratory (BCL) at LaQue was established to conduct biofouling control experiments. Once-through ambient temperature

* Program Technical Manager, David Taylor Naval Ship Research and Development Center, Bethesda, Maryland.

** Associate Professor, U. S. Naval Academy, Annapolis, Maryland 21402, USA

***Corrosion Scientist, LaQue Ctr for Corrosion Technology, Inc., Wrightsville Beach, North Carolina 28480, USA

seawater is supplied to the BLC test system via a titanium pump and a non-metallic seawater distribution system. Interruptions in seawater flow due to mechanical failure or electrical power outage are minimized by use of an emergency power generator in conjunction with an auxiliary non-metallic pump. The seawater distribution system and non-metallic test loop piping have been designed to maintain a seawater flow rate in excess of 4 feet per second (fps) to minimize the attachment and growth of macrofouling organisms.

A computer data acquisition system controls the operation of all automatic cleaning operations and acquires and analyzes heat transfer data from up to 18 test loops simultaneously. Real time data acquisition and analysis permits evaluation of cleaning method effectiveness on an instantaneous basis. The frequency and duration of cleaning can thus be easily optimized for any given set of operation conditions. Prior cleaning procedures are given in Appendix 1.

A modified version (Gavin et al (1)) of the Carnegie-Mellon University heat transfer monitor (Fetkovich et al (2)) was employed that permits extremely sensitive measurement of heat transfer resistance of fouling films that form on tube surfaces in flowing seawater. The HTM consists of a one inch tube with copper blocks attached to the outside. The internal assembly of an HTM is installed in an insulated PVC housing during operation. With seawater flowing through the tube, one set of blocks is heated two degrees Centigrade with respect to a reference block at ambient seawater temperature. By switching off the heat and monitoring the thermal decay of the heated blocks, a cooling curve is obtained. An exponential fit of the cooling curve data yields a time constant directly proportional to the fouling resistance. The relatively small temperature differential required for this technique permits instantaneous, frequent measurement of fouling resistance without affecting the continued growth of the fouling film.

Heat Transfer Tests

The test program employed three previously described HTM's. The final test matrix shown in Table 1 describes a set of experiments intended to identify the effect of seawater velocity, tube surface geometry and cleaning technique on biofouling rate. Four test periods were identified during which low, intermediate and high seawater velocities were evaluated on the one inch diameter HTM's. For the initial test phases I and II, the operating seawater velocity was selected to produce an equal pressure drop (average wall shear stress) for both smooth and enhanced one inch HTM tubes. For test phases III and IV, operating velocities in the one inch smooth or enhanced HTM tubes were selected to produce an average wall shear stress equal to the value for a 5/8 inch diameter smooth or enhanced tube operated at a velocity of 5 fps (10 fps for high velocity flush cleaning).

Results were evaluated continuously during the course of the test program. Changes in the test plan were authorized to make the most effective use of the high rate of fouling at LaQue during the summer months. Between each phase of the program the AL-6X and titanium HTM tubes were cleaned and reconditioned employing the procedure identified in Appendix I.

RESULTS

Heat Transfer Results

Heat transfer resistance data in the following figures are expressed in terms of the calculated fouling factor, R_f , in units of $\text{hr ft}^2 \text{ } ^\circ\text{F/Btu}$ versus calendar date. Average daily seawater temperature versus date is included in

Figure 1 for reference; seawater temperature has been shown in previous Ocean Thermal Energy Conversion (OTEC) studies to be the most significant environmental parameter affecting biofouling at LaQue.

Phase I. Heat transfer data for the three HTM's operated at the lowest seawater velocity are shown in Figures 2-4. Figure 2 shows data for all three units superimposed; fouling factor data are compared for both AL-6X HTM's in Figure 3 and for both smooth tube HTM's in Figure 4.

The fouling factor exceeded 12.0×10^{-4} on all three units by day 17, which is indicative of relatively thick biofilms. Between day 17 and 25, several large fluctuations occurred in the heat transfer data, somewhat more dramatically on the enhanced tube HTM than the smooth tube HTM's, that could be attributed to sloughing of the biofilm layer.

Phase II. Heat transfer data acquired from the three HTM's exposed to the intermediate velocity during Phase II are shown in Figure 5.

Excellent agreement of fouling rate was observed for the two smooth tube HTM's operated at 6.8 fps. The fouling factor exceeded 6.0×10^{-4} in approximately 20 days on both units. The Korodense unit, operated at 5.6 fps, fouled at a slightly higher rate than the smooth tube HTM's. By day 20, R_f for the Korodense HTM had increased to approximately 8.0×10^{-4} . On day 22, however, a sudden decrease in R_f from 9.0×10^{-4} to 3.2×10^{-4} was observed, indicative of sloughing of the biofilm. This result was the basis for the subsequent evaluation in Phase III of significant velocity increases as a method for biofouling control.

Phase III. High velocity seawater was evaluated as a possible biofouling control method in Phase III. The operating seawater velocities in the one inch diameter smooth or enhanced HTM's were selected to give an average wall shear stress equal to the value for an equivalent 5/8 inch smooth or enhanced tube at a velocity of 5 fps (10 fps for high velocity flush cleaning). Upon R_f reaching 6.0×10^{-4} on each unit, the flow rate was increased to twice the normal rate for various time intervals. Between each interval, R_f was measured to determine the relative effectiveness of each successive high velocity cleaning cycle.

Heat transfer data for all three test units are shown combined in Figure 6 and individually in Figures 7-9. In Figure 6, note that R_f increased at approximately the same rate for all three HTM's through day 15, even though the enhanced unit was operated at 6.0 fps compared to 5.4 fps for the smooth tube units. Thereafter, high velocity cleaning cycles were performed on the individual HTM's as the measured R_f reached 6.0×10^{-4} .

High velocity cleaning was conducted for successive time intervals of 5, 10 and 60 minutes initially; cleaning cycles performed after October 1, were for 5 and 60 minute intervals. This is indicated in Figures 7-9 by three open circle data points representing the initial cleaning cycles and two open circle data points representing the 5 and 60 minute cycles.

The combined results in Figure 6 suggest generally that high velocity cleaning cycles become progressively less effective on both smooth and enhanced tube surfaces. The individual test unit data in Figures 7-9 show this even more specifically. The effectiveness of the initial 5 minute cleaning cycle on all three HTM's diminished with repeated cleaning, as well as the

minimum R_f achievable with cumulative cleaning intervals. Phase III was terminated when R_f measured on the enhanced HTM could not be reduced below 5.3×10^{-4} after 65 minutes total cleaning.

A similar phenomenon has been observed in previous OTEC biofouling programs at both coastal and open ocean test sites. Repetitive cleaning methods for titanium that do not completely remove the biofilm result in retention of a microbiological "conditioning" film on the tube surface. This film, consisting primarily of microbiological exopolymers, enhances the rate of biofouling during subsequent cleaning cycles and becomes increasingly more resistant to removal(4).

Open Ocean Titanium Fouling Data. Open ocean biofouling studies off the coast of Puerto Rico (Argonne National Laboratory Report (3)) were conducted from February 1980, to March 1981, by the Center for Energy and Environmental Research (CEER). Seawater, typically 26-28°C year round, was pumped through titanium tubed HTM's at a nominal flow rate of 6.0 fps. The fouling factor increased to approximately 4.0×10^{-4} in 80 days, or approximately 0.05×10^{-5} per day as shown in Figure 10. This compares to fouling rates on smooth titanium tubes at LaQue during the summer months of 0.35 to 0.40×10^{-4} R_f units per day.

On day 80 in the Puerto Rico test, an inadvertent increase in seawater velocity resulted in removal of most of the biofilm. Flow rate increases from 6.0 fps to 12.0 fps for 30 minutes duration were performed routinely thereafter to evaluate high velocity as a cleaning technique. Open circles in Figure 10 represent R_f measured after high velocity cleaning. Upon completion of high velocity cleaning, the HTM tubes were manually brushed to remove remaining biofilm and return R_f as close as possible to zero. These data confirm the present Phase III results which show that high velocity cleaning becomes progressively less effective with repeated cleaning cycles.

Phase IV. An alternate approach to biofouling control for condensers required a fresh water lay-up for 72 hours upon R_f reaching 6.0×10^{-4} on all three HTM's. This was followed immediately by a return to normal seawater velocity and the addition of 5.0 ppm chlorine continuously for 48 hours. This procedure was performed twice during Phase IV to compare reproducibility of results.

Heat transfer resistance data for this final series of tests are shown in Figure 11. The R_f data shown with open symbols represent measurements made before, during, or after the fresh water lay-up/chlorine procedure. Data recorded as solid, dashed, or dotted lines represent daily R_f measurements in the interim between cleaning treatments.

The first cleaning cycle was performed on October 7-12. Immediately following the chlorine treatment, R_f measurements indicated a reduction in heat transfer resistance from approximately 6.0×10^{-4} to less than 0.50×10^{-4} on all three HTM's. A high velocity cleaning cycle at twice the normal seawater velocity following the chlorine treatment did not result in a further reduction of R_f .

Normal seawater flow was resumed on all three HTM's to demonstrate the effect of the fresh water lay-up/chlorine treatment on subsequent fouling. Approximately 25 days continuous seawater exposure was required for R_f to increase to 6.0×10^{-4} on all three units. This rate of fouling is typical for new, clean HTM's exposed to warm seawater.

The lay-up procedure was repeated on November 6-11, with nearly identical results. All three test monitors indicated a final R_f of less than 0.50×10^{-4} following fresh water lay-up and chlorination. An interim heat transfer

measurement immediately following fresh water lay-up, but prior to the chlorine treatment, indicated a reduction in R_f from approximately 6.0×10^{-4} to 5.0×10^{-4} . Thus, the most significant reduction in R_f occurred as a result of chlorination.

DISCUSSION

A comprehensive review of heat transfer results from Phases I-IV indicates about equal biofouling rates on both the Wolverine "Korodense" enhanced tube surface compared to conventional smooth tubes when operated at the same seawater velocities. Where the seawater velocities are adjusted for equal pressure drop (i.e., higher velocity in the smooth tubes), heat transfer data suggest that the rate of fouling was equal to or slightly higher in the enhanced tube compared to the smooth tube.

Periodic increases in seawater velocity to greater than 10.0 fps are initially effective in removing biofilm on titanium and AL-6X condenser tubes, but become progressively less effective with time of exposure. Previous biofouling data from LaQue have demonstrated the "conditioning" effect of repeated cleaning cycles on smooth titanium tubes. The biofouling film becomes increasingly more difficult to remove with repeated use of manual brushes, sponge rubber balls, or as demonstrated in Phase II, with repeated, high velocity cleaning cycles.

Shock chlorination following fresh water lay-up was shown to be effective in removing biofilms on titanium and AL-6X. The long term effectiveness of this treatment, however, must yet be demonstrated. Repeated shock chlorination cycles may decrease in effectiveness as has been found for repeated mechanical cleaning methods.

Examination of the enhanced tube results indicates that biofilm accumulates preferentially in the recessed area between the interior "ridges"; this suggests that further tests may be necessary to quantify biofouling rates with respect to degree of enhancement. A relatively light enhancement was evaluated on the AL-6X Korodense HTM. More severe enhancements, which may be considered for further improvement in heat transfer efficiency, could result in different rates of fouling.

Open ocean heat transfer data from a potential OTEC site off the coast of Puerto Rico have been compared to coastal biofouling data from LaQue. The results are characteristically similar from the two locations for titanium tubes cleaned by comparable techniques. The coastal biofouling data reproduce the open ocean results, but on a compressed time scale. These results support the investigation of biofouling at coastal sites to gain insight into biofouling processes and cleaning methods for both coastal and open ocean application.

A complicating, and as yet undefined, biofouling condition might occur when titanium condensers are operated alternately between open ocean and coastal harbor waters, and in seawater of varying ambient temperatures. Biofouling data on smooth titanium exist for warm and cold coastal water, and warm open ocean water. There is an absence of biofouling data, however, for cold open ocean and alternating exposure conditions. Further experimental work is required to adequately describe biofouling on smooth and enhanced titanium condenser tubes under these conditions.

CONCLUSIONS AND RECOMMENDATIONS

- o Daily heat transfer resistance measurements made during all four phases of the test program show no significant difference in the rate of biofouling between smooth and enhanced (Korodense) tubes.

- o High velocity seawater was shown to be initially effective in removing biofilm from the HTM tube surfaces, but became progressively less effective with successive cleaning cycles.
- o Chlorination shock treatment was found to be effective in controlling biofouling on titanium, but requires additional evaluation of long term effectiveness. Tube surface enhancement did not inhibit the overall effectiveness of the chlorine treatments.
- o Future tests are recommended to determine the effect of more severe enhancement on the rate and extent of biofouling. It is possible that condenser tube enhancement may inhibit the build-up of biofouling beyond a certain thickness due to increased seawater turbulence at the tube surface.
- o The effect of alternating exposure to surface harbor water and deep open ocean water has not been determined for titanium condenser tubes, and should be confirmed by further evaluation.

REFERENCES

1. Gavin, A. P., Kuzay, T. M., Benson, P. H., 1980, "Biofouling and Corrosion Measurements Using OTEC-1 Modules," 7th Ocean Energy Conference, Washington, D.C.
2. Fetkovich, J., Fette, C.W., Findlay R.W., "A System for Measuring the Effect of Fouling and Corrosion on Heat Transfer under Simulated OTEC Condition". DOE Report No. COO-4041-10.
3. Argonne National Laboratory Report, 1981, OTEC Biofouling, Corrosion and Materials Program.
4. Biofouling, Corrosion and Materials Workshop, Jan 1979, Rosalyn, Virginia, USA.

TABLE 1 - Final Test Matrix

Test Phase	Exposure (days)	Seawater Temp(°C)	Seawater Velocity (fps) 1" tube	
			Smooth	Enhanced
I	25	24-29	3.4	2.8
II	24	24-28	6.8	5.6
III*	30	20-26	5.4 10.7	6.0 11.9
IV**	35	16-20	5.4	6.0

* Cleaning Procedure: On R_f reaching 6.0×10^{-4} , all three HTM's were flushed by increasing seawater velocity to the indicated value for up to 2 hours.

** Cleaning Procedure: On R_f reaching 6.0×10^{-4} , all three HTM's were layed-up with distilled water for 72 hours. This was followed by the indicated seawater velocity with 5.0 ppm chlorine for 48 hours.

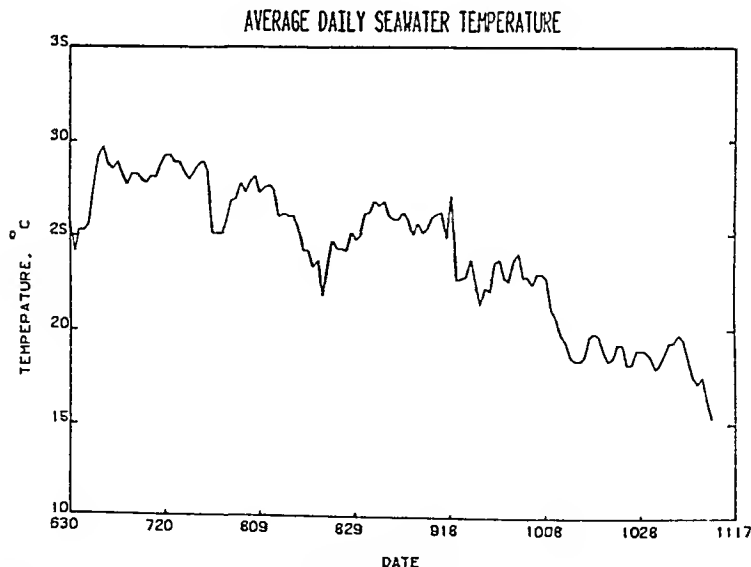


Figure 1 - Average daily seawater temperature between June 30 and November 11.

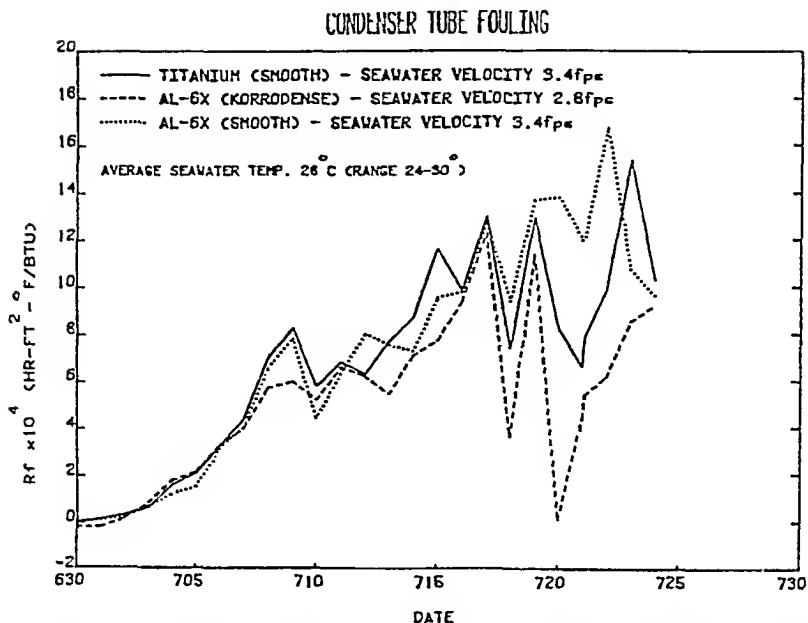


Figure 2 - Combined R_f versus time data for three HTM's during Phase I. Seawater velocity on enhanced tube was selected to produce an average wall shear stress (pressure drop) equivalent to the smooth tube value.

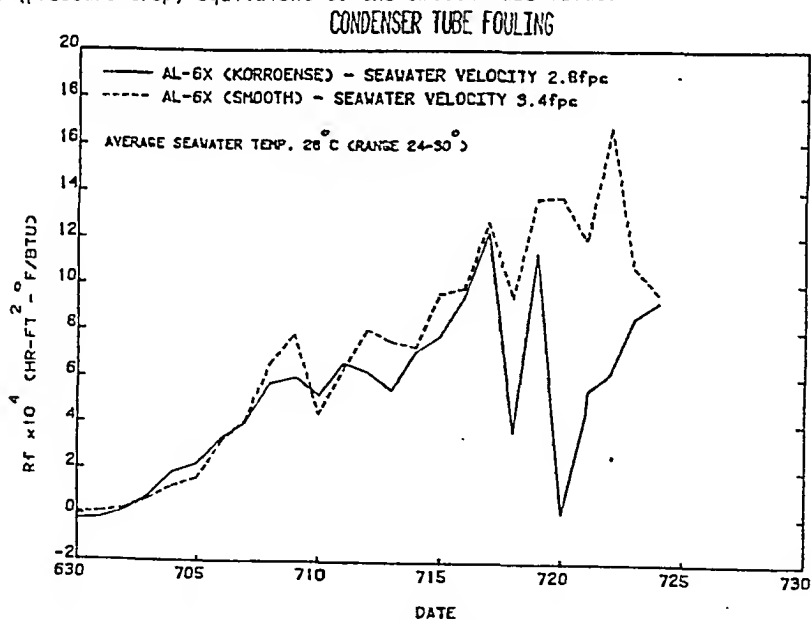
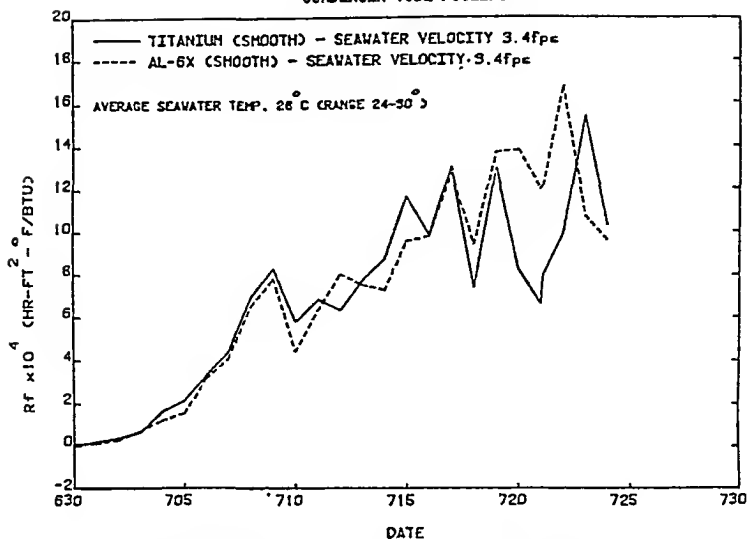
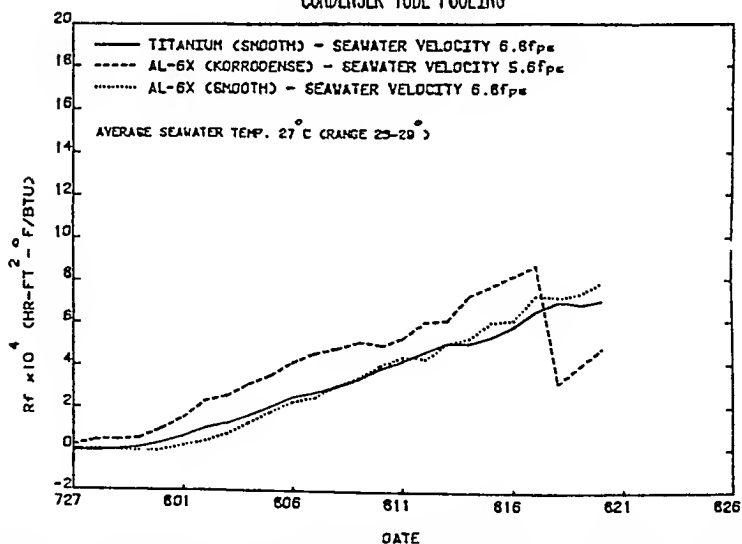


Figure 3 - Phase I R_f data for smooth and enhanced AL-6X

CONDENSER TUBE FOULING

Figure 4 - Phase I R_f data for AL-6X and titanium smooth tubes

CONDENSER TUBE FOULING

Figure 5 - Combined R_f versus time data for three HTM's during Phase II. Seawater velocity on the enhanced tube was selected to produce an average wall shear stress (pressure drop) equivalent to the smooth tube value.

CONDENSER TUBE FOULING

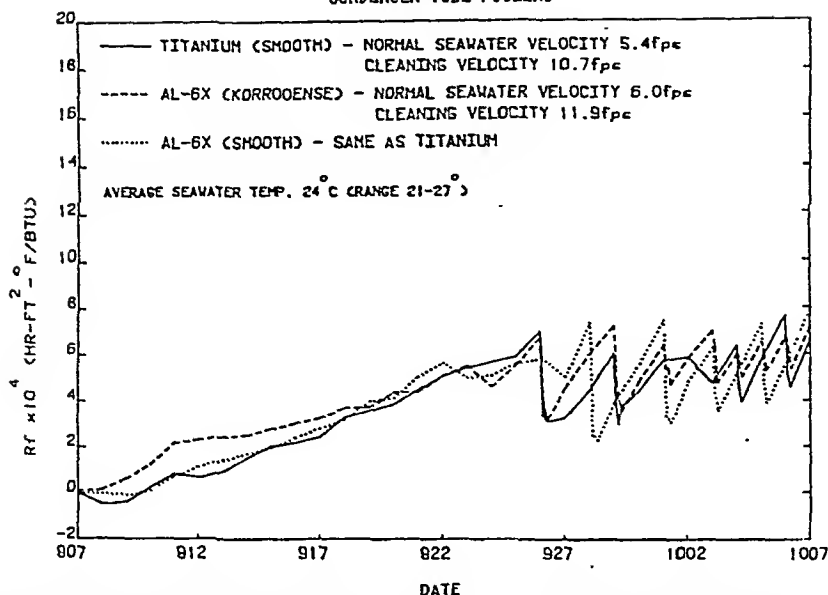


Figure 6 - Combined R_f versus time data for three HTM's during Phase III. Seawater velocity selected to produce an average wall shear stress equal to the value for a 5/8 inch tube operated at 5.0 fps

CONDENSER TUBE FOULING

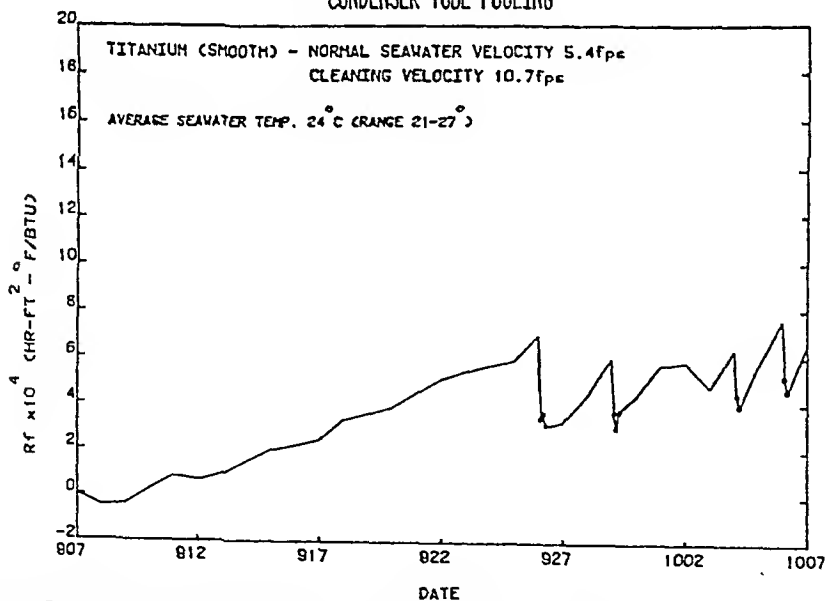


Figure 7 - Phase III R_f data for smooth titanium showing the value of R_f measured after 5, 10 and 60 minute cleaning intervals at high velocity for the first two cycles and 5 and 60 minute cleaning intervals for the last two cycles

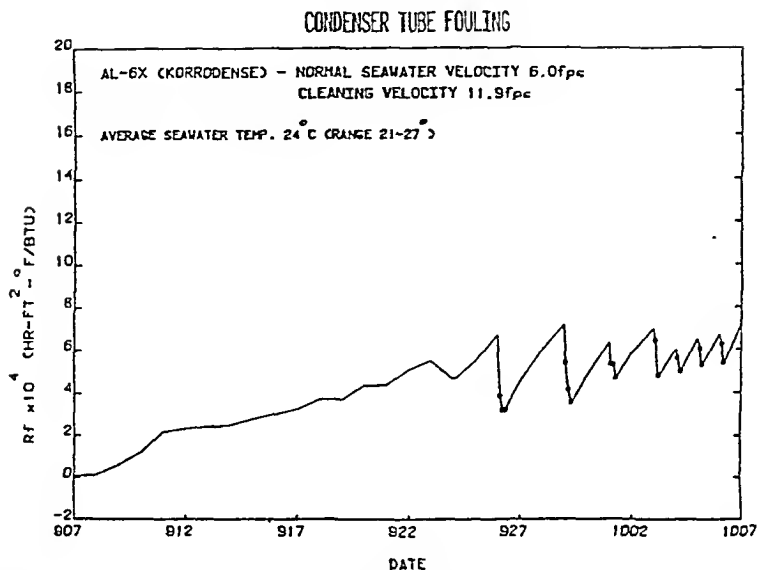


Figure 8 - Phase III R_f data for the enhanced AL-6X HTM subjected to high velocity cleaning for 5, 10 and 60 minute intervals for the first two cycles and 5 and 60 minute intervals during the remaining cleaning cycles

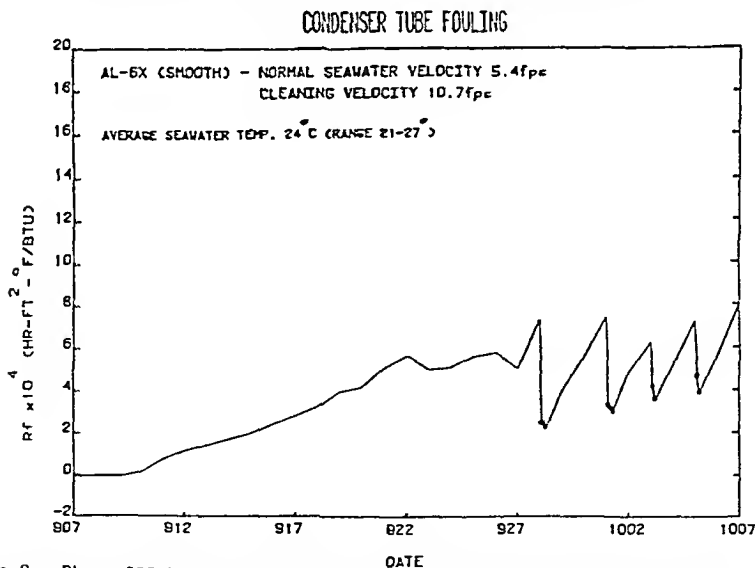


Figure 9 - Phase III R_f data for smooth AL-6X subjected to high velocity cleaning for 5, 10 and 60 minute intervals for the first two cleaning cycles and 5 and 60 minute intervals during the last two cycles

CEER-OTEC RESEARCH PLATFORM - PUNTA TUNA, PR

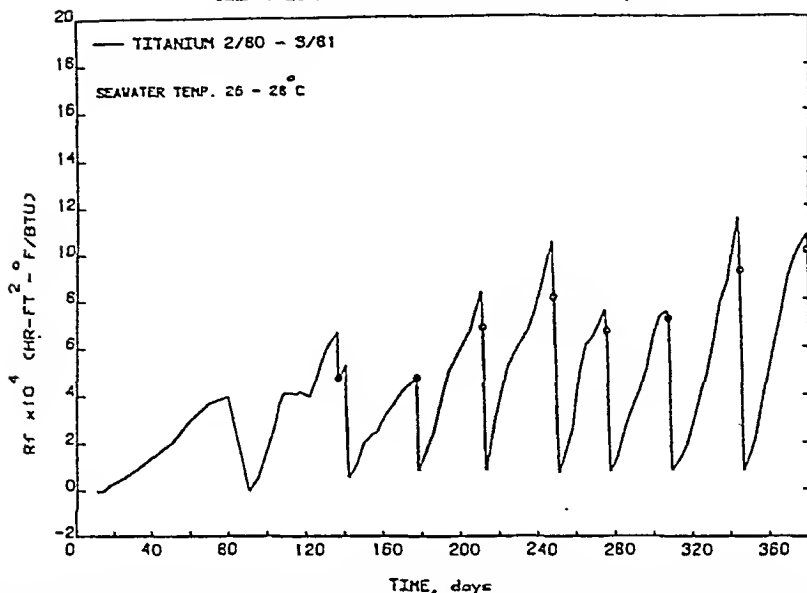


Figure 10. - Fouling data for titanium exposed to warm, open ocean water off the coast of Puerto Rico pumped from a depth of approximately 100 feet. Open circles represent Rf measured after 30 minutes at a seawater velocity of 12.0 fps.

CONDENSER TUBE FOULING

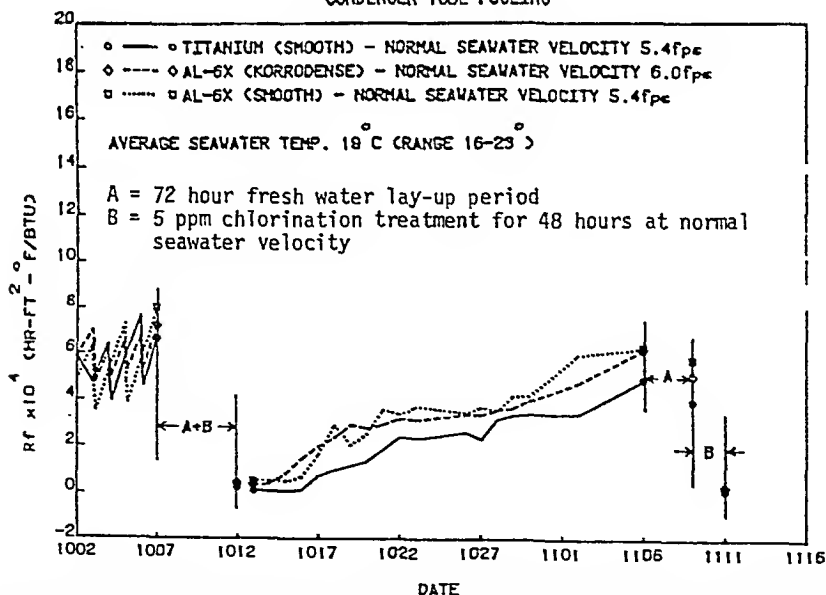


Figure 11 - Combined Rf data for three HTI's during Phase IV. A fresh water lay-up/shock chlorination treatment was evaluated twice during this phase. Open symbols represent individual Rf measurements made before, during or after treatment.

APPENDIX 1 - Titanium Pipe Cleaning Procedure

1. If degreasing is necessary for new pipe and tube test sections, the test sections will be soaked in acetone followed by freshwater rinse.
2. To remove hard fouling, the pipe section will be soaked in 20% by volume glacial acetic acid solution for 12 hours. The pipe sections will then be scrubbed with a soft brush and/or ramrod/cloth and rinsed with large quantities of freshwater.
3. Piping sections will then be immersed in an aqueous alkaline cleaning solution. Time periods of treatment may be varied depending upon the severity and type of soiling agent and original pipe condition. Specimens will be soaked in an aqueous solution of 20% (by weight) sodium hydroxide (NaOH) at room temperature for 30 minutes. All specimens will then be thoroughly rinsed.
4. Pipe sections will then be subjected to an acid pickling procedure. Specimens will be soaked in an aqueous solution of 20% (by volume) concentration nitric acid (HNO_3) at room temperature for 30 minutes.
5. Pipe samples will be thoroughly rinsed and then replaced into the test system if no pitting or corrosion products are evident.

AERATION AND DEAERATION IN A CONDENSER

I. Olikar and D. Katsman

Theoretical aspects of aeration and deaeration in a power plant condenser are discussed, including mass condensation, condensate flowdown, the air cooling section, and cooling water temperatures. Measures to improve deaeration are presented, with particular emphasis on tube bank design; adequate vacuum related to heat load; injection points for makeup, drains and vents; and use of bubbling deaerating devices. The advantages of multipressure condensers for deaeration are discussed, and a condenser configuration incorporating features of both single and multi-pressure designs is proposed.

INTRODUCTION

To ensure the integrity of the power plant water-steam systems, it is necessary not only to reduce the corrosion products in these systems but also to eliminate the causes of corrosion. The main cause of corrosion is oxygen which induces iron and copper oxide formation.

Field tests indicate that oxygen content increases as the condensate passes through the feedwater train. Therefore, oxygen must be kept at a minimum throughout the condensate/feedwater system, particularly in power plants not equipped with deaerators.

Tightness of vacuum system components can reduce air ingress considerably although achievement of absolute integrity does not appear possible. Non-condensable gases are introduced with the make-up, drain, vent and cooling water and with the exhaust steam. In-leakage also occurs through equipment that is not in service during some modes of the plant operation. Therefore, other methods providing system integrity must be introduced. Of these, the most important is the improvement of condenser deaerating capability. The condenser must function as a deaerator.

OXYGEN CONCENTRATIONS IN CONDENSATE

Since different interpretations of the character of the aeration/deaeration process in the condenser lead to different recommendations for condenser design, consideration of where and how oxygen concentration takes place is important.

Burns & Roe, Inc., Oradell, New Jersey, USA

According to Kirsh's theory (1), at 100% heat load, oxygen content is low in the area of mass condensation but higher at the condensate outlet because of admixing of the main condensate with aerated condensate flowing down from the air cooler. Also according to this theory, the oxygen content increases at low load because the mass condensation area decreases and condensate passes through a larger air-cooling area.

The steam-air mixture passes through two zones in the tube bank. In the zone of mass condensation, the steam-air mixture temperature essentially does not change, while the heat transfer coefficient and density of heat flow decrease substantially because of the increase in air concentration and decrease in flow velocity. In the zone of air cooling, the heat transfer coefficient and density of heat flow essentially do not change, while the steam-air mixture temperature decreases considerably because of a decrease in the partial steam pressure, and subcooling takes place. In the mass condensation zone, the heat transfer coefficient and density of heat flow decrease much more at low load than at 100% load. Under these conditions, the decrease in log mean temperature difference (LMTD) may be such that the cooling surface will be entirely used for mass condensation, and subcooling will not occur. On the other hand, when LMTD increases or remains the same at low load as at 100% load, the subcooling area increases. To preclude enlargement of the subcooling area, some operators decrease cooling water flow rate according to heat load. Nevertheless, oxygen content increases in the condensate.

According to Grishuk's theory (2) based on Henry's Law, the condensate is enriched by oxygen throughout the tube bank. In the main part of the bank, where steam with a minimum amount of oxygen moves downward at high velocity relative to the condensate, the latter captures gas bubbles mechanically, and a finely dispersed suspension of bubbles and condensate flows down to the hotwell. The final amount of gas bubbles relates to retention time of the condensate in the lower portion of the condenser. According to this theory, oxygen content is proportionate to the heat load. The condensate retention time does not improve deaeration unless high partial steam pressure is provided in the low part of the condenser or the condensate is treated in a deaerating device. Tests of condensers not equipped with deaerating devices show practically constant oxygen concentrations regardless of retention times from 100 to 10 sec according to Olikier and Permyakov (3).

Sklover's theory (4) considers the fact that condensate flowing down from tube to tube is exposed to both the mechanical and thermal effects of steam moving in the intertube spaces. The particles of condensate flowing to the hotwell can either gain heat until they reach the steam temperature of the local partial pressure in the surrounding steam-air mixture and release dissolved oxygen, or they can be subcooled and absorb oxygen from the surrounding steam-air mixture. The final oxygen content of the condensate in the hotwell depends on the characteristics of the steam-air mixture above the condensate surface.

It is logical to consider the aeration process in relation to mass steam condensation, with film build-up on the tubes, and the influences of such factors as condensate flowdown through the tube bank, the air cooler section, and circulating water temperature.

During mass condensation a film is formed around the condenser tubes. The outside surface of the film is at a temperature close to the steam temperature of the local partial pressure and the inside surface is close to the tube outside temperature. In this unbalanced state, the condensate absorbs gases from the surrounding steam-air mixture as a result of molecular and turbulence

diffusion. The gas concentration is higher on the boundary between the gas and liquid phases. Molecules of non-condensable gases, together with steam, transfer to the film in amounts which can be dissolved according to Henry's Law. The remainder of gases diffuses outward toward the steam-air mixture surrounding the condensate film, thus increasing the concentration of gases close to the surface of the film. However, this boundary layer is affected by steam flow, and high velocity steam flow will remove the stratified layer of concentrated gases.

As soon as film forms on the tube, it starts to cool and, theoretically, could absorb more oxygen. However, constantly forming new condensate stratifies on the existing film, isolating it from the steam-air mixture and preventing it from dissolving more oxygen. Thus, the concentration of dissolved oxygen in all boundary layers of condensate can be considered equal to the equilibrium oxygen content of its local partial pressure according to Henry's Law. This relationship is also affected by steam-air mixture velocity, heat load, and partial pressure of the non-condensable gases.

At 100% load, the relative air content in the exhaust steam is within 0.01% for condensers with high integrity and as much as 0.05% for condensers with poor integrity. Calculations in Figure 1 include both cases. This process takes place at mass condensation regardless of tube bundle design of air removal equipment.

Oxygen concentration in the condenser output often significantly exceeds calculated estimates even with proper air removal equipment operation. This is caused by absorption of oxygen while the condensate is flowing down to the hotwell past tube bank zones having different partial pressure of gases. Condensate drops (or films) falling down from the tubes are treated mechanically and thermally by the steam flow, which moves the drops toward the cooling surface. Contact between the drop and the steam effects the heat transfer. The steam is condensed on the drops and the latter are heated to a temperature close to that of saturated steam at the local partial pressure. Heat transfer is accelerated by the mass transfer rising from the film inner layers to the water boundary surface and through the phase boundary space. This process is followed by gas desorption from the film. The main resistance to gas desorption is in the liquid phase. The amount of absorbed gases depends on the air content in the steam, steam velocity, heat and mass transfer coefficients, mass transfer area, and duration of phases.

The mass transfer coefficient is a function of Reynolds number characterizing the movement of the condensate over the film on the tube surfaces. The critical Reynolds number at which the condensate flow ceases to be laminar and begins to cause turbulence in the film is somewhere above 60 according to Kytateladze (5). When the condensate flows down vertically, the Reynolds number is less than 50 even in the low tube rows, which corresponds to a laminar condition. However, under the influence of the moving steam, the condensate does not flow down vertically and the stream is turbulent.

Depending on the relative air content in the steam, different aeration conditions are present. At low velocities and laminar conditions, the newly formed condensate stratifies on the film surface, and gas equilibrium occurs. In turbulent conditions, continued transfer of condensate particles takes place within the layer of film, and intensive gas absorption occurs as the condensate flows to the hotwell.

In peripheral paths of the tube bank where high steam velocity combines with minimum air content, the aeration of condensate is insignificant because of low partial air pressure on the tube surface. In the depth of tube bank where the greater part of the steam is already condensed, the remaining steam-air mixture has a high relative air content and, therefore, forms condensate of high air content. The condensate formed in regions with small relative air content mixes with the new condensate, and the overall air concentration may be increased. This increase may be insignificant if the flow of the main condensate is laminar. However, if the flowdown is turbulent, the concentration of oxygen may be appreciable.

In the lower part of the tube bank, desorption of gases earlier dissolved in the condensate is caused by upflow steam with low partial gas pressure. However, this beneficial effect may be eliminated if the condensate bridges the intertube spaces, the condensate subcools, and the steam flow rate is reduced.

The condensate mechanically captures gas bubbles and the resultant finely dispersed suspension of bubbles flows into the hotwell. A steam-air mixture can also be injected into the hotwell with the falling condensate. This steam condenses, and gas absorption takes place in the hotwell. If not released, the gases will be pumped out with the condensate.

Normally, at constant heat load and pressure increase, condenser pressure drop decreases in relation to the reduction of specific volume of flow. The increase in condenser total pressure drop is mainly attributable to the increased pressure drop in the air cooler. The associated pressure drop can decrease condenser efficiency, including subcooling of the condensate. When the condensate flows freely down through the air cooler, pressure drop increases. In addition, the LMTD increases throughout the tube bank to the point where subcooling may occur.

Tests of condensers at different cooling water temperatures from 1°C to 25°C at heat loads close to 100% load do not confirm the accepted opinion that deaeration is diminished by cold cooling water according to Konovalov et al. (6). However, from 50% to lower heat loads, cooling water temperature decrease substantially contributes to degradation of tube bank deaeration capability. This is directly related to the redistribution of the heat loads over the zones of the tube bank. The greater mass condensation takes place in the upper part of the tube bank, and inundation and blanketing by non-condensable gases occur in the lower regions.

Cooling water velocity affects the overall heat transfer coefficient at different water temperatures. At a high cooling water temperature an increase in velocity increases the heat transfer coefficient, but at a cold cooling water temperature an increase in water velocity has no significant effect on heat transfer coefficient.

MEASURES TO IMPROVE DEAERATION

The deaerating capability of the condenser depends on high integrity in the vacuum system; adequate air removal equipment at any heat load; tube bank design; adequate vacuum related to the heat load; careful introduction of make-up, drains and vents; and presence of deaerating devices.

To improve the deaerating capability of the tube bank, the following must be taken into consideration: relative uniformity of heat load on periphery of tube bank, efficient air cooler layout, avoidance of non-condensable gas build-up, and proper conditions below tube bank.

Relative uniformity of the heat load on the periphery of the tube bank can be achieved by a suitable configuration of the steam passages and the number of tube rows from the periphery to the points where the steam-air mixture is accumulated before it enters the air cooler section. The velocity of the exhaust steam entering the peripheral rows should not exceed 60 m/s. Above this velocity, the forces on the drops around the tube circumference might be balanced; this would lead to bridging or condensate hold-up according to Reference (7).

The passages around the tube bank periphery should provide uniform steam flow throughout, including the lower tubes. For a large tube bank, wide access lanes should be provided for the steam to penetrate deep within the condenser shell. A criterion for access lane width might be that the steam velocity in the lane should not exceed the velocity at entry to the tube bank periphery.

The steam should be passed through 12 to 20 tube rows in one direction and, after mass condensation, the steam-air mixture should be accumulated in an unrestricted area for distribution into the air cooler. The number of tube rows should be based on the frictional pressure loss corresponding to the reduction in steam temperature. This results from the temperature difference between the steam and cooling water, and the condensation rate.

In a two-pass condenser, the first pass of circulating water usually flows through the top tube bank, which therefore is capable of condensing the most steam. With a high rise in water temperature, the steam side conditions are noticeably worse in the second pass because of low steam velocity in the entry of the tube bank, heavy inundation, and lower mean temperature difference. In the second pass, oxygen content in the condensate is significant, particularly at low load.

To preclude overloading the air ejector with uncondensed steam, it is necessary to provide a section of air cooling tubes between the steam-air mixture accumulation zone and the point where the air-vapor mixture leaves the condenser. The air cooler should be shielded from condensate carry-over. Passes over the tubes in the air cooler should be baffled to ensure a reasonably high velocity of the steam-air mixture. Also, the steam should not bypass into the exit duct or reheat the extracted air-vapor mixture. Devices such as tubes plugged on the ends and slotted on the bottom can help carry non-condensable gases toward the suction portion of the air cooler.

Collectors at an intermediate level in the tube bank for channeling the condensate toward the periphery have been found to reduce aeration. Tests show that installation of tubes inclined to the horizontal give best results according to Sklover and Byevich (8). Deaeration has been increased in condensers where the tubes are installed at a 4 or 5 degree angle to the horizontal and the main condensate flows along the tubesheet in a thick layer. Even in spaces close to the tubesheets where the air content in the steam-air mixture is high, intensive gas absorption does not take place because of the fast flowdown and small contact surface according to Tyshakov and Promyslov (9).

In order to completely release the gases dissolved in the condensate, it is necessary to provide the following conditions in the low part of the condenser: (1) Partial pressure of wet steam above the condensate level should be practically equal to the total pressure of steam-air mixture; that is, the gas content above the condensate level should be minimal. To achieve this, passages must be sufficiently large for free access of exhaust steam to the lower part of the condenser. (2) Since most of the gas in the hotwell is in

the undissolved state, the condensate should be retained for a sufficient time for bubbles to rise to the surface. The release of small bubbles can only be accomplished by a deaerating device. (3) Air in-leakage below the condensate level must be prevented.

It is important to maintain the steam-air mixture velocity at low loads close to that of 100% load so as to decrease the diffusion rate of non-condensable gases toward the condensate film. The best way to achieve this is by increasing the vacuum at low heat loads when the exhaust steam velocity increases due to the higher specific volume.

Maintenance of a deeper vacuum at low heat load than at 100% load increases efficiency of operation of the turbine and helps to prevent non-uniform heating of the low pressure section.

Entrance points and distribution arrangements for make-up water, heater drains, and air vents significantly influence the deaerating performance of the condenser. Although preheating of make-up water has been suggested to reduce dissolved oxygen, only deaeration by steam jets can provide adequate air removal. It is desirable to pass the make-up water through such a deaerating device before introducing it into the condenser; otherwise, it is necessary to install a deaerating device in the condenser hotwell. Make-up water should be introduced into the steam space above the tube bank through an atomizing device so that its temperature is increased close to that of the saturated steam.

All drains should also be introduced through atomizing devices. Drains at temperatures below saturated steam temperature should be introduced above the tube bank; drains above saturated steam temperature should be introduced between the tube bank and the hotwell. Dissolved oxygen content in drains cascaded to the condenser should not exceed 20 ppb.

Individual vent lines from heaters are preferable to a cascaded system because fewer bubbles enter small lines and better flow occurs through separate lines. Vents should be introduced into the zone immediately before the air cooler.

Regardless of all preventive efforts, some oxygen is dissolved in the condensate, particularly at low load. The only effective way to remove this oxygen is by installation of a bubbling or jet deaerating device. Both operate well at full load, but the jet device may be inefficient at low load if an inadequate quantity of exhaust steam is available.

In a jet deaerating device, the condensate passing through perforated trays breaks into droplets when it falls. Exhaust steam passes through the streams, and the liberated gases are vented to the air cooler. The principle of a bubbling deaerating device is multiple reheating of the condensate above the saturation temperature corresponding to condenser pressure, and subsequent flashing. Figure 2 plots results of condenser tests without deaeration, and with jet and bubbling devices. The effect of the bubbling device is superior, especially at low load. A bubbling device has the added advantage that it can be rendered temporarily inoperative if oxygen removal is satisfactory without additional deaeration.

MULTI-PRESSURE CONDENSERS AND DEAERATION

An important advantage of a multi-pressure condenser is its ability to deaerate "cold" condensate with "hot" exhaust steam. In this case, deaeration in the "hot" condenser similar to that in a typical deaerator can be achieved, and oxygen content in the condensate is less at any plant load.

Multi-pressure condensers are widely used with turbines having two, three and even four LP cylinders. A multi-pressure condenser provides for lower average mean back pressure than is achieved with a single pressure condenser at the same cooling water flow rate and temperature. Accordingly, the turbine unit capacity increases by 0.2 to 0.4%. The advantages of a multi-pressure condenser are most manifest when the turbine load is reduced because the available energy in the last stages can substantially compensate for the decreased load.

Multi-pressure condensers do not achieve useful gain in applications where the turbine last stage blades are heavily loaded and the vacuum approaches choking or maximum design pressures. In fact, the gain in the first LP turbine cylinder/first condenser stage may be less than the losses in the next LP turbine cylinder/condenser according to Coit (10). Immense cooling surfaces are required particularly for nuclear plants. Space for such large condensers is restricted by both the foundation columns and the LP turbine flow sections so they are not as widely used as single pressure condensers. In a nuclear power plant, with approximately twice the exhaust steam flow rate of a similar fossil plant, the size of a multi-pressure condenser is often prohibitive.

For any power plant, cooling water temperature and even flow rate may vary widely for the same guaranteed power output. Under such changeable environmental conditions, a single pressure condenser does not accommodate an increase in turbine efficiency or condenser deaerating capability.

A condenser configuration incorporating the advantages of both multi-pressure and single pressure condenser configurations is shown in Figure 3 for a typical 1000 MW PWR power plant comprising three LP turbine cylinders. Condenser tube layout is transverse to the turbine shaft. The condenser is arranged with two circulating water flows, each pumped separately through the condenser to the discharge channel. To ensure equalization of pressure, the condensers are connected by steam crossover ducts.

When back pressure of the LP turbine elements is between choking and maximum design pressure, the two circulating water regulation valves would be fully open. When maximum design pressure is reached in the center LP turbine, the regulating valve would be closed to the extent needed to increase flow to the center condenser and thus decrease its back pressure. At times when the outboard LP turbine elements are below choking pressure, the steam crossover passage between condensers would be partially opened to increase back pressures. These features would ensure the efficiency of the power plant at any circulating water flow and temperature encountered throughout the year.

Condensate from the outboard condensers would be pumped through atomizing devices into the steam space of the center condenser where it would mix with the exhaust steam from the center LP turbine, heated, and deaerated. The center condenser would raise the condensate temperature and thus increase balance-of-plant efficiency. To ensure air removal from the "hot" condenser, steam-air vapor would be transferred to the outlet of the air removal section of the corresponding "cold" condenser and discharged from the region near the circulating water inlet.

Consider the operating conditions of the outboard and center condensers from the standpoints of aeration and deaeration. In the outboard condensers, the colder cooling water causes more non-uniformity of the heat load along the tube bank than occurs in the center condenser, where cooling water temperature is 7° to 10°C higher. Non-uniformity of heat load causes inundation and blanketing of air, particularly in the lower section of the tube bank. Though the deeper vacuum in the outboard condensers should result in decrease of

oxygen concentration in the condensate at mass condensation, the high relative air content in the steam can overcome this positive effect and actually increase oxygen concentration. This high relative air content in the outboard condensers is explained by the fact that all make-up, drains, and vents are introduced here, and more air in-leakage can occur because of the deeper vacuum. Condensate from air coolers of the outboard condensers has a higher oxygen concentration because the air removal system operates from the center condenser through the outboard condensers. That portion of condensate with high gas concentration increases the total oxygen content after mixing with the main condensate.

At introduction of "cold" condensate through atomizing devices from the outboard condensers into the steam space of the "hot" condenser, the condensate temperature rises close to the exhaust steam temperature. Gas bubbles form at this moment because the sum of partial pressures of dissolved gases and steam reaches or exceeds the pressure inside the atomized condensate drops. This effect is similar to that when water enters a vacuum deaerator and instantaneous separation of most of the gases from the water takes place. Up to 90% of dissolved oxygen can be released at this moment according to Oliker (11).

CONCLUSION

Oxygen concentration in the condensate during mass condensation increases at reduced heat loads regardless of tube bank and air removal equipment design. The oxygen concentration at this stage of condensation relates to vacuum system integrity and condenser pressure.

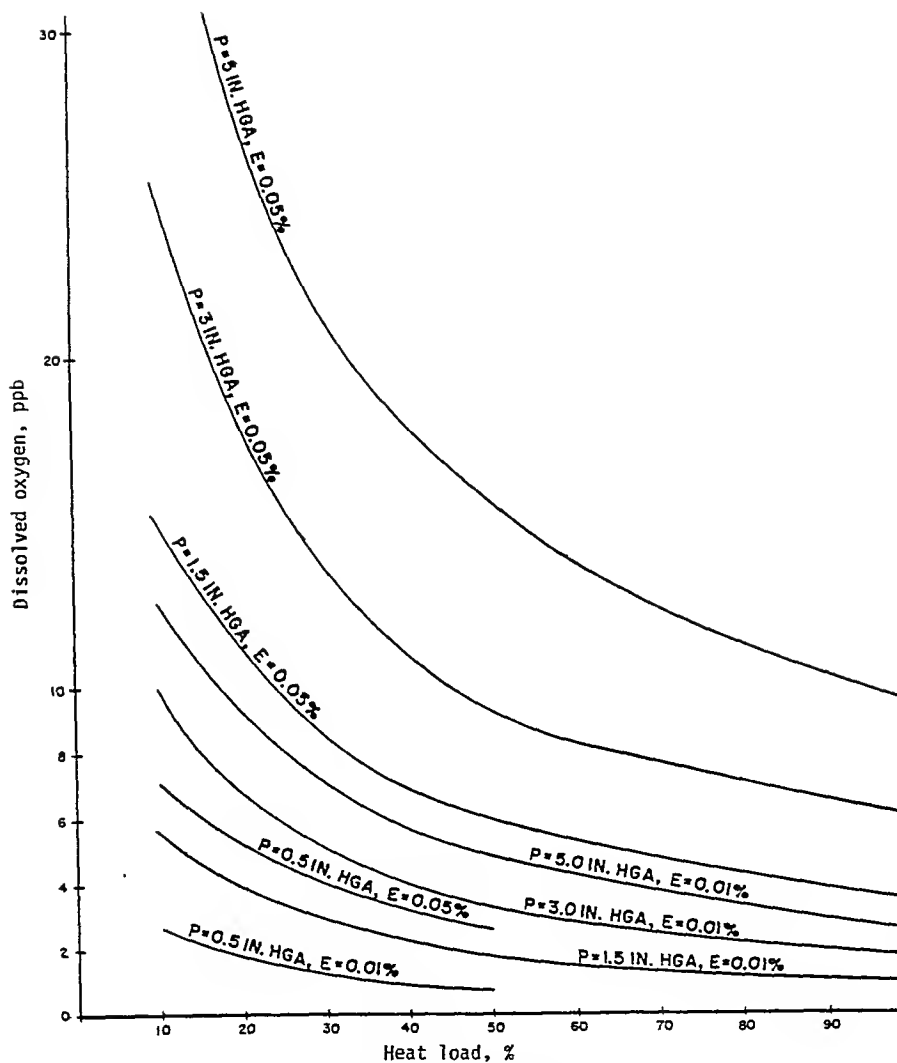
Oxygen concentration after mass condensation may increase considerably in a poorly designed condenser. The oxygen concentration immediately after mass condensation can be maintained or even decreased in a condenser with uniformity of heat load along the tube bank, proper air cooler layout, and deaerating capability in the lower part of the condenser.

A multi-pressure condenser provides considerably improved deaerating capability at any seasonal water temperatures and flow rates, and turbine load conditions.

REFERENCES

1. Kirsh, A.K. Deaeration process in condensers of large steam turbines, *Teploenergetika*, 1962 (10).
2. Grishuk, J.K. Oxygen absorption by condensate in a steam condenser. *Teploenergetika*, 1961 (3).
3. Oliker I. and Permyakov, V. Thermal deaeration of water in power plants. *Energiya*, Leningrad, 1972.
4. Sklover G.G. et al, Deaerating capability of vacuum steam condenser. *Teploenergetika*, 1969 (12).
5. Kytateladze, S.S. Fundamentals of heat transfer. *Nayka*, Novosibirsk, 1970.
6. Kononov G.M. et al, The operation efficiency and an assessment of steam turbine condenser designs as a result of field tests. *Teploenergetika*, 1972 (7).

7. Power condenser heat transfer technology. Edited by P.L. Marto and R.H. Nunn. McGraw-Hill, 1981.
8. Sklover G.G. and Byevich, A.V., Investigation of steam condensation in inclined tube bank. Teploenergetika, 1978 (6).
9. Tyshakov N.S. and Promyslov, A.A. Investigation of aeration and deaeration in a condenser. Energomachinostroenie, 1981 (4).
10. Coit, R.L. Design trends in utility feedwater heaters and condensers. Combustion, 1975 (2).
11. Oliker, I. Vacuum deaeration of water - an effective method for preventing corrosion. Corrosion, Vol. 33, No. 3 1975.



E = relative air content in the steam, %

P = condenser pressure, in Hga

Figure 1. Oxygen concentration at mass condensation

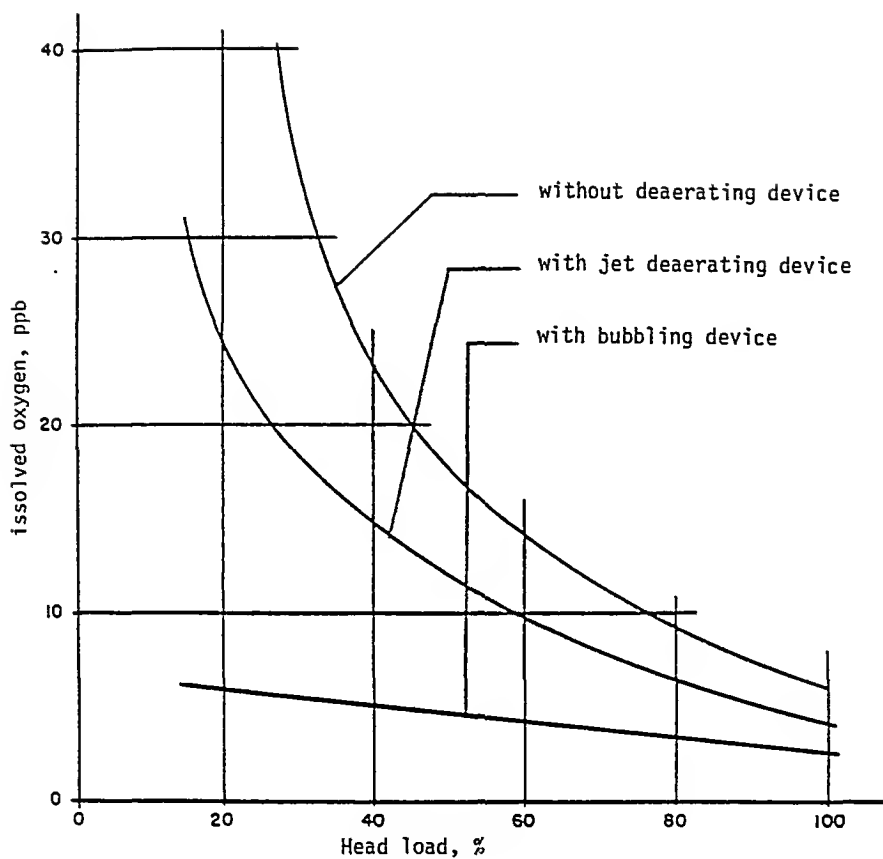


Figure 2. Condenser deaerating capability

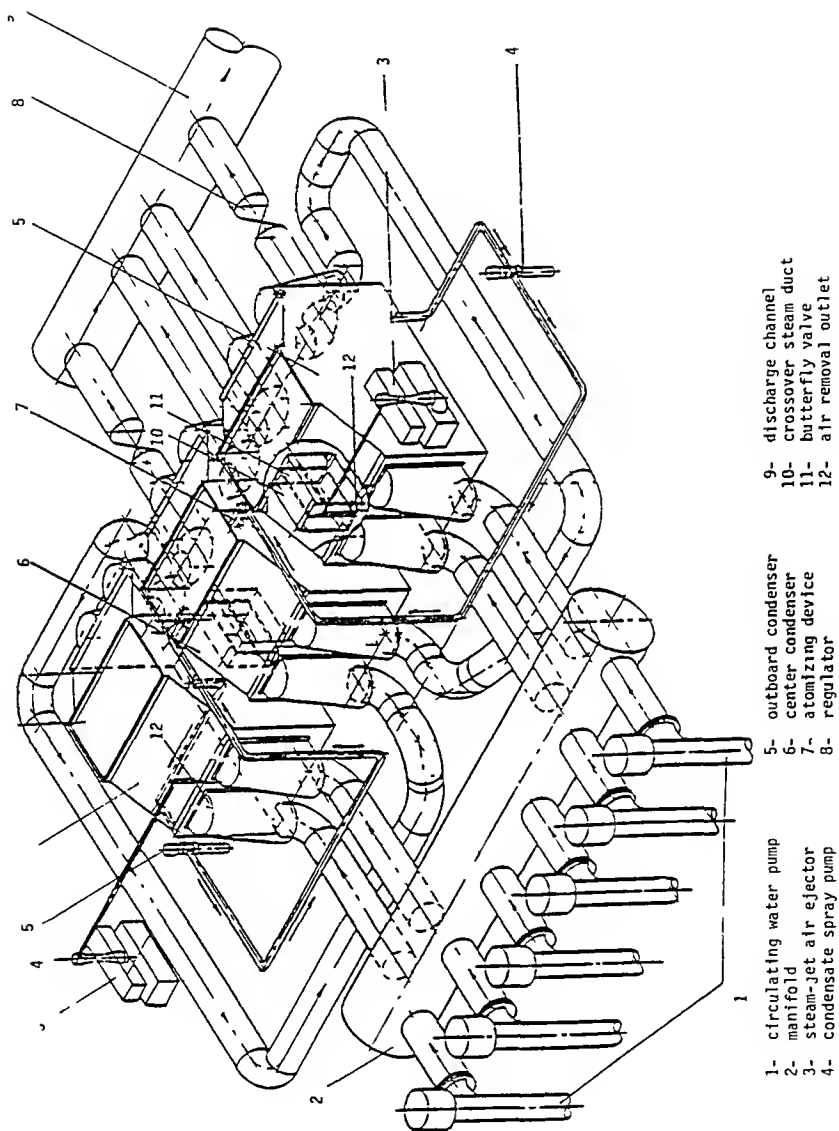


Figure 3 Multi-pressure condenser configuration

AUXILIARY CONDENSERS VS MAIN CONDENSER FOR BOILER FEED PUMP TURBINE-DRIVERS

B. Bornstein*

Condensing turbine-drivers for boiler feed pumps may exhaust to the plant's main condenser or to separate auxiliary condensers. The latter arrangement offers greater freedom in locating the feed pump-driver train and may also improve efficiency. However, each auxiliary condenser requires its own ancillary equipment. The layout and operating advantages of each arrangement are examined. Capital costs for drivers in the same location are found not to differ significantly. Auxiliary condensers perform more advantageously in plants with low main turbine exhaust pressures.

INTRODUCTION

In US central stations, nearly all fossil-fuel fired units larger than 350 MWe and light-water moderated nuclear units larger than 700 MWe employ turbine driven feedwater pumps (1), (2). The turbine-drivers are generally of the condensing type (2).

Condensing turbine-drivers may exhaust to the main condenser or to separate auxiliary condensers. Westinghouse Electric Corporation states that it has encountered about the same number of applications for each arrangement (1). Brown-Boveri, however, contends that if plant efficiency is included in the evaluation the economics will favor the auxiliary condensers, and claims to have encountered only few turbine-drivers that exhaust to the main condenser (2). Yet, nearly all turbine-drivers in central stations designed by the author's company exhaust to the main condenser.

The object of this paper is to examine the performance and capital costs associated with each arrangement to determine relative merits.

PERFORMANCE

Turbine-drivers exhausting to the main condenser require an interconnecting duct. Figure 1 is an example. This duct is eliminated if the drivers exhaust into auxiliary condensers as the

*Bechtel Power Corporation, P.O. Box 3965, San Francisco, California 94119

latter are usually connected directly to the driver (see Figure 2). Elimination of the duct yields a performance advantage by reducing turbine-driver exhaust pressure. A further reduction in driver exhaust pressure is obtained if the auxiliary condensers are operated at a lower pressure than that in the main condenser. Reduction of driver exhaust pressure reduces its steam consumption and thus increases main turbine output. The following discusses these advantages in detail.

Eliminating the exhaust duct also eliminates its pressure loss penalty. The magnitude of this penalty depends on the selected duct size, duct flow rate, and main condenser pressure. A random examination of heat balance calculations by major turbine manufacturers and consultants reveals a near-universal use of a 12.70 mm (0.50 inch) Hg pressure difference between the driver exhaust flange and main condenser. This value is used at all loads and at all condenser pressures. The origin of the 12.70 mm (0.50 inch) Hg is obscure, and its use at all load and pressure conditions does not make sense.

Figure 3 shows exhaust duct pressure losses for a selected 500 MWe unit, plotted versus main condenser pressure, for the arrangement shown in Figure 1. Pressure losses are shown for three duct sizes and were calculated at constant turbine-driver efficiency, with the necessary steam flows to obtain equal driver output at all condenser pressures. The curves clearly demonstrate that for any arrangement there is, at most, only one condenser pressure at which duct pressure loss equals 12.70 mm (0.50 inch) Hg at a given load. Relatively large ducts, for instance, the 2.1 m (7 ft) duct of Figure 3, may never experience a pressure loss as high as 12.70 mm (0.50 inch) Hg. That is because this loss could only occur if the main condenser was operated at such a low pressure that the main turbine exhaust would be in a choking condition.

Generally, the straight length of the exhaust duct has a minor effect on its pressure loss. Fittings and condenser entrance loss are the largest contributors. Steam entering an auxiliary condenser also incurs an entrance loss although, in practice, it is probably of small consequence; however, the author has no firm data on the subject. The method of calculating exhaust duct pressure loss has been described elsewhere (3). For a selected duct size, the pressure loss penalty should be based on the condenser pressure chosen for the evaluation.

The use of auxiliary condensers may yield a performance advantage as their operation is independent of the main condenser. An auxiliary condenser may be sized to operate at any desired pressure, subject only to the limitations of the available cooling water temperature. In addition to eliminating the exhaust duct pressure loss, this arrangement offers the possibility of operating the turbine-drivers at a lower exhaust pressure than the pressure prevailing in the main condenser. This further enhances the performance benefits resulting from the use of auxiliary condensers.

For the selected 500 MWe unit, the benefits obtained from the elimination of the exhaust duct and the use of auxiliary

condensers may be assessed by reference to Figure 4. This figure shows the effect on turbine electrical output of differential pressure between turbine-driver exhaust and main condenser at the driver's rating point. Negative differentials apply only when turbine-driver auxiliary condensers are used. While positive differentials are also applicable to this arrangement, plant economics are unlikely to justify the use of auxiliary condensers designed to operate at pressures higher than those prevailing in the main condenser. Therefore, the positive differentials pertain to the arrangement in which the turbine-drivers exhaust to the main condenser via an interconnecting duct. The curves in the figure are based on a constant turbine-driver output and efficiency at rated driver exhaust pressure. The constant efficiency presupposes the availability of an ideally sized driver exhaust end for every selection.

Figure 4 shows that a given pressure differential has a larger influence on turbine electrical output at lower main condenser pressures. This is because the change in turbine-driver steam demand, for a given change in rated driver exhaust pressure, is larger at lower pressures. (The steam demand is not shown in Figure 4.) The larger change in steam demand produces a larger change in plant electrical output. For example, at a 127.00 mm (5.00 inch) HgA main condenser pressure, decreasing the rated driver exhaust pressure from 142.24 mm (5.60 inch) HgA to 127.00 mm (5.00 inch) HgA ($\Delta P = 15.24$ mm (0.60 inch) Hg) reduces the drivers' steam demand by about 0.375 kg/s (3000 lbm/h) and increases the plant output by 280 kWe. At a 50.80 mm (2.00 inch) HgA main condenser pressure, a decrease from 66.04 mm (2.60 inch) HgA to 50.80 mm (2.00 inch) HgA ($\Delta P = 15.24$ mm (0.60 inch) Hg) reduces the drivers' steam demand by about 0.631 kg/s (5000 lbm/h) and increases the output by 408 kWe. In practice, the increased output shown for main condenser pressures of 50.80 mm (2.0 inch) HgA or lower may not apply. This is because ideally sized driver exhaust ends for low pressures are uneconomical and rating pressures below 50.80 mm (2.0 inch) HgA are seldom economically justified (3).

The performance advantage resulting from the elimination of the duct may be gauged by assuming an average main condenser operating pressure of 76.20 mm (3.00 inch) HgA. For the 1.8 m (6 ft) diameter duct of Figure 3, a 76.20 mm (3.00 inch) HgA main condenser pressure produces a 7.62 mm (0.30 inch) Hg pressure loss. The elimination of this duct will result, according to Figure 4, in an increased output of about 175 kWe. Using auxiliary condensers that operate merely at pressures slightly lower than the main condenser pressure would further increase the output. Since the worth, in 1985 US dollars, of just 175 kWe will likely range between \$320,000 and \$580,000 (see Appendix), the performance benefits from the elimination of the exhaust duct and the use of auxiliary condensers could be substantial. It is noteworthy that the benefit from eliminating the exhaust duct tends to increase as average main condenser pressure decreases. This is because lower condenser pressures impose a higher specific volume on the exhaust steam. This necessitates the use of larger, and costlier, exhaust ducts, or operation with higher exhaust losses. Operation at lower average main condenser pressures, therefore, provides larger incentives to eliminate the duct.

Auxiliary condensers, operating at pressures below those prevailing in the main condenser, produce drains which, when returned to the main condenser hotwell, reduce the condensate temperature and thus adversely affect station electrical output. The magnitude of this effect was calculated and found to be relatively small. At the unlikely turbine-driver rating pressure of 38.10 mm (1.50 inch) HgA (i.e., a main condenser pressure of 50.80 mm (2.00 inch) HgA and a ΔP of -12.70 mm (-0.50 inch) Hg), the 410 kWe benefit indicated on Figure 4 is reduced to 400 kWe. For the same ΔP , the effect becomes even less significant at higher condenser pressures. The values plotted in Figure 4, therefore, neglect the effect of condensate cooling.

An auxiliary condenser suffers from the "inability to function as an acceptable deaerator...and...is generally designed and guaranteed for an oxygen content of the condensate of 0.03 cubic centimeters per liter or 0.01 cubic centimeters per liter" (4). These guaranteed quantities apply to full load conditions. Oxygen concentrations increase as load decreases. The auxiliary condenser's inability to deaerate properly is particularly acute during startup. Its drains must, therefore, be further deaerated in the main condenser. Oxygen content normally guaranteed for the main condenser is 0.005 cubic centimeters per liter and one manufacturer reports that the measured oxygen content for his condensers, at full load, is 0.002 cubic centimeters per liter (4).

The need to deaerate auxiliary condenser drains in the main condenser dictates that they enter the latter above or in the upper portion of its tube bundle. This will generally necessitate the use of auxiliary condensate pumps. If a multipressure main condenser with condensate reheating is used, auxiliary condenser drains may be routed directly to the lowest pressure shell below the tube bundle. Deaeration is then accomplished due to the reheating. Routing the drains to that lower elevation may permit dispensing with the auxiliary drain pumps because of the increase in available static head.

Auxiliary condensers also require a separate air removal system. In an evaluation, the performance penalties associated with the operation of this system, although secondary in magnitude, should be included.

The employment of auxiliary condensers precludes the use of a separate reheating hotwell with its attendant benefits. Separate reheating hotwells, as distinct from the condensate reheating system mentioned above, utilize part or all of the turbine-driver's exhaust steam to reheat the condensate in the main condenser. The extraction flow to the lowest pressure feedwater heater is thereby reduced, thus increasing electrical output. The operating and economic ramifications of this arrangement were detailed in a previous study (5). The study demonstrated, however, that the benefits of separate reheating hotwells are most pronounced at high main-turbine exhaust pressures and are substantially reduced as exhaust pressure decreases. This trend is opposite that encountered in Figure 4, which shows that an auxiliary condenser or any device which reduces turbine-driver exhaust pressure has the greatest benefit at low main-turbine exhaust pressures. Also, as pointed out earlier, the benefit of

eliminating the exhaust duct increases as exhaust pressure decreases. Therefore, if the main turbine operates mostly at relatively high exhaust pressures, as might be the case with plants that utilize cooling towers, the use of separate reheating hotwells for auxiliary turbine exhaust may be advantageous. Main turbines operating mostly at relatively low pressures are more likely to favor auxiliary condensers for their turbine-drivers.

On the circulating water side, the auxiliary condensers are arranged in parallel with the main condenser. From point of supply to point of return, the circulating water pressure loss in the auxiliary condenser loop always equals the pressure loss in the main condenser loop. Since the selection of the main condenser is not appreciably influenced by the auxiliary condensers, the pressure loss in the former determines the loss in the latter. Two-pass or multishell multipass condensers have an advantage here. Their higher pressure loss permits the use of longer secondary loops. This extends the range and, therefore, increases the number of possible locations for the auxiliary condensers.

Matching auxiliary to main condenser loop pressure loss presents one of the more intractable problems associated with auxiliary condensers. The problem has two components. First, actual circulating water flows may not equal the intended ones. Besides, it is hard to ascertain whether the intended flow rates are actually obtained, as circulating water flows are difficult to measure. Second, even if the existence of a mismatch in design flows can be ascertained, remedial action is difficult as such action would rely on the throttling of one or more flows. The throttling of circulating water flows is operationally awkward and introduces a performance penalty. Since the justification for using auxiliary condensers may, in some cases, have stemmed in large measure from the enhanced performance anticipated from their use, their advantage could depend on the skill of the designer in predicting the actual pressure loss in the auxiliary condenser loop.

c

Plants with auxiliary condenser loops, whose main condensers utilize syphon recovery systems, could be more vulnerable to loss of syphon, especially when an auxiliary loop is removed from or restored to service. Such an eventuality can be avoided, however, with proper system design and appropriate operating procedures.

EQUIPMENT

Turbine driven boiler feed pumps exhausting to the main condenser, are restricted to its vicinity, and their location is dictated, in large measure, by the available routing for their driver's exhaust ducts. The elimination of these ducts and the employment of auxiliary condensers increases the range of feasible pump locations and may enhance plant layout. The largest dividend due to the use of auxiliary condensers may, indeed, result from the increased freedom in locating the feed pump-driver train. This aspect of the analysis, however, is beyond the scope of this investigation, whose objective is to compare exhaust alternatives for feed pump-driver trains in the same location.

The layouts of the principal equipment and associated piping for the two arrangements under consideration are shown in Figures 1 and 2. In Figure 1, the pumps and drivers are installed at mezzanine level and exhaust downward into a space above the condensate level and below the tubes in the main condenser hotwell. Installing the driver at the mezzanine level also facilitates the collection of various driver drains. Exhausting downward is advantageous as it permits easy maintenance access from above, using the main crane or auxiliary hoists. The downward exhaust also allows the employment of a separate reheating hotwell which, as mentioned earlier, may be advantageous.

Figure 1 shows each auxiliary turbine exhausting through a pressure balanced "T" expansion joint arrangement to the main condenser hotwell. A motor-operated butterfly valve serves to isolate the driver from the condenser during maintenance.

Figure 2 depicts the boiler feed pump drivers, installed at mezzanine level, each mounted on an auxiliary condenser. Three pumps, one for each auxiliary condenser and one common spare, are provided to convey the auxiliary condensers' drains to the main condenser for additional deaeration.

Each auxiliary condenser must have an air removal system. For the purposes of this study, it was assumed that each condenser is furnished with air ejectors sized in accordance with the Heat Exchange Institute's recommendations (6). Thus, each condenser is equipped with a $0.0236 \text{ std m}^3/\text{s}$ (50 SCFM) hogging ejector and a $0.0024 \text{ std m}^3/\text{s}$ (5 SCFM) steam jet ejector. These are not shown in Figure 2.

Table 1 shows the capital cost components that might typically be included in an auxiliary condenser evaluation. The costs shown in the table depend greatly on equipment layout and prevailing labor rates. Capital costs for the scheme with drivers exhausting to the main condenser are shown to exceed those for the scheme using auxiliary condensers by \$70,000. However, the accuracy of the estimates and their sensitivity to variations in layout and labor costs limits the conclusion's general applicability. Although a recent study (7) also showed that capital costs favored auxiliary condensers, a previous study (2) found that capital costs favored exhausting to the main condenser. Most likely, for a fixed feed pump-driver train location, capital costs for the two schemes do not differ greatly. Therefore, if the performance gain resulting from the employment of auxiliary condensers is substantial, their use is indicated. Any advantage, due to the layout improvement they afford, will enhance their desirability. Conversely, design circulating water flows in the main and auxiliary condenser loops may be difficult to realize. Furthermore, their ancillary systems add complexity and some may require more maintenance. Therefore, auxiliary condensers should not be employed for small performance gains unless the incentive is buttressed by substantial layout gains.

TABLE 1 - Comparative Capital Costs¹ for a Selected 500 MWe Plant,
Expressed in January 1985 US Dollars.

	Drivers Exhausting to Main Condenser	Drivers Exhausting to Auxiliary Condensers
Main condenser	170,000	Base
Auxiliary condensers	Base	380,000
Exhaust ducts and isolating valves	375,000 ²	Base
Auxiliary turbines	60,000 ³	Base
Circulating water system	Base	55,000
Air removal system	Base	70,000
Auxiliary condenser drains system	<u>Base</u>	<u>30,000⁴</u>
Total comparative cost	70,000	Base

Notes:

1. All costs include installation.
2. Includes \$100,000 for installation labor. This amount could be lower, depending on the extent of duct shop assembly.
3. Assumes that drivers will be rated at an exhaust pressure 12.70 mm (0.50 inch) Hg higher than those exhausting to an auxiliary condenser.
4. Includes hotwell level control valves and pump discharge check valves, which are not shown in Figure 2.

CONCLUSIONS

1. The performance benefits of auxiliary condensers are most pronounced in plants that operate at relatively low main-turbine exhaust pressures.
2. For the same feed pump-driver train location, there is, most likely, no significant difference in capital costs between the scheme that utilizes auxiliary condensers and the one in which the drivers exhaust to the main condenser.
3. The use of auxiliary condensers affords more freedom in the location of the feed pump-driver train. This may substantially reduce capital costs in favor of auxiliary condensers.

APPENDIXThe Worth of Incremental Electrical Output

Incremental electrical output may be evaluated by a number of methods. In one, a desired net electrical output is postulated and held constant. Thus, for this output, any change in electrical efficiency is translated into a corresponding change in equipment size (i.e., capital costs) and fuel consumption. This method, which leads to relatively low assessments for efficiency, will be used here.

In a different method, a fixed plant heat input is postulated, and efficiency changes are translated into changes in plant electrical output. This differential output is evaluated at replacement energy rates. Although entirely legitimate, this method, by definition, places a higher premium on efficiency than the previously discussed method. If an investment can be justified based on the former method, its justification will be even more pronounced when higher efficiency-cost figures are employed. The use of lower efficiency-assessment figures for the auxiliary condenser analysis is, therefore, more conservative.

Mid-1978 capital costs of a 500 MWe coal-fired plant, conforming to the US Environmental Protection Agency's June 1979 New Source Performance Standards, have been estimated to range between 808 and 990 US dollars per installed kWe (8). These costs were escalated to the year 1985 in the following manner:

Escalation for coal-fired plants between June 1978 and December 1981, based on historical data compiled by the author's company, is 36.5%. Assumed escalation for the years 1982 through 1984 is 9% per annum.

∴ Range of capital costs in January 1985:

$$1.365(1.09)^3 \cdot 808 = \$1428/\text{kWe}$$

$$1.365(1.09)^3 \cdot 990 = \$1750/\text{kWe}$$

Assume that an incremental kWe costs 85% of an average kWe (9).

∴ Range of incremental capital costs in January 1985:

$$0.85 \cdot 1428 = \$1214/\text{kWe}$$

$$0.85 \cdot 1750 = \$1488/\text{kWe}$$

To calculate the cost of fuel associated with an incremental kWe, the following was assumed:

Plant heat rate = 2.9307 kJ/kWs (10,000 Btu/kWh)

Plant load factor = 70%

Fixed charge rate = 20%

Range of levelized* fuel costs = \$1.89 to \$5.69 per million kJ
(\$2.00 to \$6.00 per million Btu)

(Note: at \$34/bbl, oil costs $\frac{34.00}{6.2 \cdot 10^6} = \5.48 per million kJ, or

$$\frac{34.00}{5.9 \cdot 10^6} = \$5.76 \text{ per million Btu})$$

For \$1.89 per million kJ (\$2.00 per million Btu):

$$\begin{aligned} \text{Fuel cost} &= 2.9307 \text{ kJ/kWs } (8760 \cdot 0.70 \cdot 3600) \text{ s/yr} \cdot \$1.89/10^6 \text{ kJ} \cdot 1/0.20 \\ &= 10^4 \text{ Btu/kWh } (8760 \cdot 0.70) \text{ h/yr} \cdot \$2.00/10 \text{ Btu} \cdot 1/0.20 \\ &= \$613/\text{kWe} \end{aligned}$$

For \$5.69 per million kJ (\$6.00 per million Btu), fuel cost =
(6/2) 613 = \$1839/kWe

The total cost of an incremental kWe, therefore, ranges between:

$$1214 + 613 = \$1827/\text{kWe}$$

and

$$1488 + 1839 = \$3327/\text{kWe}$$

*For a series of annual costs, P_1, P_2, \dots, P_n , the levelized cost is defined as the sum of the present worthsⁿ of the annual costs. Thus, the levelized cost

$$P_L = \frac{P_1}{(1+i)} + \frac{P_2}{(1+i)^2} + \dots + \frac{P_n}{(1+i)^n}.$$

where i = discount rate and n = number of years for which the study is conducted.

For 175 kWe, the performance advantage, expressed in 1985 US dollars, ranges between:

$$175 \cdot 1827 = \$319,725$$

$$175 \cdot 3327 = \$582,225$$

ACKNOWLEDGEMENTS

The author is indebted to Messrs. J. T. Phillips and R. L. Ward of Southern Engineering Company and Mr. T. K. Pullen of Ecolaire Incorporated for their advice during the course of the preparation of this paper. However, responsibility for its contents rests solely with the author.

Thanks are due also to Mr. S. A. Marder of the Bechtel Power Corporation for his editorial help.

REFERENCES

1. Coit, R. L., "Design Trends in United States Utility Feedwater Heaters and Condensers," Combustion, February 1975.
2. Muhlhauser, H., "Modern Feed Pump Turbines," Brown Boveri Review, October 1971.
3. Bornstein, B., and Harris, L., "Selecting an Optimum Rating for Feed Pump Turbine Drivers," ASME 78-JPGC-Pwr-4.
4. Palmer, W. E., and Pullen, T. K., "Steam Condensers for Central Station Mechanical Drive Turbines," 1968 Proceedings of the American Power Conference, Vol. 30, pp. 458-468.
5. Harris, L., and Bornstein, B., "Condensate Reheating and Separate Reheating Hotwells for Central Station Main Condensers," ASME 78-JPGC-Pwr-14.
6. Heat Exchange Institute Standards, Standards for Steam Surface Condensers, seventh edition, Tables 4 and 5.
7. Mounts, J. G., "BFP Turbine Exhaust Auxiliary Condenser versus Main Condenser," 1979 Proceedings of the American Power Conference, Vol. 41, pp. 528-533.
8. Bechtel Power Corporation, Coal-Fired Power Plant Capital Cost Estimates, EPRI Report PE 1865, Project TPS 78-810, Final Report, May 1981, p. 2-3.
9. Ibid, p. 6-21.

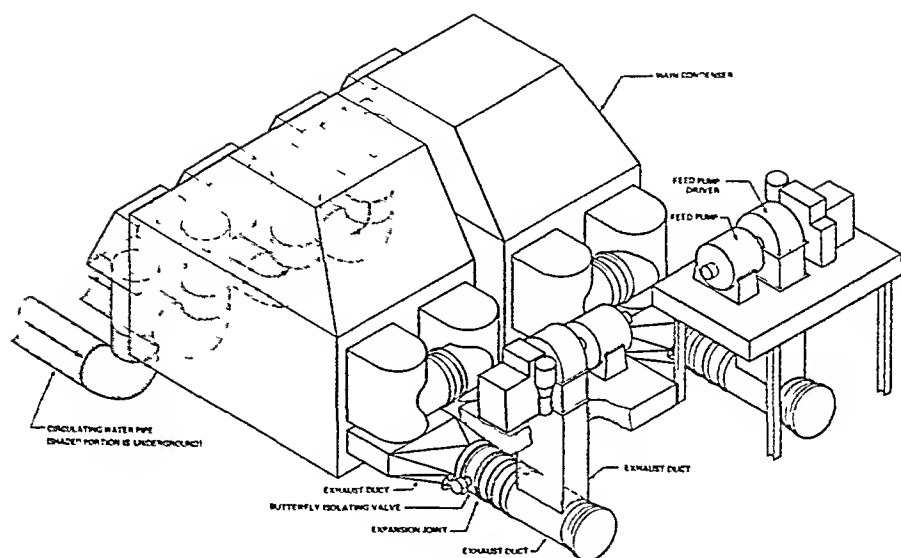


FIGURE 1. FEED PUMP TURBINES EXHAUSTING TO MAIN CONDENSER

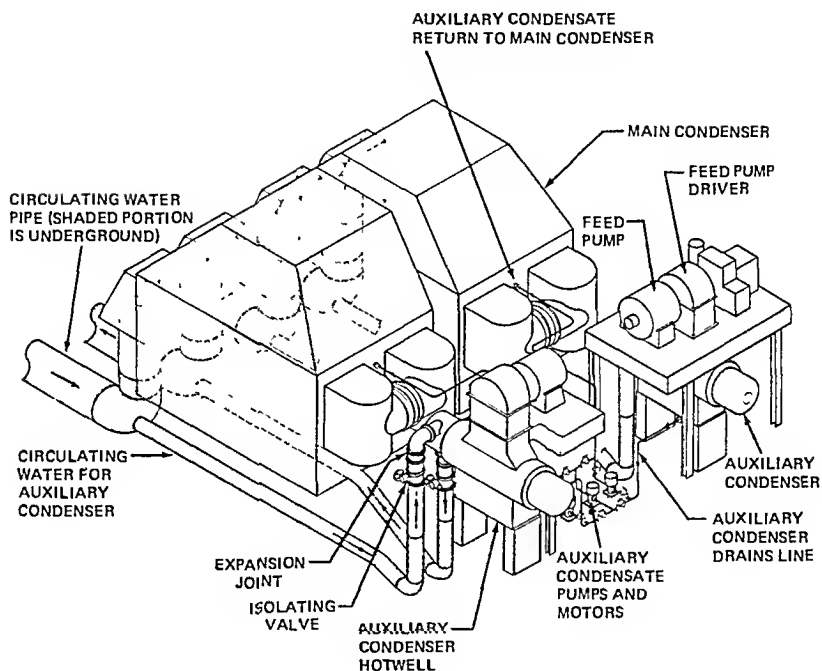


FIGURE 2. FEED PUMP TURBINES EXHAUSTING TO AUXILIARY CONDENSERS

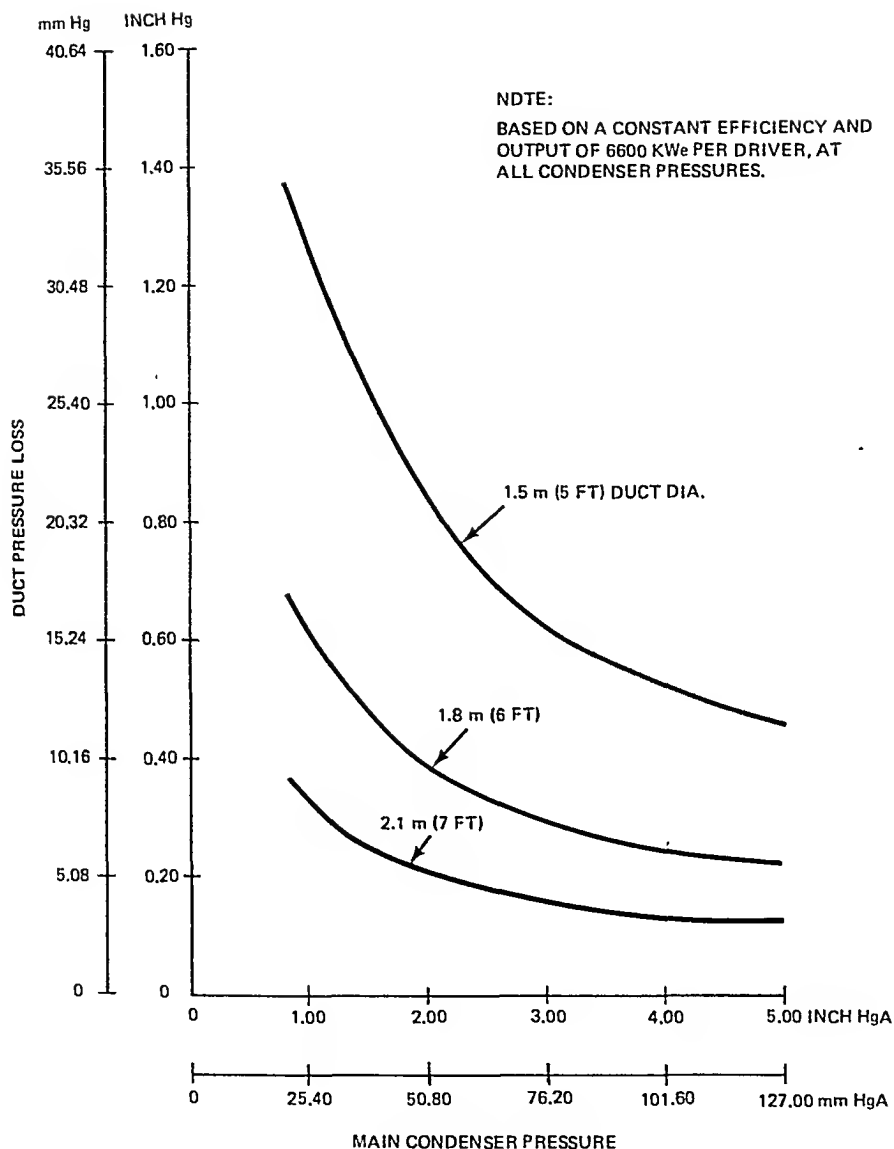
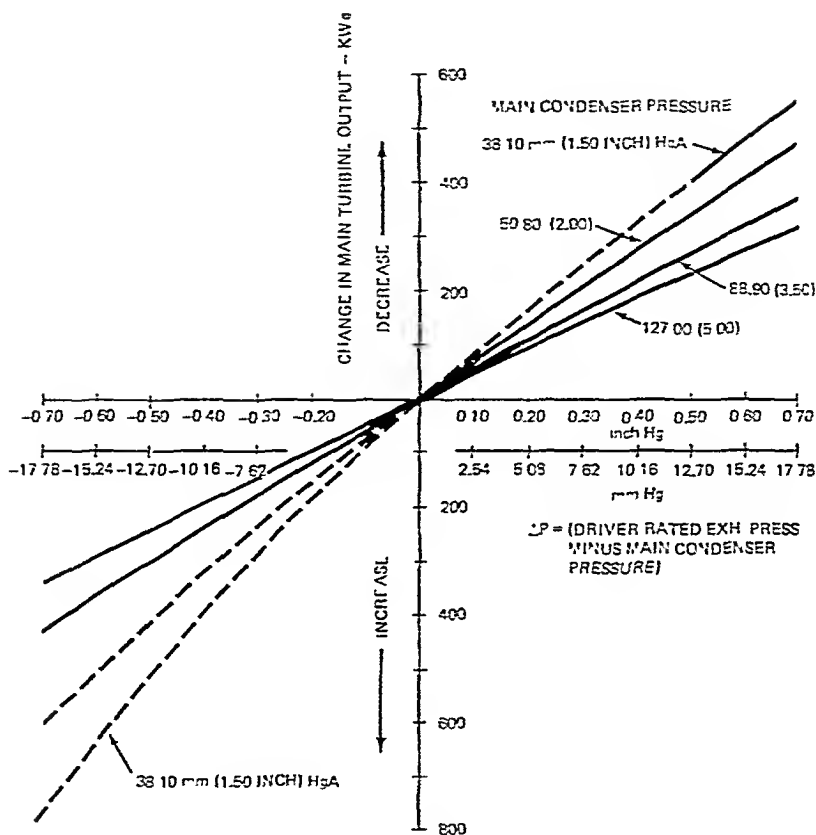


FIGURE 3. PRESSURE LOSS IN TURBINE DRIVER EXHAUST DUCT
FOR A SELECTED 500 MWe PLANT



NOTES

1. MAIN TURBINE IS TANDEM-COMPOUND 4-FLOW 68 cm (26 INCH) LAST-STAGE BLADES 5500 RPM, WITH INITIAL STEAM CONDITIONS OF 165.5 BAR GAUGE 540°C/540°C (2400 PSIG 1000°F/1000°F)
2. CURVES ARE FOR MAIN TURBINE OPERATING WITH VALVES WIDE OPEN AND AT 5% OVER RATED THROTTLE PRESSURE.
3. TURBINE-DRIVER OUTPUT AND EFFICIENCY ASSUMED CONSTANT AT ALL EXHAUST PRESSURES
4. DOTTED LINES SHOW PERFORMANCE CHANGES THAT MAY NOT BE ATTAINABLE IN PRACTICE.

FIGURE 4. EFFECT OF BOILER FEED PUMP TURBINE-DRIVER EXHAUST PRESSURE AT RATING ON MAIN TURBINE OUTPUT FOR A SELECTED 500 MWe PLANT

ASSESSING THE EFFECT OF STAINLESS STEEL TUBES ON
CONDENSER PERFORMANCE AND INTEGRITY

Jack R. Maurer*
Frank H. Berendsen**

The condenser tube is the primary barrier to the intrusion of aggressive environments into power generation feedwater systems. Its cost, integrity and performance are key items in the attempt to provide and improve economical, reliable and efficient service.

This paper will review the introduction, growth and innovations provided by stainless steel tubing during the past quarter century in the United States. Particular emphasis will be given to the newer corrosion resistant alloys (AL-6X and AL 29-4C) specifically developed for the more aggressive marine environments. The characteristics of various alloys which make them suitable for condenser service will be reviewed with emphasis on corrosion resistance, heat transfer, vibration, installation techniques for strength and tightness and galvanic interactions between materials.

INTRODUCTION

The past quarter century has seen a number of changes in the manner of producing electrical power, the cost and availability of fuels, environmental concerns, conservation and in other areas. These have greatly affected the design and operation of the condenser since this equipment plays an important role in each of these areas.

The major component in the condenser is the tubing. It provides a thin barrier to a harsh, aggressive environment that can cause considerable harm to the balance of the plant if that barrier is breached. Its performance also affects the cost of producing electricity. Interactions between tubing and the balance of the condenser also affect the cost, efficiency and reliability of the entire system.

Stainless steels were introduced as condenser tubing in the United States in the mid-1950's. Initially, these alloys were used to solve specific problems such as steam impingement erosion, ammonia corrosion and to provide resistance to acid mine waters. Relatively high costs and anticipated poor heat transfer performance kept the development and use at a "low level" for a decade. More recently, however, highly competitive costs, recognized heat transfer performance, and new high technology alloys designed for extremely aggressive environments have increased the usage of these materials.

BACKGROUND

Over 700 million linear feet of stainless steel tubing are now in use in power plant condensers in the United States. Most of this is Type 304, a basic 18% chromium, 8% nickel austenitic stainless steel, used in fresh, industrial mine and cooling tower applications. A small amount of Type 316, which contains

*Allegheny Ludlum Steel Corporation, Brackenridge, Pennsylvania, U.S.A.

**Allegheny Ludlum Steel Corporation, Dusseldorf, West Germany

about 2 1/2% molybdenum, is also used on these applications. Type 316 was originally considered for marine environments, but this application proved too severe. The introduction of the newer high technology alloys such as AL-6XTM and AL 29-4CTM provided materials with the necessary performance characteristics for these areas. A relatively new ferritic stainless steel, Type 439, is also being used as an alternate to Type 304 in condensers and offers several advantages as feedwater heaters and finned moisture separator reheater tubing. The typical chemical analysis and mechanical properties of these alloys are provided in Tables 1 and 2.

TABLE 1 - Typical Chemical Analysis of Condenser Alloys

Alloy	Composition (Wt. Percent)			
	Cr	Ni	Mo	Ti
304	18	8	-	No
316	17	12	2.5	No
AL-6X	20	24	6	No
AL 29-4C	29	-	4	Yes
439	18	-	-	Yes

TABLE 2 - Typical Mechanical Properties

Alloy	Condition	.2% YS (MPa)	TS (MPa)	% E (5.08 cm)
304	Annealed	241	586	60
316	Annealed	276	586	50
AL-6X*	As-Welded	427	627	30
	Annealed	290	558	50
AL 29-4C*	As-Welded	648	683	18
	Annealed	531	648	26
439*	As-Welded	539	565	20
	Annealed	352	510	40

*These alloys are supplied in both conditions.

AL-6X alloy has been in service since 1970. Twenty-eight condensers are now completely tubed with this alloy representing 30 million linear feet. Applications cover a wide variety of exposures, including four nuclear units. Several million tube inserts have been installed of this material to protect the inlet ends of soft erosion-prone brass alloy tubes. The chromium plus molybdenum content provides a high chloride, seawater resistant material. AL 29-4C alloy has been in service since 1980 and is the chosen alloy for nine installations using 7 million linear feet. It is more resistant to aggressive

TM Trademark of Allegheny Ludlum Steel Corporation

environments and because of its leaner alloy content, is less expensive. Both alloys were chosen because of the advantages they offered over titanium tubes, and in most cases represented a solution to the catastrophic failure of brass or cupro-nickel tubes.

Type 439 has been used in four applications, two industrial and two utility condensers, one of which is a 665 MW nuclear unit. The most widespread application of the alloy in utility service has been as integrally finned moisture separator reheater tubes (1), (2). Over 7 million feet have been installed, mostly as replacements for carbon steel and 90-10 cupro nickel in the United States and is now being specified for many additional units throughout the world. The advantage of a ferritic stainless steel, in addition to its other attributes, is stress corrosion cracking resistance. This property may lead to increased usage in feedwater heaters where some failures of this type have already been experienced with Type 304 (but not in condenser applications).

If one omits the misapplication of Type 316 in seawater units where most tubes have now been replaced, the stainless steels have an exceptional record. Less than 0.1% of all the tubes installed since 1957 have failed. The only complete failure to-date resulted from cleaning the Type 304 tubes with "inhibited" hydrochloric acid, a very poor practice (similar to cleaning copper tubes with nitric acid). A second unit is reported in difficulty as a result of an exceptionally long outage (six months) with the tubes filled with stagnant water.

The primary failure modes for stainless steels (where they do occur) have been pitting/crevice corrosion, and vibration damage. The severity of the cooling water environment (chlorides) and the tendency toward deposit formation or biofouling are the primary causes of localized corrosion. The newer alloys (AL-6X and AL 29-4C) were specifically designed to overcome these problems. Vibration damage is more of a design problem and severity is a function of a material's modulus of elasticity and tube wall thickness.

Two recent seminars sponsored by the Electric Power Research Institute (3), (4) considered the problem of condenser tube failure and their prevention. The vast majority of discussions were devoted to problems with copper alloy tubes since this is where most problems have occurred. There was little to discuss concerning the stainless steels and titanium, not because of lack of exposure and service experience, but because of lack of problems. This was further confirmed in a recent study by Rios and Shorr (5) who concluded that both Type 304 and Type 316 would meet the basic forty-year life criteria even under such adverse exposure conditions imposed by the concentration of corrosives in cooling tower applications.

HEAT TRANSFER

One of the major drawbacks to the development of stainless steel tubes has been the heat transfer factors assigned to these materials. When comparisons are made to the thermal conductivity coefficients of copper base alloys, the stainless steels appear to have a major disadvantage. This is carried through in many analyses, even though they take into account some of the surface films and other resistances to heat flow.

The Heat Exchange Institute (HEI) sets the standards in the United States. The standards for material and gage factors were based on tests at the Lehigh University calorimeter. Despite obvious shortcomings detailed by Wenzel (6), little has been done to establish realistic design criteria. In his paper Wenzel describes the basic problem with admiralty brass when shelf-aged (stored

after manufacture) for a period of time which results in a minimum performance loss of at least 10 percent. The problem is not "aging" in a metallurgical sense but corrosion product formation (oxides or refractory type scales) which definitely affects the performance of the more susceptible brass alloys, but not stainless steel or titanium. The report also lists as a systematic error the failure to arrive at a steady state condition, yet the short tests performed (8 hours) have no hope of reaching a true steady state despite the relatively ideal conditions of the laboratory, because the tube materials have not reached a steady state with their environment.

While the data is now two decades old, the work of McAllister and his co-authors (7) at Lamar provide a much more realistic approach to heat transfer through condenser tube walls. Their studies show the effect of exposure on the overall heat transfer coefficient of different alloys. Tests reported in their paper cover a 120-day exposure but the author has received data from Dr. McAllister for 550-days of exposure. Figure 1 illustrates the effect of this "exposure aging" where initially the heat transfer through brass tubes exceeded that through stainless steel, but the greater effect of "exposure" (fouling and corrosion) on brass soon reversed their positions.

A further analysis of the Lamar paper shows that the effects are not limited only to admiralty brass, but include all the copper alloys tested with similar performances from the various stainless steels which were tested. Some of these curves are shown in Figure 2.

The excellent heat transfer performance results of stainless steels, competing with copper alloys have been shown on several occasions. Long (8) was one of the first, reporting on his experiences with Type 304 tubes in the first all-stainless units where his data showed stainless steel was operating at better than 100% clean which meant the material and gage factors were in error. Salomon (9) provided some insight to the excellent performance of one of the newer alloys, AL-6X, in its first complete installation.

We believe there is now sufficient evidence to show that the stainless steels will perform at least to the same level as copper base alloys once the material has achieved a steady state with the environment. There are three time periods; the initial phase when the lack of corrosion product film allows the copper alloys to perform more efficiently, the second phase where near stable conditions exist and the various alloys perform similarly and the final phases where the stainless alloys may actually out-perform the copper. Time periods for the various phases will vary depending on the severity of the environment and time it takes for corrosion product film to form, but "steady state" conditions are normally achieved within 18 months.

There is no question that the work done by the HEI is valuable and provides a base line for some evaluation, but the commonly used practice to assign "better" cleanliness factors to stainless designs is a compounded error. The "shelf-aged" or "exposure aged" condition is the base line and should be investigated in depth.

It is also unfortunate that the calorimeter at Lehigh University is no longer being used to evaluate materials. Since this work was discontinued several years ago, a number of new alloys (AL-6X, AL 29-4C, Type 439 and others) have appeared and a significant number of applications have been made of each. This type of information is sorely needed for future design and application if utilities are to make sound engineering decisions regarding material selection and then use them most efficiently.

VIBRATION

One of the most important attributes of stainless steels is their high modulus of elasticity ($29 - 31 \times 10^6$) which permits the use of thin walled tubes for both initial and replacement applications. The most common application for stainless steel in the United States is 22 BWG (.028" or .7 mm). This was established by Allegheny Ludlum in 1957 and over 98% of all tubes installed are of this gage. Heavier gages have been used but this is not an economically sound decision since heat transfer is reduced and the cost of the tubes is increased. The most common thickness for seamless copper alloys is 18 BWG (.049" or 1.25 mm) and 20 BWG (.035" or .9 mm) for welded 90-10 cupro nickel.

An analysis of vibration failure susceptibility based on Coit's (10) formula of:

$$L = 9.5 \frac{EI}{\rho V^2 D} \quad 1/4$$

when:

L = tube spacing, mm (in.)

E = tube material modulus of elasticity, N/m² (psi)

I = tube cross sectional moment of inertia, mm⁴ (in.⁴)

ρ = turbine exhaust steam density, kg/m³ (lb./ft.³)

V = average exhaust steam velocity at condenser inlet,
m/s (ft./s)

D = tube diameter, mm (in.)

and by keeping diameter, velocity, density and tube spacing constant for a given situation, provides the following comparison in Table 3.

TABLE 3 - Minimum Wall Thickness to Prevent Vibrational
Damage for a Specific Application

<u>Tube Material</u>	<u>Minimum Wall Thickness</u>	
	<u>mm</u>	<u>in.</u>
Admiralty	1.07	0.042
Titanium	1.07	0.042
90-10 Cu Ni	0.84	0.033
Type 304	0.51	0.020
AL-6X	0.51	0.020
Type 439	0.48	0.019
AL 29-4C	0.48	0.019

This is of considerable importance for retrofit units with fixed tube support sheets. It permits the use of thin gage stainless steel to replace heavier walled copper alloy tubes without the need of additional support. The use of titanium would necessitate additional and repositioned supports, stiffeners, dampeners (stakes), or heavier walled tubes. In one recent application, a utility in the United States paid a \$7 million premium to use titanium over AL-6X alloy, not including the cost of an extended outage to accomplish the changes, not a very cost effective solution.

INSTALLATION

The integrity of the condenser and its influence on the reliability of the entire plant is not only affected by the choice of materials and the designs that incorporate them into a functioning system, but also on the methods, procedures and quality of installation techniques. If one hopes to achieve a high degree of reliability, it is important that tube installation be given major consideration.

Recent publications have dealt with the subject in some depth (11), (12), far beyond the scope of this paper. The author would like to touch on only a few of these aimed to promote a higher quality installation. The subjects to be covered briefly are shipment and storage of tubes, tube and support sheet preparation, rolling or expansion, and flaring.

A great deal of care is taken to select and specify materials and to insure they are made under controlled conditions. Boxing may also be specified in great detail. On far too many occasions, tubes are shipped and stored with little control prior to installation. They have been known to arrive in rail cars submerged under water or are stored in areas where streams can overflow or ground depressions can trap rain water and cover tubes. This has occurred where specifications insisted tubes be rinsed in zero chloride water, following processing. On other occasions, boxes have been stored partially opened, under bridges, heavily salted in winter months to melt ice and snow.

Retubed units often create problems as a result of corrosion and deposits between tubes and tube support sheet holes. The old tubes are frequently difficult to remove and new tubes are inserted without adequately preparing holes by removing the buildup. Difficulties at this point are sometimes compounded by hitting the tube ends with sledges or wooden beams to drive them into the unit.

Roller expansion is one of the key factors for reliable condenser operation. Tight, strong joints are intended with a minimum of tube and tubesheet damage. To achieve this, it is imperative that proper expanders be used (five rolls are better than three rolls) with material properties and geometrics in mind. Tube expansion should be limited to prevent distortion of the tubesheet. Procedures designed to produce repetitive results with built-in quality checks are absolutely necessary. Planned rolling sequences are also necessary to tie-in the tubesheets, reducing distortion and keeping stresses to a minimum.

Probably the two most misunderstood concepts in this area are wall thinning and the effects of grooves. Formulas to determine the amount to expand most often develop their answer based on a percentage of the tube wall thickness. Hard tube materials such as titanium and the stainless steels do not "thin" as expanded into condenser tubesheets. Any thinning that does occur is simply the result of stretching the tube to a new and greater diameter. The only measurable dimension after rolling is the inside diameter of the tube. This is a key variable and must be controlled since distortion of the tubesheet

is a compounding error not easily corrected once initiated.

Grooves in tubesheet holes are frequently required by specification to increase the holding strength of the joint. This may well be a successful approach for softer materials such as brass alloys which can be expanded into the grooves, but for harder materials such as the stainless steels and titanium, we have found that the greater the amount of groove area, the lower the pull-out strength of the joint. Wyzalek and Obermaier (13) recently reported their experiences which confirm those of the author (14). One possible approach that appears successful in substantially increasing the joint strength without over-rolling and distorting the tubesheet is the use of an anaerobic sealing and locking compound.

Another historic practice that is slowly changing is the use of flared ends. There was a need for this design feature when units were tubed with erosion prone alloys, but the newer materials have eliminated that need. The author has never seen an example of inlet-end erosion, whatever the velocity where a stainless steel or titanium tube has been used. Flaring requires special machining of the tubesheets and an extra operation during the installation of the tubes, at a considerable cost penalty with no advantage gained.

GALVANIC CORROSION

One of the few topics of concern when using the newer alloys has been the potential problem of galvanic corrosion between tubes, tubesheets and water boxes. The data resulting from research performed at Ocean City Research sponsored by Allegheny Ludlum Steel Corporation and others (15), (16), (17) provide the most definitive work yet published in this area. This research provides an understanding of what is occurring and also provides direction in reducing, solving and eliminating the problem.

When stainless steels and titanium are used in fresh water environments with Muntz Metal, naval brass, or aluminum bronze tubesheets, there have been no problems because of the extremely low conductivity of the electrolyte. This changes dramatically when the tubes are produced from the very noble metals and used in seawater cooled condensers. The effect, if not controlled, can result in excessive corrosion of the tubesheets. Table 4 illustrates the results of tests where forty foot tubes were coupled to representative tubesheet areas and exposed to full strength seawater at 7 fps and the less noble metal was allowed to corrode under the influence of galvanically accelerated conditions.

TABLE 4 - Corrosion Rate of Tubesheets Based on Weight Loss Measurements

<u>Couple</u>	<u>Corrosion Rate mm/yr.</u>
AL-6X/904L	0.00864
AL-6X/Muntz	2.80
AL-6X/Al Bronze	1.07
Ti 50A/Muntz	6.96
Ti 50A/Al Bronze	3.20
90-10 Cu Ni/Muntz	0.846

A more insidious problem is the dealloying effects resulting from the galvanic couples. This is a problem because the true extent of the damage is camouflaged from the viewer. These are described in Table 5 in terms of a measurable rate and more graphically in Figure 3 where the extent of dezincification of Muntz metal tubesheets coupled to titanium and AL-6X tubes is displayed.

TABLE 5 - Maximum Dezincification Rate of Muntz Metal Tubesheets Coupled to Noble Tube Materials

<u>Couples</u>	<u>Maximum Dezincification Rate, mm/yr.</u>
AL-6X/Muntz	16.1
Ti 50A/Muntz	25.8

This type of attack is more insidious since it frequently goes un-noticed until considerable damage has occurred. In one operating unit with titanium tubes and Muntz tubesheets, dezincification to the extent of 3/4" depth occurred in a few months. The redeposition of copper as a soft, spongy mass with little strength or integrity masks the seriousness of the situation and sometimes goes undetected until major problems arise.

Knowledge of the problem and mechanisms which create it, provides possible solutions. For those units tubed with AL-6X alloy in the United States, several corrective measures have been used successfully. The best solution is to use compatible materials and in this case Type 316 has been found to be an excellent tubesheet material in several seawater applications with no detected pitting, crevice corrosion or other problems in over six years of operation. Other tubesheet possibilities are 904L, 317LX and 254SMO but these are more expensive. Impressed current cathodic protection systems have also been used successfully. Coatings have been used with mixed success and are probably best when coupled with an impressed current cathodic protection system. There is increasing evidence that some of the systems may be introducing new and unexpected problems making it imperative to properly design and control impressed current cathodic protection systems if they are to operate successfully.

CONCLUDING REMARKS

There exists today, a variety of tube materials for condenser applications, some more successful in preventing problems than others but each with its own advantage and disadvantage. As a group, the stainless steels have proven themselves, for over a quarter of a century, to be the best combination of all factors. Most frequently the stainless alloys have been used in the more difficult applications and in particular in those areas where other materials have failed or given unsatisfactory performance. The newer, high technology stainless alloys have extended this level of service to include some of the most aggressive environments, coupled with the most demanding requirements for integrity and efficiency.

This paper has briefly reviewed the development and attributes of the various stainless alloys, as well as some of the more pertinent aspects of their application. No single material has ever, or will ever prove to be completely adequate for all situations, but when the stainless steels are given a complete and realistic evaluation, they offer the most attractive potential to meet the requirements of today's demanding power plant designs.

REFERENCES

1. Gibson, J., 1981, "Redesign and Replacement of Connecticut Yankee MSR Tube Bundles", Joint Power Conference, St. Louis, Missouri, U.S.A.
2. Kratz, J., and Minard, P., and Weinberg, D., 1982, "Alloy Selection Considerations and Service Experience of the First In-Service 439 Stainless Steel MSR Tube Bundles", Joint Power Conference, Denver, Colorado, U.S.A.
3. Conference Proceedings, 1981, "Prevention of Condenser Failures-The State of the Art", EPRI, Palo Alto, California, U.S.A.
4. Conference Proceedings, 1981, "Prevention of Condenser Failures-The State of the Art", EPRI, Arlington, Virginia, U.S.A.
5. Rios, J., and Shorr, S., 1982, "Performance of Stainless Steel Tubes in Condensers Associated with Cooling Towers", ASM Power Conference, Hershey, Pennsylvania, U.S.A.
6. Wenzel, L., 1962, "Measurement of the Performance of Condenser Tubes", American Power Conference Proceedings, Chicago, Illinois, U.S.A.
7. McAllister, R., Eastham, D., Dougharty, N., and Hollier, M., 1961, Corrosion 17, 579t.
8. Long, E., 1959, "Experience with the Use of Stainless Steel Condenser Tubes", 20th Water Conference, Pittsburgh, Pennsylvania, U.S.A.
9. Salomon, J., 1977, "Improved Condenser Performance at Bridgeport Harbor Station", EEI Prime Movers Meeting, Kansas City, Missouri, U.S.A.
10. Coit, R., 1972, "Design Trends in United States Utility Feedwater Heaters and Condensers", Inco Power Conference, Lausanne, Switzerland.
11. Boyd, G., 1982, "Some Considerations for Tubing Condensers in the Field", Nuclear Engineering Conference, Portland, Oregon, U.S.A.
12. EPRI Report NP2371, 1982, "Condenser Tubing Criteria Manual".
13. Wyzalek, L., and Obermaier, H., 1982, "Evaluation of New Tube Alloys for Condenser and Heat Exchanger Service", Joint Power Conference, Denver, Colorado, U.S.A.
14. Maurer, J., and Vuillaume, D., 1982, "High Technology Materials for the High Technology Requirements of Marine Fossil and Nuclear Steam Condensers", SFEN Condenser Colloquium, Avignon, France.
15. Kuester, C., Maurer, J., and Gehring, G., 1980, "Effective Tube Length-A Consideration of the Galvanic Performance of Marine Heat Exchanger Materials", CORROSION/80, Chicago, Illinois, U.S.A.
16. Gehring, G., and Kyle, R., 1982, "Galvanic Corrosion of Selected Tubesheet/Tube Couples Under Simulated Seawater Condenser Conditions", CORROSION/81, Toronto, Canada.

17. Gehring, G., and Kyle, R., 1982, "Galvanic Corrosion in Surface Condensers Tubed with Either Stainless Steel or Titanium", CORROSION/82, Houston, Texas, U.S.A.

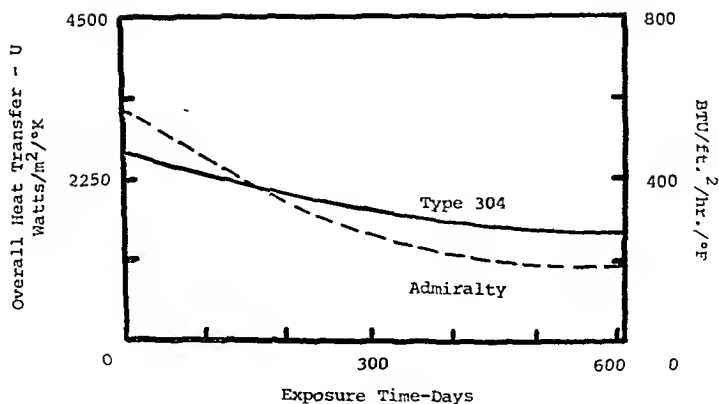


Figure 1 Effect of Exposure on the Heat Transfer of Two Alloys Over an Extended Period

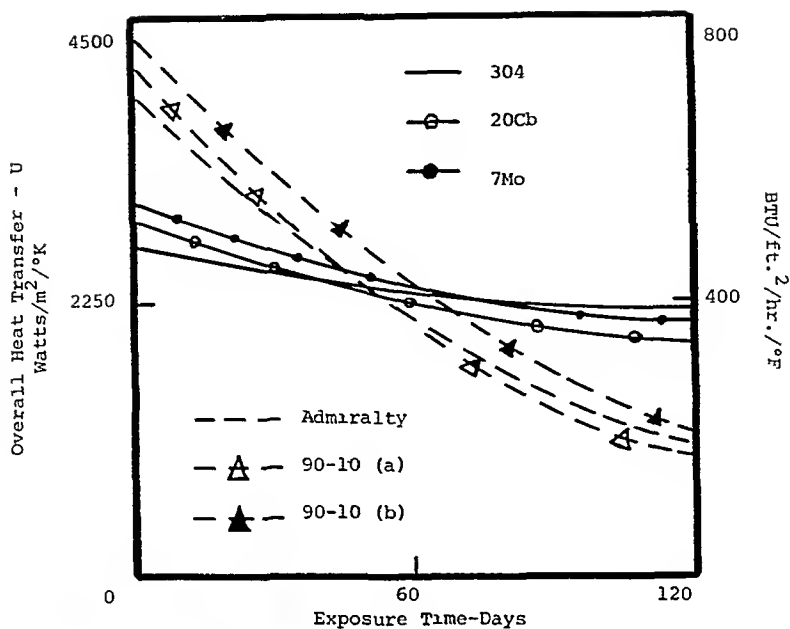


Figure 2 Effects of Exposure on Heat Transfer Performance of Similar Alloys

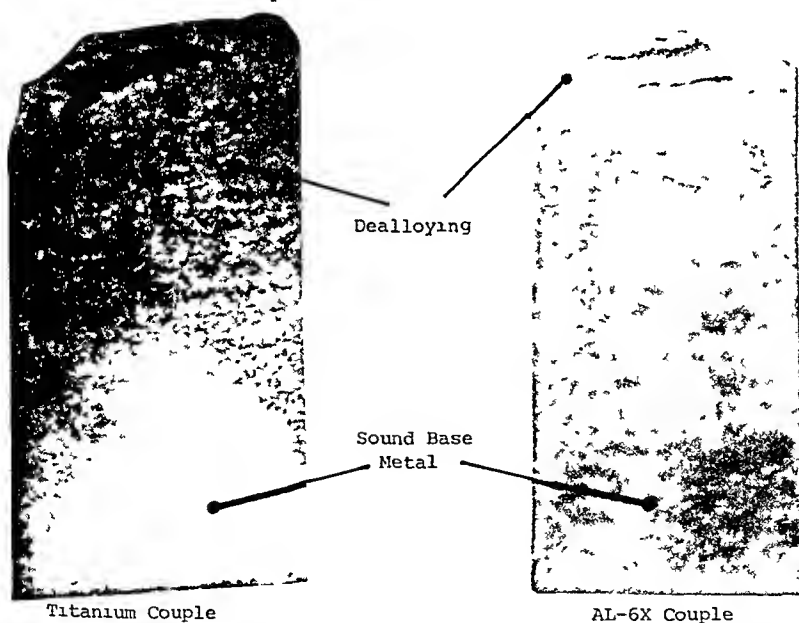


Figure 3 Cross Section of Muntz Tubesheets After Coupling with Tube Materials for Seven Months in Seawater

THE WYLFA CONDENSERS - CONSTRUCTION AND OPERATIONAL
PROBLEMS AT A NUCLEAR POWER STATION

F. John L. Bandon*

Nuclear power stations because of their lower operating costs compared to the fossil fuelled stations are operated as the base load component of the system. Thus, high load factors are sought and in the case of Wylfa power station with its once-through boilers a very strict chemical regime is required. Condenser leaks therefore represent a charge against a safe and economic system of generation. The paper describes the operating regime at Wylfa Power Station.

INTRODUCTION

The commercial nuclear power stations built in the U.K. have been operated as the base load of the C.E.G.B. system because of their low fuel costs compared to coal and oil-fired stations. It is thus apparent that any loss of output or availability of these stations has to be minimised.

Wylfa Nuclear Power Station was the last of the Magnox design to be built under the first nuclear programme announced in 1955 by a Government White Paper (Cmd 9389).

The 1,000 MW station is located on the North West coast of the Isle of Anglesey, North Wales, its output being connected to the 400kV national grid network, via a single, double-circuit line to the mainland 35km away.

The twin reactor station was designed with prestressed concrete pressure vessels, the boilers being an integral part. The boilers have been designed to operate on the once-through mode, and therefore the chemical conditions are extremely strict. Thus, any contamination such as condenser leaks must be speedily dealt with.

The paper describes briefly the construction of the condensers of the four turbines and details some operational problems encountered, such as the condenser leaks mentioned above, together with other operational problems on vacuum conditions, etc. It is not the purpose of this paper to discuss the advantages of the construction or the thermal design, but merely to relate how correct operation and maintenance of these essential parts of the steam cycle at a power station like Wylfa have upon the economics of the electrical output.

Wylfa Power Station, C.E.G.B., N.W. Region

Description of the Plant

The generating plant at Wylfa Power Station consists of four steam turbines each designed to give a gross output of 335 MW. The turbines are tandem compound, four cylinder units running at 3,000 r.p.m. and operating on a single pressure steam cycle. Each turbine comprises one double-flow high pressure (h.p.) cylinder and three double-flow low pressure (l.p.) cylinders. The turbine and the generator rotors are solidly coupled throughout and axial location is by a single thrust-bearing which is fitted in the pedestal between the h.p. cylinder and the first l.p. cylinder. A 'bridge type' condenser integrally mounted with the l.p. casings is employed.

The single steam pressure cycle decided upon for the particular reactor design with the adoption of a once-through boiler gave a steam operating temperature at the turbine stop valves of 333°C, at 38.7 bar.

These steam conditions however, required the use of reheat because the degree of wetness for the last row of blades, (91.5cms long on a 2.54m mean diameter and with a tip speed of 542m/sec) would have been unacceptable. Two stages of reheat are used, steam being bled from the higher stages of the h.p. cylinder and the temperature of the h.p. exhaust steam and reheater outlet steam being 103°C and 123°C respectively. The degree of wetness on the last row of l.p. blades being 8½%, exhausting into the condenser at 982m bar of vacuum (29.0 ins Hg.). This results in a generated power output of 250 MW per set when on full load conditions, the steam flow per turbine being 1.36 million kg of steam per hour. The steam conditions and hence the power output of the four sets are lower than the designed value due to the limitation of the reactors gas outlet temperature to 360°C, following the discovery of on-load steel corrosion in the earlier magnox stations.

The Bridge Condenser

Each turbine has one main condenser to take the six l.p. exhausts. There are six completely separate waterways on the C.W. side, but the steam side is common to all six l.p. exhausts. It is therefore possible to shut off and drain one of the six waterways at a time to attend to tube leaks or other defects whilst the set is on load, although there is a small reduction in set output and thus a financial penalty.

The 'bridge condenser' spans the distance between the h.p. cylinder and the alternator and the design results in considerable reduction in overall length and basement depth if compared with earlier conventional condensers employing a separate condenser shell for each cylinder. The design also ensures a short path from the last row of l.p. blades to condenser chamber inlet and of such a large area that pressure losses at the l.p. exhaust are minimal.

Aluminium/brass tubes are expanded into a double tube plate at both ends of the condenser and the differential expansion is accommodated by a bellows between the condenser shell and the tube plates on one side. A total of 3,296 aluminium/brass tubes are connected to the top tube plate, the bottom having 3,438 tubes. The tubes are expanded or 'rolled in' to the tubeplates at each end, the inlet end bellmouthed for improved flow (Figs. 1 and 2). In order to ensure adequate drainage, the tubes are 'hogged' when located in the holes in the support plates. Each tube at its inlet end is fitted with a plastic ferrule insert which is designed to promote a slightly turbulent flow through the tube, i.e. 2 metres/second. Double tube plates are used and the space between them filled with feed water supplied from a head tank. The

pressure ensures that any leak at the tube fixings would be of feed water into either the circulating water or into the condensate to prevent contamination of the boiler feed water. The once-through mode of boiler operation requires a very stringent chemical regime

Circulating Water Cooling

Each condenser is supplied with "screened" sea-water, via six motorised inlet valves from a common supply culvert. The water is discharged to a common outlet culvert through six motorised outlet valves. To provide a positive pressure, the water discharges over a weir at the end of the culvert thus protecting the culvert structure from surge pressures and at the same time providing a syphon.

The total flow of sea water pumped by the four C.W. pumps provided is 240 million litres per hour with the station on full load.

Operational Aspects

The operating regime for nuclear power stations is to supply the base load component of the National Grid system demand. This is because of their low operating fuel costs and thus it is important for such stations to achieve high standards of availability or load factor. Further, it is also important for optimum efficiency and to minimise costs to operate all the plant at its correct operating parameters. These parameters in so far as they affect the cost analysis of availability loss, are understood by the operating staff who ensure that the sets run within their normal operating conditions. At full load the vacuum is within the range 965 mbar - 1000 mbar (28.5 - 29.5 ins Hg) dependent upon sea water temperatures i.e. summer and winter conditions. The graph in Fig 3 shows the variation over a period of one year of the sea water (inlet temperature). As the design was for an inlet temperature not greater than 11°C, some financial penalty results during the summer months, but is offset during the winter months.

To allow the staff of the Central Control Room (C.C.R.) to monitor any condenser changes which might relate to loss of performance, the following parameters can be displayed on demand, via a data processing system. Exhaust steam temperature, C.W. inlet and C.W. outlet temperatures, vacuum (p.s.i. absolute and inches Hg) and C.W. pump motor current. In general, experience has found changes in these parameters to be only minimal, except for the high C.W. inlet temperature already mentioned and some small losses due to condenser water boxes being incorrectly primed. Under normal operation the C.W. pass inlet valves are fully open, while the C.W. pass outlet valves are normally 60% open. This has been found to give the optimum position for seeking to maintain prime in the passes over a range of tide levels. Outside these changes, occur others of a more severe nature. One of these is the abnormal conditions which can arise on the plant during adverse weather conditions. At certain times of the year, if the wind on the Anglesey coast is from the North West and approaching Force 7 or above, it will bring in large masses of seaweed which has to be washed from the drum screens by additional sprays of water from water hoses to prevent loss of vacuum due to a heavy restriction in flow rates. Such events occur usually in the autumn or early winter and have caused two very serious load reductions in the station's operating history.

When returning a turbine to service following an outage for major remedial work such as the bi-annual overhaul, problems do arise in obtaining the correct vacuum conditions because of some defect which defies more than a

normal time to find. Examples of this would be air leaks in expansion bellows, thermocouple points or drain plugs, ejector defects, etc. The pressure conditions on the condenser and the condensate feed train before running the turbine to speed are such as to make leak searching difficult, such difficulties heightened by a rising condensate temperature, as under these conditions the condensate is on a by-pass or recirculation loop.

In the station's ten years of operation the loss of a set due to low vacuum conditions has been extremely rare. The condensers are fitted with a vacuum trip (operates at 610 mbar (24 ins Hg.)) and this device is checked weekly.

Because of the danger of boiler tube corrosion the most important single problem connected with the Wylfa condensers is that of conductivity increase. The boilers operate in the once-through mode and thus for protection the station is committed to a policy of shut-down of a particular set should the conductivity exceed $0.3 \mu\text{S}/\text{cm}$, and the sodium content exceed $10 \mu\text{g}$ per litre, although of course, operator action will have been taken before that point is reached.

Thus, condenser leaks play a major part in the station's performance, not only because direct losses of output can result, but because of the vital importance to ensure a very high degree of purity of the boiler feed water. Contamination of the feed water by the ingress of sea water from the condenser cooling water due to condenser tube leaks is therefore very serious.

Normally, one condenser pass can be isolated when the set is on load, to discover and repair the offending tube. A loss of generator output also results. This loss can amount to between 5 and 10 MW depending whether the pass isolated is an end pass or not. A smaller loss of output results from isolating an intermediate or centre pass because although the steam flowing over the tubes is from a common chamber of all three l.p. cylinders, there is a sharing of steam with adjacent passes on either side, whereas on an end pass, all the steam passes to the inner pass thus causing a larger power loss.

The condensate system employs further chemical conditioning by means of a 100% polishing plant placed between the extraction pump first stage discharge and the extraction pump final discharge. The conditions require a normal running level of between 0.06 to $0.2 \mu\text{S}$ per cm. conductivity and within 0.5 to $2.0 \mu\text{g}$ per litre for sodium. (Comparable figures for a drum type boiler would be $0.2 \mu\text{S}/\text{cm}$ for conductivity and about a factor of 1000 higher for sodium than for the once-through boiler.

Any increase beyond this range requires prompt operator action to identify the offending condenser pass and isolate it. Instrumentation is provided in the C.C.R. and at a Chemical Control Centre. A 12-point conductivity monitoring recorder is installed as commercial equipment covering the six passes on both East and West ends of the condenser to give early diagnosis and thus assist quick removal of an offending pass from service. Usually, no problem exists in identifying which of the six passes has a tube leak, but intermediate passes can be troublesome because of some tendency of carry-over of contaminated steam from one pass to another.

Earlier, mention was made of the double tube plate arrangement at each end of the individual passes designed to protect the condensate from contamination. The arrangement is shown in Fig. 4 and indicates the four possible ways that a leak path may find a route into the condensate:-

- (a) the tube wall in the steam space;
- (b) the tube plate/tube expanded joints and the tube wall within the inter-space;
- (c) the inner tube plate/outer tube plate joint (including bolt joints;
- (d) the tube plates/condenser shell joint.

The leaks of the type (a) and (d) will usually be found by the foam method. Leaks of the type (b) and (c) usually mean a loss of demineralised water which is the sealing fluid in the double tube plate being supplied from a header tank with a 20 metres minimum head. The header tank has fitted a low level alarm which would indicate urgent action. Head checks are made by shutting off the make-up flow to the header tank and noting the fall over a period of time. Once a leak is established each tube plate is checked by isolating in turn. The actual location of this type of leak can only be determined by baving the set off load and using nltrasonic means.

The demineralised water pipework between the cast iron water box and the connection to the brass tube plate is semi-flexible to allow for expansion, and the condition of this pipework sometimes requires remedial work.

Once the pass is identified then swift action is taken to isolate by closing the air suction valve, inlet and outlet C.W. valves and draining the pass. A manually operated vent valve is provided as a vacuum breaking valve during the draining of the water boxes, the same valve being used to vent the water boxes to the atmosphere during the initial filling of the condenser pass to achieve prime.

The leak location method used at Wylfa is the foam method, the repair procedure being to plug both ends of the leaking tube with nylon plugs, thus making it redundant. The length of outage for a leak swiftly found is about 6 hours (this will equate to 45 MWh and a loss to the Board of over £1,000 in replacement generation). (1982)

If the foam process does not yield positive results after several attempts the operating staff may resort to applying sawdust to the pass, but it must be emphasised that this can only really be a temporary measure brought about by the need for that extra generation, or because of other factors such as prominent evidence of a more serious leak in one of the other five passes. In order to safeguard the turbine (vibrations etc.,) only one pass is taken out of service at any one time. For the start-up of the turbine to achieving 3,000 r.p.m., six passes must be in service although it is permissible in conditions of a particularly bad leak to run up with one pass full, but isolated. The station has been in operation for over ten years, the number of tubes plugged are as follows:-

T/A No.	1	2	3	4
	830	1257	990	380

This represents less than 2½%, which is a good condenser performance and with negligible effect on turbine performance or lack of output. The running hours on No. 4 set are much lower than the other 3 sets and this in some ways accounts for the lower number of tubes plugged.

The seawater is mostly clean having only a low suspended solids burden and most of the leaks have been as a result of impingement attack, erosion-

corrosion initiated by mussel shells and other hard sea debris lodging in the tubes. The leak rate in the first five years of operation had been relatively high.

In 1975 ferrous sulphate dosing was introduced. This was attempted firstly by using experimental equipment to overcome any obvious shortcomings, but became a permanent feature of dosing for each condenser. It has had a beneficial effect on the leak rate, reducing leaks to an average of one to two per month. The rich iron oxide layer used to protect the tubes had some heat transfer penalty, giving a reduction in condenser vacuum and thus generation loss. Calculations have suggested this figure to be about 1 MW per set, but nevertheless on balance, the case for ferrous sulphate dosing has been made.

Finally, before the advent and success of ferrous sulphate dosing, the station had considered re-tubing each condenser with titanium tubes, a massive undertaking in both capital and plant outage costs.

Tests have been conducted during outages to measure any possible damage to the internal surface of the tubes by eddy current measurement, under a trade name 'Probalog'. This involves driving a plug connected to a wire carrying an electrical signal down the tube and recording the trace caused by changes of resistance on a recording chart. This is not a simple operational exercise and is performed by the C.E.G.B's scientific staff. The results to date have confirmed the advantages of ferrous sulphate dosing.

The exposed cast iron and steel surfaces of the water boxes are coated with a rubberised paint to overcome any possible problems of an erosion/corrosion nature. Remedial work is done to ensure the coating is kept in good condition because damage can occur when personnel with equipment enter the passes during leak searching periods. Damage to the coatings occurs at the weak points on the internal parts of the water box shape i.e., corners and similar places where the full thickness of coating is not easily applied and thereby becomes particularly difficult to ensure full protection.

Fouling

Some fouling of the tubes by sedimentation does occur from the suspended solids burden of the sea water, the particles acting as a catalyst precipitating chemical reactions.

Tube cleaning by manual means takes place bi-annually by a system known as 'bulleting'. This involves firing a nylon plug down individual tubes with a compressed air gun from East end to West end, tube by tube ensuring some cleaning, but also checking for blockages. Non-emergence of the bullet at the receiving end requires either attempts made to unblock by "rodding out" or failure to clear will require the tube to be sealed at each end by plugs in the normal leak repair manner, because failure to do so may lead to a leak when the set is generating.

The position of the passes in the inlet culverts is such that passes '1F' and '3F' are adjacent to the ends of the two inlet culverts. The depth of the culverts at these points is reduced because of the reduced flow, but it has become an area where stones, shells and other marine impediments build up and this does possibly account to some degree to a greater number of leaks in the tubes associated with these two passes. The debris is removed during the time of the bi-annual outage of the two associated sets.

Chlorination

Chlorination takes place during the summer months and injection is made to the two inlet culverts at a rate of 135 kg/hour. The chlorination plant as installed was intended to inject also at each inlet pass, but it was found much simpler and cheaper to inject at the two culvert inlet points only. The magnitude of the residual chlorine in the water at the C.W. pass inlet water boxes governs the dose rates and thus the need to inject at a point adjacent to the water boxes was found not to be required. In other words, the chlorine injection at the above injection points gives a level of residual chlorine which affords effective protection.

Priming

One final aspect of the operation of these condensers mentioned concerns loss of prime to the passes. Through the cycle of tides the negative pressure at the top of the passes varies and for periods during low tide it becomes more negative and an increase in the release of dissolved gases causes a reduction in vacuum and thereby a loss of MW output. In order to maintain all passes in the fully primed state, an Operator routine is established to check each shift that these passes are not suffering from lack of the correct amount of water flow by opening the vent valve on each pass and ensuring the correct conditions.

Conclusion

Wylfa Nuclear Power Station has contributed over 50,000 million units of electricity to the National Grid in its 10 years of operation. It has a lifetime load factor of 56.5% (1982) which would have been much higher, but for some difficult boiler engineering problems which had to be overcome in the middle 1970's. In fact, such has been the improvement, that annual load factors of over 80% have been achieved over the last three years. The state of the boiler tubes has been, and will be, a critical dimension in the remaining years of its history and thus the strict chemical regime mentioned must be adhered to. As the major ingress of contamination is from sea water, correct condenser operation is an all important factor. The percentage loss of tubes due to leakage and subsequently made redundant by plugging, occurred mainly in the days before ferrous sulphate dosing, which has had an exceptionally beneficial effect on the station's performance. The decision for this system instead of the expensive titanium tube replacement has been proven. The degree of vigilance on the part of operating staff cannot be too highly stressed, and I believe it true that much urgency is also put on a swift conclusion being arrived at to ensure condenser leaks are quickly found, repaired and the guilty pass returned to service. With the station generating its units possibly cheaper than any other station with the possible exception of the Hinkley Point A G R, a full load condition each 24 hours is continually sought. I believe this paper illustrates the excellent operational policy of the station and the C E G B, and, that all operating staff are fully aware of that policy and direction.

Acknowledgements

I wish to record my thanks to the C E G B, North Western Region and the Station Manager, Wylfa Power Station for permission to present this paper and my appreciation to colleagues who have given help and useful criticism in its preparation.

18 January 1983

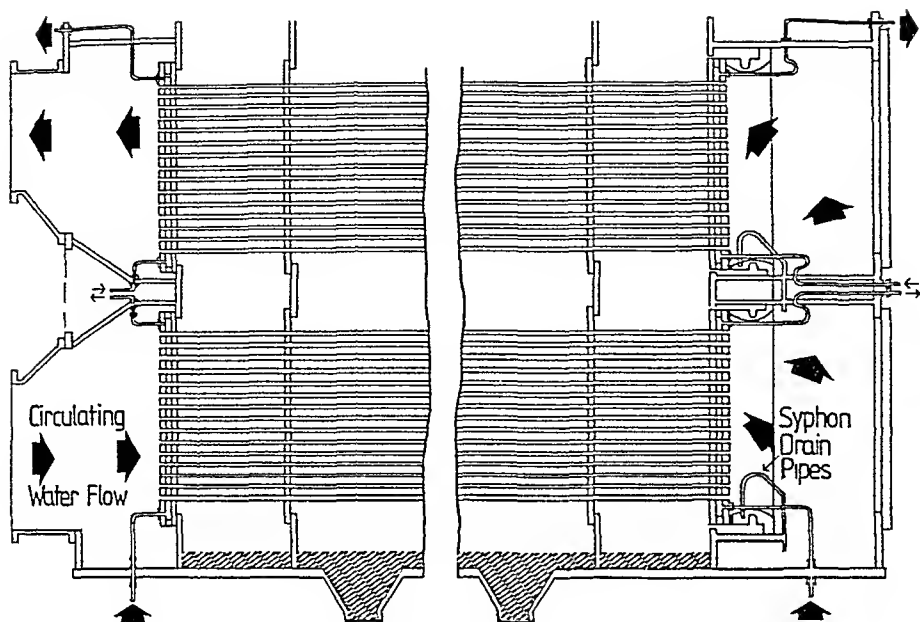


Figure 1 Section through Condenser and Water Boxes.

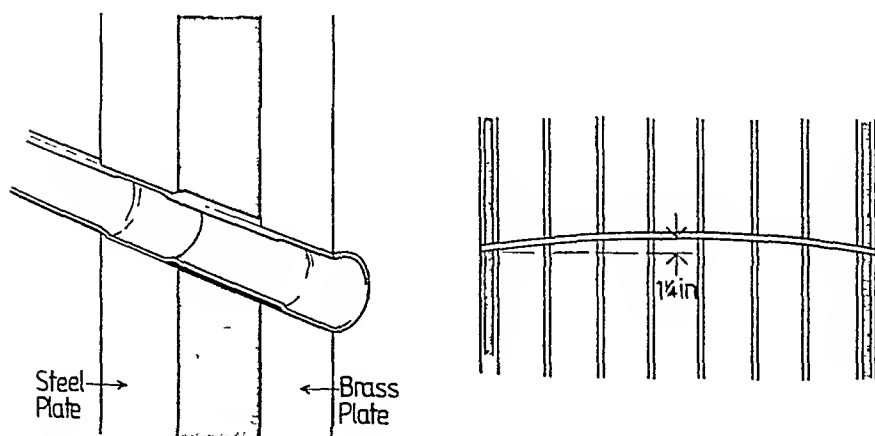


Figure 2 Detail of Tube-ends and Tube Bowing for Drainage.

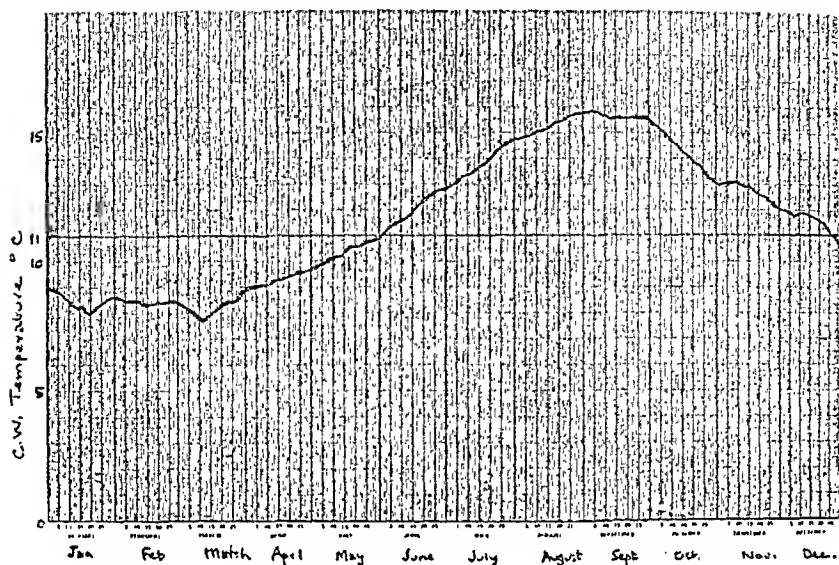


Figure 3 Mean annual variation of Sea Water Temperature.

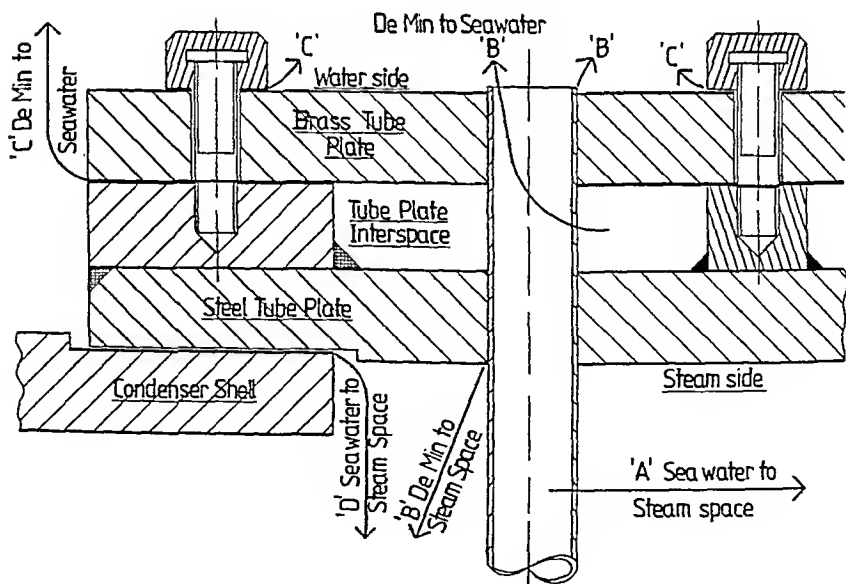


Figure 4 Types of leaks in the Wylfa Condensers.

PROCESS CONDENSERS

Theory

A REVIEW OF SOME RECENT DEVELOPMENTS IN CONDENSATION THEORY

R. G. Owen* and W. C. Lee**

Recent developments in the theory of condensation are discussed in relation to the design of equipment for condensing duties. For both tubeside and shellside condensation, improvements are described in the methods for predicting flow regimes, pressure drop and heat transfer in the condensate film. Developments in the prediction methods for multi-component condensation, including the effect of non-condensing gas, are considered. Also reviewed are recent improvements in predicting flow phenomena and heat transfer during direct contact condensation.

INTRODUCTION

This paper attempts to give a brief review of some of the recent developments in the theory of condensation. The review is strongly biased towards the engineering aspects of condensation: those aspects which are directly applicable to the design of condensing equipment for industrially important fluids.

In their own defence, the authors do not claim that the review is comprehensive, definitive or exhaustive. The limited space available has forced the authors to be selective in their choice of topics and of references. Inevitably, there are reliable and authoritative papers which are neither discussed nor referenced.

The main thrust of this paper is a review of the information available for the design of shell and tube condensers for chemical-process and oil-refinery application. The emphasis is on the developments which have occurred over the past ten years and this paper thus updates a previous review by Butterworth [1]. This review does not include either dropwise condensation or the molecular-kinetic resistance occurring at the vapour-liquid interface, despite their importance in some circumstances. Also omitted is discussion of wet-wall desuperheating, condensation on enhanced heat transfer surfaces, fog formation, condensation of vapours of immiscible condensates and the calculation of mean temperature differences in condensers.

* Technical Manager, Heat Transfer and Fluid Flow Service, Harwell

** Department of Mechanical Engineering, Queen Mary College, London University, England.

In deciding which papers and methods to include in this paper, priority has been given to soundly-based theories or to empirical formulae suitable for use in design methods. Where different authors have correlated or analysed similar data in apparently unrelated ways, an attempt is made to show how the methods relate.

FLOW PATTERNS

Flow Patterns for Tubeside Condensers

Horizontal tubes. An indication of the changing flow patterns which can exist during condensation in a horizontal tube has been given by Palen et al [2] and by Breber et al [3] from visual observation of condensation in a glass tube. The sequence of flow patterns from vapour inlet to outlet depends on the liquid loading (i.e. total flowrate) as shown in Figure 1. This figure shows that there are two distinct regimes for condensation inside a horizontal tube: that in which the flow is vapour shear controlled and that in which the flow is gravity controlled. When vapour shear controls the flow, the flow pattern is usually annular and the condensate film thickness is primarily determined by the axial vapour shear force at the vapour-liquid interface. There is usually entrainment of the condensate into the vapour phase in the form of droplets and also circumferential variation in condensate film thickness although the predominant velocity component in the condensate film is axial. As condensation proceeds, the condensate flowrate increases and the vapour flowrate correspondingly decreases and the effect of gravity on the flow pattern becomes more important. In gravity-controlled flow, the condensate drains from the top and sides of the tube to the bottom and flows along the bottom of the tube. There may be waves on the thick film flowing along the bottom of the tube and these waves may form frothy surges or may bridge the tube to give slug flow. Thus in gravity-controlled flow, there is significant variation in the circumferential thermal resistance of the condensate layer because of the large variation in the thickness of the condensate film around the tube.

For condensing flow in horizontal tubes the transition from shear-controlled flow (i.e. annular flow) to gravity-controlled flow (i.e. stratified-wavy or slug flow) is thus very important. It is worth examining and comparing the various criteria available in the literature for predicting this transition. Palen et al [2] suggest characterising this transition using a parameter which is the ratio of the shear force to the gravitational force on the condensate film. This approach had previously been suggested by Quandt [4] and also by Golan and Stenning [5] for flow regimes in vertical tubes. This idea has also been used by Wallis [6] in analysing the transition from slug (or churn) flow to annular flow in vertical tubes to predict the flooding velocity.

Palen et al [2] have plotted their data, together with those of Soliman and Azer [7,8] and those of Traviss and Rohsenow [9], as a function of the dimensionless superficial gas velocity, \dot{v}_g^* , where

$$\dot{v}_g^* = \frac{p_g^{1/2} \dot{v}_g}{\sqrt{g D (\rho_l - \rho_g)}} \quad (1)$$

and where D is the tube diameter and \dot{v}_g is the superficial gas velocity.

This plot is shown in Figure 2. From this diagram Palen et al infer that the transition from shear-controlled flow (annular, semi-annular) to gravity-controlled flow (semi-annular wave, wave etc.) falls between values of \dot{v}_g^* of 0.5 and 1.5. Support for this idea can be found from the flow pattern map of Fisher et al [10]. In Figure 3 the Fisher et al map has been redrawn with co-ordinates of \dot{v}_g^* and \dot{v}_g^* . The transition from annular flow to slug flow and that from annular flow to wavy flow occur at a dimensionless gas superficial velocity just exceeding unity. This value falls within the transition range suggested by Palen et al. Moreover, the transition between the annular-dispersed flow pattern and the stratified-wavy flow pattern has been found by Taitel and Dukler [11], using simple physical modelling, to be a function of \dot{v}_g^* and the Lockhart-Martinelli [12] parameter X (sometimes called the Martinelli parameter) defined as

$$X = \left[\frac{dp_F/dz}{dz} \right]_f \left/ \left[\frac{dp_F}{dz} \right]_g \right. \right]^{1/2} \quad (2)$$

where $[dp_F/dz]_{f,g}$ are respectively the local frictional pressure gradients for the liquid and gas phases flowing alone in the tube. As shown in Figure 4, Taitel and Dukler [11] have obtained a relationship between \dot{v}_g^* and X for the transition between annular and stratified flow. For the small values of X which are typical of annular flow, the annular stratified transition occurs roughly at a dimensionless gas velocity of approximately unity.

It is worthwhile examining whether there is any supporting evidence for this simple transition model from experimental studies of condensing flows. Such studies have been made by Traviss and Rosenhow [9] and by Soliman and Azer [7,8] for refrigerants and by Jaster and Kosky [13] for low pressure steam-water. Traviss and Rosenhow found that for refrigerant 12, this transition occurred at a condition of

$$F_1 = 2025 \quad \text{where } F_1 = \frac{u_f^2}{g\delta} \quad (3)$$

where u_f and δ are respectively the mean liquid velocity and film thickness if the flow were annular. For low pressure steam-water condensation, Jaster and Kosky [13] proposed the following alternative criteria:

$$\begin{aligned} \text{for annular flow,} & \quad F_2 \geq 29 \\ \text{for transition flow,} & \quad 5 < F_2 < 29 \\ \text{for stratified-type flow,} & \quad F_2 \leq 5 \end{aligned}$$

where

$$F_2 = \frac{\tau_w}{(p_f - p_g) g \delta} \quad (4)$$

In equation (4), τ_w is the wall shear stress and δ is the annular flow film thickness as before. Butterworth [1] has shown that the criterion of Traviss and Rosenhow agrees quite well with the criterion of Jaster and Kosky. This has been simply done by taking the middle value of F_2 for transition to be

In deciding which papers and methods to include in this paper, priority has been given to soundly-based theories or to empirical formulae suitable for use in design methods. Where different authors have correlated or analysed similar data in apparently unrelated ways, an attempt is made to show how the methods relate.

FLOW PATTERNS

Flow Patterns for Tubeside Condensers

Horizontal tubes. An indication of the changing flow patterns which can exist during condensation in a horizontal tube has been given by Palen et al [2] and by Breber et al [3] from visual observation of condensation in a glass tube. The sequence of flow patterns from vapour inlet to outlet depends on the liquid loading (i.e. total flowrate) as shown in Figure 1. This figure shows that there are two distinct regimes for condensation inside a horizontal tube: that in which the flow is vapour shear controlled and that in which the flow is gravity controlled. When vapour shear controls the flow, the flow pattern is usually annular and the condensate film thickness is primarily determined by the axial vapour shear force at the vapour-liquid interface. There is usually entrainment of the condensate into the vapour phase in the form of droplets and also circumferential variation in condensate film thickness although the predominant velocity component in the condensate film is axial. As condensation proceeds, the condensate flowrate increases and the vapour flowrate correspondingly decreases and the effect of gravity on the flow pattern becomes more important. In gravity-controlled flow, the condensate drains from the top and sides of the tube to the bottom and flows along the bottom of the tube. There may be waves on the thick film flowing along the bottom of the tube and these waves may form frothy surges or may bridge the tube to give slug flow. Thus in gravity-controlled flow, there is significant variation in the circumferential thermal resistance of the condensate layer because of the large variation in the thickness of the condensate film around the tube.

For condensing flow in horizontal tubes the transition from shear-controlled flow (i.e. annular flow) to gravity-controlled flow (i.e. stratified-wavy or slug flow) is thus very important. It is worth examining and comparing the various criteria available in the literature for predicting this transition. Palen et al [2] suggest characterising this transition using a parameter which is the ratio of the shear force to the gravitational force on the condensate film. This approach had previously been suggested by Quandt [4] and also by Golan and Stenning [5] for flow regimes in vertical tubes. This idea has also been used by Wallis [6] in analysing the transition from slug (or churn) flow to annular flow in vertical tubes to predict the flooding velocity.

Palen et al [2] have plotted their data, together with those of Soliman and Azer [7,8] and those of Traviss and Rohsenow [9], as a function of the dimensionless superficial gas velocity, \dot{v}_g^* , where

$$\dot{v}_g^* = \frac{p_g^{\frac{1}{2}} \dot{v}_g}{\sqrt{g D (\rho_l - \rho_g)}} \quad (1)$$

and where D is the tube diameter and \dot{v}_g is the superficial gas velocity.

This plot is shown in Figure 2. From this diagram Palen et al infer that the transition from shear-controlled flow (annular, semi-annular) to gravity-controlled flow (semi-annular wave, wave etc.) falls between values of \dot{v}_g of 0.5 and 1.5. Support for this idea can be found from the flow pattern map of Fisher et al [10]. In Figure 3 the Fisher et al map has been redrawn with co-ordinates of \dot{v}_l and \dot{v}_g . The transition from annular flow to slug flow and that from annular flow to wavy flow occur at a dimensionless gas superficial velocity just exceeding unity. This value falls within the transition range suggested by Palen et al. Moreover, the transition between the annular-dispersed flow pattern and the stratified-wavy flow pattern has been found by Taitel and Dukler [11], using simple physical modelling, to be a function of \dot{v}_g and the Lockhart-Martinelli [12] parameter X (sometimes called the Martinelli parameter) defined as

$$X = \left[\frac{dp_F}{dz} \right]_l / \left[\frac{dp_F}{dz} \right]_g \quad (2)$$

where $[dp_F/dz]_{l,g}$ are respectively the local frictional pressure gradients for the liquid and gas phases flowing alone in the tube. As shown in Figure 4, Taitel and Dukler [11] have obtained a relationship between \dot{v}_g and X for the transition between annular and stratified flow. For the small values of X which are typical of annular flow, the annular stratified transition occurs roughly at a dimensionless gas velocity of approximately unity.

It is worthwhile examining whether there is any supporting evidence for this simple transition model from experimental studies of condensing flows. Such studies have been made by Traviss and Rosenhow [9] and by Soliman and Azer [7,8] for refrigerants and by Jaster and Kosky [13] for low pressure steam-water. Traviss and Rosenhow found that for refrigerant 12, this transition occurred at a condition of

$$F_1 = 2025 \quad \text{where } F_1 = \frac{u_l^2}{g \delta} \quad (3)$$

where u_l and δ are respectively the mean liquid velocity and film thickness if the flow were annular. For low pressure steam-water condensation, Jaster and Kosky [13] proposed the following alternative criteria:

$$\begin{aligned} \text{for annular flow,} & \quad F_2 \geq 29 \\ \text{for transition flow,} & \quad 5 < F_2 < 29 \\ \text{for stratified-type flow,} & \quad F_2 \leq 5 \end{aligned}$$

where

$$F_2 = \frac{\tau_w}{(\rho_l - \rho_g) g \delta} \quad (4)$$

In equation (4), τ_w is the wall shear stress and δ is the annular flow film thickness as before. Butterworth [1] has shown that the criterion of Traviss and Rosenhow agrees quite well with the criterion of Jaster and Kosky. This has been simply done by taking the middle value of F_2 for transition to be

17 so that

$$\frac{F_2}{F_1} \approx 8 \times 10^{-3} \quad (5)$$

However, dividing equation (4) by equation (3) gives

$$\frac{F_2}{F_1} \approx \frac{\tau_w}{\rho_L u_L^2} = \frac{\tau_w (1 - \epsilon_g)^2}{\rho_L \hat{v}_L^2} \quad (6)$$

where ϵ_g is the void fraction and \hat{v}_L is the superficial velocity of the liquid phase (i.e. the velocity if it occupied the whole tube). The wall shear stress τ_w can be calculated from

$$\tau_w = \frac{f_L}{2} \rho_L \hat{v}_L^2 \phi_L^2 \quad (7)$$

where the two-phase frictional multiplier ϕ_L^2 may be approximated by

$$\phi_L^2 = \frac{1}{(1 - \epsilon_g)^2} \quad (8)$$

Combining equations (6), (7) and (8) yields

$$\frac{F_2}{F_1} = \frac{f_L}{2} \quad (9)$$

The friction factor f_L is that obtained if the liquid alone were flowing in the tube. Although the friction factor is not strictly constant, it does not vary very greatly and a value of $f_L/2$ of 8×10^{-3} is reasonable, thus making equations (5) and (6) compatible.

While it has thus been shown that the criterion of Traviss and Rosenhow for the transition from shear-controlled flow to gravity-controlled flow is compatible with the criterion of Jaster and Kosky, it has yet to be proved that either of these criteria are compatible with the simple formulation suggested by Palen et al [2]. However, it is possible to perform such a comparison as follows: in equation (4), the wall shear stress τ_w may be calculated from

$$\tau_w = \frac{f_g}{2} \rho_g \hat{v}_g^2 \phi_g^2 \quad (10)$$

where ϕ_g^2 is a two-phase frictional multiplier and the film thickness δ is approximated by

$$\delta = \frac{D}{4} (1 - \epsilon_g) \quad (11)$$

Equations (10) and (11) may be substituted into equation (4) to give:

$$F_2 = 2 f_g \dot{v}_g^*{}^2 \left[\frac{\phi_g^2}{1 - \epsilon_g} \right] \quad (12)$$

where the term in square parentheses in equation (12) is a function of the Lockhart-Martinelli parameter X . The friction factor f_g is that obtained if the gas phase alone were flowing in the tube. Although this friction factor is not strictly a constant it does not vary very greatly and a value of 7.5×10^{-3} has been chosen.

Equation (12) may be rearranged to yield

$$\dot{v}_g^* = \left[\frac{F_2}{2 f_g} \right]^{\frac{1}{2}} \frac{(1 - \epsilon_g)^{\frac{1}{2}}}{\phi_g} \quad (13)$$

where the annular flow limit corresponds to a value of F_2 of 29 and the stratified flow limit corresponds to a value of F_2 of 5.

For low pressures, the Lockhart and Martinelli expression for void fraction may be given in the form (Butterworth [14]):

$$(1 - \epsilon_g) = \frac{1}{(1/A + 1)} \quad \text{where } A = 0.28 X^{0.71} \quad (14,15)$$

and where X is the Lockhart-Martinelli parameter defined in equation (2). It is therefore possible using equation (13) to evaluate values of \dot{v}_g^* which correspond to the annular and to the stratified limits of Jaster and Kosky. For low pressures this is done in Table 1 for a range of values of X .

TABLE 1 - Values of \dot{v}_g^* corresponding to annular flow and stratified flow transition criteria of Jaster and Kosky; at low pressures

X	$(1 - \epsilon_g)$	ϕ_g	$\frac{(1 - \epsilon_g)^{\frac{1}{2}}}{\phi_g}$	\dot{v}_g^* at annular flow transition	\dot{v}_g^* at stratified flow transition
0.01	0.0105	1.21	0.0847	3.45	1.55
0.1	0.0518	1.73	0.130	5.32	2.38
1	0.219	4	0.117	4.77	2.14
10	0.589	17.32	0.044	1.81	0.81
100	0.880	121	0.00775	0.32	0.14
Recommended values of Palen et al [2]				1.5	0.5

At pressures near the critical pressure, the void fraction term in equation (13) may be expressed (Butterworth and Hewitt [15]) as:

$$(1 - \epsilon_g) = \frac{1}{\left[\frac{1}{B} + 1 \right]} \quad \text{where } B \approx X^{1.11} \quad (16,17)$$

Thus it is possible to calculate values of \dot{v}_g^* which correspond to the annular flow and stratified flow limits of Jaster and Kosky. For pressures near the critical pressure, these are given in Table 2 for a range of X values.

TABLE 2 - Values of \dot{v}_g^* corresponding to annular flow and stratified flow transition criteria of Jaster and Kosky; at pressures near the critical point

X	$(1 - \epsilon_g)$	ϕ_g	$\frac{(1 - \epsilon_g)^{1/2}}{\phi_g}$	\dot{v}_g^* at annular flow transition	\dot{v}_g^* at stratified flow transition
0.01	0.0060	1.32	0.0587	2.39	1.07
0.1	0.0720	2.04	0.131	5.37	2.41
1	0.5	4.92	0.143	5.86	2.63
10	0.928	20.9	0.0461	1.88	0.84
100	0.994	140	0.00712	0.29	0.13
Recommended values of Palen et al [2]				1.5	0.5

In Tables 1 and 2, the two-phase frictional multiplier ϕ_g^2 has been evaluated from (Wallis [6]),

$$\phi_g^2 = \left\{ (1 + X^{2/m})^{m/2} \right\}^2 \quad (18)$$

where $m = 4$ at low pressure and $m = 8/7$ at pressures near the critical pressure.

Tables 1 and 2 demonstrate that the Jaster and Kosky [13] criteria predict higher values of \dot{v}_g^* for both the annular and for the stratified transitions than those recommended by Palen et al [2]. This is so for a range of X values from 0.01 to 10 but at higher X values (>10) there is a tendency for the Jaster and Kosky criteria to give \dot{v}_g^* values lower than those recommended by Palen et al. However, considering the uncertainties in defining flow patterns, and the large scatter in the available experimental data, there is thus a considerable measure of agreement between the criteria of Traviss and Rosenhow, Palen et al, Jaster and Kosky and Taitel and Dukler.

Perhaps the most recent investigation of the shear to gravity controlled flow transition is that of Soliman [16]. Eight data sets corresponding to different test fluids of R-113, R-12 and steam and to tube diameters in the range 4.8 mm to 15.9 mm were used to test the predictions of the available methods. None of the available methods gave predictions which were fully consistent with all of these data. Soliman therefore proposed a new correlation:

$$Re = 10.18 Fr^{0.625} Ga^{0.313} (\phi_v/X)^{-0.938} \quad \text{for } Re_f \leq 1250 \quad (19a)$$

$$\text{and } Re = 0.79 Fr^{0.962} Ga^{0.481} (\phi_v/X)^{-1.442} \quad \text{for } Re_f > 1250 \quad (19b)$$

$$\text{where } Ga = \frac{g D^3}{\nu_l^2} \text{ is the Galileo number,} \quad (20)$$

$$Fr = 0.25 Re_l \left(\frac{u^*}{\delta^+} \right)^{1.5} / \sqrt{g \nu_l} \quad (21)$$

where δ^+ is given by equation (34).

$$\text{In equation (19), } \phi_v = 1 + 1.09 X^{0.039}. \quad (22)$$

A comparison of the Soliman [16] correlation with others described previously is given in Figure 5 for adiabatic air/water flow in a 1 inch tube at atmospheric pressure.

Vertical tubes. Vertical downwards cocurrent flow is more common than upwards flow in industrial condensers. The main characteristic of vertical downwards flow is the existence of the annular flow pattern for a wide range of flow conditions, as shown in Figure 6. The best available map for downwards flow is that of Golan and Stenning [5] which was derived from data for air-water systems. An attempt was made by Oshinowo and Charles [17] to generalise the map of Golan and Stenning but there was some conflict between the experimental data of the two sets of workers. There is thus some doubt about the accuracy and generality of the Golan and Stenning map and it should be used with caution.

Shellside Flow Patterns

Although there have been many flow pattern studies of adiabatic and condensing flow inside tubes, there has only been one systematic study of shellside flow patterns. This is the study of Grant and Murray [18,19] in which flow patterns were observed for adiabatic air-water flow in a model heat exchanger with a rectangular shell and 30° triangular tube layout.

A schematic diagram of the experimental heat exchanger used in this study is given in Figure 7. Three segmental baffles were used, giving four baffle spaces on the shellside. In 1972, Grant and Murray investigated vertical (up and down) flow across the four baffled crossflow sections of the model exchanger and, in 1974, they obtained data for flow patterns and for pressure drop in horizontal crossflow with the same model exchanger turned sideways so that the baffle cuts were vertical.

Five flow patterns were observed. A spray flow pattern occurred at high mass qualities with liquid carried along by the gas as a spray. At low mass qualities bubbly flow occurred with the gas distributed as discrete bubbles in the liquid phase. For vertical up and down flow in the model heat exchanger, chugging flow was observed under certain conditions. In chugging flow, intermittent slugs of liquid were propelled through the model by the gas phase. With the exchanger in a horizontal orientation, a stratified spray flow was observed in which the liquid and gas tended to separate with liquid flowing along the bottom of the model. The gas was entrained as bubbles in the liquid layer and also liquid droplets were carried along by the gas as a spray. Also observed for the model in a horizontal orientation was a stratified flow in which the liquid and gas were completely separated.

The observed flow patterns are illustrated in Figure 8 and the flow pattern maps for horizontal flow and for vertical flow obtained from these observations are given in Figure 9. The parameters used as ordinates in these maps are those of Baker [21] modified according to Bell et al [22]. The map is essentially a plot of superficial gas velocity versus superficial liquid velocity, with each of the superficial velocities multiplied by a physical property parameter. The superficial velocity is defined as the volumetric flux of the phase divided by the average flow cross-sectional area. The shellside flow pattern map of Grant and Murray [19] for horizontal flow is compared with the original Baker map for tubeside flow in Figure 10. A similarity between the two maps may be observed, with the shear-controlled and gravity-controlled regimes falling in about the same regions both for tubeside and for shellside flow. The similarity between the shellside and tubeside maps for horizontal flow leads one to speculate that use of the simple $\frac{v_g}{v_l}$ criterion of equation (1) may be adequate in determining the transition between shear and gravity controlled conditions in shellside flows. There is, however, little evidence available to support (or refute) such a conjecture.

A similar comparison has been made between the flow pattern map of Grant and Murray [18] for vertical flow and that of Hewitt and Roberts [23] for flow in vertical tubes. This is given in Figure 11 and, again, shear-controlled and gravity-controlled regions fall in similar areas for both types of flow.

Although the Grant and Murray flow pattern map is the only one currently available, it is based solely on observations of adiabatic flow and no flow pattern maps have yet been derived for shellside condensing flow. Furthermore, the experiments of Grant and Murray examined idealised crossflow in a rectangular geometry. For two-phase flow on the shellside of heat exchangers there will be leakage of fluid through the spaces between the tubes and the baffles and between the baffles and the shell. These leakages are coupled to phase separation so that the composition of the leakage streams may differ from that of the main crossflow stream. These effects increase the uncertainty in predicting shellside flow patterns in operating heat exchangers.

PRESSURE DROP IN CONDENSING FLOW

Tubeside Pressure Drop

Tubeside pressure drop is obtained by integrating the local pressure gradient over the length of the tube. The local pressure gradient is the sum of the frictional, accelerational and gravitational components as given by

$$\frac{dp}{dz} = \left[\frac{dp_F}{dz} \right] + \frac{d}{dz} \left\{ \dot{m}^2 \left[\frac{(1-x)^2}{\rho_f (1-\epsilon)} + \frac{x^2}{\rho_g \epsilon} \right] \right\} + g \left\{ \rho_g \epsilon_g + (1-\epsilon_g) \rho_l \right\} \cos \phi \quad (23)$$

where ϕ is the angle of the direction of flow from vertically upwards. In condensing flow, the accelerational term leads to a pressure recovery.

The frictional pressure gradient is usually calculated from frictional pressure drop correlations such as those of Lockhart and Martinelli [12] or Soliman et al [26]. However, these correlations may not accurately predict the measured pressure distribution in condensing flow. For example, Figure 12 gives a comparison of the predictions of these two models with the experimental data of Traviss et al [27] for R-12 condensing in a horizontal tube. An alternative approach [28,29] is to use an annular flow model of the type developed by Whalley and co-workers [30]. This annular flow approach also

permits calculation of the local void fraction ϵ_g which is required for the evaluation of the accelerational and gravitational components of pressure gradient.

Whichever method is used for calculating the frictional pressure gradient, account must be taken in condensing flow of the effect of mass transfer to the vapour/liquid (V/L) interface. The adiabatic frictional pressure gradient is corrected by a factor θ_F such that;

$$\frac{dp_F}{dz} = \left[\frac{dp_F}{dz} \right]_{\text{NMT}} \cdot \theta_F \quad (24)$$

$$\text{where } \theta_F = \frac{\phi_F}{1 - \exp(-\phi_F)} \quad \text{and} \quad \phi_F = \frac{\dot{m}_c (U_g - U_i)}{\tau_i} \quad (25)$$

and where $[dp_F/dz]_{\text{NMT}}$ is the frictional pressure gradient in the absence of mass transfer to the V/L interface, \dot{m}_c is the condensing mass flux and U_g and U_i are the axial velocities of the vapour phase and the V/L interface respectively. Equation (25) is based on the "film theory" of heat, mass and momentum transfer (see a later section of this paper) [31,32]. In some cases of high condensing rate, the mass transfer to the V/L interface can increase the frictional component of pressure gradient by as much as a factor of 2 over that for the corresponding adiabatic flow.

Where the flow is shear controlled it is usual to assume, both for horizontal as well as for vertical tubes, that the shear stress is uniform around the circumference. Although not strictly correct for horizontal flow [33] this assumption permits the interfacial shear stress τ_i to be calculated from

$$\frac{dp_F}{dz} = \frac{4}{d} \tau_i \theta_F \quad (26)$$

where θ_F is the mass transfer correction factor given in equation (25).

Shellside Pressure Drop

A shell and tube condenser has shellside cross baffles whose purpose is both to direct the shellside flow across the tube bundle and to provide support for the tubes. After each crossing of the bundle, the flow is turned in the baffle window to recross the bundle. The most common type of baffle is the single-segmental type as shown in Figure 13. Although the baffles are used to induce crossflow of the tube bundle, the baffles are not absolutely efficient in this respect. This is because various gaps must be left in order that the exchanger can be constructed. For example, the holes in the baffles through which the tubes must pass must be slightly larger than the tube o.d. and the baffle diameter must be less than the shell i.d. This allows some of the flow to leak through the gaps. In addition, the tube bundle does not completely fill the shell and some flow can bypass the bundle by flowing between the bundle and the shell.

Measurements of shellside pressure drop in an idealised heat exchanger without leakage and bypass (see Figure 7) have been made by Grant [20]. He

considered the crossflow zone and the window-flow zone separately as is the usual procedure for shellside studies. The results were correlated using an approach originated by Chisholm [34] for two-phase flow inside tubes

$$\frac{\Delta p}{\Delta p_{l0}} \approx 1 + (\gamma^2 - 1) \left\{ B x^{\frac{2-n}{2}} (1-x)^{\frac{2-n}{2}} + x^{2-n} \right\} \quad (27)$$

where Δp is the two-phase frictional pressure drop, Δp_{l0} is the pressure drop if the total flow were flowing with liquid properties and x is the quality. The parameter γ is given by

$$\gamma^2 = \Delta p_{go} / \Delta p_{l0} \quad (28)$$

where Δp_{go} is the pressure drop obtained if the total flow were flowing with the gas properties. The index n is that in the Blasius type expression relating the friction factor to the Reynolds number for single phase flow. The values of B were obtained empirically and are shown in Table 3.

TABLE 3 - Values of B for Use in Equation (27)

	Horizontal	Vertical
Crossflow { spray and bubbly	0.75	1.0
stratified and stratified spray	0.25	-
Window-flow ($n = 0$)	$2/(\gamma+1)$	0.25

Figure 14 gives an example of Grant's comparisons between the data and the empirical equation. Here a parameter ψ is used in the plot where

$$\psi = \frac{\Delta p / \Delta p_{l0} - 1}{\gamma^2 - 1} \quad (29)$$

This form was chosen because $\psi = x$ corresponds to homogeneous flow. Although results were obtained only for low pressure, air-water systems, the form of equation (27) has been shown by Chisholm [34] to apply more generally.

The crossflow and windowflow pressure drops calculated from equation (27) are for an idealised condenser and must be corrected for leakage and bypass. This may be done, for example, by the method proposed by Bell [35]. For pressure drop in the crossflow zone:

$$\Delta p_{ACTUAL} = \Delta p_{IDEAL} F'_B F'_L \quad (30)$$

where F'_B and F'_L are bypass and leakage correction factors respectively. These factors are given in Figure 15. The ideal window-flow pressure drop may be corrected in a similar manner.

The procedure given above is typical of those produced before the advent of economical and powerful computers. As shown in Figure 16, the more recent methods utilise the power of modern computers to solve the flowrates of the main (i.e. crossflow and windowflow), bypass and leakage streams. These methods treat the shellside flow as though it were an electrical network in which current corresponds to flowrate, electrical potential corresponds to pressure and electrical resistance corresponds to flow resistance. Correlations or theoretical models are used to evaluate the flow resistance characteristics of the various streams. In some of these recent methods (e.g. Moore [47] and Palen and Taborek [44]), the procedure starts at the vapour inlet and steps along the shell to the outlet. In other methods (e.g. Johnston and Wills [48]) calculations are done simultaneously for the complete exchanger. These latter methods should provide a more accurate treatment of end spaces, bundle bypassing and of axial leakage than the former methods but at the penalty of additional computing cost. Many of these more recent methods are proprietary. However unsatisfactory this may seem from a purely academic viewpoint, the expense involved in developing and validating a shellside procedure deters research organisations from disclosing detailed information.

HEAT TRANSFER ACROSS THE CONDENSATE FILM

Downflow in Vertical Tubes and on Flat Plates

When a stationary vapour condenses on a vertical surface, the condensate film in the uppermost part of the surface is laminar. If the Reynolds number of the condensate film attains a value of approximately 1600 to 2000 the film becomes turbulent. In the region of laminar flow, the classical Nusselt analysis [50] is applicable. In the turbulent flow region, Colburn [51] has obtained an analytical solution by assuming that all the thermal resistance of the turbulent film is in a thin laminar sublayer adjacent to the wall. Colburn's result indicates that the heat transfer coefficient increases with increasing film Reynolds number.

When significant vapour shear is present, two effects are observed, viz: (1) vapour shear tends to thin the film thereby increasing the heat-transfer coefficient, and (2) the laminar-turbulent transition occurs at lower film Reynolds numbers. For film condensation with vapour shear, several theoretical solutions [52-56] are available. The studies of Rohsenow et al [52], Dukler [53] and Lee [54] take account of the effect of interfacial shear stress in reducing the transition Reynolds number of the condensate film and utilise a turbulent viscosity variation similar to that in single-phase pipe flow. These analyses indicate that the heat-transfer coefficient increases with film Reynolds number raised to the power 0.2 in the turbulent region.

Blangetti and Schlunder [55,56] have improved the analysis of the turbulent region by utilising a turbulent viscosity profile which accounts for the reduction in turbulent viscosity close to the vapour-liquid interface. They found that the heat-transfer coefficient in the turbulent region depends on the film Reynolds number raised to the power 0.4. Figure 17 compares the results of the Blangetti and Schlunder theory with experimental data for water and for a high-Prandtl number fluid, MWA. Both the Blangetti and Schlunder [55,56] and the earlier [52-54] models may also be used to give a more accurate solution than that of Colburn [51] for the zero vapour shear limit.

Horizontal Tubes

Different types of theoretical model are used for condensation in horizontal tubes, depending on whether the flow is gravity or vapour shear controlled. Methods for identifying the transition from gravity-controlled flow to shear-controlled flow have already been discussed. In the gravity-controlled region it is usually assumed that the flow is stratifying with the condensate running down the side walls and collecting in the bottom of the tube. The condensate layer in the bottom of the tube flows under the action of vapour shear or hydraulic gradient. However, this assumption of stratifying flow in the gravity-controlled region may not be valid at high liquid loading when the flow is usually of the slugging type. In the vapour shear-controlled region many theoretical models are available in which the flow is assumed to be annular with axial flow of the condensate film and no stratification.

The models for heat transfer during stratifying condensation are modifications to the Nusselt theory [50] for condensation outside tubes:

$$\alpha_L = 0.725 \Omega \left\{ \frac{\lambda_L^3 \rho_L (\rho_L - \rho_g) g \Delta h_v}{\eta_L D (T_1 - T_w)} \right\}^{\frac{1}{4}} \quad (31)$$

where Ω is a correction term which gives Nusselt's result if set to 1.0. D is taken as the tube internal diameter here. The correction factor is less than one for in-tube condensation because of the layer of condensate at the bottom of the tube which makes that region less effective for heat transfer. Typically, Ω is about 0.8. Different methods for calculating Ω have been given by several authors [13,57,58].

The annular-flow models for the heat-transfer coefficient may be written in the following form

$$\alpha_L = \rho_L u^* c_{pL} / T^+ \quad (32)$$

where u^* is the wall "friction velocity" given by $(\tau_w/\rho_L)^{\frac{1}{2}}$ and T^+ is a dimensionless film temperature drop which depends on the dimensionless film thickness, δ^+ (i.e. $\rho_L u^* \delta / \eta_L$), and the condensate Prandtl number, Pr_L . Relationships for T^+ are normally calculated using some form of Martinelli analogy [59] and the following results [13], with minor variations [27,60-62], are obtained by this method:

$$T^+ = Pr_L \delta^+ \quad \text{for } \delta^+ \leq 5 \quad (33a)$$

$$T^+ = 5 \left[Pr_L + \ln \left\{ 1 + Pr_L \left[\frac{\delta^+}{5} - 1 \right] \right\} \right] \quad \text{for } 5 < \delta^+ \leq 30 \quad (33b)$$

$$T^+ = 5 \left[Pr_L + \ln (1 + 5 Pr_L) + \frac{1}{2} \ln \frac{\delta^+}{30} \right] \quad \text{for } \delta^+ > 30 \quad (33c)$$

Before equation (33) may be used, relationships are required which give δ^+ in terms of known quantities. These are usually obtained by integrating the velocity profile across the film. The velocity profile is often

calculated by assuming the same turbulent viscosity profile as that for single-phase liquid flow in the tube with the same wall shear stress. The following simple relationships were obtained by Kosky and Staub [61]:

$$\delta^+ = (Re_\ell/2)^{\frac{1}{2}}, \quad Re \leq 1250 \quad (34a)$$

$$\delta^+ = 0.0504 Re_\ell^{0.875}, \quad Re > 1250 \quad (34b)$$

where Re_ℓ is the liquid superficial (or liquid film) Reynolds number given by

$$Re_\ell = (1-x) \dot{m} D / \eta_\ell \quad (35)$$

Equations (33) and (34) give T^+ as a function of liquid Reynolds and Prandtl numbers as is shown in Figure 18. Also shown in this figure is a simplified relationship obtained by Carpenter and Colburn [63] which is

$$T^+ = 23.3 Pr_\ell^{\frac{1}{2}} \quad (36)$$

The shear stress τ_w is calculated from the two-phase frictional pressure gradient as already discussed.

The annular-flow type models would generally be expected to apply at high flow rates and a different model by Boyko and Kruzhilin [64] is frequently found to work in these circumstances. Their equation for the local heat-transfer coefficient is

$$\alpha_\ell = 0.021 \frac{\lambda_\ell}{D} Re_{\ell o}^{0.8} Pr_\ell^{0.43} \left\{ 1 + x \left[\frac{p_\ell}{p_g} - 1 \right] \right\}^{\frac{1}{2}} \quad (37)$$

where $Re_{\ell o}$ is the liquid Reynolds number defined by $\dot{m} D / \eta_\ell$. Butterworth [1] has compared this equation with the above annular flow models by transforming equation (37) to the same form as equation (32) using the following homogeneous flow equation for the wall shear stress:

$$\tau_w = 0.023 Re_{\ell o}^{-0.2} \left\{ 1 + x \left[\frac{p_\ell}{p_g} - 1 \right] \right\} \frac{\dot{m}^2}{\rho_\ell} \quad (38)$$

This results in the following equation for T^+

$$T^+ = 7.22 (1-x)^{-0.1} Re_\ell^{0.1} Pr_\ell^{0.57} \quad (39)$$

The group $(1-x)^{-0.1}$ only varies slightly over the range of interest (e.g. it is 1.0 at $x = 0$ and is 1.49 at $x = 0.98$) and may be approximated as 1.17 for all circumstances giving

$$T^+ = 8.5 Re_\ell^{0.1} Pr_\ell^{0.57} \quad (40)$$

This equation is compared with other annular flow models in Figure 18. Close agreement may be observed for high Re_f .

Annular flow models give heat-transfer coefficients which are typically 5 to 15 times the corresponding all-liquid heat transfer coefficients.

Shellside

Neglecting vapour shear effects, the Nusselt [50] equation for the heat-transfer coefficient outside a single horizontal tube has been well substantiated since its derivation in 1916. This equation is number (31) above with Ω taken as 1.0 and D as the tube outside diameter.

The average coefficient for a vertical row of tubes is generally less than that given by equation (31) because of condensate from higher tubes falling onto the lower ones and thereby reducing the coefficients on the latter. If it is assumed that the condensate flows from tube to tube in a continuous sheet, as shown in Figure 19, and that the flow remains laminar, extensions to the Nusselt analysis give

$$\bar{\alpha}_{LN} / \alpha_{L1} = N^{-1/4} \quad (41)$$

where $\bar{\alpha}_{LN}$ is the mean coefficient for N tubes. The coefficient α_{L1} is that for the top tube as calculated by equation (31). Berman compared equation (41) (and others) with a range of experimental data and found a tendency for most of the data to lie above the theoretical curve. This is attributed to the following:

- the actual condensate flow is as illustrated in Figure 19 and this pattern is more favourable to heat transfer;
- it is likely that in a few of the experiments, some of the tubes encountered large vapour velocities which tended to increase the coefficient as a result of vapour shear effects. (Vapour shear effects are discussed further below.)

An alternative method to equation (41) has been proposed by Kern [65] and this gained much popularity amongst designers of shell-and-tube condensers despite there having been little attempt to substantiate the method with experimental data. This method gives

$$\bar{\alpha}_{LN} / \alpha_{L1} = N^{-1/6} \quad (42)$$

Grant [66] has, however, shown that the Kern relationship is in close agreement with the Grant and Osment method [67] which is based on experimental data. Butterworth [68] has shown that the empirical equations of both Grant and Osment [67] and Kern [65] are in close agreement with that proposed by Short and Brown [69]. The equation of Short and Brown may be expressed by;

$$\frac{\bar{\alpha}_{LN}}{\alpha_{L1}} = 1.24 N^{-1/4} \quad (43)$$

This result is equivalent to

$$\frac{\alpha_{LN}}{\alpha_{L1}} = \left\{ \frac{\Gamma_N}{Y_N} \right\}^{-\frac{1}{4}} \quad (44)$$

where Γ_N is the condensate drainage from the N^{th} tube and Y_N is the condensate generated on the N^{th} tube. Equation (44) agrees closely with that of Grant and Osment [67]

$$\frac{\alpha_{LN}}{\alpha_{L1}} = \left\{ \frac{\Gamma_N}{Y_N} \right\}^{-0.223} \quad (45)$$

Figure 20 shows the Kern equation (solid line) compared with equation (43) (broken line) derived from Short and Brown's equation. Equation (43) is only valid for large values of N but it is possible to derive numerical values for low N . These are shown as the points on Figure 20. It may be seen that there is extremely good agreement between Kern's result and the Short and Brown empirical equation.

The analysis given above is relevant to laminar condensate films. However for large tube bundles, film Reynolds numbers may become sufficiently large for a transition to turbulent flow to occur. Butterworth [68] presents a tentative method for such cases. However no experimental data are as yet available to test this tentative method.

The above discussion relates to condensation with sufficiently low vapour velocity that vapour shear effects on the condensate film are negligible compared with gravitational effects. Shell and tube condensers, however, often operate with high vapour velocities and the effect of vapour shear must be taken into account. In baffled shellside condensers the vapour flow is usually horizontal although, in crossflow condensers, vertical downflow of vapour is more common. As a first step towards understanding the condensation of vapour in crossflow over a tube bundle, several studies have considered the simpler case of condensation on a single isolated tube in a uniform vapour stream.

Single tube studies in crossflow condensation. Shekriladze and Gomelaouri [70] have analysed the case of downward vapour flow over an isolated tube. They obtained an expression which fitted both the gravity-dominated and the vapour shear-dominated conditions:

$$\alpha_L = 0.64 E [1 + (1 + 1.69 F)^{\frac{1}{2}}]^{\frac{1}{2}} \quad (46)$$

where α_L is the mean heat-transfer coefficient for the tube,

$$E = \left(\lambda_L^2 \rho_L u_g / \eta_L D \right)^{\frac{1}{2}} \quad (47)$$

$$\text{and } F = g D \eta_L \Delta h_v / (u_g^2 \lambda_L \Delta T) \quad (48)$$

When vapour shear forces are dominant, equation (46) reduces to:

$$\alpha_L = 0.9 E \quad (49)$$

The above equations were derived using the assumption that there is no separation of the boundary layer as it flows around the tube. By considering the most forward position at which the boundary layer could separate and by ignoring heat transfer in the region beyond the separation point, equations (46) and (49) are modified to

$$\alpha_f = 0.416 E [1 + (1 + 9.47 F)^{\frac{1}{2}}]^{\frac{1}{2}} \quad (50)$$

$$\alpha_f = 0.59 E \quad (51)$$

Since the pioneering work of Shekriladze and Gomelauri, a significant amount of further work has been performed on crossflow condensation on an isolated tube [71-80]. Fujii et al [71] have provided a more thorough solution which yields the formula;

$$\alpha_f = E X [1 + 0.276 F/X^4]^{\frac{1}{2}} \quad (52)$$

$$\text{where } X = 0.9 (1 + 1/G)^{1/3} \quad (53)$$

$$\text{and } G = \Delta T \lambda_f (\rho_f \eta_f / \rho_g \eta_g)^{\frac{1}{2}} / (\eta_f \Delta h_v) \quad (54)$$

Fujii et al [71] solved the governing equations by numerical methods. Equation (52) is an empirical fit to the numerical solutions. The maximum difference between the numerical solutions and equation (52) is 5%. For $G \gg 1$, the result becomes independent of G . For $G > 10$, equation (52) is in close agreement with equation (46). Recent analyses [73,75] are refinements of the work of Fujii et al [71] and give results which differ only slightly from equation (52).

Equations (46) and (52) may be used to evaluate the extent to which vapour shear increases the heat-transfer coefficient. In Figure 21, the ratio of the heat-transfer coefficient with vapour shear to that for gravity-controlled condensation is plotted against the reciprocal of the parameter F . The reciprocal of F is used as the abscissa so that increasing values of the abscissa correspond to increasing vapour velocity. It is clear from Figure 21 that theory correctly predicts the heat-transfer coefficients for low and moderate vapour velocity (i.e. $1/F < 10$). The region of high velocity (i.e. $1/F > 10$), however, is still unclear. The accuracy of the data of Nicol and Wallace [77,78] is suspect since the measurements were taken when significant amounts of air were present in the steam. Further accurate data is therefore needed to confirm the theoretical predictions at high vapour velocities.

While equations (46) and (52) were obtained for vapour downflow, Honda and Fujii [72] have shown that the results for horizontal vapour flow are almost identical to those for vapour downflow. Hence equations (46) and (52) should also be applicable to horizontal vapour flow.

Tube bundle studies in crossflow condensation. The physical processes involved during crossflow condensation within a tube bundle are more complex than those for an isolated tube. The vapour flow within the bundle is not uniform and condensate inundation occurs. Moreover the vapour velocity decreases as the vapour progresses through the bundle while the effects of inundation become more important. Condensate films may be laminar on some

tubes and turbulent on others.

Owing to the complexity of the problem, little theoretical analysis has been done. However, a number of experimental investigations [79,81-87] have been performed. Fujii et al [82] found that their data for horizontal steam flow could be correlated in terms of the single-tube equation (i.e. equation (52)),

$$\alpha_L = K E X [1 + 0.276 F/X^4]^{\frac{1}{4}} \quad (55)$$

where $K = 1.0$ for the staggered bundle and $K = 0.8$ for the in-line bundle. More recently Fujii [86] reported extensive measurements for steam in horizontal, downward and upward flows in staggered and in-line bundles. These results were found to be in fair agreement with a semi-empirical correlation for single-tube data, see Figure 22. The difference between the data for horizontal and downward flows is only slight while the data for upward flow are somewhat lower than these. No appreciable difference was found between the data for the staggered and in-line bundles.

While equation (55) predicts the data of Fujii et al [82] satisfactorily, a general design method could utilise equation (50) for the effect of vapour shear and the Kern [65] method for condensate inundation,

$$\bar{\alpha}_{LN} = 0.416 E [1 + (1 + 9.47 F)^{\frac{1}{4}}]^{\frac{1}{4}} \cdot N^{-1/6} \quad (56)$$

However, this method does not take into account the interaction between the vapour flow and condensate inundation. It should, however, be conservative since some condensate may be entrained in the vapour flow thus reducing the amount of condensate inundation.

McNaught [87] has adopted a different approach which takes account of the combined effect of vapour velocity and inundation. The method uses an empirical correlation based on the Lockhart-Martinelli parameter (refer equation (2)) for two-phase forced-convection heat transfer,

$$\bar{\alpha}_{LN} = (\alpha_{SHEAR}^2 + \alpha_{GRAVITY}^2)^{\frac{1}{2}} \quad \text{where} \quad \alpha_{SHEAR} = \bar{\alpha}_L \cdot a (1/X)^b \quad (57)$$

a and b are empirical constants and $\bar{\alpha}_L$ is the mean heat-transfer coefficient for the liquid phase flowing alone in the bundle. In equation (57) $\alpha_{GRAVITY}$ is calculated using equation (45). McNaught [87] compared equations (56) and (57) with a limited dataset for condensation of steam on staggered and in-line bundles [79] in Figure 23. Equation (57) showed better agreement with the limited data [79] than equation (56), with equation (56) being conservative with respect to most of the data.

When applying the above methods to the design of process shellside condensers, account must be taken of bypass, leakage and window effects as already discussed in relation to shellside pressure drop. Hence using the method proposed by Bell [35]

$$\alpha_{ACTUAL} = \alpha_{IDEAL} F_B F_L F_W \quad (58)$$

where F_B , F_L and F_W are bypass, leakage and window correction factors

respectively. They are evaluated in a similar manner to the correction factors for pressure drop.

The more recent flowstream methods [44,47] solve simultaneously for the flowrates the crossflow, windowflow leakage and bypass streams. The crossflow flowrate thus computed may be used directly in the evaluation of the shellside condensing coefficient.

HEAT AND MASS TRANSFER WITH MIXTURES

Three types of method are available for the analysis of heat and mass transfer during the condensation of mixtures. In order of increasing rigour and complexity, these methods are;

- (i) Simplified, approximate methods in which the condensation process is assumed to pass through a series of equilibrium states. These equilibrium states comprise a condensation curve which is usually expressed in the form of a plot of condensing temperature T versus the cumulative heat release rate Q .
- (ii) "Film theory" methods in which primary consideration is given to heat and mass transfer in the gas phase. Concentration and temperature differences between the bulk vapour and the vapour-liquid interface are assumed to occur across a thin laminar film adjacent to the interface. This assumption may sound remote from the conditions prevailing in industrial equipment which are usually designed to ensure turbulent flow of the condensing fluid. But in a highly turbulent flow there is little resistance to mass transfer in the main body of the fluid and the principal resistance is confined to a thin film of fluid adjacent to the condensing surface. The situation is idealised by assuming a thin film in which the movement is wholly laminar and, outside this film, a highly turbulent region in which the concentration and temperature gradients are negligible. A one-dimensional analysis is performed for the flow normal to the condensing surface and the thickness of the thin laminar film is usually obtained from correlations of experimental data.
- (iii) Boundary layer methods in which analytical or numerical methods are used to solve the boundary-layer equations which describe the heat and mass transfer processes in the gas phase. These methods start at the most upstream point and march downstream. At the present time, these methods are only available for simple geometrical configurations and for simple mixtures (e.g. one vapour condensing in the presence of a non-condensing gas). Extension of boundary-layer methods to more complex geometries, such as condensation in tube banks, is not straightforward. Moreover, the amount of computation increases markedly with the number of condensing components.

The simplified approximate methods are already widely used by industry. The "film theory" methods are used by industry for some applications such as condensation of a vapour from a non-condensing gas. However, "film theory" methods are not yet used widely for complex mixtures. Boundary-layer methods, although giving the promise of greatest accuracy, are still primarily research tools.

Simplified Approximate Methods

The methods of Silver [88] and Bell and Ghaly [89] for the condensation of vapour mixtures may be written as

$$\frac{1}{a_{\text{eff}}} = \frac{1}{a_l} + \frac{Z}{a_g} \quad (59)$$

The parameter Z was introduced by Bell and Ghaly and is the ratio of heat removal for sensible cooling of the gas phase to the total heat removal:

$$Z = d\dot{Q}_g / d\dot{Q} \quad (60)$$

Equations (59) and (60) may be regarded as rigorous as written since the only approximation introduced is the comparatively minor one that all the heat released in cooling the condensate layer has to cross the whole of that layer. Loss of rigour occurs in practice when the equations are used because the following three further assumptions are then made:

- (1) Equation (60) is evaluated on the basis of an equilibrium condensation curve.
- (2) a_g is not corrected for mass transfer effects.
- (3) a_g is not corrected for two-phase flow effects (e.g. waves on the condensate layer).

Assumption (3) is usually conservative while (2) is non-conservative. Assumption (1) can be either safe or unsafe dependent on the circumstances. While assumptions (2) and (3) can be removed without difficulty [90,91], assumption (1) cannot without going to the much more complicated methods described in the next section.

"Film Theory" Methods

Condenser design using the "film theory" methods involve calculating the local heat and mass transfer rates and integrating these local rates over the condenser length using differential mass and energy balances [92]. The energy flux at any local point is given by

$$\dot{q} = \dot{q}_g + \sum_{j=1}^n \dot{n}_j \Delta \tilde{h}_j \quad (61)$$

where

$$\dot{q}_g = a_g \left\{ \frac{\phi_T}{\exp \phi_T - 1} \right\} (T_g - T_l) \quad (62)$$

and

$$\Delta \tilde{h}_j = \Delta \tilde{h}_{vj} + \tilde{c}_{pgj} (T_g - T_l) \quad (63)$$

\dot{q}_g is the sensible heat flux calculated using Ackermann [93]

analysis. \dot{q}_g is responsible for the cooling of the bulk gas core. Sardesai [94] observed that Ackermann analysis predicts the experimental vapour temperature profile within an accuracy of $\pm 10\%$.

The condensation flux \dot{n}_j of any component is given by

$$\dot{n}_j = \dot{J}_{jb} + \tilde{y}_{jb} \dot{n}_t \quad (64)$$

The mass transfer models used to calculate \dot{J}_{jb} can be classified into 2 categories; interactive models and non-interactive models.

There are two interactive models: Toor's [95] linearised theory and Krishna-Standart model [96]. The interactive models give the diffusion fluxes, \dot{J}_{jb} , as

$$(\dot{J}_b) = [B] \left\{ \frac{[\phi]}{\exp [\phi] - \tau_L} \right\} (\tilde{y}_b - \tilde{y}_1) \quad (65)$$

The elements of matrix $[B]$ can be obtained from the binary mass-transfer coefficients β_{jk} for all the component pairs and the bulk vapour composition. The elements of the high flux correction matrix are a function of the condensation fluxes and are calculated iteratively. Sardesai [94] and Panchal [97] found that the predictions of Krishna-Standart method and Toor's linearised theory were within $\pm 1\%$ for a range of experimental conditions.

The non-interactive methods are also known as effective diffusivity methods. The diffusion flux of any component is assumed to be a function of driving force of that component only and is given by

$$(\dot{J}_b) = D_{eff} (\tilde{y}_b - \tilde{y}_1) \quad (66)$$

The effective diffusivity may be defined in several ways. Two commonly used definitions are

$$(i) D_{k,eff} = \delta_{k,n} \quad k=1, 2, \dots, n-1 \quad (67)$$

The effective diffusivity is equal to binary diffusivity with respect to a fixed component n

$$(ii) D_{k,eff} = (1 - \tilde{y}_{kb}) / \left(\sum_{\substack{j=1 \\ j \neq k}}^n \tilde{y}_{jb} / \delta_{jk} \right) \quad (68)$$

This is the Wilke equation [98].

Of the two "film theory" multicomponent condensation methods, the interactive (Krishna-Standart) method is more complex than the non-interactive (effective diffusivity) method. The computational time decreases with decreasing complexity of the method and it may be useful to employ a less complex method if the difference between their predictions is within acceptable limits. The Krishna-Standart method and the effective diffusivity method (equation (67)) become identical at high concentration of non-condensing gases. Also, the effective diffusivity method (equation (68)) is

identical to Krishna-Standart method when a single component is condensing in the presence of $(n-1)$ non-condensing gases.

Sardesai [94] and Deo [99] have carried out experimental validation of Krishna-Standart and effective diffusivity methods in vertical condensers for ternary systems using a range of components of widely different molecular weights. It was found that the Krishna-Standart method predicted the experimental condensation rates within an accuracy of $\pm 10\%$. The difference between the Krishna-Standart method and the effective diffusivity method was less than 20%. Comparisons of both the simplified, approximate methods and the film theory with experimental data are also available from McNaught*.

Recent research has also been directed at providing robust and efficient algorithms for the solution of the governing equations for film theory models [100,101].

Boundary Layer Methods

The boundary layer methods currently available deal primarily with the simplest case of condensation of vapour from a non-condensing gas. The boundary layer equations are solved by similarity, numerical or integral methods. For example, Sparrow et al [102], Schrock [103], Koh [104], Fujii et al [105] and Rose [106] have obtained solutions for condensation of a flowing vapour from a non-condensing gas on a flat plate. Rose [107] and Lee and Rose [108] have considered the case of condensation from a flowing vapour-gas mixture on an isolated tube. Much work is required to extend these methods for application to complex geometries (such as condensation in tube banks) and for treating mixtures with many condensing and non-condensing components.

DIRECT CONTACT CONDENSATION

When condensation occurs directly on a subcooled liquid and the heat of condensation is primarily absorbed in raising the temperature of the subcooled liquid, the process is termed direct contact condensation. If the liquid is exposed to the vapour for a sufficiently long time, it will asymptotically attain the saturation temperature of the vapour whence condensation will cease. Figure 24 shows typical temperature profiles for direct contact condensation of (a) a pure miscible vapour, (b) a pure immiscible vapour, and (c) a multi-component mixture (which may include a non-condensing gas). In (a) and (b) the major thermal resistance is in the liquid phase while in (c) there may be significant resistances in both the liquid and vapour phases.

Use of direct contact condensers in sea-water desalination, in conventional and geothermal power plants and, more recently, in emergency core cooling and pressure suppression systems for nuclear reactors, have stimulated a considerable amount of research which has mainly focussed on the following:

- (1) condensation on droplets and sprays,
- (2) condensation on falling films or sheets of liquid,
- (3) condensation in subcooled liquid pools.

* McNaught, J.M. (1981) "An assessment of design methods for condensation of vapours from a non-condensing gas". Seminar on "Advances in Heat Exchangers". Int. Centre for Heat and Mass Transfer, Dubrovnik, Yugoslavia.

Condensation on Droplets and Sprays

Theoretical models have been developed for the condensation of pure vapours (both miscible and immiscible with the drop) [109-113] and vapour-gas mixtures [114-116]. In the theoretical modelling [109-116], it is generally assumed that (a) the drops are spherical, (b) convection within the drop is negligible (except in [114-116]), and (c) the surface temperature of the drops as they emerge from the nozzle is the saturation temperature. Brown [109] obtained a simple analytical result for the mean drop temperature as a function of time and drop diameter,

$$\frac{T_{\ell 2} - T_{\ell 1}}{T_g - T_{\ell 1}} = 1 - \frac{6}{\pi^2} \sum_{n=1}^{\infty} \left\{ \frac{1}{n^2} \exp \left(- \frac{4 n^2 \pi^2 \kappa t}{D^2} \right) \right\} \quad (69)$$

This equation is shown graphically in Figure 25. For other fluids, the time required to achieve a desired duty is,

$$t = t_W \kappa_W / \kappa \quad (70)$$

It is evident from Figure 25 that the drops which are smaller than 1 mm attain the saturation temperature of the condensing vapour in no more than a few tenths of a second. In such a short time, the drops would only have travelled a distance of a few nozzle diameters. Thus most of the condensation occurs in the near nozzle region where jet break-up and droplet formation are taking place. Beyond this region, the drops interact with the vapour and with each other only hydrodynamically [117-119].

More recent numerical studies have considered the effect on heat transfer rate of the drop growth rate [110], drop size distribution [111], the thermal resistance of the condensate film [112], the drop and vapour velocities [113], convection within the drop [114-116] and the gas-phase resistance [114-116]. The importance of these effects will depend on the drop size and the presence of non-condensing gases, and the physical properties of the coolant used.

Condensation on Falling Films or Sheets of Liquid

Theoretical solutions have been developed for the condensation of pure vapours (both miscible [120-121] and immiscible [122] with the coolant) and binary miscible vapour mixtures [123]. In the theoretical formulations, it is generally assumed that the condensate film completely wets the sheet of subcooled liquid. The sheet is divided into two regions as shown in Figure 26. In the figure, the line $y = 0$ may either be considered as the centre line of the falling sheet of liquid or as a solid wall, in the case of the falling film. In [120,121,123], the line $y = 0$ was assumed to be isothermal, whereas in [122] it was assumed to be adiabatic. For the condensation of a pure vapour on a falling film, the total length of the plate, z_{final} , required for the complete use of the heat capacity of the coolant is given by [122]:

$$z_{\text{final}} = 55.9 \text{ Ja}^{0.6} \text{ Pr}_\ell^{-0.144} \text{ Pr}_f^{1.35} \text{ Re}_f^{4/3} (\nu_\ell/\nu_f)^{1/8} \quad (71)$$

This empirical expression fits numerical solutions to within $\pm 10\%$ and is applicable to situations in which $(\nu_\ell/\nu_f) < 0.2$ and $(\lambda_\ell/\lambda_f) > 0.3$.

In [123] consideration was given to the condensation of a binary vapour mixture on falling sheets on liquid. The general trends observed were similar to those found in film condensation of binary mixtures on a cooled wall [124-126].

Condensation in Subcooled Liquid Pools

Condensation of vapour by sparging into a pool of subcooled liquid is used for suppressing large amounts of vapour in the event of plant malfunction. It is also used for the direct steam heating of a process fluid. Variations in the injection configuration, flowrate, pool subcooling and other properties, result in distinct behaviour patterns [127,128] which can broadly be classified as:

- (a) Bubbling - the vapour bubbles through the pool with little or no condensation.
- (b) Chugging - this is an irregular process which has four consecutive stages;
 - (i) vapour flow forces liquid out of the injection pipe,
 - (ii) a bubble grows at the end of the pipe,
 - (iii) the bubble collapses,
 - (iv) the liquid surges into the pipe.

Large pressure pulses occur during chugging.

- (c) Oscillatory - a regular oscillatory process with pressure variations approaching the level attained in chugging.

Figure 27 shows a flow pattern map obtained for steam at about 100 kPa [128].

Early theoretical investigations [129-136] assumed the bubbling flow pattern and were motivated by applications to sea-water desalination and geothermal power plants. The systems studied included one and two (immiscible) components with or without non-condensing gas. In these studies, the main assumptions made were: (a) the flow field around the spherical vapour bubble is given by the potential flow theory; (b) the bubble rises at a constant velocity; and (c) a thin condensate film on the inner surface of the bubble continuously drains into a pool at the bottom of the bubble. The bubble collapse rate is given by [136] as:

$$\frac{D}{D_0} = \left[1 - \left\{ \frac{3 \sqrt{2}}{4 \pi \Delta h_v} \frac{P_l - P_g}{\rho_l \rho_g} C_2 \right\} / D_0^{3/2} t \right]^{2/3} \quad (72)$$

where C_2 is a complex function of fluid properties and the difference between the saturation and liquid temperatures and D_0 is the initial diameter.

With the exception of [133,134], the work in references [129-136] is for the case of a single bubble. In [133,134] Sideman considered the case of a bubble train. In this case, the bubble frequency is an important parameter affecting both the temperature field and the bubble rise velocity. Future work to improve the hydrodynamic modelling, particularly for multiple bubble trains, and the modelling of the effect of non-condensing gas are needed.

More recent work has been directed at understanding the chugging phenomenon. Sargis and co-workers [137-139] have developed analytical models to investigate steam chugging phenomena in light water reactor pressure suppression pools. The models are based on fundamental mass, momentum and energy conservation equations in both phases and include empirical descriptions of the motion and behaviour of the interface between phases. These investigations have resulted in several computer codes, e.g. CHUG and SAMPAC, which are able to reproduce both qualitatively and quantitatively the measurements of laboratory-scale experiments in small tanks.

CONCLUSIONS

This review has revealed significant recent progress in many aspects of condensation theory. However, it is surprising that a number of fundamental issues are still unresolved and that there is a continuing lack of information on some important aspects of design.

Many important processes relevant to condenser design have not been discussed in this review. For example, the topics of condensation on enhanced heat-transfer surfaces, condensation of immiscible liquids, wet wall desuperheating, fogging and the calculation of mean temperature differences in condensers have been omitted entirely. For further information on these topics, the reader is referred to the papers by Butterworth [1], Bell and Panchal [140], Collier [141], Marto and Nunn [142] and Nakayama [143].

SYMBOLS USED

[B]	matrix of multicomponent mass-transfer coefficients ($\text{kmol/m}^2\text{s}$)
c_p	specific heat capacity (J/kg K)
C_p	specific molar heat capacity (J/kmol K)
D	diameter (m)
D	multicomponent diffusion coefficient (m^2/s)
dp_T/dz	local frictional pressure gradient (N/m^3)
E	dimensionless parameter defined in equation (47) (-)
F	dimensionless parameter defined in equation (48) (-)
F_B	bypass correction factor (-)
F_L	leakage correction factor (-)
F_W	window correction factor (-)
Fr	Froude number defined in equation (21) (-)
F_1	dimensionless parameter defined in equation (3) (-)
F_2	dimensionless parameter defined in equation (4) (-)
f	friction factor (-)
G	dimensionless parameter defined in equation (54) (-)
G_a	Galileo number defined in equation (20) (-)
g	gravitational acceleration (m/s^2)
\mathbf{I}_L	diagonal unit matrix (-)
J_j	molar diffusive flux of component j ($\text{kmol/m}^2\text{s}$)
Ja	Jakob number (-)
\dot{m}	mass flux ($\text{kg/m}^2\text{s}$)
\dot{m}_c	condensing mass flux ($\text{kg/m}^2\text{s}$)
N	Number of tubes in a vertical row (-)
\dot{n}	molar flux ($\text{kmol/m}^2\text{s}$)
Pr	Prandtl number (-)
p	pressure (Pa)
Q	cumulative heat release rate from condensing stream (W)
\dot{q}	heat flux ($\text{W/m}^2 \text{K}$)
Re	Reynolds number (-)
T	temperature (K)

T^+	dimensionless film temperature drop (-)
t	time (s)
U	axial velocity (m/s)
u	mean velocity (m/s)
u^*	friction velocity (m/s)
\dot{v}	superficial velocity (m/s)
\dot{v}^*	dimensionless superficial velocity (-)
X	Martinelli parameter defined in equation (2) (-)
x	quality (-)
\tilde{y}_j	vapour mole fraction of component j (-)
Z	factor defined in equation (60) (-)
z	axial co-ordinate (m)

Greek

α	heat-transfer coefficient ($W/m^2 K$)
β_{jk}	mass-transfer coefficient for components j and k ($kg/m^2 s$)
Γ_N	condensate drainage from the N^{th} tube in a bundle (kg)
γ	dimensionless parameter defined in equation (28) (-)
γ_N	condensate generated on the N^{th} tube in a bundle (kg)
Δh_v	specific enthalpy of evaporation (J/kg)
$\tilde{\Delta h}_v$	specific molar enthalpy of evaporation (J/kmol)
Δp	pressure drop (Pa)
ΔT	temperature difference (K)
δ	film thickness (m)
δ	binary mass diffusion coefficient (m^2/s)
δ^+	dimensionless film thickness defined in equation (34) (-)
ϵ_g	void fraction (-)
η	viscosity (Ns/m^2)
θ_F	mass-transfer correction factor defined in equation (25) (-)
κ	thermal diffusivity (m^2/s)
λ	thermal conductivity ($W/m K$)
ν	kinematic viscosity (m^2/s)
ρ	density (kg/m^3)
σ	surface tension (N/m)
τ	shear stress (N/m^2)
ϕ^2	two-phase frictional multiplier(-)
$[\phi]$	elements of high flux correction matrix (-)
ϕ_T	heat-transfer rate factor (-)
χ	dimensionless parameter defined in equation (53) (-)
ψ	dimensionless parameter defined in equation (29) (-)
Ω	factor in equation (31) (-)

Subscripts

b	bulk
eff	effective
f	falling film
g	gas
go	when total flow has gas properties
i	vapour-liquid interface
l	liquid (i.e. condensate)
lN	value for the N^{th} tube in a vertical row
lo	when total flow has liquid properties
$l1$	top tube of bundle; also inlet conditions (see equation (69))
$l2$	exit conditions (see equation (69))
t	total
W	water
w	wall

Superscripts

- mean
 ~ molar

REFERENCES

1. Butterworth, D., 1977, "Developments in the Design of Shell-and-Tube Condensers", ASME, Paper 77-WA/HT-24.
2. Palen, J.W., Breber, G. and Taborek, J., 1979, Heat Transfer Engg., 1, 2, 47-57.
3. Breber, G., Palen, J.W. and Taborek, J., 1980, Trans. ASME, 102, 471-476.
4. Quandt, E., 1965, "Analysis of Gas-Liquid Flow Patterns", Chem. Engg. Prog. Symp. Series, 61, 57, 128.
5. Golan, L.P. and Stenning, A.H., 1969, "Two-Phase Vertical Flow Maps", Proc. Instn. Mech. Engrs., No. 184, Part 3c, 108-114.
6. Wallis, G.B., 1969, "One-Dimensional Two-Phase Flow", McGraw-Hill, New York.
7. Soliman, H. and Azer, N.Z., 1971, ASHRAE Trans., 77, 1, 210-224.
8. Soliman, H. and Azer, N.Z., 1974, "Visual Studies of Flow Patterns During Condensation Inside Horizontal Tubes", Proc. 5th Int. Heat Transfer Conf., Tokyo, Paper Csl.6, 3, 241-245.
9. Traviss, D.P. and Rosenhow, W.M., 1973, ASHRAE Trans., 79, 2, 31-39.
10. Fisher, S.A., Harrison, G.S. and Pearce, D.L., 1978, "Instrumentation for Localised Measurements with Fast Response in Liquid/Vapour Flows", Symposium on Measurements in Polyphase Flows, ASME Winter Annual Meeting, San Francisco, 73-80.
11. Taitel, Y. and Dukler, A.E., 1976, AIChE J., 22, 1, 47-55.
12. Lockhart, R.W. and Martinelli, R.C., 1949, Chem. Engg. Prog., 45, 39-48.
13. Jaster, H. and Kosky, P.G., 1976, Heat Mass Transfer, 19, 95-99.
14. Butterworth, D., 1975, Int. J. Multiphase Flow, 1, 845-850.
15. Butterworth, D. and Hewitt, G.F., 1977, "Two-Phase Flow and Heat Transfer", Oxford University Press.
16. Soliman, H.M., 1982, Can. J. Chem. Engg., 60, 4, 475-481.
17. Oshinowo, T. and Charles, M.E., 1974, Can. J. Chem. Engg., 52, 25-35.
18. Grant, I.D.R. and Murray, I., 1972, "Pressure Drop on the Shellside of a Segmentally Baffled Shell and Tube Heat Exchanger with Vertical Two-Phase Flow", NEL Report No. 500.

19. Grant, I.D.R. and Murray, I., 1974, "Pressure Drop on the Shellside of a Segmentally Baffled Shell and Tube Heat Exchanger with Horizontal Two-Phase Flow", NEL Report No. 560.
20. Grant, I.D.R., 1975, "Flow and Pressure Drop with Single- and Two-Phase Flow on the Shellside of Segmentally Baffled Shell and Tube Heat Exchangers", in "Advances in Thermal and Mechanical Design of Shell and Tube Heat Exchangers", NEL Report 590, 1-22.
21. Baker, O., 1954, Oil and Gas Journal, 53, 185-195.
22. Bell, K.J., Taborek, J. and Fenoglio, F., 1970, Chem. Engg. Prog. Symp. Series, 66, 102, 150-163.
23. Hewitt, G.F. and Roberts, D.N., 1969, "Studies of Two-Phase Flow Patterns by Simultaneous X-Ray and Flash Photography", Report AERE-M 2159, UKAEA, Harwell.
24. Mandhane, J.M., Gregory, G.A. and Aziz, K., 1974, Int. J. Multiphase Flow, 1, 537-553.
25. Weisman, J., Duncan, D., Gibson, J. and Crawford, T., 1979, Int. J. Multiphase Flow, 5, 437-462.
26. Soliman, M., Schuster, J.R. and Berenson, P.J., 1968, Trans. ASME, 90, 2, 267-276.
27. Traviss, D.P., Baron, A.B. and Rohsenow, W.M., 1971, "Forced Convection Condensation Inside Tubes", Dept. of Mech. Engg., MIT, Report No. DSR 72591-74.
28. Owen, R.G., Sardesai, R.G. and Butterworth, D., 1981, "Two-Phase Pressure Drop for Condensation Inside a Horizontal Tube", Symp. on Advancement in Heat Exchangers, Int. Centre for Heat and Mass Transfer, Dubrovnik.
29. Sardesai, R.G., Owen, R.G. and Pulling, D.J., 1982, "Pressure Drop for Condensation of a Pure Vapour in Downflow in a Vertical Tube", Proc. 7th Int. Heat Transfer Conf., Munich, Paper Cs23.
30. Whalley, P.B., Azzopardi, B.J., Hewitt, G.F. and Owen, R.G., 1982, "A Physical Model for Two-Phase Flows with Thermodynamic and Hydrodynamic Non-Equilibrium", Proc. 7th Int. Heat Transfer Conf., Munich, Paper Cs29.
31. Mickley, H.S., Ross, R.C., Squyers, A.L. and Stewart, W.E., 1954, "Heat, Mass and Momentum Transfer for Flow Over a Flat Plate with Blowing or Suction", Report No. NACA-TN-3208.
32. Bird, R.B., Stewart, W.E. and Lightfoot, E.N., 1962, "Transport Phenomena", Wiley, New York.
33. Pearce, D.L., 1977, "Development of the Horizontal Annular Flow Model: Axial Shear Stresses at the Wall", Private Communication.
34. Chisholm, D., 1973, Int. J. Heat Mass Transfer, 16, 347-358.

35. Bell, K., 1963, "Final Report of the Co-Operative Research Program on Shell and Tube Heat Exchangers", Univ. Delaware, Engineering Experimental Station, Bulletin No.5.
36. Short, B.E., 1947, ASME, Paper 47-A-105.
37. Short, B.E., 1943, "Heat Transfer and Pressure Drop in Heat Exchangers", Univ. of Texas, Publ. No.4324.
38. Tinker, T., 1947, ASME, Paper 47-A-130.
39. Tinker, T., 1948, Trans. ASME, 89-116.
40. Donohue, D.A., 1949, Ind. Engg. Chem., 41, 11, 2499-2511.
41. Williams, R.B. and Katz, D.L., 1952, Trans. ASME, 74, 1307-1320.
42. Kern, D.Q., 1950, "Process Heat Transfer", McGraw-Hill, New York.
43. Buthod, A.P., 1960; Oil and Gas Journal, 58, 67-82.
44. Palen, J.W. and Taborek, J., 1969, Chem. Engg. Prog. Symp. Series, 65, 92, 55-63.
45. Parker, R.O. and Mok, Y.I., 1968, Brit. Chem. Engg., 13, 3, 366-368.
46. Grant, I.D.R. and Murray, I., 1972, Private Communication.
47. Moore, M.J.C., 1979, Private Communication.
48. Johnston, D. and Wills, M.J.N., 1981, Private Communication.
49. Johnston, D. and Wills, M.J.N., 1982, Private Communication.
50. Nusselt, W., 1916, Z.V.D.I., 60, 27, 541-546 and 60, 28, 569-575.
51. Colburn, A.P., 1934, Trans. Am. Inst. Chem. Engrs., 30, 187-193.
52. Rohsenow, W.M., Webber, J.H. and Ling, A.T., 1956, Trans. ASME, 78, 1637-1643.
53. Dukler, A.E., 1960, Chem. Engg. Prog. Symp. Series, 56, 30, 1-10.
54. Lee, J., 1964, AIChE J., 10, 4, 540-544.
55. Blangetti, F.L. and Schlunder, E.U., 1978, "Local Heat Transfer Coefficients on Condensation in a Vertical Tube", Proc. 6th Int. Heat Transfer Conf., Toronto, 2, Paper CS-10, 437-442.
56. Blangetti, F.L. and Schlunder, E.U., 1979, "Local Heat Transfer Coefficients in Film Condensation at High Prandtl Numbers", in "Condensation Heat Transfer", ASME/AIChE, 17-25.
57. Chaddock, J.B., 1957, Refriger. Engg., 65, 4, 36-41 and 90-95.
58. Chato, J.C., 1962, ASHRAE J., 4, 2, 52-60.

59. Knudsen, J.G. and Katz, D.L., 1958, "Fluid Dynamics and Heat Transfer", McGraw-Hill, New York.
60. Alfman, M., Staub, F.W. and Norris, R.H., 1960, Chem. Engg. Prog. Symp. Series, 56, 30, 151-159.
61. Kosky, P.G. and Staub, F.W., 1971, AIChE J., 17, 5, 1037-1043.
62. Bae, S., Maulbetsch, J.S. and Rohsenow, W.M., 1970, "Refrigerant Forced-Convection Condensation Inside Horizontal Tubes", MIT Report No. DSR 72591-71.
63. Carpenter, E.F. and Colburn, A.P., 1951, "The Effect of Vapour Velocity on Condensation Inside Tubes", Proc. Instn. Mech. Engrs., Gen. Disc. Heat Transfer, 20-26.
64. Boyko, L.D. and Kruzhilin, G.N., 1967, Int. J. Heat Mass Transfer, 10, 361-373.
65. Kern, D.Q., 1958, AIChE J., 4, 2, 157-160.
66. Grant, I.D.R., 1972, "Film Condensation of Pure Vapours", in "Notes for Condensation and Condensers Course", Birniehill Institute, NEL.
67. Grant, I.D.R. and Osment, B.D.J., 1968, "The Effect of Condensate Drainage on Condenser Performance", NEL Report No.350.
68. Butterworth, D., 1981, "Inundation Without Vapor Shear", in "Power Condenser Heat Transfer Technology", Ed. Marto, P.J. and Nunn, R.H., 271-278.
69. Short, B.E. and Brown, H.E., 1951, "Condensation of Vapours on Vertical Banks of Horizontal Tubes", Proc. Instn. Mech. Engrs., Gen. Disc. Heat Transfer, 27-31.
70. Shekriladze, I.G. and Gomelauri, V.I., 1966, Int. J. Heat Mass Transfer, 9, 581-591.
71. Fujii, T., Uehara, H. and Kurata, C., 1972, Int. J. Heat Mass Transfer, 15, 235-246.
72. Honda, H. and Fujii, T., 1974, Proc. 5th Int. Heat Transfer Conf., Tokyo, 3, 299-303.
73. Fujii, T., Honda, H. and Oda, K., 1979, "Condensation of Steam on a Horizontal Tube", in "Condensation Heat Transfer", ASME/AIChE, 35-43.
74. Lee, W.C., 1982, "Filmwise Condensation on a Horizontal Tube in the Presence of Forced Convection and Non-Condensing Gas", Ph.D Thesis, Queen Mary College, London University.
75. Lee, W.C. and Rose, J.W., 1982, "Film Condensation on a Horizontal Tube - Effect of Vapour Velocity", Proc. 7th Int. Heat Transfer Conf., Munich, Paper Cs17.
76. Gogonin, I.I. and Dorokhov, A.R., 1971, Heat Transfer Soviet Research, 3, 6, 157-161.

77. Nicol, A.A. and Wallace, D.J., 1974, "The Influence of Vapour Shear Force on Condensation on a Cylinder", Symp. on Multi-Phase Flow Systems, Instn. Chem. Engrs., Symp. Ser. No.38, Paper D3, I-19.
78. Nicol, A.A. and Wallace, D.J., 1976, "Condensation with Appreciable Vapour Velocity and Variable Wall Temperature", Symp. on Steam Turbine Condensers, NEL Report No.619, 27-38.
79. Nobbs, D.W. and Mayhew, Y.R., 1976, "Effect of Downward Vapour Velocity and Inundation on Condensation Rates in Horizontal Tube Banks", Symp. on Steam Turbine Condensers, NEL Report No.619, 39-52.
80. Gogonin, I.I. and Dorokhov, A.R., 1976, J. Appl. Mech. Tech. Phys., 17, 2, 252-257.
81. Fuks, S.N. and Zernova, E.P., 1970, Thermal Engg., 17, 3, 84-90.
82. Fujii, T., Uehara, H., Hirata, K. and Oda, K., 1972, Int. J. Heat and Mass Transfer, 15, 247-260.
83. Ivanov, O.P., Butyrskaya, S.T. and Mamchenko, V.O., 1972, Heat Transfer Soviet Research, 4, 6, 143-149.
84. Kutateladze, S.S., Gogonin, I.I., Dorokhov, A.R. and Sosunov, V.I., 1979, Thermal Engg., 26, 5, 270-273.
85. Gogonin, I.I. and Sosunov, V.I., 1981, Theor. Found. Chem. Engg., 15, 2, 125-129.
86. Fujii, T., 1981, "Vapor Shear and Condensate Inundation", in "Power Condenser Heat Transfer Technology", Ed. Marto, P.J. and Nunn, R.H., 193-223.
87. McNaught, J.M., 1982, "Two-Phase Forced Convection Heat Transfer During Condensation on Horizontal Tube Bundles", Proc. 7th Int. Heat Transfer Conf., Munich, Paper Cs21.
88. Silver, L., 1947, Trans. Inst. Chem. Engrs., 25, 30-42.
89. Bell, K.J. and Ghaly, M.A., 1973, AIChE Symp. Series, 69, 131, 72-79.
90. McNaught, J.M., 1979, "Mass-Transfer Correction Terms in Design Methods for Multicomponent/Partial Condensers", in "Condensation Heat Transfer", ASME/AIChE, 111-118.
91. Price, B.C. and Bell, K.J., 1974, AIChE Symp. Series, 70, 138, 163-171.
92. Krishna, R. and Panchal, C.B., 1977, Chem. Engg. Sci., 32, 7, 741-745.
93. Ackermann, G., 1937, Ver. D. Ing. Forschungsheft, 8, 382, 1-10.
94. Sardesai, R.G., 1979, "Studies in Condensation", Ph.D. Thesis, UMIST.
95. Toor, H.L., 1964, AIChE J., 10, 448 and 460.
96. Krishna, R. and Standart, G.L., 1976, AIChE J., 22, 2, 383-389.

97. Panchal, C.B., 1977, "Multicomponent Transfer Processes in Condensation", Ph.D. Thesis, UMIST.
98. Wilke, C.R., 1950, Chem. Engg. Prog., 46, 95.
99. Deo, P.V., 1979, "Condensation of Mixed Vapour", Ph.D. Thesis, UMIST.
100. Krishnamurthy, R. and Taylor, R., 1981, "Algorithms for the Calculation of Interphase Mass and Energy Transfer in Multicomponent Systems", Proc. HTFS Res. Symp., Paper RS404.
101. Webb, D.R. and Taylor, R., 1982, Chem. Engg. Sci., 37, 1, 117-119.
102. Sparrow, E.M., Minkowycz, W.J. and Saddy, M., 1967, Int. J. Heat Mass Transfer, 10, 1829-1845.
103. Schroppel, J., 1981, Int. J. Heat Mass Transfer, 24, 165-170.
104. Koh, J., 1962, "Laminar Film Condensation of Condensable Gases and Mixtures on a Flat Plate", Proc. 4th USA Nat. Cong. Appl. Mech., 2, 1327-1336.
105. Fujii, T., Uehara, H., Mihara, K. and Kato, Y., 1977, "Forced Convection Condensation in the Presence of Non-Condensables - A Theoretical Treatment for Two-Phase Laminar Boundary Layer", Univ. Kyushu, Res. Inst. Ind. Sci., Report No.66, 53-80.
106. Rose, J.W., 1980, Int. J. Heat Mass Transfer, 23, 539-546.
107. Rose, J.W., 1981, "Condensation in the Presence of Non-Condensing Gases", in "Power Condenser Heat Transfer Technology", Ed. Marto, P.J. and Nunn, R.H., 151-162.
108. Lee, W.C. and Rose, J.W., 1983, "Comparison of Calculation Methods for Non-Condensing Gas Effects in Condensation on a Horizontal Tube", Proc. Int. Symp. Condensers - Theory and Practice, UMIST.
109. Brown, G., 1951, "Heat Transmission by Condensation of Steam on a Spray of Water Drops", Proc. Instn. Mech. Engrs., General Disc. Heat Transfer, London, 49-52.
110. Ford, J.D. and Lekic, A., 1973, Int. J. Heat Mass Transfer, 16, 61-64.
111. Lekic, A., Bajramovic, R. and Ford, J.D., 1976, Can. J. Chem. Engg., 54, 399-402.
112. Jacobs, H.R. and Cook, D.S., 1978, "Direct Contact Condensation on a Non-Circulating Drop", Proc. 6th Int. Heat Transfer Conf., Toronto, 2, 389-393.
113. Lekic, A. and Ford, J.D., 1980, Int. J. Heat Mass Transfer, 23, 1531-1537.
114. Kulic, E., Rhodes, E. and Sullivan, G., 1975, Can. J. Chem. Engg., 53, 252-258.
115. Kulic, E. and Rhodes, E., 1977, Can. J. Chem. Engg., 55, 131-137.

116. Kulic, E. and Rhodes, E., 1978, "Heat Transfer Rates to Moving Droplets in Air/Steam Mixtures", Proc. 6th Int. Heat Transfer Conf., Toronto, Paper FB-34, 1, 469-474.
117. Dix, G.E., 1979, "BWR Core Spray Distribution", 7th USA Nuclear Regulatory Commission Water Reactor Safety Research Information Meeting, Gaithersburg.
118. Sandoz, S.A., Myers, L.L., Sutherland, W.A., Schumacher, D.G. and Dix, G.E., 1979, "Core Spray Design Methodology Confirmation Tests", Gen. Electric Co., Report No. Nedo-24712.
119. Sandoz, S.A. and Sutherland, W.A., 1980, "Core Spray Performance", 19th Nat. Heat Transfer Conf., ASME, "Experimental and Analytical Modelling of LWR Safety Experiments", Orlando, 109-114.
120. Murty, N.S. and Sastri, V.M.K., 1974, "Condensation on a Falling Laminar Liquid Film", Proc. 5th Int. Heat Transfer Conf., Tokyo, Paper Csl.4, 3, 231-235.
121. Murty, N.S. and Sastri, V.M.K., 1976, Can. J. Chem. Engg., 54, 633-635.
122. Jacobs, H.R. and Bogart, J.A., 1980, "Condensation on Immiscible Falling Films", ASME/AICHE Heat Transfer Conf., Orlando, Paper 80-HT-110.
123. Tamir, A., Taitel, Y. and Schlunder, E.U., 1974, Int. J. Heat Mass Transfer, 17, 1253-1260.
124. Sparrow, E.M. and Marschall, E., 1969, Trans. ASME, 91, 205-211.
125. Denny, V.E. and Jusionis, V.J., 1972, Int. J. Heat Mass Transfer, 15, 2143-2153.
126. Marschall, E. and Hickman, R.S., 1973, Trans. ASME, 95, 1-5.
127. Sargis, D.A., Masiello, P.J. and Stuhmiller, J.H., 1979, "A Probabilistic Model for Predicting Steam Chugging Phenomena", in "Condensation Heat Transfer", ASME/AICHE, 85-91.
128. Chan, C.K. and Lee, C.K.B., 1982, Int. J. Multiphase Flow, 8, 1, 11-20.
129. Sideman, S. and Hirsch, G., 1965, AIChE J., 11, 1019.
130. Isenberg, J.A. and Sideman, S., 1970, Int. J. Heat Mass Transfer, 13, 997-1010.
131. Isenberg, J.A., Moalem, D. and Sideman, S., 1970, "Direct Contact Heat Transfer with Phase Change: Bubble Collapse with Translatory Motion in Single and Two-Component Systems", Proc. 4th Int. Heat Transfer Conf., Paris, 5, 258-268.
132. Moalem, D. and Sideman, S., 1971, Int. J. Heat Mass Transfer, 14, 2152-2156.
133. Moalem, D., Sideman, S., Orell, A. and Hetsroni, G., 1972, "Condensation of Bubble Train - An Approximate Solution", in "Progress in Heat and Mass Transfer", Pergamon Press, Oxford, 6, 155-178.

134. Moalem, D. and Sideman, S., 1973, Int. J. Heat Mass Transfer, 16, 2305-2319.
135. Moalem, D. and Sideman, S., 1973, Int. J. Heat Mass Transfer, 16, 2321-2329.
136. Jacobs, H.R., Fannar, H. and Beggs, G.C., 1978, "Collapse of a Bubble of Vapour in an Immiscible Liquid", Proc. 6th Int. Heat Transfer Conf., Toronto, 2, 383-388.
137. Sargis, D.A., Stuhmiller, J.H. and Wang, S.S., 1979, "Analysis of Steam Chugging Phenomena", Report EPRI NP-962, 1.
138. Sargis, D.A., Masiello, P.J., Stuhmiller, J.H. and Wang, S.S., 1981, "Analysis of Steam Chugging Phenomena", Report EPRI NP-1305, 1.
139. Wang, S.S. and Stuhmiller, J.H., 1981, "Analysis of Steam Chugging Phenomena", Report EPRI NP-1305, 4.
140. Bell, K.J. and Panchal, C.B., 1978, "Condensation", Proc. 6th Int. Heat Transfer Conf., Toronto, 6, 361-375.
141. Collier, J.G., 1981, "Convective Boiling and Condensation", McGraw-Hill, U.K.
142. Marto, P.J. and Nunn, R.H., 1981, "Power Condenser Heat Transfer Technology", Hemisphere Pub. Corp., New York.
143. Nakayama, W., 1982, "Enhancement of Heat Transfer", Proc. 7th Int. Heat Transfer Conf., Munich, 1.

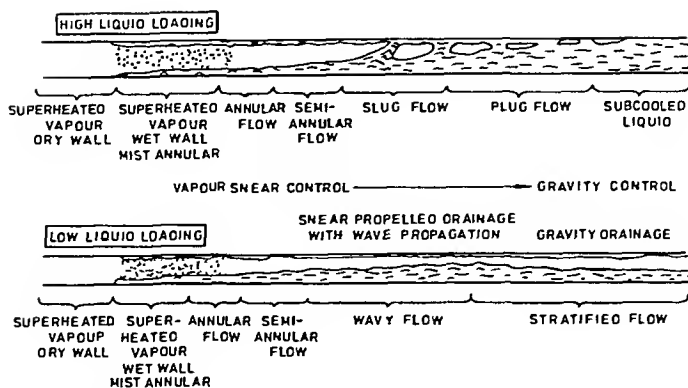


FIG.1. ILLUSTRATION OF FLOW PATTERNS IN TUBESIDE CONDENSATION

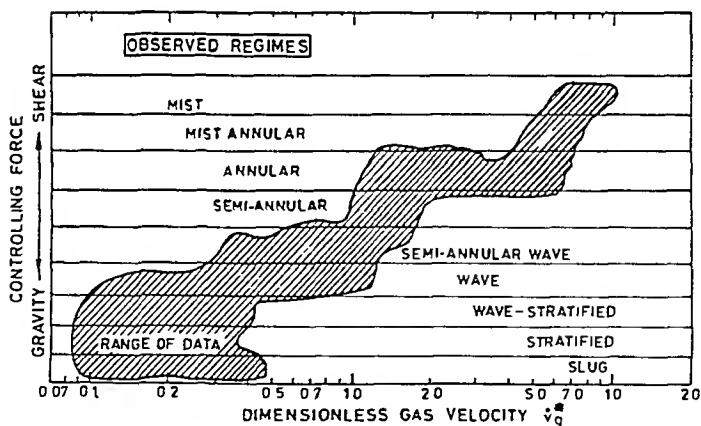


FIG. 2. CONDENSATION FLOW REGIMES AS A FUNCTION OF THE DIMENSIONLESS SUPERFICIAL GAS VELOCITY

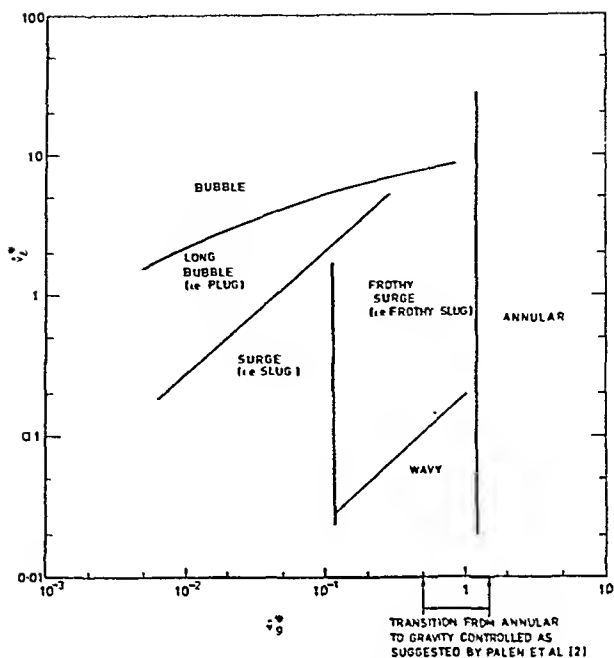


FIG 3 FISHER ET AL [10] FLOW PATTERN MAP PLOTTED ON CO-ORDINATES OF DIMENSIONLESS GAS AND LIQUID VELOCITIES

$$F = \hat{v}_g \rho_g^{1/2} / \sqrt{(\rho_L - \rho_g) g D} = \hat{v}_g^* \quad ; \quad T = \left[\frac{dp_F/dz}{(\rho_L - \rho_g) g} \right]^{1/2} \quad ; \quad K = \left[\frac{\rho_g \hat{v}_g^2 \hat{v}_L}{(\rho_L - \rho_g) g \frac{1}{2}} \right]^{1/2} \quad X = \left[\frac{dp_F/dz}{dp_F/dz_g} \right]^{1/2}$$

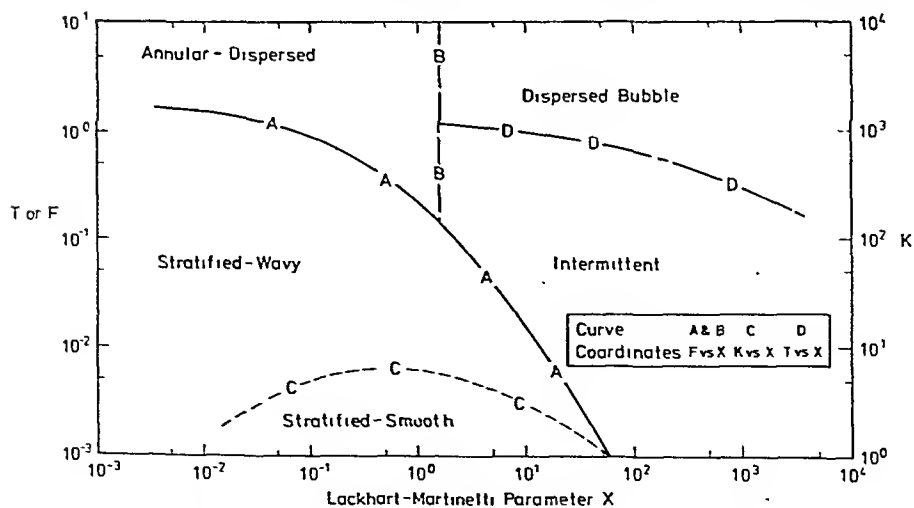


FIG 4 THE FLOW PATTERN MAP OF TAITEL AND DUKLER [11].

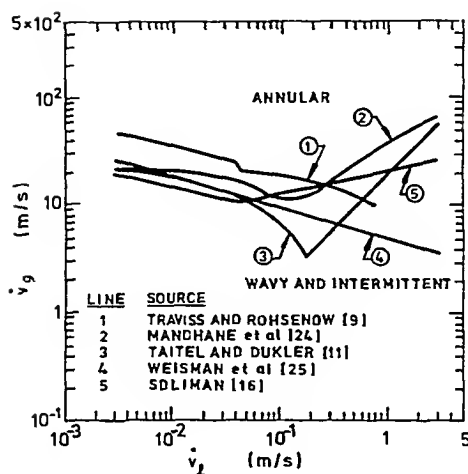


FIG. 5 COMPARISON BETWEEN DIFFERENT TRANSITION CRITERIA FOR WATER FLOW IN A 25.4 mm I.D. HORIZONTAL TUBE AT STANDARD (25°C) CONDITIONS.

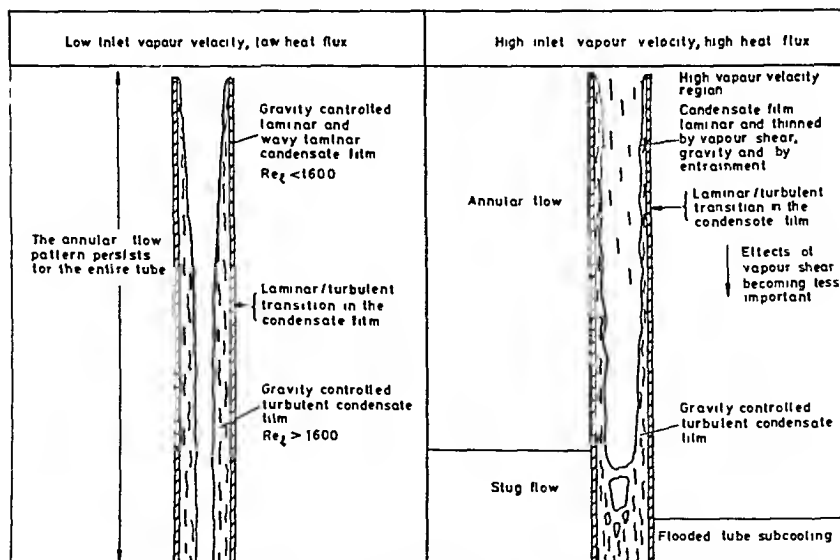


FIG 6 FLOW PATTERNS IN VERTICAL TUBES FOR DOWNFLOW CONDENSATION

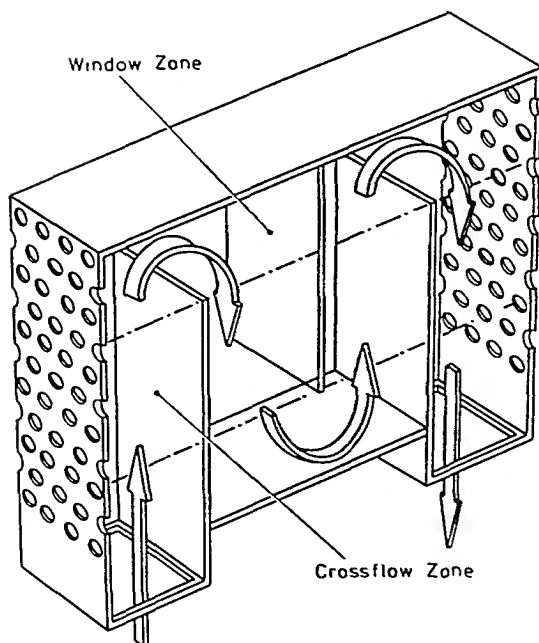


FIG 7 EXPERIMENTAL HEAT EXCHANGER OF GRANT AND MURRAY [18,19].

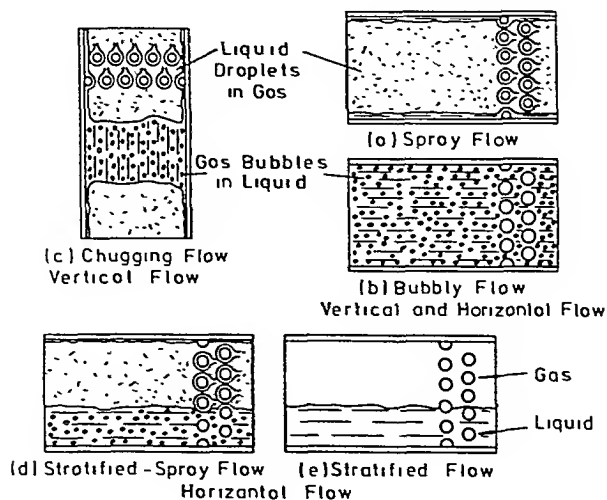


FIG. 8 SHELL-SIDE TWO-PHASE FLOW PATTERNS OBSERVED BY GRANT [20].

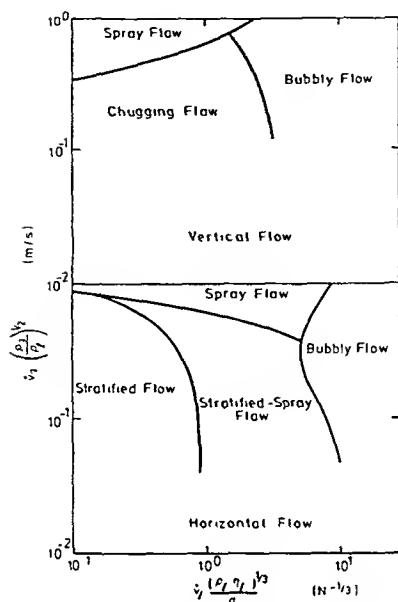


FIG 9 SHELL-SIDE FLOW PATTERN MAPS OBTAINED BY GRANT [20]

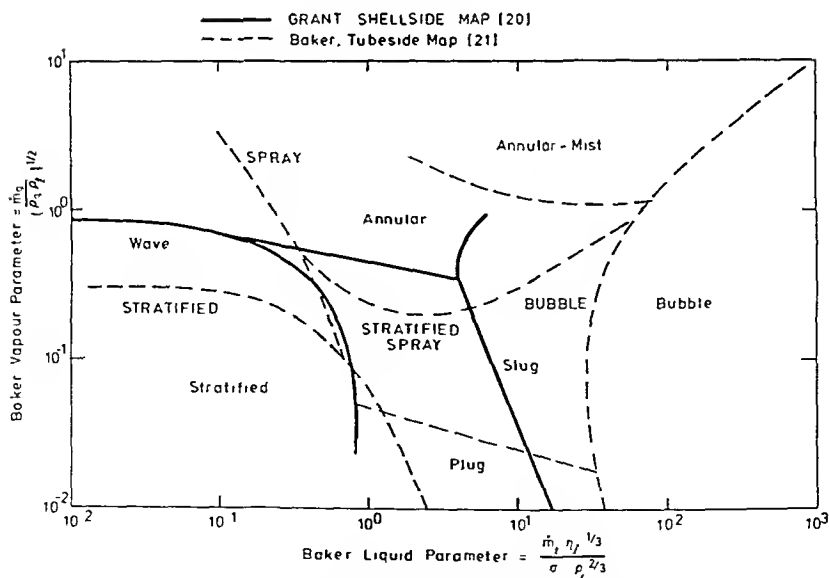


FIG 10 COMPARISON OF THE GRANT SHELLSIDE FLOW PATTERN MAP WITH THAT OF BAKER FOR TUBESIDE FLOW

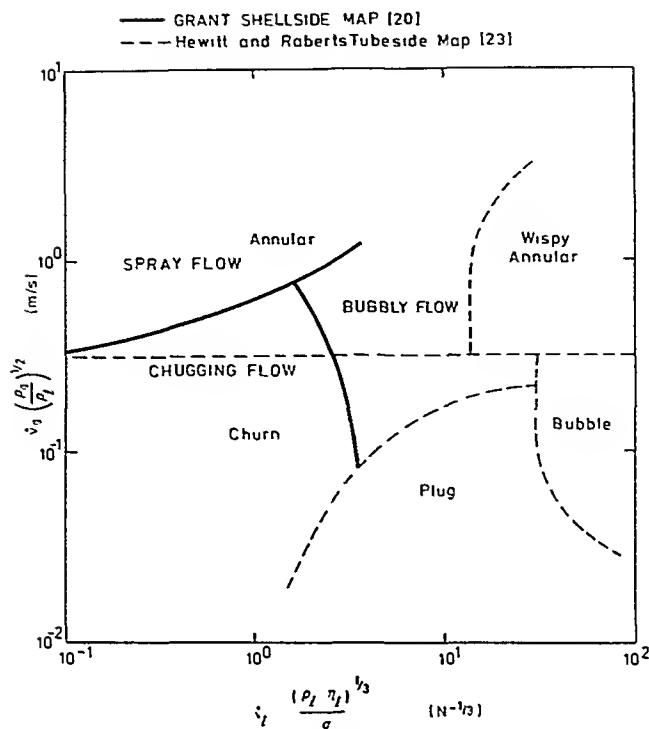


FIG. 11 VERTICAL FLOW OF AIR/WATER AT ATMOSPHERIC PRESSURE

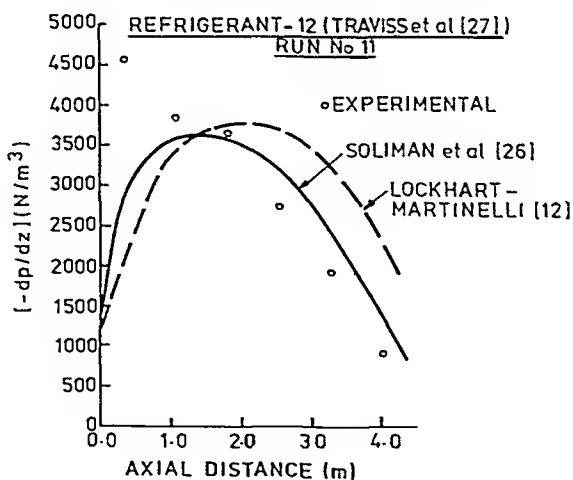


FIG. 12. THE VARIATION OF PRESSURE GRADIENT ALONG A CONDENSER TUBE.

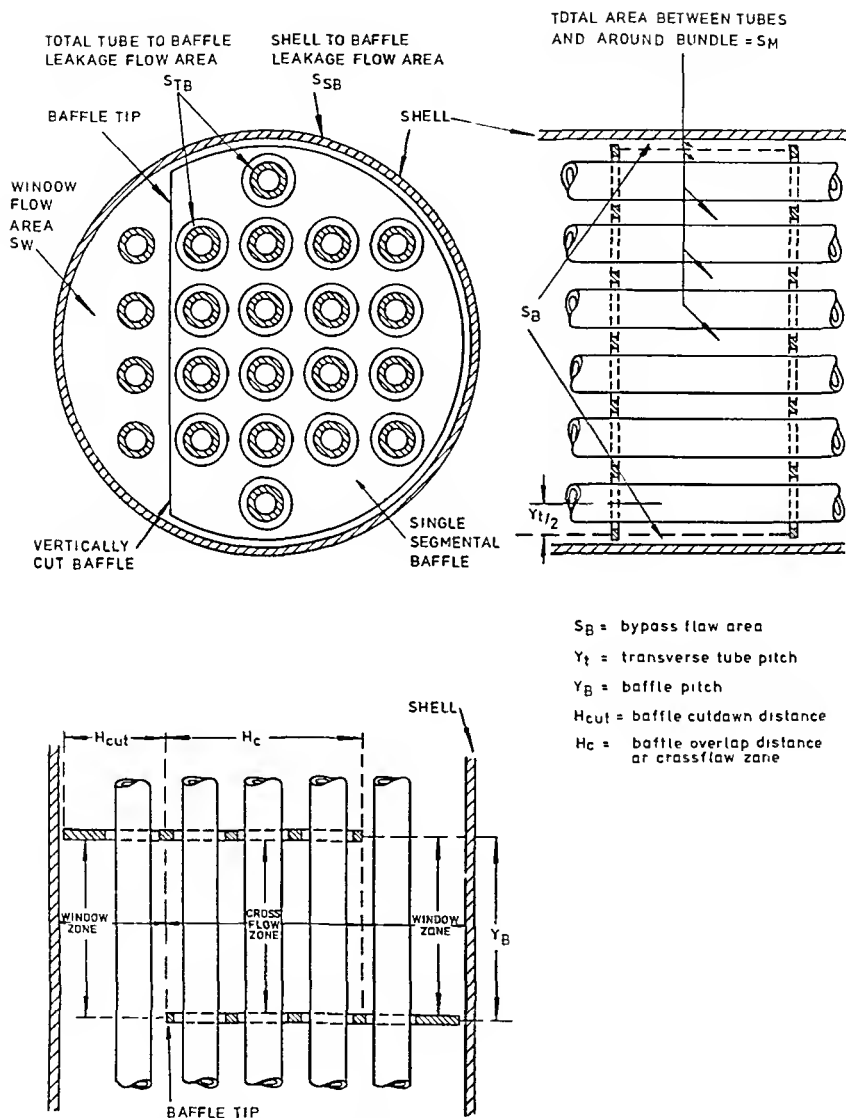


FIG. 13 BAFFLE SPACE GEOMETRY IN A SHELL AND TUBE CONDENSER
(1st ANGLE PROJECTION)

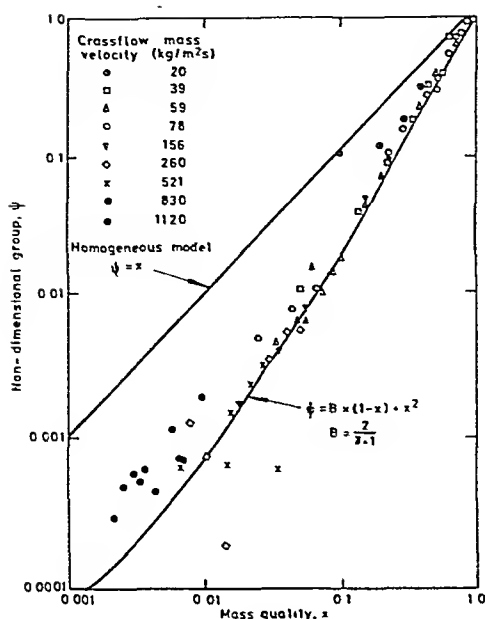


FIG 14 TWO-PHASE PRESSURE DROP IN WINDOW ZONE
(HORIZONTAL SIDE-TO-SIDE FLOW)

S_M = crossflow flow area, taken near equator of tube bundle

S_L = total leakage flow area = $S_{TB} + S_{SB}$

S_{SB} = shell to baffle leakage flow area

S_B = bypass flow area

S_{TB} = tube-to-baffle leakage flow area

Re_c = crossflow Reynolds number

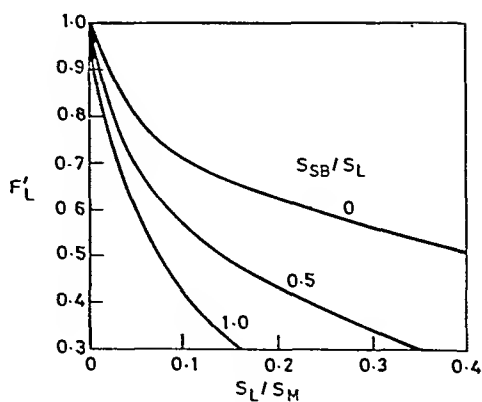
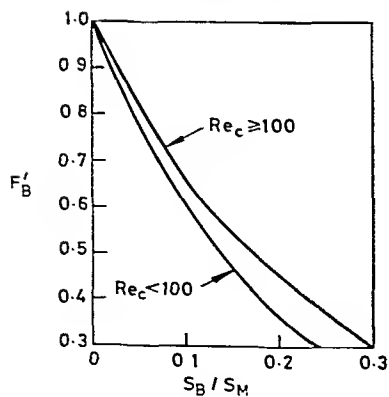


FIG 15 BELL [35] CORRECTION FACTORS FOR SHELLSIDE PRESSURE DROP

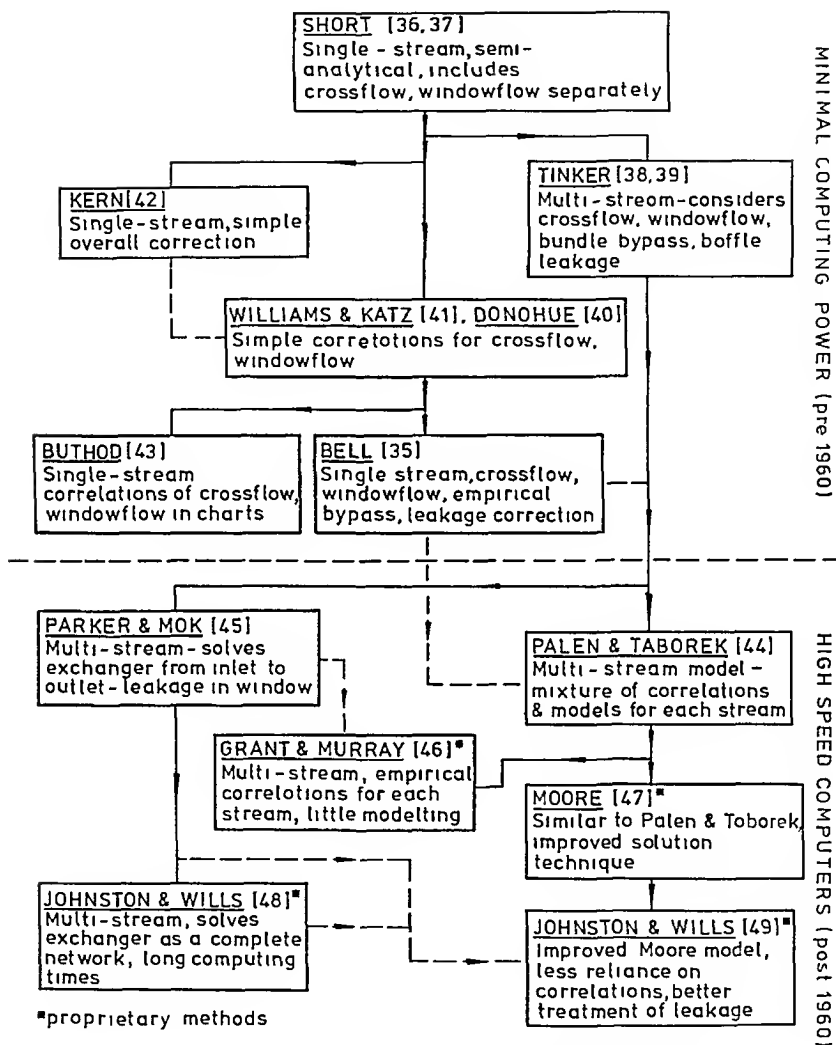
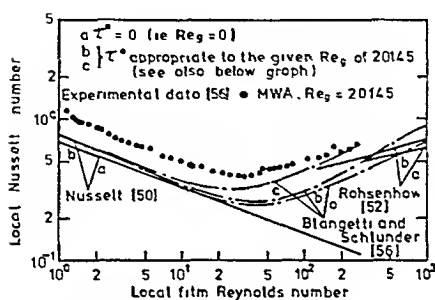
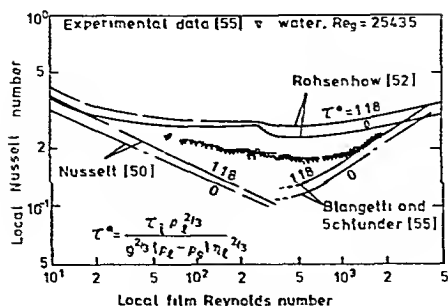


FIG 16 DEVELOPMENT OF SHELLSIDE PRESSURE DROP PREDICTION METHODS



legend: {
 b temperature profile development not explicitly accounted for
 c temperature profile development included

FIG. 17. CONDENSING NUSSULT NUMBERS INSIDE A VERTICAL TUBE AS A FUNCTION OF CONDENSATE FILM REYNOLDS NUMBER, AFTER BLANGETTI AND SCHLUNDER [55,56].

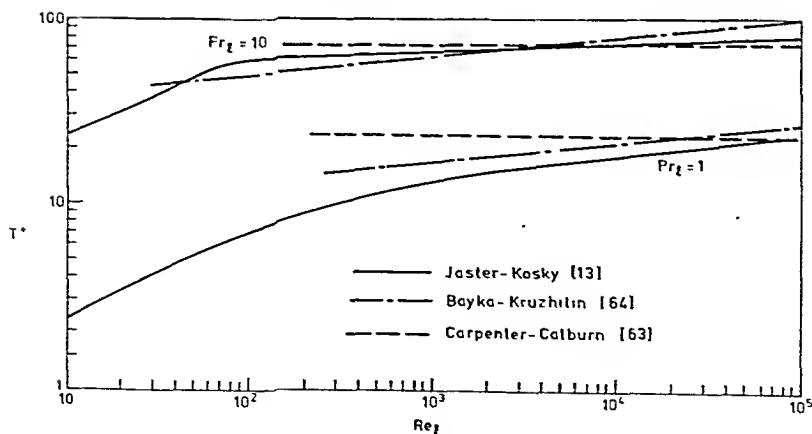


FIG 18 A COMPARISON OF METHODS FOR CALCULATING T^* (AFTER BUTTERWORTH [1])

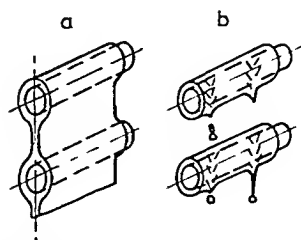


FIG. 19. DOWNWARD FLOW OF CONDENSATE.
a) according to Nusselt; b) actual flow pattern.

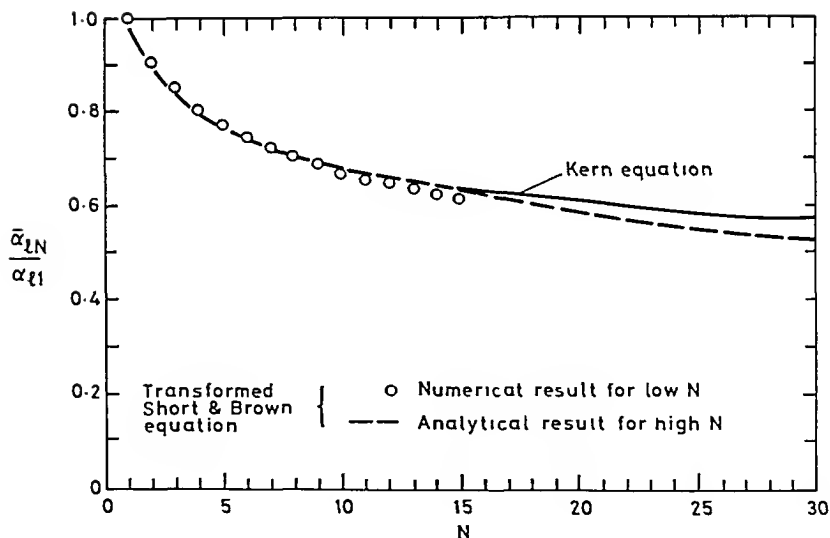


FIG. 20. COMPARISON OF KERN METHOD FOR INUNDATION
WITH THE SHORT AND BROWN METHOD.

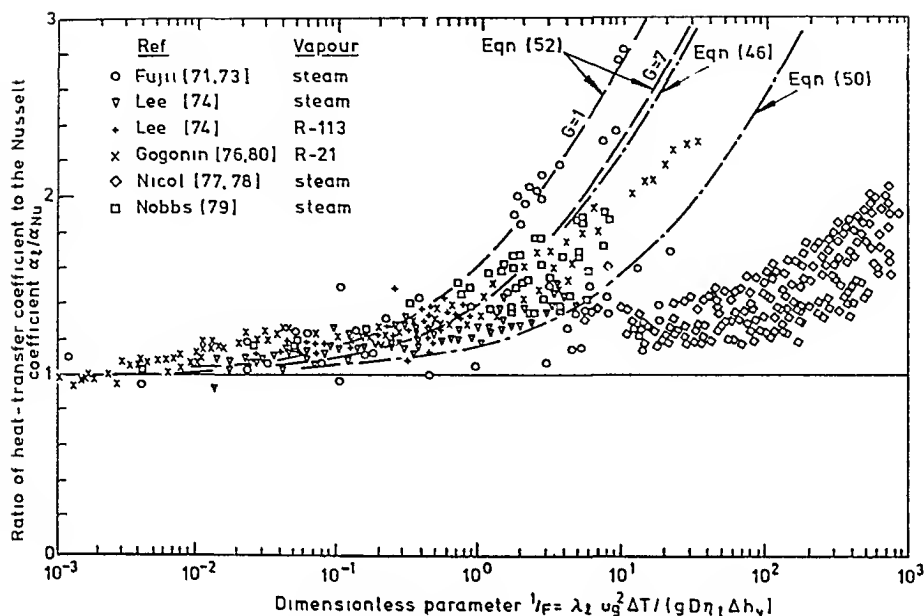


FIG 21 COMPARISON OF SINGLE-TUBE MEASUREMENTS WITH THEORY

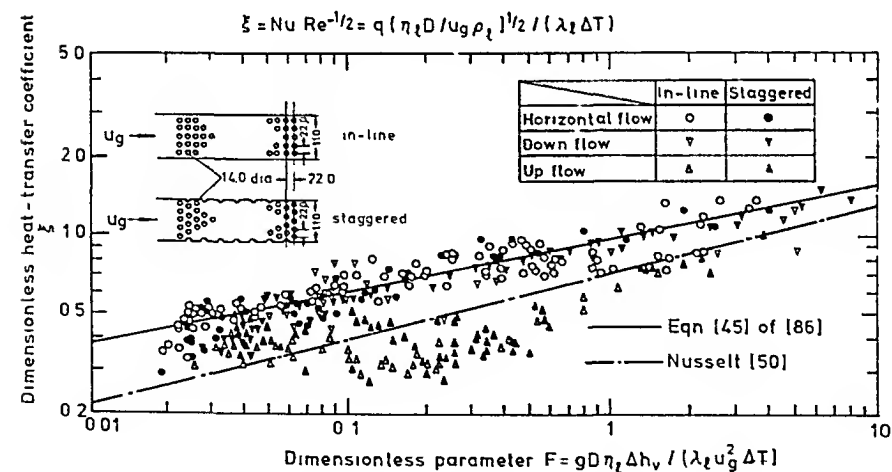
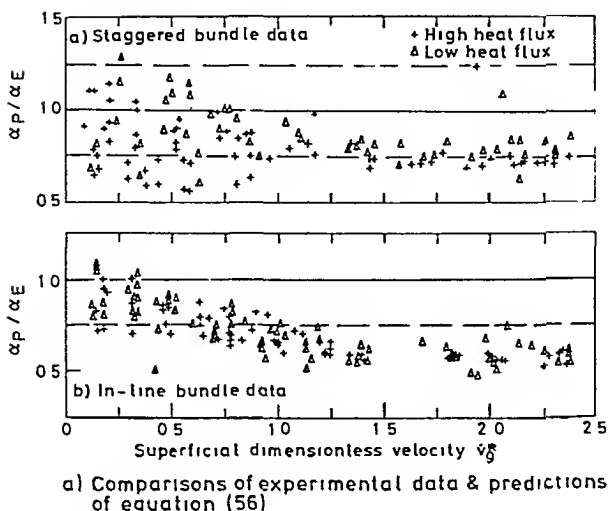
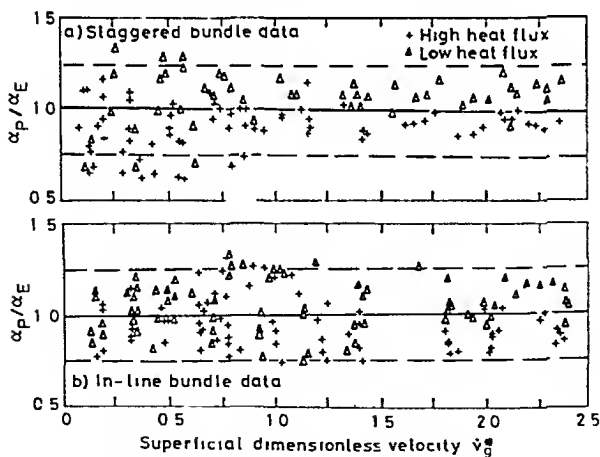


FIG 22 RELATIONSHIP BETWEEN DIMENSIONLESS HEAT TRANSFER COEFFICIENT AND F FOR HORIZONTAL, DOWNWARD AND UPWARD FLOW IN IN-LINE AND STAGGERED BANKS [AFTER FUJII [86)]



a) Comparisons of experimental data & predictions of equation (56)

α_P = predicted heat transfer coefficient
 α_E = experimental heat transfer coefficient



b) Comparisons of experimental data & predictions of equation (57)

FIG 23 COMPARISON OF PREDICTED & MEASURED HEAT-TRANSFER COEFFICIENTS FOR THE COMBINED EFFECT OF INUNDATION & VAPOUR SHEAR (AFTER McNAUGHT [87])

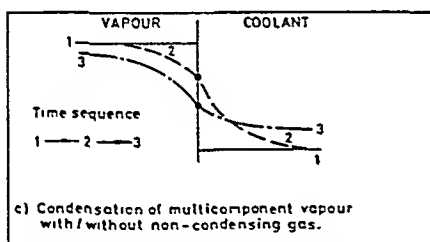
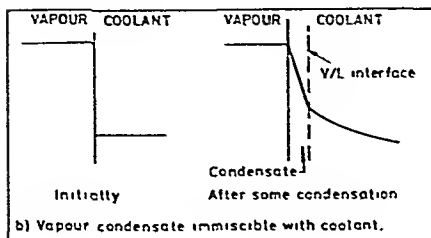
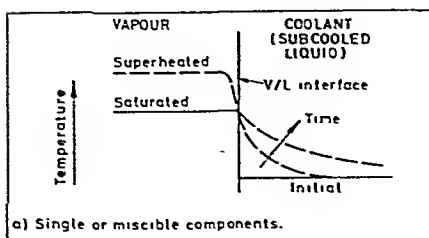
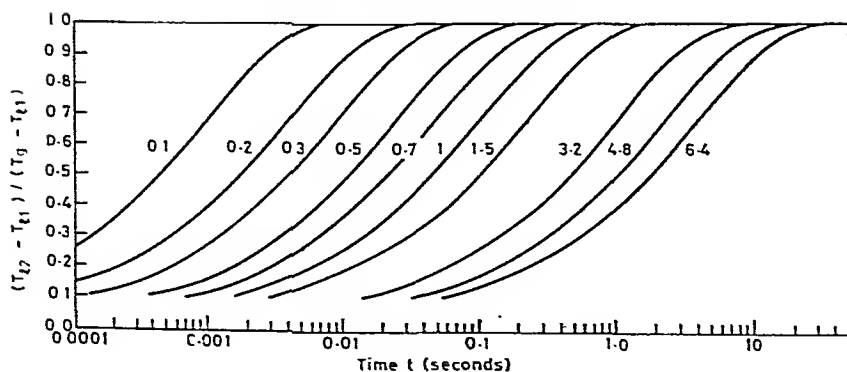


FIG 24. TEMPERATURE PROFILES DURING DIRECT-CONTACT CONDENSATION

FIG. 25. TIME OF HEATING FOR SPHERES OF WATER WITH THERMAL DIFFUSIVITY OF $1.68 \times 10^{-7} \text{ m}^2 \text{ s}^{-1}$. THE NUMBERS ON THE CURVES GIVE THE DROP DIAMETERS IN mm. (AFTER BROWN [109]).

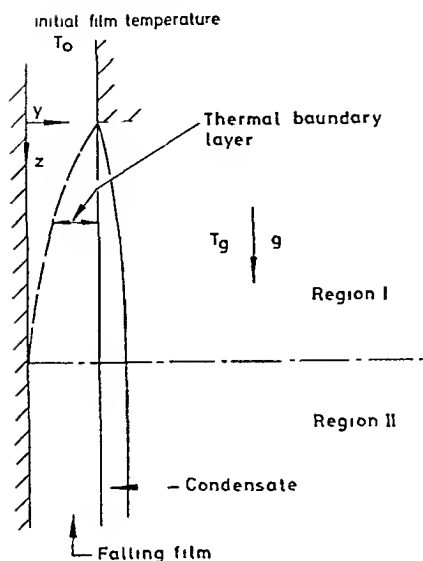


FIG. 26 PHYSICAL MODEL FOR CONDENSATION ON FALLING FILMS OF LIQUID AFTER JACOBS [122]

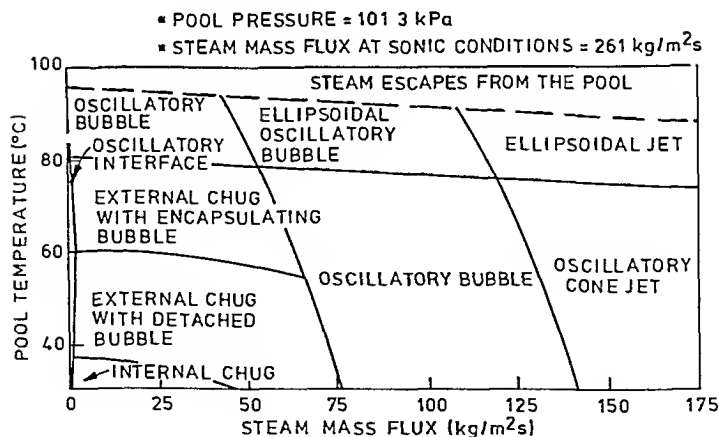


FIG. 27. FLOW PATTERN MAP FOR CONDENSATION OF STEAM IN A SUBCOOLED WATER POOL. (AFTER CHAN AND LEE [128]).

FORCED CONVECTION CONDENSATION OF REFRIGERANTS INSIDE A VERTICAL ANNULUS

A. Cavallini^{*}, S. Frizzerin^{*}, and L. Rossetto^{*}

Experimental data on local heat transfer coefficients and pressure drops are reported for refrigerants R-11 and R-113 condensing in the shear dominated regime inside an annular vertical duct. These data are compared with results from an analysis similar to that established for forced convection condensation inside pipes; calculated heat transfer data are conservative, with a mean deviation around 15%. Similar predictions can be obtained from semiempirical equations proposed for circular ducts.

INTRODUCTION

Figure 1 is a schematic diagram of the experimental apparatus used to measure the mean and local heat transfer coefficients and the pressure drops for saturated condensing pure vapours of refrigerants R-11 and R-113. The condensation occurs in forced convection conditions, on the outside surface of the inner pipe of a vertical annular duct, with internal diameter $D_1 = 24$ mm, external diameter $D_2 = 38.5$ mm and total length of the condensing section $L = 2$ m. The apparatus and the general procedure used in the tests have already been extensively described by Cavallini et al. in reference (1), where the mean heat transfer coefficients on the whole test heat transfer surface have been considered; the comparison of these values with the predictions from semiempirical correlations or theoretical analyses available in the open technical literature and applicable to the phenomenon under study has given the following results:

- Butterworth's theoretical analysis (2) overestimates the experimental results within 50%;
- the semiempirical equation proposed by Shah (3) underestimates the experimental data within 20 - 25%;
- both Cavallini - Zecchin's and Boyko - Kruzhilin's semiempirical equations (4),(5) underestimate the experimental data within 15%, with a better aggregation of the points for this last equation.

In this present study the pressure drop values and the local heat transfer coefficients are given; the experimental results are compared with the values predicted by an approximate fluid-dynamic analysis applied to the annular section here considered and suggested for safe design predictions and with values given by the Boyko-Kruzhilin's semiempirical equation. This equation in

* Istituto di Fisica Tecnica, Università di Padova, 35100 Padova, Italy.

fact, among the many proposals in literature concerning the prediction of the heat transfer coefficients, has turned out to be the most suitable in the operative conditions regarding the mean data on the whole heat transfer surface.

EXPERIMENTAL PROCEDURE

The general experimental procedure undertaken in the tests is extensively described in reference (1).

With regard to the local heat transfer coefficients on the condensing surface, these have been calculated by measuring the saturation pressure of the condensing vapour, the local temperature on the heat transfer area and the heat transfer flux density.

The methods for measurement of the saturation pressure and the surface temperature have been described in the previous paper (1). Heat flow rate, has been computed along ten successive condensing sections of equal area, by measuring the cooling water flow rate and the relative temperature rises. The water cools the condensing section by flowing in a bayonet type configuration (1); measurement of the temperature rise is carried out only in the downwards flow of water in direct contact with the heat transfer surface in the outside annulus of the bayonet. In estimating the heat flow rate in each section the temperature rise of the cooling water flowing upwards in the inner bayonet pipe is taken into account. Those rises have been computed by numerical solution of the energy equation and are checked against the total temperature variation measured between inlet and outlet of the bayonet.

In the annulus of the bayonet the temperature rises in each section have been measured using two independent copper-constantan thermocouples, directly inserted in the cooling water; for the final computation the mean values of the two independent readings have been taken. Direct differential temperature readings between successive thermocouples were obtained. Helicoidal continuous inserts give a high degree of turbulence and of mixing in the annular section of the cooling bayonet.

To measure the thermocouple e.m.f. a digital multimeter with a $1 \mu\text{V}$ resolution was used; special care has been taken in avoiding spurious e.m.f. in the measuring circuit, as more extensively described by Cavallini et al. in (6).

The pressure drops were measured in three adjacent sections in the experimental duct, each 0.6 m long beginning at 0.1 m from the entrance.

In Table 1 the ranges of the operating conditions relative to the experimental data considered in this work are given.

FLUID-DYNAMIC ANALYSIS

Following the approach for condensation of pure vapours inside circular pipes adopted by Kosky and Staub (7) and Traviss et al (8), the flow model con-

TABLE 1 - Ranges of parameters for the experimental runs.

	R-11	R-113
Number of data-points	120	190
Pressure, p (kPa)	144 - 104	134 - 109
Vapor quality	0.987 - 0.426	0.986 - 0.144
Heat flux density, \dot{q} (W/m^2)	71200 - 14300	100900 - 14700
Mass velocity, \dot{m} ($\text{kg/m}^2 \text{ s}$)	198 - 43.4	217 - 66.4
Superficial vapor velocity, w_v (m/s)	23.7 - 2.37	24.6 - 1.19
Temperature difference, ΔT (K)	18.1 - 5.5	37.7 - 7.1

sidered is a separated flow one, with the liquid flowing as a film along the internal surface of the inner pipe of the annulus (heat transfer area). Further the assumption of constant shear stress throughout the liquid film is made.

Applying the Von Karman momentum - heat transfer analogy to calculate the liquid layer thermal resistance, one gets to the following expression for the Nusselt number:

$$\text{Nu} = \frac{\alpha D_h}{\lambda_f} = \frac{1}{T^+} \frac{\rho_f D_h c_f}{\lambda_f} u_{\tau 1} \quad (1)$$

where the dimensionless parameter T^+ can be written, assuming the Von Karman universal velocity distribution inside pipes to hold for the liquid layer, as a function of δ^+ as:

$$\begin{aligned} T^+ &= \delta^+ \text{Pr}_f & \delta^+ \leq 5 \\ T^+ &= 5 \left[\text{Pr}_f + \ln(1 + \text{Pr}_f (\delta^+/5 - 1)) \right] & 5 < \delta^+ < 30 \\ T^+ &= 5 \left[\text{Pr}_f + \ln(1 + 5 \text{Pr}_f) + 0.495 \ln(\delta^+/30) \right] & \delta^+ \geq 30 \end{aligned} \quad (2)$$

while in turn the dimensionless film thickness δ^+ may be obtained, for the proposed model, from the liquid layer Reynolds number Re_f by the relations (see ref. (7)):

$$\begin{aligned} \delta^+ &= \left(\frac{\text{Re}_f}{2} \right)^{0.5} & \text{Re}_f \leq 1145 \\ \delta^+ &= 0.0504 \text{Re}_f^{7/8} & \text{Re}_f > 1145 \end{aligned} \quad (3)$$

For Nusselt number calculations through equation (1) it is therefore necessary to evaluate the friction velocity on the heat transfer surface $u_{\tau_1} = \sqrt{\tau_1/\rho_l}$, and therefore the relative value of the shear stress τ_1 .

To evaluate the shear stress on the inner surface τ_1 , one can first calculate the wall shear stress for adiabatic two-phase flow with the same flow parameters, assuming equal values on the inside and outside surface of the annulus ($\tau_{1ad} = \tau_{2ad}$). This assumption underestimates the final value of the shear stress at the condensing wall, bringing about a conservative evaluation of the heat transfer coefficient, while only slightly affecting the calculation of the pressure gradient; an alternative procedure is under development. The method proposed by Friedel (9) for the evaluation of the frictional component of two-phase pressure drop in vertical pipes with downward flow is used:

$$\phi_{l0}^2 = \left(\frac{dp_f}{dz} \right)_{ad} / \left(\frac{dp_f}{dz} \right)_{l0} = C + 48.6 x^{0.8} (1-x)^{0.29} \left(\frac{\rho_l}{\rho_v} \right)^{0.9} \left(\frac{\eta_v}{\eta_l} \right)^{0.73} \left(1 - \frac{\eta_v}{\eta_l} \right)^{7.4} Fr_{tp}^{0.03} / We_{tp}^{0.12} \quad (4)$$

$$\text{with } C = (1-x)^2 + x^2 (\rho_l \xi_{vo} / \rho_v \xi_{lo})$$

The friction factors for single phase flow ξ_{vo} and ξ_{lo} are calculated for the specific annulus as Deubel (10).

Therefore:

$$\tau_{1ad} = \tau_{2ad} = - \left(\frac{dp_f}{dz} \right)_{ad} \frac{D_h}{4} \quad (5)$$

To take into account the effect of the mass transfer at the liquid-vapour interface during condensation, the shear stress at the inner surface has finally been calculated according to Mickley et al (11):

$$\frac{\tau_1}{\tau_{1ad}} = \frac{H}{1 - e^{-H}} \quad (6)$$

where:

$$H = \frac{\alpha (T_s - T_w) (\bar{u}_v - u_i)}{\Delta h_v \tau_{1ad}} \quad (7)$$

The mean vapour velocity \bar{u}_v is calculated considering the vapour flow cross sectional area, while the interface velocity u_i is evaluated according to the assumed universal velocity profile in the liquid film.

To calculate the pressure gradient along the condensing section one must again refer to the separated flow model considered above. Therefore:

$$\frac{dp}{dz} = \frac{dp_f}{dz} + g_n \left[\psi \rho_v + (1-\psi) \rho_l \right] - \frac{1}{2} \frac{d}{dz} \left[\frac{x^2}{\rho_v \psi} + \frac{(1-x)^2}{\rho_l (1-\psi)} \right] \quad (8)$$

with z oriented in the direction of flow. For $\delta \ll (D_2 - D_1)$ the void fraction ψ can be given by the relation:

$$\psi = 1 - 4 \delta \frac{D_1}{D_2^2 - D_1^2} \quad (9)$$

while the frictional component of the pressure gradient is obtained by the equation:

$$\frac{dp_f}{dz} = (\tau_1 D_1 + \tau_2 D_2) \frac{4}{D_2^2 - D_1^2} \quad (10)$$

with τ_1 from equation (6) and $\tau_2 = \tau_{2ad}$ from equation (5).

COMPARISON BETWEEN THE COMPUTED AND EXPERIMENTAL DATA

The diagram in figure 2 shows the comparison between the values of Nusselt numbers measured in the ten experimental sections and the corresponding values calculated by the theoretical analysis described in the above paragraph. The theoretical results, obtained at the computer by successive approximations, refer to the local experimental flow conditions; the liquid and vapour properties are estimated at the local saturation temperature. As one can see, the theoretical analysis tends to underestimate the experimental values: the standard deviation for the 190 tests on R-113 is 0.184, while for the 120 tests on R-11 the standard deviation is 0.149.

The diagram in figure 3 shows the comparison between the pressure drops (difference between inlet and exit pressures) measured in the three adjacent condensing sections each 0.6 m long, and the corresponding values estimated with the procedure shown in the above paragraph, locally applied to each section increment 20 cm long, and referring to the local experimental conditions. In evaluating the data in figure 3 one should keep in mind that the pressure drop calculation, according to equation (8), derives from the algebraic sum of three terms of the same order of magnitude, one of which (frictional component) opposite in sign to the other two (gravity and momentum components).

In the following diagrams (figure 4 and 5) the measured local Nusselt numbers are compared with the corresponding values calculated through the present analysis, in four tests chosen to represent the general trend of data. The ope-

TABLE 2 - Operating conditions for tests of Fig. 4 and Fig. 5.

Run No.	114	122	127	135
Fluid	R-113	R-113	R-11	R-11
Pressure at inlet, p_{in} (kPa)	129	119	137	134
Mass velocity, \dot{m} (kg/m ² s)	110	217	74.3	173
Vapour flow quality, x	.953-.232	.967-.473	.974-.551	.980-.661
Temp. difference, ΔT (K)	34.1-30.6	24.1-21.8	15.3-14.3	12.3-10.7

rative conditions relative to the four tests in fig. 4 and 5 are given in Table 2. These graphs point out the general regular trend of this analysis to underestimate the test results.

In the open literature several semiempirical correlations are suggested to evaluate the heat transfer coefficients for a pure vapour condensing at high velocity inside pipes. Amongst these the Boyko-Kruzhilin's one (5), which was already found suitable to predict the mean heat transfer coefficients for the annular section (1), is considered here. The Boyko-Kruzhilin's equation is the following:

$$Nu = 0.024 Re_{LT}^{0.8} Pr_L^{0.43} \sqrt{1 - x + x \rho_L / \rho_v} \quad (11)$$

The comparison between the experimental local Nusselt numbers and the corresponding values estimated through equation (11) (applied to the local experimental values of the flow parameters) is shown in fig. 6; in this case too the liquid and vapour properties have been computed at the saturation temperature. Fig. 6 diagram shows also that the Boyko-Kruzhilin's equation tends to underestimate the experimental data with standard deviation equal to 0.124 for refrigerant R-113 and 0.173 for refrigerant R-11. A similar trend was found by applying the semiempirical equation proposed by Cavallini-Zecchin (4), which too showed to be in fair agreement with the mean values of the Nusselt numbers (1).

In all computations the values used for the thermophysical properties of refrigerants R-11 and R-113 are those published by the International Institute of Refrigeration (12), (13).

CONCLUSIONS

The theoretical analysis given for the evaluation of the local heat transfer coefficients for R-11 and R-113 vapours condensing in forced convection on the inner surface of an annulus, derived from the ones already proposed for condensation inside circular pipes, turns out to be adequate to predict the experimental results considered in this paper with a mean deviation of about 15%

on the safe side; not forgetting the nature of the problem even the pressure drops prediction may be considered satisfactory. Similar predictions in regard to the local heat transfer coefficients can be obtained with Boyko-Kruzhilin's and Cavallini-Zecchin's semiempirical correlations.

SYMBOLS USED

c = specific heat capacity (J/kg K)

D = diameter (m)

$D_h = D_2 - D_1$ equivalent (hydraulic) diameter (m)

F = cross-sectional area of the channel (m²)

$Fr_{tp} = \dot{m}^2 / g_n D_h \rho_{tp}^2$ two phase Froude number

$g_n = 9.80665$ (m/s²) acceleration of gravity

Δh_v = specific latent heat of vaporization (J/kg)

L = length (m)

\dot{m} = mass flux density (kg/m² s)

\dot{M} = mass flow rate (kg/s)

$Nu = \alpha D_h / \lambda_\ell$ Nusselt number

p = pressure (N/m²)

$Pr = c \eta / \lambda$ Prandtl number

\dot{q} = heat flux density (W/m²)

$Re_\ell = 4 \dot{M} (1-x) / \pi D_1 \eta_\ell$ Reynolds number of the liquid film

Re_{LT} = liquid Reynolds number defined as $\dot{M} D_h / \eta_\ell F$

T = temperature (K)

u = velocity (m/s)

$u_\tau = \sqrt{\tau / \rho_\ell}$ friction velocity (m/s)

w_v = superficial vapour velocity (m/s)

$We_{tp} = \dot{m}^2 D_h / \rho_{tp} \sigma$ two phase Weber number

x	= vapour flow quality
z	= space coordinate (m)
α	= heat transfer coefficient ($\text{W/m}^2 \text{ K}$)
δ	= thickness of the condensate film (m)
δ^+	= $\delta u_{\tau}/\nu$
Δ	= difference
ΔT	= $T_s - T_w$ (K)
η	= dynamic viscosity (kg/m s)
λ	= thermal conductivity (W/m K)
ν	= kinematic viscosity (m^2/s)
ξ	= friction factor
ρ	= density (kg/m^3)
ρ_{tp}	= $1/(x/\rho_v + (1-x)/\rho_l)$ (kg/m^3)
σ	= surface tension (N/m)
τ	= shear stress (N/m^2)
ψ	= void fraction

Subscripts

ad	= adiabatic
f	= frictional component
i	= at the liquid-vapour interface
in	= at inlet
l	= liquid
lo	= at the same total mass flux having the liquid properties
s	= saturation

- tp = two phase
- v = vapour
- vo = at the same total mass flux having the vapour properties
- w = wall
- 1 = at the internal diameter of the annulus
- 2 = at the external diameter of the annulus

REFERENCES

1. Cavallini, A., Frizzerin, S., and Rossetto, L., 1982, "Condensation of Refrigerants inside Annuli", Proceedings of the Seventh International Heat Transfer Conference, München, Fed. Rep. of Germany.
2. Butterworth, D., 1983, "Film Condensation of Pure Vapour", Heat Exchanger Design Handbook, Hemisphere Publishing Corp., New York, U.S.A.
3. Shah, M.M., 1979, Int. J. Heat Mass Transfer, 22, 547.
4. Cavallini, A., and Zecchin, R., 1974, "A Dimensionless Correlation for Heat Transfer in Forced Convection Condensation", Proc. 5th Int. Heat Transfer Conference, Tokyo, Japan.
5. Boyko, L.D., and Kruzhilin, G.N., 1967, Int. J. Heat Mass Transfer, 10, 361.
6. Cavallini, A., Frizzerin, S., and Rossetto, L., 1981, "Forced Convection Condensation of R-11 and R-113 in Annuli", Ist. Fisica Tecnica dell'Università di Padova, Italy, Report No. 106.
7. Kosky, P.G., and Staub, F.W., 1971, A.I.Ch.E. Journal, 17, 1037.
8. Traviss, D.P., Baron, A.B., and Rohsenow, W.M., 1971, "Forced-Convection Condensation inside Tubes", M.I.T., Cambridge, Mass., U.S.A., Rep. No. DSR 72591-74.
9. Friedel, L., 1979, 3R international, 18, 485.
10. Deubel, K., 1964, Diss. TU Darmstadt, Fed. Rep. of Germany.
11. Mickley, H.S., Ross, R.C., Squyers, A.L., and Stewart, W.E., cited in Bird, R.B., Stewart, W.E., and Lightfoot, E.N., 1960, "Transport Phenomena", Wiley, New York, U.S.A., 658.
12. 1982, "Thermodynamic and physical properties of R 11", International Institute of Refrigeration, Paris, France.

13. 1982, "Thermodynamic and physical properties of R 113", International Institute of Refrigeration, Paris, France.

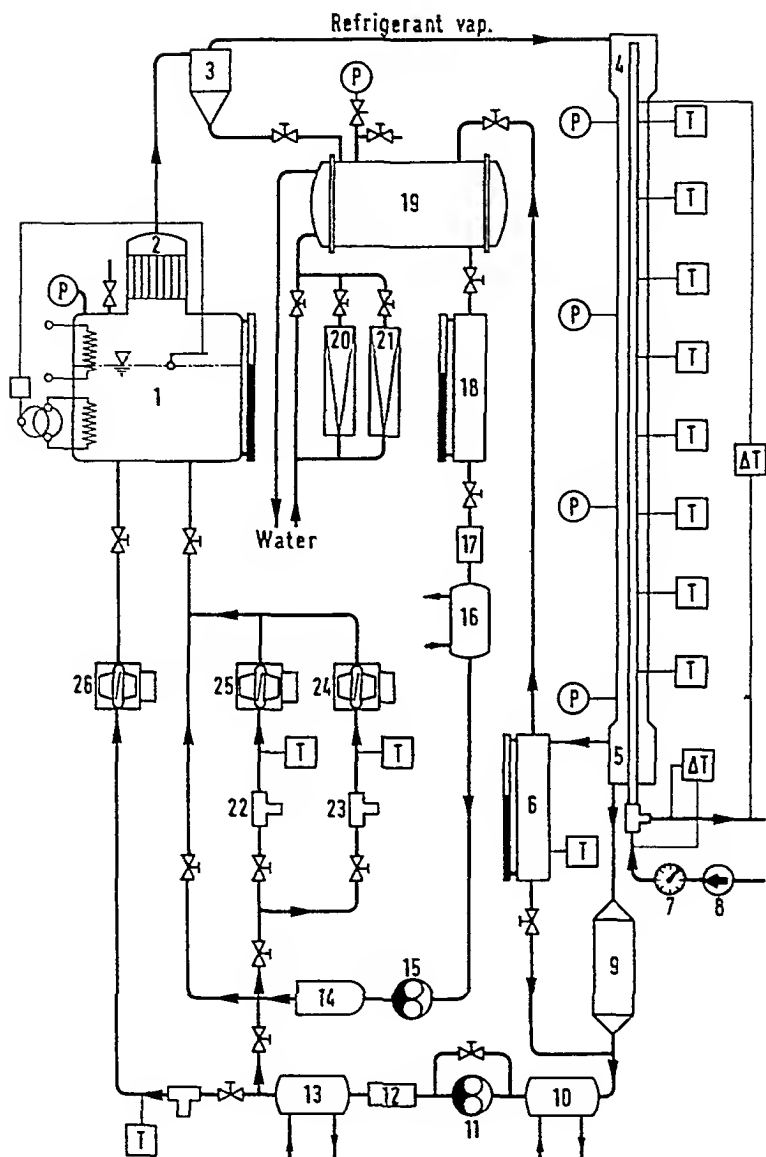


Figure 1 Scheme of the test facility

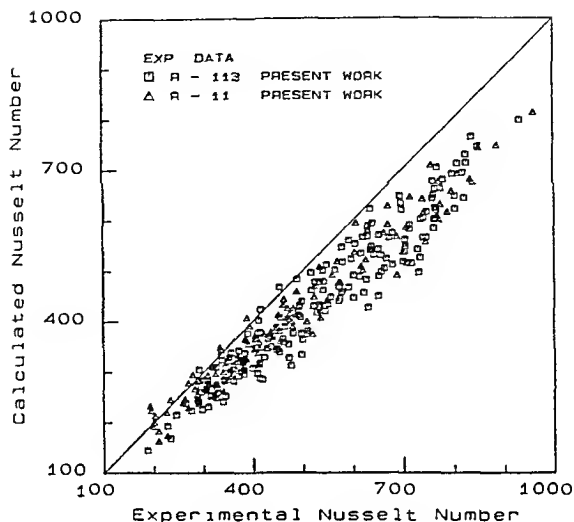


Figure 2 Measured local Nusselt Numbers compared with values calculated from the analysis outlined in the text.

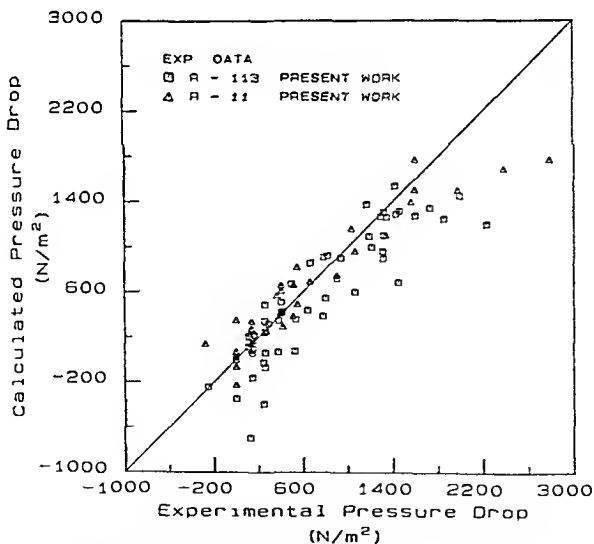


Figure 3 Measured pressure drops compared with values calculated from the analysis outlined in the text

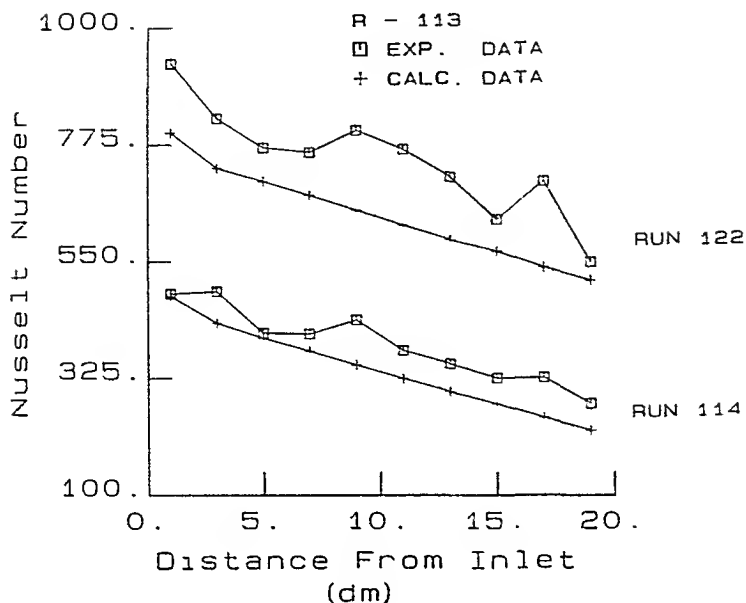


Figure 4 Measured local Nusselt Numbers and corresponding values calculated from the analysis outlined in the text

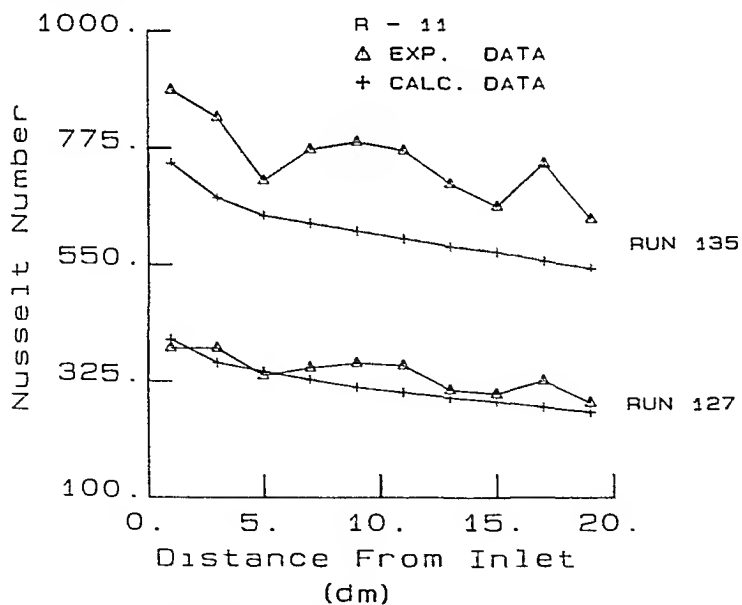


Figure 5 Measured local Nusselt Numbers and corresponding values calculated from the analysis outlined in the text

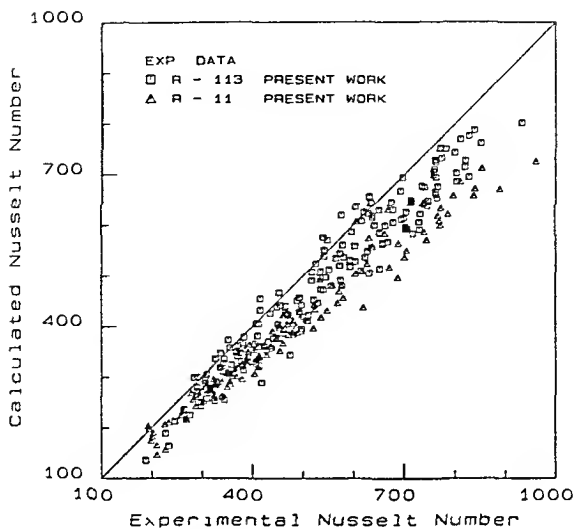


Figure 6 Measured local Nusselt Numbers compared with values calculated from Boyko-Kruzhilin equation

EFFECT OF PITCH-DIAMETER RATIO AND BY-PASS LANES ON PRESSURE LOSS IN
CONDENSER TUBE BANKS

N.K. Lee*, Y.R. Mayhew*, M.A. Hollingsworth*

Conditions in a condenser were modelled by using air flowing over porous tubes with suction to simulate condensation. Data are presented for pressure drop across banks of tubes with a pitch-diameter ratio of 1.5 and compared with previous data for 1.25. By-pass lanes were later incorporated and pressure drops for lanes alone and lane-bank combinations are presented, together with mass flow distributions between lane and bank.

INTRODUCTION

The design of steam condensers is nowadays often carried out using computer programs, but the designs achieved are no better than the validity of the input data permits, and the data for steam-side pressure loss are frequently unreliable. This unreliability arises because meaningful values for pressure drop are difficult to obtain in real condensers and most measurements have therefore been done using air. The experiments reported herein are no exception to this, but the effect of condensation has been simulated by making the tube bank with porous tubes and sucking appropriate amounts of air from the cross-flow. The resulting pressure drops therefore exhibit the effects of mass transfer but unencumbered by the two-phase effect of inundation.

The rig enabled pressure losses to be measured for flow across three different arrays of tubes, in-line square, equilateral triangle and triangular constant-gate (Fig. 1) with seven tubes across the flow and up to seven tube rows in the flow direction. Measurements with and without suction were made with transverse pitch-diameter ratios of 1.25, 1.375 and 1.5. Results for the 1.25 have been reported in (1) and in full detail in (2); results for the 1.5 pitch are reported herein. The full results for the 1.5 pitch as well as those for the intermediate pitch of 1.375 will be reported in (3).

On completion of the tests for banks of tubes which filled the test duct, the rig was modified to enable the effect of longitudinal by-pass lanes to be studied. By-pass or access lanes are used in many condensers to lead the vapour directly to a downstream part of the tube bank, but the overall pressure loss and distribution of flow between lanes and their adjacent tube banks are not well documented. Tests were carried out to establish the overall pressure loss and the distribution of mass flow for lane-bank combinations in which one,

*Department of Mechanical Engineering, University of Bristol.

two and three rows of tubes were removed to form the lane. Measurements to date have been restricted to banks with a transverse pitch-diameter ratio of 1.25 having seven rows of tubes across the flow in in-line square, equilateral triangle and triangular constant-gate arrays.

The effect upon pressure loss of a by-pass lane in a tube bank is reported by Bell (4). In his paper covering extensive experimental work for single phase flow without suction, Bell gives a correlation

$$\frac{\Delta p_{LB}}{\Delta p} = \exp(-CF) \quad (1)$$

where Δp_{LB} = pressure loss for a tube bank with by-pass lane,

Δp = pressure loss for a bank which completely spans the duct (see Notation for precise definition of Δp),

C = constant; 5 for laminar flow, 4 for turbulent flow.

The definition of fractional by-pass area, F, used by Bell, and adopted by the present authors, is the ratio of the by-pass area to the total area of the lane-bank configuration, see Fig. 2,

$$F = \frac{S_T - S_{CF}}{S_T} \quad (2)$$

An alternative approach to that of Bell was adopted by Wilson (5). The loss in the tube bank alone was evaluated from a correlation for flow over a tube bank without suction, and the pressure loss for the by-pass lane alone was determined from a correlation for flow through a channel. The two pressure losses were then reconciled by allowing for a mass flow crossing between by-pass lane and tube bank.

The predictions of Bell are compared with the results, both with and without suction, obtained by the present authors; their data for pressure drop in by-pass lanes are compared with the predictions of Wilson.

EXPERIMENTAL APPARATUS AND METHOD

The basic rig for tube banks with a transverse pitch-diameter ratio of 1.25 is fully described in (2). The rig was altered to allow it to accommodate tubes at a pitch-diameter ratio of 1.5 but in all other respects it was unchanged.

The principal airflow was generated by a two-stage centrifugal fan and passed through a settling region and a filter before entering the contraction which accelerated it into the parallel-sided working duct containing the porous tubes. These tubes were 150 mm long and 19 mm in outside diameter and completely spanned the duct. The tubes were of sintered bronze and of a sufficiently low permeability for the pressure drop across their walls, when suction was applied, to be greatly in excess of any pressure differences around the tube created by the cross-flow, this ensured a suction flow which was reasonably uniform circumferentially. Adjustable restrictors at the outlet enabled the flow into each tube to be controlled, and the total flow from each transverse row could be controlled separately and measured by means of a standard orifice before it passed into a common plenum chamber and then into a multi-stage centrifugal exhauster which discharged it to atmosphere. Tests were performed with both constant mass flow, and also with constant suction parameter, $\gamma = (\bar{v}/u_H)(Re_H)^2$, for all rows in the bank.

Static pressure tapings were located in the wall of the duct 5 tube diameters upstream of the first row and 30 diameters downstream of the last, where the flow had settled and a linear pressure gradient had been re-established. The pressure loss between the tapings for the empty duct was measured and this was subtracted from the pressure loss with the tubes installed, using values at the mean mass flow to allow for the flow lost by suction.

Tube banks with seven tubes across the flow (six full tubes and a half tube on the upper and lower walls) and up to seven tubes in the direction of flow were used.

Modification of the Rig for By-pass Lanes

A by-pass lane could have been formed by removing one or more of the central longitudinal rows in the bank, but this would have left banks of tubes only a few rows across on either side of the lane - quite unrepresentative of the situation in real condensers. The lane was therefore formed by removing a row, or rows, adjacent to the upper wall of the duct so that the upper wall represented the line of symmetry along the centre of a lane. This left a minimum of 5 rows of tubes across the flow for the widest lane used - equivalent to a by-pass lane every ten rows across the flow when symmetry is taken into account, see Fig. 2. The narrowest lane was formed by taking out the row of half-tubes attached to the upper wall of the duct, equivalent to removing one row of complete tubes from a bank to leave $6\frac{1}{2}$ tubes either side. Larger lanes were formed by removing further rows, giving the following range of by-pass lanes.

No. of rows removed	Form of bank array	Equivalent full lane width (in rows)	Equivalent bank width either side (in rows)	F	Nomenclature
$\frac{1}{2}$	Triangular	1	$6\frac{1}{2}/7$	0	1T
$\frac{1}{2}$	Square	1	$6\frac{1}{2}$	0.278	1S
$1\frac{1}{2}$	Triangular	3	$6\frac{1}{2}/6$	0.278	3T
$1\frac{1}{2}$	Square	3	$5\frac{1}{2}$	0.577	3S
$2\frac{1}{2}$	Triangular	5	$5\frac{1}{2}/6$	0.454	5T
$3\frac{1}{2}$	Triangular	7	$5\frac{1}{2}/5$	0.577	7T

For this work the banks always contained 7 rows of tubes in the direction of flow.

To enable the upper wall to be regarded as a line of symmetry, it was important that the boundary layer on the upper wall at the approach to the working duct should be removed. This was done by using the contraction made for the pitch-diameter ratio of 1.5, installing the tubes at a pitch-diameter ratio of 1.25, and bleeding the flow at the top of the duct to atmosphere via a control valve. A yaw-meter, placed in the vertical (pitch) plane, was used to establish that the flow approaching the bank and by-pass lane remained parallel. Figure 3 shows the arrangement.

The flow leaving the by-pass lane could be separated from that leaving the

bank by means of a splitter plate that butted up to the rear of the last tube adjacent to the lane and ran in close fitting grooves in the side walls of the working duct downstream of the tube bank. This flow was passed to one calibrated orifice, whilst the flow from the bank passed to another calibrated orifice. Both orifices were followed by control valves which enabled the flows through the lane and the bank to be controlled independently. The position of the splitter plate could be altered to suit differing lane depths, whilst the separator at the exit of the working duct ensured that each of the two flows was always directed to the appropriate orifice. Splitter plates could also be placed ahead of the tube bank, covering a length of 7 tube diameters, and between tubes in the longitudinal row adjacent to the by-pass lane. This enabled pressure drops and mass flows to be measured in two configurations, shown in Fig. 4.

Configuration A

This arrangement enabled the pressure drop in the by-pass lane alone, Δp_L , to be established. The downstream control valves were adjusted to ensure that the flow approaching the upstream splitter plate was parallel, which was checked by a further yaw meter ahead of the upstream splitter plate. The pressure drop across the bank alone could also be measured to verify that it agreed with the data in (2). This configuration was used without suction.

Configuration B

This arrangement represents a by-pass-bank combination in which the flow is free to distribute itself between the two. Tests were carried out both with and without suction, and the downstream control valves were adjusted to equalise the bank and by-pass pressure drops. Previous tests had shown that the empty duct velocity distribution at entry to the test section was flat, save for a boundary layer on the lower wall, and so by comparing the overall mass flow with the two downstream components, \dot{M}_{Be} and \dot{M}_{Le} , the proportion of flow diverted into the by-pass lane could be established. It was not possible, however, to establish what proportion of the by-pass flow entered it from within the tube bank and what proportion was diverted into the lane ahead of the bank.

RESULTS FOR BANKS OF TUBES

It is only possible in this paper to give a representative sample of the results obtained, but sufficient are included to bring out the essential points. The complete set of results will be included in (3).

Without Suction

Tests were performed without suction on banks of six and seven rows across the flow, using both smooth tubes and internally sealed porous tubes to establish any effects of surface roughness. The measured pressure drop was corrected for empty duct pressure loss and then expressed as a pressure coefficient per row, ξ_p , by dividing by the dynamic head and the number of rows.

Following normal practice the dynamic head was based on the velocity in the narrowest gap between the tubes, u_{max} , giving

$$\xi_p = \frac{\Delta p}{\frac{1}{2} \rho u_{max}^2 N} \quad (3)$$

Figure 5(a) shows the results for in-line square arrays; data from the

present tests are compared with data for a pitch-diameter ratio of 1.25 from (2) and both sets of data are compared with a correlation suggested by Butterworth (6). There is little evidence of any surface roughness effect and pressure coefficients for the seven row banks are generally only slightly lower than for the six row banks. The larger pitch-diameter ratio of 1.5 gives rise to substantially lower pressure coefficients, as might be expected, and below a Reynolds number of about 60 000 they follow a similar trend of falling with Re_{max} . Above this value there is a surprising change; ξ_p now begins to rise with Re_{max} , and when Re_{max} is 90 000 ξ_p is approaching the value for $P_y/D = 1.25$. (It is unfortunate that with the larger area working duct used for the larger values of P_y/D the maximum Re_{max} was limited to about 90 000.) Although the results for the smaller pitch agree well with Butterworth's correlation, those for the larger pitch agree less well; nevertheless the discrepancy is only 13% at the most. Other correlations, by Zukauskas (7), and ESDU (8), fit the data with varying degrees of agreement, but none exhibit the rise in pressure coefficient at high Re_{max} with the larger pitch.

Data for equilateral triangle arrays, Fig. 5(b), show trends identical with those for in-line square including the rise at high Re_{max} for the larger pitch, putting the correlation seriously in question at those values.

Data for the less common triangular constant-gate array are not shown in this report but they exhibit exactly the same features as the other two arrays, once again exhibiting a rise in pressure coefficient for $Re_{max} > 70\ 000$ when P_y/D is 1.5. Generally speaking, all correlations fit the data for this type of array relatively poorly.

With suction

When suction is applied the measured pressure drop is reduced by the pressure rise caused by the loss in momentum. The pressure drops, Δp , used to obtain the pressure coefficients quoted herein have been corrected for this by having the momentum pressure rise added to the measured values. The suction also causes u_{max} to vary throughout the bank, which leads to problems with data reduction. Throughout the work the attempt was made to reduce the data with suction in such a way that it agreed with data for no-suction, and this was found to be best brought about by using a mean dynamic head, $\frac{1}{2}\rho u_{max}^2$, in

$$\frac{1}{2}\rho \bar{u}_{max}^2 = \frac{1}{2}\rho_m \left[\frac{1}{2}(u_{max,l}^2 + u_{max,e}^2) \right] \quad (4)$$

where suffices l and e refer to entry and exit of the bank respectively. Thus the pressure coefficient with suction, ξ_p , is defined as

$$\bar{\xi}_p = \frac{\Delta p}{\frac{1}{2}\rho \bar{u}_{max}^2} \quad (5)$$

The data cover a suction range from $\gamma = 0$ to 5 for a Reynolds number range of $Re_{max} = 20\ 000$ to 140 000 over a seven row bank, using both constant γ and constant mass extraction; this corresponds to a fractional mass extraction rate from 0.11 at high Re_{max} , low γ , to 0.98 at low Re_{max} , high γ .

Figures 6(a) and (b) give results for the complete range of suction for

in-line square and equilateral triangle arrays for constant γ ; the data for constant mass extraction follows a similar pattern. At all Reynolds numbers above the lowest, the data for all suction rates, when presented as $\bar{\xi}_p$, are seen to be virtually independent of suction rate and to agree reasonably well with the no-suction data, although tests could not be carried out above $Re_{max} = 70\,000$ because of equipment limitations. At the lowest Reynolds number, of about 20 000, the pressure coefficients diverge somewhat from this convenient trend and show a fairly marked dependence upon suction rate, at least for equilateral triangular banks, and consequently diverge from the no-suction values. This divergence is seen to be inconsistent, giving $\bar{\xi}_p > \xi_p$ for in-line square banks and $\bar{\xi}_p < \xi_p$ for equilateral triangle banks. Two points should be noted when assessing the low Re_{max} data, however. The fractional mass extraction rate is large for a given γ under these conditions so that the situation is rather extreme, and the measured pressure drops, and indeed all experimental readings, were very small.

Note that the measured pressure drop, Δp , corrected for momentum loss, falls with increasing suction at any given inlet value of Re_{max} . In order to establish whether this fall is merely due to the drop in local velocity or also due to delayed separation, a prediction was made for the pressure drop, based on a row-by-row calculation using no suction data for the appropriate local value of Re_{max} , and hence u_{max} . It was found that the value predicted in this way corresponded closely with the experimental value for the in-line array but overestimated the pressure drop for the triangular array, particularly for the more "open" array with $P_y/D = 1.5$. This suggests that for the more open triangular array, and to a lesser extent for the more tightly packed array (2), the separation point is delayed by suction, but for the square arrays the separation point is little affected by suction.

RESULTS FOR BANKS WITH BY-PASS LANES

All the data presented here are for $P_y/D = 1.25$.

Without suction

Typical experimental results for pressure drop vs. Reynolds number, Re_D , for a complete bank, a lane, and a lane-bank combination are shown in Fig. 7(a). This figure is for a lane formed by removing three longitudinal rows from an equilateral triangle bank, 3T. The pressure drop for the lane alone is seen to be negligible compared with that for the bank alone, and hardly greater than that for an equivalent smooth duct (5). For the lane-bank combination the pressure drop is seen to lie between the pressure drops for the lane and bank alone.

Pressure drop data for by-pass lanes alone, formed by removing tubes from triangular arrays, are given in Fig. 7(b) as pressure coefficient, ξ_p vs. Reynolds number, Re_D , where Re_D is based on the diameter of the tubes removed to form the lane. ξ_p is based on u_{max} , where u_{max} is the velocity that would have occurred between tubes had they not been removed to form the lane. This makes it directly comparable with ξ_p for a bank having the same approach velocity.

Pressure coefficients for lane-bank combinations, ξ_p , are shown in Fig. 8(a) for in-line square arrays and in Fig. 9(a) for equilateral triangle arrays. Tests were carried out with and without the rear splitter plate and both series of tests gave similar results, indicating that the splitter plate did not materially affect the flow. ξ_p is seen to be considerably greater than Bell's relation would suggest, except for the 1T configuration. For this case, however, Bell's method breaks down as it gives $F = 0$ and therefore $\Delta p_{LB} = \Delta p$. In addition, for this very narrow lane, the accuracy of the experimental data is doubtful owing to the relatively large effect of the thickening boundary layer on the wall forming the line of symmetry.

As the flow in the duct approaches the lane-bank combination the velocity profile becomes distorted and the velocity of that part of the flow which is approaching the by-pass lane increases. The mass flow entering the by-pass lane is thus greater than the nominal mass flow at entry, \dot{M}_{L1} , where the nominal flow is based upon a uniform velocity of approach so that

$$\dot{M}_{L1} = \frac{S_L}{(S_L + S_B)} \times \text{total mass flow entering the lane-bank combination} \quad (6)$$

where S_L is the area of the duct occupied by the lane and S_B the area occupied by the bank, see Fig. 2. Likewise, the nominal mass flow entering the bank, \dot{M}_{B1} , is given by

$$\dot{M}_{B1} = \frac{S_T}{(S_L + S_B)} \times \text{total mass flow entering the lane-bank combination} \quad (7)$$

That proportion of the nominal mass flow entering the tube bank which is transferred to the by-pass lane, ϕ , is defined as

$$\phi = \frac{\dot{M}_{Le} - \dot{M}_{L1}}{\dot{M}_{B1}}$$

where \dot{M}_{Le} is the mass flow leaving the by-pass lane. Note that, without carrying out detailed traverses, it is not possible to distinguish the flow that crosses into the by-pass lane from within the bank from that which is diverted into the lane ahead of the bank resulting from the inequality of the resistances of the lane and the bank. Nevertheless, ϕ represents that proportion of the flow that is diverted, by one means or another, away from, or out of, the bank by the presence of the by-pass lane.

Values of ϕ for all the lane widths tested are shown plotted against Re_D in Figs. 8(b) and 9(b). ϕ is seen to depend heavily upon the transverse width of the lane relative to the transverse width of the bank, but to be largely independent of Reynolds number. Save for the narrowest lane, for which the data are unreliable, between 40 and 70 per cent of the flow which would otherwise pass through the tube bank is diverted into the by-pass lane. For banks with more than 7 rows of tubes in the flow direction the proportion will be even greater.

With suction

The data for lane-bank combinations with suction is limited as work is still in progress, but preliminary results for pressure coefficient vs. Re_D for in-line square banks in which one row and three rows (1S and 3S) have been removed to form the lane are shown in Fig. 10(a). The pressure drop has again

been non-dimensionalised using $\frac{1}{2} \rho_m \bar{u}_{\max}^2$, as was used for banks alone, and this is seen to have the effect of collapsing the pressure coefficient, $\bar{\xi}_p$, particularly well for the wider lane. For the narrow lane, 1S, the pressure coefficient with suction is seen to be lower than the no-suction value, even for low suction rates ($\gamma = 1$), and at low Re_D the fall in $\bar{\xi}_p$ with increasing suction is quite marked. The experimental values are again substantially greater than those predicted by Bell.

The effect of suction on the flow distribution is shown in Fig. 10(b); as might be expected, ϕ falls with suction but even at the highest suction rates $\phi > 0$, i.e. the lane is still carrying more than its share of the flow approaching the lane-bank combination based on the relative lane and bank areas S_L and S_B . This is probably caused principally by diversion of the flow ahead of the lane-bank combination because suction will reduce, or even reverse, the flow into the lane from within the bank. It must be noted that values for ϕ will depend critically upon the number of transverse (across the flow) rows in the bank. If this number is very large, ϕ will become negative even for moderate suction rates.

CONCLUSIONS

Data are presented in this report for the pressure drop on the steam side of shell and tube condensers with a tube pitch-diameter ratio of 1.5. The tests were carried out in air using suction into porous tubes to simulate condensation, and the work is a continuation of a similar study for a pitch-diameter ratio of 1.25 reported in (1) and (2).

For in-line square arrays the pressure drop expressed as a pressure coefficient based on the arithmetic mean dynamic head in the tube bank, $\bar{\xi}_p$, was found to be independent of suction parameter, γ , when $\gamma \geq 1.0$, and to depend upon the flow Reynolds number in a manner which followed closely the correlation of Butterworth up to the maximum attainable Reynolds number $Re_{\max} = 70\ 000$ based on the velocity in the minimum cross-sectional area between tubes. Similar data for flow without suction, $\gamma = 0$, shows somewhat lower values of pressure coefficient at low Re_{\max} with an unexpected rise for $Re_{\max} > 70\ 000$.

A similar trend is found for equilateral triangle banks, save that in this instance the data do not collapse well at low Re_{\max} and under these conditions $\bar{\xi}_p$ is found to fall steadily with γ .

Preliminary data for banks that contain by-pass lanes suggest that predictions based on Bell substantially underestimate the pressure coefficient. Data for flow with suction suggest that non-dimensionalising the pressure drop with the arithmetic mean dynamic head once again produces pressure coefficient which are largely independent of suction rate, but suitable correlations must await more data.

ACKNOWLEDGEMENTS

The work reported here constitutes an extension of an earlier substantial programme of research. The authors wish to thank S.E.R.C. for their support which made this extension possible.

NOTATION

D	Outside diameter of tubes
F_L	Ratio of by-pass cross-sectional area to total cross-sectional area
\dot{M}	Mass flow rate
N	Number of rows of tubes in flow direction
P_y	Pitch between tube centres in the transverse (across the flow) direction
Δp	Overall static pressure drop across tube bank corrected for empty duct loss Δp_{st} and, with suction, for momentum loss $\{= \Delta p_{measured} - \Delta p_{st} - \rho_m(u_1^2 - u_e^2); \text{ see Ref. (1), eqn. (4)}\}$
Re_D	Reynolds number based on the mean "free-duct" velocity u_1 of the flow entering the working section $(= \rho_m u_1 D / \eta)$
Re_{max}	Reynolds number based on $u_{max,1}$ $(= \rho_m u_{max,1} D / \eta)$
Re_N	Reynolds number based on the "free-duct" approach velocity to the Nth row $(= \rho_m u_N D / \eta)$
S	Cross-sectional area across the working duct
u	Velocity of flow in the longitudinal direction
\bar{u}	Mean velocity given by $\{\frac{1}{2}(u_1^2 + u_e^2)\}^{\frac{1}{2}}$
\bar{v}	Mean velocity of the sucked air at the tube outer surface, normal to the surface
ϕ	Proportion of flow approaching the tube bank which is transferred to the by-pass lane $\{= (\dot{M}_{Le} - \dot{M}_{LL}) / \dot{M}_{TL}\}$
ξ_p	Pressure coefficient for flows without suction, based on u_{max} $(= \Delta p / \frac{1}{2} \rho_m u_{max}^2)$
$\bar{\xi}_p$	Pressure coefficient for flows with suction, based on the arithmetic mean dynamic head $(= \Delta p / \frac{1}{2} \rho_m \bar{u}_{max}^2)$
γ	Suction parameter based on "free-duct" approach velocity to Nth row $\{= (\bar{v} / u_N) Re_N^{\frac{1}{2}}\}$
ρ_m	Mean density of the flow

Suffixes

T, CF	Refer to bank and by-pass areas, see Fig. 2
L, B	

1,...,N,... Refers to entry to 1st,..., Nth,... tubes in flow direction

e Refers to exit from last tubes in flow direction

max Means that velocity has been scaled from "free-duct" to minimum cross-sectional area

REFERENCES

1. Lee, N.K., Hollingsworth, M.A. and Mayhew, Y.R., 1982, "Simulation of condenser pressure losses by porous tubes with suction", Proc. 7th Int. Ht. Trans. Conf., Paper Cs 18, Munich, Fed. Rep. of Germany.
2. Lee, N.K., 1981, "Simulation of Condenser Pressure Losses by Porous Tubes with Suction", Ph.D. Thesis, University of Bristol.
3. Lee, N.K., 1983, "Further Data on Condenser Pressure Losses by Porous Tubes with Suction", to be published.
4. Bell, K.J., 1963, "Final Report of the Co-operative program on Shell and Tube Heat Exchangers", J. Delaware Eng. Exp. Stn. Bull., No. 5, Newark, Delaware.
5. Wilson, J.L., 1974, "N.E.L. Two-dimensional Condenser Computer Program", Report No. 619, Natl. Eng. Lab., East Kilbride, Scotland.
6. Butterworth, D., 1978, Int. J. Heat Mass Trans., 21, 253.
7. Žurauskas, A.A., 1972, "Heat Transfer from Tubes in Cross-Flow", Advances in Heat Transfer, Vol. 8, 93-160.
8. E.S.D.U., 1979, Data Item No. 79034, Eng. Sci. Data Unit, 251-9 Regent Street, London.

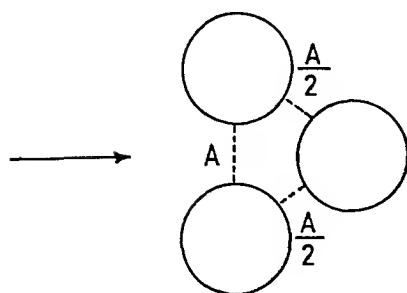
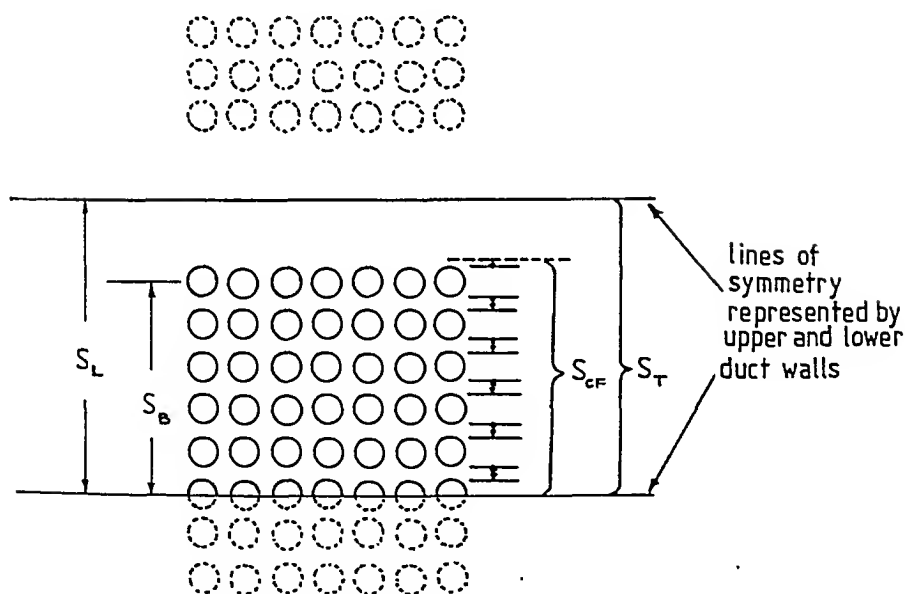


FIG.1 TRIANGULAR CONSTANT-GATE ARRAY



S_{CF} = minimum crossflow area + half the minimum clearance

S_T = S_{CF} + by-pass lane width

FIG.2 BY-PASS LANE NOMENCLATURE

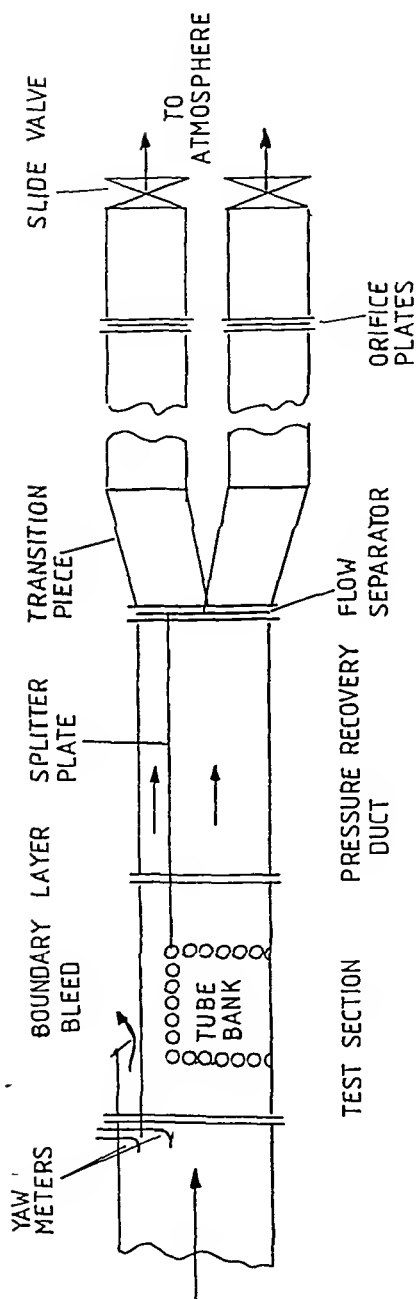
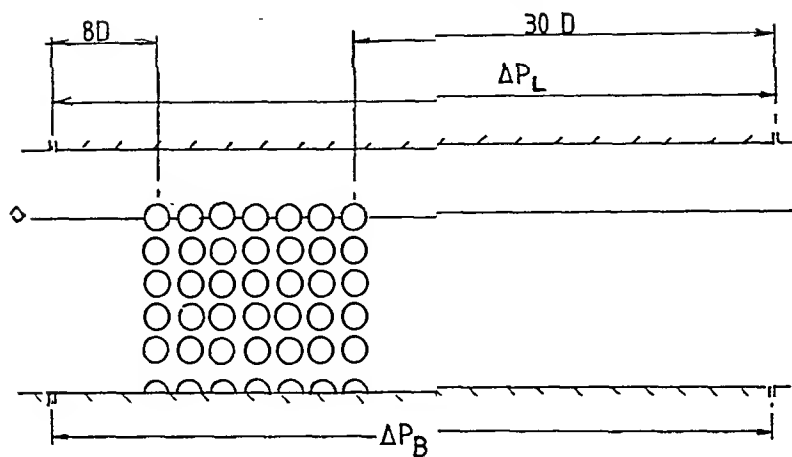
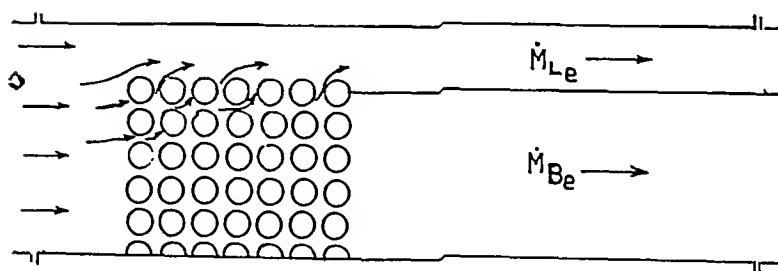


FIG 3 EXPERIMENTAL RIG FOR BY-PASS LANES



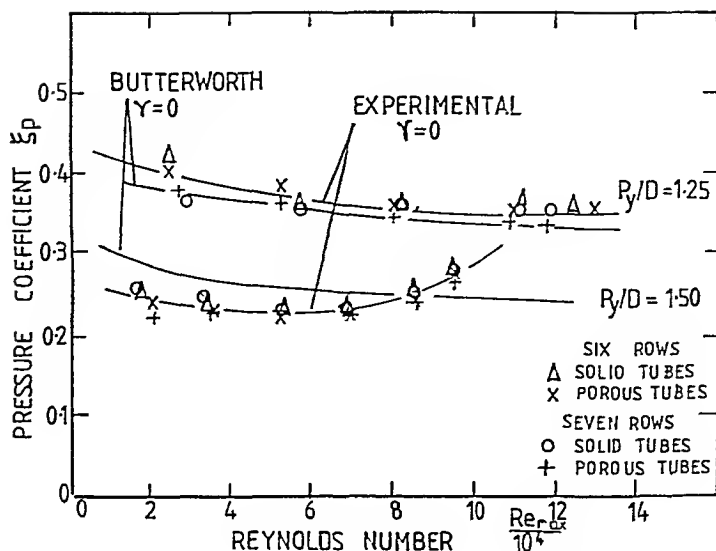
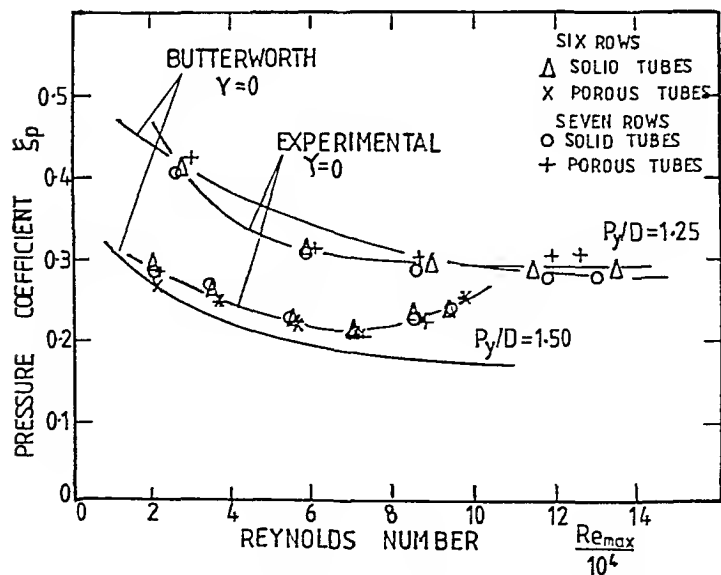
CONFIGURATION A

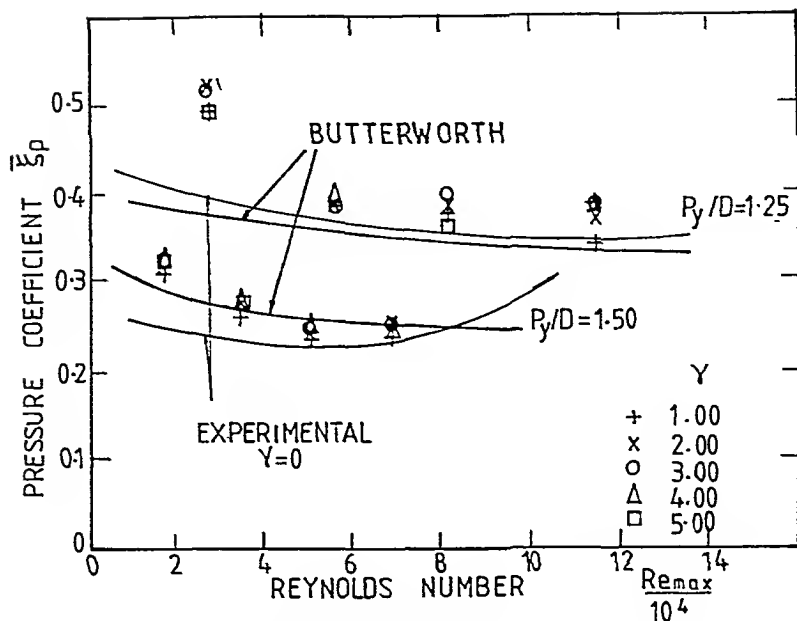
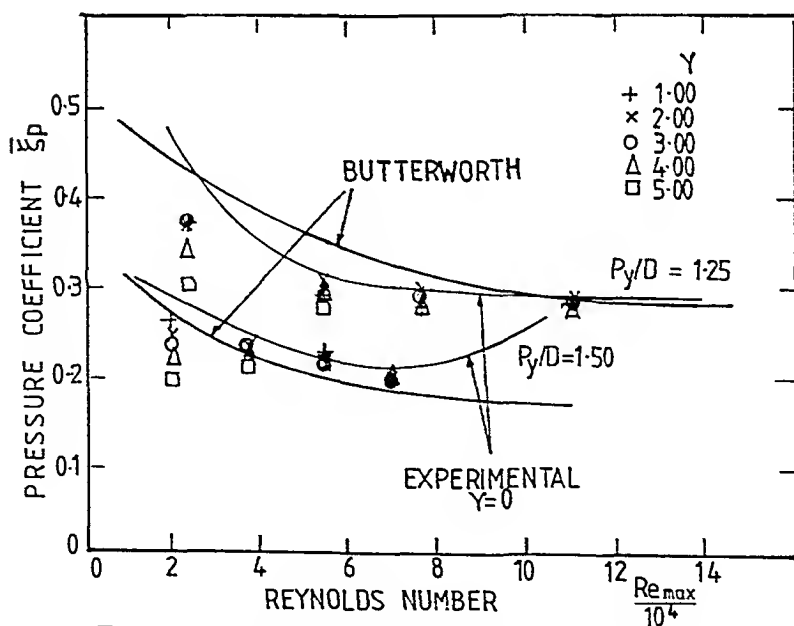


CONFIGURATION B

FIG 4

BY-PASS TESTS

FIG 5(a) ξ_p FOR IN-LINE SQUARE BANKS WITHOUT SUCTIONFIG 5(b) ξ_p FOR EQUILATERAL TRIANGLE BANKS WITHOUT SUCTION

FIG 6(a) $\bar{\xi}_p$ FOR IN LINE SQUARE BANKS WITH CONSTANT SUCTION PARAMETERFIG 6(b) $\bar{\xi}_p$ FOR EQUILATERAL TRIANGLE BANKS WITH CONSTANT SUCTION PARAMETER

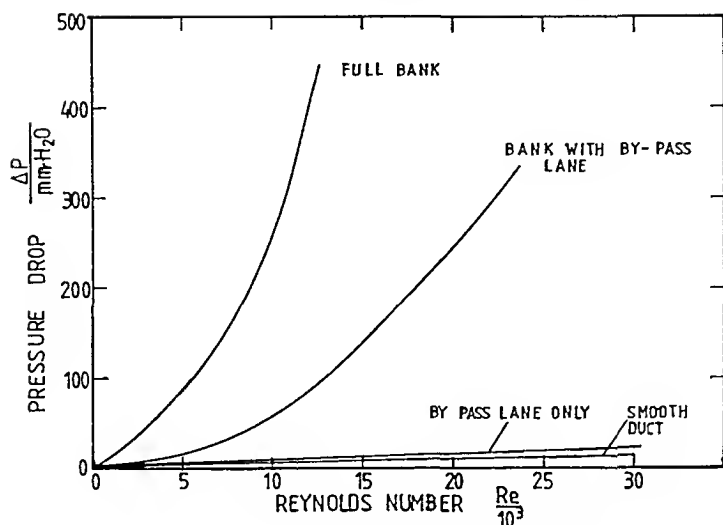


FIG 7(a) ΔP FOR EQUILATERAL TRIANGLE BANKS WITHOUT SUCTION
 $P_y/D=1.25$, 3T

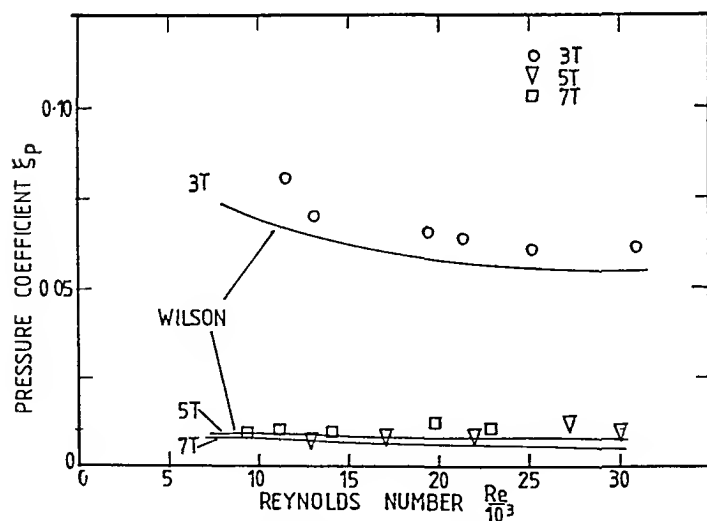


FIG 7(b) ξ_p FOR BY-PASS LANES FORMED IN EQUILATERAL-TRIANGLE BANKS

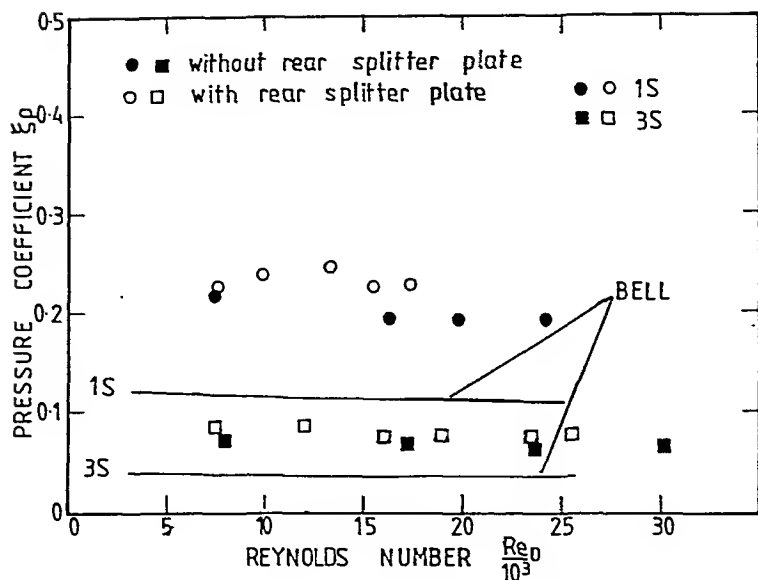


FIG 8 (a) ξ_p FOR IN-LINE SQUARE BANKS WITH BY-PASS LANES, $\gamma=0$

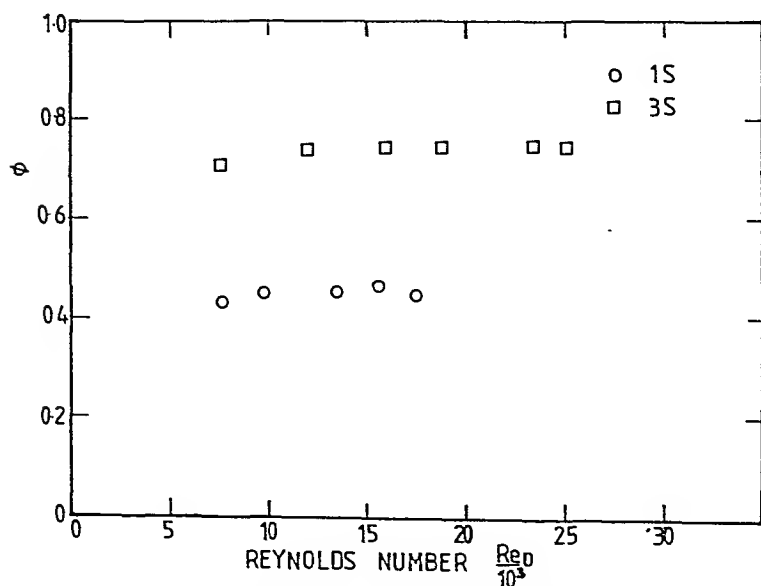


FIG 8 (b) ξ FOR IN-LINE SQUARE BANKS WITH BY-PASS LANES, $\gamma=0$

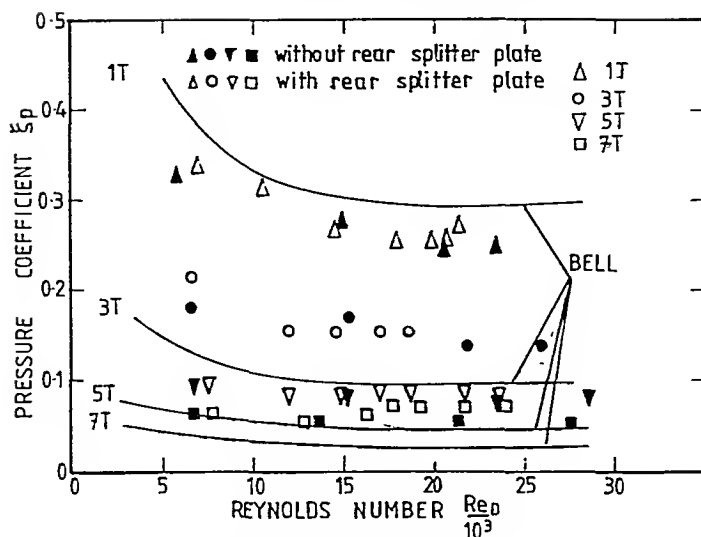


FIG 9(a) ξ_p FOR EQUILATERAL TRIANGLE BANKS WITH BY-PASS LANES, $\gamma=0$

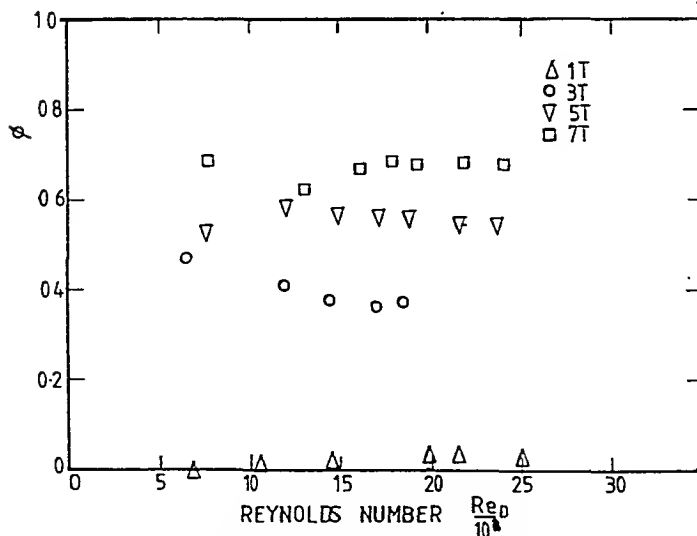


FIG 9(b) ϕ FOR EQUILATERAL TRIANGLE BANKS WITH BY-PASS LANES $\gamma=0$

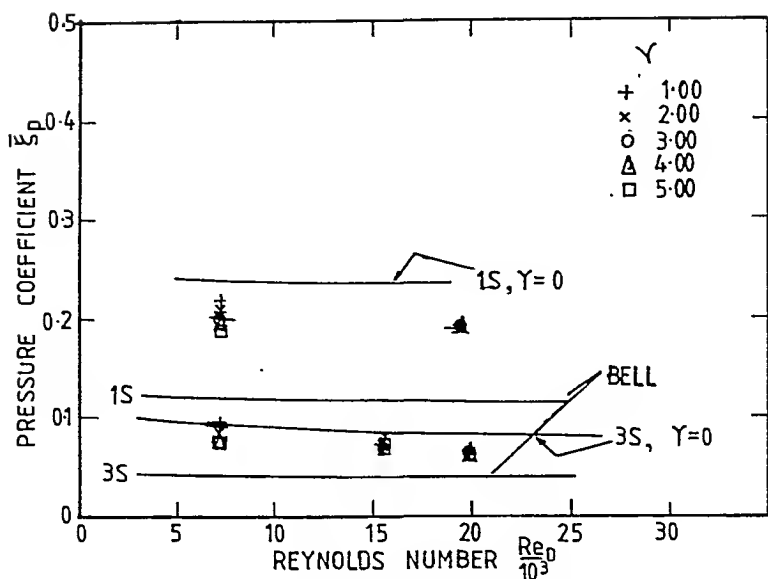


FIG 10(a) $\bar{\xi}_p$ FOR IN-LINE SQUARE BANKS WITH SUCTION AND BY-PASS LANES

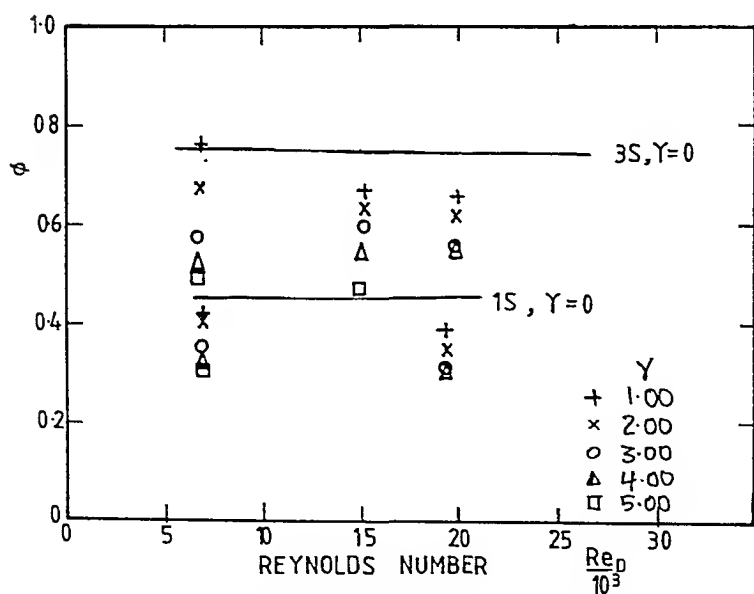


FIG 10(b) ϕ FOR IN-LINE SQUARE BANKS WITH SUCTION AND BY-PASS LANES

COMPARISON OF CALCULATION METHODS FOR NON-CONDENSING GAS EFFECTS IN CONDENSATION ON A HORIZONTAL TUBE

W.C. Lee* and J.W. Rose*

Various methods are discussed for calculating the mass-transfer resistance due to the presence of a non-condensing gas in a vapour flowing normal to, and condensing on, a horizontal tube. The different methods are compared with each other and with experimental data for several vapour-gas combinations. Simple equations based on boundary-layer theory are found to be in good agreement with the data. The 'stagnant film model', utilizing the 'Chilton-Colburn analogy', is generally conservative but may give relatively large errors.

INTRODUCTION

For condensation in the presence of a non-condensing gas, the "effective gas-phase resistance" may, in principle, be calculated by solving the relevant conservation equations for the vapour flow over the condensing surface. In recent years several numerical solutions, based on the boundary-layer equations, have been obtained. The results, however, are not generally available in a readily useable form. In contrast, a widely-used calculation method, which adopts a simple model of the flow near the condensing surface and utilizes an imperfect analogy between corresponding heat and mass-transfer problems, is relatively straightforward but the reliability of results obtained is less certain.

For the case of forced convection condensation on a horizontal tube, two separate theoretical studies have led to approximate expressions, based on boundary-layer solutions, for calculating the temperature drop in the vapour resulting from the presence of a gas. These expressions should give more accurate predictions than the simple model. In the present paper, the various prediction methods are compared with each other and with experimental data for a wide range of circumstances.

MASS-TRANSFER COEFFICIENT AND SHERWOOD NUMBER

In this paper the surface mass-transfer coefficient, β , is defined in terms of the *diffusive* component of the *mass* flux and the difference in *mass* fraction, thus

$$m_{DV} = - \rho_o D (\partial W_v / \partial y)_o = \beta (W_{vo} - W_{vw}) \quad (1)$$

*Department of Mechanical Engineering, Queen Mary College (Univ. London)

where m_{vy} is the *outward* (from the surface) diffusive component of the vapour flux, i.e.

$$\beta = - \rho_0 D (\partial W_v / \partial y)_0 / (W_{v0} - W_{v\infty}) \quad (2)$$

For a 2-constituent mixture

$$W_v + W = 1 \quad (3)$$

so that β may also be written

$$\beta = - \rho_0 D (\partial W / \partial y)_0 / (W_0 - W_\infty) \quad (4)$$

The dimensionless mass-transfer coefficient or Sherwood number is defined

$$Sh = \beta d / \rho D \quad (5)$$

For condensation of a vapour in the presence of a non-condensing gas, the condition that the surface is impermeable to the gas gives

$$m_v = \beta (W_{v\infty} - W_{v0}) / (1 - W_{v0}) = \beta (W_0 - W_\infty) / W_0 \quad (6)$$

where m_v is the *inward* (towards the surface) total vapour mass flux or condensation rate at the vapour-condensate interface. Equations 5 and 6 give

$$Sh = \frac{m_v d}{\rho D} \left(\frac{W_0}{W_0 - W_\infty} \right) \quad (7)$$

CALCULATION METHODS

Stagnant film model

This method uses the model of a 'stagnant' vapour-gas layer, separating the bulk flow and the surface of the condensate, in which only one-dimensional, laminar motion, normal to the surface, occurs. On this basis one readily obtains

$$\tilde{m}_v = \tilde{\beta}^* \ln \left(\frac{1 - \tilde{W}_{v0}}{1 - \tilde{W}_{v\infty}} \right) = \tilde{\beta}^* \ln \left(\frac{\tilde{W}_0}{\tilde{W}_\infty} \right) \quad (8)$$

where subscripts $_0$ and $_\infty$ relate respectively to the condensate surface and the bulk flow, i.e. the inner and outer surfaces of the 'film', and

$$\tilde{\beta}^* = \tilde{\rho} D / \delta \quad (9)$$

where δ is the film thickness. In practice $\tilde{\beta}^*$ is obtained from

$$\tilde{\beta}^* = \frac{\alpha}{M_\infty c_p} \left(\frac{Pr}{Sc} \right)^{2/3} \quad (10)$$

which stems from the work of Colburn and co-workers (1-3).

Equation 10 may be 'deduced' as follows:

Except at low Prandtl numbers, heat-transfer problems can often be represented approximately by

$$Nu = Pr^{1/3} \psi(Re) \quad (11)$$

where the function $\psi(Re)$ depends on the geometry. Under certain circumstances the appropriately non-dimensionalised energy and diffusion equations, together with the boundary conditions (except that on v_0), of the corresponding heat- and mass-transfer problems are identical. Thus, for the limiting case when $v_0 \rightarrow 0$, ($v_0 = 0$ in the heat transfer problem) we have, for the mass-transfer problem

$$Sh = Sc^{1/3} \psi(Re) \quad (12)$$

The Reynolds number function is the same in equations 11 and 12 and division gives

$$\beta = \frac{\alpha}{c_p} \left(\frac{Pr}{Sc} \right)^{2/3} \quad (13)$$

where β is the mass-transfer coefficient defined by

$$\beta = \frac{\dot{m}_{DV}}{\bar{W}_{VO} - \bar{W}_{V\infty}} = - \frac{\rho_o D (\partial \bar{W}_v / \partial y)_o}{\bar{W}_{VO} - \bar{W}_{V\infty}} \quad (14)$$

A corresponding 'molar mass-transfer coefficient' is

$$\tilde{\beta} = \frac{\tilde{m}_{DV}}{\bar{W}_{VO} - \bar{W}_{V\infty}} = - \frac{\tilde{\rho}_o D (\partial \tilde{W}_v / \partial y)_o}{\bar{W}_{VO} - \bar{W}_{V\infty}} \quad (15)$$

It follows from the above definitions that

$$\beta = M_\infty \tilde{\beta} \quad (16)$$

and equation 13 gives

$$\tilde{\beta} = \frac{\alpha}{M_\infty c_p} \left(\frac{Pr}{Sc} \right)^{2/3} \quad (17)$$

which may be compared with equation 10.

Equation 8 is sometimes written

$$\tilde{m}_v = \tilde{\beta}^* \frac{\phi}{(e^\phi - 1)} (\tilde{W}_{V\infty} - \tilde{W}_{VO}) + \tilde{W}_{V\infty} \tilde{m}_v \quad (18)$$

$$\text{where } \phi = \tilde{m}_v / \tilde{\beta}^* \quad (19)$$

$\tilde{\beta}^*$ is referred to as the 'low-flux mass-transfer coefficient' and the quantity $\phi/(e^\phi - 1)$, which tends to unity for $\tilde{m}_v \rightarrow 0$, is described as a 'high-flux correction factor'. This practice appears to offer little advantage and is somewhat misleading in that it might be taken to imply that a correction has been made for the fact that $\tilde{\beta}^*$, when obtained from equation 10, is only correct for the limiting case $v_0 \rightarrow 0$ i.e. zero condensation rate†.

† The surface impermeability condition for the gas gives $m_v = -\rho v_0$

Acrivos-Mills (4,5)

Acrivos (4) considered the problem of boundary-layer flow over arbitrary surfaces with inward mass transfer. Specifically, he investigated the limiting case of strong suction where $W_0/W_\infty \rightarrow \infty$. His results indicate that

$$Sh_L Re^{-1/2} = C \left\{ \frac{W_0 Sc}{2W_\infty (1+Sc)} \right\}^{1/2} \quad (20)$$

where Sh_L relates to the limiting case considered and C depends on the potential velocity distribution at the 'edge' of the vapour-gas boundary layer. Acrivos also drew attention to the fact that the asymptotic result was not too badly in error, for cases where exact solutions were available, even for the opposite extreme $W_0/W_\infty \rightarrow 1$, and proposed a simple interpolation formula for the general case

$$Sh = \{Sh_0^{3/2} + [(1 - \frac{W_\infty}{W_0}) Sh_L]^{3/2}\}^{2/3} \quad (21)$$

where Sh_0 is the Sherwood number when $v_0 = 0$ and can be obtained from a solution of the corresponding heat-transfer problem by replacing Nu by Sh_0 and Pr by Sc . In many cases expressions of the type

$$Sh_0 Re^{-1/2} = A Sc^n \quad (22)$$

are adequate (6). By dividing equations 20 and 22 we obtain

$$\frac{Sh_L}{Sh_0} = C_1 \frac{Sc^{-n}}{\{2(W_\infty/W_0)(1 + Sc^{-1})\}^{1/2}} \quad (23)$$

Mills et al (5) used equation 23 with $n = 0.4$, together with their experimental data for steam-air mixtures, to obtain a value of 2.22 for C_1 .

It may be noted that, though the form of equation 23 implies the adoption of equation 22 for Sh_0 , Mills et al. apparently used the alternative expression

$$Sh_0 = 0.43 + 0.53 Re^{1/2} Sc^{0.31} \quad (24)$$

when analysing the data. Values of Sh given by equations 21 and 23 are, for a wide range of Re , virtually the same when using equation 22 with appropriate values of A and n , and when using equation 24 for Sh_0 .

Rose (7)

Rose (7) used existing heat-transfer solutions for the problem of boundary-layer flow with surface suction, to obtain solutions for the corresponding mass-transfer problem. For flow on a horizontal plane surface, the 'analogy' is exact, i.e. the appropriately non-dimensionalized energy equation and the boundary conditions (including that on v_0) for the heat-transfer problem are identical to those for the diffusion equation in the mass-transfer problem. Existing numerical solutions for the heat-transfer case were used to obtain a relatively simple expression for the Sherwood number in the mass-transfer case. When this was applied to condensation on a horizontal plane surface, excellent agreement with detailed numerical solutions of the condensation problem (8-10) was found.

In the case of flow over a cylinder the required heat-transfer results are only available for the limiting cases of zero and infinite surface mass-transfer rates. An equation having the same form as that for the flat plate case, and satisfying the known limiting conditions, was used to obtain the corresponding result for the mass-transfer problem, which may be written

$$\text{Sh Re}^{-1/2} = \{ [1 + 2.28 \text{Sc}^{1/3} (W_o - W_\infty) / W_\infty]^{1/2} - 1 \} W_o / 2(W_o - W_\infty) \quad (25)$$

Equation 25 was found to be in excellent agreement with data for condensation of steam on horizontal tubes in the presence of air (5,11,12).

NEW MEASUREMENTS

Extensive experimental data have recently been obtained (13,14) for condensation of steam and R-113, each in the presence of both air and hydrogen, flowing vertically downward over a horizontal tube. The tube could be viewed to ensure that the filmwise mode of condensation prevailed throughout all tests. Two copper tubes, having diameters 12.5 mm and 25.3 mm, were used. Surface temperatures at four positions were obtained from thermocouples embedded in the tube wall. The heat flux was obtained from coolant measurements which were checked in preliminary tests, against values obtained by collecting condensate. The vapour mass flow rate was obtained from the electrical power input to the boiler. The mass flow determination incorporated a correction for the relatively small thermal loss from the apparatus which was established by preliminary measurements where all of the vapour supplied to the test section was condensed and measured.

The non-condensing gases were supplied, via flowmeters, to the boiler. Excellent agreement was found between the vapour composition given by the vapour and gas flow rates and that determined from pressure and temperature measurements in the test section. As well as confirming the reliability of the composition measurements, this attests to the accuracy of the vapour flow rate determination and, in turn, that of the vapour velocity.

The approximate ranges of the variables used were:- pressure 4 - 124 kPa, heat flux 12 - 465 kW/m², vapour velocity 0.3 - 26 m/s, mole fraction of non-condensing gas 0.1% - 35%. The vapour-gas combinations used gave a range of Schmidt number of approximately 0.05 to 0.5. For the R-113-hydrogen case $\text{Sc} = 0.05$, for R-113-air and steam-hydrogen $\text{Sc} = 0.2$ and for steam-air $\text{Sc} \approx 0.5$.

Pure vapour measurements were made for the same ranges of vapour velocity and pressure in order to evaluate the thermal resistance of the condensate film. These data were found to be in excellent agreement with a theoretically-based correlation (of steam data only) given by Fujii et al. (15), which may be written

$$\text{Nu Re}^{-1/2} = 0.91 (g^2 d \rho_L \mu_L h_{fg}^2 / u_\infty^3 Q^2)^{0.13} \quad (26)$$

The comparison of the pure vapour data with equation 26 is shown in Fig.1.

When analysing the vapour-gas data, equation 26 was used to determine the temperature drop across the condensate film for the observed vapour velocity and heat flux. An iterative procedure, evaluating condensate properties at the reference temperature

$$T^* = (2/3)T_w + (1/3)T_o \quad (27)$$

was adopted for this purpose. The interface gas mass fraction was found from the equilibrium condition

$$W_o = \frac{P - P_{\text{sat}}(T_o)}{P - (1 - (M_v/M_g))P_{\text{sat}}(T_o)} \quad (28)$$

COMPARISONS

In the Acrivos-Mills case, for convenience, we shall use

$$Sh_o = 0.57 Re^{1/2} Sc^{1/3} \quad (29)$$

When using equation 29 for Sh_o , equations 21 and 23 give $Sh Re^{-1/2}$ independent of Re . The Acrivos interpolation formula (equation 21) with equations 23 and 29 may be expressed

$$Sh Re^{-1/2} = 0.57 Sc^{1/3} \left[1 + \left\{ \frac{1.57(1 - \frac{W_o}{W_\infty}) Sc^{0.1}}{(\frac{W_o}{W_\infty})^{1/2} (1+Sc)^{1/2}} \right\}^{3/2} \right]^{2/3} \quad (30)$$

The error in Sh , introduced by using equation 29 rather than a more accurate correlation, where the coefficient and index of Re depend on Re , is less than 5% for $40 < Re < 10^4$.

Equations 25 and 30 are compared in Fig.2 for $Sc = 0.05, 0.2, 0.5$. It may be seen from Fig.2 that the two equations do not differ greatly within the range of the experimental data, the largest discrepancy occurring at the lowest value of Sc .

In Fig.3 the data (13,14) are compared with equation 25. When evaluating the experimental values of Sh , Re and Sc , the density and viscosity of the vapour-gas mixture were taken as the arithmetic means of the values for the bulk and at the condensate surface. The diffusion coefficient was evaluated at $(T_o + T_\infty)/2$. The mass flux was taken as Q/h_{fg} and h_{fg} was evaluated at T_o . Full details of the properties and sources are given in (13).

The data are seen to be smooth, consistent and in very good agreement with the theoretical result. It may be noted that the data exhibit a clear Schmidt number dependence, in line with theory, and that the steam-hydrogen data are in close agreement with the R-113-air results which have similar values of Schmidt number.

In Fig.4 the steam-air data are compared with the earlier measurements of Mills et al (5) and Fujii (12,16). Also shown is the correlation of steam-air data given by Berman (11) which, as shown by Rose (7), may be written

$$Sh Re^{-1/2} = \frac{0.455 W_o (1 - 0.378 W_\infty)^{0.933}}{(W_o - W_\infty)^{1/3} W_\infty^{0.6} (1 - 0.378 W_o)^{2/3}} \quad (31)$$

It is seen that the different data sets are in good agreement with each other and are well represented by equation 25. The fact that the Berman correlation agrees less well with the data given in Fig.4 for higher values of W_∞ , and behaves incorrectly when W_o/W_∞ approaches unity, suggests that the data

used for the correlation did not extend to these conditions.

In Fig.5 results obtained on the basis of the stagnant film model are compared with equation 25 and the experimental data. When equation 8 is expressed on a mass basis and, for heat transfer with flow over a solid cylinder we take

$$Nu = 0.57 Re^{1/2} Pr^{1/3} \quad (32)$$

in order to determine α and hence β^* from equation 10, we obtain

$$Sh Re^{-1/2} = \frac{0.57 Sc^{1/3} (1 + rW_\infty - W_\infty)}{1 - (W_\infty/W_0)} \ln \left\{ \frac{W_0}{W_\infty} \cdot \frac{(1 + rW_\infty - W_\infty)}{(1 + rW_0 - W_0)} \right\} \quad (33)$$

where r is the ratio of molar masses M_v/M_g . It is apparent from Fig.5 that the stagnant film model agrees less well with the data than the boundary-layer theory result. While the stagnant film model prediction is generally seen to be conservative, the error (underestimate) in the mass-transfer coefficient can be quite large, particularly at high values of W_0/W_∞ (low bulk gas concentration and high condensation rate), low Schmidt numbers and when the molar mass ratio, M_v/M_g is not close to unity. Comparison of equations 25 and 33 show that for $W_0/W_\infty = 100$, equation 33 underestimates the mass-transfer coefficient by a factor between about 3 and 15 for the range of parameters used.

CONCLUSION

Equation 25 is recommended for prediction of non-condensing gas effects in condensation on a horizontal tube on the basis that it

- (i) is based on boundary-layer theory; no experimental condensation data have been used in its derivation,
- (ii) agrees well with an alternative approximate theoretical result for wide ranges of the relevant parameters,
- (iii) agrees closely with the experimental data,
- (iv) is the simplest of the three calculation methods considered.

A convenient equation for use in practical calculations is obtained by substituting for Sh from equation 7 in equation 25 to obtain the relationship between the condensation rate and the gas mass fractions in the bulk and at the condensate surface thus:-

$$m_v d/\rho D = 0.5 Re^{1/2} \{ [1 + 2.28 Sc^{1/3} (W_0 - W_\infty)/W_\infty]^{1/2} - 1 \} \quad (34)$$

For given bulk vapour conditions and given tube-wall temperature, equation 34 may be used with a suitable equation for the condensate film (e.g. equation 26) to determine the interface gas mass fraction W_0 and temperature T_0 (which satisfy the equilibrium condition, equation 28) so that the value of m_v given by equation 34 is equal to Q/h_{fg} given by the equation for the condensate. Convenient iterative schemes, giving W_0 , T_0 , m_v and Q , may be devised.

Finally it may be noted that, while the stagnant film model is generally conservative, the errors can be quite large. The magnitude of the errors found for this case, i.e. condensation of a vapour in the presence of a non-condensing gas on a single horizontal tube, may serve as a guide to errors which might be expected when this model is used in other cases i.e. different geometries or multi-constituent condensation.

SYMBOLS USED

- A = constant, see equation 22
 C = constant, see equation 20
 C_1 = constant, see equation 23
 c_p = isobaric specific heat capacity of mixture
 D = diffusion coefficient
 d = tube diameter
 g = gravitational acceleration
 h_{fg} = specific enthalpy of evaporation
 k_L = thermal conductivity of condensate
 M = molar mass
 M_∞ = bulk molar mass of mixture
 M_g = molar mass of gas
 M_v = molar mass of vapour
 m_{DV} = diffusive component of outward surface mass flux of vapour
 \bar{m}_{DV} = diffusive component of outward surface mole flux of vapour
 m_v = mass flux of vapour (towards the surface) at the vapour-condensate interface, i.e. condensation rate per area
 \bar{m}_v = mole flux of vapour (towards the surface)
 n = constant, see equation 22
 Nu = Nusselt number
 P = pressure
 P_{sat} = saturation pressure
 Pr = Prandtl number
 Q = heat flux
 r = M_v/M_g
 Re = Reynolds number, $(u_\infty \rho d / \mu)$
 \bar{Re} = "two-phase Reynolds number", $(u_\infty \rho_L d / \mu_L)$
 Sc = Schmidt number
 Sh = Sherwood number defined in equation 5
 Sh_L = Sherwood number in the limiting case when $W_O/W_\infty \rightarrow \infty$
 Sh_O = Sherwood number in the limiting case when $v_O = 0$
 T = temperature
 T_w = outside wall temperature of tube
 T_O = temperature at vapour-condensate interface
 T_∞ = free-stream temperature
 T^* = reference temperature defined in equation 27
 u_∞ = free-stream approach velocity

- v_o = velocity component (outward) normal to surface
 W = mass fraction of gas
 W_o = value of W at the vapour-condensate interface
 W_∞ = free-stream value of W
 W_v = mass fraction of vapour
 W_{vo} = value of W_v at the vapour condensate interface
 $W_{v\infty}$ = free-stream value of W_v
 \tilde{W} = mole fraction of gas
 \tilde{W}_o = value of \tilde{W} at the vapour-condensate interface
 \tilde{W}_∞ = free-stream value of \tilde{W}
 \tilde{W}_v = mole fraction of vapour
 \tilde{W}_{vo} = value of \tilde{W}_v at the vapour-condensate interface
 $\tilde{W}_{v\infty}$ = free-stream value of \tilde{W}_v
 y = distance measured normal to the surface
 α = surface heat-transfer coefficient
 β = surface mass-transfer coefficient, defined in equation 2
 $\tilde{\beta}$ = 'molar surface mass-transfer coefficient', defined in equation 15
 $\tilde{\beta}^*$ = 'low-flux mass-transfer coefficient', defined in equation 9
 δ = film thickness in stagnant film model
 μ = viscosity of mixture
 μ_L = viscosity of condensate
 ρ = density of mixture
 $\tilde{\rho}$ = molar density of mixture
 ρ_L = density of condensate
 ρ_o = density of mixture at vapour-condensate interface
 ϕ = $\tilde{m}_v/\tilde{\beta}^*$

REFERENCES

1. Colburn, A.P. and Hougen, D.A., 1934, Ind. Engg. Chem., **26**, 1178-1182.
2. Chilton, T.H. and Colburn, A.P., 1934, Ind. Engg. Chem., **26**, 1183-1187.
3. Colburn, A.P. and Drew, T.B., 1937, Trans. Am. Inst. Chem. Eng., **33**, 197-215.
4. Acrivos, A., 1960, AIChE Journal, **6**, 410-414.
5. Mills, A.F., Tan, C. and Chung, D.K., 1974, "Experimental study of condensation from steam-air mixtures flowing over a horizontal tube: overall condensation rates", Proc. 5th Int. Heat Transfer Conf., Tokyo, Vol.5, Paper CTL5, 20-23.
6. McAdams, W.H., 1951, "Heat transmission", McGraw Hill.

7. Rose, J.W., 1980, Int. J. Heat Mass Transfer, 23, 539-546.
8. Koh, J.C., 1962, "Laminar film condensation of condensible gases and gaseous mixtures on a flat plate", Proc. 4th USA Nat. Cong. Appl. Mech. Vol.2, 1327-1336.
9. Sparrow, E.M., Minkowycz, W.J. and Saddy, M., 1967, Int. J. Heat Mass Transfer, 10, 1829-1845.
10. Fujii, T., Uehara, H., Mihara, K. and Kato, Y., 1977, "Forced convection condensation in the presence of non-condensables - a theoretical treatment for two-phase laminar boundary-layer", Univ. Kyushu Res. Inst. Ind. Sci. Report No. 66, 53-80 (in Japanese).
11. Berman, L.D., 1969, Thermal Engineering, 16, 95-99.
12. Fujii, T., Honda, H., Oda, K. and Kawano, S., 1979, "Forced convection condensation from steam-air mixtures on a horizontal tube", Proc. 16th Japanese Heat Transfer Symp., Paper C103, 331-333 (in Japanese).
13. Lee, W.C., 1982, "Filmwise condensation on a horizontal tube in the presence of forced convection and non-condensing gas", Ph.D. Thesis, University of London.
14. Lee, W.C. and Rose, J.W., paper in preparation.
15. Fujii, T., Honda, H. and Oda, K., 1979, "Condensation of steam on a horizontal tube - the influence of oncoming velocity and thermal condition at the tube wall", in "Condensation Heat Transfer", Proc. 18th Nat. Heat Transfer Conf., San Diego, 35-43.
16. Fujii, T., 1981, "Vapor shear and condensate inundation: an overview", in "Power Condenser Heat Transfer Technology", ed. Marto P.J. and Nunn, R.H., Hemisphere, 193-223.

APPENDIX 1 - Some relations between mass and molar quantities for a 2-constituent mixture

Nomenclature

M	molar mass
r_{12}	M_1/M_2
r_{21}	M_2/M_1
W	mass fraction
\bar{W}	mole fraction
ρ	density
$\bar{\rho}$	molar density (moles/volume)

subscripts

- 1,2 denote constituents 1 and 2; unsubscripted quantities relate to the mixture

$$W_1 + W_2 = 1$$

$$\tilde{W}_1 + \tilde{W}_2 = 1$$

$$W_1 = \tilde{W}_1 / (r_{21} + \tilde{W}_1 - r_{21} \tilde{W}_1)$$

$$\tilde{W}_1 = W_1 / (r_{12} + W_1 - r_{12} W_1)$$

$$M = \rho / \bar{\rho}$$

$$= M_1 \tilde{W}_1 + M_2 \tilde{W}_2$$

$$= M_1 (r_{21} + \tilde{W}_1 - r_{21} \tilde{W}_1)$$

$$= M_1 / (r_{12} + W_1 - r_{12} W_1)$$

APPENDIX 2 - Approximate ranges of parameters used in the experiments

Ref.	mixture	$\frac{P}{\text{kPa}}$	$\frac{d}{\text{mm}}$	T_∞/K	T_w/K	$\frac{u_\infty}{\text{m/s}}$	100 W_∞	Re	Sc
(13,14)	steam-air	4-103	12.5 - 25.3	301 - 373	291 - 364	0.3 - 26	0.1 - 32	227 - 2330	0.48 - 0.53
(13,14)	steam-hydrogen	4-102	12.5 - 25.3	300 - 373	294 - 355	0.3 - 17	0.1 - 5.7	130 - 1040	0.15 - 0.34
(13,14)	R113-air	101 - 104	12.5	318 - 321	284 - 303	0.5 - 1.8	0.04 - 1.6	3200 - 15700	0.17 - 0.21
(13,14)	R113-hydrogen	103 - 124	12.5	318 - 320	285 - 301	0.5 - 0.9	0.02 - 0.3	3290 - 7340	0.038 - 0.056
(5)	steam-air	8.5 - 18	19.1	307 - 333	2.8* - 25.6*	0.3 - 0.9	0.1 - 7.8	40 - 150	0.5 - 0.53
(12,16)	steam-air	3.7 - 8.6	37.2	300 - 313	5* - 15*	2.5 - 71	0 - 20	500 - 9000	0.46 - 0.53

$$*(T_\infty - T_w)/K$$

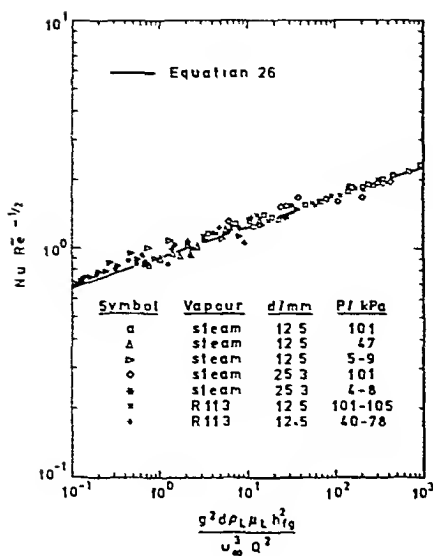


Figure 1 Pure vapour results (13,14)

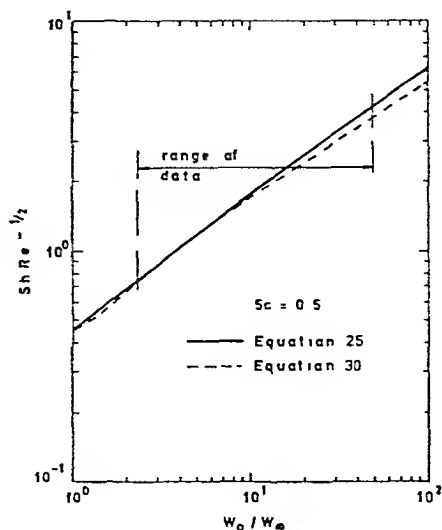


Figure 2a Comparison of boundary-layer solutions

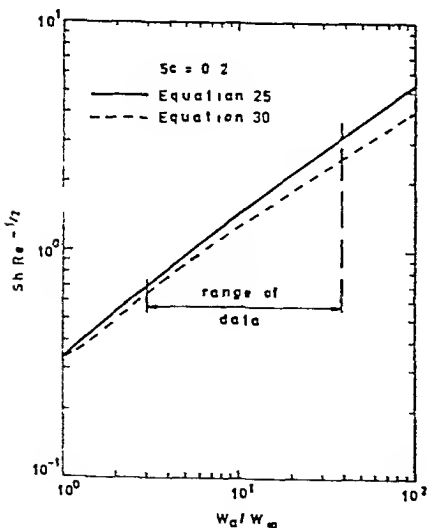


Figure 2b Comparison of boundary-layer solutions

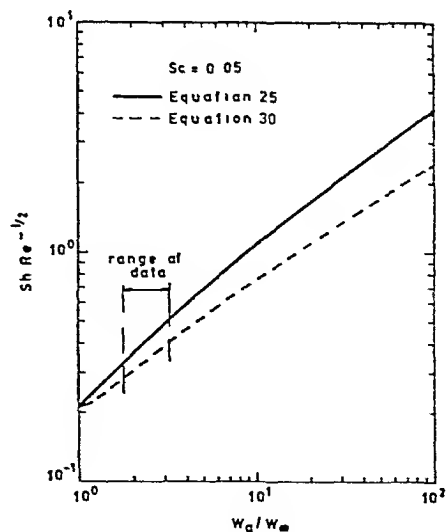


Figure 2c Comparison of boundary-layer solutions

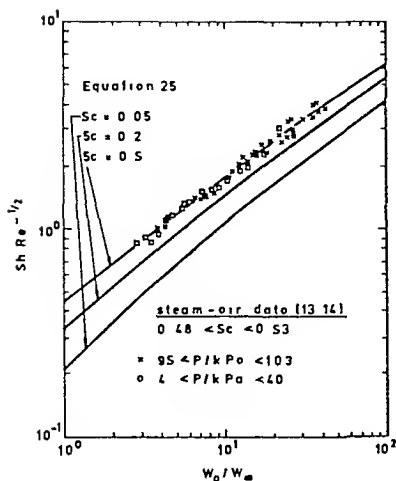


Figure 3a Comparison of equation 25 with experimental data

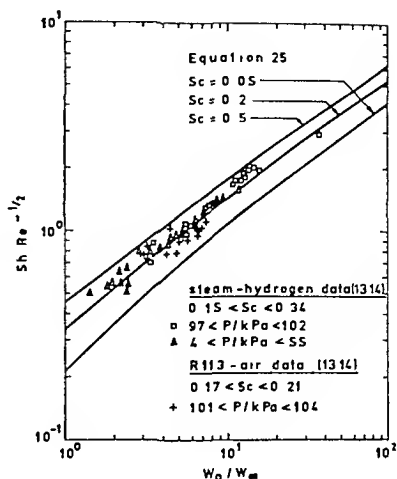


Figure 3b Comparison of equation 25 with experimental data

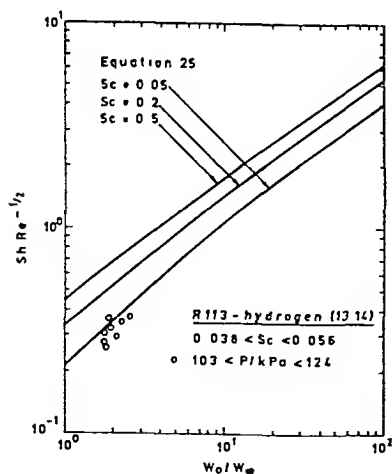


Figure 3c Comparison of equation 25 with experimental data

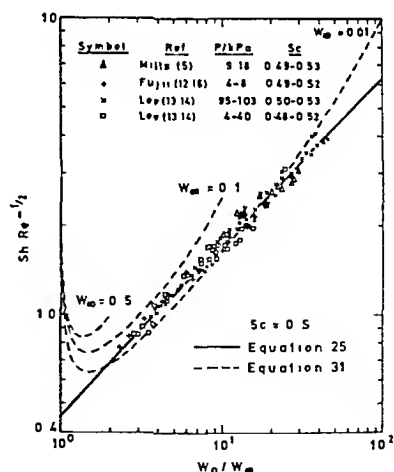
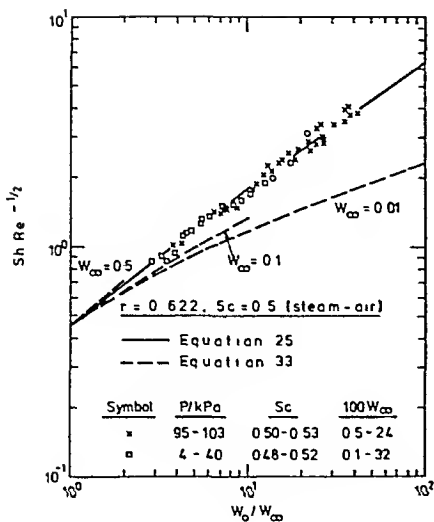
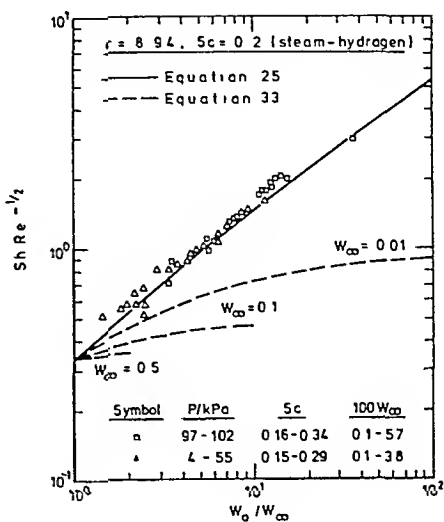


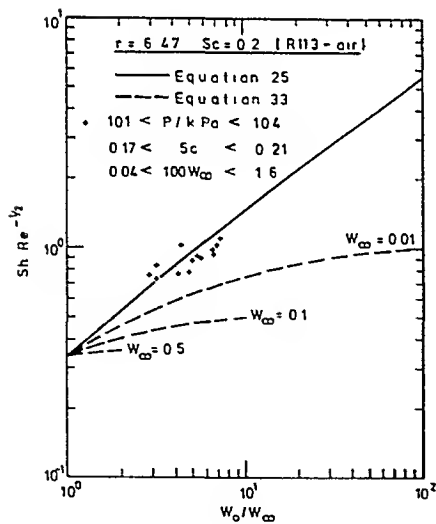
Figure 4 Comparisons for steam-air case



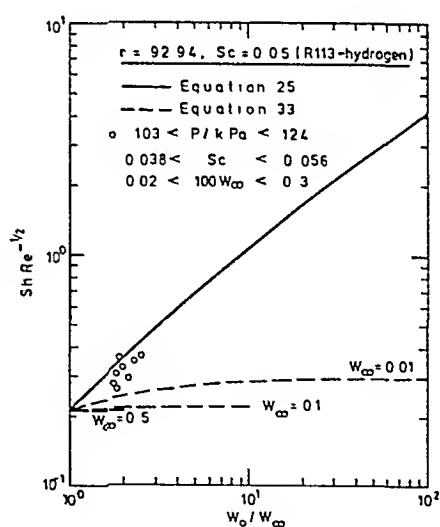
(a)



(b)



(c)



(d)

Figure 5 Comparisons with stagnant film model

CONDENSATION OF SINGLE AND MIXED VAPOURS FROM A NON-CONDENSING GAS IN FLOW OVER A HORIZONTAL TUBE BANK

A.K. Shah and D.R. Webb *

Experimental work is reported on condensation of methanol and methanol-water mixtures from nitrogen, carbon dioxide and refrigerant-12 in turbulent downwards flow across a bank of fifty horizontal tubes. It is shown that the Chilton-Colburn analogy between heat and mass transfer can be applied successfully to the prediction of condensation rates and heat loads. However the prediction of gas side temperature drop, essential if fogging is to be anticipated appears to be strongly influenced by heat transfer to condensate falling between the tubes. Evidence is presented to show that advanced methods of describing multi-component diffusion do not necessarily lead to improved prediction of condensation rates.

INTRODUCTION

The design of heat exchangers to condense vapours from a non-condensing gas is of considerable industrial importance. This condensation process has been extensively studied theoretically and experimentally. However the majority of these studies apply to condensers of simple geometry (condensation inside and outside single tubes or on a flat plate) and little work is reported for condensation over tube banks. Such studies are expensive because of the very high heat loads in condensation over a tube bank of even modest dimensions and are difficult to interpret because of the complicated flow pattern. Not only does the cross sectional area of vapour flow vary but the liquid condensate flow pattern is irregular due to inundation effects where condensate drips from higher to lower tube rows.

Fogging, a condition in which condensation occurs in a bulk supersaturated vapour, may lead to poor recovery of that vapour and entrainment problems and must be avoided in practical condensers. It is clear that conditions for its occurrence are only realistically studied in a bank of tubes where the environment is as similar to that of the practical condenser as possible. Further most prior studies have been concerned with binary condensation. It is known that the rigorous description of mass transfer in multicomponent systems (containing three or more constituents) is complicated by the possibility of diffusional interactions, and such effects have not previously been studied in condensation over a tube bank.

The present study has therefore been undertaken to extend the experimental data available on condensation of binary and multicomponent vapour mixtures over a tube bank. Particular attention has been paid to the prediction of the temperature profile in the gas phase, essential if fogging conditions are to be recognised.

* Department of Chemical Engineering, UMIST, Sackville St., Manchester, U.K.

The experimental work presented is in three parts. In a short preliminary study measurements are reported of heat transfer rates in cooling a pure gas and in condensation of a single vapour. Such studies are useful in determining the relative importance of the various resistances to heat transfer, and in assessing the validity of existing correlations for the prediction of these resistances. The second part of the work is concerned with the case of condensation of a vapour from a non-condensing gas, while the third deals with the multicomponent condensation of two vapours from a non-condensing gas.

PREVIOUS WORK

The only relevant work which appears to have been reported on the condensation of vapours and vapour mixtures from a non-condensing gas onto a tube bank is that of Schrodt and Gerhard, (15a) and (15b). Their work is limited to the condensation of water vapour and mixtures of water vapour and methanol from air over a vertically mounted bank of tubes. They were able to demonstrate the applicability of the Chilton Colburn Analogy (2) to their results and to justify the assumption of vapour-liquid equilibrium at the condensate surface. In the case of two condensing vapours, predictions of rates of condensation were not good ranging from 37 to 99% of the experimentally measured rate with a mean of about 70%.

Their work is significantly extended in the present study. A bank of horizontally mounted tubes is investigated so that effects arising from condensate drainage from row to row will be measured. The condenser consists of fifty tubes all carrying cooling water compared with the five 'active' tubes of their study. A far wider range of non-condensing gases has been studied and a more rigorous treatment of the mass transfer process is used.

Experimental conditions were chosen so that the vapour side processes should be controlling but it was necessary to predict the resistances of coolant and condensate so that the vapour side resistance could be obtained from the overall resistance.

There is a rather extensive literature on condensation of saturated single vapours over tube banks. Young et al (24) were apparently the first to measure rates of condensation in this geometry. Refrigerant 12 was condensed in downwards flow over five horizontally mounted tubes in a vertical plane. Their extensive data was used to check the classical treatment of Nusselt (12) which gives the following expression for the heat transfer coefficient of the j th row of a set of tubes arranged in a vertical plane.

$$\alpha_{L,j} = 0.725 \left\{ j^{\frac{3}{4}} - (j-1)^{\frac{3}{4}} \right\} N_c^{\frac{1}{4}} = K_j N_c^{\frac{1}{4}} \text{ where } N_c = \frac{\lambda^3 \rho_L (\rho_L - \rho_V) g \Delta h_v}{\eta d_o (T_I - T_w) \tilde{M}} \quad (1)(2)$$

Young et al provided a set of coefficients, K_j , which gave the best fit to their experimental data and these differ appreciably from the values of Nusselt.

	K_1	K_2	K_3	K_4	K_5
Nusselt	0.725	0.493	0.436	0.401	0.375
Young	0.655	0.576	0.551	0.498	0.464

Soling (18) commenting on the work of Young et al pointed out that Nusselt had assumed constant temperature driving force, $(T_I - T_w)$, and that the values of K_j should be modified according to,

$$K_j = 0.725 \left\{ \left[1 + \sum_{k=1}^{j-1} R_{fk} \right]^{\frac{1}{4}} - \left[\sum_{k=1}^{j-1} R_{fk} \right]^{\frac{1}{4}} \right\} \text{ where } R_{fk} = \frac{(T_I - T_w)_1}{(T_I - T_w)_k} \quad (3)(4)$$

Many further studies of condensation of pure saturated vapours over tube banks have been reported, for example, by Short & Brown (17), Turek (22) and Dornieden (5). The above studies of Young and Nusselt were found to be sufficiently accurate for the purposes of this study and subsequent work has not been evaluated.

There is a tremendous body of work to allow the prediction of heat transfer coefficients for single phase flow inside tubes. The equation of Grant et al (8) was found to give excellent results,

$$Nu_c = 0.00123 Re_c Pr_c^{0.42} \{1 + 25 Re_c^{-0.27}\} \quad (5)$$

The tubes of the condenser were relatively short and a correction was made for end effects according to the following correlation due to Boelter et al (1).

$$\alpha_c = \alpha_c' (1 + 6d_i/L) \quad (6)$$

Multicomponent mass transfer is complicated by the possibility of diffusional interaction where the rate of transfer of each individual species may depend upon all the independent concentration gradients present in the system. As pointed out by Toor (20), this can lead to unexpected effects; for example species may transfer in the opposite direction to their own concentration gradient, (viewed of course in the appropriate reference frame where there is no net transfer of mass or moles). Toor (21) and Stewart and Prober (19) showed how multicomponent mass transfer rates could be calculated, and Krishna and Standart (10) have provided an alternative and somewhat more rigorous treatment. In recent years considerable experimental evidence has indicated that these 'advanced' methods do in general lead to slightly better predictions of condenser performance particularly where there is a necessity to predict individual rates of condensation rather than total rates. However for the most part a traditional approach based on a generalisation of Colburn and Drew (3) will be adequate for design purposes; Sardesai (14) and Deo (4).

In this work the simpler approach of Colburn and Drew, generalised so that it should be appropriate for multicomponent mixtures, has been used in analysis of the multicomponent vapour results. However the data has also been analysed using the more rigorous methods and a comparison is provided to justify the use of the simpler method.

Thus this paper reports on the accuracy that can be achieved in predicting multicomponent condenser performance on the basis of data that has been measured with single vapours or gases and binary mixtures.

DESIGN MODEL

Consider a superheated gas-vapour mixture flowing downwards over a bank of tubes arranged on a triangular pitch (See Fig. 1). The temperature of the coolant is everywhere low enough to provide a tube surface temperature below the saturation temperature of the gaseous mixture, a condition essential to provide the temperature and concentration gradients for heat and mass transfer.

In Fig. 1 the idealised flow structure around the j th row of tubes in a tube bank with a total of n rows is shown. Liquid condensate arriving at the j th row originates at row $(j-2)$ and because of the staggered arrangement of tubes drips to row $(j+2)$. It will be assumed that the tube surface is wetted and the condensate forms a continuous film. In the arrangement shown the condensate forms into parallel and separate streams which in general have different flowrates depending on the rates of condensation on the tubes above. Tube rows 1 and 2 are exceptional in that there is no condensate dripping from above. The vapour flow is essentially vertical with minor deviations around the tubes. In traversing the j th row, heat and mass transfer takes place to the coolant. However it is clear that the proximity of vapour and droplets of condensate, subcooled relative to the vapour, might lead to additional transfer and the failure of the simple model described below. The coolant may flow upwards or downwards through the tube bank (counter or cocurrent with respect to the vapour) and in Fig. 1 is depicted as flowing into and out of the bank in succeeding rows. In this work cocurrent (downwards) flow of coolant was studied.

The Colburn and Drew equations (3) are adapted for this model of the condenser behaviour, first for one condensing vapour and later extended for two. There are three dependent variables, vapour-gas temperature, T_{gj} , the single condensable vapour (subscript A) flowrate, G_{Agj} , cooling water temperature, T_{cj} , in the difference equations which describe the downstream change of conditions from row to row (subscript j gives number of tube row) through the condenser. For simplicity these variables are assumed to take their average value in each horizontal plane of tubes. For the j th row, (See Figure 2)

$$\text{Vapour gas temperature, } T_{gj} = \frac{T_{gj}^{\text{in}} + T_{gj}^{\text{out}}}{2.0} \quad j = 1, n \quad (7)$$

$$\text{Condensable vapour molar flowrate, } G_{Agj} = \frac{G_{Agj}^{\text{in}} + G_{Agj}^{\text{out}}}{2.0} \quad j = 1, n \quad (8)$$

$$\text{Coolant Temperature, } T_{cj} = \frac{T_{cj}^{\text{in}} + T_{cj}^{\text{out}}}{2.0} \quad j = 1, n \quad (9)$$

The following difference equations describe the development of T , G_{Ag} and T_c with exchanger area, A , for the j th row in terms of the driving forces between gas phase (subscript g) and interface (subscript I).

Gas Temperature

$$-(G_{Bg} + G_{Agj}) \tilde{C}_{pgj} \frac{\Delta T_{gj}}{\Delta A_j} = \alpha_{gj}^* (T_{gj} - T_{Ij}) \quad j = 1, n \quad (10)$$

where the gas film heat transfer coefficient to the tube, α_{gj}^* is corrected by the Ackermann factor ϕ_j

$$\alpha_{gj}^* = \alpha_{gj} \frac{\phi_j}{\exp \phi_j - 1}; \quad \phi_j = \frac{N_{Aj} \tilde{c}_{pAj}}{\alpha_{gj}} \quad (11), (12)$$

and \tilde{c}_{pA} and \tilde{c}_{pg} are molar specific heat capacities of component A and gas mixture respectively.

Condensable flowrate

$$-\frac{\Delta G_{Aj}}{\Delta A_j} = N_{Aj} = \beta_{gj} \ln \left\{ \frac{1 - y_{AIj}}{1 - y_{Agj}} \right\} \quad j = 1, n \quad (13), (14)$$

where the molar rate of mass transfer, N_A , to condensate is given as the product of gas film mass transfer coefficients, β_g , and molar driving force.

Cooling Water Temperature

$$G_c \tilde{c}_{pc} \frac{\Delta T_c}{\Delta A_j} = \alpha_{oj} (T_{wj} - T_{cj}) \quad j = 1, n \quad (15)$$

where G_c is the molar flowrate and \tilde{c}_{pc} the specific heat capacity of the coolant and α_{oj} the overall heat transfer coefficient between wall and coolant. The two condensate stream flowrates, distinct depending on whether they originated at tube row 1 or 2 may now be calculated at a plane immediately below the j th row.

$$G_{1Aj}^{out} = \sum_{k=1,3,5}^j N_{Ak} \Delta A_k \quad G_{2Aj}^{out} = \sum_{k=2,4,6}^j N_{Ak} \Delta A_k \quad (16), (17)$$

The vapour composition in the j th tube row is given as

$$y_{Agj} = G_{Agj} / (G_{Bg} + G_{Agj}) \quad (18)$$

The interfacial temperature, T_{Ij} , and the wall temperature, T_{wj} , may be obtained from the continuity of the energy flux across the interface.

$$\alpha_{oj} (T_{wj} - T_{cj}) = \alpha_{lj} (T_{Ij} - T_{wj}) = \alpha_{gj}^* (T_{gj} - T_{Ij}) + N_{Aj} \{ \tilde{\Delta h}_{vA} + \tilde{c}_{pA} (T_{Ij} - T_{lj}) \} \quad (19)$$

where

$$\alpha_{gj}^* = \alpha_{gj} \exp(\phi_j) \quad (20)$$

The rigorous prediction of the 'mixing average' temperature, T_{lj} , of the condensate would require a knowledge of the velocity distribution in the liquid film which is probably turbulent and certainly distorted by the effect of droplets impinging from above. For simplicity the average temperature is used,

$$T_{lj} = (T_{wj} + T_{Ij}) / 2.0 \quad (21)$$

Heat and mass transfer coefficients for the gas film, α_{gj} and β_{gj} , have been predicted using the Chilton-Colburn analogy.

$$J_{Hj} = \frac{\alpha_{gj} S Pr^{2/3}}{\tilde{c}_{pg} (G_{Bg} + G_{Agj})} = J_{Dj} = \frac{\beta_{gj} S Sc^{2/3}}{(G_{Bg} + G_{Agj})} = a Re_j^b \quad (22)$$

$$\text{where } Sc = \nu/D_{AB}; \text{ Pr} = \nu/\alpha; \text{ Re} = d_e(G_{Bj} + G_{Agj})\tilde{M}_{gj}/\eta \quad (23), (24)$$

and S is the minimum flow area for vapour flow.

There are $(3n+3)$ unknowns on the R.H.S. of equations (7) to (9). Three of these are specified as design variables, usually inlet vapour flowrate, G_{Agl}^{in} , inlet vapour temperature, T_{gl}^{in} , and inlet cooling water temperature, T_{cl}^{in} . Equations (10), (13) and (15) are the $3n$ equations, which allow the determination of the unknowns and the design of the condenser.

The coefficients, 'a' and 'b', of equation (22) have been determined from experimental data for cooling of a pure gas and binary condensation as described in Section 5. Material and energy balances over the test condenser may be written,

$$\text{Condensation Rate} = (G_{Agl}^{in} - G_{Agn}^{out}) = G_{1\&n}^{out} + G_{2\&n}^{out} \quad (25)$$

$$\text{Energy transferred} = G_{c} \tilde{c}_{pc} (T_{cn}^{out} - T_{cl}^{in}) = G_{Bg} \tilde{c}_{pB} (T_{gl}^{in} - T_{gn}^{out}) +$$

$$G_{Agl}^{in} \left[\tilde{h}_{vA}^* + \tilde{c}_{pA} \{T_{gl}^{in} - T_{1n}^{out}\} \right] - G_{Agn}^{out} \left[\tilde{h}_{vA}^* + \tilde{c}_{pA} \{T_{gn}^{out} - T_{2n}^{out}\} \right] \quad (26)$$

where * refers to the reference state of saturation at the condensate outlet temperature.

In the latter part of the paper, concerned with multicomponent condensation, subscript A will refer collectively to the condensing components, referred to by the individual subscripts, C and D. Subscript B will continue to be used for the non-condensing gas. Then the molar flowrate of condensing species, G_{Ag} , and the total condensation flux, N_A , will be given as,

$$G_{Ag} = G_{Cg} + G_{Dg}; \quad N_{Ag} = N_{Cg} + N_{Dg} \quad (27), (28)$$

Some care must be taken over physical properties which are subscripted A since averaging of the properties of the condensing species C and D may be either on a molar basis or a molar flux basis. The appropriate averaging is clear from the context. Thus in the expression for the Ackermann correction factor averaging is clearly on a molar flux basis,

$$\phi = \frac{N_A \tilde{c}_{pA}}{\alpha_g} = \frac{N_C \tilde{c}_{pC} + N_D \tilde{c}_{pD}}{\alpha_g} \quad \text{with } \tilde{c}_{pA} = N_C \tilde{c}_{pC} + N_D \tilde{c}_{pD} / N_A \quad (29), (30)$$

With these definition equations (7) to (13) apply unchanged.

The addition of a second condensing species modifies equations which describe mass transfer. Individual rates of transfer of C and D will be given by equations of identical form to equation (14) but the mass transfer coefficients must be defined in terms of the appropriate diffusivity and the interfacial compositions must be evaluated using an appropriate thermodynamic

relationship to account for liquid non-ideality. Thus for component C

$$N_C = \beta_{CB} \ln \left\{ \frac{1 - y_{CI}}{1 - y_{CG}} \right\} \quad (31)$$

$$\text{where } J_D = \frac{\beta_{CB} S Sc_{CB}^{2/3}}{(G_{Bg} + G_{Ag})} = a Re^b \text{ and } Sc_{CB} = \frac{\nu}{D_{CB}} \quad (32)(33)$$

Similar equations must be written also for component D.

The interfacial compositions were evaluated with the assumption of thermodynamic equilibrium, thus,

$$y_{CI} P_T = \gamma_C x_{CI} P_{CI}^0$$

where, the activity coefficient, γ_C , is to account for the non-ideality of the liquid. In this work γ_C was estimated using the Wilson (23) equation.

It is clear that the composition of the vapour by mole fraction requires that equation (18) be written individually for species C and D and this in its turn requires an additional difference equation of the same form as (13) to describe the change in flowrate of one of the species C and D. Thus

$$\frac{\Delta G_{CG}}{\Delta A} = -N_C - N_{Cd} \text{ with } y_{CG} = G_{CG}/(G_{Bg} + G_{Ag}) \quad (34)(35)$$

With these modifications the design problem becomes identical to that of the case of binary condensation. There is of course an extra difference equation required to follow the change of downstream conditions through the condenser, this being equation (35).

In the study of multicomponent condensation the equations as modified above are used in a purely predictive manner. Known experimental conditions at the vapour/gas inlet are used as the boundary conditions to solve the four difference equations (involving gas and coolant temperatures, total vapour gas flowrate and the flowrate of one condensing species) from row to row through the condenser.

TEST APPARATUS

The condenser consists of fifty stainless steel tubes (of 0.0127m OD, 0.0109m ID and length 0.18m) arranged horizontally on a 0.025m equilateral triangular pitch (Figure 3). The tubes are arranged in 9 rows of 6 and 5 tubes alternately. The rows with 5 tubes were completed by including two dummy half tubes at the wall so that the gas flow pattern should be similar in all rows. The total heat exchanger area based on the outside diameter of the tubes is 0.36m².

tion produces a liquid mixture and its composition must be determined. Liquid mixtures were analysed for composition by simultaneous measurement of density and refractive index.

The above measurements allow the mass and energy balances, equations (25) and (26), to be checked. In all the runs reported both the mass and energy balances agreed within 10%. This is consistent with the stated precision of the measurements and estimated losses of mass by leakage of condensate and of energy by natural convection to the surroundings.

ANALYSIS OF EXPERIMENTAL RESULTS AND DISCUSSION

The main body of the experimental work was concerned with condensation of vapours from a non-condensing gas. However shorter studies of gas cooling and condensation of a pure vapour were carried out to gain experimental information which would be useful in assessing the reliability of the correlations available in the literature for gas side, condensate and coolant heat transfer coefficients.

Experiments on Gas Cooling

Nineteen experimental runs were carried out on cooling of nitrogen, and are fully reported in Shah (16). Typically the heat load, which was calculated from the change in temperature of the gas, lies between 1 and 2kW, corresponding to a cooling between 15 and 40°C. An accurate energy balance was not possible because the coolant temperature rise was too small. The coolant heat transfer coefficient, (usually 30 to 40 times larger than the gas film coefficient) was calculated from the equation of Grant (8) and hence could be backed out of the overall coefficient to give the gas side coefficient. ^{1/3}The results are presented graphically in Figure 5 as a plot of log (Nu/RePr) versus log (Re) and the data have been fitted by linear regression to give the coefficients of the correlation,

$$J_H = Nu/RePr^{1/3} = a Re^b$$

The values of a and b obtained over these runs are compared with values quoted in the literature in the following table. Agreement of all correlations is good ($\pm 10\%$) in the range considered. Agreement of experimental results with the quoted values of McAdams (11) is particularly close ($\pm 2\%$).

Source	a	b
Grimson (9)	0.513	-0.437
McAdams (11)	0.330	-0.400
Eng. Sci. Data (6)	0.272	-0.365
Zukauskas (25)	0.357	-0.400
Ramamurthy (13)	0.407	-0.408
This work	0.315	-0.396

COEFFICIENTS OF $J_H = a Re^b$

It is clear from the table that the values of 'b' are in good agreement in four of the six sources. Thus in the analysis of the data presented on condensation of a single vapour from a non-condensing gas, values of 'a' will be determined for a value of $b = -0.4$. The effect of condensate on vapour side heat and mass transfer should then be apparent from the variation of coefficient 'a'.

Experiments on Condensation of a Pure Vapour

A total of twenty six experimental runs were carried out on the condensation of a pure vapour equally divided between methanol and isopropanol. In all cases the condenser was operated in a loaded condition with a substantial fraction of the vapour generated passing to the knockout condenser. In this series of experiments the heat transfer resistance of the condensate film and of the coolant were of very similar magnitude so that neither resistance can be measured in isolation; It was unfortunately not possible to vary operating conditions so that one resistance should dominate.

The experimental results are reported in Shah(16). Examination of the data shows that the heat load was varied between about 6 and 16kW and the vapour side Reynolds Number between 1,000 and 2,000. The heat loads estimated on the basis of both the vapour and coolant sides are reported and it can be seen that the energy balance agrees in all cases within 10%, (See also Figure 6).

The experimental data were used to assess some of the correlations available in the literature. A condenser rating calculation was carried out on a row to row basis using the correlations described in the Section on PREVIOUS WORK. The correlation of Grant et al corrected for the small L/d ratio by the equation of Boelter et al was used to predict the heat transfer coefficient of the coolant. The condensate heat transfer coefficient was predicted by both the methods of Nusselt and Young. In the case of the Nusselt method a temperature driving force correction was made in accordance with the proposal of Soling but the calculations based on Young's work used the coefficients he obtained (reported above) without a temperature correction. In this way the performance of the condenser could be predicted and these predictions are now compared with the performance measured directly.

The condenser rating calculations are reported in full in Shah(16) and presented graphically in Figures 6 and 7. Figure 6 shows the comparison of experimental and predicted heat loads. It is clear that in all runs better results are obtained using Young's experimental coefficients, K_c , rather than the theoretical values of Nusselt in equation (1). Secondly the data relating to methanol are better predicted than the data measured with isopropanol. The experimental procedure was improved in the later work with methanol compared with the earlier work with isopropanol by installation of automatic data logging and this may account for some of the better agreement with methanol. Further the overall temperature driving force was far higher with isopropanol and the coefficients of Young have not been corrected for temperature as proposed in Equation (4). This correction tends to reduce the predicted heat load and will probably explain the discrepancy between the two data sets. No particular significance is therefore attached to the apparently better predictions of data obtained with methanol. The trends of

Figure 6 are exactly followed by Figure 7 where predicted and experimentally based overall heat transfer coefficients, α , are compared.

In conclusion, the performance of the test condenser was predicted within about 15% using correlations taken from the literature for the case of condensation of a pure vapour. In the next set of experimental measurements reporting condensation of a vapour from a non-condensing gas, the heat loads achieved were usually about 50% of those reported in this section. This implies a gas side resistance to heat transfer approximately the same as that of condensate and coolant combined. The above error in predicting the resistance of condensate and coolant should therefore contribute less than 10% error to the value of a gas side heat transfer coefficient obtained from a measured overall coefficient. This was regarded as acceptable for the purposes of this study.

Experiments on Condensation from a non Condensing Gas

A total of 35 experimental runs were carried out on the condensation of vapours from a non-condensing gas, divided between 3 systems

	<u>No. of runs</u>
1) Methanol and Nitrogen	(m = 11)
2) Methanol and Carbon Dioxide	(m = 13)
3) Methanol and Refrigerant 12	(m = 11)

The experimental data are reported in full in Shah (16) for each system listed.

All experimental data were tested to ensure that the overall energy balance, equation (26) was satisfied within $\pm 10\%$. This energy balance which is presented graphically in Figure 8, is based directly on measured quantities. The data were analysed as described in the section on the DESIGN MODELS. For each system an optimisation was carried out over all runs with that system. This involved the selection of the value of 'a' in equation (23) which minimised the objective function

$$\sum_{k=1}^m \left\{ \sum_{j=1}^9 \{ \Delta T_{cj}^{\text{out}} \}_k + \{ \Delta T_{gn}^{\text{out}} \}_k \right\}$$

where $\{ \Delta T_j^{\text{out}} \}_k$ is the difference between predicted and experimentally measured outlet temperature of the jth row for the kth run with a particular system, subscript c for coolant and g for gas. There are of course 9 tube rows and the number of runs with each system are summarised in the above list. For the purpose of this optimisation the exponent b was taken as -0.4 which was justified above. The heat transfer coefficients of condensate and coolant were predicted by the methods verified in the previous section; Young's method for the liquid, Grant's correlation for the coolant.

The validity of this approach may be judged from the comparison of experimental and predicted heat loads as shown in Figure 8. It is clear that the heat load is predicted within $\pm 10\%$ in nearly every individual run.

The experimentally measured and predicted condensation rates are compared in Figure 10. Since the major contribution to the heat load is the latent heat of condensation, and the overall heat load is accurately predicted it would be expected that condensation rates would not be in serious error and this is confirmed in Figure 10. The condensation rates are predicted within $\pm 15\%$ in most cases.

The experimentally measured and predicted temperature drops in the gas phase, ΔT_g , are presented in Figure 9. It is clear that temperature drop in the gas phase is rather poorly predicted, always 10% smaller than that measured and sometimes as much as 30% smaller. This occurs despite the fact that during the optimisation procedure the value of a in the Chilton-Colburn correlation is considerably increased over the value found for cooling of nitrogen as shown in the following Table.

System	Model
Methanol-Nitrogen	0.380
Methanol-Carbon dioxide	0.374
Methanol-Refrigerant 12	0.484
Nitrogen (single gas)	0.315

$$\text{COEFFICIENTS OF } J_H = a \text{Re}^{-0.4}$$

The particular objective function chosen ascribes equal importance to all measured temperature differences, each run including 9 based on coolant and one based on gas. In a second optimisation (not reported here), only overall coolant and gas temperature differences were included in the optimisation. The prediction of the gas temperature drops was improved but only at the expense of the heat load and this was not regarded as acceptable. This latter effect arises through the analogy. An increase in the J_H value and hence the J_D value leads to an increase in the predicted mass transfer rate and an over prediction of the heat load. This seems to indicate that it is not the analogy itself which is at fault but rather that there is some additional mechanism leading to transfer of sensible heat from the vapour phase.

In conclusion the observed temperature drops can only be explained by some additional mechanism of heat transfer between vapour and condensate. This mechanism does not appear to be associated with a condensate induced enhancement of the vapour side heat and mass transfer processes since this would lead in its turn to overprediction of the heat load. Rather it would appear that there is transfer of heat to subcooled condensate droplets falling between the tubes. Exploratory calculations have shown that such a mechanism can account for the observed gas temperature drop without significantly affecting the predicted heat load.

Experiments on Multicomponent Condensation of Two Vapours from a Non-Condensing Gas

Three sets of data are reported each measured with a different system as follows.

I) Water vapour-methanol-nitrogen	25	No. of runs
II) Water vapour-methanol-carbondioxide	25	
III) Water vapour-methanol-refrigerant 12	22	

These data are used to assess a design procedure based on the correlations verified by the measured data on gas cooling, condensation of pure vapours and of a single vapour from a non-condensing gas. Accordingly Young's method was used for the condensate coefficient, Grant's correlation for the coolant coefficient and the Chilton-Colburn Analogy with 'a' and 'b' taken as 0.33 and -0.41 respectively.

The measured data are fully reported in Sbahi (16). It is apparent that the gas side Reynolds Number was varied from 2,000 to 20,000 based on outside tube diameter with a heat load from 4 to 11 kW. The vapour composition was varied as widely as was practical with water vapour making up between 0.1 and 0.2 and methanol between 0.4 and 0.8 by mole fraction. These vapour compositions were realised from three water-methanol mixtures of about 70%, 50% and 30% water by volume respectively. Condensation rate was varied from about 10 to 25 kg/hr. Shah's thesis (16) gives measured heat loads based on coolant and gas-vapour side measurements respectively. These can be seen to agree within 10%.

The data were analysed by three models of multicomponent mass transfer, (only one of which is described in detail in the section on the DESIGN MODEL).

- (1) The method of Toor (21).
- (2) The method of Krishna & Standart (10).
- (3) An effective diffusivity model based on Colburn and Drew (3).

Of these the first two are 'advanced' models in that they account for the multicomponent mass transfer process in a rigorous manner. Good agreement was achieved in all cases. Typically gas phase temperature drops (of the order of 15-20K) were predicted within 0.5K, outlet vapour-gas compositions within 0.005 m.f., heat loads within 7% and condensate compositions and flow-rates within 10% irrespective of the mass transfer model used. One such comparison is presented in Figure 11. This shows the total condensation rate as predicted by the Krishna-Standart and Effective Diffusivity methods. In this particular case the simpler model is in better agreement with experiment. This contrasts with the recent work of Deo (4) and Sardesai (14) where the 'advanced' models were uniformly better. It is perhaps significant that their work was carried out in condensation onto a vertical tube of short length where molecular transport would be relatively more important.

The model described in this paper for predicting heat and mass transfer is evaluated now using the multicomponent data. Predicted temperature drops are compared in Figure 12 which applies for the system water vapour-methanol-refrigerant 12. Clearly gas phase temperature drops are underestimated by the same margin as they were for binary systems, that is by about 30 to 40%. The success of the proposed design model as applied to all the data of this study, is shown in Figures 13-15. Taking each Figure in turn it is seen that for the majority of data points,

- (i) Condensate composition is predicted within $\pm 20\%$ (Figure 13)
- (ii) Condensation rates are predicted within $\pm 20\%$ (Figure 14)
- (iii) Heat loads are predicted within $\pm 15\%$ (Figure 15)

CONCLUSIONS

Experimental measurements are reported on gas cooling and condensation over a horizontal tube bank. Measured values of the coefficients of the Chilton-Colburn analogy were in good agreement with published values in experiments of gas cooling. Good accuracy was also achieved in predicting the combined heat transfer coefficient of coolant and condensate in condensation of pure vapours using published correlations.

The Chilton-Colburn analogy was also successful in predicting heat load, condensation rate and condensate composition in condensation of binary and multicomponent vapours but failed to predict the temperature drop of the gas phase within acceptable limits in both systems.

There is clear evidence that an additional mechanism is present in the system studied whereby sensible heat is transferred from the gas phase. This will have important implications with respect to the prediction of fogging.

It is apparent that the more rigorous models of the multicomponent mass transfer process due to Toor (21) and Krishna and Standart (10) perform no better than a simple effective diffusivity model under the conditions of the present study.

NOMENCLATURE

A	- heat exchange area (m^2)	n	- number of rows
A _j	- heat exchanger area of all tubes in jth row (m^2)	N	- molar flux of condensation ($kmol/m^2s$)
a	- coefficient in correlation for J_H	N _c	- Nusselt grouping of equation 2
b	- exponent in correlation for J_H	Nu	- Nusselt Number
\tilde{c}_p	- molar specific heat capacity (J/kmolK)	p ^o	- Vapour Pressure (kN/m^2)
d _o	- outside tube diameter (m)	Pr	- Prandtl Number
d _i	- inside tube diameter (m)	P _T	- System Pressure (kN/m^2)
d _e	- equivalent diameter (m)	Re	- Reynolds Number
D _{AB}	- binary diffusivity (m^2/s)	R _f	- temperature ratio of equation 4
G	- molar gas or vapour flowrate (kmol/s)	S	- 'Window' flow area of vapour (m^2)
g	- gravitational acceleration (m/s^2)	T	- temperature (K)
$\Delta \tilde{h}$	- molar latent heat (J/kmol)	x	- mole fraction in liquid
J _H , J _D	- Chilton Colburn J factors	y	- mole fraction in gas
j	- row number counted from gas inlet	<u>Greek Symbols</u>	
K	- constant in equation 1	α	- heat transfer coefficient (W/m^2K)
L	- tube length (m)	α	- thermal diffusivity (m^2/s)
m	- number of runs	β	- mass transfer coefficient ($kmol/m^2s$)
\tilde{M}	- molecular weight (kg/kmol)	γ	- activity coefficient

Δ	- increment of following quantity	<u>Subscripts</u>	
λ	- thermal conductivity (W/m K)	A	- component A, condensing vapour
η	- viscosity (kg/m s)	B	- component B, non-condensing gas
ν	- kinematic viscosity (m^2/s)	C	- component C, condensing vapour, 1 of 2
ρ	- density (kg/m^3)	c	- relating to coolant
Σ	- summation	D	- component D, condensing vapour, 2 of 2.
ϕ	- Ackermann correction factor	d	- relating to droplet
<u>Superscripts</u>		e	- equivalent
.	- modified heat transfer coefficient	g	- relating to gas
/	- uncorrected quantity	i	- inside
*	- reference state	I	- relating to interface
in	- inlet condition	j	- row number
out	- outlet condition	i, k	- indexes
		l	- relating to liquid condensate
		o	- overall
		v	- relating to vapour
		w	- relating to wall

REFERENCES

- Boelter, L.M., Young, G. and Iverson, H.W., N.A.C.A. Tech. Note 1451, (1948)
- Chilton, J.H. and Colburn, A.P., Ind. Eng. Chem., **26**(1), 1183, (1934)
- Colburn, A.P. and Drew, T.B., Trans. A.I.Ch.E., **33**, 197, (1937)
- Deo, P.V., Ph.D. Thesis, University of Manchester, (1979)
- Doroieden, M., Chemie Ing. Techn., **44**(1), 269, (1972)
- Engineering Science Data, "Convective heat transfer during cross flow of fluids over plain tube banks", Item No. 73031, ESDU, London, (1973)
- Fair, J.R., Petro. Chem. Engr., **33**(9), 57, (1961)
- Grant, I.D.R. and Osment, B.D.J., N.E.L. Report No. 350, E. Kilbride, (1968)
- Grimson, E.D., Trans. ASME, **59**, 583, (1937)
- Krishna, R., and Standart, G.L., A.I.Ch.E.J., **22**(2), 383, (1976)
- McAdams, W.H., "Heat Transmission", McGraw Hill, New York, (1954)
- Nusselt, W., Ver. Deutsch. Ind., **60**, 541, (1916)
- Ramamurthy, P.A., Ph.D. Thesis, UMIST, (1976)
- Sardesai, R.G., Ph.D. Thesis, UMIST, (1979)
- Schrodt, J.T. and Gerhard, E.R., Ind. Eng. Chem. Fundl., **4**(1), 46, (1965)
- Schrodt, J.T. and Gerhard, E.R., Ind. Eng. Chem. Fundl., **7**(2), 281, (1968)

16. Shah, A.K., Ph.D. Thesis, UMIST, (1981)
17. Short, B.E. and Brown, H.E., Proc. Gen. Disc. of Ht. Trans., London, (1951)
18. Soling, S.P., Trans ASME, 64, 793, (1942)
19. Stewart, W.E. and Prober, R., Ind. Eng. Chem. Fundl., 3, 224, (1964)
20. Toor, H.L., A.I.Ch.E.J., 3, 198, (1957)
21. Toor, H.L., A.I.Ch.E.J., 10(4), 448, (1964)
22. Turek, K., Chemie, Ing. Techn., 44(1), 280, (1972)
23. Wilson, G.M., J. Am. Chem. Soc., 86, 127, (1964)
24. Young, F.L. and Wohlenburg, W.J., Trans ASME, 64, 787, (1942)
25. Zukauskas, A., Advances in Ht. Transfer, 8, 93, (1972)

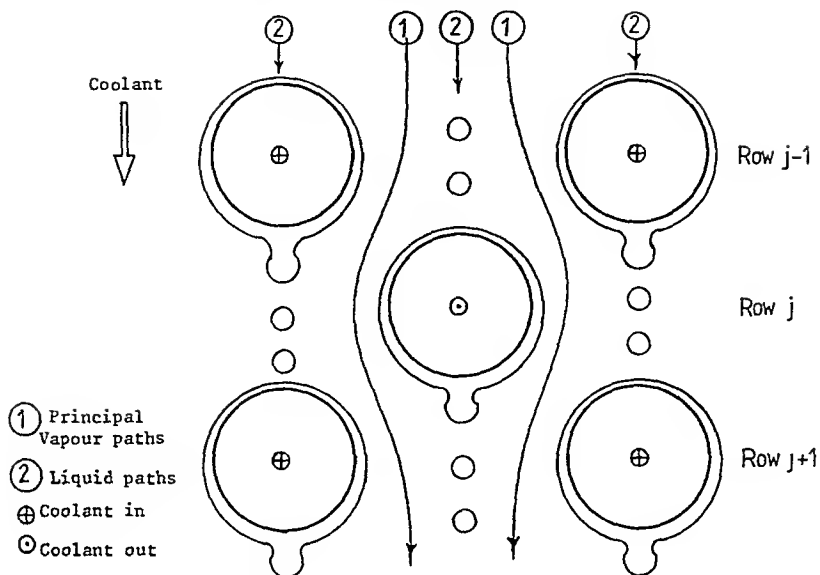


FIGURE 1 IDEALISED FLOW PATTERN

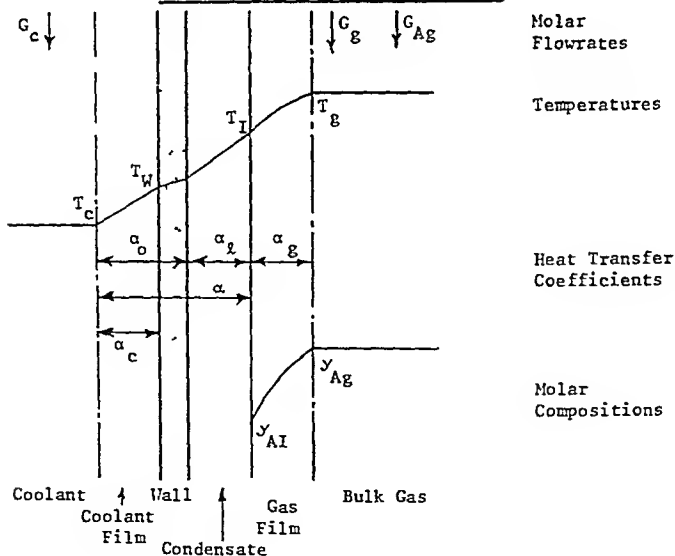


FIGURE 2 IDEALISED FILM MODEL OF HEAT AND MASS TRANSFER

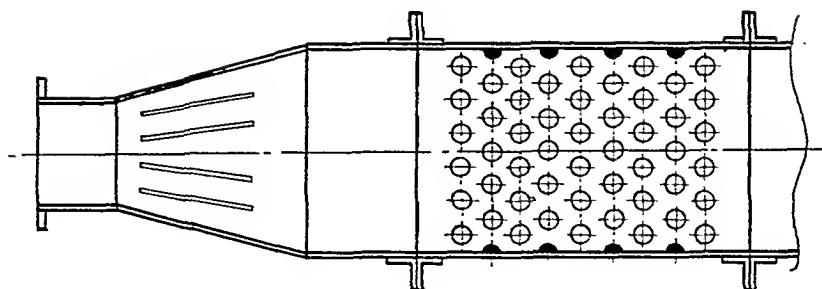


FIGURE 3 SECTION THROUGH TUBE BUNDLE

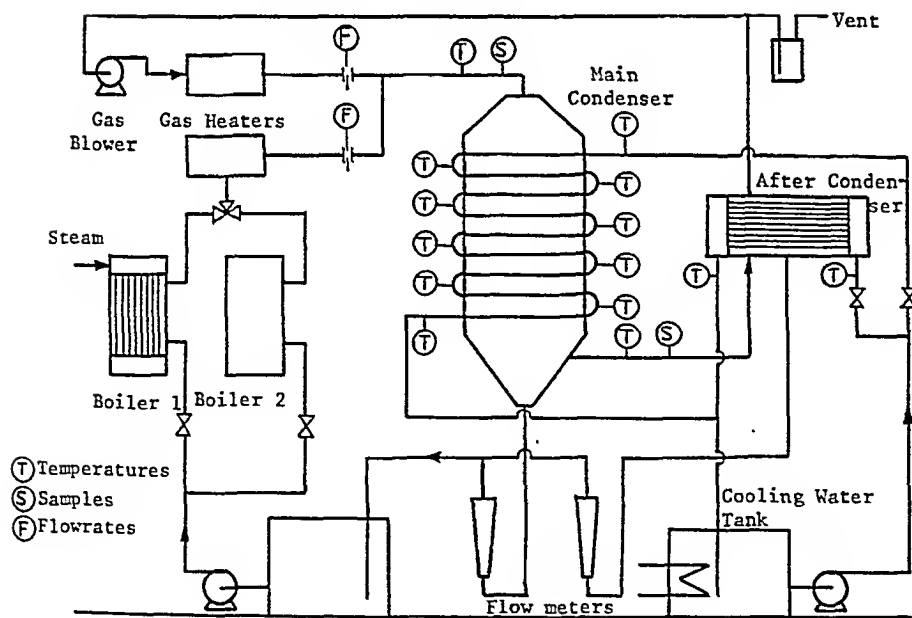


FIGURE 4 EXPERIMENTAL FLOWSHEET

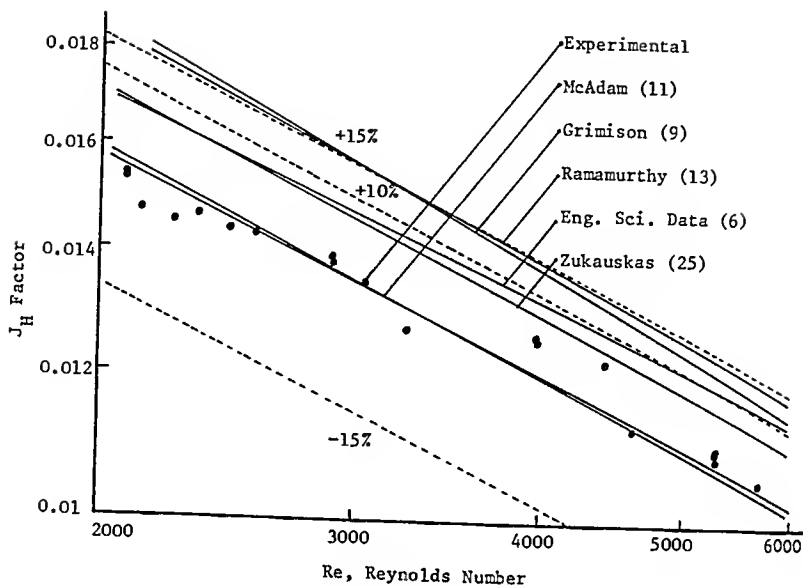


FIGURE 5 J_H FACTORS FOR COOLING OF A SINGLE GAS

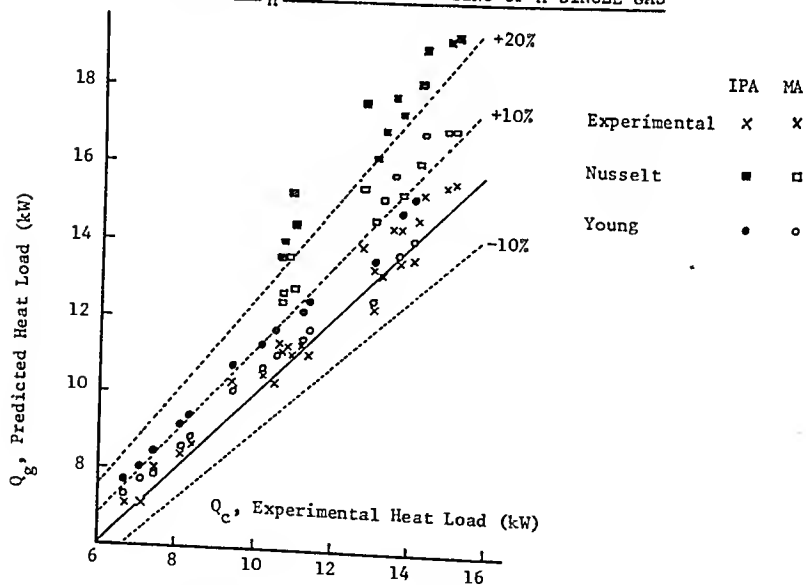


FIGURE 6 HEAT LOADS: CONDENSATION OF A PURE VAPOUR

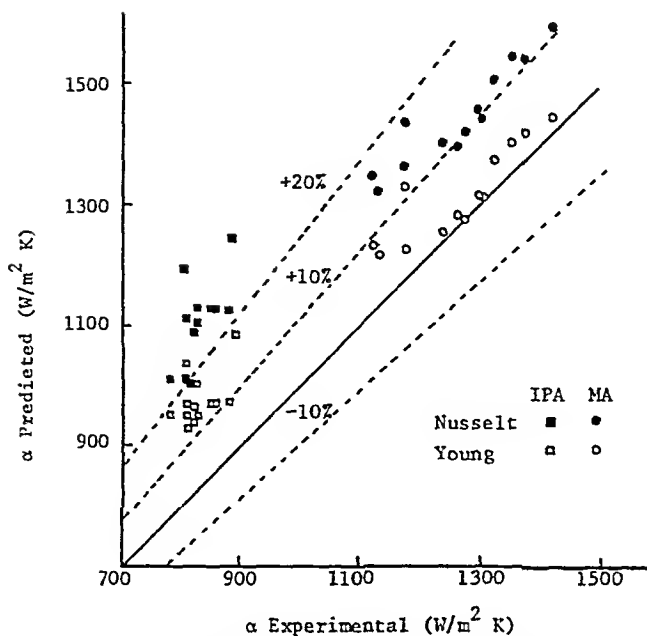


FIGURE 7 OVERALL HEAT TRANSFER COEFFICIENT
CONDENSATION OF PURE VAPOURS

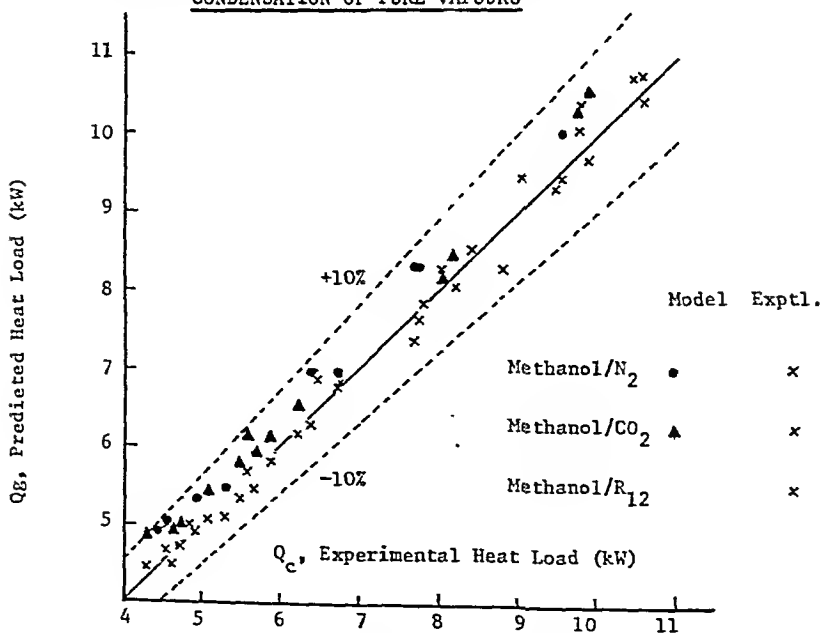


FIGURE 8 COMPARISON OF HEAT LOADS

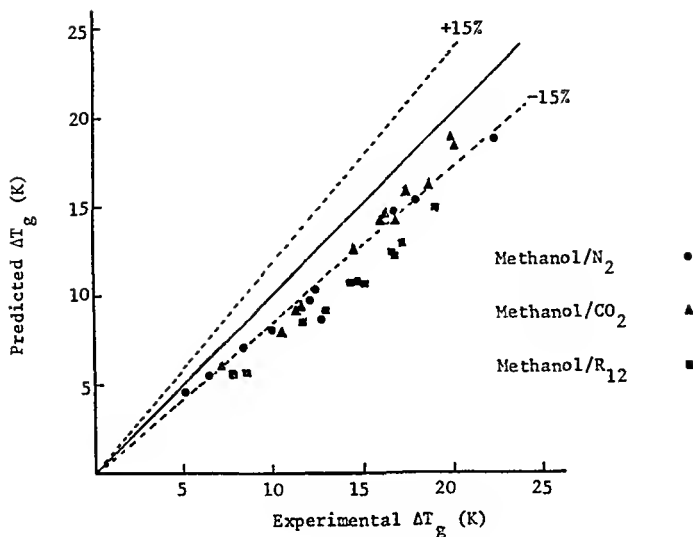


FIGURE 9 COMPARISON OF GAS PHASE TEMPERATURE DROP

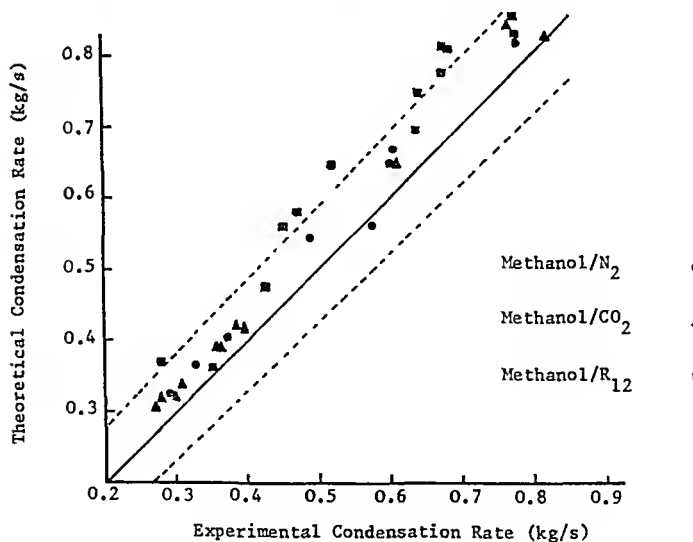


FIGURE 10 COMPARISON OF CONDENSATE FLOWRATE

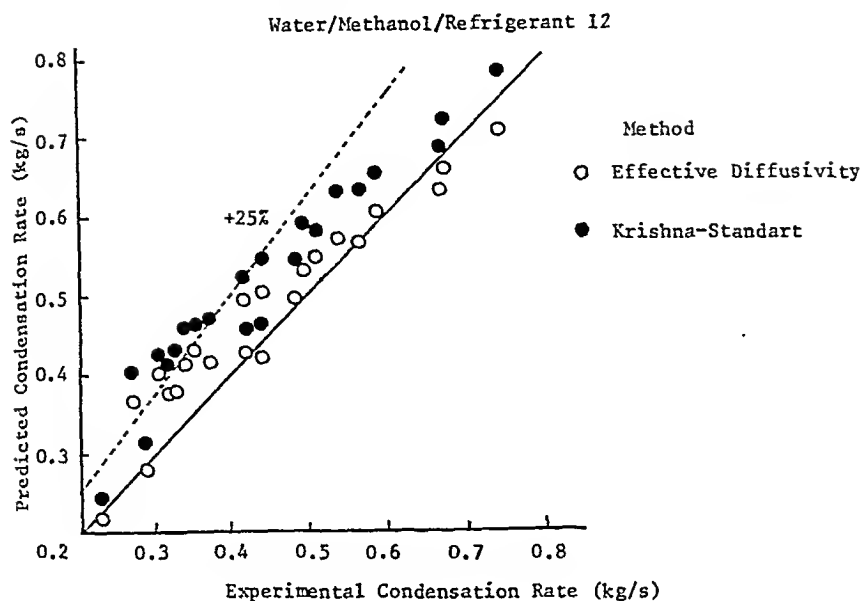
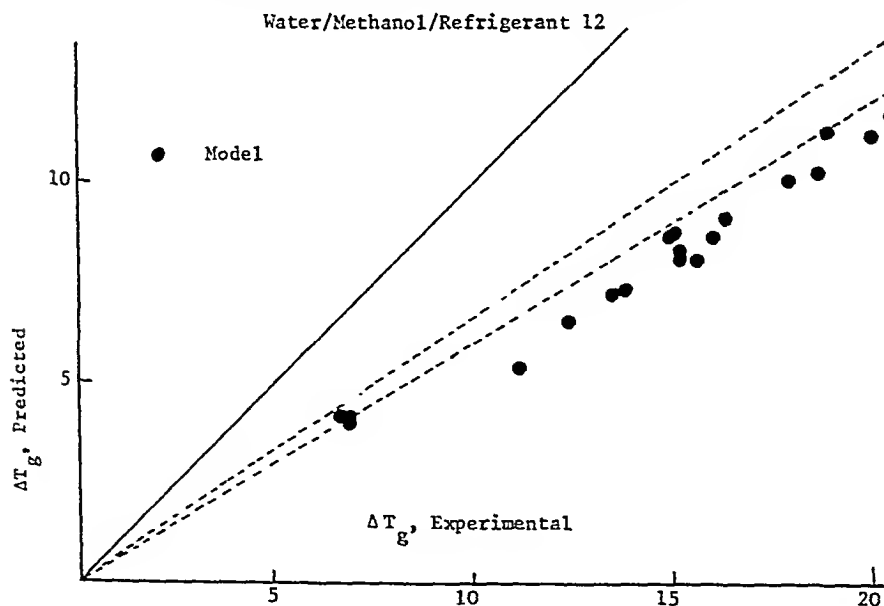


FIGURE 11 COMPARISON OF MASS TRANSFER MODELS

FIGURE 12 COMPARISON OF GAS PHASE
TEMPERATURE DROPS

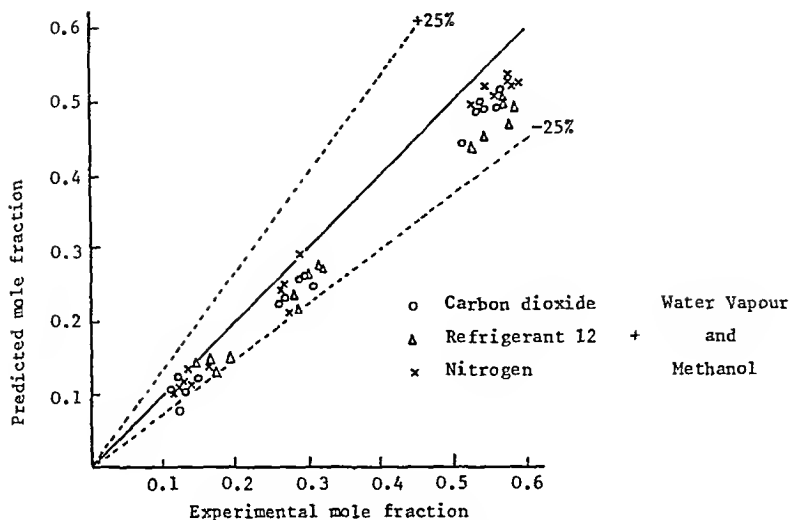


FIGURE 13 COMPARISON OF CONDENSATE COMPOSITION

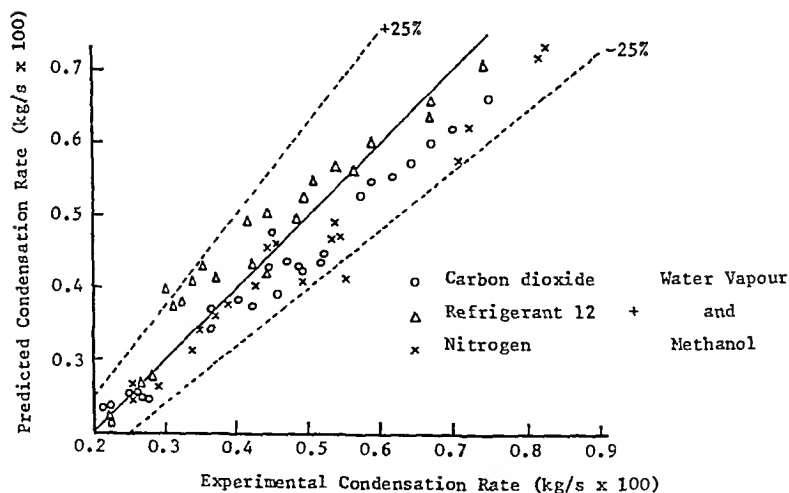


FIGURE 14 COMPARISON OF CONDENSATION RATES

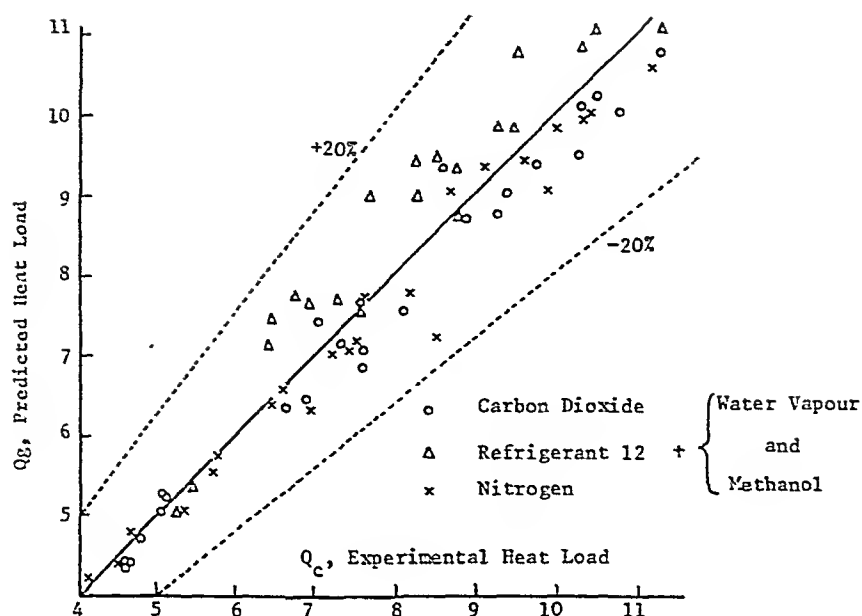


FIGURE 15 COMPARISON OF HEAT LOADS

A NEWTON-LIKE ALGORITHM FOR THE EFFICIENT ESTIMATION OF RATES OF MULTI-COMPONENT CONDENSATION BY A FILM MODEL

R. Taylor, A. Lucia and R. Krishnamurthy*

A new algorithm is proposed for calculating the rates of mass and energy transfer during the condensation of multi-component mixtures using a film model. The features of the algorithm are that the vapour-liquid equilibrium and the mass and energy transfer rate calculations are converged simultaneously using a combination of Newton's method and a quasi-Newton update. The hybrid algorithm compares very favourably with other methods in terms of cost and robustness. Moreover, the procedure permits all currently available methods of calculating rates of mass transfer in multicomponent mixtures to be used with almost no difference in cost.

INTRODUCTION

Existing methods for designing heat exchangers to condense multicomponent mixtures are of two basic kinds equilibrium methods, such as those of Kern (1), Silver (2) and Bell and Ghaly (3), and the differential methods that have been developed following the original work of Colburn and Drew (4). In the latter methods a set of differential material and energy balance equations are integrated numerically along the length of the condenser. Each step of the integration requires the local mass and energy transfer rates to be calculated. While the equilibrium methods are widely used, the differential methods are more soundly based and appear to be attracting increasing interest (5-15).

All of the differential methods cited above employ equations based on a film model to calculate the transfer rates. That the non-linear equations that constitute the model can be solved is obvious from the growing literature in this area; how they can efficiently be solved for routine use in design calculations is the main subject of this paper, the layout of which is as follows. First, we place the film model in context and follow with a review of the pertinent equations. A discussion of the computational problems involved precedes a description of a new Newton-like algorithm for solving non-linear equations, developed recently by Lucia and Macchietto (16). We then show how it can be applied to the multicomponent condensation problem, some numerical results are presented and we conclude with some remarks concerning the use of multicomponent mass transfer models in design. The notation used here is, by and large, that used by Webb and McNaught (11), whose review should be consulted for more discussion of the condensation process and the equations used to model it.

*Department of Chemical Engineering, Clarkson College of Technology, Potsdam, New York 13676, U.S.A.

A MODEL OF MULTICOMPONENT CONDENSATION

A typical multicomponent condensation problem specification will include the vapour inlet flow rate, temperature, pressure and composition and the coolant inlet temperature; a total of $n+3$ variables in an n component system. To be determined by calculation are the corresponding quantities in the outlet streams and, in a design calculation, the size of condenser that gives them.

Material and Energy Balance Equations

As always with chemical process calculations, we start from the appropriate material and energy balance equations which, in the differential methods, are constructed around a section of the condenser of area dA (4-12).

$$\frac{d\dot{N}_{ig}}{dA} = -\dot{n}_i = -\frac{d\dot{N}_{if}}{dA} \quad (1)$$

$$\dot{N}_g \bar{c}_{Pg} \frac{dT_g}{dA} = -\dot{q}_g \quad (2)$$

$$\dot{N}_c \bar{c}_{Pc} \frac{dT_c}{dA} = \pm \dot{q}_w \quad \begin{array}{l} + \text{ co-current} \\ - \text{ counter-current} \end{array} \quad (3)$$

where \dot{N}_{ig} and \dot{N}_{if} are the molar flow rates of species i in the vapour phase and condensate respectively. The \dot{n}_i are the constituent molar fluxes, positive if condensation actually occurs, zero for non-condensing species and negative if evaporation takes place. \dot{q}_g is the conductive heat flux out of the bulk vapour and \dot{q}_w is the heat flux across the condenser tube wall.

For condenser design or simulation calculations equations (1-3) are cast into difference form (e.g. $dT/dA \rightarrow \Delta T/\Delta A$) and advanced numerically starting from the vapour inlet. If the coolant flow is counter to the vapour/condensate flow, then an estimate of the coolant outlet temperature must be supplied (and either it or \dot{N}_c altered if the predicted inlet temperature is unrealistic). Each step of the integration requires the determination of the local mass and energy fluxes, \dot{n}_i , \dot{q} . The equations that permit this calculation are the subject of the next sections.

Mass Transfer in Multicomponent Gas/Vapour Mixtures

The analysis of mass transfer in multicomponent gas/vapour mixtures starts from the Maxwell-Stefan equations (17)

$$\frac{d\tilde{y}_i}{d\eta} = \sum_{k=1}^n \frac{\tilde{y}_i \tilde{n}_k - \tilde{y}_k \tilde{n}_i}{\beta_{ik}} = \sum_{k=1}^n \frac{\tilde{y}_i j_k - \tilde{y}_k j_i}{\beta_{ik}} \quad (4)$$

where the β_{ik} are binary mass transfer coefficients. The molar fluxes, \tilde{n}_i , are related to the molar diffusive flux, j_i by

$$\tilde{n}_i = j_i + \tilde{y}_i \tilde{n}_t \quad ; \quad \tilde{n}_t = \sum_{i=1}^n \tilde{n}_i \quad (5)$$

Equations (4) suggest that a variety of interaction effects such as reverse or osmotic diffusion are possible in multicomponent mixtures (but not in binaries) if the binary mass transfer coefficients are not all the same.

Indeed, investigating the influence of these interaction effects on condensation rates has been the specific objective of several recent studies (7-10,12) and criteria for assessing their significance have been proposed (15,18).

Even for a film model of steady state mass transfer there are several solutions of equations (4) which have been used in condenser simulation calculations. The solutions can be divided into three groups.

(1) Methods of the effective diffusivity type which neglect interaction effects. The diffusion fluxes, J_1 are calculated from (17)

$$J_1 = \beta_{1\text{eff}} \frac{\phi_1}{e^{\phi_1-1}} (\bar{y}_{1g} - \bar{y}_{1I}) \quad ; \quad \phi_1 = \dot{n}_1 / \beta_{1\text{eff}} \quad (6)$$

where $\beta_{1\text{eff}}$ is the effective mass transfer coefficient, most commonly chosen as β_{1g} . Equation (6) is an exact solution of equation (4) in the limit that $\bar{y}_n \rightarrow 1$, $\bar{y}_1 \rightarrow 0$, a condition sometimes approached at the condenser outlet.

(11) Methods which account for interaction effects and which are implicit in the \dot{n}_1 (or \dot{n}_1). The method of Krishna and Standart (19), based on an exact solution of equations (4), and the solution of the linearised equations due to Toor (20) and to Stewart and Prober (21) are in this category. In these methods the diffusion fluxes are given by a matrix equation of the form (17, 19,22)

$$(J_g) = [B'](\bar{y}_g - \bar{y}_I) = [B][\phi]\{\exp[\phi] - 'I, \}^{-1}(\bar{y}_g - \bar{y}_I) \quad (7)$$

where $[B']$ and $[B]$ are square matrices of order $n-1$ of multicomponent diffusive mass transfer coefficients. The structures of $[B]$ (which depends on the \bar{y}_1 and β_{1j}) and $[\phi]$ (which depends on the \dot{n}_1 and β_{1j}) are given in (11,19,22)

In all of the methods in the above categories the \dot{n}_1 are obtained from equation (5) upon specification of an appropriate determinacy condition. In condensation, this is usually the requirement that the energy flux be continuous across the vapour-liquid interface (see below).

(111) Methods which account for interaction effects and are explicit in the \dot{n}_1 (if the \bar{y}_{1g} , \bar{y}_{1I} and determinacy condition are available). There are two methods in this category, due to Krishna (23,24) and to Taylor and Smith (25) (as a generalisation and modification of a method due to Burghardt and Krupiczka (26)) and the \dot{n}_1 are given by an equation of the form

$$(\dot{n}) = [B]\Xi(\bar{y}_g - \bar{y}_I) \quad (8)$$

Here, $[B]$ is a matrix of multicomponent total mass transfer coefficients (see (27) for possible structures of $[B]$) and Ξ is a scalar correction factor (unity in Krishna's (23,24) method) that depends only on the boundary conditions and flux ratios or stoichiometric coefficients (25,27).

The method used has an important bearing on the algorithm used to compute the fluxes and, more importantly, on the actual results obtained. There can be no doubt that the Krishna-Standart (19) method is the most soundly based. Unfortunately, it is also the most involved computationally and, if repeated substitution of the \dot{n}_1 is used, convergence may sometimes be slow or not occur at all. Stable algorithms and efficient methods of computing the matrix functions involved are essential for design calculations and are described in detail in (28-30). The linearised theory involves similar matrix computations

but is rather more stable (31). Obviously, the "explicit" methods do not have any convergence problems.

A thorough statistical comparison of the various methods was recently made by Smith and Taylor (27). They compared the fluxes predicted by several approximate methods to the fluxes predicted by an exact solution for some 10,500 problems with each of 23 real ternary gas mixtures exhibiting a very wide range of physical properties. It was found that, on average, the linearised equations give rise to a completely negligible error, the method of Taylor and Smith (25) has an average error of around 10% in mixtures containing inert species and was marginally superior to or equivalent to the linearised equations in all other cases, the model of Krishna (23,24) gives good results if the driving forces are low and the effective diffusivity methods give good estimates of all of the fluxes only rarely.

We shall return, later in this paper, to the question of which method should be used. For definiteness, we formulate the algorithm for methods of type (i) and (ii) above; i.e. those which calculate the j_i rather than the \dot{n}_i . The extension to the "explicit" methods is quite straightforward.

The Liquid Phase

A description of mass transfer in the liquid phase is not usually required in condensation where the principal resistance to mass and energy transfer resides in the vapour phase. One of two extreme conditions is assumed to hold (6,7,11):

(i) The liquid phase is completely mixed with regard to composition, corresponding to infinite liquid phase mass transfer coefficients, and the liquid composition calculated from a material balance along the flow path

$$\bar{x}_{iI} = \dot{N}_{iI} / \sum_{k=1}^n \dot{N}_{kI} \quad (9)$$

(ii) The liquid phase is completely unmixed, corresponding to zero liquid phase mass transfer coefficients. In this case the interfacial composition is given by the relative rates of condensation

$$\bar{x}_{iI} = \dot{n}_i / \sum_{k=1}^n \dot{n}_k \quad (10)$$

The former is applicable to vertical condensers, the latter to horizontal and at the inlet to vertical devices (6,11). There is also some evidence that the final design is insensitive to whichever extreme is chosen, particularly if non-condensing species are present in the mixture (12).

Equilibrium and Energy Transfer

The conditions at the interface become completely specified by assuming equilibrium to exist there and by the requirement that the energy flux be continuous across it. Thus

$$\bar{y}_{iI} = K_i \bar{x}_{iI} \quad (11)$$

where $K_i = f(T_I, P, \bar{x}_{iI}, \bar{y}_{iI})$ are the equilibrium ratios and

$$\begin{aligned}\dot{q}_w &= \alpha_{ol} (T_I - T_C) = \alpha_L (T_I - T_W) = \alpha_C (T_W - T_C) \\ &= \dot{q}_g + \sum_{i=1}^n \dot{n}_i \tilde{c}_{pi} (T_g - T_I) + \sum_{i=1}^n \dot{n}_i \Delta \bar{h}_{vi}\end{aligned}\quad (12)$$

$$\dot{q}_g = \alpha_g \frac{\epsilon}{\epsilon - 1} (T_g - T_I) \quad ; \quad \epsilon = \frac{\sum_{i=1}^n \dot{n}_i \tilde{c}_{pi}}{\alpha_g} \quad (13)$$

α accounts for the resistance to heat transfer in the coolant and the tube wall, α_L is the heat transfer coefficient for the condensate and $1/\alpha_{ol} = 1/\alpha_C + 1/\alpha_L$. α_g is the gas phase heat transfer coefficient.

Transport and Physical Properties in Condenser Design

Condenser design based on the foregoing equations requires extensive physical property data. Specifically, the following are required

- (i) Density: vapour at T_g and T_f , liquid at T_L , coolant at T_C
- (ii) Heat capacity: vapour at T_g and T_f , liquid at T_L , coolant at T_C
- (iii) Viscosity: vapour at T_g and T_f , liquid at T_L , coolant at T_C
- (iv) Thermal conductivity: vapour at T_f , liquid at T_L , coolant at T_C
- (v) Diffusion coefficients: vapour at T_f
- (vi) Partial molar enthalpies: vapour at T_I , liquid at T_I
- (vii) K-values: at T_I

Heat and binary mass transfer coefficients are normally evaluated from appropriate correlations; the Chilton-Colburn $j_H = j_D = f(\text{Re})$, which we have used here, is one example. Webb and McNaught (11) summarise other correlations that are commonly used for these calculations.

In compiling the list above, we note that Reynolds numbers are evaluated at bulk conditions. Often Prandtl and Schmidt numbers are likewise evaluated but sometimes (as here) film average conditions are used (11). Methods of estimating these properties are described by Reid et al (32).

THE COMPUTATIONAL PROBLEM

Given the bulk vapour temperature, pressure and composition and the coolant temperature (specified at the inlet and calculated from (1-3) thereafter, physical and transport property estimation methods and appropriate equilibrium data, what is the best way to compute the fluxes so that equations (1-3) can be advanced a step further. The equations to be solved are non-linear and must, therefore, be solved by some iterative process. The most difficult problem is the calculation of the fluxes at the vapour inlet since there is, at first, no information with which to start the iterations. At downstream positions good estimates of all quantities involved in equations (4-13) become available from the solution obtained for the preceding step. Thus, whichever of the two extremes of condensate mixing is used to characterise downstream conditions, it is the unmixed case which always must be solved first.

To Tear or Not to Tear? That is the First Question

To our knowledge, all other algorithms described in the literature employ some kind of tearing strategy to solve the condensation equations. Equation tearing involves iteratively solving a subset of the complete set of governing equations for a subset (the tear variables) of the complete set of unknowns. Within the loop that determines how the tear variables are to be re-estimated all other equations are satisfied exactly. Thus, if the remaining subset of equations also requires iteration (or, possibly, further tearing), the end result is a series of nested iteration loops. For example: Krishna et al. (7) solve the mass and energy transfer rate equations (by repeated substitution of the \dot{n}_i) and the vapour-liquid equilibrium calculations (bubble point calculations) within an outer loop on $n-1$ of $\tilde{x}_{i,1}$ and T_1 . Other tearing algorithms, those of Price and Bell (5) and of Webb and coworkers (11,13,15), involve up to three levels of iteration loop.

One problem with tearing is the number of times physical properties must be evaluated (several times per outer loop iteration) if temperature and composition dependent physical properties are used. It is the physical properties calculations that generally dominate the cost of chemical design problems (32) (the present problem is no exception). A second problem can arise if the inner iteration loops are difficult to converge. We noted above that the Krishna-Standart (19) method of calculating the \dot{n}_i has convergence problems and the difficulties of converging $\tilde{y}_{i,1} = K_i \tilde{x}_{i,1}$ (all i) are well known. All of these problems have been encountered in solving by tearing the example problems described below. We wonder what point there is to requiring subsets of the complete set of equations to be satisfied exactly (by iteration) when the estimate of the tear variables does not pertain to the solution. We suggest that a better strategy is to solve all of the equations simultaneously by guessing enough unknown variables to permit all other quantities appearing in equations (4-13) to be calculated explicitly and by not requiring any of the equations to be satisfied until complete convergence has been achieved. This approach is followed in our proposed algorithm which converges the vapour-liquid equilibrium calculations and the mass and energy transfer rate calculations at the same time.

Variations on a Theme: Newton's Method and Related Fixed Point Algorithms

If the first step of the algorithm to find \dot{n}_i and \dot{q} involves the guessing of the unknowns, the heart of it is the method used to re-estimate them if the initial guess was wrong. Newton's method (or the Newton-Raphson method) is one of the oldest yet most reliable algorithms for solving a system of non-linear equations. A new variation on this classic theme is the basis of the method proposed here.

Let $(f) \equiv (f(X))$ denote any collection of equations, non-linear in (X) , the collection of variables, with solution $(f) = (0)$. The direct prediction Newton correction is given by a solution of the equations linearised about the current estimate (X_k) of (X)

$$[J_k](X_{k+1} - X_k) = - (f(X_k)) \quad (14)$$

where $[J_k]$ is the Jacobian matrix with elements

$$J_{ij} = \partial f_i / \partial X_j \quad (15)$$

If a problem with Newton's method exists, it is the computation of $[J]$.

For most engineering applications of reasonable complexity, complete derivative information is rarely available in analytical form. Consequently, finite differences must be used to approximate all or part of $[J]$. In most cases, the unavailable derivatives involve derivatives of physical properties [e.g. $\partial K/\partial T$, $\partial K/\partial x_i$]. Finite difference approximations of these derivatives can enormously increase the cost of solution because many more physical property calculations are required. Further, neglect of these derivatives generally increases the number of iterations or can even cause failure (16).

One way to avoid the repeated calculation of $[J]$ is to use a "quasi-Newton" method (see Dennis and Moré (34) for a recent review of these methods). Broyden's (35) method, for example, builds an approximation $[J'_k]$ to $[J_k]$ from the formula

$$[J'_{k+1}] = [J'_k] + \{[(Y) - [J'_k](S)](S)^T\}/(S)^T(S) \quad (16)$$

where $(Y) = (f(X_{k+1}) - f(X_k))$ and $(S) = (X_{k+1} - X_k)$. Schubert's (36) method is an extension of the Broyden method that preserves any known sparseness in $[J]$. The quasi-Newton correction is given by a solution of the linear system (14) with $[J'_k]$ replacing $[J_k]$.

Unfortunately, quasi-Newton methods are not without problems. The first is that they are not scale invariant (Newton's method is) and may, as a result, perform poorly or fail on problems that are ill-conditioned. This is an important consideration in chemical engineering applications where material and energy balance equations almost always are part of the model. This particular subset of equations usually exhibit poor scaling. To a lesser extent, the need to supply an initial approximation to $[J]$ can sometimes be a problem. If the initial approximation is poor, it can increase the number of iterations or even, as we shall see, cause failure. Quasi-Newton methods appear to be more susceptible than is Newton's method to this problem.

A Hybrid Method

A judicious combination of Newton's method and a quasi-Newton update can, as shown recently by Lucia and Macchietto (16), be a very efficient means of solving the kinds of equations found in chemical process calculations. In what they call the hybrid method, the Jacobian matrix is divided into two parts, a computed part, $[C_k]$, and an approximated part, $[A_k]$. Thus,

$$[J_k] = [C_k] + [A_k] \quad (17)$$

$[C_k]$ consists of any partial derivatives for which analytical expressions exist. $[A_k]$ is made up of any terms that contain unavailable partial derivative information such as $\partial K/\partial x_i$. In the hybrid approach, $[C_k]$ is computed in each iteration while $[A_k]$ only is updated from an initial approximation using the Broyden or Schubert methods. The correction to (X_k) again is provided by equation (14) with $[J_k]$ given by equation (17).

It is easy to see that other well-established fixed-point iterations can be incorporated within the framework of equation (17). For example, if $[A_k]$ is null for each k then $[J_k] = [C_k]$, the classical Newton method. If, on the other hand, $[C_k] = 0$ and $[A_k]$ is defined by finite difference approximations, then we have a finite difference Newton method. If $[C_k]$ is a constant matrix and this time, $[A_k]$ is defined by Schubert's or Broyden's method, then, of course, we have a quasi-Newton method. Finally, if $[C_k]$ is not a constant matrix and $[A_k]$ is defined by Eq. (16), then we have the hybrid method.

APPLICATION TO CONDENSER DESIGNVariables and Functions

Our first task is to identify all of the variables in equations (6-13) that are not initially known. They are the \tilde{y}_{iI} , T_I , the \hat{n}_i and T_w . The \tilde{y}_{iI} and T_I are selected as iteration variables for three reasons: (i) so that K -values and partial molar enthalpies can be calculated, (ii) so that the diffusion and heat conduction fluxes can be calculated, equations (6,7,12,13) and (iii) so that those physical properties that are calculated at film average conditions can be properly evaluated. Any one of these reasons is sufficient to demand the selection of the \tilde{y}_{iI} and T_I . However, the first two are particularly important. The fluxes, \hat{n}_i , are chosen so that the high flux correction factors for diffusion and heat transfer can be calculated without iteration and so that the composition of an unmixed condensate is known. The last variable, T_w , is included whenever the heat transfer coefficients in the condensate and coolant are evaluated at the appropriate average temperatures (for example, $\alpha_i = f(T_i)$, $T_i = \frac{1}{2}(T_w + T_I)$). The vector of variables, (X) , is chosen to be

$$(X)^T \equiv (\hat{n}_1, \hat{n}_2, \dots, \hat{n}_n, \tilde{y}_{1I}, \tilde{y}_{2I}, \dots, \tilde{y}_{n-1,I}, T_I, T_w)$$

The vector of functions corresponding to (X) is chosen to be

$$(f)^T \equiv (M_1, M_2, \dots, M_{n-1}, H_1, E_1, E_2, \dots, E_n, H_2)$$

with

$$M_i = \sum_{j=1}^{n-1} B_{ij} \Delta \tilde{y}_j + \tilde{y}_{ig} \hat{n}_t - \hat{n}_i \quad i=1,2,\dots,n-1 \quad (18)$$

$$H_1 = \alpha_g \cdot f(\epsilon) \cdot (T_g - T_I) + \sum_{i=1}^n \hat{n}_i \Delta \tilde{h}_{vi} - \alpha_{oi} (T_I - T_c) \quad (19)$$

$$E_i = K_i \tilde{x}_{iI} - \tilde{y}_{iI} \quad i=1,2,\dots,n \quad (20)$$

$$H_2 = \alpha_i (T_I - T_w) - \alpha_c (T_w - T_c) \quad (\text{downstream}) \quad (21)$$

where

$$\Delta \tilde{y}_i = \tilde{y}_{ig} - \tilde{y}_{iI} ; f(\epsilon) = \epsilon e^\epsilon / (e^\epsilon - 1) \quad (22)$$

At the inlet where no condensate exists equation (21) must be modified to read

$$H_2 = T_I - T_w \quad (\text{inlet}) \quad (23)$$

M_i represents the degree to which the mass transfer rate equations are not satisfied, H_1 and H_2 represent the departure from continuity of the energy fluxes across the vapour/liquid interface and the tube wall respectively and the E_i describe the departure from equilibrium at the interface. These equations apply to both extremes of condensate mixing.

As a demonstration of exactly which terms are included in $[C]$ and which in $[A]$ (and to aid the programming of the algorithm), we give below the complete derivatives of these equations.

$$dH_1 = \sum_{k=1}^n \left[\sum_{j=1}^{n-1} \frac{\partial B_{1j}}{\partial \dot{n}_k} \Delta \tilde{y}_j - \delta_{1k} + \tilde{y}_{1g} \right] d\dot{n}_k + \sum_{k=1}^{n-1} \left[-B_{1j} + \sum_{j=1}^{n-1} \frac{\partial B_{1j}}{\partial \tilde{y}_{kI}} \Delta \tilde{y}_j \right] d\tilde{y}_{kI} \\ + \left[\sum_{j=1}^{n-1} \frac{\partial B_{1j}}{\partial T_I} \Delta \tilde{y}_j \right] dT_I \quad i=1, 2, \dots, n-1 \quad (24)$$

$$dH_1 = \sum_{k=1}^n \left[\Delta \tilde{h}_{vk} + \tilde{c}_{pk} (T_g - T_I) f'(\epsilon) + \left(-(T_I - T_c) \frac{\partial \alpha_{ol}}{\partial \tilde{x}_{kI}} + \sum_{i=1}^n \dot{n}_i \frac{\partial \Delta \tilde{h}_{vi}}{\partial \tilde{x}_{kI}} \right) \frac{\partial \tilde{x}_{kI}}{\partial \dot{n}_k} \right] d\dot{n}_k \\ - \left[\alpha_{ol} + \alpha_g \cdot f(\epsilon) - (T_g - T_I) \frac{\partial (\alpha_g f(\epsilon))}{\partial T_I} + (T_I - T_c) \frac{\partial \alpha_{ol}}{\partial T_I} + \sum_{i=1}^n \dot{n}_i \frac{\partial \Delta \tilde{h}_{vi}}{\partial T_I} \right] dT_I \\ - \frac{(T_I - T_c) \frac{\partial \alpha_{ol}}{\partial T_w}}{\frac{\partial \alpha_{ol}}{\partial T_w}} \cdot dT_w + \sum_{k=1}^{n-1} \left[f(\epsilon) (T_g - T_I) \frac{\partial \alpha_g}{\partial \tilde{y}_{kI}} + \sum_{i=1}^n \dot{n}_i \frac{\partial \Delta \tilde{h}_{vi}}{\partial \tilde{y}_{kI}} \right] d\tilde{y}_{kI} \quad (25)$$

$$dE_1 = \sum_{k=1}^n \left[K_1 \frac{\partial \tilde{x}_{1I}}{\partial \dot{n}_k} + \tilde{x}_{1I} \frac{\partial K_1}{\partial \tilde{x}_{kI}} \cdot \frac{\partial \tilde{x}_{kI}}{\partial \dot{n}_k} \right] d\dot{n}_k + \sum_{k=1}^{n-1} \left[\tilde{x}_{1I} \frac{\partial K_1}{\partial \tilde{y}_{kI}} - \delta_{1k} + \delta_{1n} \right] d\tilde{y}_{kI} \\ + \tilde{x}_{1I} \frac{\partial K_1}{\partial T_I} \cdot dT_I \quad i=1, 2, \dots, n \quad (26)$$

$$dH_2 = \left[\alpha_l + (T_I - T_w) \frac{\partial \alpha_l}{\partial T_I} \right] \cdot dT_I - \left[\alpha_c + \alpha_l - (T_I - T_w) \frac{\partial \alpha_l}{\partial T_w} + (T_w - T_c) \frac{\partial \alpha_c}{\partial T_w} \right] dT_w \\ + (T_I - T_w) \sum_{k=1}^n \left[\frac{\partial \alpha_l}{\partial \tilde{x}_{kI}} \cdot \frac{\partial \tilde{x}_{kI}}{\partial \dot{n}_k} \right] d\dot{n}_k \quad (\text{downstream}) \quad (27)$$

$$dH_2 = dT_I - dT_w \quad (\text{inlet only}) \quad (28)$$

where

$$f'(\epsilon) = \partial f(\epsilon) / \partial \epsilon = e^\epsilon (e^\epsilon - 1 - \epsilon) / (e^\epsilon - 1)^2 \quad (29)$$

$$\frac{\partial \tilde{x}_{1I}}{\partial \dot{n}_k} = (\dot{n}_t \delta_{1k} - \dot{n}_1) / \dot{n}_t^2 \quad (\text{unmixed}), \quad \frac{\partial \tilde{x}_{1I}}{\partial \dot{n}_k} = 0 \quad (\text{mixed}) \quad (30)$$

and δ_{1k} is the Kronecker delta.

The terms underscored by an unbroken line contain a partial derivative of a heat or mass transfer coefficient or of a K-value or enthalpy. Non-zero derivatives of the heat and mass transfer coefficients arise whenever these coefficients are evaluated at film average conditions. The derivatives $\partial B_{ik} / \partial \tilde{y}_{kI}$, for example, will be non-zero if the binary mass transfer coefficients, β_{1k} , are calculated using the film average Schmidt number. This particular derivative will also be non-zero if the linearised theory or the explicit methods are used to calculate the \dot{n}_1 even if the β_{1j} are not

evaluated at average conditions. The K-values are quite strongly temperature dependent and composition dependent to a degree influenced by the non-ideality of the mixture. Most of these derivatives do not admit to being straightforward and, accordingly, they are relegated to [A]. Some are quite negligible but others have an important affect on the numerical performance. The term $\partial E_{ij} / \partial n_k$ (underscored by a broken line) is readily calculated for all mass transfer methods except the Krishna-Standart method. In practice, the inclusion of this term does not seem to affect the numerical performance. The remaining terms are assigned to [C] which has the structure shown in Table 1. Broken lines indicate a sequence of elements, enclosed areas a submatrix of elements which form a natural group. The submatrix $[\partial E_{ij} / \partial n_k]$, for example, is null if the condensate is completely mixed. [A] is full except for the column corresponding to T_w as variable, the row corresponding to H_2 as function and the submatrix $[\partial E_{ij} / \partial n_k]$ if the condensate is unmixed.

The Algorithm

1. Set k, the iteration counter, to zero. Initialize (X_0) and $[A_0]$ (see below). Decide upon a convergence tolerance, t say.
2. Calculate $(f(X_k))$. A possible route is
 - (a) If the condensate is unmixed, calculate \tilde{x}_{iI} from (10)
 - (b) Calculate average compositions and temperatures
 - (c) Calculate all physical properties and K-values etc.
 - (d) Calculate the diffusion fluxes from (6,7)
 - (e) Calculate the energy fluxes from (12,13)
 - (f) Calculate $(f(X_k))$ from (18-22)
3. Calculate $[C_k]$ from (24-30).
4. Check for convergence. If $||f|| \leq t$ stop. Otherwise continue.

TABLE 1 - Structure of [C].

f/X	\dot{n}_1	\dot{n}_2	..	\dot{n}_{n-1}	\dot{n}_n	\tilde{y}_{1I}	\tilde{y}_{2I}	..	$\tilde{y}_{n-1,I}$	T_I	T_w
M_1	x				x	x					
.											
M_{n-1}	x				x						
H_1	x										
E_1	x				x	-1				x	x
.											
E_{n-1}	x				x					x	
E_n	x				x	1				x	
H_2										x	x
H_2										1	-1

downstream
inlet only

The conclusion I draw from this is that it is the quality of the engineer that determines the success of his designs and that a really good engineer can rise above the level of the tools available to him in the performance of his task. I certainly welcome the improvement in the quality of the information and techniques available to us to these 30-some years. But it is also true that all of these advances will be completely offset if there is a corresponding decline in the quality of the engineering training and judgement that uses them. And unfortunately there are some trends implicit in modern technology and indeed arising from the very power of the tools that we have at our control to give pause for consideration. This point will be returned to later.

In the sections below, I have introduced a number of topics in which substantial development has occurred in the condenser design application area in recent years. To some extent the sections are not separable and indeed are not really organizable in a linear fashion. Therefore there will be some overlap and cross sections between the various topics.

DEVELOPMENT OF COMPUTER PROGRAMS FOR CONDENSER RATING AND DESIGN

Pointwise Calculations

The combination of the vast increase in understanding of fundamental mechanisms of two phase flow and heat transfer and the expansion of computer capabilities has resulted in the development of design methods based upon the calculation of pointwise conditions over the course of the condensing process and the integration of these pointwise conditions over the entire condenser. These programs have been mainly, but not solely, developed for shell and tube heat exchangers. But even there the wide variety of geometries available to the designer and the wide range of condensing problems in the process industries require the programs to be extremely large and complex. The accumulation and introduction of the basic thermodynamic equilibrium and physical properties information needed to solve the more complex multicomponent problems alone is a major task and generally more time-consuming than the actual calculation of the exchanger performance. But there is no doubt that these programs give much more detailed and accurate predictions of the actual conditions in the piece of equipment. In the hands of a competent engineer, this detail may provide warning of potentially unsatisfactory operation under various conditions and may suggest better condenser configurations to be employed.

Design Logic for Condensers

The most comprehensive computer programs available for condenser calculations at this time are, in essence, rating programs. That is, the program will predict the performance of a dimensionally-specified condenser when vapor and coolant streams are introduced at specified flow rates and conditions into the condenser. In order to convert the rating program into a design program, one must introduce an algorithm which will successively modify the configuration of the condenser, rerating each configuration until the "optimal" configuration is found. At present, the form of this design modification algorithm is not well-set. The corresponding case for a purely sensible heat exchanger with a specified design pressure drop is relatively straightforward, such that the successive modifications better utilize the available pressure drop. (Though it should be noted that this begs the question of whether or not the specified pressure drop was any place close to "optimal".) However, in the case of a condenser, it is not necessarily optimal to design to use the entire allowable pressure drop. The greater the pressure drop, the lower the

condensing pressure, and therefore the lower the local temperature difference. Not only may this lead to a larger condenser, but if the pressure drop is underestimated by the program the resulting design may be incapable of totally condensing the vapor or achieving the desired outlet conditions. One needs to introduce this kind of logic either into the computer program, or into the intuitive judgement of the engineer working with the computer program which in turn requires a highly interactive program. Unfortunately, the present condenser design programs tend to be so massive that they do not operate well in an interactive mode and hence lead to a very tedious design optimization procedure. Incidentally, it should be noted that there is no substitute for good engineering judgement in this case.

Desuperheating and Subcooling

The presence of considerable superheat in the incoming vapor and/or the requirement that the exiting condensate be substantially subcooled introduces further complications into the program. There are generally conservative ways of handling desuperheating if one is only concerned to provide enough heat transfer surface. However, if one wishes to know the exact location of the onset of condensation, the problem can become quite formidable because it must be interlocked with the coolant temperature profile as well. In general, there are no significant fundamental questions involved.

The problem is more complicated if one insists upon substantial subcooling of the condensate within the same shell in which condensation is occurring. (For several reasons, the author is firmly convinced that a separate subcooler is much the preferable way to go if substantial subcooling is required, but this opinion does not seem to be shared by any large number of process engineers.) The presence of a substantially subcooled liquid phase in a condenser raises some problems concerning mixed natural and forced convection flows, condensation on subcooled liquid interfaces, and the hydrodynamics of segregated two-phase flows in complex geometries. These topics require a good deal more fundamental study as well as mathematical modeling. Methods to incorporate a significant subcooled zone into present condenser rating programs should be approached cautiously and conservatively until these fundamental studies are available.

EXPERIMENTAL DATA SOURCES

Fundamental Studies

While some very distinguished workers in the field of fluid mechanics and heat and mass transfer have expressed the opinion that many important problems can be solved in a purely theoretical fashion with the use of sufficiently large computers, I think that most of us would agree that a great deal of experimental work of a very fundamental nature is still required to resolve the many outstanding issues that underlie the successful design of condensers. Fortunately, there are many university and government laboratories around the world that are extremely competent and capable in carrying out these small-scale fundamental studies. While one can point to areas in which one would like to see more data, it is probably not in fundamental work that the greatest concern about our data requirements must lie.

Small Equipment Studies

Carefully taken experimental information on representative heat transfer equipment is necessary both to guide the development of the rating and design methods and to verify the validity of those methods for a reasonable range of

operating parameters. Such information is now quite generally available through proprietary research organizations, such as HTFS and HTRI, at what must be regarded as very nominal cost to the user. However, such studies are very expensive in terms of dollars per individual test. The experimental equipment, particularly the test loops and the associated instrumentation and data reduction equipment, is expensive; the cost of the trained technical personnel is high; and the utilities costs are becoming an increasingly important factor in limiting the scale of these experiments. But even so, the equipment under the best of these conditions is only at the lower range of the size of the equipment used in large-scale process plants. Extrapolation of the data from the small-scale units, however carefully designed and scaled to large scale equipment, must be done very carefully. Much more work remains to be done in this area, particularly as more fundamental information is made available for incorporation in advanced computer models of this equipment. However, the organizations for obtaining and appropriately processing this information do exist and again it seems not to be the area of major concern for the future.

Large Equipment Studies

The process industries are moving toward increasingly larger heat exchangers. This trend is caused not only by the increasing capacity of individual process units, but also by the desire for maximum efficiency and energy recovery and conservation. As one moves to large equipment, phenomena that before were of minor significance become much more critical. For example, two phase flow regime patterns conceivably can be quite different in large diameter equipment unless one has the scaling laws just right. Interaction between fluid at the top and bottom of a large horizontal shell-side condenser is more limited and very probably further removed from the equilibrium state than in a corresponding small unit. Yet design methods that were developed on small-scale equipment or even a university laboratory experiment are being applied to the design of these large units. And there are very few large scale test data available with a sufficient degree of accuracy to verify whether or not these methods are producing adequate designs. The data are even less adequate to determine individual effects upon the overall performance, and it is this kind of information that is so vital for the improvement of existing design methods.

The problem of course, is that the already expensive experiments carried out at HTRI and HTFS at thermal duties on the order 10^7 Btu/hr become almost prohibitive when one is talking in the range of 10^8 to 10^9 Btu/hr characteristic of modern process units. It would be ideal if one could set up carefully-controlled, well-instrumented experiments on process equipment in the plant, but this is generally not compatible with the goal of the plant to make a profit by operating at a tightly constrained set of operating conditions. And the cost of instrumentation required to obtain reasonably accurate data is prohibitive except under special conditions. There are in fact only a very few instances available where large-scale process equipment has been tested under adequately controlled conditions to allow verification of the design methods. Two such examples that come to mind are the Raft River Geothermal Plant (6) and the OTEC 1 Ocean Thermal Experiment (7).

The Raft River experiment used isobutane as the working fluid for a low temperature (300°F) brine heat source in a fairly conventional Rankine cycle. The plant was rated at approximately 5 megawatts electrical net with a corresponding thermal load on the condenser of about 35 megawatts. The X-shell condenser was well-instrumented with the cooperation of HTRI, and it is hoped that the results will give us some idea of the shell side performance for a typical light hydrocarbon fluid. A final report has not yet appeared on these experiments.

The OTEC-1 experiment involved testing the evaporator and condenser for an Ocean Thermal Energy Conversion plant, using warm sea water as the heat source and cold sea water as the heat sink, installed on a ship anchored off Hawaii in 1981. The equipment was rated at 40 megawatts thermal corresponding to approximately 1 megawatt electrical net. The working fluid was ammonia condensing on the shell side of an X shell condenser approximately 9 feet in diameter and 50 feet long. The equipment was extremely well instrumented (though not all of the individual tube monitors became operational during the course of the experiment), and the data obtained were in excellent agreement with the design predictions on both a local as well as an overall basis.

Both of these large-scale experiments were on pure components and operated only over a very narrow range of conditions corresponding to those expected in a full-scale plant. It would be highly desirable, for the reasons given above, if there were opportunities to test other large-scale equipment (especially configurations other than X shells) over a wider range of operating conditions and particularly for more complex mixtures. It is in this area that our greatest data needs exist now and in the foreseeable future.

TWO-PHASE FLOW PROBLEMS AND NEEDS

Pressure Drop Prediction

We have come along way from the situation represented (by exclusion) in Kern's book regarding two-phase pressure drop prediction. Curiously enough, the methods existing at that time are still recognized as being among the most generally applicable, if not the most precise under a narrow range of conditions. Perhaps in those days, the central importance of pressure drop prediction to two-phase heat exchanger design was not as well recognized as it is now. In any event, great progress has been made in developing further the pressure drop methods and incorporating them into design programs. There is, however, still a great need for additional information on the shell-side two-phase flow phenomena, with particular reference to distinguishing between pressure drop effects and correlations for crossflow and for axial flow. And again, the problem of scale enters in; methods and approximations suitable for small equipment may fail entirely when applied to large equipment, particularly when the potential hydrostatic head and friction effects are a significant fraction of the absolute pressure existing in the system.

Flow Pattern Prediction

Great progress has been made in the quantification of flow pattern prediction both for flow inside tubes and the much more difficult problem of flow outside tubes. Flow regime predictions for flow inside tubes is probably on a satisfactory foundation for present design purposes with the work of Taitel and Dukler and many others (8) in the open literature and the more proprietary work of HTRI and HTFS.

Flow patterns on the shell side have been studied notably by Grant and Murray at the National Engineering Laboratory (9), and these works have certainly greatly amplified our ability to deal with shell side flow distribution problems. However, much more work remains to be done in this area in order to understand the effects of parallel flow vs crossflow phenomena and how they interact. It is probable that none of these flows can be considered fully developed within a piece of equipment, and this suggests that one may discover quite different phenomena for large diameter shells compared to small diameter shells, even for the same values of the scaling parameters.

A problem of particular interest here which will be referred to in greater detail in the next section is that of side-to-side flow as opposed to up and down flow in a conventional E shell condenser.

Two-Phase Flow Distribution

The process engineer is often tempted to put a two-phase flow into a heat exchanger having a multiplicity of parallel flow channels which may or may not be interconnected along the length. Worse, he usually assumes for computational purposes that the two phases distribute in aliquot fractions into each channel. There is no proven way to accomplish this at this time (short of "one channel-one pump"), and this disparity between expectation and realization can lead to very serious consequences. A detailed example or two will be given later, but one can certainly say that this is a major problem deserving of some research to at least establish the limits and parameters of the maldistribution in some common geometries (such as box headers on air-cooled exchangers).

DEVELOPMENTS IN CONDENSER CONFIGURATION AND OPERATIONAL PRACTICES

Shell and Tube Configurations

Horizontal Cut Baffles. As noted in the previous section, there is a growing impression that horizontal cut baffles may in fact give superior operational performance compared to the more conventional vertical cut baffles, especially in those regions of the condenser where the vapor velocities are not sufficient to entrain a substantial portion of the liquid phase. The suspicion exists that the effect is that the vapor, by being forced to flow down underneath the baffle cut on every other baffle, must stir up the liquid and entrain a portion of it while maintaining a degree of thermodynamic equilibrium. Presumably the heat transfer coefficient for the lower tubes is also improved. Thermodynamic equilibrium in this case means both temperature equilibrium, which operates in all cases including pure components, and composition equilibrium, which is vital in multicomponent condensers. Evidently, there is a small increase in pressure drop associated with this configuration, but this would be a small price to pay in many applications. A more quantitative understanding of flow patterns and the associated vapor-liquid interaction mechanisms would be of the greatest importance in identifying the area of applicability for this configuration. It might be noted that there is no law that says that one cannot combine vertical baffle cuts in the beginning of the condensation process with horizontal cuts at the end of the process.

Variable Baffle Spacing. It has long been recognized, as a theoretical possibility at least, that there might be some advantage to varying the baffle spacing for shell-side condensation in such a way as to keep the vapor velocity up and secure the advantages of vapor shear control of the condensation heat transfer process at an acceptable penalty in pressure drop. The author is not fully confident that the precision of our pressure drop and heat transfer calculations is sufficient to do this with a high degree of confidence, but this has not stopped this design from being occasionally proposed and at least one proprietary computer rating program will accept this kind of information as input and dutifully carry out the calculations. Clearly, as our capabilities to predict the heat transfer and fluid dynamics of the situation improve, so will the opportunity to knowledgeably incorporate this design option.

RODBaffle® Construction. The RODBaffle® construction is a proprietary design in which the tubes are supported on all four sides by a set of four grids of rods spaced typically six to eight inches apart (10). The design was originally put forth to eliminate the possibility of vibration arising from high velocity cross-flow on the shell side, but it was later realized that this configuration also gives extremely low pressure drop. In the case of a condenser, where the heat transfer coefficient tends to be quite good even in the absence of shear effects on the condensate film, the low pressure drop was recognized as a potentially great advantage for such applications as vacuum condensers. The design particularly lends itself to single pass construction on the tube side (coolant side) and is therefore attractive in the design of partial condensers in which it is important to knock out as much of the condensable component from the effluent noncondensable gas as possible. Low-finned tubes have been used in this design with no apparent operational difficulties.

Annular Distributors. A major loss of pressure in condensers occurs at the inlet in introducing the vapor into the shell. This is especially serious in vacuum condensers and quickly became noticeable when designing RODBaffles for vacuum operation. The annular distributor - an annular vapor channel around the outside of the shell of the condenser proper and admitting vapor into the condenser through slots cut in the shell around the periphery of the tube field - was found to solve this problem and in addition provide a built-in impingement plate without the removal of any tubes. The annular distributor was a standard design feature on all kinds of shell and tube exchangers manufactured by C. F. Braun and Co. until they went out of that business, but has always been regarded as a high-cost feature. However, the cost is very much reduced if one builds up the annular distributor by welding together cut steel plate sections rather than using the hot rolled knuckles developed by Braun. In any case, the low pressure drop, uniform distribution, and the freedom in placement of the nozzles relative to the baffle spacing have made this construction feature an almost standard item in RODBaffle exchanger design and in many other condenser applications as well.

Air Cooled Exchangers

Changing Role for Air-Cooled Application. It is particularly interesting from an historical point of view to compare the role of air-cooled heat exchangers at the time of Kern's book compared to their role in present technology. In the 1950's the air-cooled exchanger was being actively pushed for application in the area of rejection of high temperature waste heat. That phrase rings curiously anomalous to our ears now, there being no such thing as "high temperature waste heat". But at the same time, the diminishing availability of surface water as the ultimate heat sink for low temperature heat rejection has brought new attention to the air-cooled heat exchanger for this service.

Air is everywhere available and so far has not been subjected to the same kind of restrictions upon its effluent thermal conditions as water supplies now are. The result is we must now look at the design of air-cooled heat exchangers in quite a different context from that of only a relatively few years ago. Instead of worrying about the mechanical design problems of a heat exchanger operating at very high temperatures and not having to worry too much about the thermal-hydraulic aspects on the tube side because of the very large temperature differences, we now are much more concerned about the achievement of uniform thermal-hydraulic conditions across the tube field and with matching the air-side capabilities to the tube-side flow distribution.

Flow Distribution and Close Temperature Approach Considerations. Since the air-cooled exchanger is now being used for rejecting heat at temperatures very close to ambient temperature, it is important to understand in detail the relationship between the process fluid flow in the tubes and the air flow temperature profiles exterior to the tubes. Maldistribution of the fluid to be condensed among the tubes leads to a mismatch in the capacity of the air to remove the heat and the amount of heat that must be removed from each tube. A tube running rich in vapor will have a higher duty required to fully condense the vapor than will a tube which has less vapor flow in it. The problem is exacerbated if one attempts to take a two-phase mixture and redistribute it among the tubes on a second pass through the exchanger for example. There is no known way to guarantee that each tube will receive equivalent amounts of vapor and liquid. The result is, in the case of a multicomponent mixture, a certain amount of fractionation taking place at the turnaround and, for all condensing applications, the situation that vapor-rich tubes will not be washed by enough air to pick up the enthalpy that needs to be removed for complete condensation. One, of course, would like very much to know about the mechanics of the distribution of a two-phase mixture exiting from a number of rows of tubes in parallel and flowing into another number of tubes in parallel. That information does not now exist and it does not seem likely that it will be forthcoming in a reliable form in the foreseeable future. Therefore, the present designer has little choice but to design very conservatively, e.g., to condense in a single pass or in a single set of U tubes. Other approaches are possible, but depend upon the insight and judgement of the engineer once again.

Protection Against Freeze-up. Closely related to the above problems in air-cooled condensers is the protection against freeze-up when the ambient air temperature is below the freezing point of the liquid being condensed. It should be pointed out here that the danger to the successful operation of the heat transfer equipment arises not from the reduction in the overall heat transfer coefficient because of formation of a solid phase inside the tubes; indeed, the problem is that the heat transfer is too good rather than deteriorated. Rather the problems are that the tube is subject to mechanical damage because of the formation of a solid phase less dense than the liquid phase (a situation almost unique to steam condensers) or to the formation of a pocket of noncondensed gas and substantially subcooled liquid near the exit of the bottom-most tubes in the air-cooled condenser. The noncondensable gas - liquid interface can give rise to accelerated corrosion effects (especially severe in the case of the air-water system) and to the possible occurrence of a recurrent water hammer resulting from the presence of a body of subcooled liquid which occasionally may come in contact with the noncondensed vapor.

Numerous techniques have been proposed for eliminating or minimizing this problem but all of them represent substantial capital and/or operational cost penalties against the heat exchanger. Ideally, one would like to control the distribution of the vapors to be condensed among the tubes to be just equal to that which can be condensed in the tube, but all the techniques have been proposed along this line are in principle effective only at one air temperature. Most of the proposed solutions to this problem depend upon the ability of the designer in some way to modify the air temperature so as to bring it into a range in which the problem is no longer severe (though in principle it can never be completely eliminated). The "ultimate" solution to this is to build the air-cooled heat exchanger into a house in which the ambient air temperature is controlled by recirculation, a technique commonly used in polar regions, for example. This works, but at the cost of making this structure a much more expensive component of the system than the heat exchanger itself.

"New" Exchanger Applications

Plate Exchangers. Gasketed plate heat exchangers have been around a long time for liquid-to-liquid heat exchange (10) and have recently substantially expanded their scope of application with the development of sweet water to sea water heat rejection systems for plants located on or near the ocean. Interest in their application in condensing vapors of modest pressures (on the order of five to ten atmospheres) was perhaps spurred by the Ocean Thermal Energy program. Gasketed plate exchangers were successfully used as the ammonia condenser on Mini-OTEC, a state and privately funded experiment off Hawaii, which in 1979 produced the first demonstrable net energy production from an OTEC cycle (11). The condenser in this case was working with saturated ammonia at a pressure of approximately 6 atma. The gasketed plate heat exchanger because of the close clearances between the plates results in relatively very high shear stresses and correspondingly high pressure drops and heat transfer coefficients. It is not applicable to the case of low density, low pressure vapors, but may have a range of applications heretofore unused. The plate exchanger may be of particular interest in situations in which there is a possibility of operational upsets causing substantial fouling of the heat transfer surface since the plate exchanger can be stripped down relatively easily for cleaning. They are also of particular interest for condensation of corrosive vapors since plate heat exchangers are generally substantially less expensive than shell and tube heat exchangers of the same thermal capacity if alloy construction is required.

Spiral Plate Exchangers. Spiral plate exchangers have been used for some time as internal condensers in distillation columns because of their natural cylindrical symmetry. By directly coupling the column to the condenser without intervening piping, pressure drop may be minimized, a vital consideration in vacuum operation. Manufacturing techniques for spiral plate exchangers have enabled the increase in size of these heat exchangers to accommodate the increase in capacity of vacuum distillation columns. Again, spiral plate exchangers will generally cost less in alloy construction than the corresponding shell and tube exchanger (12).

Operational Considerations

Close Temperature Approaches. The desire for increased thermodynamic efficiency in process plant heat exchangers and the increasing use of air as a cooling medium have both resulted in the reduction of temperature approaches to very small values in condensers. Accordingly, much more care must be paid to matching the enthalpy removal profiles of the vapors to be condensed with the enthalpy absorption capability of the coolant flow. Furthermore, care must be taken to ensure close contact between the vapor and the liquid phases in multi-component condensation particularly in order to minimize the departure from thermodynamic equilibrium. Particular care is required when dealing with a two-phase mixture and trying to distribute it among a number of parallel channels as noted above. It is probably fair to say at this point that there is no satisfactory method for doing this within the normal context of close temperature approach heat exchanger design.

Feed-Effluent Exchangers. Feed-effluent exchangers - exchangers designed to exchange heat between an incoming feed stream and an effluent product stream whether it be from a distillation column or a chemical reactor or other piece of process equipment effecting a temperature change between the streams - are venerable items in the lexicon of the chemical engineer, but they seem to have achieved a new popularity with the onset of the energy crisis. As may be guessed from the above, there are many configurations and situations

which may be described as feed-effluent exchangers in the process industries, but those which attract the most attention (because they impose the most severe problems) are typically exchanger systems in which the hot stream enters as a superheated vapor or two-phase fluid condensing and exchanging heat against an incoming liquid which undergoes vaporization during its passage through the exchanger. If these systems are to achieve the desired goal of maximum heat recovery, it follows that they tend to exchange heat over wide temperature ranges, but with small temperature differences between the two streams. Several considerations follow from this: accurate prediction of the vapor-liquid equilibrium and enthalpy relationships as a function of temperature is essential for the successful design and operation of this equipment if it is to achieve the desired terminal temperature differences. And the heat exchangers involved must either be countercurrent or multiple shells in series.

The problem of accurate thermodynamics is probably beyond the scope or control of either the process engineer or the heat exchanger designer. Nevertheless, they should be on their guard against accepting at face value information in these areas which has a possible uncertainty approximating that of the precision of the calculations which they wish to carry out. The question of configuration of the exchanger and the possible uncertainties introduced by flow distribution considerations are very much in the province of at least the heat exchanger designer. He should consider the actual possible degree of departure from true countercurrent flow or the ideal flow situations assumed in the design of multiple shell systems, and provide a degree of resilience (which has become the academically respectable term for a system which will work in spite of the blunders of the designer and/or operator). Again we are faced with the final reliance coming upon the quality of the engineering insight and judgement on the part of the designer. One mechanical development of relatively recent times that helps a great deal in this regard is that of the high pressure, high temperature bellows or expansion joint which can be used particularly on the tube side piping internal to the shell, to absorb the thermal expansion differential in the typical feed-effluent exchanger arising from the very great temperature ranges involved in each fluid.

ENHANCED SURFACES

Finned Tubes

Low-finned tubes have long been used in shell and tube heat exchangers for a variety of services where the shell side heat transfer coefficient was less than perhaps half of the tube side coefficient; this situation is very common in water-cooled condensers, for example. The finned surface turns out to be at least as good as prime surface in its effective heat transfer coefficient, at least for fluids with low surface tensions. Fluids with high surface tensions, such as water (and one has to think very hard to come up with process fluids which fall into anything like the same category) on the other hand, bridge the fins and in fact sharply reduce the effective condensing heat transfer coefficient. Undoubtedly, there is much more to be learned of the effects of vapor shear superimposed upon the fin surface condensing heat transfer coefficient and the proper relationship of the fin efficiency or fin resistance to the condensation process. And undoubtedly surface tension-driven flows are extremely important in determining the hydrodynamics of the film on the surface and its thickness and therefore the local heat transfer coefficient. New tubes with a much finer fin spacing have been introduced and also shown to be effective. However, the major problems remaining in these areas, while certainly worthy of further study, are probably not of a nature to make major changes in the design procedures or effectiveness of the surface.

Grooved and Corrugated Surfaces. The above statement probably cannot be made with regard to the various kinds of grooved and corrugated surfaces that have been proposed and tested in condensers. Work at Oak Ridge National Laboratory (13) in support of work on both the geothermal and ocean thermal energy projects have shown that vertical axially grooved tubes ("Gregorig surface") give condensing heat transfer coefficients on the order of five to ten times those obtainable with a corresponding plain tube. The effect has been studied by several workers on a single tube recognizing that surface tension forces resulting from the changing radius of curvature on the surface give rise to very thin films of condensate on the convex surfaces and therefore very high heat transfer coefficients on those surfaces. The difficulty is that these tubes tend to be self-defeating. Their very high heat transfer coefficients result in a rapid accumulation of condensate draining in the concave channels, which quickly tend to flood out the high heat transfer coefficient convex surfaces. Several proposals have been made for the removal of the accumulated liquid such as skirts which will throw that liquid outwards off of the tube and then allow the buildup of a new condensate film. Most of these studies have been carried out on a single tube in which the liquid, when thrown out, does not further enter into the heat transfer process. However, in a multi-tube bundle, one would anticipate that the liquid that was thrown outwards would very probably immediately impact upon an adjacent tube and simply contribute to its local condensate buildup. Some testing has been done with multi-tube bundles and the effects have been at least very attractive if not as spectacular as those for the single tube. Before the process industries are in a position to benefit from this kind of surface, a good deal more large scale study needs to be done as well as to consider the interaction of these tubes with such essential mechanical elements as tube support plates.

Plate Fin Exchangers. Plate fin exchangers, or matrix exchangers as they are sometimes called, are another example of a piece of equipment which has a long honorable history of successful application in spite of the dearth of two-phase pressure drop and heat transfer information. These exchangers, with their very large ratio of heat transfer area to volume and consequently high NTU ratings, have been one of the mainstays of the cryogenic processing industry. Yet virtually no two-phase flow studies had been made on these units until the last half dozen years. Most of this work has been done by Robertson and co-workers (15) at HTFS and Harwell and only now is only beginning to appear in the literature. We may expect to see computer design programs coming more generally available and reliable as this fundamental information can be incorporated into the design programs.

However, the main problem in the application of plate fin exchangers is to secure as nearly as possible uniform distribution among the many parallel channels and often among several exchangers in parallel. There are numerous patents reported for the distributors for introducing simultaneously liquid and vapor flows into the channels in aliquot proportions. None of these devices work adequately, and conventional design practice is to only attempt to introduce a single phase into any given set of channels. Because of the very close temperature approaches and very tight enthalpy balancing that is necessary for good energy efficiency in cryogenic processes, the greatest care must be taken in piping units in parallel so that they all have reasonably equivalent flow rates through them. This problem is made more difficult by the fact that both valves and instrumentation are eliminated wherever possible in cryogenic plants because of the difficulty of maintaining them inside the cold box. Additionally, what one might gain in uniformity of flow distribution by a flexible valving system one would likely lose by the pressure losses through the valves. This problem of flow maldistribution is

one that has been very little explored, in the open literature at least.

MULTICOMPONENT/NONCONDENSABLE PROBLEMS

Improvement in Fundamental Basis

The problem of heat and mass transfer in condensation of multicomponent mixtures, with or without a noncondensable gas, has long been studied from a fundamental point of view. Generally acceptable design procedures for condensation of a single component from a noncondensable gas and condensation of a miscible binary mixture were already available to Kern and were cited by him. However, the more common general problem of many components has only recently moved into the position where it is becoming tractable computationally at a level that can be considered for inclusion in condenser design programs. Most of the credit for this must go to Professor Standart and his successors, including Professors Krishna and Webb here at Manchester. I think that we shall shortly see condenser design programs incorporating these fundamental procedures, at least as far as the vapor phase transport is concerned. However, there are still some problems remaining with the apparently not-inconsiderable multicomponent transport effects in the condensate phase, which does not admit to some of the simplifications that are possible with the vapor phase. This is a very active area of work and is progressing much faster than I think most of us would have predicted ten years ago.

Immiscible Condensation

Many condensers for multicomponent mixtures produce a condensate having two immiscible phases. There have been many small scale laboratory experiments measuring the average heat transfer coefficient for the condensate phase. These data are then generally correlated in terms of a weighted average of the coefficients for each of the liquid phases alone. The results are generally adequate for design purposes but the basis of the calculation is in principle unrelated to the actual hydrodynamics. For one thing, the small scale of most of these experiments tells us very little about the general nature of the flow patterns to be expected even for pure gravity-driven drainage on a vertical surface. Perhaps the first paper to contribute significantly to this aspect of the problem was by Polley and Calus (16). However, nothing seems to have been done to this point in the vapor shear-controlled or transition flow regimes. Current design methods still rely upon the very simple formulations of the type suggested by Bernhardt et al. (17). It is not to be expected that major changes will occur in either design or application as a result of more work in this area, but certainly it would greatly facilitate our understanding and at least possibly provide us a better handle on operational problems.

Thermodynamic and Physical Property Data Needs. In a very real sense when dealing with multicomponent mixtures, our operational capabilities are limited not so much by the thermal-hydraulics of the situation as by the thermodynamic and particularly vapor-liquid equilibrium relationships. Certainly reliable thermodynamic information is necessary but not sufficient for good heat exchanger design. And nowhere is that more true than in the condenser design area. Of necessity, process engineers have become fairly adept at predicting the properties of very complex and even undefined mixtures of substances that keep cropping up in their processes. But there is a never-ending need for further improvements in this area, a need which is probably easier to justify on economic grounds than much of the research that is done in heat and mass transfer. Perhaps all that the thermal-hydraulic specialist can do here is to lead the cheering section for his colleagues who are doing what so often appears to be mundane work in these areas,

but which is nonetheless vital to our own efforts.

SUMMARY

In the foregoing pages the author has very briefly and broadly brushed over a number of topics of current interest in the design and application of process condensers. While it is clear that there is still much work that needs to be done in order to refine our procedures and simplify and optimize our operations, it is also true that process engineers, heat exchanger designers, and operators working together and working intelligently have been able to solve successfully all of the problems that have been put to them.

It is important that we - and especially management - recognize that the key factor in both our past and our future successes is still the well-trained and responsible engineer and that improvements in such tools as computer-oriented design procedures can never take the place of the education and responsibility provided by the engineer. Our best computer programs are fully capable of producing teratomorphs, and our only protection against having these paper monsters turned into expensive metal ones is the design engineer who has a pretty good idea of what the heat exchanger ought to look like before he ever goes to the computer to design one. With all of the advances in computer design methods, it is important to remember that we must continue to have engineers as good as those working in Don Kern's day.

REFERENCES

1. Kern, D. Q., 1950, "Process Heat Transfer", McGraw-Hill Book Co., New York USA.
2. Schlunder, E. U., Ed., 1982, "Heat Exchanger Design Handbook", Hemisphere Publishing Corporation, Washington, USA.
3. Colburn, A. P., and Hougen, O. A., 1934, Ind. Eng. Chem., 26, 1178.
4. Colburn, A. P., and Drew, T. B., 1937, Trans. AIChE, 33, 197.
5. Silver, L., 1947, Trans. Inst. Chem. Eng., 25, 30.
6. Blien, C. J., 1982, Presentation at HTRI Technical Advisory Committee Meeting, Pasadena, California.
7. Lorenz, J. J. Yung, D., Howard, P. A., Panchal, C. B., and Poucher, F. W., 1981, "OTEC-1 Power System Test Program: Performance of One-Megawatt Heat Exchangers", Argonne National Laboratory, USA, Report No. ANL/OTEC-PS-10.
8. Taitel, Y., and Dukler, A. E., 1976, AIChE J., 22, 47.
9. Grant, I. D. R., and Murray, I., 1975, "Flow and Pressure Drop with Single and Two-Phase Flow on the Shellside of Segmentally Baffled Shell-and-Tube Heat Exchangers, Advances in Thermal and Mechanical Design of Shell-and-Tube Heat Exchangers", National Engineering Laboratory, East Kilbride, Scotland, Report No. 590.
10. Shall, W. M., and Young, R. K., 1979, Heat Trfr. Eng., 1, No. 2, 21.

11. Marriott, J., 1971, Chem. Eng., April 5.
12. Owens, W. L., and Trimble, L. C., 1980, "Mini-OTEC Operational Results", Conference Proceedings "Seventh Ocean Energy Conference", Washington, USA 2, 14.1-1.
13. Minton, P. E., 1970, Chem. Eng., May 4.
14. Murphy, R. W., and Domingo, N., 1982, "Field Tests of 2- and 40-Tube Condensers at the East Mesa Geothermal Test Site", Oak Ridge National Laboratory, USA, Report No. ORNL-5852.
15. Proceedings, Sixth International Heat Transfer Conference, Toronto, Canada, 471.
16. Bernhardt, S. H., Sheridan, J. J., and Westwater, J. W., 1972, AIChE Symposium Series, No. 118, 68, 21.
17. Krishna, R., and Standart, G. L., 1976, AIChE J., 22, 383.

GRAVITY CONTROLLED CONDENSATION ON A HORIZONTAL LOW-FIN TUBE

R. G. Owen*, R. G. Sardesai[‡], R. A. Smith** and W. C. Lee^{‡‡}

Published data are used to derive a general method for predicting the degree of liquid retention during condensation on a horizontal low-fin tube. This general method for predicting condensate retention permits extension of the Beatty and Katz [1] heat transfer model to include the effects of retained condensate. The predictions of the extended model are compared with published heat transfer data. These data are for the condensation of methyl chloride, sulphur dioxide, propane, n-butane, n-pentane, acetone, water, refrigerant-11, refrigerant-12 and refrigerant-22. It is found that the extended model can predict the mean condensate heat transfer coefficient for all data within $\pm 30\%$.

INTRODUCTION

Integral-fin tubes with low fins have application in condensers used in the petrochemical, power, refrigeration and air-conditioning industries. These tubes will permit higher condensation rates than plain tubes and this may yield advantages in reducing the size, weight and cost of the condenser. These advantages are particularly important where space and weight are expensive, e.g. in offshore oil and gas production and in marine applications. Integral-fin tubes may also be used to increase the capacity of an existing condenser by retubing. They are also employed to hold tube-side velocity within a desired narrow range as is required for glycol injection in gas treatment plants.

Figure 1 illustrates the main features of integral-fin tubing. It is common practice to provide plain sections of the tube where the tube passes through baffles. This is necessary to provide a reasonably tight fit to support tubes and to avoid damage to the fins as a result of tube vibration. Fin-densities range from 200 to 1600 fins/metre. When integral-fin tubes were originally introduced, the fin-densities were in the lower end of this range but there has been a trend in recent years towards the use of tubes with high fin-densities. The surface area of the outside of an integral fin tube varies with fin height and spacing but is typically about 3 times that of the corresponding plain tube.

* Engineering Sciences Division, AERE Harwell, Oxon. OX11 0RA

‡ Engineering Sciences Division, AERE Harwell (now with Heat Transfer Research Inc., Alhambra, California, U.S.A.)

** Consultant to the Heat Transfer and Fluid Flow Service (HTFS)

‡‡ Post-doctoral Fellow at Queen Mary College, London.

Integral-fin tubes may be usefully employed wherever the resistance of the condensing fluid on the outside of the tube is controlling or is a significant fraction of the overall resistance. Thus, integral fin tubes are more commonly employed for condensing refrigerants and hydrocarbons than for condensing steam. This is because organic liquids have a lower latent heat and a lower thermal conductivity than water. Thus, the resistance of the condensing fluid is relatively higher when condensing organic vapours than when condensing steam.

The enhanced performance of the integral-fin tubes is due to a combination of the following effects:

- (1) There is an increase in heat transfer area on the condensing side per unit length of the tube. However, in calculating the effective area of the tube, the fin-efficiency must be taken into consideration.
- (2) There may be an increase in the condensate film heat transfer coefficient. This increase arises because the flanks of the fins provide vertical or nearly vertical surfaces for which the condensation coefficient is higher than that for the base tube. There may be further improvement in heat transfer due to the effect of surface tension thinning the condensate film on the tips and on the flanks of the fins. Also the greater surface area leads to a lower heat flux and hence to a thinner film.

In 1948, Beatty and Katz [1] developed a simple analytical model to predict the condensation coefficient on horizontal integral-fin tubes. Although this model is over 30 years old and is quite simple, it still appears to be the best available. The model assumes that all the condensate is gravity drained and that there is no condensate retained between the fins due to the effect of surface tension. However, it may be expected that surface tension forces would inhibit the drainage of the condensate from between the fins and cause a portion of the inter-fin space to be filled with condensate. The performance of the Beatty and Katz [1] model has been tested by a number of groups of workers [1,2,3,4,5]. It has been found that the model adequately predicts the heat transfer coefficient when the condensate retention is not important. However, where condensate retention is important, Rudy and Webb [5] have observed that the Beatty and Katz [1] model tends to overpredict the mean coefficient.

The objectives of this paper are;

- (i) To develop a general method for predicting the degree of condensate retention between the fins.
- (ii) To use this method in modifying the Beatty and Katz [1] model to account for the effects of retained condensate.
- (iii) To test the performance of the improved model against all available data.

THE BEATTY AND KATZ MODEL [1]

This model accounts separately for condensation on the fins and for condensation on the base tube between the fins. The model assumes that the condensate flow is laminar and gravity-controlled and that there is no effect of surface tension in thinning the condensate film or in retaining the condensate between the fins. In evaluating the heat transfer coefficient, the

base tube is treated as a plain horizontal tube and the flanks of the fins are treated as plain vertical surfaces. The Nusselt [6] film condensation equations appropriate to a horizontal tube and to a vertical flat surface are used in the forms given in equations (1) and (2) respectively.

$$a_H = 0.725 \left\{ \frac{\lambda_L^3 \rho_L (\rho_L - \rho_g) g \Delta h_v}{\eta_L \Delta T} \right\}^{\frac{1}{4}} \left[\frac{1}{d_r} \right]^{\frac{1}{4}} \quad (1)$$

$$a_V = 0.943 \left\{ \frac{\lambda_L^3 \rho_L (\rho_L - \rho_g) g \Delta h_v}{\eta_L \Delta T} \right\}^{\frac{1}{4}} \left[\frac{1}{X} \right]^{\frac{1}{4}} \quad (2)$$

where d_r is the root diameter of the finned tube.

The value of X in equation (2) is given by Beatty and Katz as

$$X = \frac{\pi (d_o^2 - d_r^2)}{4 d_o} \quad (3a)$$

where d_o is the outside diameter of the finned tube. X is physically interpreted as the average vertical fin height over the diameter d_o . Equation (2) shows that a_V is proportional to $X^{-\frac{1}{4}}$. Using this minus one quarter dependency, X should, in principle, be calculated from equation (3b)

$$X^{-\frac{1}{4}} = \frac{4}{\pi (d_o^2 - d_r^2)} \int_{A_f} Z^{-\frac{1}{4}} dA \quad (3b)$$

where A_f is the area of the flanks of the fins per length of the tube, i.e.

$$A_f = \frac{\pi}{2} (d_o^2 - d_r^2) N \quad (4)$$

and Z is the vertical height of the fin. Equation (3b) gives a larger value of X than equation (3a) but for a typical case, e.g. $d_o = 19.1$ mm and $d_r = 15.9$ mm the difference in X determined by (3a) and (3b) is only 6.6% [5]. This gives a negligible difference in a_V .

The total heat flow is the sum of that on the exposed portion of the base tube and that on the vertical fins. Thus the composite condensing coefficient based on the effective total surface area, A_{eff} , is a_T where

$$a_T = \frac{A_r}{A_{eff}} a_H + \frac{\phi A_f}{A_{eff}} a_V \quad (5)$$

where $A_{eff} = A_r + \phi A_f$, (6)

ϕ = fin efficiency,

and A_r = area of the exposed portion of the base tube and the area of the tips of the fins. This is approximated by taking it to be the area of a plain tube with diameter equal to the root diameter of the finned tube.

From equations (1), (2), (5) and (6)

$$\alpha_T = 0.725 \left(\frac{\lambda_f \rho_f (\rho_f - \rho_g) g \Delta h_v}{\eta_f \Delta T} \right)^{\frac{1}{4}} \left\{ \frac{A_r}{A_{eff}} \frac{1}{d_r^{\frac{1}{4}}} + 1.3 \frac{\phi A_f}{A_{eff}} \frac{1}{X^{\frac{1}{4}}} \right\} \quad (7a)$$

Hence;

$$\alpha_T = 0.725 \left(\frac{\lambda_f \rho_f (\rho_f - \rho_g) g \Delta h_v}{\eta_f \Delta T} \right)^{\frac{1}{4}} \left[\frac{1}{d_e^{\frac{1}{4}}} \right] \quad (7b)$$

$$\text{where } \frac{1}{d_e^{\frac{1}{4}}} = \left[\frac{A_r}{A_{eff}} \frac{1}{d_r^{\frac{1}{4}}} + 1.3 \frac{\phi A_f}{A_{eff}} \frac{1}{X^{\frac{1}{4}}} \right] \quad (8)$$

The constant 0.725 in equation (7a) was modified to a value of 0.689 by Beatty and Katz [1] in order to give the best fit to their own experimental data. Hence the final form of the Beatty and Katz [1] model is

$$\alpha_T = 0.689 \left(\frac{\lambda_f \rho_f (\rho_f - \rho_g) g \Delta h_v}{\eta_f \Delta T} \right)^{\frac{1}{4}} \left[\frac{1}{d_e^{\frac{1}{4}}} \right] \quad (9)$$

The Beatty and Katz model, given in equation (9), does not account explicitly for the effect of surface tension which: (i) increases the local heat transfer coefficients by thinning the condensate film on the tips and flanks of the fins; (ii) causes condensate to be retained in the spaces between the fins. However, it is possible that the reduction of the constant from 0.725 to 0.689 empirically accounted for the reduction in heat transfer coefficient due to condensate retention.

AVAILABLE EXPERIMENTAL DATA

A number of published reports are available in which experimental measurements have been made of heat transfer coefficients for condensation on integral-fin tubes. These studies are listed in Table 1, which gives the fluids and the tube geometries used. The data are for fluids which span a range of surface tension from 5×10^{-3} to 75×10^{-3} N/m and liquid densities from 500 to 1500 kg/m³. Fin heights range from 0.9 to 8.7 mm and fin densities from 250 to 1610 fins/metre. The ratio of fin height to root diameter (z/d_r) ranges from 0.045 to 0.548.

The study of Beatty and Katz [1] indicated that equation (9) correctly predicted the mean condensate heat transfer coefficient. The maximum fin density used in this study was 630 fins/metre. Katz et al [2] also found that the Beatty and Katz [1] model predicted their data within $\pm 10\%$. Katz and Geist [3] studied condensation on 6 finned tubes in a vertical row. For organic fluids, the Beatty and Katz [1] model was able to predict the condensation coefficient for the top tube within 14%.

As indicated in Table 1, data are also available from Pearson and Withers [4] and Carnavos [7]. Rudy and Webb [5] tested the Beatty and Katz [1] model against the above sources of data and observed that the model performed fairly accurately when condensate retention between fins was small but tended to

TABLE 1 - Summary of Experimental Data Sources

Data Source	Geometry			Test Fluids
	Root diameter of tube (mm)	Fin height (mm)	Fin density (fins/metre)	
Beatty and Katz [1]	15.8 - 19.5	1.47 - 8.66	257 - 608	Methyl Chloride n-pentane Sulphur dioxide Propane Refrigerant 22 n-butane
Katz and Geist [3]	15.8	1.59	591	Refrigerant 12 n-butane Acetone Water [*]
Carnavos [7]	16.3	1.32	1060	Refrigerant 11
	17.6	0.79	1610	
Pearson and Withers [4]	15.8	1.42	1024 748	Refrigerant 22

* The water data of Katz and Geist [3] were considered to be unreliable and hence were not included in Figures 4, 5 and 6. The data were considered unreliable because of the occurrence of partial dropwise condensation and because of the presence of non-condensing gas.

overpredict the mean film coefficient when the condensate retention was high.

Clearly, there is a need to modify the Beatty and Katz [1] model to account for retention of condensate. However, in order to do this, it is first necessary to develop a general method for predicting the degree of condensate retention.

CONDENSATE RETENTION BETWEEN FINS

Rudy and Webb [5] have studied the degree of condensate retention for a range of fluids and finned tube geometries. The degree of condensate retention, θ , is the fraction of the tube perimeter which is filled with retained condensate. The degree of condensate retention can be calculated* from the condensate retention angle β shown in Figure 2. Experiments were performed by Rudy and Webb to measure the degree of retention during condensation, for a range of condensation rates. Measurements were also made of condensate retention for a static condition with no condensation occurring. Rudy and Webb [5] observed that the condensate retention angle, β , is very weakly dependent on the condensation rate. The simplifying assumption is therefore made in this paper that β is independent of the condensation rate and is equal to that for a static condition with no condensation occurring. The

* θ is equal to $\beta/180$ where β is measured in degrees.

theoretical analysis given below therefore deals specifically with the static condition.

Consider the space between two adjacent fins of an integral fin tube. Let a liquid of density, ρ_ℓ , and surface tension, σ_ℓ , subtend an angle β ($0 < \beta < 180^\circ$) as shown in Figure 2. At the lowest point of the tube, there will be a balance between the surface tension force acting vertically and the downward force resulting from the weight of the retained condensate. The surface tension force acting at the outer edge of the adjacent fins over an elemental circumferential length Δy is given by $2 \sigma_\ell \Delta y$. The downward force of liquid is given by $[\rho_\ell g (d_o/2) (1 - \cos \beta) \Delta y w]$ where w is the width of the inter-fin space. Hence, the force balance is;

$$\frac{\sigma_\ell}{\rho_\ell g d_o w} = \frac{1}{4} (1 - \cos \beta) \quad (10)$$

For a tube of fin density N fins/metre, the fin pitch is $1/N$ metres. The inter-fin space, w , will be a fraction, Y of the fin pitch. Hence

$$w = \frac{Y}{N} \quad (11)$$

From equations (10) and (11)

$$\frac{\sigma_\ell N}{\rho_\ell g d_o Y} = \frac{1}{4} (1 - \cos \beta) \quad (12)$$

The dimensionless group $(\sigma_\ell N / \rho_\ell g d_o Y)$ is denoted by ζ .

Equation (12) is valid until the condensate retention angle reaches 180° . Once this angle is reached, no additional condensate can be retained because the inter-fin space is then completely filled with condensate. Hence equation (12) is only valid in the range $0 < \beta < 180^\circ$. Thus, if the inter-fin space is full of retained condensate;

$$\zeta \geq \frac{1}{2}; \quad \theta = 1 \quad (13a)$$

and if the inter-fin space is partially filled with retained condensate;

$$\zeta < \frac{1}{2}; \quad \theta = \frac{\cos^{-1}(1 - 4\zeta)}{180} \quad (13b)$$

Equation (13) is compared with the data of Rudy and Webb [5]* in Figure 3. Good agreement is obtained.

* Geometrical details of the integral-fin tubes used by Rudy and Webb are not included in their paper. However, they were supplied to the authors in a private communication from Thomas Rudy. These details are also included in the Ph.D. Thesis of Dr. Rudy.

THE MODIFIED BEATTY AND KATZ MODEL

The Beatty and Katz model has been extended in a simple way to account for the presence of retained condensate. In extending the model it is assumed that;

- (i) The Beatty and Katz model, in its original form, is applicable to the upper portion of the tube where there is no retained condensate. The area of this portion is $(1-\theta) A_{eff}$. Hence in the upper portion of the tube, neglecting variations of the local heat transfer coefficient with height, the heat transfer coefficient a_U is given by;

$$a_U = 0.725 \left\{ \frac{\lambda_f^3 \rho_f (\rho_f - \rho_g) g \Delta h_v}{\eta_f \Delta T} \right\}^{\frac{1}{4}} \left[\frac{1}{d_e} \right]^{\frac{1}{4}} \quad (14)$$

- (ii) In the lower portion of the tube with area θA_{eff} , the inter-fin space is flooded with retained condensate and condensation occurs both on the surface of the retained condensate and on the tips of the fins. The effective thermal resistance on the condensing side is equivalent to the sum of the following two resistances in series;

- (a) the thermal resistance arising from condensation on a plain tube of diameter d_o . This corresponds to a heat transfer coefficient a_C given by;

$$a_C = 0.725 \left\{ \frac{\lambda_f^3 \rho_f (\rho_f - \rho_g) g \Delta h_v}{\eta_f \Delta T} \right\}^{\frac{1}{4}} \left[\frac{1}{d_o} \right]^{\frac{1}{4}} \quad (15)$$

- (b) the combined resistance of the fins and retained condensate. These provide parallel paths for heat flow. The simplifying assumption is made that heat flow is purely radial and that the heat is transferred across the retained condensate by conduction only. In some cases, this conservative assumption may underestimate heat transfer through the retained condensate.

An effective thermal conductivity over the fin height may thus be determined on an area-averaged basis for low fins as;

$$\lambda_{eff} = (1 - Y) \lambda_f + Y \lambda_f \quad (16)$$

The heat transfer coefficient of the combined fin-retained condensate region is thus

$$a_f = \frac{\lambda_{eff}}{z} \quad (17)$$

In the lower portion of the tube the effective heat transfer coefficient is thus

$$a_L = \left(\frac{1}{a_f} + \frac{1}{a_C} \right)^{-1} \quad (18)$$

where α_F is given by equation (17) and α_C by equation (15).

The average heat transfer coefficient, α_T , for the whole tube having an effective area, A_{eff} , is thus an area average of coefficients for the upper and lower portions. Hence

$$\alpha_T = (1 - \theta) \alpha_U + \theta \alpha_L \quad (19)$$

where α_U is given by equation (14) and α_L by equation (18).

COMPARISON OF THE IMPROVED BEATTY AND KATZ MODEL WITH EXPERIMENTAL DATA

The available experimental data which are listed in Table 1 have been used to test both the original model of Beatty and Katz and the improved model outlined above.

Figure 4 gives a comparison of all data with the original Beatty and Katz model as given in equation (9). In this figure, the abscissa is the dimensionless group ζ which correlates the degree of condensate retention between the fins. The available data have ζ values in the range from zero to 0.234. This corresponds to θ values from zero to 0.48. For this range of data the Beatty and Katz model performs adequately although there is a trend towards overprediction at high ζ values. Rudy and Webb [5] have suggested modifying the original model of Beatty and Katz by neglecting heat transfer in the lower part of the tube which contains the retained condensate;

$$\text{i.e. } \alpha_T = \alpha_{BK} (1 - \theta) \quad (20)$$

where α_{BK} is the heat transfer coefficient of the original Beatty and Katz model as given in equation (9)

The performance of the Rudy and Webb [5] modification to the Beatty and Katz model is shown in Figure 5. In this case, underprediction of the mean condensate film coefficient occurs when a significant amount of condensate is retained between the fins. This underprediction implies that there is significant heat transfer in the region of retained condensate.

The performance of the improved model given in equation (19) is shown in Figure 6*. This model is able to predict all available data within $\pm 30\%$ for the entire range of ζ values. For the range of data currently available, the improved model does not appear to have a significant advantage over the original model of Beatty and Katz. However, the improved model, by explicitly accounting for the effects of retained condensate, should be more accurate in situations where an appreciable fraction of the tube is flooded with retained condensate. In order that the improved model may be fully tested there is thus a need for further experimental data with significant condensate retention and for data covering a wider range of fin height.

The above analysis considers condensation on a single horizontal integral-fin tube. When condensation occurs on a bundle of horizontal finned tubes, the effect of condensate inundation must be taken into account. The

* Whereas Figure 4 uses the constant of 0.689 in the Beatty and Katz model, Figures 5 and 6 use a value of 0.725. This is done to avoid any possible double accounting of condensate retention.

data of Rudy and Webb [5] has shown that the degree of condensate retention is, to a first approximation, independent of the condensate loading on that tube. Hence, the effect of inundation may be evaluated using the conventional method* for banks of plain tubes but using equation (19) to calculate the heat transfer coefficient of the top tube in a vertical row. This result is only applicable, however, where the condensate film remains laminar.

CONCLUSIONS

- (1) It has been shown that a dimensionless number, which is the ratio of surface tension to gravity forces in the condensate film, can quantify the degree of condensate retention on integral-fin tubes.
- (2) Figure 4 indicates that condensate retention may not be ignored in evaluating the heat transfer performance of integral-fin tubes. Figure 5 shows that there is a significant amount of heat transfer in the region of retained condensate. The effect of condensate retention can be included in the heat transfer model of Beatty and Katz [1] using the above dimensionless number.
- (3) It has been shown that an improved Beatty and Katz model which explicitly accounts for condensate retention can predict all the available data within $\pm 30\%$.

ACKNOWLEDGEMENTS

This work was carried out as part of the HTFS General Research Programme funded by the Materials and Chemicals Requirements Board of the United Kingdom Department of Industry.

SYMBOLS USED

- A = area (m^2)
- A_{eff} = effective area of integral-fin tube (m^2) (see equation 6)
- d = diameter (m)
- g = acceleration due to gravity (9.81 m/s^2)
- Δh_v = latent heat of vaporisation (J/kg)
- N = fin density (fins/metre)
- ΔT = temperature difference across the condensate film (K)
- w = width of inter-fin space (m)
- X = average vertical fin height (defined in equation 3) (m)
- Δy = elemental circumferential length around the tube (m)
- z = radial fin height (m)

* The conventional method is where $a_N = a_{\text{TOP}} \times (1/N)^m$ where a_N is the mean coefficient over N tubes, a_{TOP} is the coefficient for the top tube and m is an index (typically 1/6).

- z = vertical height of the fin at any diametrical position (m)
 α = heat transfer coefficient ($\text{W/m}^2 \text{ K}$)
 β = condensate retention angle (degrees)
 γ = ratio of inter-fin space and fin pitch ($= wN$) (dimensionless)
 ζ = dimensionless number = $\left[\frac{\sigma_{\ell} N}{\rho_{\ell} g d_o \gamma} \right]$
 η = viscosity (Ns/m^2)
 θ = fraction of tube with retained condensate (dimensionless)
 λ = thermal conductivity (W/m K)
 ρ = density (kg/m^3)
 σ = surface tension (N/m)
 ϕ = fin efficiency (dimensionless)

Subscripts

- e = equivalent
 eff = effective
 f = fin
 H = horizontal
 i = internal
 ℓ = liquid (i.e. condensate)
 L = lower portion of the tube flooded with retained condensate
 o = outside of fin tips
 r = root
 T = average for the whole tube
 U = upper portion of the tube free of retained condensate
 v = vertical

REFERENCES

- [1] Beatty, K.O. Jr. and Katz, D.L., 1948, "Condensation of vapors on outside of finned tubes", Chemical Engineering Progress, 44, (1), January, 55-70.
- [2] Katz, D.L. et al, 1947, "Condensation of Freon-12 with finned tubes, Part I, Single horizontal tubes", Journal of the ASRE, March, 211-217.
- [3] Katz, D.L. and Geist, J.M., 1948, "Condensation on six finned tubes in a vertical row", Transactions ASME, November, 908-914.
- [4] Pearson, J.F. and Withers, J.G., 1969, "New finned tube configuration improves refrigerant condensing", ASHRAE Journal, June, 77-82.
- [5] Rudy, T.M. and Webb, R.L., 1981, "Condensate retention of horizontal integral-fin tubing", Advances in Enhanced Heat Transfer, Presented at the 20th National Heat Transfer Conference, Milwaukee, Wisconsin, August 2-5.
- [6] Nusselt, W., 1916, "Surface condensation of water vapour", Z. Ver. dt. Ing., 60, (27), 541-546 and 60, (26), 569-575.
- [7] Carnavos, T.C., 1980, "An experimental study: Condensing R-11 on augmented tubes", ASME Paper No. 80-HT-54.

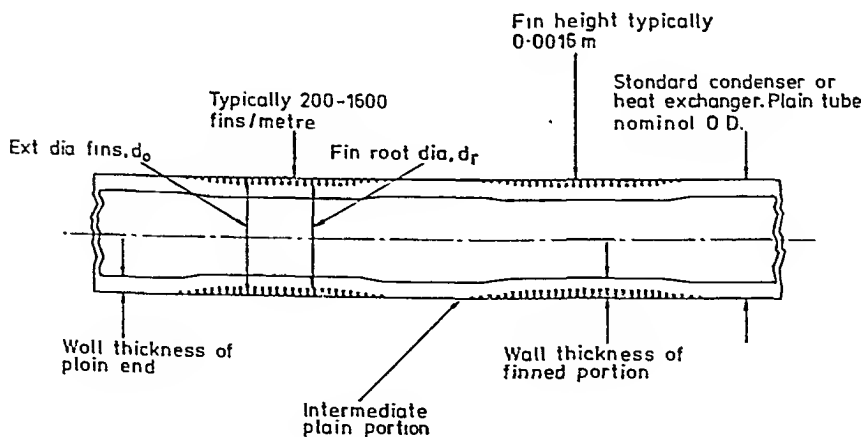
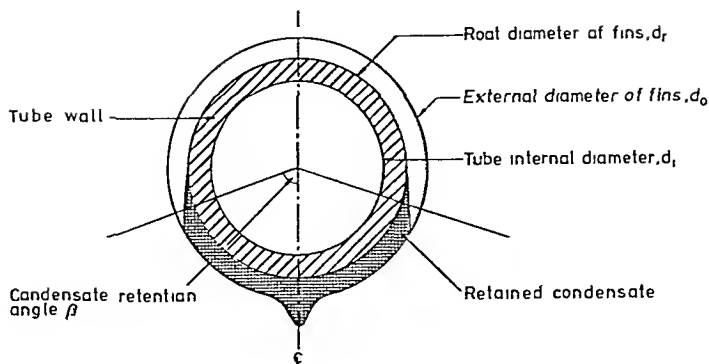
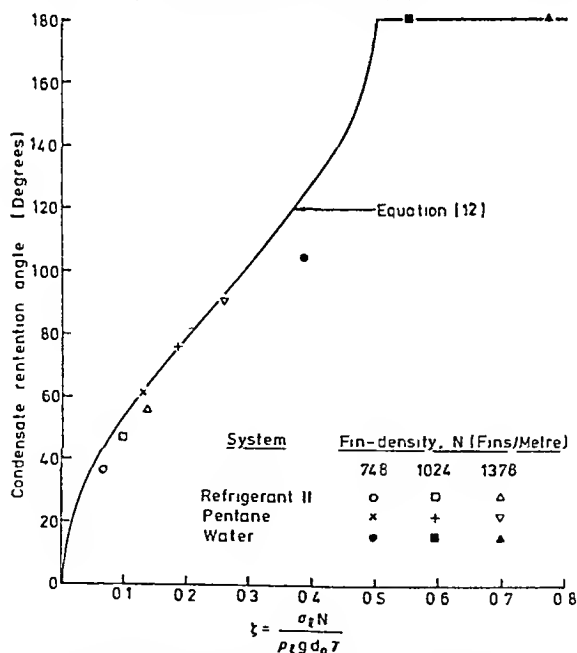


FIG.1.MAIN FEATURES OF INTEGRAL -FIN TUBING

Cross-section of integral - Fin Tubing.FIG 2 THE DEGREE OF CONDENSATE RETENTION IN INTEGRAL - FIN TUBING
(AFTER RUDY AND WEBB [5])FIG 3 CONDENSATE RETENTION ANGLE PLOTTED AS A FUNCTION
OF DIMENSIONLESS NUMBER $\frac{\sigma_t N}{\rho_t g d_o T}$ FOR THE DATA OF
RUDY AND WEBB [5]

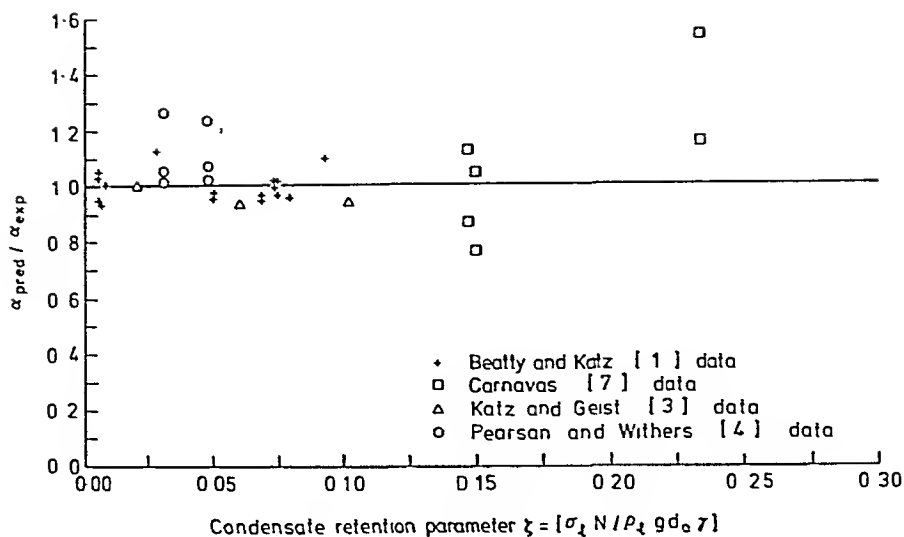


FIG 4 COMPARISON OF EXPERIMENTAL DATA WITH PREDICTIONS OF THE ORIGINAL BEATTY AND KATZ (1948) MODEL

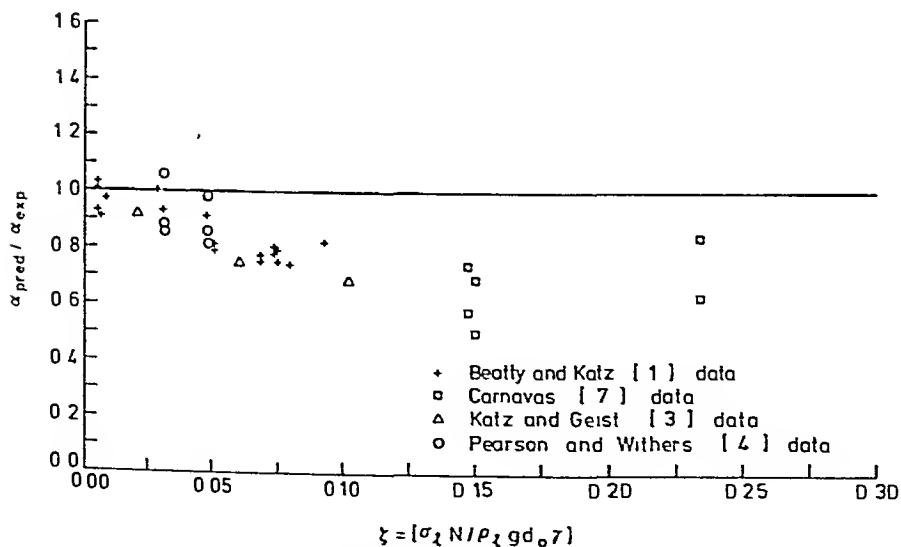


FIG 5 COMPARISON OF EXPERIMENTAL DATA WITH PREDICTIONS OF BEATTY AND KATZ MODEL AS MODIFIED BY RUDY AND WEBB (1981)

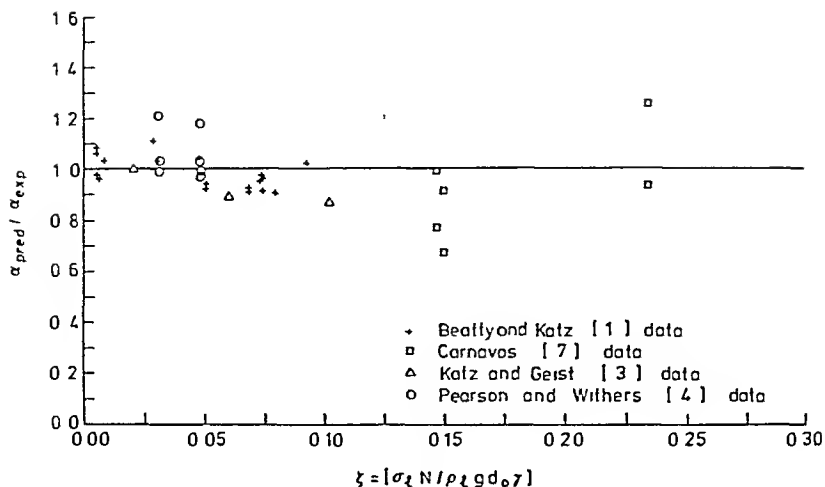


FIG 6 COMPARISON OF EXPERIMENTAL DATA WITH PREDICTIONS OF EXTENDED BEATTY AND KATZ MODEL AS GIVEN BY EQUATION (19)

CONDENSATION OF PURE FLUIDS ON HORIZONTAL FINNED TUBE BUNDLES

Ishihara, K. I., Palen, J. W. *

A method is proposed to predict the local shellside finned tube condensation heat transfer coefficients for pure fluids. The heat transfer process during condensation is separated into a vapor shear-controlled flow regime and a gravity-controlled flow regime. The latter is further differentiated into a laminar film region and a turbulent film region. In previous methods, the heat transfer coefficients were calculated based on empirical corrections to the Nusselt equation. The new method is based on a more realistic modeling of condensation process. Substantial improvement is obtained in the prediction of existing data. Because of the proprietary nature of the research work, it was necessary to omit the final values of some of the constants used in the correlations. However, the basic procedures are presented.

INTRODUCTION

This paper presents in principle calculation procedures for shellside finned tube condensation of pure vapors.

The new procedures make use of the technique of dividing the condensation process into controlling regimes and providing reasonable mechanistic correlational models for each regime. The salient features of the flow regimes for either plain or finned tube shellside condensation can be described as follows:

- Gravity-Controlled Flow Liquid drains vertically under gravity. Three flow regimes are plausible for this case:
 1. Laminar film flow where the Nusselt equation applies, but must be adapted to finned geometry.
 2. Rippled film flow where the Nusselt equation can be empirically modified.
 3. Turbulent film flow where the Nusselt equation does not apply. A new method was developed to be analogous to the method used for tubeside flow.
- Shear Controlled Flow The liquid is blown off the tubes by high velocity vapor. The Nusselt equation for laminar draining condensate does not apply. A new method was developed based on a convective type correlation.

* Heat Transfer Research, Inc., Alhambra, California, USA

• **Transition Flow** The heat transfer coefficient for this regime is prorated from the results of the gravity controlled and shear-controlled regimes. A shellside flow regime parameter is used to determine which flow regime is controlling. This parameter was developed as the ratio of the vapor shear force to the gravitational force on fluid.

SINGLE FINNED TUBE THEORY

The essence of the Katz-Beatty method [1] for single finned tubes is the simultaneous application of the Nusselt theoretical equation for flat plates and for plain horizontal cylinders. The horizontal plain tube equation is applied to the root area of a finned tube and the vertical plate equation is applied to the vertical fin surface of a finned tube. For the root area, the Nusselt equation for a single horizontal tube is applied as follows by using the root diameter of a finned tube, D_{FR} .

$$h_T = 0.725 \left[\frac{k_L^3 \rho_L (\rho_L - \rho_V) g \lambda}{\mu_L \Delta T_C (D_{FR})} \right]^{1/4} \quad (1)$$

For the vertical finned surface, the Nusselt equation for a vertical plate is applied as follows using the height of an equivalent vertical plate, H_M .

$$h_F = 0.943 \left[\frac{k_L^3 \rho_L (\rho_L - \rho_V) g \lambda}{\mu_L \Delta T_C (H_M)} \right]^{1/4} \quad (2)$$

The term H_M is defined by Equation (3) and physically represents the height of a rectangle with the width of D_{OF} having an area equal to the vertical surface of one side of a fin.

$$H_M = \frac{\pi}{4} \left[\frac{(D_{OF})^2 - (D_{FR})^2}{(D_{OF})} \right] \quad (3)$$

The equation for an entire finned surface can be written by using the Nusselt equation for a horizontal plain tube and replacing the plain tube diameter with an effective diameter of a finned tube, D_{EF} , to be determined through the use of Equations (1), (2), and (3).

$$h_g = 0.725 \left[\frac{k_L^3 \rho_L (\rho_L - \rho_V) g \lambda}{\mu_L \Delta T_C (D_{EF})} \right]^{1/4} \quad (4)$$

The derivation for D_{EF} is as follows.

The condensation heat transfer rate, Q , on a finned tube can be expressed as

$$\begin{aligned} Q &= h_g (A_{EQ}) \Delta T_C \\ &= h_T (A_{RO}) \Delta T_C + h_F (A_{FO}) \Omega \Delta T_C \end{aligned} \quad (5)$$

where A_{RO} root surface area per unit of length

A_{FO} finned surface area exclusive of root area per unit of length

Ω fin efficiency. This can be assumed as 1 except for low thermal conductivity metals coupled with high heat transfer coefficients.

A_{EQ} equivalent heat transfer area of a finned tube per unit of length

$$= A_{RO} + \Omega (A_{FO}) \quad (6)$$

Rearranging Equation (5) and substituting h_T , h_F , and h_g from Equations (1), (2), and (4), respectively, the following relationship for the effective diameter of a finned tube, D_{EF} , may be obtained

$$\left(\frac{1}{D_{EF}} \right)^{1/4} = \frac{A_{RO}}{(D_{FR})^{1/4} (A_{EQ})} + \frac{1.3 \Omega (A_{FO})}{(H_M)^{1/4} (A_{EQ})} \quad (7)$$

Thus, Equation (4) with D_{EF} defined by Equation (7) gives a condensation heat transfer coefficient for a single horizontal finned tube. The above analysis is completely theoretical with the exception of the definition of H_M by Equation (3) which is reasonable but nonetheless somewhat arbitrary. However, Equation (4) gave surprisingly good results for condensation of organic vapors on single horizontal low finned tubes at low vapor velocity. This equation also was found to give surprisingly good prediction of condensation on tube bundles despite the fact that it was developed for a single tube under laminar condensate flow with negligible vapor velocity effect. Therefore, Equation (4) is suggested as a shortcut method for quick rating of finned tube bundles to determine an approximate average coefficient. However, for local heat transfer coefficient evaluation, a more sophisticated approach is required, and it is likely that there will be cases for which the single tube shortcut approximation will give very poor results.

EXTENSION TO FINNED TUBE BUNDLES

Equation (4) was derived for a single horizontal finned tube. For tube bundle application, two alternative methods were recommended, i.e., the ΔT_c form and the Reynolds number form.

• ΔT_c Form. The modified Nusselt equation was originally developed for plain tube bundles to take into account the effect of number of tubes in a vertical row. The same equation was adapted for finned tube bundles by replacing the plain tube diameter with D_{EF} as defined in Equation (7).

$$h_g = 0.725 \left[\frac{k_L^3 \rho_L (\rho_L - \rho_V) g \lambda}{\mu_L \Delta T_c (D_{EF})} \right]^{1/4} \frac{1}{(N_{RV})^m} \quad (8)$$

The original analysis by Nusselt shows that $m = 1/4$. However, Young and Ward [2] found that the data from various sources indicated that the correction factor of $1/(N_{RV})^{1/4}$ was too severe, and they introduced a correction factor, C_N , to be multiplied to the above original Nusselt equation (with $m = 1/4$) to account for a turbulence effect as follows:

$$h_g = 0.725 \left[\frac{k_L^3 \rho_L (\rho_L - \rho_V) g \lambda}{\mu_L \Delta T_c (D_{EF})} \right]^{1/4} \frac{C_N}{(N_{RV})^{1/4}} \quad (9)$$

Pearson and Withers [3] used the above Young and Ward formulation for the correlation of their data with Freon 22 condensing on low integral S/T type finned tube bundles. They found that with $N_{RV} = 4$ results were within 5 percent of the Katz Beatty correlation with full Nusselt tubebow correction [Equation (8) with $m = 1/4$]. Specifically, C_N was found to be 0.969 for tubes with 26 fins per in. and 0.949 for tubes with 19 fins per in. The data are all in the low vapor velocity flow region, all tubeside controlling, and with only four tubes in a vertical row it is not possible to determine the real significance of a tubebow correction. It is doubtful, therefore, whether these precise values would hold for other fluids or other bundle geometries so the realistic conclusion is that the original correlation held rather well for these new data. This type of formulation is an improvement on the previous approaches of arbitrarily adjusting the power on the number of tubebows to agree with the data, but is not as flexible in dealing mechanistically with the effects of a turbulent condensate film as is required for general method.

● Reynolds Number Form The temperature difference ΔT_c can be eliminated by applying the heat balance for the tube bundle

$$\begin{aligned} W_c \lambda &= (h_g) (\Delta T_c) (A_{EQ}) (L) (N_{TT}) \\ &= (h_g) (\Delta T_c) (\pi) (D_{EF}) (A_{TF}) (L) (N_{TT}) \end{aligned} \quad (10)$$

where W_c condensate flow rate
 L tube length
 N_{TT} total number of tubes
 A_{TF} effective heat transfer area ratio

$$= \frac{A_{EQ}}{\pi (D_{EF})} \quad (11)$$

As discussed above, the theoretical analysis of Nusselt for a plain tube bundle shows that the exponent m for tuberow correction is $1/4$. Replacing the plain tube diameter with the effective diameter for finned tube, the equation which is the same as Equation (8) with $m = 1/4$ is expressed as

$$h_g = 0.725 \left[\frac{k_l^3 \rho_l (\rho_l - \rho_v) g \lambda}{\mu_l \Delta T_c (D_{EF}) (N_{RV})} \right]^{1/4} \quad (12)$$

Substituting ΔT_c from Equation (10) into Equation (12) and rearranging the equation, the following Reynolds number form for laminar flow condensation heat transfer equation is obtained

$$h_g = 1.51 (k_l) \left[\frac{\rho_l (\rho_l - \rho_v) g}{\mu_l^2} \right]^{1/3} (Re_g)^{-1/3} (A_{TF})^{1/3} \quad (13)$$

The Reynolds number is defined in the same way as for plain tubes

$$Re_g = \frac{4\Gamma}{\mu_l} \quad (14)$$

$$\text{where } \Gamma = \frac{(W_c) (N_{RV})}{(L) (N_{TT})} \quad (15)$$

The factor $(A_{TF})^{1/3}$ in Equation (13) has the effect of modifying the Reynolds number so that the liquid loading is distributed over the finned surface thereby thinning the liquid film

The Nusselt analysis for a tube bundle given by Equation (12) assumes that the condensate film remains laminar for the entire tube bundle regardless of the value of N_{RV} . It imposes extreme penalties for large bundles. Actually, it is logical to assume that the condensate film will remain laminar only for a given number of tuberows and then become turbulent as the condensate Reynolds number exceeds a critical value. The condensate critical Reynolds number for a vertical row of plain tubes was assumed to be roughly around 800 for staggered arrays based on the analysis of the single phase friction factor curves for ideal tubebanks. However the presumed critical Reynolds number varies considerably with tube layout and pitch ratio. Theoretically, after the critical Reynolds number has been reached in flow down the tube bank, the condensing coefficient should begin to increase with Reynolds number, reflecting the effect of increasing turbulence.

The above theoretical approach, either ΔT_c form or Reynolds number form, accounts for the thinning of the condensate over a greater surface area of finned tube (see Figure 1) and thus results in much higher heat transfer coefficients, which was confirmed by data. However, since the classical Nusselt equation was developed for laminar film flow regime where vapor shear effect is negligible, this method was later proved by HTRI data to be too conservative at high vapor velocity.

• **Vapor Shear Effect** In an earlier (now obsolete) proprietary method for finned tube bundles, the vapor shear effect was accounted for conservatively by an empirical relationship which was referred to as the vapor shear correction factor, F_v , given by Equation (16). This factor was a multiplier to the modified Nusselt equation and came into effect for $Re_v > 30\,000$.

$$F_v = \left[1 + 1.5 \exp \left\{ \frac{-1.5 (10^5)}{Re_v} \right\} \right]^{2.5} \quad (16)$$

where the vapor Reynolds number, Re_v , is given by

$$Re_v = \frac{(D_{EQ}) (W_t) (y)}{(\mu_v) (S_{NETX})} \quad (17)$$

where W_t total flow rate

y vapor weight fraction

S_{NETX} net crossflow area for tube bundle

D_{EQ} projected equivalent diameter of a finned tube

Later analysis showed that the shear-controlled condensation regime for finned tubes could be correlated by a convective heat transfer model as was done for plain tubes, providing a much more logical method, which is described in a later section.

• **Condensate Retention Effect** Another important consideration in finned tube condensation is the effect of liquid retention on finned tubes (see Figure 2). This effect produces a tendency toward poor performance for fins with high surface tension liquids and high fin surface density. The effect of the condensate retention in grooves between fins was correlated as a function of fin geometry and liquid properties based on a theoretical approach by Katz et al [4] with empirical adjustment. In the original HTRI methods this was expressed as the thermal resistance factor, r_c , due to the retained condensate, and was given by

$$r_c = A_1 [1 + \tanh (\Lambda_T - 2.5)]^2 \quad (18)$$

where $\Lambda_T = B_g \left(\frac{\sigma g_c}{\rho_l g} \right)$ (19)

$$B_g = (N_f) \left[\frac{4 (D_{OF}) - 2 (D_{FR}) + \frac{2}{(N_f)}}{\frac{\pi}{4} \left((D_{OF}^2 - D_{FR}^2) \right)} \right] \quad (20)$$

Note B_g has the dimension of L^{-2} , and A_r is dimensionless

This thermal resistance factor was then used to find the liquid retention correction factor, F_r , as given by

$$F_r = \frac{1}{1 + (r_c)(h_g)} \quad (21)$$

The earlier method, which may still be used as a quick approximation, consisted of applying the corrections for velocity and condensate retention to the gravity-controlled film heat transfer coefficient as follows

$$h_{cf} = h_g (F_v)(F_r) \quad (22)$$

where h_g gravity-controlled condensation coefficient calculated from the Nusselt type equations with the effective finned tube diameter, D_{EF} , given by Equation (7)

F_r condensate retention correction For light hydrocarbon, and other fluids with low surface tension, $F_r \approx 0.8 - 1.0$ for typical low integral finned tubes F_r can be as low as 0.2 for water¹

F_v vapor shear correction from Equation 16, should be conservative

IMPROVED NEW APPROACH

The concept of separating gravity-controlled and shear controlled mechanisms, which was first successfully applied for tubeside condensation, is used in shellside condensation for finned tubes as well as plain tubes

In most practical cases, the vapor velocity is high enough to produce shear-controlled flow when condensation begins at the entrance of the condenser. Then there is a transition to gravity-controlled flow as more condensation takes place and the vapor velocity decreases. In the following discussion, the gravity-controlled laminar mechanism is discussed first to illustrate the difference between the new approach and the previous method

Gravity Controlled Flow Regime

Figure 3 illustrates the idealized flow situation of gravity-controlled regime for finned tubes. As will be discussed in the next section, the gravity controlled flow regime is defined as that for which vapor shear forces are negligible and all flow is vertically downward with the properties of the liquid film determined by gravity-dominated hydrodynamics. It is postulated that the following heat transfer regions can exist in the gravity-controlled flow regime

• **Laminar Film and Rippled Film Flow Region** If the vapor velocity is small and the vapor shear force is negligible, the condensate liquid flows downward from one tubewall to another. If the liquid Reynolds number is low enough the film is laminar and the modified Nusselt relation applies to the number of tubes in a vertical row. The heat transfer coefficient may be expressed for finned tubes by a Reynolds number form based on the work of Beatty and Katz [1] and Young and Ward [2]

$$Nu_{gR} = 1.51 (C_{fr}) (Re_g)^{-1/3} (A_{fr})^{1/3} \quad (23)$$

where $Nu_{gR} = \left(\frac{h_{gR} \ell}{k_g} \right) \left[\frac{\mu_g^2}{\rho_g (\rho_g - \rho_v) g} \right]^{1/3} \quad (24)$

Development is aided by analogy to a previously developed proprietary correlation for shellside plain tube condensation

$$\frac{h_s D_{EQ}}{k_f} = C (Re_s)^a (Pr_f)^b F_{tp} \quad (32)$$

Equation (32) is the Dittus Boelter type convective equation corrected by a factor F_{tp} which relates the two phase shear force to that for liquid flowing alone. For shellside flow it is well known that a direct analogy between pressure drop and heat transfer does not hold because of momentum change losses outside the thermal boundary layer, resulting in less effect on heat transfer. This trend is expected to be more pronounced for finned tubes than plain tubes because of more complicated geometry of finned tubes.

However, some functional relationship between heat transfer and pressure drop should still hold as it does in single phase flow.

The convection factor F_{tp} for shear-controlled crossflow finned tube bundle is therefore

$$(F_{tp})_x = \left[1 + \frac{C_x}{(\lambda_{tt})_x} + \frac{1}{(\lambda_{tt})_x^2} \right]^n \quad (33)$$

where $(\lambda_{tt})_x$ the Martinelli two phase flow parameter at local crossflow condition

C_x Chisholm C factor adapted for crossflow two phase pressure drop [13]

Here, the exponent, n , in Equation 33 is theoretically 0.5 for ideal conversion of momentum to heat transfer. The value of n should be determined empirically for finned tube bundles, and will be less than 0.5.

The majority of shellside condensers in practical use are baffled exchangers. The new methods described in the preceding sections apply only to the crossflow section of a tube bundle. However, special treatment for the window flow heat transfer coefficient is necessary only for the shear-controlled flow regime in window flow area, because the assumed mechanisms of the gravity-controlled heat transfer apply to either crossflow or window flow sections of tube bundles as long as the vapor shear forces are negligible. In the absence of data for finned tube windowflow, it is suggested that F_{tp} for windowflow be based on plain tube data. This is likely to produce a lower value for the windowflow coefficient than the crossflow coefficient which is reasonable due to the longitudinal flow component. It is possible that some additional penalty should be applied to the coefficient especially for viscous liquids to account for ineffective heat transfer in the fin grooves in longitudinal flow. However, for good designs, the amount of longitudinal flow with radial finned tubes should be minimized and this effect, therefore, should not be a significant one.

COMPARISON WITH DATA

The data used for comparison consist of 351 runs for pure components. The evaluation presented in this paper does not include an extensive new set of data for finned tube bundles taken since 1979. Five different bundle geometries are included consisting of two ideal tube banks, one baffled bundle, and two nonbaffled bundles. The pertinent description of the condensers is given in Table 1. Fluids used in the test include n-pentane, steam, acetone, isopropanol, Freon 113 and Freon 22, covering a wide range of physical properties. Freon 22 runs were taken from a published article by Pearson and Withers [3].

• **Developed Turbulent Region** As the gravity-controlled draining condensate film becomes turbulent due to dripping and splashing with increasing condensate loading, the heat transfer mechanism is postulated to be the convective type and can be expressed as a form analogous to that for turbulent flow down a vertical surface. Kirkbride [9] has correlated the turbulent film condensation data measured by Badger et al. [10] for vertical downflow on pipe as

$$\left(\frac{h_{gt}}{k_L} \right) \left[\frac{\mu_L^2}{\rho_L^2 g} \right]^{1/3} = 0.0133 (Re_g)^{0.4} \quad (26)$$

Labuntsov [11] has presented a correlation for downflow on vertical surface which is supported by extensive test results as

$$\left(\frac{h_{gt}}{k_L} \right) \left[\frac{\mu_L^2}{\rho_L^2 g} \right]^{1/3} = 0.01725 (Re_g)^{1/4} (Pr_L)^{1/2} \quad (27)$$

A proprietary correlation for horizontal plain tubes has the following form

$$\left(\frac{h_{gt}}{k_L} \right) \left[\frac{\mu_L^2}{\rho_L (\rho_L - \rho_v) g} \right]^{1/3} = A_2 (Re_g)^{1/3} (Pr_L)^{1/3} \quad (28)$$

It is possible to adapt the correlation developed for plain tubes to finned tube application. However, the hypothetical film thickness of plain tube condensation should be reduced by the finned tube area ratio, A_{TO} , defined by Equation (31) to obtain the equivalent film thickness for finned tube. Therefore, the Nusselt expression for turbulent condensate film heat transfer can be given as

$$Nu_{gt} = A_3 (Re_g)^{1/3} (Pr_L)^{1/3} (A_{TO})^{1/3} \quad (29)$$

$$\text{where } Nu_{gt} = \left(\frac{h_{gt}}{k_L} \right) \left[\frac{\mu_L^2}{\rho_L (\rho_L - \rho_v) g} \right]^{1/3} \quad (30)$$

$$A_{TO} = \frac{A_{RO} + A_{FO}}{\tau (D_{EQ})} \quad (31)$$

All the condensation heat transfer correlations proposed in the gravity-controlled flow regime are summarized in Figure 4 as a combined curve incorporating the proposed mechanistic models for each of the condensation regions for the case of a 3/4-in OD (nominal), 19 fins/in, integral low-finned tube bundle with 45 degree tube layout angle, as an example.

Shear-Controlled Flow Regime

At high vapor velocity, the thickness of the condensate film on the tubes is determined by the shear force on the film rather than by gravity, and the film is normally turbulent. This mechanism is illustrated in Figure 5. The Nusselt type formulation no longer applies, and a new correlating form based on the groups significant to convective heat transfer should be used. Hence, the tubewall effect is eliminated. Also, in the limit it should not matter whether the flow is downflow or crossflow.

TABLE 1 - Finned tube bundle geometry specifications

Bundle	Number of Tubes	Flow Type Code (*)	Nominal Tube OD		Tube Pitch Ratio	Tube Layout Angle	Average Number of Tubes in Vertical Row	Number of Fins per Unit Length (°)		Number of Data Points
			in	mm				in	m	
518 1	72	a	5/8	15.9	1.300	45	4.5	19	748	93
518 2	72	a	5/8	15.9	1.300	45	4.5	19	748	140
519	33	a	5/8	15.9	1.300	45	4.5	19	748	25
C2 (†)	660	b	1/2	12.7	1.375	45	15.0	19	748	71
19 (‡)	60	c	3/4	19.0	1.250	30	4.0	26	1 024	10
26 (‡)	60	c	3/4	19.0	1.250	30	4.0	26	1 024	12

Notes (*) Flow Types a Ideal tube bank, horizontal crossflow of vapor

b Baffled bundle, horizontal crossflow plus windowflow

c Nonbaffled bundle, gravity downflow

(†) HTRI bundle, 11.24 in (285 mm) baffle spacing, 45.8 percent vertical baffle cut

(‡) Ref 3 bundle, refrigeration type

(°) Standard Wolverine type low fin geometry

The final results are summarized in Figure 6 as the plot of the error ratio against the average vapor Reynolds number (evaluated at the mean vapor weight fraction of the inlet and outlet)

It can be seen that the range of average Re_v covered by the data was from 200 to 100 000 and that the majority of points are well predicted

CONCLUSIONS AND RECOMMENDATIONS

A method for predicting local shellside condensate film heat transfer coefficients on finned tubes has been developed based on the concept of controlling condensation mechanisms for local conditions of vapor shear and liquid film turbulence. The new developments presented in this paper are

- Use of a modified Katz Beatty approach for the finned tube effects in gravity-controlled flow
- A new model incorporating a Prandtl number effect for gravity-controlled transition flow
- Use of an empirically developed condensate retention correction to penalize high surface tension fluids
- Use of a Dittus Boelter type convective equation in shear-controlled flow

I.CHEM.E. SYMPOSIUM SERIES NO. 75

Based on the comparison with 351 data points from ideal tube banks, a baffled condenser and a nonbaffled condenser, the new method shows substantial improvement in the prediction of heat transfer coefficients over any previous approach. However, further refinements may be necessary as additional data become available, especially in the following respects:

- a. Data on large commercial-sized units with diverse fluids.
- b. Visual data for shellside two-phase flow aimed at confirming and/or developing better flow regime maps.

As a special consideration, the ideal plain tube bank data of Hawes [12] were recently reviewed. These data are for very high velocity vapor (greater than 75 ft/sec) and very high vapor quality (greater than 0.9) and show that in this region the heat transfer coefficient can decrease with increasing velocity. This indicates an additional heat transfer mechanism not covered in this report which may be due to effective superheating from excessive pressure drop, viscous dissipation, and loss of liquid film on part of the tube surface. Since the effect can exist only for an insignificant entrance region in an actual condenser, the consideration of the mechanism involved is interesting but rather academic. However, this effect will be further investigated, if possible, during planned experimentation on shear-controlled condensation in baffled bundles.

It should also be noted that, while the condensing heat transfer coefficient is usually greater in shear-controlled flow than in gravity-controlled flow, this is not always the case since, under some conditions, there can be hindrance of free drainage of the condensate due to the vapor velocity which increases the condensate film thickness and decreases the coefficient. This effect has been observed in the methods shown here and will also be further investigated.

ACKNOWLEDGEMENT

The authors are grateful to the Technical Committee of HTRI for permitting publication of this paper.

NOMENCLATURE

The consistent sets of units to use for both the US Customary and SI systems are given in the following nomenclature. Unless otherwise noted, all the heat transfer coefficients used in this report are referred to shellside area, i. e., based on tube outside area including finned surface. (Due to lack of time, it was not possible to convert symbols to format recommended by the International Centre for Heat and Mass Transfer. The following symbols are consistent with current US practice).

- A_1 = condensate retention constant ($\text{m}^2 \text{ K/W}$)
- A_2 = turbulent film constant, plain tubes
- A_3 = turbulent film constant, finned tubes
- a = exponent
- A_{EQ} = equivalent heat transfer area of a finned tube per unit of length (m^2/m)
- A_{FO} = finned area exclusive of root area for one tube per unit of length (m^2/m)

- A_{OIR} = ratio of total outside finned tube area to tube inside area
 A_{If} = effective area ratio for low finned tube
 A_{TO} = finned tube area ratio
 A_{RO} = root area for one tube per unit of length (m^2/m)
 b = exponent
 B_g = parameter for liquid retention correction (m^{-2})
 C = constant
 C_{lr} = correction to the Nusselt equation due to rippling of the laminar film to account for higher heat transfer
 C_N = tubeword correction factor for tube bundle condensation heat transfer coefficient
 $(C_p)_l$ = liquid heat capacity ($J/kg\ K$)
 C_x = crossflow C factor
 D_{EF} = effective diameter for condensation on a finned tube (m)
 D_{EQ} = projected equivalent diameter for finned tube (m)
 D_{FR} = root diameter of finned tube at the base of the fin (m)
 D_{OF} = over fin diameter (m)
 F_H = fin height (m)
 F_r = liquid retention correction factor
 F_{tp} = two phase convection factor
 $(F_{tp})_x$ = two-phase correction factor for crossflow
 $(F_{tp})_w$ = two phase correction factor for windowflow
 F_v = vapor shear correction factor
 g = acceleration of gravity ($9.81\ m/s^2$)
 g_c = conversion factor (1)
 h_{cf} = heat transfer coefficient for the condensate film ($W/m^2\ K$)

- h_f = condensation heat transfer coefficient for vertical surface of a fin ($\text{W/m}^2 \text{ K}$)
- h_g = condensing heat transfer coefficient in gravity-controlled film ($\text{W/m}^2 \text{ K}$)
- h_{gl} = condensation heat transfer coefficient for gravity-controlled laminar flow ($\text{W/m}^2 \text{ K}$)
- h_{gt} = condensation heat transfer coefficient for gravity-controlled turbulent film ($\text{W/m}^2 \text{ K}$)
- h_t = condensation heat transfer coefficient for root area of a finned tube ($\text{W/m}^2 \text{ K}$)
- h_s = condensing heat transfer coefficient in shear-controlled flow ($\text{W/m}^2 \text{ K}$)
- h_M = mean height of finned area (m)
- k_l = liquid thermal conductivity (W/m K)
- L = tube length (m)
- L_F = mean fin thickness (m)
- m = exponent
- n = exponent on $(F_{tp})_x$ equation
- N_F = number of fins per unit tube length (1/m)
- N_{RV} = number of tubes in a vertical row (average for circular bundle)
- $(N_{RV})_e$ = effective number of tubes in a vertical row
- N_{TT} = total number of tubes in the bundle or bank
- Nu_g = Nusselt number for gravity-controlled flow regime
- Nu_{gl} = Nusselt number for gravity-controlled laminar film
- Nu_{gt} = Nusselt number for gravity-controlled turbulent film
- Pr_l = liquid Prandtl number
- Q = total heat duty (W)
- r_c = thermal resistance factor ($\text{m}^2 \text{ K/W}$)

Re_g = Reynolds number for gravity-controlled liquid film

Re_s = Reynolds number for shear-controlled liquid film

Re_v = vapor Reynolds number

S_{NETX} = net crossflow area for tube bundle (integral average for circular bundle) (m^2)

W_c = condensation flow rate (kg/s)

W_t = total flow rate (kg/s)

$(X_{tt})_x$ = Martinelli two phase parameter for crossflow

y = weight fraction vapor

Greek Letters

Γ = liquid loading (flow rate/length)

ΔT_c = temperature difference between wall and bulk of condensing fluid (K)

λ = latent heat of vaporization (J/kg)

Λ_T = parameter for liquid retention correction

μ_l = liquid viscosity (Ns/m^2)

μ_v = vapor viscosity (Ns/m^2)

ρ_l = liquid density (kg/m^3)

ρ_v = vapor density (kg/m^3)

σ = liquid surface tension (N/m)

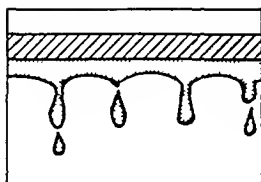
Ω = fin efficiency

REFERENCES

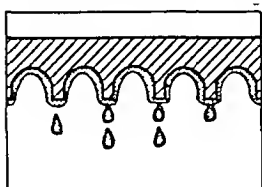
- 1 Beatty, K O, Jr and Katz, D L. (1948) "Condensation of Vapors on Outside of Finned Tubes," Chem Eng. Prog., 44, No 1
- 2 Young, E H, and Ward D J, Nov 1957 "How to Design Finned Tube Shell and Tube Heat Exchangers, Part 2 Design of Finned Tube Condensers," The Refining Engineer, 7-10
- 3 Pearson, J F and Withers, J G, June 1969 "New Finned Tube Configuration Improves Refrigerant Condensing," ASHRAE Journal

- 4 Katz, D L., Hope, R C , and Datsko, S C , written August 1946, reproduced April, 1947 "Liquid Retention on Finned Tubes," Dept of Eng Research, University of Michigan, Ann Arbor, Michigan, Project M592, Wolverine Tube Division, Calumet & Hecla Consolidated Copper Company
- 5 Dukler, A E , and Bergelin, O P , (1952) "Characterstics of Flow in Falling Liquid Films," Chem Eng Prog , 48, 557
- 6 Kutateladze, S S , 1963 "Fundamentals of Heat Transfer," Edward Arnold, London
- 7 Gngull, U , (1952) "Warmeubergang bei Film Kondensation," Forsch Gebiete Ingenieurw , 18, 10
- 8 McAdams, W H , (1954) "Heat Transmission," 3rd Edition, McGraw Hill, New York
- 9 Kirkbride, C G , (1934) "Heat Transfer by Condensing Vapor on Vertical Tubes," Ind Eng Chem , 26, 425
- 10 Badger, W L., Monrad, C C , and Diamond, H W , (1930) "Evaporation of Caustic Soda to High Concentrating Means of Diphenyl Vapors," Ind Eng Chem , 22, 700
- 11 Labuntsov, D A , (1960) "Heat Transfer During Condensation of Steam on a Vertical Surface in Conditions of Turbulent Flow of a Condensate Film," Inzhenerno Fizicheski Zhurnal, 3, No 8, 3-12
- 12 Hawes, R I, 1976 "Effect of Vapor Crossflow Velocity on Condensation," NEL Report No 619, National Engineering Lab , E Kilbride, Glasgow
- 13 Ishihara, K , Palen, J W , and Taborek, J , (1979) "Critical Review of Correlation for Predicting Two Phase Flow Pressure Drop Across Tube Bundles," Heat Trans Eng 1, No 3 , 1979

Liquid Film on Bottom of Plain Tube



Liquid Film on Bottom of Finned Tube



Thinner Film; Improved Drainage

Figure 1 Illustration of enhanced heat transfer for finned tubes in gravity-controlled flow

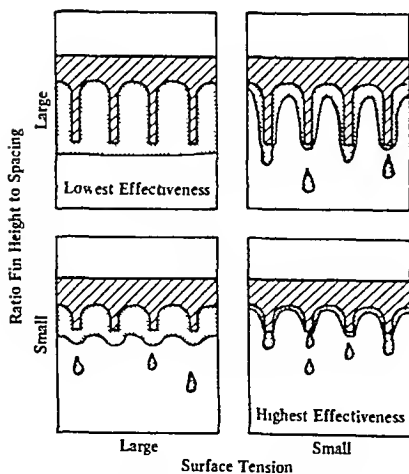


Figure 2 Condensate retention effect as a Function of fin geometry and fluid


Flow Situation		Proposed Heat Transfer Model
Laminar Film		Nusselt Model (Function of effective area ratio, A_{ef})
		Prorated Correction
Ruppled Film		Modified Nusselt Model (Function of Prandtl Number)
Transition		Constant Nusselt Number (Function of Actual Area Ratio, A_{p0} and Prandtl Number)
Turbulent Film		Convective Model (Dittus-Boelter type convective correlation)

Figure 3 Gravity-controlled flow model for finned tubes

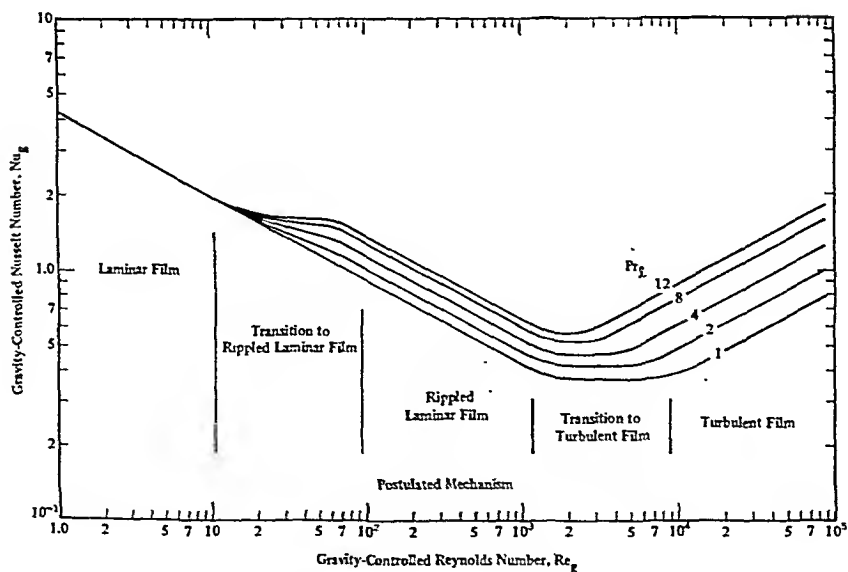


Figure 4 Generalized prediction of local condensation heat transfer coefficient, gravity-controlled film, horizontal finned tube bundle, 45° layout, 3/4 inch (19.05 mm) outside tube diameter, 19 low fins per inch.

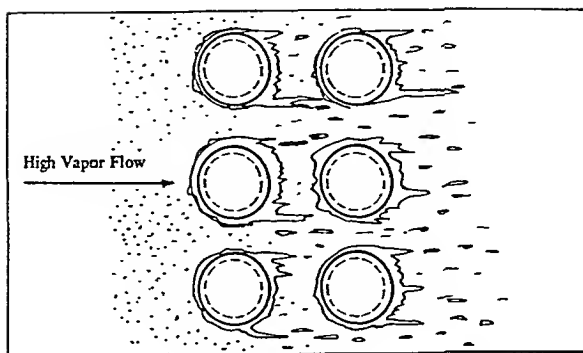


Figure 5 Vapor shear-controlled condensation on bank of finned tubes

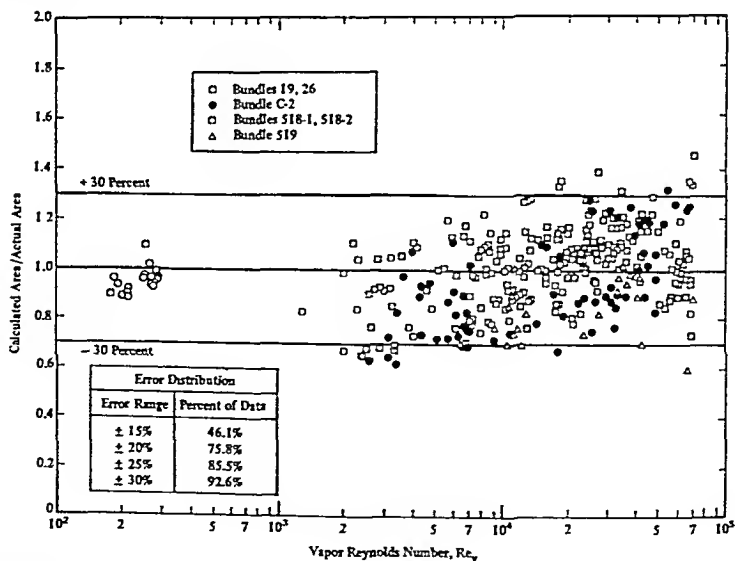


Figure 6 Error ratio plot

AN ASSESSMENT OF DESIGN METHODS FOR MULTICOMPONENT CONDENSATION AGAINST DATA FROM EXPERIMENTS ON A HORIZONTAL TUBE BUNDLE

J M McNaught*

Two types of design method, (a) Silver's method, based on a pre-determined temperature/enthalpy relationship and (b) film theory mass-transfer models, are compared and assessed against the data of Shah and Webb for condensation of one or two vapours from a non-condensing gas on a horizontal tube bundle. This study supplements previous work which considered multicomponent condensation inside a vertical tube. Silver's method yields satisfactory heat load predictions that are not significantly poorer than those of the more complex and rigorous mass-transfer models. The mass-transfer model gives the more accurate prediction of outlet condensate composition, though neither model is wholly satisfactory.

INTRODUCTION

The objective of this paper is to compare and assess design methods for multicomponent condensation against the experimental data of Shah and Webb (1,2) for condensation of one or two vapours from a non-condensing gas on a horizontal tube bank. A similar comparison was made in a previous paper⁽³⁾ for condensation inside a vertical tube, and it also contains a description and analytical comparison of the two types of design method considered: Silver's and those based on mass-transfer models. The interest in extending the in-tube experiments to a horizontal tube-bank lies mainly in the different hydrodynamic conditions.

DESIGN METHODS

In the method used by Silver⁽⁴⁾ and almost universally applied in condenser design, the condensation rate is evaluated implicitly by calculating the sensible heat-transfer rate from the gas-phase and adopting the approximation of a pre-determined temperature/enthalpy relationship. This relationship is usually obtained from the integral condensation curve, in which it is considered that the vapour mixture and accumulated condensate are well-mixed and in equilibrium at the same temperature. With the film-theory mass-transfer correction, justified on theoretical⁽⁵⁾ and experimental⁽³⁾ grounds, applied to the dry-gas heat-transfer coefficient α_g , the equation for the local overall heat-transfer coefficient α_o is:

*Heat Transfer and Fluid Flow Service,
National Engineering Laboratory, East Kilbride, Glasgow, United Kingdom

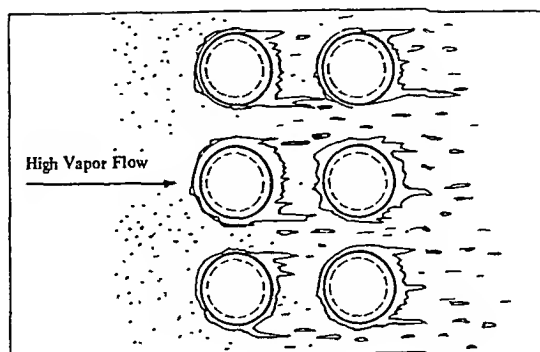


Figure 5 Vapor shear-controlled condensation on bank of finned tubes

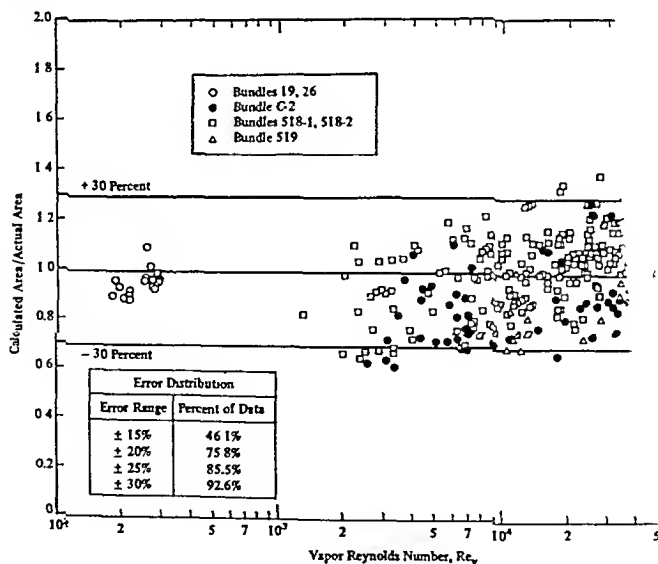


Figure 6 Error ratio plot

$$\frac{1}{\alpha_{ov}} = \frac{1}{\alpha_f} + \frac{1}{\alpha_g} \frac{dQ_g}{dQ_T} \quad (1)$$

Here Q_g and Q_T represent the sensible heat-transfer rate from the gas phase and the total heat-transfer rate respectively according to the temperature/enthalpy relationship.

A more advanced approach is adopted in the application of film-theory mass-transfer models, as in the Colburn-Hougen⁽⁶⁾ and Colburn-Drew⁽⁷⁾ methods for binary systems, and the matrix model of Krishna and Standart⁽⁸⁾ for multi-component systems. In this method condensation rates are calculated explicitly using mass-transfer coefficients and concentration driving forces. The condensation curve concept is not used, and the downstream development of temperature and concentration profiles is entirely determined by integration of local heat- and mass-transfer rates.

An essential difference between the two approaches is that in Silver's method the phases are considered to be in equilibrium at the bulk gas-phase temperature, while in the mass-transfer models the equilibrium state occurs at the condensate-vapour interfacial temperature. The methods therefore predict different liquid concentration profiles. The results of the in-tube study⁽³⁾ showed that the mass-transfer models gave a significantly superior prediction of condensate composition, and it was concluded that the method represents a consistent model of the heat- and mass-transfer processes which can be applied in design with greater confidence than Silver's method.

The increased rigour of the mass-transfer models is of course only achieved through the expenditure of increased computing time and effort, and the input of diffusivities. It is of great importance to continue to assess the benefits of the method against experimental data. A condensing stream is often directed to the shellside of a shell-and-tube heat exchanger, and the tube bundle data of Shah and Webb^(1,2) clearly provide a relevant test under different hydrodynamic conditions from the in-tube study.

TEST APPARATUS AND SYSTEMS

The test condenser and other apparatus are fully described by Shah and Webb⁽²⁾. The condenser has 50 stainless steel tubes of 0.0127 m o.d., 0.0109 m i.d. and of length 0.18 m. The tubes are horizontal on a 0.025 m equilateral triangular pitch in nine rows of six and five tubes alternately. There are half-tubes on the walls to prevent bypassing.

The experiments considered here cover condensation of one or two vapours from a non-condensing gas. The binary systems are methanol-nitrogen, methanol-carbon dioxide, methanol-Refrigerant 12 and isopropanol-nitrogen with a total of 43 runs. The ternary systems involve condensation of water and methanol from the non-condensing gases nitrogen, carbon dioxide and Refrigerant 12, and water-isopropanol-nitrogen giving a total of four systems and 80 runs. In this comprehensive set of data the vapour composition and heat load were varied as widely as possible.

ANALYSIS OF EXPERIMENTAL RESULTS

Computer programs were written to simulate the condenser performance from the measured inlet conditions. The differential equations describing the downstream development of conditions were integrated numerically using a Runge-Kutta method. This is in contrast to Shah's⁽¹⁾ analyses which employed a row-to-row difference method. In the simulation a correlation of the form

$$j_H = \frac{Nu_g}{Pr_g^{1/3} Re_g} = a Re_g^b \quad (2)$$

was applied to evaluate the dry-gas heat-transfer coefficient α_g . The values $a = 0.315$ and $b = -0.396$ obtained by Sheh⁽¹⁾ from experiments on cooling nitrogen in the same apparatus were applied to all of the condensing systems. The Chilton-Colburn analogy was used to obtain the mass-transfer coefficient in the usual way from

$$\beta_g = \frac{\alpha_g}{\tilde{c}_{p,g}} \left(\frac{Pr_g}{Sc_g} \right)^{1/3} \quad (3)$$

For consistency the coolant resistance was evaluated using the same correlation, that of Allen and Eckert⁽⁹⁾, as was used by Shah and Webb in correlating the dry-gas heat-transfer coefficient in the same apparatus. For the same reason a tube-side fouling resistance of $0.000176 \text{ m}^2\text{K/W}$ was applied. The condensate heat-transfer coefficient was obtained using Nusselt's equation for the top row with an inundation correction for subsequent rows from Grant and Osment's⁽¹⁰⁾ correlation.

The two methods used in the simulations were:

a Silver's method, with wet-wall desuperheating assumed at entry. The temperature/enthalpy relationship was evaluated at the saturation temperature T_d and a correction applied to account for the additional heat flux due to desuperheating. The local overall heat-transfer coefficient α_{ov} defined by

$$q_w = \alpha_{ov}(T_d - T_o) \quad (4)$$

is then given by

$$\frac{1}{\alpha_{ov}} = \frac{1}{\alpha_f} + \frac{1}{\alpha_g^*} \frac{Z(T_d - T_S)}{T_d - T_S + Z(T_G - T_d)} \quad (5)$$

where the gradient $Z (= dQ_G/dQ_T)$ was evaluated at T_d from the integral condensation curve. The equation describing the downstream development of the saturation temperature is

$$\dot{M}_g c_{p,g} dT_d/dA = -\alpha_g^*(T_d - T_S). \quad (6)$$

This, together with the integral condensation curve, is sufficient to determine the downstream development of the bulk compositions. The actual bulk gas-phase temperature profile is given by

$$\dot{M}_g c_{p,g} dT_g/dA = -\alpha_g^*(T_g - T_S). \quad (7)$$

b Mass-transfer models, with a Colburn-Hougen⁽⁶⁾ approach for binary systems and the matrix model of Krishna and Standart for ternary systems. In the Colburn-Hougen method the vapour molar flux is given locally by

$$\dot{n}_V = \beta_g \ln \frac{1 - \tilde{y}_{VS}}{1 - \tilde{y}_{VG}} \quad (8)$$

with β_g obtained from equation (3). The matrix model applied to condensation represents a multi-component generalisation of the Colburn-Hougen approach. Application of the model to condensation from ternary systems is described by Krishna and Panchal⁽¹¹⁾. The assumption of perfect mixing in the liquid phase, which corresponds to integral condensation in Silver's method, was adopted. A few sample runs confirmed that there was virtually no difference between this assumption and the alternative of no-mixing in the small scale of the test condenser. Equation (7) was applied to obtain the bulk gas-phase temperature profile, and for the molar flowrate \dot{N}_{g1} of each component in the gas phase

$$d\dot{N}_{g1}/dA = -\dot{n}_1 \quad (9)$$

COMPARISON OF PREDICTION AND EXPERIMENTAL RESULTS

In this section overall measurements of heat load and condensate flowrate and composition are compared with the predictions of the methods described above. Such comparisons are only valid in partial condensation if the test condenser is large enough to prevent undue magnification of local errors in prediction, whilst avoiding an excessive relative variation in the overall heat-transfer coefficient. The data considered here satisfy this criterion.

Single Vapour with Non-condensing Gas

Comparisons of the predictions of the Colburn-Hougen⁽⁶⁾ method and Silver's⁽⁴⁾ method (including the film-theory mass-transfer correction) with the reported measurements of Shah⁽¹⁾ of overall heat load and condensation rate are shown in Figures 1 and 2.

The abscissa is the mean value of the parameter F , defined in Reference 3 as the ratio of the molar fluxes obtained from the Colburn-Hougen and Silver methods. It is given locally by:

$$F = \frac{\tilde{c}_{p,g} B (\tilde{c}_{p,v} / \tilde{c}_{p,g})^{(1/Le^3)}}{\tilde{c}_{p,v} B - 1} \sim \frac{1}{T_G - T_S} \frac{\tilde{y}_{VG} - \tilde{y}_{VS}}{T_G - T_S} \left/ \frac{1}{P} \left(\frac{dP_{VG}}{dT} \right)_{SAT} \right. \quad (10)$$

$$\text{where} \quad B = \frac{1 - \tilde{y}_{VS}}{1 - \tilde{y}_{VG}} \quad (11)$$

The parameter F gives a measure of local differences in prediction between the Colburn-Hougen and Silver methods for the same bulk conditions. Overall differences are smaller.

There is little difference between the total heat load predictions of the two methods. The methanol data are predicted to within ± 15 per cent by the Silver (with the mass-transfer correction) and Colburn-Hougen methods, though

the isopropanol data are less well predicted. However Shah⁽¹⁾ reports that these data were obtained in a preliminary study before the experimental procedures and data acquisition systems were fully developed, and are therefore less reliable than the methanol data.

The Colburn-Hougen method yields a slightly better prediction of condensation rate than Silver's method. The predictions of both methods for the methanol data are generally within ± 20 per cent of the measurements. The isopropanol-nitrogen data are again less well predicted.

Two Vapours with Non-condensing Gas

A comparison of predicted and measured heat load for the ternary data is shown in Figure 3. The abscissa is the condensate mole fraction of water, and it illustrates the wide range of composition over which the data were gathered. With the exception of the water-isopropanol-nitrogen data, which are subject to the same uncertainty as the isopropanol-nitrogen data, most of the data are predicted by both the Silver and matrix methods to within ± 10 per cent.

A quantity which gives a fair representation of the ability of the methods to predict outlet condensate composition is the ratio of the component liquid molar flowrates $\dot{N}_{L,1}/\dot{N}_{L,2}$, given alternatively by $\tilde{x}_1/(1 - \tilde{x}_1)$. Predicted/measured values of this quantity are displayed in Figure 4, where the subscript 1 refers to water. It is clear that the matrix method gives the more accurate prediction of composition, with the quantity $\dot{N}_{L,1}/\dot{N}_{L,2}$ generally predicted to within ± 25 per cent. Silver's method can however give quite inaccurate predictions of condensate composition, with errors of up to 70 per cent in $\dot{N}_{L,1}/\dot{N}_{L,2}$.

DISCUSSION

The results from the single vapour/non-condensing gas studies are similar to those of the previous in-tube paper⁽³⁾. Provided that wet-wall desuperheating is properly accounted for, Silver's method gives total heat load predictions that are not significantly poorer than those of the Colburn-Hougen method. The condensation rate predictions of Silver's method are only marginally poorer, but this is a reflection of the systems studied. In the in-tube study, Silver's method gave significantly poorer predictions of condensation rate for values of F (equation (10)) less than about 0.8; in the present study the minimum value of F is around 0.85.

Similarly, there is little difference between the errors in the total heat load predictions of Silver's method and the matrix method in the ternary study. As would be expected from the different approaches to the phase equilibrium state of the methods, there are considerable differences in the predictions of condensate outlet composition. The measured composition generally lies between the Silver and matrix method predictions, with the matrix method giving the better prediction over the whole composition range. It is not to be expected that the fractional condensation curve concept (used in Silver's method) would provide an accurate representation of condensate composition profiles. Since phase equilibrium is unrealistically considered to occur at the bulk gas-phase temperature Silver's method tends to over-estimate the condensate composition of the less volatile component. However, the indication from the results is that the apparently more realistic

mass-transfer model, in which it is considered that phase equilibrium occurs at the interface between the vapour and liquid on the tubea, does not provide a wholly satisfactory representation, though it is closer to the measurements. Certainly the condensate composition predictions are poorer than those observed by Sardesai⁽¹²⁾ for vertical in-tube condensation.

One possible explanation is that there is significant further phase change, not well represented by film theory, due to direct contact of vapour and condensate. It is significant that Shah and Webb^(1,2) were able to substantially improve their predictions of the bulk gas-phase temperature drop by including a simple model of heat- and mass-transfer to condensate droplets in the free spaces between the tube rows. Further support for this suggestion comes from the measurements of condensate outlet temperature, which are generally well in excess of the predicted condensate surface temperatures. In addition it is possible that film theory is less representative of mass-transfer to the disturbed liquid films on horizontal tube bundles than to a vertically falling film on the inside of a tube.

Though an improved mass-transfer model taking into account mass transfer to droplets by some mechanism other than film theory can be envisaged, the adequacy of the heat load predictions means that the incentive to proceed in this direction is not strong.

CONCLUSIONS

Data from condensation of one or two vapours from a non-condensing gas on the outside of a horizontal tube bundle have been compared with the predictions of design methods based on

- a a predetermined temperature/enthalpy relationship (Silver's method), and
- b film theory mass-transfer models (Colburn-Hougen, Krishna and Standart).

There is little difference between the errors in the total heat load predictions of the methods, provided that wet-wall desuperheating is realistically modelled in Silver's method and the film-theory mass-transfer correction is applied. The heat load predictions are satisfactory, being generally within ± 20 per cent of the measurements.

The measured condensation rates for the single vapour/non-condensing gas systems are well predicted by both methods. The conditions of the experiments are such that differences between Silver's method and the Colburn-Hougen method would be expected to be small.

Neither Silver's method nor the film-theory mass-transfer model accurately predicts the outlet condensate composition in the ternary data, though the mass-transfer model is closer to the measurements. The measured composition lies between the predictions of the methods and the indication is that the film-theory picture of mass transfer to a smooth condensate surface on the tubes is supplemented by further phase interactions.

ACKNOWLEDGEMENT

This paper is presented by permission of the Director, National Engineering Laboratory, Department of Industry.

The work was carried out under the research programme of the Heat Transfer and Fluid Flow Service and was supported by the Materials and Chemicals Requirements Board of the Department of Industry, United Kingdom. This paper is Crown copyright.

SYMBOLS USED

- A = Surface area (m^2)
 B = Parameter defined by equation (11)
 c_p = Specific heat capacity (J/kg K)
 F = Parameter defined by equation (10)
 j_H = J-factor for heat transfer
 Le = Lewis number ($= Sc/Pr$)
 \dot{M} = Mass flowrate (kg/s)
 \dot{N} = Molar flowrate (kmol/s)
 \dot{n} = Molar flux (kmol/ m^2s)
 Nu = Nusselt number
 P = Total pressure (N/ m^2)
 p = Partial pressure (N/ m^2)
 Pr = Prandtl number
 Q = Heat-transfer rate (W)
 q = Heat flux (W/ m^2)
 Re = Reynolds number
 Sc = Schmidt number
 T = Temperature (K)
 \tilde{x} = Mole fraction (liquid phase)
 \tilde{y} = Mole fraction (vapour phase)
 Z = Gradient dQ_G/dQ_T

- α = Heat-transfer coefficient ($\text{W/m}^2 \text{ K}$)
 β = Mass-transfer coefficient ($\text{kmol/m}^2 \text{ s}$)

SUBSCRIPTS

- d = Equilibrium
 f = Condensate + wall + fouling + coolant
 G = Bulk gas phase
 g = Gas phase
 i = Component identifier
 o = Coolant
 ov = Overall
 S = Condensate surface
 SAT = Saturation condition
 T = Total
 V = Vapour
 W = Wall

SUPERSCRIPTS

- ~ = Molar quantity
 • = Correction for mass transfer

REFERENCES

- 1 Shah, A. K., 1981, "Condensation of vapours on a horizontal tube bank", PhD Thesis, University of Manchester, Institute of Science and Technology, UK.
- 2 Shah, A. K. and Webb, D. R., 1983, "Multicomponent condensation in downwards flow over a horizontal tube bank", Conference Proceedings "Condensers - Theory and Practice", Manchester, UK.
- 3 McNaught, J. M., 1981, "An assessment of design methods for condensation of vapours from a non-condensing gas", Conference Proceedings "Advancement in heat exchangers - 1981 ICHMT International Seminars", Dubrovnik, Yugoslavia.
- 4 Silver, L., 1947, Trans. Instn Chem. Engrs, 25, 30.

- 5 McNaught, J. M., 1979, "Mass-transfer correction terms in design methods for multi-component/partial condensers." Condensation Heat Transfer, 18th Nat. Heat Transfer Conf., San Diego, Calif., 6-8 August 1979, New York: ASME.
- 6 Colburn, A. P. and Hougen, O. A., 1934, Ind. Engng Chem., 26, 1178.
- 7 Colburn, A. P. and Drew, T. B., 1937, Trans. Am. Instn Chem. Engrs. 33, 197.
- 8 Krishna, R. and Standart, G. L., 1976, AIChEJ. 22(2), 383.
- 9 Allen, R. W. and Eckert, E. R. G., 1964, J. Heat Transfer 86(3), 301.
- 10 Grant, I. D. R. and Osment, B. D. J., 1968, "The effect of condensate drainage on condenser performance", National Engineering Laboratory, East Kilbride, Glasgow, UK, NEL Report No 350.
- 11 Krishna, R. and Panchal, C. B., 1977, Chem. Engng Sci. 32, 741.
- 12 Sardesai, R. G., 1979, "Studies in condensation", PhD Thesis, University of Manchester, Institute of Science and Technology, UK

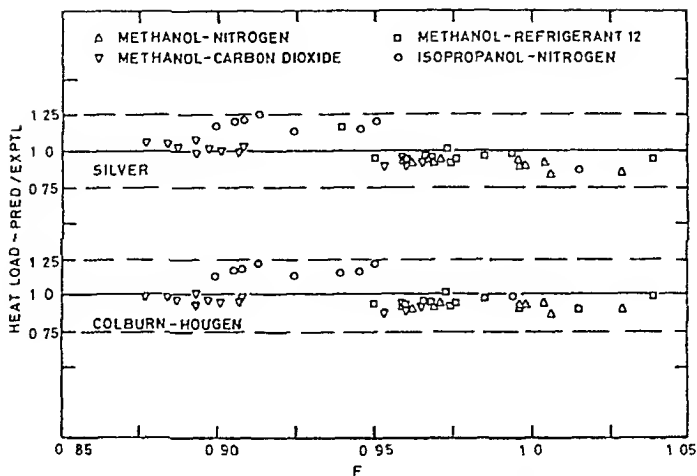


FIG 1 COMPARISON OF PREDICTED AND MEASURED HEAT LOAD
—BINARY SYSTEMS

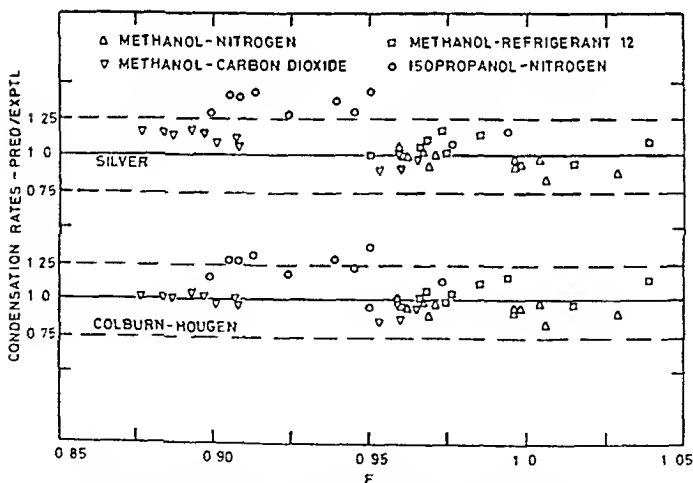


FIG 2 COMPARISON OF PREDICTED AND MEASURED
CONDENSATION RATE—BINARY SYSTEMS

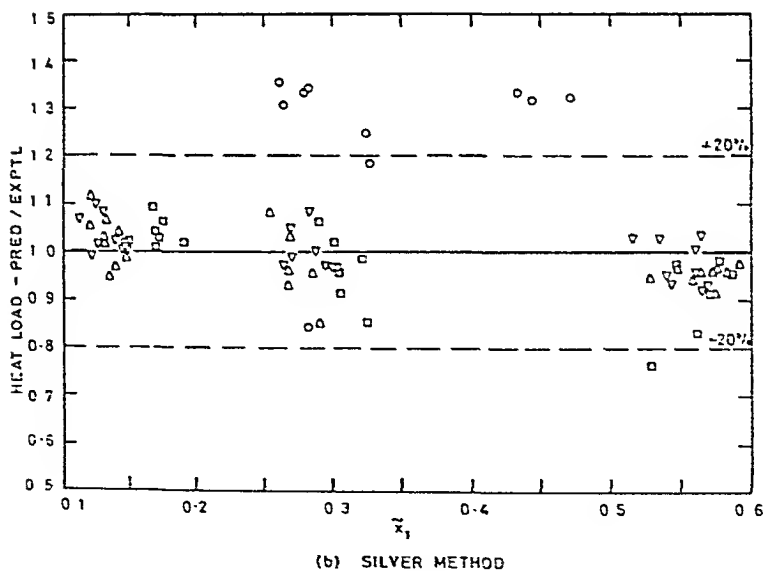
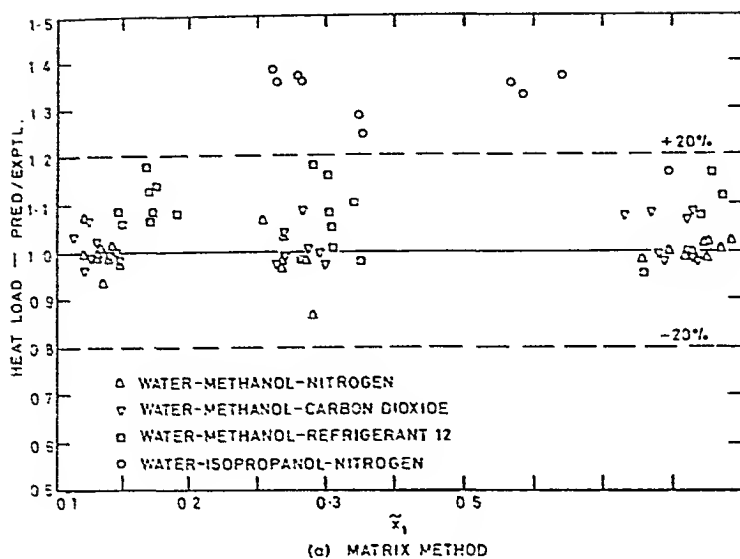
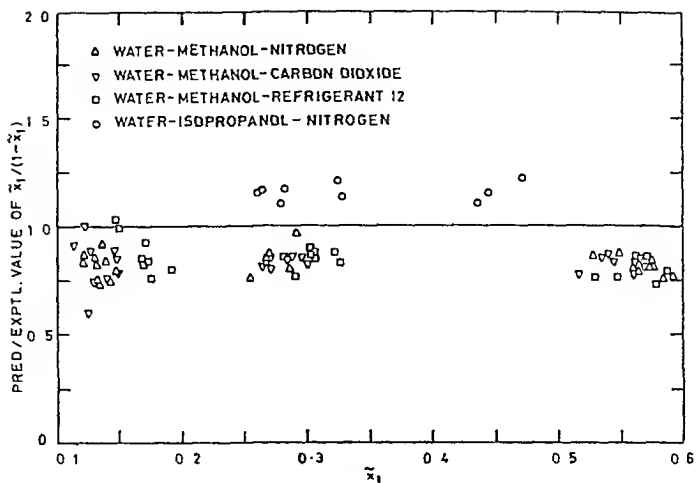
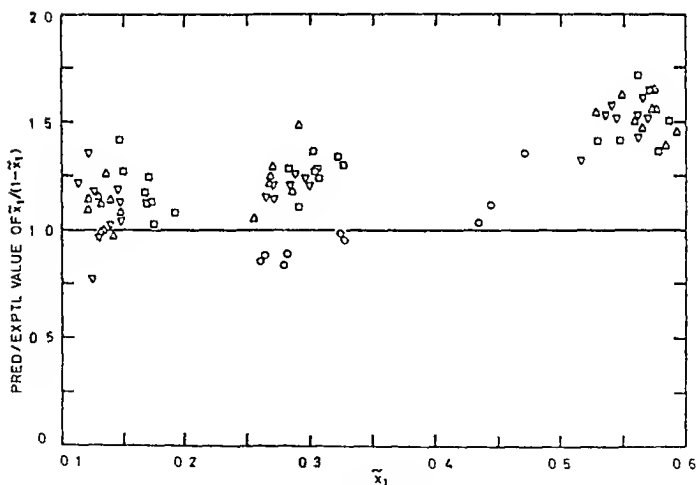


FIG 3 COMPARISON OF PREDICTED AND MEASURED HEAT LOAD - TERNARY SYSTEMS



(a) MATRIX METHOD



(b) SILVER METHOD

FIG 4 COMPARISON OF PREDICTED AND MEASURED OUTLET CONDENSATE COMPOSITION -TERNARY SYSTEMS

A METHOD OF IMPROVING THE PERFORMANCE OF AN IN-TUBE CONDENSER

J A R Henry, I D R Grant, C D Catchin*

A method of improving the performance with in-tube condensation is demonstrated. A slice of a typical kettle reboiler with R-12 boiled by condensing steam is used in the demonstration, where the use of tube inserts improved the reboiler performance by as much as 75 per cent. An explanation for the poor performance is provided, and the method of sizing inserts to remove it is given. Simple theory is used to show the likely degree of steam-side maldistribution and how it is affected by geometry.

INTRODUCTION

During the study of shell-side boiling in shell-and-tube heat exchangers it became clear that the performance was poorer than expected. Investigation revealed flow maldistribution on the tube side where the heating medium, steam, was being condensed at sub-atmospheric pressure.

With in-tube condensation, maldistribution on the tube side can occur for various reasons, for instance due to tubes of different lengths. This case was the subject of papers by Boiko and Kruzhilin^(1,2). Another reason is that each tube is subject to a different temperature difference as in air-cooled condensers^(3,4) or in reheaters⁽⁵⁾. None of these likely causes was present in this study and it was suspected that the kinetic head of the supply steam was to blame since pressure drop is known to be small during condensation.

TEST SECTION

A slice of the kettle reboiler used as a test section is shown in Fig. 1 and its main dimensions are given in Table 1. Refrigerant R-12 is boiled on the outside of the bundle being heated by condensing steam inside the tubes. The steam, which forms a constant temperature source of heat, enters the upstream header as shown in Fig. 1 by an axial nozzle and hence to each of the tubes in the bundle. Each tube discharges its condensate to a common downstream header which is also connected to a vent pump to remove any non-condensable gases. The total condensate flowrate is measured to determine the heat load of the bundle. The heat load of nine individual tubes is measured by extending the tubes through the header as shown in Fig. 1. These tubes are attached to separators which are also connected to the vent pump. The condensate collected in each separator is measured to give the heat load of each tube.

*National Engineering Laboratory, East Kilbride, Glasgow, United Kingdom

The boiling fluid, R-12, enters the bottom of the kettle shell in a slightly subcooled condition and the vapour produced, with liquid carryover, leaves by the top nozzle to a condenser. Sufficient liquid is supplied to keep the tube bundle flooded, any excess being removed at the side nozzle. The boiling pressure and hence the temperature was kept constant for all the tests reported here.

BUNDLE PERFORMANCE

Tests were carried out for a range of temperature differences between the steam and R-12 by varying the steam temperature. These steam temperatures correspond to a range of condensing pressures all below atmospheric. The results of the tests are shown in Fig. 2 in which the total condensing rate is shown as a function of the condensing temperature.

The condensing rate is very much less than simple methods (based on in-tube condensation and pool boiling) would predict and led to a detailed examination of the bundle using the individual tube connections. This showed that tubes on the outside rows performed badly while tubes at the centre were much better than the bundle average. Tubes between the outer and inner rows had a very varied performance between these limits from test to test. Following these tests the upstream and downstream headers were opened for examination and it was noticed that tubes on the outside rows were dry at outlet and wet at inlet, which is opposite to what is expected. This observation along with the individual tube measurements confirmed that steam was penetrating the centre tubes of the bundle by virtue of its kinetic head, allowing steam to enter both ends of the outer tubes. This leads to gas blanketing of the outer tubes and subsequent loss in performance. As in practice an impingement plate was installed in the inlet header opposite the inlet steam nozzle to improve the distribution of steam to the bundle. This had no apparent effect as shown in Fig. 2 on the overall condensing rate of the bundle. More surprising however was the observation from individual tube measurements that the performance of the centre and outside rows had been reversed. Steam now penetrated the outside rows, returning into the centre tubes.

Clearly the impingement plate was insufficient, in this case, to destroy the kinetic head and hence cure the maldistribution. It was therefore decided to install at entry to each tube an insert which would increase the pressure drop over the tube bundle hence making the kinetic head of the entry steam less significant. This has been suggested for obvious cases of maldistribution⁽⁶⁾ but is rarely carried out in practice.

The way in which the inserts are sized is described in Appendix 1.

BUNDLE PERFORMANCE WITH TUBE INSERTS

The performance of the bundle with tube inserts is also shown in Fig. 2. The condensing rate at a given steam temperature is increased over that of the plain bundle by as much as 75 per cent. It should be noted that the bundle performance is enhanced over the entire range of steam temperature. This indicates that the improved flow distribution is obtained regardless of the flowrate. From equation (1.3) in Appendix 1 this is not surprising since

$$\Delta p_f \propto \frac{1}{2} \rho_v u_N^2.$$

This improved performance is due to the elimination of gas pockets. These cannot be removed by increasing the rate of venting from the outlet header, as this was tried in the course of the present tests.

Fig. 2 also shows that the scatter of data obtained without inserts has been considerably reduced. This is presumably due to the random way in which gas pockets formed between the inner and outer tube rows in the absence of inserts.

OTHER BUNDLE GEOMETRIES

It might be thought that the phenomena observed in these tests is a result of the short tube length and that longer tubes used in practice will tend to reduce maldistribution. Simple theory presented in Appendix II suggests that if momentum effects are predominant then lengthening the tubes can make maldistribution worse. The likely degree of maldistribution of the test section used in this study (without inserts) is shown in Fig. II.1.

If U-tube bundles are used for in-tube condensation then different sized inserts will be required because of the different tube lengths. A method of sizing these inserts is given in Appendix III.

CONCLUSIONS

- 1 Observation shows that in-tube flow distribution with condensation in a tube bundle is greatly influenced by inlet kinetic head since the friction and momentum pressure changes tend to cancel each other.
- 2 A simple impingement plate opposite the shell inlet nozzle did not give any noticeable improvement in distribution.
- 3 The performance of this kettle reboiler slice at a given overall temperature difference is almost doubled by the installation of inserts. These provide a controlling pressure drop on the condensing side, thus giving good distribution and eliminating gas blanketing of the condensing surface.
- 4 The improvement occurs through the entire range of steam flowrate.
- 5 A method is given of sizing the inserts for a particular duty.
- 6 A method of sizing inserts for use with U-tube bundles is also given.

ACKNOWLEDGEMENT

This paper is presented by permission of the Director, National Engineering Laboratory, Department of Industry.

The work was supported by the Materials and Chemicals Requirements Board of the Department of Industry, United Kingdom. This paper is Crown copyright.

SYMBOLS USED

- d = tube inside diameter
 f = friction factor

l = tube length
 \dot{M} = mass flowrate
 \dot{m} = mass flux
 Δp = pressure change
 S = cross sectional area
 u = velocity
 GREEK
 ρ = density

SUBSCRIPTS

AV = average
 f = friction
 i = insert
 L = liquid
 m = momentum
 MAX = maximum
 N = nozzle
 T = tube bundle
 V = vapour

LIST OF REFERENCES

- 1 Boiko, L. D. and Kruzhilin, G. N., 1965, "Heat-transfer conditions with steam condensing in tubes connected in parallel." Teploenergetica, Vol. 12, No 5, pp 63-67. Thermal Engng, Vol. 12, No 5, pp 74-79.
- 2 Boiko, L. D. and Kruzhilin, G. N., 1967, "Heat transfer and hydraulic resistance during condensation of steam in a horizontal tube and in a bundle of tubes." Int. J. Heat Mass Transfer, Vol. 10, No 3, pp 361-373.
- 3 Berg, W. F. and Berg, J. L., 1980, "Flow patterns for isothermal condensation in one-pass air-cooled heat exchangers." Heat Transfer Engng, Vol. 1, No 4, pp 21-31.
- 4 Rozenman, T. and Fundyk, J., 1974, "Effect of unequal heat loads on the performance of air-cooled condensers." AIChE Symp. Ser., Vol 70, No 138, pp 178-184.

- 5 Henry, J. R., 1969, "A computer program for use in reheater design." NEL Report No 426. East Kilbride, Glasgow: National Engineering Laboratory.
- 6 Forgo, L., 1970, "The causes of poor heat transfer in shell-and-tube heat exchangers during condensation of saturated steam." Brennst.-Wärme-Kraft, 1967, 19(1), pp 20-23. English Trans.: AERE-Trans. 1132. Harwell, Berks. AERE Information Branch, March 1970. Edinburgh: H.M. Stationery Office, 1970.
- 7 Fraas, A. P. and Ozisic, M. N. 1965, "Heat exchanger design." John Wiley and Sons, Inc., London.

A P P E N D I X ISIZING THE INSERTS

In order to size the inserts it is useful to consider the effect which the kinetic head has on distribution. This can be done as suggested by Fraas and Ozisic⁽⁷⁾ who relate the maximum flow through a particular tube to the mean flow by the relationship

$$\frac{\dot{M}_{MAX}}{\dot{M}_{AV}} = \sqrt{\left(\frac{\Delta p_T \pm \frac{1}{2} \rho_V u_N^2}{\Delta p_T} \right)} \quad (I.1)$$

where Δp_T is the overall tube bundle pressure drop, and

$\frac{1}{2} \rho_V u_N^2$ is the kinetic head at exit from the inlet nozzle.

To be conservative, $\frac{1}{2} \rho_V u_N^2$ should take the same sign as Δp_T .

Equation (I.1) assumes that the entire inlet nozzle dynamic head impinges on the tube plate, as would happen with an axial nozzle. If an impingement plate were used or a radial nozzle, then possibly less than the full impact would be obtained, and hence different distribution.

The tube bundle pressure drop can be written as

$$\Delta p_T = \Delta p_f + \Delta p_m + \Delta p_i \quad (I.2)$$

where Δp_f and Δp_m are the friction and momentum components of pressure drop, and

Δp_i is the pressure drop through the proposed insert.

In a condensing system, Δp_f and Δp_m are of opposite sign and hence tend to cancel each other, resulting in the small pressure drop which is often observed.

In order to size the insert it is conservative to assume that

$$\Delta p_f + \Delta p_m = 0$$

which gives

$$\frac{\dot{M}_{MAX}}{\dot{M}_{AV}} = \sqrt{\left(\frac{\Delta p_i + \frac{1}{2} \rho_V u_N^2}{\Delta p_i} \right)}. \quad (I.3)$$

Hence for the maximum flow not to differ from the mean by more than 5 per cent

$$\Delta p_i \leq 10 \times \frac{1}{2} \rho_V u_N^2. \quad (I.4)$$

To be further conservative, the inserts in the present case were sized such that

$$\Delta p_i = 15 \times \frac{1}{2} \rho_V u_N^2. \quad (I.5)$$

A P P E N D I X I IEFFECT OF GEOMETRY ON TUBE-SIDE DISTRIBUTION

Equation (I.1) showed how the tube-side distribution could be related to the pressure drop and incoming kinetic head. It is enlightening to pursue this further, by considering the way in which friction and momentum interact, and how they are affected by the dynamic head of the flow issuing from the inlet nozzle.

The total pressure drop through the tube, ignoring entry and exit losses can be written as

$$\Delta p_T = \Delta p_f + \Delta p_m. \quad (\text{II.1})$$

Ignoring the presence of condensate, the mean frictional pressure change can be calculated from

$$\Delta p_f = - \frac{f \lambda \dot{m}_T^2}{d \rho_v} \quad (\text{II.2})$$

where \dot{m}_T is the tube-side mass flux.

Assuming the quality to be unity at inlet and zero at outlet, the momentum pressure change can be evaluated from

$$\Delta p_m = \dot{m}_T^2 \left(\frac{1}{\rho_v} - \frac{1}{\rho_L} \right) \quad (\text{II.3})$$

and for $\rho_L \gg \rho_v$ this may be simplified to

$$\Delta p_m = \frac{\dot{m}_T^2}{\rho_v} \quad (\text{II.4})$$

Hence the total pressure change through the tube is

$$\Delta p_T = \frac{\dot{m}_T^2}{\rho_v} \left(1 - \frac{f \lambda}{d} \right). \quad (\text{II.5})$$

The inlet nozzle kinetic head KH is

$$KH = \frac{1}{2} \rho_v u_N^2 = \frac{1}{2} \frac{\dot{m}_N^2}{\rho_v} \quad (\text{II.6})$$

where \dot{m}_N is the nozzle mass flux; that is from continuity

$$\dot{m}_N S_N = \dot{m}_T S_T \quad (\text{II.7})$$

and S_N and S_T are the flow areas of the nozzle and tube bundle respectively.

From equation (II.6) and (II.7)

$$KH = \frac{1}{2} \left(\frac{S_T}{S_N} \right)^2 \frac{\dot{m}_T^2}{\rho_v}. \quad (\text{II.8})$$

Substituting equations (II.5) and (II.8) in equation (I.1) and rearranging gives the relationship

$$\frac{\dot{N}_{MAX}}{\dot{N}_{AV}} = \sqrt{\left\{ 1 \pm \frac{\frac{1}{2} \left(\frac{S_T}{S_N} \right)^2}{\left(1 - \frac{f l}{d} \right)} \right\}}. \quad (\text{II.9})$$

This is a function which takes the form shown in Fig. II.1, and has a discontinuity where $fl/d = 1$; that is where the friction and momentum components balance each other. It is at that condition that the tube bundle would be most susceptible to the nozzle kinetic head.

Fig. II.1 shows that most in-tube condensers could suffer from the effects of maldistribution. The location of the kettle reboiler test section is shown in Fig. II.1 indicating a large degree of maldistribution in the absence of inserts.

A P P E N D I X I I I

SIZING INSERTS FOR USE WITH U-TUBE REBOILERS

In order to prevent gas blanketing, the quality at exit from each tube should be zero. This can be achieved by allowing each tube to take steam in proportion to its length, by varying the diameter of the insert orifice as

$$d_i = \bar{d}_i \left(\frac{l}{\bar{l}} \right)^{\frac{1}{2}} \quad (\text{III.1})$$

where \bar{d}_i is the diameter of orifice required to satisfy the pressure drop from equation (I.5).

This is fitted to tubes of average length \bar{l} . The other tubes of length, l_i are fitted with inserts of diameter, d_i .

T A B L E 1

DIMENSIONS OF KETTLE REBOILER

Shell diameter (m)	0.84
Tube diameter (m)	0.0191
Tube pitch (m)	0.0254
Tube arrangement	Square
Tube length (m)	0.254
Tube bundle diameter (m)	0.375
Number of tubes	177
Nozzle diameter (m)	0.154

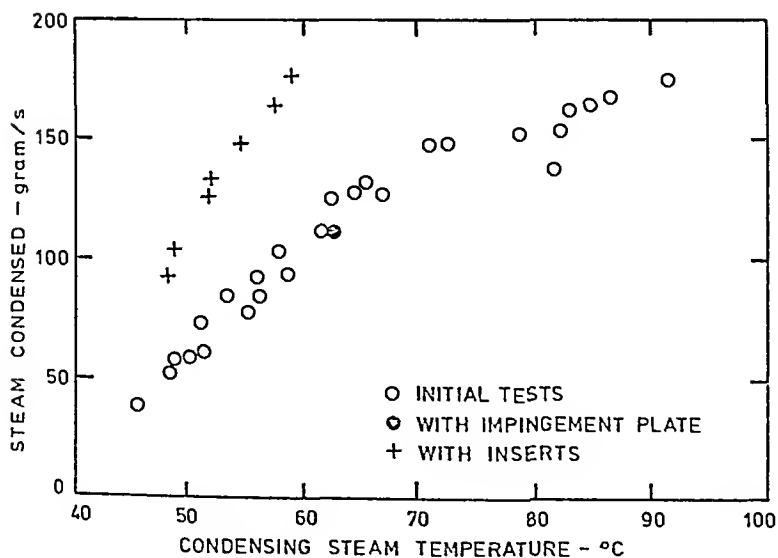
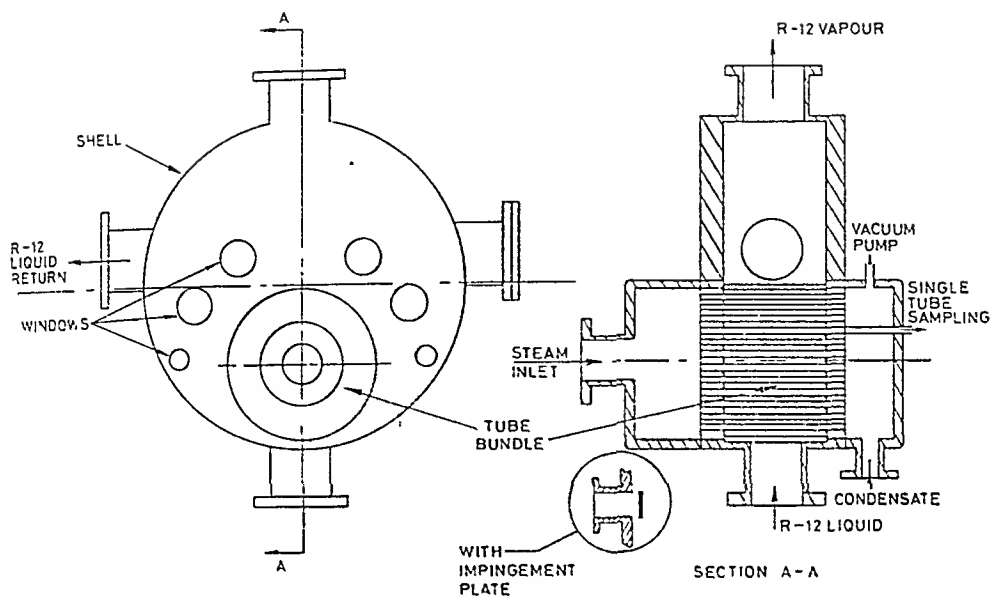


FIG 2 CONDENSING RATE AS A FUNCTION OF STEAM TEMPERATURE

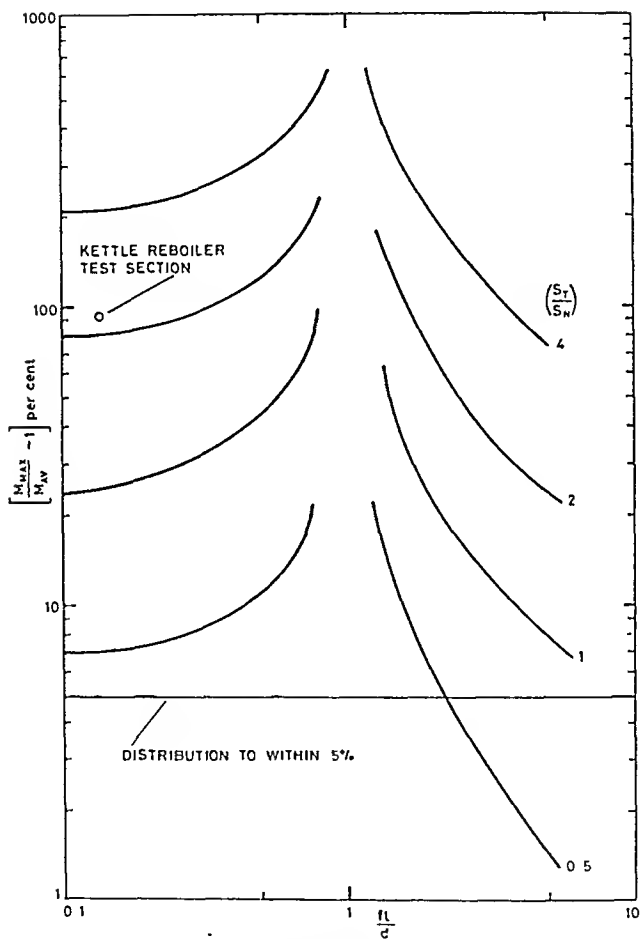


FIG II 1 FLOW DISTRIBUTION AS A FUNCTION OF GEOMETRY

THE PREVENTION OF TUBE FAILURE IN HIGH INTEGRITY CONDENSERS

P.D.Hills* D.Henderson* R.R.Cowell⁺

Failures of mild steel tubes are reported on chlorine partial condensers due to corrosion from the treated cooling water. A low water design velocity compounded by throttling of the water flow for control led to deposits of dirt which prevented access of the treatment chemicals to the metal surface. Several alternative courses of action to prevent recurrence of the problem are discussed and evaluated. These range from improved inspection procedures to complete redesign of the system. The requirements of very high integrity led to the redesign of the condenser using corrosion resistant materials.

INTRODUCTION

Distillation of chlorine is sometimes required to remove heavy impurities. This is done on three plants in ICI at a pressure of 12-14 bar abs, giving a condensing temperature of 40-50°C, allowing the use of cooling tower water as the cooling medium. As the downstream processes use chlorine vapour, partial condensers are used.

Plant A was designed in 1970. The condenser designed was a vertical fixed tube sheet shell and tube exchanger with chlorine condensing in down-flow in the tubes and cooling water flowing up through an E Type shell. Mild steel was used throughout but to provide high integrity the tubes were of 12 swg and a double tubesheet construction was used.

The chlorine vapour from the partial condenser passes to a reactor and it is essential for the smooth operation of the reactor that the feeds to it are steady. The control scheme adopted for the distillation column to provide this steady flow involved flow control of the steam to the boiler and control of the still head pressure by throttling the cooling water flow to the condenser (Fig 1). From the process control standpoint this has proved very satisfactory.

* ICI PLC, Engineering Department, Northwich.
⁺ ICI PLC, Mond Division, Runcorn.

When Plant A was uprated, four years after commissioning, the original condenser was replaced by a unit with nearly twice the effective area, based on the results of a high load trial which indicated severe fouling of the small unit. This fouling was assumed at the time to be largely on the Chlorine side, but subsequent evidence suggests that it was more likely to be on the water side.

Plant B was built 6 years after Plant A. The Chlorine still was based on the design for Plant A but is smaller as the throughput is lower. For layout reasons a horizontal condenser was chosen, still with chlorine in tube. A single tubesheet with welded tube-tubesheet joints was adopted.

Plant C was built ~ 8 years after Plant A. For this unit a vertical condenser similar to that of Plant A was chosen. To provide high integrity, explosion welded tube-tubesheet joints were used.

The cooling waters for all three plants have similar anti-corrosion treatments consisting of pH control, synergised chromate, polyelectrolyte dispersants and chlorination to control bio-fouling.

HISTORY OF TUBE FAILURES

About four years after the uprating the large condenser on Plant A failed in operation, some six weeks after it had passed a routine inspection and pressure test during the annual plant shutdown. Note that visual inspection of the shell-side was not possible due to the fixed tube sheet construction, and that ultrasonic tube thickness measurements were not made.

Subsequent examination revealed that a group of 14 tubes had failed close to the inner bottom tube plate. Several tubes were drawn and examined and showed significant corrosion, including pitting, on the water side, particularly in the areas just above the tube plate and each baffle. Some sediment was found on the tubes. There was slight thinning on the process side, particularly at the tube inlets.

In order to get the plant back on line, the small condenser, which had been left in the plant after installation of the large unit, with the tube-side under a nitrogen blanket and the shellside drained of cooling water and blanked off, was pressure tested and then reconnected to the still. Three days after start up this unit also failed. Subsequent examination showed a pattern of tube thinning similar to the large unit. Two tubes had failed completely.

In order to restart Plant A the spare condenser from Plant B, which had not yet been used, was installed on Plant A and the plant run with this exchanger for some 12 weeks while the large condenser was retubed. It is worth noting that although this exchanger is only 65% of the size of the large unit, plant output was not restricted.

The spare Plant B condenser was replaced in Plant A by the large Plant A unit, which had been completely retubed. The latter was inspected after 20 months service using ultrasonic thickness measurements backed up by selected tube withdrawal. The tube had suffered significant general corrosion on the water side to a greater level than had been observed on the previous occasions on Plant A. As before there was additional local corrosion at baffles and tubesheet. Because of the level of corrosion the exchanger was considered to be in an unsuitable condition to be put back in service.

The Plant C condenser failed after only 10 monthly operation in a similar manner to Plant A.

Surprisingly, the original Plant B condenser showed only localised corrosion in the lower tubes although its twin, when used on Plant A, experienced a corrosion rate which would indicate a useful life of only 2 years, considerably worse than when in Plant B service.

CAUSES OF CORROSION

At temperatures below about 100°C , mild steel is the usual material to contain dry chlorine. However, wet chlorine is exceedingly aggressive to most materials. Particular care is taken in the design of equipment handling chlorine to prevent any interaction between the chlorine and any water containing stream. The weak points in a heat exchanger from this point are generally the tube to tubesheet joints. Single expanded joints are not suitable. The Plant A exchangers used double tube sheets with tubes expanded into each sheet, but this form of construction is not now liked, mainly due to the difficulty of checking that a satisfactory joint has been made to the inner tubesheet. Conventional welded joints, such as were used on the Plant B units, have the disadvantage of requiring a greater tube pitch. The explosion welded technique, as used on Plant C, does not have this disadvantage. No problems were experienced on any of the condensers due to contamination of the chlorine through the tubesheet joints.

In general mild steel is a suitable material for use in inhibited cooling tower water but can only be 'guaranteed' if there is good water flow and if the correct level of inhibiting chemicals is maintained.

The main problem in this respect is solids deposition and though the situation can be improved by attention to details like filters etc. and by using best design features such as correct baffle spacing, neither of the above make the application fully predictable without good flow.

If sedimentation does occur then corrosion of mild steel can be expected behind such deposits even with an otherwise adequate concentration of corrosion inhibitors, as the deposits prevent access of the chemicals to the metal surface.

Cooling tower water on the shell side of an exchanger always presents a potential for localised corrosion as it is impossible completely to avoid 'dead spots' where dirt deposits can accumulate, although good design can reduce this likelihood. Good design includes ensuring an adequate water velocity at all times in all areas of the exchanger. ICI codes recommend a minimum cooling water velocity on the shell side of an exchanger of 0.6 m/s.

The Plant A condenser was designed for a maximum cooling water flow corresponding to a velocity in the bundle of only 0.35 m/s. The corresponding figure for Plant B is 0.11 m/s and for Plant C is 0.17 m/s.

The problem is aggravated by the control scheme used for the stills, and the excessive design fouling resistance used. For example, the combined design fouling resistance used for Plant C was $0.0034 \text{ m}^2 \text{ }^{\circ}\text{C/W}$ which would correspond to a dirt film thickness of $\sim 4 \text{ mm}$! The exchangers were sized for full plant output with high summer cooling water inlet temperature and a high fouling resistance. The water flowrate needed for the case of winter operation with a clean exchanger under turndown conditions can be 3 or 4 times less than design. In general it is considered bad practice to control the

- a) It was significantly more expensive than the alternatives.
- b) It would incur increased maintenance charges.
- c) It involved more alterations to plant pipework and occupied more space than the existing system.
- d) The reliability of the total system would be reduced.
- e) It would require more attention from plant personnel to ensure that the required level of treatment chemicals was maintained. Of particular concern was the possibility that there would be a leak of the circulating water through the recirculating pump glands, which would be made up with non-treated water, requiring the addition of further chemicals. If this were not done this scheme would be little better than the original system.

Change of Exchanger Materials of Construction

When we originally considered alternative materials, after the first failure, Cupro-nickel or Monel were suggested. However, our Materials Group stated that these materials would also be prone to corrosion under the low velocity cooling water conditions. Although the rate of corrosion would be expected to be less than for mild steel, they could not quantify the improvement to be expected. Because of this, this solution was not then followed up.

Later, Hastelloy 'C' was proposed as an alternative material. This has the advantages of excellent resistance to corrosion by cooling water under any conditions of flow, inhibitors and solids deposition, and good resistance to even wet chlorine should a small mechanical leak appear. The basic high cost of the material could be offset by the following factors:

- a) The fouling coefficient on the chlorine side was expected to be low, whereas a high figure had been used previously.
- b) The water side fouling coefficient was reduced by designing with a reasonable water velocity and because Hastelloy 'C' is intrinsically less prone to fouling than mild steel. A reasonable water velocity also ensured a good film coefficient.
- c) As there was no need for a corrosion allowance on either side, thin walled tubing (20-22 swg) could be used.
- d) As the unit is expected to have a life in excess of ten years a spare was not required.

Exchangers with Hastelloy 'C' tubes were designed; the unit for Plant A had an effective surface of only 55% of the original 'large' condenser.

Comparison of Alternative Schemes

Table 1 shows the estimated costs of six alternative schemes for Plant A. The figures given are only the initial capital cost of each scheme.

TABLE 1 - Initial Capital Cost of Alternative Schemes for Plant A

	Description of Scheme	Initial Cost
A	Retain existing unit, provide spare, inspect annually and retube every 1-2 years depending on results of inspection.	£ 42,000
B	As A but spare unit designed for improved water velocity. Retube every 1-4 years.	£ 34,000
C	Install U-tube condenser with chlorine in the shell, spare tube bundle, inspect annually and retube every 2-4 years.	£ 68,000
D	Retain existing unit, provide spare, install booster pumps and recycle system. Inspect every 1-2 years and retube every 2-4 years. (See Figure 3)	£ 54,000
E	Closed circuit cooling system. (See figure 2)	£106,000
F	Install Hastelloy C exchanger without spares.	£ 60,000

Schemes A-D would require regular inspection including a full ultrasonic inspection of every tube at an estimated cost of £4,000 to £8,000 depending on size. They also require periodic re-tubing at an estimated cost of £10-20,000. The additional costs of a plant shutdown are not included in these figures.

Schemes D and E would incur additional maintenance charges, because of the pumps, the need to check treatment chemicals levels etc.

Scheme F is technically the most satisfactory solution for the following reasons:

- It offers the highest integrity. Hastelloy C is resistant to cooling water (even untreated) and to wet and dry chlorine. Even if a failure were to occur it would only result in a small leak which would not rapidly enlarge as happens with mild steel.
- The installation is simple, involving minimal change to the existing equipment.
- The present still control system, which has given satisfactory performance, can be retained.
- There is no need for a spare.
- There will be less maintenance and less need to open up the chlorine system for inspection.

In addition to these technical advantages, it can be seen that over a reasonable working life for the plants the Hastelloy C units are likely to have a lower total cost considering both capital and operating charges. We have therefore proceeded with the design and procurement of the new units.

CONCLUSIONS

Low water velocities lead to fouling and corrosion, even in well treated cooling water systems. Significant overdesign and the use of high fouling factors make low velocities more likely.

"The use of a high fouling factor at the design stage is liable to be a self-fulfilling prophesy."

Designers should be aware of the potential problems of high cooling water turndown in winter. Designs should be checked for these conditions as well as the peak load summer conditions usually used for design.

A highly corrosion resistant (and hence expensive) material of construction was recommended for this duty because a major tube failure was unacceptable, and because due to the interaction of chlorine and water, any minor failure would rapidly escalate into a major one.

Although this paper has been written around a series of incidents on a chlorine duty, similar problems could be expected wherever the process fluid becomes much more corrosive when wet. Examples of other systems include HCl, HF, SO₃, and concentrated sulphuric acid, all of which are frequently handled in mild steel when in the dry state.

ACKNOWLEDGEMENTS

We would like to thank ICI PLC for permission to publish this paper. We are grateful to our many colleagues in ICI Mond Division and Engineering Department for their help and advice during the course of this project.

REFERENCE

1. Chin, T.G., October 1979, Hydrocarbon Processing, 145.

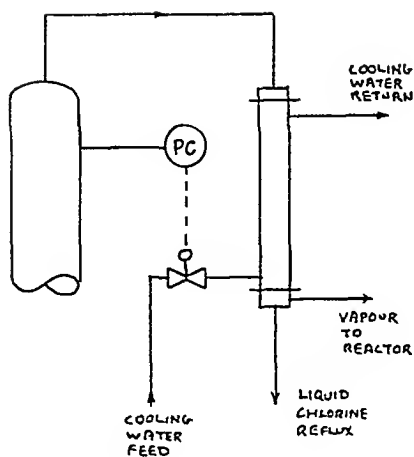


Figure 1 Chlorine Still Pressure Control System

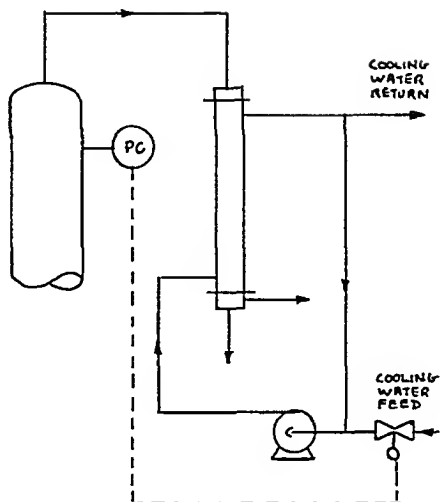


Figure 2 Recirculated Cooling Water System

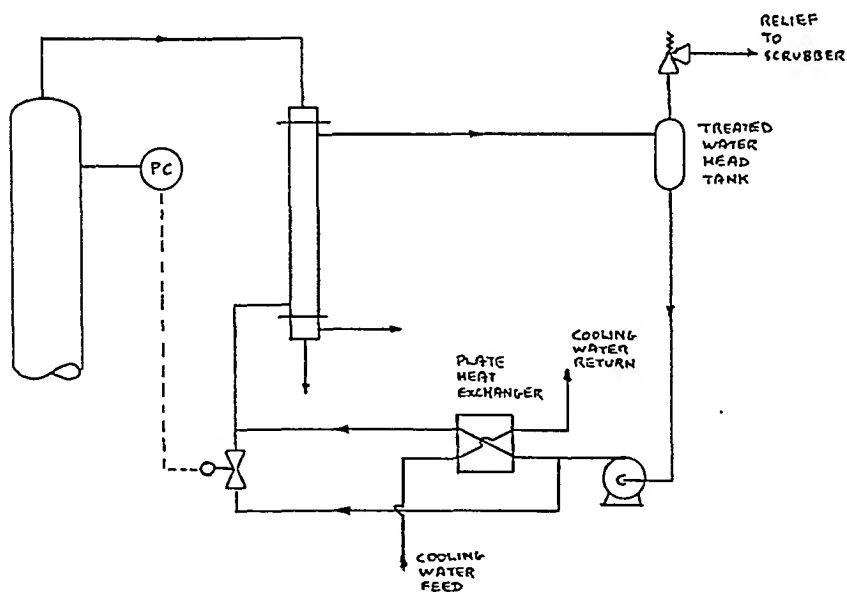


Figure 3 Indirect Cooling System

CONDENSATION DUTIES IN PLATE HEAT EXCHANGERS

H. Kumar*

Whereas plate heat exchangers (PHE's) are not normally considered for condensation duties, this paper highlights practical applications for which the PHE is particularly effective. The operation of PHE's is described and their characteristics defined. Considerations are then given to condensation duties which have been successfully achieved in PHE's and principles behind calculation methods are outlined.

INTRODUCTION

The use of PHE's for liquid/liquid heat transfer duties is now well understood by heat transfer engineers. Because of its high heat transfer coefficients, it normally provides very economic designs particularly for corrosion-resistant materials of construction. As a condenser the commonest application for plate heat exchangers is for heating process by steam. For example, in milk pasteurisers, the product is heated to a pasteurising temperature of 72°C. Normally this is done using hot water, but in several cases steam is employed to avoid large power dissipation in pumping hot water. To ensure 'gentle' heating of milk, steam would be under vacuum at say, 75°C. The more common use for PHE's is with pressurised steam heating the process fluid which is almost invariably liquid. Economic designs are obtained provided that a 'reasonable' pressure loss is allowed for the condensing medium. If too low a pressure drop is available, condensation will occur on only part of the plate length, i.e. not all the surface area will be utilised.

In the following sections, the operation of PHE's as condensers is described first followed by an outline of basic calculation methods.

OPERATION AS CONDENSERS

A simple arrangement is shown in Fig 1 depicting a single pass arrangement for both process and condensing media which flow in alternate passages. Although Fig 1 shows counter-flow, co-flow may be used. The number of passages will be determined by heat load and pressure drop considerations.

Because of the modular nature of PHE's plates have fixed port sizes. When port velocities are high, it is sometimes necessary to adopt double entry for the vapour to reduce velocities and hence pressure and temperature drops

*APV Company Limited, Crawley

in the port. Such an arrangement is depicted in Fig 2. As an alternative a special design of plates may be used where instead of the normal circular port, a D-shaped port is employed giving a bigger flow area in the vapour manifold. The normal and special designs are shown in Fig 3.

Fig 4 shows an arrangement where the process medium is in two passes. The point to note here is that the first process pass flows countercurrent to the condensing medium whereas the second pass is concurrent. Also, because vapour is condensing against process at different temperatures in the two passes, the rates of condensation will vary and many of the steam passages will not be fully loaded. These must be carefully considered in any design calculations.

Another facet of PHE's is the passage flow geometry. These geometries are normally designed for liquid/liquid heat transfer and are formed by shallow corrugations giving flow gaps of between 3 to 5.5 mm. Coupled with the induced turbulence generated by the complex geometry, these narrow gaps give very high heat transfer on the process side. Assuming that the process medium is water, film coefficients as high as 15 to 20 kW/m²K are obtainable.

However, the small interplate spacing dictates a careful examination of vapour side pressure loss. Two examples of experimental steam coefficients and pressure drops are given below both for counter-flow. Example 2 is for a smaller temperature difference. The overall coefficients given have been calculated assuming isothermal condensation and using a log mean temperature difference. The actual mean temperature difference will be smaller because of condensing pressure drop, and therefore the coefficients below appear artificially low.

TABLE 1 - Examples of Experimental Condensing Coefficients

	Example 1	Example 2
Steam inlet gauge pressure (kPa)	70	70
Waterside velocity (m/s)	0.98	0.49
Heat flux (kW/m ²)	150.4	51.5
Steam condensed/passage (kg/s)	0.0474	0.0168
Steam pressure loss (kPa)	37	8.6
Overall coefficient (kW/m ² K)	5.8	5.0

Pressure Drop

In order to calculate the condensing pressure drop, the plate length is split into several zones. In each zone, the liquid and vapour component pressure drops ΔP_l and ΔP_g are calculated from individual single phase correlations obtained from tests.* The liquid data in turbulent flow is in the form

$$f = \frac{A}{Re} I \quad (1)$$

A typical value for I is 0.2 and A may vary between 3 and 0.5 dependent

* ΔP_l is the pressure drop if the liquid fraction were to flow alone over the entire cross-section. ΔP_g is the vapour fraction counterpart.

on the trough geometry. The hydraulic diameter d is defined as

$$d = \frac{4 \times \text{Volume between plates}}{\text{The Wetted surface area}} \quad (2)$$

The vapour phase pressure drop for steam is expressed empirically as

$$\Delta P_g = \frac{B}{\rho_g} (m)^{1.7} \quad (3)$$

B is a constant unique for each plate and varies between 2×10^6 and 150×10^6 dependent on plate geometry, i.e. trough configuration, gap, flow length and width. The two-phase pressure loss is then calculated using the Lockhart-Martinelli (1) approach as follows

$$X = \sqrt{\frac{\Delta P_l}{\Delta P_g}} \quad (4)$$

The parameter ϕ_l (or ϕ_g) is obtained from Fig 5 and the two-phase pressure drop ΔP_t is given by

$$\begin{aligned} \Delta P_t &= \phi_g^2 \Delta P_g \\ \text{or} \quad \Delta P_t &= \phi_l^2 \Delta P_l \end{aligned} \quad (5)$$

Heat Transfer

Condensation in a PHE may be considered analogous to condensation inside vertical tubes. The PHE method follows that suggested by Akers et al (2) for tubes. This is based on converting the two-phase mixture into an equivalent liquid flow which will exert the same shearing force on the condensate film.

The shear τ_g is due to the interaction between the vapour core and the liquid film.

$$\tau_g = f_g \frac{G_g^2}{2 \rho_g} \quad (6)$$

The vapour core may be replaced with a liquid whose flow (C_l) yields the same shear, i.e.

$$\tau_g = f_l \frac{G_l^2}{2 \rho_l} \quad (7)$$

$$\therefore G_l = G_g \left(\frac{\rho_l}{\rho_g} \right)^{1/2} \left(\frac{f_g}{f_l} \right)^{1/2} \quad (8)$$

The total pseudo-liquid flow is therefore G_v plus the actual liquid flow, and this may be used in the single phase heat transfer correlation to find the coefficient. The heat transfer equation will typically take the form

$$Nu = C Re^x Pr^{0.33} \left(\frac{\mu_b}{\mu_w} \right)^{0.14} \quad (9)$$

In turbulent flow x lies between 0.65 and 0.8. A typical value is 0.7. The factor C may vary between 0.1 and 0.3 dependent on the trough geometry.

The methods above have been incorporated into PHE programs and have been successfully used to verify experimental data. A sample plot of predicted versus experimental overall coefficient is presented in Figure 6.

CONCLUSIONS

Provided that moderate pressure drops are available, PHE's will give good condenser designs. By applying analogy to tubular correlations, it has been possible to develop a satisfactory design method for pure vapour condensing in PHE's.

SYMBOLS USED

ΔP_L	= Pressure drop for liquid fraction flowing over entire cross-section (Pascals).
ΔP_g	= Pressure drop for vapour fraction flowing over entire cross-section (Pascals).
ΔP_t	= Two-phase pressure drop (Pascals).
X	= Lockhart-Martinelli parameter.
ϕ	= Lockhart-Martinelli multiplier.
τ	= Shear stress.
f	= Fanning friction factor.
G	= Mass flux.
ρ	= Density, (kg/m^3)
A	= Constant in equation (1).
I	= Index in equation (1)
d	= Hydraulic diameter.
B	= Constant in equation (3).
m	= Channel mass flow rate (kg/s).
C	= Constant in equation (9).
Re	= Reynolds number.

Nu	= Nusselt number.
Pr	= Prandtl number.
μ_b	= Bulk viscosity.
μ_w	= Wall viscosity.
Suffix l	= Liquid.
Suffix g	= Vapour.

REFERENCES

1. Lockhart, R.W., Martinelli, R.C., Chem. Eng. Prog. 1949, 45(1), 39.
2. Akers, W.W., Deans, H.A., Crosser, O.K., Chem. Eng. Prog. Symposium Series 1959, 55(29), 171.

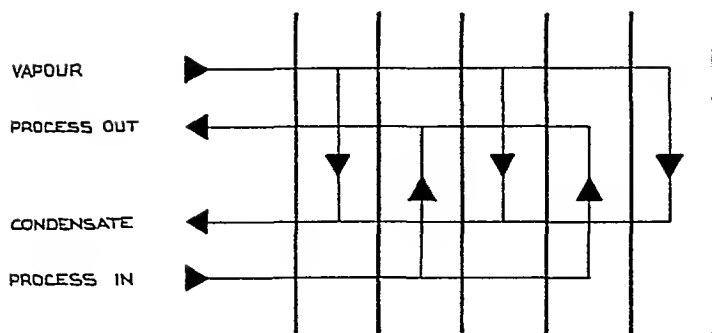


Figure 1: Single Pass Arrangement in Counter-flow

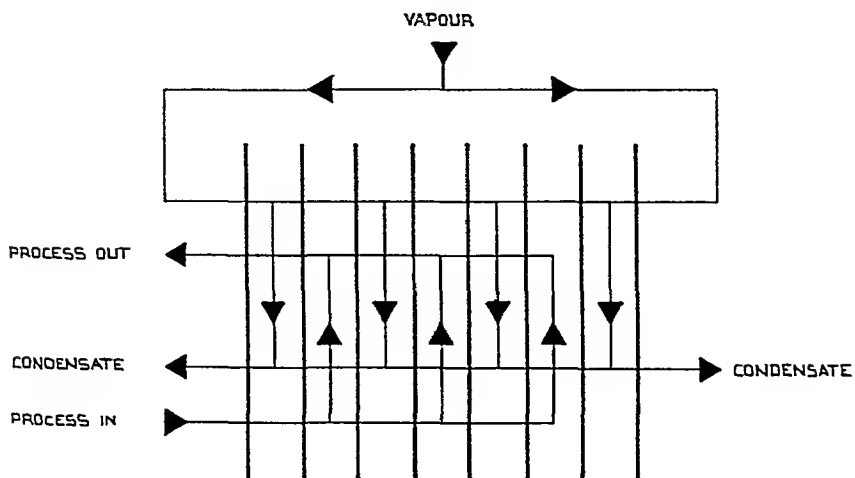


Figure 2: Double Entry for Vapour

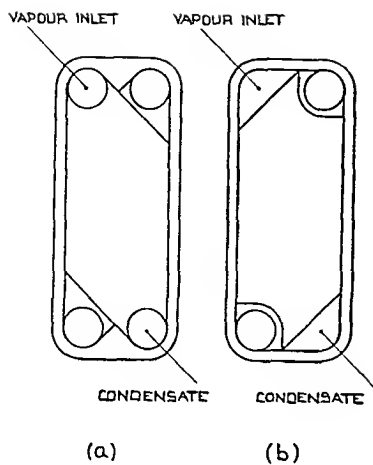


Figure 3 (a) Normal Ports and, (b) Special Vapour Ports

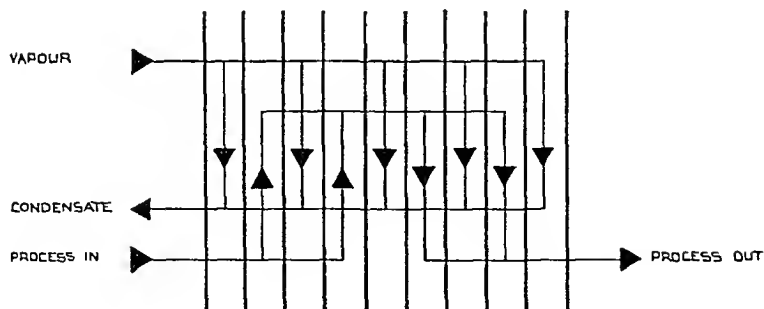


Figure 4: Two Passes for Process Medium

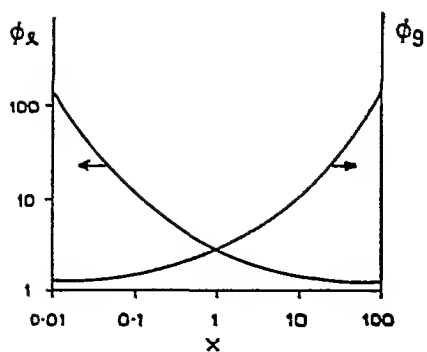


Figure 5 ϕ v X Liquid and Vapour
Fractions Turbulent

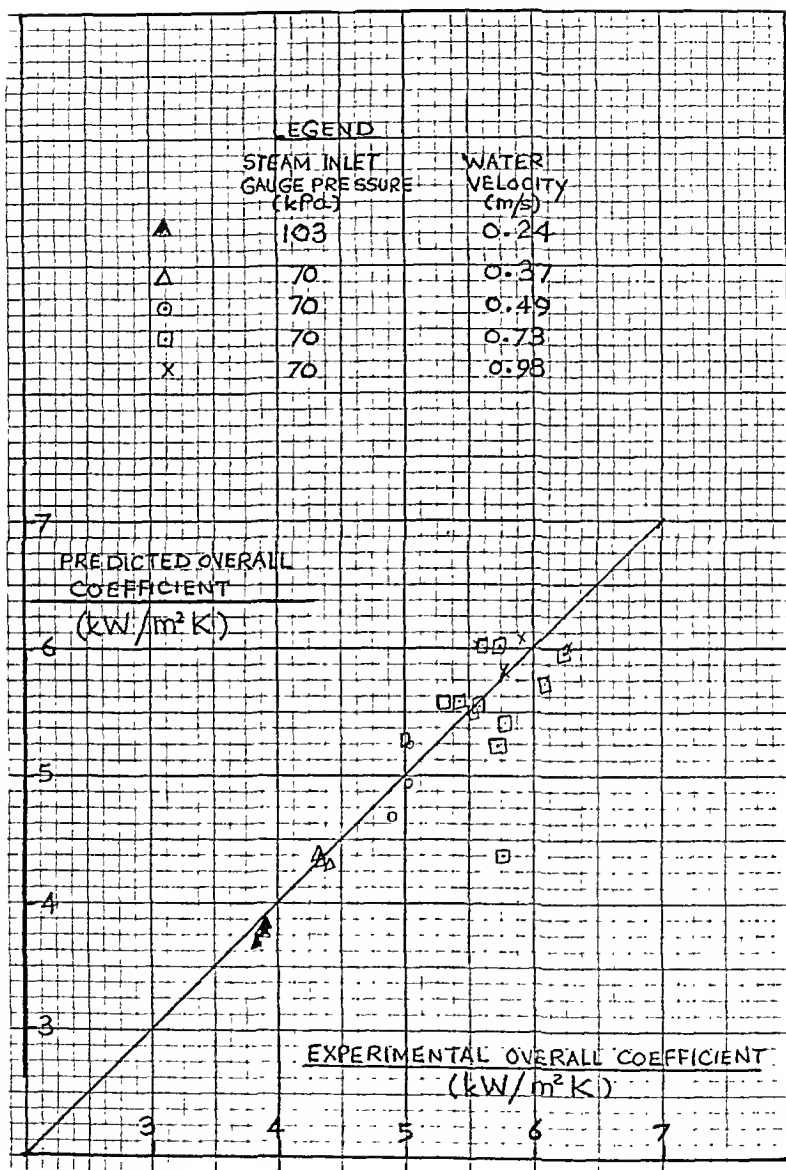


Figure 6: Predicted versus experimental overall coefficients

DISCUSSION

DISCUSSION POWER CONDENSERS - THEORY

Mr. F.J.L. Bindon¹ Professor Fujii's and Dr. Nunn's papers, (1) and (2), appeared to me, in my capacity as an operator, to be advocating tubewise enhancement with almost the sole objective of giving a condenser smaller in physical size for a given output, thus resulting in a saving of capital cost.

I felt that the questions of fouling and pumping power were not put into the financial equation, neither was the redundancy required for the number of tubes where tube leaks may arise from a hostile environment. In other words, we get a better heat transfer geometry from enhancement, but at what cost?

Professor T. Fujii² My present view is that capital cost will be saved by devising such ideal tube arrangements that all cooling tubes bring their capability fully into play, on the premise that tube leakage and fouling can be prevented by proper counterplans. From this point of view more accurate knowledge concerning the effect of air upon heat transfer, characteristics of pressure drop, condensate inundation etc. is required.

I am rather too conservative to adopt enhanced tubes. The figures in Table 3 show that the physical size of the tube banks composed of enhanced tubes is not as small as may be expected from the heat transfer characteristics of a corresponding single tube. However, enhancement of shell side heat transfer can be effective for an air cooling zone. It is very difficult for me to comment on total cost, because I have no practical experience in condenser design.

Professor R.H. Nunn³ We thank Mr. Bindon for his comment which serves to highlight a most important point that perhaps deserved more emphasis in our paper. While not wishing to diminish the critical nature of the question of cost, our work has focussed upon the effectiveness of thermal enhancement methods. We have mentioned some possible "costs" such as pumping power, cleaning, structural factors, and manufacturability; and many of these receive attention in the references provided. In the end, of course, the question of value for money is closely related to the application. We have, in effect, declined to write a "financial equation".

Although our sample calculations have used length reduction as a measure of goodness in designing with enhancement, we would like to point out that such methods can lead to other beneficial effects. In Ref. 44, for example, a case is described in which heat duty is maintained with a 20% reduction in tube count. In the absence of enhancement this would require a 70% increase in bundle length and a 26% increase in weight. With enhancement, however, the length increase is negligible and the weight actually decreases slightly. Thus enhancement might be used to alleviate packaging problems. In other instances, steam-side pressure losses might be reduced through judicious application of enhancement. The sufficiency of the merits of adjustments such as these will finally depend upon the premiums to be placed upon the costs as well as the benefits.

1 Wylfa Power Station, C.E.G.B., N.W. Region, U.K.

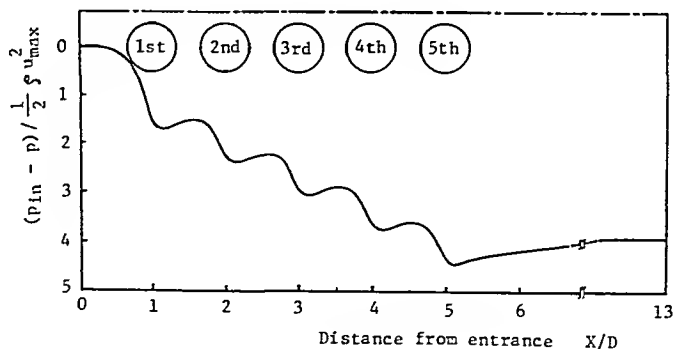
2 Research Institute of Industrial Science, Kyushu University, Kasuga, Fukuoka 816, Japan

3 Dept. of Mech. Eng., Naval Postgraduate School, Monterey, California, U.S.A.

Dr. Y.R. Mayhew⁴ I would like to congratulate Professor Fujii on an excellent and useful Keynote Paper, Paper (1), and would like to comment on the information on pressure drop given in his Table 2, which relates to his References (34) and (35). We do have complete, and provide some, data for pressure drop for single rows in those References. It is very important to distinguish between pressure drop across a single row, and pressure drop across the first row of a bank. For the former we provide data which we consider very reliable, for the latter it is very difficult to provide meaningful data because measurements are subject to considerable fluctuations, and moreover they are very sensitive to location of the pressure tappings between the first and second rows. It is for this reason that Reference (35) only provides relatively qualitative information on the latter.

In making comparisons of pressure coefficients in general, and between 'real-condensation' and 'simulation' data in particular, extreme care must be taken to ensure that the measured pressure drops have been normalised in the same way: what u or u_{\max} has been used in the denominator, and how has it been averaged in a 'suction' situation across a bank. It might be safer to compare values of pressure drop (corrected for momentum loss due to 'suction') rather than pressure coefficients. What is worrying is not only the disagreement between the 'Core-Part' column, say, lines 1 and 5, but that it appears that the disagreement goes the wrong way - one would have expected that two-phase flow (inundation) effects would reverse the sense of the disagreement. But there is a marked difference in the pitch-diameter ratios which might explain the discrepancy. The explanation may be that, in tightly packed banks, vapour-flow separation on the rear of a tube is hardly affected by suction.

Professor T. Fujii⁵ Many thanks for your valuable comments, almost all of which I agree with. The following figure shows an example of numerically calculated pressure distributions along a centre line between tubes in an in-line square tube bank, pitch-diameter ratio 1.5x1.5, $Re = u_{\max} D / \nu = 120$.



⁴ Dept. of Mech. Eng., University of Bristol, Bristol, U.K.

⁵ Research Institute of Industrial Science, Kyushu University, Kasuga, Fukuoka 816, Japan

The physical meaning of the pressure coefficient for each row in a bank is somewhat uncertain. However, you can see that the pressure coefficient for the 1st row can be extracted from the pressure gradient of the 2nd to the end row, if relative location of the pressure tappings are consistent, at least in a practical sense.

In a future publication I will discuss the reference value of u and the relation between pressure drop and pressure coefficient after making similar theoretical calculations for tube banks with suction, although such calculations are restricted to laminar flow at present. If you could provide the data for the same diameter, pitch-diameter ratio and Reynolds number range as those in our condensation test, because it is more difficult to carry out real-condensation tests than simulation tests with air suction, the question would be solved. Without a reliable knowledge of pressure drop we cannot pursue reasonable condenser design.

Mr. F.J.L. Bindon⁶ Fig. 8 in paper 4, presented by Dr. R.T. Deam, shows a strong periodic variation of steam and water temperature due to the presence of the sagging plates. Is this due to the temperature difference between the sagging plates and the condenser tubes, or is it due to the physical surface of the sagging plate?

Is Dr. Deam suggesting that such a number of tube plates gives rise to improved steam ejector performance due to the instability of the way in which the condensate droplets flow?

J.G. Andrews, R.T. Deam & J. Smalley⁷ The figure shows a strong periodic variation in vapour mixture temperature. The hypothesis we put forward is that water running down the tube plates entrains an air rich boundary layer which is transported downwards with the water. This mechanism will improve air removal if the air suction port is placed in a position which takes advantage of this effect.

Dr. J.W. Rose⁸ It seemed to me, from the presentations, that in none of papers 4, 5, 6 and 7 was a free-convection or buoyancy effect included. Because of relatively large density differences between regions of high and low concentration, it would seem that free convection should play an important role in determining the location of 'air pockets' within a condenser.

J.G. Andrews, R.T. Deam & J. Smalley⁹ The effect of buoyancy is included in the calculation of " λ ", the air entrainment coefficient, when we consider the Natural Convection Case and derive λ from the work of Sparrow and Lin. The details of the calculation were not included in the paper, due to lack of space, but the overall results are discussed under the heading Natural Convection Past a Vertical Plate.

As far as determining the location of "air pockets" in real condensers is concerned, the air transport mechanisms are insufficiently understood to make any general statement about the relative importance of buoyancy.

6 Wylfa Power Station, C.E.G.B., N.W. Region, U.K.

7 C.E.G.B., Marchwood Engineering Laboratories, Marchwood, Southampton, U.K.

8 Dept. of Mech. Eng., Queen Mary College, University of London, U.K.

9 C.E.G.B., Marchwood Engineering Laboratories, Marchwood, Southampton, U.K.

S. Al-Sanca, N. Rhodes & D.G. Tatchell¹⁰ Our mathematical model does not include terms to account for buoyancy effects. However, the calculations reported in the paper are for a relatively small condenser, the height is 0.78m, and mixture velocities are fairly high over most of the tube nest. I therefore believe that convection would dominate in this particular case.

In power station condensers operating at full load, a similar situation would probably prevail. At part load, however, free-convection may become more important and could be worth including in the model.

G. Beckett, B.J. Davidson & J.A. Ferrison¹¹ If by buoyancy you mean the difference in density between the steam alone and the air this should have little effect on the position of the 'air pockets' since the densities of steam and air are of similar magnitude. The pressure distribution throughout the tube nest determines the location of the 'air pockets'. If one were to include gravity terms for the gas phases alone when calculating pressure drops a significantly more accurate result would not be obtained since frictional pressure drop and momentum terms dominate this calculation in large power condensers where velocities are high outside the air pockets; the frictional term, for example, is several orders of magnitude larger than the gravity term. If, however, relative densities of air/steam/condensate mixtures were to be examined, significant differences occur but unfortunately knowledge of pressure drops in such mixtures is incomplete. Hopkins et al, Paper 10, however, mention in their paper at this symposium a correlation of steam pressure drop in presence of condensate and under the influence of a gravitational field.

C. Caremoli¹² No free convection or buoyancy effect is included in the numerical model presented in paper 6.

Some tests have been done including a buoyancy effect and it does not seem that free convection should play an important role in determining the location of "air pockets".

¹⁰ CHAM Ltd., Bakery House, High Street, Wimbledon, U.K.

¹¹ CERL, Kelvin Avenue, Leatherhead, Surrey, U.K.

¹² Electricité de France, quai Watier 78400, CHATOU, FRANCE

DISCUSSION POWER CONDENSERS - PRACTICE

W. Burrough¹ Has the author of Paper 16, J.R. Maurer, any experience of condenser tube change from traditional material to stainless steel where erosion due to abrasive silts, etc. have been the cause of failure? Has stainless steel given the required protection, whether in full tube form or insert?

J.R. Maurer² Stainless steels offer excellent resistance to the erosive effects of sand, silt, turbulence, etc. Data developed by several sources indicate the excellent performance of these alloys under extreme velocity conditions (up to 140 ft. per second). These materials have performed well in service exposures such as the Mississippi River where the softer brass alloys have suffered substantial wear and failure. Tube inserts of AL-6X have been used to control the erosive effects of inlet end turbulence for over a decade with total resistance to erosion attack. In my quarter of a century experience, I have never seen a stainless steel condenser tube with erosion damage on the inside surface and have only heard of a few instances where wet or high pressure steam has roughened the outside surface.

¹ W. Burrough, Alcan Lynemouth Ltd., Ashington, Northumberland, U.K.

² J.R. Maurer, Allegheny Ludlum Steel Corp., Brackenbridge, Pennsylvania, U.S.A.

DISCUSSION PROCESS CONDENSERS - THEORY

Dr. R.G. Sardesai¹ I have a question for Professor Cavallini, Paper 19, over the use of the Friedel equation.

Dr. Owen reports in his keynote paper that adiabatic correlations for frictional pressure gradient give a reasonable prediction of the overall pressure drop but they do not give the correct distribution of pressure along the channel. In your paper, you use the Friedel frictional pressure gradient correlation to give the local wall shear stress which is then used both to calculate the pressure drop and the heat transfer coefficient. Could you say whether the Friedel correlation was derived using data for condensing flows, and whether this correlation gave the correct pressure distribution along the channel in your tests.

Professor A. Cavallini² Friedel, Ref. (9), quotes that his correlation was derived from a data bank of about 25000 friction pressure drop results of various single and two component mixtures taken during unheated flow under widely varied test conditions. The correlation used is specifically given for vertical downward flow.

We did not see a definite trend of deviation between our experimental data and the calculated ones by the Friedel correlation. Experimental values were equally distributed about the calculated ones.

Dr. P.D. Hill³ In paper 20 the authors, Lee, Mayhew and Hollingsworth, have used suction to simulate condensation in order to be "unencumbered by the two phase effect of inundation". In a real condenser the effects of inundation have a marked effect on pressure drop and cannot be ignored. How do the authors propose to incorporate the results of their research into the design of real condensers?

Lee N.K., Mayhew Y.R. & Hollingsworth M.A.⁴ There is no easy answer to Dr. Hill's question, and further work would have to be carried out. The difficulty is that simulation via suction cannot be combined experimentally with two-phase flow. Ideally we would like to carry out two-phase flow experiments without suction on our rig, suitably modified (who is prepared to finance it?). The way forward would then be to study what method of 'superposition' of the two sets of data, single-phase with suction and two-phase without suction, provides agreement with real condenser data.

1 Heat Transfer Research Inc. (HTRI). Alhambra, California, USA.

2 Istituto di Fisica Tecnica, Università di Padova, 35100 Padova, Italy

3 ICI PLC, Brunner House, Northwich, Cheshire, U.K.

4 Dept. of Mechanical Engineering, University of Bristol, Bristol, U.K.

Dr. I.D.R. Grant⁵ In considering Paper 20 I would also like to comment on two-phase flow effects which are not modelled in this experiment and complicate further the prediction of pressure loss in a real condenser. I have noticed that if a homogeneous type mixture of air and water is introduced into a channel containing a tube bundle with a bypass lane the liquid transfers to the bypass lane. This maldistribution (or separation) of liquid and hence gas flow across the channel results in a considerable decrease in pressure loss.

Lee N.K., Mayhew Y.R. & Hollingsworth M.A.⁴ The nature of our response to Dr. Grant's very interesting comments must be similar to our reply to Dr. Hill. Separate two-phase flow experiments with by-pass lanes are needed to establish pressure drops and redistribution of flow of the liquid and gaseous phases between the bank and the lane. The problem is more difficult because, although we looked at the effect of suction, we only needed to look at the redistribution of flow of one phase. Clearly, by-pass experiments in this area will add a further dimension to the solution of this problem.

Dr. M.J.N. Wills⁶ Continuing the discussion of Paper 20, I would point out that in classical studies of tube-bundle bypassing, it has generally been considered that the crossflow region extends outside the tube-bundle to a distance equivalent to half the minimum clearance between the tubes. Have you considered moving the splitter plate towards the wall of the exchanger to try and ascertain the distance at which the interface between crossflow and bundle bypassing occurs in practice.

Lee N.K., Mayhew Y.R. & Hollingsworth M.A.⁴ In reply to Dr. Wills we would say that there appears to be some logic in defining the mass flow parameter ϕ in terms of mass flows which relate to areas S_{CF} and S_T rather than S_L and S_B as has been done in the paper (See Fig.2). The net effect of such redefinition would be to shift any correlation such as those given in Figs. 9(b) and 10(b). This would appear to be of little practical consequence, provided a user extracts information in the same manner in which it has been correlated. The classical studies put the boundary of the bank in the position mentioned by Dr. Wills in the course of adoption of an arbitrary definition useful in correlating results rather than for any fundamental reasons, and no more can be expected when flow patterns are as complicated as near a by-pass lane.

What seems to have been suggested, however, is to search for a dividing plane between the two regions considered at which interaction ceases. It seems unlikely that such a plane exists, and while redistribution goes on, the flow in the by-pass lane must continue to readjust itself right across the lane (except at the wall or on a line of symmetry).

Experiments on flow visualisation carried out since the Conference unfortunately proved of little use in showing up flow redistribution. Detailed velocity traverses, rather than the shifting of the splitter plate, may prove more revealing.

Dr. M. Rowe⁷ In my opinion the work performed by Dr. Lee and his co-workers was both useful and necessary. However could the authors offer an explanation as to why the measured pressure loss coefficients for tube banks with bypass lanes were more than expected from previous predictions?

5. National Engineering Laboratory, East Kilbride, Glasgow, U.K.

6. Heat Transfer and Fluid Flow Service, Harwell, Oxon, U.K.

7. CERL, Leatherhead, Surrey, U.K.

Lee N.K., Mayhew Y.R. & Hollingsworth M.A.⁴ Dr. Rowe's question can, we must assume, only relate to the earlier work of our Ref.(4), because Wilson's predictions were theoretically based.

We have no explanation to offer other than pure speculation. Although Ref.(4) and a predecessor provide information on correlations, they provide no hard information on the experimental arrangements from which the experimental data were derived. Although we have tried to obtain some of the original M.Sc. theses some considerable time ago, we are still struggling with this problem! Did they suck away the by-pass lane boundary layer at entry to the bank as we did? This may well have a marked effect on pressure drop and flow distribution.

We also believe that in Ref.(4), banks of 10×10 tubes were used rather than 5 or 6×7 as in our rig. We do not think that this can explain the discrepancies, but we may be wrong. If we are wrong, then our results cannot be generalised by the method used, but neither can those of Ref.(4).

D. Butterworth⁸ I would make a brief comment on Paper 21. I notice that the authors use the phrase "stagnant-film model" for what most other people refer to as "the film model". I believe that the use of the word "stagnant" is incorrect, because there is certainly flow across the film when there is mass transfer present. Also, there is usually a superimposed velocity parallel to the interface. The assumptions we are making in the model are as follows:

- (1) Conditions in the film only vary in the direction perpendicular to the interface and not parallel to the interface.
- (2) The film is laminar.
- (3) Conditions outside the film are constant.

The trick then is to choose the thickness of the film so that we get answers which agree with data or with other more complex models. One assumption concerning the thickness which often works very well indeed, is that the film thickness is the same with and without mass transfer.

In view of the above, my preferred title for this model is "equivalent laminar film model". I would be grateful for your comments on this.

W.C. Lee⁹ and J.W. Rose¹⁰ Replying to Mr. Butterworth, we would like to say that we have no special preference for the term 'stagnant-film model' which is found frequently in the literature. If 'stagnant' implies that all velocities are zero, it is not perhaps the best name. Equation (8) of our paper is easily obtained if it is assumed that the motion is purely one-dimensional and normal to the surface. The same equation may also be obtained in the presence of velocity parallel to the surface if it is assumed that the molar velocity parallel to the surface ($\bar{u} = \bar{n}/\bar{\rho}$) and the composition of the vapour-gas mixture are independent of distance along the surface. These assumptions, together with that of laminar flow and that the 'film' has finite thickness, probably cannot be satisfactorily covered by any short title. "Couette film model" has been suggested.

8. HTFS, Harwell, Oxon, U.K.
9. GEC Energy Systems LTD., Leicester, U.K.
10. Department of Mechanical Engineering, Queen Mary College (University of London)

Nomenclature

\tilde{m} mole flux of mixture parallel to the surface
 $\tilde{\rho}$ molar density of mixture

Dr. R. Taylor¹¹ In Paper 21, Lee and Rose have, in effect, compared several different methods of correcting "low flux mass transfer coefficients" for the effect of a finite rate of condensation of a single vapour in the presence of a non-condensing gas. Their work provides a simple and soundly-based equation for estimating the "high flux mass transfer coefficient" that is in good agreement with the available experimental data. However, their comparison with film theory is misleading because it is based on an inappropriate equation. The following remarks are offered in order to clarify these statements:

Regardless of the model of mass transfer (film, boundary layer or other) and of the units used (mass, molar or other), the rate of condensation is given by the following expression

$$\text{Condensation Rate} = \text{Diffusion Flux} + \text{Convective Flux} \quad (1)$$

per unit area

All models of mass transfer yield expressions for the diffusion flux of the form

$$\text{Diffusion Flux} = \text{High Flux Mass Transfer Coefficient} \times \text{Driving Force} \quad (2)$$

with

$$\text{High Flux Mass Transfer Coefficient} = \text{Low Flux Mass Transfer Coefficient} \times \text{High Flux Correction Factor} \quad (3)$$

It is important to recognise that the mass transfer coefficient is defined with respect to some reference velocity. Mass average and molar average velocities are the reference velocities most commonly used in engineering(1). For the case of interest here (a binary mixture with one non-transferring species) the mass average velocity, u^0 , is

$$u^0 = W_v \tilde{m}_v / \rho_v \quad (4)$$

and the molar average velocity is

$$u^* = \tilde{W}_v \tilde{m}_v / \tilde{\rho}_v \quad (5)$$

Equation LR1 (equation 1 in the paper by Lee and Rose) implicitly defines a mass transfer coefficient, β , in mass units relative to the mass average velocity. Equation LR14 implicitly defines a mass transfer coefficient, β , in molar units relative to the molar average velocity. The simple correspondence between them, equation LR16, does not hold unless $u^0 = u^*$ (true if the molecular masses of the vapour and gas are the same) since $m_{Dv} \neq \tilde{m}_{Dv} M$

Buried within the boundary layer equations of Lee and Rose is the implicit assumption of constant mass density. The film model equations which are compared to the boundary layer equations are based on the assumption of constant molar density (see (1) where these equations are derived). These two assumptions are incompatible whenever, as here, the molecular masses of the gas and vapour differ.

11. Dept. of Chem. Eng., Clarkson College, Potsdam, New York 13676, U.S.A.

It is easy to show that in mass units and assuming constant mass density the form of equation LR8 is preserved

$$m_v = \beta^* \ln \left[\frac{1-W_{v0}}{1-W_{v\infty}} \right] = \beta^* \ln \left[\frac{W_o}{W_\infty} \right] \quad (6)$$

where β^* is the low flux mass transfer coefficient defined with respect to the mass average velocity. The appropriate forms of equations LR18 and LR19 are

$$m_v = \beta^* \frac{\phi}{e^{\phi}-1} (W_{v\infty} - W_{v0}) + W_{v\infty} m_v \quad (7)$$

$$= \beta^* \frac{\phi e^{\phi}}{e^{\phi}-1} (W_{v\infty} - W_{v0}) + W_{v0} m_v \quad (8)$$

$$\text{where } \phi = m_v / \beta^* = \ln(W_o / W_\infty) \quad (9)$$

The functions of ϕ in (7,8) are the high flux correction factors given by film theory.

β^* cannot be calculated from its film theory definition ($\beta^* = \rho D / \delta$) since the film thickness δ is not normally known. In practice, the low flux coefficient is estimated from a suitable correlation of experimental mass transfer data or from a heat transfer correlation combined with the Chilton-Colburn analogy (1). We therefore introduce the low flux Sherwood number, Sh^* , defined by

$$Sh^* = \beta^* d / \rho D \quad (10)$$

and calculate it, in the present case anyway, from the correlation

$$Sh^* = 0.57 Re^{\frac{1}{2}} Sc^{\frac{1}{3}} \quad (11)$$

Lee and Rose present expressions for the high flux Sherwood number, Sh , defined by equation LR5 and related to the low flux Sherwood number by

$$Sh = Sh^* \times \text{High Flux Correction Factor } (\Xi) \quad (12)$$

It is worth emphasizing here that Sh^* is, as it should be, model independent (see the intercept on the left hand vertical axis in figures 5); only the high flux correction factor is model dependent. Thus for the Acrivos-Mills formula, comparison of equations (11,12) and LR30 shows that the correction factor, Ξ , is

$$\Xi = \left\{ 1 + \frac{[1.57(1-W_\infty/W_o) Sc^{0.1}]^{3/2}}{(1+Sc)^{1/2} (W_\infty/W_o)^{1/2}} \right\}^{2/3} \quad (13)$$

The corresponding result for the equation of Rose is a little harder to express in such a neat form but could be written down simply by dividing equation LR25 by $0.57 Sc^{1/3} (=Sh^* Re^{-1/2})$.

The correction factor obtained from the film model is the simplest of all:

$$\Xi = \frac{\ln(W_o/W_\infty)}{1 - W_o/W_\infty} = \frac{\phi e^\phi}{e^\phi - 1} \quad (14)$$

It should be noted that, unlike the corresponding result of Lee and Rose (equation LR33 divided by $0.57 Sc^{1/3}$), equation (14) is independent of the ratio of molecular masses and depends on W_o and W_∞ only in so far as they appear together as W_o/W_∞ .

It would, perhaps, be more logical to compare the methods by plotting $Sh/Sh^* = (Sh Re^{1/2} / Sh^* Re^{1/2}) = \Xi$ against W_o/W_∞ . It would then be seen that Equation (14) lies somewhat closer to equation (13) than does the erroneous result used by Lee and Rose. The correction factor given by (14) still falls below the boundary layer model (13) by a factor of $2\frac{1}{2}$ at $W_o/W_\infty = 100$ and $Sc = \frac{1}{2}$. However, this corresponds to a driving force of such magnitude that is unreasonable to expect such conditions to be maintained throughout all but the smallest condensers. In practice, the largest driving forces would be expected near the vapour/gas inlet but in the bulk of a large condenser driving forces would correspond more to the left hand side of figures 5 - the region where film theory does much better. It would be unrealistic to expect film theory to do as well as a more rigorous boundary layer model; that it does so well at lower driving forces and in other situations (1) is more important.

In view of all of the foregoing, could Dr. Lee and Professor Rose provide a corrected version of figure 5 and, also, revise their comments with regard to the film model?

Reference:

1. Bird, R.B., Stewart, W.E., and Lightfoot, E.N., 1960, "Transport Phenomena", Wiley, New York.

W.C. Lee¹² and J.W. Rose¹³

The comments below relate to consecutive paragraphs of Professor Taylor's written discussion contribution. Additional nomenclature and a figure (Fig. R1) are given at the end of this reply.

(1) We do not regard equations (25) and (34) of our paper as methods of 'correcting' anything. These equations provide an expression for the mass-transfer coefficient which is valid for both high and low mass-transfer rates.

(2) We regard Professor Taylor's equation (1) more as an aid to memory than an expression of physical principle. The following expressions for mass and mole flux in the y-direction are mutually convertible

$$m_v = \rho v W_v - \rho D \frac{\partial W_v}{\partial y} \quad (R1)$$

$$\tilde{m}_v = \tilde{\rho} \tilde{v} \tilde{W}_v - \tilde{\rho} D \frac{\partial \tilde{W}_v}{\partial y} \quad (R2)$$

Subscript v is used to denote the constituent considered, e.g. vapour. The equations, however, do not transform term by term so that, for example, what might be considered the 'diffusive flux' in the mass-based equation does not transform to the diffusive flux term in the mole-based equation.

We do not appreciate the meaning of the word "high" in Professor Taylor's equation (2). This equation seems otherwise to be the normal definition of mass-transfer coefficient.

(3) We do not understand Professor Taylor's statement that mass-transfer coefficient is defined "with respect to" a velocity. The definition we have used (which seems to us most deserving of the description 'mass') is

$$\beta = -\rho_o D (\partial W_v / \partial y)_o / (W_{vo} - W_{v\infty}) \quad (R3)$$

The analogous molar version is

$$\tilde{\beta} = -\tilde{\rho}_o D (\partial \tilde{W}_v / \partial y)_o / (\tilde{W}_{vo} - \tilde{W}_{v\infty}) \quad (R4)$$

so that

$$m_{vo} = \rho_o v_o W_{vo} + \beta (W_{vo} - W_{v\infty}) \quad (R5)$$

$$\tilde{m}_{vo} = \tilde{\rho}_o \tilde{v}_o \tilde{W}_{vo} + \tilde{\beta} (\tilde{W}_{vo} - \tilde{W}_{v\infty}) \quad (R6)$$

where quantities without subscript v denote properties of the mixture and

$$v_o = m_o / \rho_o \quad (R7)$$

$$\tilde{v}_o = \tilde{m}_o / \tilde{\rho}_o \quad (R8)$$

2 GEC Energy Systems Ltd., Leicester, U.K.

3 Department of Mechanical Engineering, Queen Mary College (University of London)

β and $\tilde{\beta}$ as defined above and in equations (14) and (15) of our paper are related by equation (16) of our paper (i.e. $\beta = M_{\infty} \tilde{\beta}$). This equation is valid whether or not the molar masses of the vapour and gas are the same, i.e. Professor Taylor is incorrect in his assertion.

(5) We agree that the boundary-layer theory result assumes uniform (mass) density and that the mole-based version of the 'film theory', with which we made comparisons, assumes uniform molar density. We do not, however, understand the statement that 'these two assumptions are incompatible', since they are not used in the same model. In order to obtain equation (33) of our paper from our equation (8) (i.e. to obtain an expression for Sherwood number in terms of mass fractions, from the mole-based version of the 'film theory') it is only necessary that the density used in the definition of Sherwood number be the same as that used in the Schmidt number in our equation (10).

(6) In our paper we did not consider the mass-based version of the 'film theory'. When the (mass) density of the mixture is assumed uniform and the velocity and composition are assumed independent of distance along the surface, the same procedure leads to

$$m_v = \frac{\rho D}{\delta} \ln \left(\frac{W_0}{W_{\infty}} \right) \quad (R9)$$

If we put $\beta = \rho D / \delta$ and use for β , the value given by equation (13) of our paper (i.e. so as to ensure that the 'film theory' gives the correct result in the zero mass-transfer limit) we obtain

$$\text{ShRe}^{-1/2} = \frac{0.57 \text{Sc}^{1/3}}{(1 - W_{\infty}/W_0)} \ln \left(\frac{W_0}{W_{\infty}} \right) \quad (R10)$$

The above equation is not the same as equation (33) of our paper. The latter (which is not 'erroneous') uses the (different) assumptions of the mole-based film theory and the final result has then been expressed in terms of mass fractions. It may be noted that the mass-based film theory indicates that $\text{ShRe}^{-1/2}$ does not depend on the molar mass ratio, r . Similarly the expression for $\text{ShRe}^{-1/2}$ in terms of mole fractions would not involve r in the case of the mole-based theory, but would involve r in the mass-based theory.

In our paper we considered only the mole-based film theory since this appeared to be more widely used than the mass-based version. The mass-based result given above is compared here (Fig.R1) with the data and the boundary-layer result. We emphasize that this is not a 'correction' of Fig.5 of our paper. As may be seen, the mass-based film theory agrees with the boundary-layer result and the experimental data better than the mole-based film theory when $r > 1$. When $r < 1$ the mole-based film theory is better.

Nomenclature

- D diffusion coefficient
- M_{∞} bulk molar mass of mixture
- m_0 mass flux of mixture at the condensate surface (y-direction)
- \tilde{m}_0 mole flux of mixture at the condensate surface (y-direction)
- m_v mass flux of vapour (y-direction)
- m_{v0} value of m_v at the condensate surface

\bar{m}_v	mole flux of vapour (y-direction)
\bar{m}_{v0}	value of \bar{m}_v at the condensate surface
Re	Reynolds number
r	molar mass ratio, vapour-to-gas
Sc	Schmidt number
Sh	Sherwood number
v	velocity component (y-direction) = total mass flux/ ρ
\bar{v}	molar velocity component (y-direction) = total mole flux/ $\bar{\rho}$
v_0	value of v at the condensate surface
\bar{v}_0	value of \bar{v} at the condensate surface
W	mass fraction of gas
W_0	value of W at the condensate surface
W_∞	free-stream value of W
W_v	mass fraction of vapour
W_{v0}	value of W_v at the condensate surface
$W_{v\infty}$	free-stream value of W_v
\bar{W}_v	mole fraction of vapour
\bar{W}_{v0}	value of \bar{W}_v at the condensate surface
$\bar{W}_{v\infty}$	free-stream value of \bar{W}_v
y	distance, distance measured normal to the surface
β	surface mass-transfer coefficient
$\bar{\beta}$	'molar surface mass-transfer coefficient'
δ	film thickness in film model
ρ	density of mixture
ρ_0	value of ρ at the condensate surface
$\bar{\rho}$	molar density of mixture
$\bar{\rho}_0$	value of $\bar{\rho}$ at the condensate surface

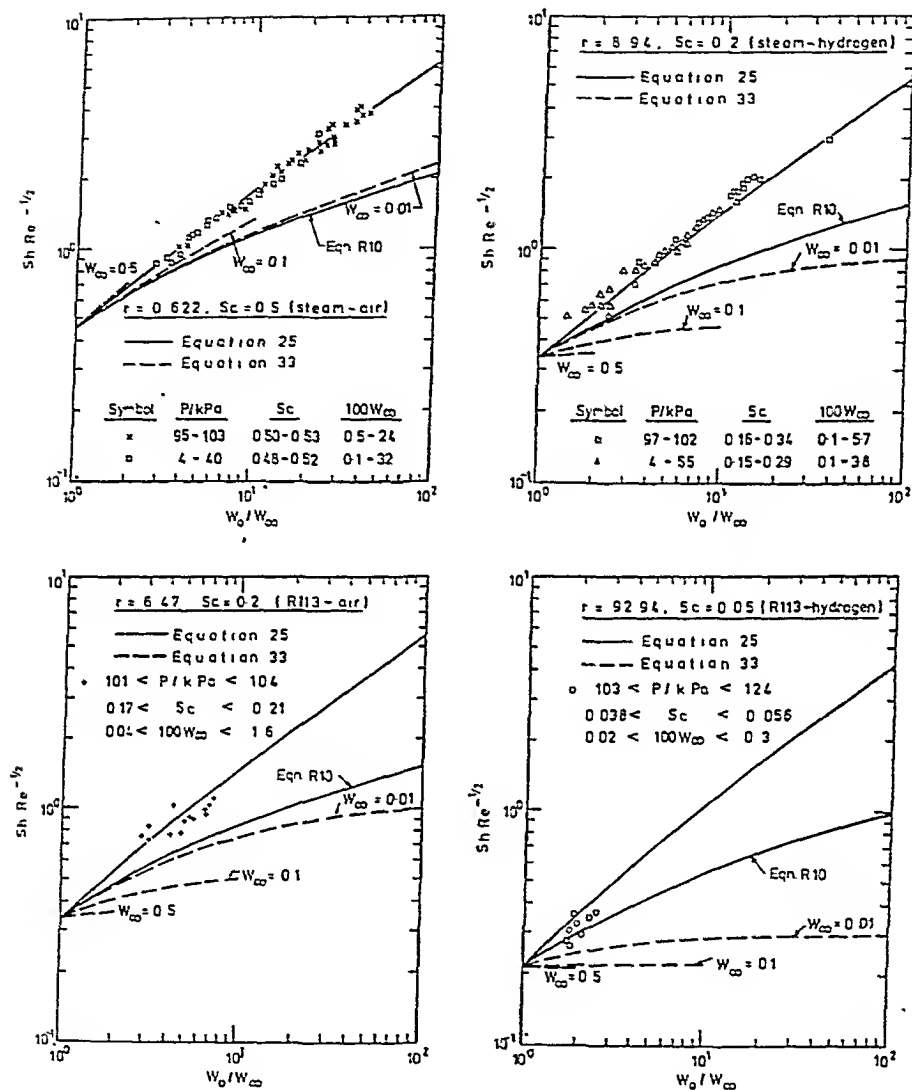


Fig.R1 Comparisons with 'stagnant film models' including mass-based version (eqn.R.10)

(W.C. Lee and J.W. Rose. Authors' reply to R. Taylor).

Dr. B.J. Davidson¹⁴ Does Dr. Taylor, author of Paper 23, find that the larger and sparser the Jacobian Matrix the more computationally efficient the algorithm becomes?

In many problems $[C_k]$ is a constant and the algorithm is then based on the Quasi-Newton method modified by Broyden & Schubert. Under these circumstances the speed of convergence depends critically on the initial guesses. Can you offer any suggestion for weakening this dependence on the initial guess?

Dr. Ross Taylor¹⁵ If Dr. Davidson's question refers to the performance of the hybrid algorithm relative to the performance of a finite difference Newton method, then the answer is a qualified "no". The hybrid algorithm seems to be approximately "x" times faster than a finite difference Newton method regardless of the size and sparsity of the Jacobian matrix. "x" seems to depend only on the application of the method (i.e. the equations being solved). The performance of the hybrid algorithm is closely related to the quantity of good derivative information that is accumulated in $[C_k]$. That is, if $[C_k]$ is a good approximation to $[J_k]$ then the hybrid algorithm will do well. If, on the other hand, $[C_k]$ bears very little resemblance to $[J_k]$ then the hybrid algorithm will be much less successful relative to a method that generates good approximations to $[J_k]$; a finite difference Newton method. It should be noted that in the condensation problems that we have solved, the Jacobian is quite small (order 10) and very nearly full. Very large and sparse Jacobians arise in the solution of, for example, multicomponent-multistage separation process problems where hundreds of equations are solved simultaneously. Some numerical results for these problems are reported by Westman and Lucia (1,2).

1. Westman, K.R., and Lucia, A., 1983, Comput. Chem. Eng., under review.
2. Lucia, A., and Westman, K.R., 1983, Proceedings of the Foundations of Computer Aided Chemical Process Design, Snowmass, Colorado, to appear.

With respect to Dr. Davidson's second question, it is our belief that most problems of a physical or engineering origin will not lead to $[C_k]$ being a constant matrix. However, if $[C_k]$ is constant, then the algorithm reverts, essentially to Broyden's or Schubert's methods. These algorithms appear quite sensitive to the initial guess and it is difficult to predict in advance how they will behave. We can offer no suggestions for weakening the dependence on the initial guess of these algorithms.

Dr. M.A. Taylor¹⁶ I have a question concerning Paper 23. In an empirical situation it is usually possible to plot data in such a way that a polynomial curve fit can be carried out within reasonable r.m.s. error. The resulting equation can then be handled mathematically with ease - e.g. differentiated or integrated, and is reasonably accurate provided one stays within the bounds of the data range. Such a procedure has been used to integrate complicated view factor data, for example.

14. CERL, Kelvin Avenue, Leatherhead, U.K.
15. Dept. of Chem. Eng., Clarkson College, Potsdam, New York, 13676, USA.
16. Britoil, 29 Bolton Street, London, W1Y 8BN. U.K.

Would it be possible, and if so practical, for a program to be written to generate spot data for the problem, curve fit it with an appropriate polynomial and then treat the equation mathematically? This procedure, if possible, would presumably be robust.

Dr. R. Taylor¹⁵ The solution to the material and energy balance equations for some chemical process by Newton's method or related methods necessarily involves the calculation (or approximation) of physical properties and their derivatives with respect to process variables like temperature and composition. Thus, a polynomial curve-fit must be able to supply accurate estimates of the properties themselves and of their derivatives.

In light of the results obtained with the hybrid approach, the work associated with polynomial curve fitting does not appear to be justified. The Schubert update does a very nice job of approximating those physical properties derivatives that are not readily available and, moreover, it's inexpensive.

Further, there is no reason to believe that a reasonable fit of any physical property (for example, K value) with respect to system variables (such as temperature and composition) implies good derivative information, even with the proper smoothness of the approximating polynomial.

For example, in the area of computer aided flowsheeting some workers are advocating simple polynomial approximations for activity coefficients of the form

$$\ln \gamma_i = a_i + b_i x_i$$

where a_i and b_i are determined by solving a least squares problem using a small number of rigorous activity coefficient values. The parameters a_i and b_i are updated as necessary.

The numerical problem associated with this approach is that it will lead to inconsistent Jacobian approximations if, as will often be the case with non-ideal systems, the activity coefficients depend strongly on the mole fraction x_k ($i \neq k$). This, in turn, can cause convergence difficulties.

If, on the other hand, a more complex approximating polynomial is used, then the fitting procedure becomes expensive. In this case, finite differencing might just as well be used.

In summary, curve fitting may be possible but it should be used with extreme care where derivatives are concerned.

Dr. Mayhew⁴ May I comment that Figure 17, of the keynote paper of Owen and Lee, Paper 18, taken from Dr. Blangetti's doctoral dissertation, carried out under Professor Schlünder, uses the following, German style definition of Reynolds number,

$$\text{Re}_L = \frac{\rho u \delta}{\eta} = \frac{\dot{m}}{\eta}$$

which is a quarter of the UK/USA-style definition based on the 'equivalent diameter' 4δ , viz.

$$\text{Re}_L = \frac{\rho u 4\delta}{\eta} = \frac{4\dot{m}}{\eta}$$

Mr. C Baker¹⁸ The work covered by Paper 18 covering high vapour shear condensation inside tubes refers to tubes of circular cross section.

Could you please suggest a method whereby the information could be modified to allow it to be applied to rectangular ducts with high aspect ratios, i.e. 5:1 to 10:1.

Would, also any further modifications be required for applications whereby the condensation only takes place on one surface of a rectangular duct.

Dr. R.G. Owen¹⁷ and Dr. W.C. Lee⁹ The methods given in the paper for shear controlled condensation apply specifically to tubes of circular cross-section. However, these methods should give predictions of reasonable accuracy for square channels provided the hydraulic diameter of the square channel is used in the analysis. Although it is possible to use these methods for rectangular channels of high aspect ratio, the accuracy of the methods will inevitably become poorer as the aspect ratio increases. Theoretical models and experimental data are both lacking for shear controlled condensation in narrow rectangular channels. The only relevant work of which I am aware is a Russian paper:

"Heat Transfer and Hydraulic Resistance during Cooling Agent Condensation in Narrow Vertical Channels" by Ivanov, O.P. and Mamchenko, V.O., Kholod, Tekh., No. 6 pp 23-28 (1973).

Where condensation takes place on only one surface of the channel it is likely that condensate from this surface will be entrained into the vapour core and that some of this condensate will be deposited onto the other surfaces of the channel. The higher the vapour shear the more vigorous these entrainment and deposition processes become. At high vapour velocities, the flow in the channel may thus be similar to that which would occur if condensation occurred on all surfaces and the prescribed methods should give a reasonable prediction of heat transfer coefficient.

Dr. R.H. Nunn¹⁹ In the film that Dr. Owen has shown I believe that I saw a fair amount of what is called "side drainage". In such flows, condensate drainage occurs in paths leading, in an intermittent way, to the sides of tubes in adjacent columns. I would like to ask if such drainage paths are important in the experience of HTFS especially in the shear-dominated regions such as illustrated (?) in the film.

Recommended reference: Eissenberg, Proc. 4th Int. Heat Transfer Conference, Paris, Vol I, HE 2.1, 1970.

(Also in Power Condenser Heat Transfer Technology.)

18. Marconi Underwater Systems Ltd., Browns Lane, Portsmouth, U.K.
19. Naval Postgraduate School, Monterey, California, U.S.A.

Dr. R.G. Owen¹⁷ and Dr. W.C. Lee⁹ This is a good question - I only I wish I had a good answer to it! There is evidence that condensate drainage in staggered banks may lead, in an intermittent way to the sides of tubes in adjacent columns. This may occur in low velocity flows as reported by Eissenberg and is also apparent in the visualisation work on high velocity flows performed at Harwell. At the present time it is unclear whether this effect plays an important role in modifying the heat transfer characteristics of the flow. As far as I am aware, none of the theoretical models of inundation currently available are sufficiently detailed to account properly for this effect.

Additional Comments by R.G. Owen¹⁷ and W.C. Lee⁹ The authors would like to thank Dr. R. Taylor for pointing out typographical errors in equations (65) and (66) of the paper. Equation (65) should be written

$$(\dot{J}_b) = [B] [\phi] \{\exp[\phi] - I_1\}^{-1} (\tilde{y}_b - \tilde{y}_i)$$

since division by a matrix is undefined. Equation (66) is dimensionally inconsistent and should read

$$(\dot{J}_b) = \tau_{\beta_{eff,j}} (\tilde{y}_b - \tilde{y}_i)$$

where $\tau_{\beta_{eff,j}}$ is a diagonal matrix of effective mass transfer coefficients and is a function of $\tau_{D_{eff,j}}$.

DISCUSSION PROCESS CONDENSERS - PRACTICE

Dr. R.T. Deam¹ Have the authors of Paper 28, any evidence to suggest the existence of similar effects of poor performance for the case of condensation outside tubes?

For condensation inside tubes would the use of a separate vent pump for each tube solve the problem, although I realise this to be impractical?

J.A.R. Henry, I.D.R. Grant, C.D. Cotchin² For condensation outside a tube bundle, as in a power condenser, the desired flow direction is not so well defined but is generally towards a vent point. Flow maldistribution can allow stagnation regions to form within the condensing surface. leading to gas blanketing and well-known loss of performance. The prevention of flow maldistribution and hence gas blanketing is not so easily achieved (eg by inserts) for condensation outside tubes where the flow is two-, or more likely, three-dimensional.

Yes, anything which results in an assertive pressure change (whether negative in the case of inserts on positive in the case of separate vent pumps) can eliminate flow maldistribution. The expense of separate vent pumps clearly precludes their use but furthermore, unless they are individually sized or throttled they may vent more vapour than is necessary.

¹ C.E.C.B., Marchwood Engineering Laboratories, Marchwood, Southampton, U.K.

² National Engineering Laboratory, East Kilbride, Glasgow, U.K.

5. Set $[J_k] = [C_k] + [A_k]$ and solve the linear system $[J_k](S_k) = -(f_k)$ for (S_k)
6. Set $(X_{k+1}) = (X_k) + (S_k)$
7. Compute $(f(X_{k+1}))$ and $[C_{k+1}]$ as in steps 2 and 3 above.
8. Define $(S) = (X_{k+1} - X_k)$ and $(Y) = (f_{k+1} - f_k) - [C_{k+1}](S)$ and update $[A]$ using Broyden's method (35) or Schubert's (36) method.
9. Increment k and return to step 4.

Step 1 probably deserves further clarification since the numerical performance is intimately related to it. In the five component problem below, we have initialised T_I and \bar{y}_{1I} as those values in equilibrium with a condensate of composition \bar{y}_{1g} . In the six component problem, which includes a sparingly soluble component, \bar{y}_{1I} is initialised as \bar{y}_{1g} . The algorithms appear to be sensitive to the initial guess of the n_1 but not to the initial guesses of the y_{1I} or T_I . We have set the \dot{n}_1 according to the units used in the calculations. Thus, if kmol/m²s are used, then the \dot{n}_1 are set initially to 10^{-4} (no component is truly non-condensable (11)). All of the foregoing applies only to the inlet. At downstream locations, the values pertaining to the solution of the previous step are used to initialise (X_0) . Two ways of initialising $[A_0]$ come to mind. The first is to use finite differences. Clearly, this is far more costly than the alternative $[A_0] = [0]$ which is used in our application of the hybrid method.

Numerical Results

The hybrid algorithm and its forebears described above have been programmed on an IBM 4341 and used to solve a number of multicomponent condensation problems. The examples for which we report numerical results are (i) a five component hydrocarbon vapour problem posed by Kern (1) and solved by Webb and McNaught (11) using an effective diffusivity method and (ii) a six hydrocarbon mixture (which includes hydrogen) solved by Krishna et al. (7) using various methods of calculating the fluxes. The specifications of these two problems are given in Table 2. Physical and transport properties have been calculated from the methods used by Webb and McNaught (11). The Chao-Seader method was used for the thermodynamic property calculations, Prandtl and Schmidt numbers are calculated at film average conditions. One change has been made in the six component problem, we do not consider hydrogen to be truly non-condensable ($\dot{n}_{H_2} \neq 0$). The convergence tolerance, t , is 10^{-6} and double precision was used in all calculations.

The performance of these algorithms and of the tearing strategy of Webb and co-workers (11,13,15) for three different methods of calculating the \dot{n}_1 is recorded in Table 3. The algorithms are identified as follows.

- (i) FDNEW: Finite difference Newton method
- (ii) HYB: The hybrid algorithm
- (iii) QNAN: Quasi-Newton method with $[J_0] = [C_0]$
- (iv) QNFD: Quasi-Newton method with $[J_0]$ given by finite difference calculations
- (v) WEBB: Tearing algorithm of Webb and coworkers (11,13,15)

Central difference approximations have been used in the finite difference calculations: The methods of calculating \dot{n}_1 are

TABLE 2 - Specification of the five and six component hydrocarbon condensation problems

Number of components	5	6
Condenser tube orientation	vertical	vertical
Vapour flow direction	down	down
Number of tubes	1324	1
Tube diameter (m)	0.0254	0.0254
Tube length (m)	2.438	1.442
Inlet vapour flow (kmol/s)		
n-Octane	0.2706	8.4×10^{-6}
n-Heptane	0.3251	4.2×10^{-6}
n-Hexane	0.0541	12.6×10^{-6}
n-Butane	0.2709	6.3×10^{-6}
Propane	0.1624	10.5×10^{-6}
Hydrogen	0.0	28.0×10^{-6}
Vapour inlet temperature (K)	413.06	345.4
Coolant temperature at top (K)	300*	283.15
Coolant flow rate (kg/s)	-	0.04376
Coolant flow direction	-	up
Heat transfer coefficients		
α_c (W/m^2K)	1700*	-
α_{oi} (W/m^2K)	-	1700*
Condensate mixing	none	none
Source of Problem	(11)	(7)

*Assumed constant throughout condenser

- (i) KS : Krishna-Standart method (19)
(ii) LT : Linearised theory (20,21)
(iii) ED : Effective diffusivity method with $\beta_{ieff} = \beta_{in}$

Note that non-condensing (or sparingly soluble) gases if present are the usual choice of species n.

It is apparent from the quoted results that algorithm HYB is, by some way, the best of those considered. We should point out that other methods involving nested iterations (7) have also been tried and found to be much less efficient. It must be said that we were unable to get the algorithm of Webb et al. (11,13,15) to solve the six component problem due solely to an unsuitable method of calculating the bubble point of a mixture containing hydrogen and not to any shortcomings of the basic strategy. Table 2 does not, however, tell the complete story. For different initial estimates of the \bar{n}_i (we have tried 10^{-3} down to 10^{-12}) both of the quasi-Newton methods fail to converge these examples. The finite-difference Newton and hybrid methods, on the other,

TABLE 3 - Numerical results for the five and six component condensation problems

Mass Transfer Method	Algorithm									
	FDNEW It	Time*	HYB It	Time*	QNAN It	Time*	QNFD It	Time*	WEBB It	Time*
5 Components : inlet										
KS	5	13.50	10	1.83	18	2.58	16	4.22	8	6.94
LT	5	13.16	12	2.05	18	2.58	18	4.40	9	6.04
ED	5	9.30	13	1.76	19	2.00	18	3.36	8	4.93
5 Components : average of 9 downstream locations										
KS	3.2	9.55	6.6	1.24	9.0	1.37	8.2	3.40	9.0	8.84
LT	3.2	9.46	6.6	1.24	8.2	1.27	8.3	3.39	8.9	6.99
ED	3.2	7.1	9.2	1.31	12.3	1.40	7.9	2.54	9.0	6.42
6 Components : inlet										
LS	7	27.98	13	2.81	20	3.59	22	9.22		
LT	7	26.68	12	2.57	20	3.46	21	6.77		
ED	6	15.85	14	2.25	20	3.04	23	5.09		
6 Components : average of 9 downstream locations										
KS	3.4	15.87	6.0	1.60	7.1	1.56	7.4	4.97		
LT	3.4	15.43	6.3	1.64	7.7	1.62	7.4	4.85		
ED	3.4	11.57	7.4	1.49	11.1	1.68	10.1	3.87		
*Time in service units (SU): 1 SU = 1 second										
It = number of iterations (outer loop in the case of WEBB)										

hand, were completely successful. We also note that simply setting $[J_k] = [C_k]$ (with $[C_k]$ defined above) (called the partial-Newton method in (16)) will sometimes work well but is just as likely to fail completely.

Many other problems derived from these two examples by changing the constituents, their number, the inlet vapour composition, flow rate and temperature and by using a different method to calculate the thermodynamic properties (UNIQUAC) have also been solved. Other, similar, problems involving both condensation and evaporation, those in refs (8,37-39), have been solved anew by adapting the approach described here. All of these examples confirm the statements above concerning the robustness and efficiency of the hybrid method compared to a finite-difference Newton method and of the disappointing and erratic performance of the quasi-Newton and partial-Newton methods.

Usage and Abuse

1. It is better to use functions which are simple differences between, for example, energy fluxes, as in equations (18-21), rather than normalised functions involving the same fluxes. The present choice of functions, equations (18-21), requires fewer iterations than any other variation we have tried (this is only relevant with the nonsymmetric quasi-Newton methods which are not scale invariant). In any case, it is easier to differentiate the functions given above.

2. We have found it quite adequate to use Broyden's method to update $[A]$ even if this matrix contains some zeroes. However, this may not always be true.

3. Derivatives of K -values with respect to T_I must be included in $[C_k]$. The major contribution to $\partial K_i / \partial T_I$ is given by the temperature derivative of the natural logarithm of the pure component fugacity. This is usually expressed in the form of an extended Antoine equation, even for thermodynamic models like UNIQUAC. Neglect of these derivatives may substantially affect (for the worse) the numerical performance.

4. It is a good idea to restrain quantities that should remain non-negative from becoming less than zero. Most physical properties subroutines do not take kindly to mole fractions less than zero.

5. If the equations are not scaled (which is our recommendation) then, when the energy balance equations, H , are converged, so are all of the other equations. This is because, if SI units are used, the various terms in the equations have the following typical orders of magnitude: $M_i = O(10^{-3}, 10^{-4})$, $H_i = O(10^4)$, $E_i = O(1)$. This fact can be used to choose an appropriate value of t , the convergence tolerance. The value used in our calculations (10^{-6}) turned out to be rather more stringent than was really necessary.

CONCLUDING REMARKS

The Last Question: Which Method to Use?

There are actually two questions to be answered here. The first concerns the choice of algorithm. The results obtained to date suggest a strong case for the use of the hybrid method of Lucia and Macchietto (16) to converge simultaneously all of the equations involved in the calculation of the local transfer rates. It is important to emphasize that the quasi-Newton algorithms are much less robust than the hybrid method. While we have solved here a fairly general condensation problem, any variation on this theme can readily be solved along the lines described above (see (5,6,8,10,12,14) for other possible applications).

The second question concerns the choice of method to predict the \dot{n}_i . It is clear (to us at least) from the now rather numerous calculations made by ourselves and others that the approximate methods that take interaction effects into account give results that, for all practical purposes, are almost indistinguishable from those obtained using the KS method. Methods which neglect interaction effects may sometimes lead to very large discrepancies. For example, the effective diffusivity method predicts outlet mole fractions that, in the six component problem, differ from the corresponding quantities obtained using the KS method by between 5 and 80%. None of the other approximate methods (and we include the explicit methods (23-25) here) give results that differ by more than a few percentage points. In fact, we have yet to find an application where the differences between any of the interactive methods are truly significant (39).

Now, an algorithm is available which effectively eliminates the convergence difficulties and more lengthy matrix computations of some of the interactive methods. It is to be noted (see Table 3) that the interactive methods do not take substantially more time than the effective diffusivity methods. Moreover, effective diffusivity methods are not always the fastest. Minor changes in specification can alter, sometimes substantially, the number of iterations required, and reverse the relative merits of the methods. Thus, although the choice of method to calculate the \dot{n}_i must remain a matter for

personal preference, it is our belief, based on the extensive statistical comparison of (27) and the present computational results, that there is no longer any justification for using methods of the effective diffusivity type to predict rates of mass transfer in gas mixtures.

ACKNOWLEDGEMENTS

This material is partially based upon work supported by the National Science Foundation under Grant Number CPE 8105516.

The authors would like to thank T. Chakravarty, H. Sardar, U. Phukan and R. Scheffe for their assistance with the computations.

SYMBOLS USED

[A]	= approximated part of Jacobian matrix
[B]	= matrix of order $n-1$ of multicomponent diffusive mass transfer coefficients ($\text{kmol/m}^2\text{s}$)
[B]	= matrix of order $n-1$ of multicomponent total mass transfer coefficients ($\text{kmol/m}^2\text{s}$)
[C]	= computed part of Jacobian matrix
\bar{c}_p	= molar specific heat capacity (J/kmol K)
c_p	= specific heat capacity (J/kg K)
E_i	= discrepancy function defined by equation (19)
(f)	= column matrix (vector) of discrepancy functions
H_i	= discrepancy function defined by equations (18,20)
j_i	= molar diffusion flux ($\text{kmol/m}^2\text{s}$)
[J]	= Jacobian matrix
K	= "K-value", vapour liquid equilibrium ratio
\dot{M}	= mass flow rate (kg/s)
M_i	= discrepancy function defined by equations (17)
\dot{n}	= molar flowrate (kmol/s)
\dot{n}	= molar flux ($\text{kmol/m}^2\text{s}$)
n	= number of components
\dot{q}	= conductive heat flux (W/m^2)
(S)	= column matrix of the corrections to (X)
T	= temperature (K)
\bar{x}	= mole fraction in condensate
(X)	= column matrix of iteration variables
\bar{y}	= mole fraction in vapour
(Y)	= column matrix of function differences

Greek Symbols

α	= heat transfer coefficient ($\text{W/m}^2\text{K}$)
S_{ij}	= mass transfer coefficient of the i - j pair ($\text{kmol/m}^2\text{s}$)

δ_{ieff}	= effective mass transfer coefficient ($\text{kmol/m}^2\text{s}$)
$\Delta \bar{h}_v$	= molar latent heat (J/kmol)
δ_{ij}	= Kronecker delta
ϵ	= heat transfer rate factor
η	= dimensionless distance across film
ϕ_i	= mass transfer rate factor in effective diffusivity method
$[\phi]$	= matrix of mass transfer rate factors in equation (7)
Ξ	= correction factor in the "explicit methods"

Subscripts

c	= pertains to coolant
f	= pertains to vapour film
g	= pertains to bulk gas/vapour phase
i	= refers to vapour/liquid interface
i,j,k,n	= species index
l	= pertains to condensate
t	= total
w	= refers to the condenser tube wall

Superscripts

.	= quantity modified by finite fluxes
~	= molar quantity

Matrix Notation

$[]$	= square matrix
$[]^{-1}$	= inverse of a square matrix
I_i	= diagonal identity matrix
$()$	= column matrix

REFERENCES

1. Kern, D. Q., 1950, "Process Heat Transfer", McGraw-Hill, New York.
2. Silver, L., 1947, Trans. Inst. Chem. Eng., **25**, 30.
3. Bell, K. J., and Ghaly, M. A., 1973, A.I.Ch.E. Symp. Ser., **69**, 72.
4. Colburn, A. P., and Drew, T. B., 1937, Trans. Am. Inst. Chem. Engrs., **33**, 197.
5. Price, B. C., and Bell, K. J., 1974, A.I.Ch.E. Symp. Ser., **70**, 163.
6. Schrodt, J. T., 1973, A.I.Ch.E.J., **19**, 753.
7. Krishna, R., Panchal, C. B., Webb, D. R., and Coward, I. C., 1976, Letts Heat and Mass Transfer, **3**, 163.

8. Krishna, R., and Panchal, C. B., 1977, Chem. Eng. Sci., 32, 741.
9. Rohm, H. J., 1980, Int. J. Heat Mass Transfer, 23, 141.
10. Bandrowski, J., and Kubaczka, A., 1981, Int. J. Heat Mass Transfer, 24, 147.
11. Webb, D. R., and McNaught, J. M., 1980, "Condensers" in Developments in Heat Exchanger Technology - I (D. Chisholm, Ed.), Applied Science Publishers, Barking, England.
12. Webb, D. R., and Sardesai, R. G., 1981, Int. J. Multiphase Flow, 7, 507.
13. Webb, D. R., and Taylor, R., 1982, Chem. Eng. Sci., 37, 117.
14. Sardesai, R. G., and Webb, D. R., 1982, Chem. Eng. Sci., 37, 529.
15. Webb, D. R., 1982, Proc. 7th International Heat Transfer Conference, Munich, 5, 167.
16. Lucia, A., and Macchietto, S., 1983, A.I.Ch.E.J., in press.
17. Krishna, R., and Standart, G. L., 1979, Chem. Eng. Commun., 3, 201.
18. Webb, D. R., Panchal, C. B., and Coward, I. C., 1981, Chem. Eng. Sci., 36, 87.
19. Krishna, R., and Standart, G. L., 1976, A.I.Ch.E.J., 22, 383.
20. Toor, H. L., 1964, A.I.Ch.E.J., 10, 448, 460.
21. Stewart, W. E., and Prober, R., 1964, Ind. Eng. Chem. Fundam., 3, 224.
22. Taylor, R., and Webb, D. R., 1980, Chem. Eng. Commun., 7, 287.
23. Krishna, R., 1979, Letts. Heat Mass Transfer, 6, 437.
24. Krishna, R., 1981, Chem. Eng. Sci., 36, 219.
25. Taylor, R., and Smith, L. W., 1982, Chem. Eng. Commun., 14, 361.
26. Burghardt, A., and Krupiczka, R., 1975, Inz. Chem., 5, 487.
27. Smith, L. W., and Taylor, R., 1983, Ind. Eng. Chem. Fundam., in press.
28. Taylor, R., and Webb, D. R., 1980, Chem. Eng. Commun., 6, 175.
29. Taylor, R., and Webb, D. R., 1981, Comput. Chem. Eng., 5, 61.
30. Krishnamurthy, R., and Taylor, R., 1982, Chem. Eng. J., 25, 47.
31. Taylor, R., 1982, Comput. Chem. Eng., 6, 69.
32. Reid, R. C., Prausnitz, J. M., and Sherwood, T. K., 1977, "Properties of Gases and Liquids", 3rd Edition, McGraw-Hill, New York.
33. Westerberg, A. W., Hutchison, H. P., Motard, R. L., and Winter, P., 1979, "Process Flowsheeting", Cambridge University Press, Cambridge.

I.CHEM.E. SYMPOSIUM SERIES NO. 75

34. Dennis, J. E., and Moré, J. J., 1977, SIAM Review, 19, 46.
35. Broyden, C. G., 1965, Math. Comp., 19, 577.
36. Schubert, L. K., 1970, Math. Comp., 24, 27.
37. Krishna, R., 1979, Letts. Heat Mass Transfer, 6, 137.
38. Krishna, R., 1981, Trans. I. Chem. E., 59, 35.
39. Taylor, R., and Noah, M. K., 1982, Letts. Heat Mass Transfer, 9, 463.

PROCESS CONDENSERS

Practice

TRENDS IN DESIGN AND APPLICATION OF CONDENSERS IN THE PROCESS INDUSTRIES

K. J. Bell*

The design and application of condensers in the process industries are undergoing rapid change in many areas, including a) more fundamentally - based design procedures incorporated into extremely flexible computer programs, b) an expanding data base from tests on large process condensers, c) several new or revived condenser configurations and design features, and d) greater attention to energy recovery possibilities and operational considerations. This paper attempts to describe and inter-relate these developments, and to suggest some promising areas for further developments.

INTRODUCTION

In attempting to assess trends in a subject area, it is highly desirable to have a well known and widely-accepted point of departure. In trying to identify such a point of departure for the process condenser area, one is virtually thrown back upon Kern's "Process Heat Transfer" (1), published in 1950. One would ordinarily have sought a more recent point in such a rapidly developing and active field, but there simply are none (until this very year with the publication of the "Heat Exchanger Design Handbook" (2)).

There are several noteworthy features about the existence of this gap. First, one may point to all the things that Kern does not have. For example, all of the correlations for condensation heat transfer coefficients derive directly from Nusselt, with no consideration of the effects of vapor shear and all that we now know or strongly suspect about two-phase flow phenomena in heat transfer mechanisms. The corresponding pressure drop calculations are entirely missing. The Colburn-Hougen (3) and the Colburn-Drew (4) treatments are there, but the general multicomponent case is treated in a fashion much more naive than even the Silver (5) method. And there is of course no mention of computers for design. So it is not hard to see even without going into detail that we have made major advances in the field of condenser design and application.

But it is also useful and indeed sobering to reflect upon the fact that large scale process plants did exist and did operate very successfully 30 years ago. And their condensers were designed using methods taken from Kern. Perhaps they were more frequently oversized or undersized than present condensers, but one is still driven to the conclusion that somebody was doing something right even with what we would now regard as rather primitive tools.

*School of Chemical Engineering, Oklahoma State University, Stillwater, Oklahoma 74078, USA.